IDŐJÁRÁS

QUARTERLY JOURNAL
OF THE HUNGARIAN METEOROLOGICAL SERVICE

VOL. 100 * NO. 1–3 * JANUARY – SEPTEMBER 1996

IDŐJÁRÁS

Quarterly Journal of the Hungarian Meteorological Service

Editor-in-Chief
G. MAJOR

Executive Editor
Ms. M. ANTAL

Editorial Office: P.O. Box 39, H–1675 Budapest, Hungary or
Gilice tér 39, H-1181 Budapest, Hungary
E-mail: gmajor@met.hu; Fax: (36-1) 290-7387
antal@met.hu

Subscription from customers in Hungary should be sent to the
Financial Department of the Hungarian Meteorological Service,
Kitaibel Pál u. 1, H-1024 Budapest

Abroad the journal can be purchased from the distributor:
KULTURA, P.O. Box 149, H–1389 Budapest

This is the 100th volume of IDŐJÁRÁS!

The first issue of IDŐJÁRÁS (the name means: weather) appeared in April of 1897, therefore in this year we are publishing our 100th volume! It is a special pleasure, that the combined No. 1–3 of volume 100th can be dedicated to Prof. Ernő Mészáros at his 60th birthday.

The journals have their own life and such a long life is really exceptional amongst the meteorological journals. We know only 4 existing journals which are older than ours: Meteorologische Zeitschrift, Monthly Weather Review, The Meteorological Magazine and The Quarterly Journal of the Royal Meteorological Society.

The basic purposes of the founder of our journal, Dr. Endre Héjas, were the following:

- *to increase the meteorological knowledge in Hungary especially in the fields of weather forecasting, climatology and agrometeorology, since he met several times not only lack of proper konowledge but even misbelieves;*
- *to help to improve the Hungarian meteorological specific language.*

Dr. Héjas was the proprietor until 1925, when the Meteorological Service was not able to support the publication anymore. The journal was taken over by the Hungarian Meteorological Society. In that time the journal became more and more scientific. In 1945 it became the official scientific journal of the Hungarian Meteorological Service. Since then it has not published popular articles but research papers only. Besides the Hungarian ones, papers appeared in English, French, German and Russian as well.

From the beginning of 1992 the only accepted language is English.

During its whole lifetime the journal always published the Chronicle section. The reports here reflect the most important events in the Hungarian and international meteorological community.

The recent policy of the journal is to publish original scientific contributions in any field of atmospheric sciences from authors of any nationality. The Editorial Board is international, its members help to keep a proper scientific level.

Professor Ernő Mészáros's scientific career

Professor Ernő Mészáros was born in Budapest, Hungary, in 1935. He finished his studies in 1957 at the University of Loránd Eötvös (Budapest) receiving a diploma in meteorology. He obtained his doctorate degree in physics in 1961 at the same university. In 1985 he became a member of the Hungarian Academy of Sciences. He is presently the President of the Department of Earth Sciences of the Academy. At the same time he is the Doctor 'Honoris Causa' of the Université de Bretagne Occidentale (Brittany, France) and a member of the 'Academia Europaea'.

For eight years he served as the Secretary of the Commission on Cloud Physics of the International Association of Meteorology and Atmospheric Physics (IUGG) and as a member of the Commission of Atmospheric Chemistry and Global Air Pollution of the same Association. He has taken an active part in the background air pollution monitoring program of the World Meteorological Organisation, mainly as the principal director of its training center in Budapest.

Professor Mészáros held research positions in the Meteorological Service of Hungary and he was director of the Institute for Atmospheric Physics of the Service between 1976 and 1990. He has published more than one hundred papers and several books on atmospheric physics and chemistry including his volume on Atmospheric Chemistry in 1981, and he was invited lecturer in Europe, U.S.A., and Africa. He served as Editor-in-Chief of IDŐJÁRÁS between 1979 and 1994.

Since 1992 he has been a professor of environmental sciences at the University of Veszprém, Department of Analytical Chemistry.

Professor Mészáros's interest covers a wide spectrum of air chemistry and physics. His major research field includes the cloud chemistry, investigation of aerosols, biogeochemical cycles of elements, atmospheric sulphur cycle in particular. He is working on the investigation of organic compounds in precipitation and aerosols.

Along with his personal research achievements, which were fundamental in many respects, Professor Mészáros's major contribution to science has also been in the areas of teaching atmospheric science as a discipline. He has been lecturing on graduate and post-graduate courses since 1974 having shown interest, understanding and enthusiasm to his students.

EDITORIAL

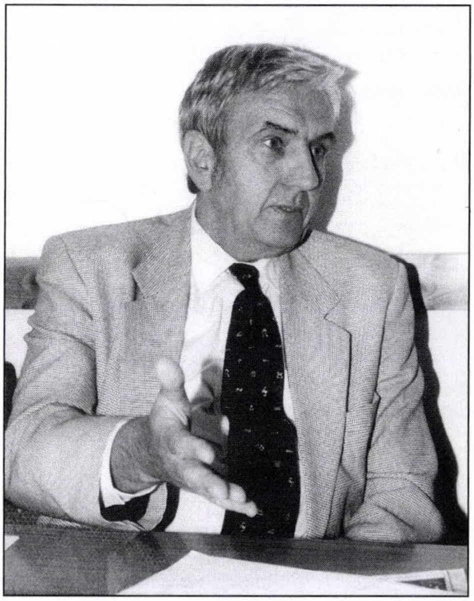

Professor Ernő Mészáros is 60

Professor Ernő Mészáros celebrated his 60th birthday in 1995. On this occasion this number of Időjárás publishes 22 papers dedicated to him by his friends and colleagues working in Hungary and in other countries. This fact confirms, that he is the best recognized scientist of the Hungarian meteorological community.

He served 16 years as Editor-in-Chief of Időjárás, the present form of our journal has been implemented by him.

Dear Ernő, all of us whish you long life and good health!

Members of the Editorial Board

Our thanks to Prof. J. Hlavay of the University of Veszprém (Hungary) for his assistance.

Contents

IDŐJÁRÁS

Quarterly Journal of the Hungarian Meteorological Service
Vol. 100, No. 1–3, January–September 1996

Aerosol climate impact in the context of global climate change

K. Ya. Kondratyev

Research Centre for Ecological Safety, Russian Academy of Science,
Nansen International Environmental and Remote Sensing Centre
18, Korpusnaya St., 197042, St. Petersburg, Russia

(Manuscript received 22 May 1995; in final form 8 September 1995)

Abstract—The Intergovernmental Panel on Climate Change Report (*IPCC*, 1990) is a most persuasive document demonstrating that the global climate change problem may only be solved in a much broader context of global change.The 1992 IPCC Supplement (*IPCC*, 1992) is a confirmation of this conclusion. The Framework Convention on Climate Change (FCCC), approved by the UN Conference on Environment and Development (UNCED) in June 1992, emphasized an urgent necessity in measures for reducing greenhouse gas emissions to the atmosphere as a critical component of the mitigation policy. The time has come now to once more assess the whole situation from the viewpoint of priorities. Since it is doubtless true that the global greenhouse warming may be compensated for by aerosol cooling to a considerable extent, it is important to analyze the reliability of relevant estimates because the assumption of pure scattering aerosols is far from reality. The results of the complex CAENEX and GAAREX field programmes conducted in Russia have been considered in this context to demonstrate the significance of aerosol absorption. Also in this context, the case of Arctic haze deserves special attention. Another important aspect is the necessity to take into account the indirect aerosol impact on climate via changes in cloud optical properties. Since global climate modelling is still at an early stage of its development, the decisive role belongs to climate observations. Optimization of the Global Climate Observing System (GCOS) with regard to combined use of conventional and satellite observations to solve climate dynamics problems in the context of global change is a must of current climate studies. Some aspects of this optimization have been considered.

Key-words: climate change, greenhouse warming, aerosol cooling, cloud optical properties.

1. Introduction

The problem of global climate change is doubtless among the most important ones humankind is presently facing (see *Gates et al.*, 1993; *Gore*, 1993; *Hansen et al.*, 1992; *Kim* and *Crowley*, 1994; *Kondratyev*, 1993a,b, 1994;

Kondratyev and *Moskalenko*, 1984; *Kondratyev* and *Cracknell*, 1995; *Kondratyev et al.*, 1995a-c; *Manabe et al.*, 1994; *Mészáros*, 1982, 1985, 1987, 1988; *Roeckner et al.*, 1995; *Schneider*, 1994; *Schwartz*, 1994; *Shaw*, 1987; *Tanre et al.*, 1984; *Taylor* and *Penner*, 1994; *Washington et al.*, 1994). In the 20th century a special value have been acquired by studies of anthropogenic impact on climate change, whose most important aspect is the assessment of the contributions of enhancing greenhouse effect and increasing content of anthropogenic aerosols in the atmosphere. There is a number of mechanisms through which aerosols affect climate, three of which are of special importance (*Kondratyev* and *Cracknell*, 1995; *Penner et al.*, 1994; *Penner*, 1995):

- Direct effect of aerosols on the radiation budget of the surface-atmosphere system through redistribution of shortwave solar radiation and infrared thermal emissions in the system due to scattering and absorption by aerosol particles, non-uniformly distributed in the atmosphere (*Box* and *Trautmann*, 1994; *Cautenet et al.*, 1992; *Charlson et al.*, 1991, 1992, 1994; *Coakley* and *Cess*, 1985; *Engardt* and *Rodhe*, 1993; *Grassl*, 1988a,b; *Hales et al.*, 1992; *Hidy* and *Wolf*, 1995; *Hunter et al.*, 1993; *Jennings*, 1993; *Karl et al.*, 1995; *Kaufman* and *Chou*, 1993; *Kiehl* and *Briegleb*, 1993; *Kiehl* and *Rodhe*, 1995; *Kondratyev*, 1991; *Langner et al.*, 1992; *Liou*, 1992; *Marchuk et al.*, 1992; *Novakov* and *Penner*, 1993; *Penner et al.*, 1994; *Preining*, 1991; *Schlesinger et al.*, 1992).
- The key role of aerosol particles in water phase transformations in the atmosphere, and in particular, in cloud formation, which is more important for atmospheric energetics than the direct effect of aerosols (*Ackerman et al.*, 1993; *Anderson et al.*, 1992; *Andreae*, 1994; *Blanchet*, 1994; *Boers et al.*, 1994; *Charlson* and *Wigley*, 1994; *Chylek* and *Hallett*, 1992; *Falkowski et al.*, 1992; *Fouquart* and *Isaka*, 1992; *Grassl*, 1975, 1992; *Hanson* and *Svenningson*, 1994; *Harshvardhan*, 1993; *Hobbs*, 1993; *Kim* and *Cess*, 1993; *King et al.*, 1995; *Kondratyev*, 1972, 1991, 1993b; *Leatich* and *Isaac*, 1994; *Lelieveld* and *Heintzenberg*, 1992; *Marchuk et al.*, 1986; *Novakov et al.*, 1994; *Parungo et al.*, 1994; *Platnick* and *Twomey*, 1994; *Raga* and *Jonas*, 1993; *Toon et al.*, 1994; *Toon*, 1995; *Twomey*, 1991). An issue of concern is the role of gas-to-particle reactions of aerosol formation (cloud condensation nuclei formation) due to natural and anthropogenic emissions to the atmosphere of compounds such as dimethylsulfide and sulphur dioxide (*Charlson et al.*, 1987; *Lawrence*, 1993; *Malin et al.*, 1993; *Putaud et al.*, 1993).
- Heterogeneous chemical processes, in particular, the disintegration of ozone molecules on the surface of aerosol particles, which affect the changes in the atmospheric gas composition (*Kondratyev*, 1989).

Complex field studies of the interaction between aerosols and radiation accomplished in different regions of the globe within the CAENEX and GAAREX programmes (*Kondratyev*, 1972, 1991) show that the aerosols absorb a considerable amount of solar radiation and thus perturb the atmospheric radiation budget to a great extent. The following problems are most urgent:

(a) Impact of dust outbreaks from arid regions on the radiative regime of the atmosphere over the continents and the oceans;

(b) Transport of aerosols to high latitudes leading to the formation of arctic haze and extended cloudiness in the Arctic (*Marchuk et al.*, 1986; *Kondratyev* and *Cracknell*, 1995; *Kondratyev et al.*, 1995). Of special importance are aerosol perturbations due to volcanic eruptions.

The most complicated problem is that of the role of radiation impact on the formation and evolution of the atmospheric aerosol field. Relationships should be studied between radiative, convective and turbulent heat and mass exchange in the processes of aerosol generation and formation, as well as the chemical composition, particle size distribution and optical properties of aerosols (*Jennings*, 1993; *Kondratyev*, 1991).

Numerical modelling of aerosol formation and global distribution requires essential advancement; further substantiation of aerosol models is necessary.

2. Modelling of aerosol properties

Modelling of aerosol properties is extremely difficult because it involves consideration of a large number of parameters affecting their variability, and also because there are no reliable criteria for choosing respective parameters. For example, the spatial and temporal variability of aerosol properties is determined by a complex set of processes of the generation, transformation and evolution of an ensemble of aerosol particles, their propagation from the sources and removal from the atmosphere. Separate consideration of these processes, which has often been the case, is incorrect, since these processes are interrelated.

The problem of aerosol modelling may be subdivided into two tasks, viz.,:

(1) Global spatial distribution of aerosols (the aerosols mass concentration field), including consideration of average characteristics of the generation, propagation and removal of particles from the atmosphere (*Kondratyev et al.*, 1983; *Kondratyev*, 1992).

(2) Local aerosol properties resulting from the effects of transformation processes of size spectra and composition of atmospheric aerosols of different origin (*Grassl*, 1974; *Ivlev*, 1982; *Mészáros*, 1981).

The processes of particle generation determine, first of all, their physical and chemical properties, and their concentration in the atmosphere, and therefore, subsequent transformation of size distribution spectra and particle removal rate from the atmosphere.

The following types of natural aerosol particles can be identified:

- Products of disintegration and evaporation of sea spray;
- Mineral dust, wind-driven to the atmosphere;
- Products of volcanic eruptions: those directly emitted to the atmosphere and resulting from gas-to-particle conversion;
- Particles of biogenic origin: those directly emitted to the atmosphere and resulting from the condensation of volatile organic compounds, e.g., terpenes, and chemical reactions taking place between them.
- Smoke from biomass burning on land;
- Products of natural gas-to-particle conversion, e.g., sulfate formed from sulfur compounds supplied by ocean surface.

Basic types of anthropogenic aerosols are particles of industrial emissions (soot, smoke, cement, road dust, etc.), as well as products of gas-to-particle conversion. Besides, part of the aerosol matter is formed by heterogeneous chemical reactions, in particular, by photocatalytic reactions.

As a result of comparatively large lifetime of aerosol particles, their transport, mixing and interaction with each other and with gaseous compounds of various substances, as well as differences in the physical and chemical properties of particles coming from various sources, are smoothed over. This results in the formation of background aerosols.

Characteristics of background aerosols vary in different atmospheric layers. This is relevant, in particular, to tropospheric and stratospheric aerosols which do not mix very well, and their particles differ considerably with regard to their composition and size distribution. There are regions in the troposphere where particles are very diverse, and this is due to relatively short lifetimes of tropospheric particles, especially in the surface layer, and also to the presence of some highly intensive sources of aerosols.

Processes of aerosol transport and removal from the atmosphere are governed by both meteorological factors, and aerosol particle properties. Processes dependent on meterological conditions involve organized convective and advective particle transport, as well as mixing due to turbulent diffusion. Individual properties of particles govern some processes of particle removal from the atmosphere, e.g. dry and wet deposition.

In the course of transport and removal of particles from the atmosphere, their size (mass) and composition are transformed due to coagulation and condensation growth, as well as to heterogeneous chemical reactions. These processes are responsible for the particle size spectrum and determine the complex refractive index value as well as the particle shape, i.e. optical properties of particles (*Ivlev*, 1982; *Kondratyev et al.*,1983).

The most essential gas-to-particle reactions affecting the formation of aerosol particles include (*Jennings*, 1993; *Kondratyev*, 1991):

- Reactions between sulphur dioxide and hydroxyl radicals which eventually lead to the formation of easily condensed sulfuric acid molecules in the presence of water molecules;
- Reactions of hydrocarbons with ozone and hydroxyl radicals, with subsequent formation of primary products with nitrogen oxides, such as peroxyacetylnitrate (PAN).

All processes of the formation and evolution of aerosol systems depend on periodical variations of solar radiation in the atmosphere and at the surface. The processes of atmospheric heating near the surface, water evaporation and chemical reactions of aerosol formation are characteristic of a pronounced diurnal variation resulting in variations of aerosol characteristics which in some cases exceed the annual variation. Considerable daily variations of anthropogenic aerosols have been observed.

Aerosol matter cycles are closely connected with hydrological processes in the atmosphere: on the one hand, clouds and precipitation play an important role in the formation, transformation and removal of aerosol particles from the atmosphere; on the other hand, aerosols are condensation nuclei whose physicochemical properties determine the microphysical processes in clouds. The fact that water vapour molecules and aerosol particles have approximately equal lifetimes has an explanation. Therefore, a more reliable knowledge of interactions between aerosols and cloud elements is necessary to better understand the processes of aerosol formation and the variability of aerosol properties in time and space.

3. Aerosol climatic impact

The relationship between climate changes due to the enhanced greenhouse effect of the atmosphere and increased aerosol concentration is strongly dependent on differences in the behaviour of anthropogenic aerosols and greenhouse gases (GHGs), caused by the spatial-temporal inhomogeneity of the aerosol distribution. These differences can be accounted for by the presence of powerful local sources, the short lifetimes of aerosols in the troposphere (of the order of several days), the photochemical particle growth processes in the presence of solar illumination, a strong interaction with natural aerosols, cloud elements and water vapour. It is the interaction between aerosols and water vapour that is first of all responsible for the limited lifetimes of both in the troposphere: about 10–15 and 6 days, respectively, as well as for their spatial-temporal inhomogeneity. The lifetimes of aerosols and water vapour are also dependent on the altitude and latitude of their location (*Ivlev*, 1982; *Kondratyev*, 1991).

It is important that anthropogenic sulfate aerosols are mostly formed at the middle latitudes of the Northern Hemisphere (Europe, U.S.A., Japan). With the total emission level of sulphur-containing gases of about 10^{14} g/year, the contribution of anthropogenic sources constitutes about 70%, out of which amount about 80% is relevant to the Northern Hemisphere, i.e. 50–60% of the total emission (*Kondratyev*, 1991). However, the efficiency of these sources in the formation of sulfate aerosols is strongly variable: from 6% to 40%. Thus, the amount of anthropogenic sulfate aerosols in the global atmosphere varies from 0.4 mg/m^2 to 2.8 mg/m^2. With the back-scattering coefficient by sulfate aerosols in the shortwave spectral region of about 10 m^2/g, the relative contribution of backscattered solar radiation will be about $4 \times 10^{-3} - 2.8 \times 10^{-2}$.

According to the estimates of Lelieveld and Heintzenberg (1992), a sulfate concentration of 0.5–2.0 mg/m^3 is responsible for a solar radiation extinction of about 0.5–1.0 W/m^2. The attenuation of solar radiation by anthropogenic sulfate aerosols must be approximately 2–2.5 times greater. Due to spatial inhomogeneity of sulfate anthropogenic aerosols, this value may vary within two orders of magnitude.

Although the role of sulfate submicron aerosols in the radiation regime of lower atmospheric layers is doubtless very important and reveals itself as cooling, it should be noted that this effect is not quite general. Data of observations obtained in the course of implementation of complex CAENEX and GAAREX programmes (*Kondratyev*, 1972, 1991) have revealed the presence of a sufficiently large amount of aerosol particles absorbing shortwave solar radiation in the troposphere, which may lead sometimes not to cooling but to radiative heating of lower atmospheric layers. In most cases, such absorption is due to the presence of soot (black carbon — BC and organic carbon — OC) and iron oxides in the aerosol matter. In polluted urban atmosphere, the contribution of soot in the mass aerosol concentration may reach 10–30%, and that of sulfate components 20–40%.

It is important that a considerable portion of soot particles is represented by small-sizes fraction (particle radius $r < 0.1$ μm). According to observational data, the modal radius of primary soot nuclei may reach 20–40 μm, whereas that of sulfate particles is in the size range of about 0.15 μm (*Kondratyev*, 1991). The coagulation of primary soot nuclei leads to the formation of fractals having a lower sedimentation rate and anomalous optical properties. If there are mineral or other aerosol particles close to a soot source of high concentration (which is also relevant to sulfate particles), primary soot nuclei are condensed on these particles forming a cover layer. The specific absorption of shortwave radiation by soot may then increase by an order of magnitude or more (*Kondratyev* and *Ivlev*, 1995).

It should also be noted that in most cases, the emissions of sulfur-containing gases, which are transformed into sulfuric acid and sulfates, are accompanied by simultaneous release of soot to the atmosphere. It is known that soot can be an effective catalyst in the process of SO_2 oxidation up to SO_4. The optical properties of non-uniform particles that are formed this way differ substantially from the optical properties of homogeneous particles. To calculate the optical characteristics of spherical particles, their modelling with polydispersive two-layer spheres has been successfully performed (*Ivlev et al.*, 1992; *Kondratyev* and *Ivlev*, 1995).

The formation of two-layer cloud particles resulting from the condensation of water vapour on particles containing soot leads, as a rule, to an increase of albedo for shortwave radiation. In such cases, clouds have a greyish-brown or brownish colour. In particular, at sufficiently large optical thicknesses, an enhancement of molecular absorption by minor gases may appear due to an increased photon path length in a cloud (*Twomey*, 1991), as well as a result of the formation of thin layer of adsorbed molecules absorbing radiation. The increase of cloud albedo may take place due to a change in the droplet size distribution with the growing concentration of CCN: the mean modal radius decreases, the number concentration of small droplets grows, and this changes the scattering function and increases the contribution of back scattering (*Kondratyev* and *Ivlev*, 1995).

Cloud formation processes are greatly affected by nitrogen oxides and their acids, whose source, to a large extent, is industrial activity. Their role is especially important in the processes of formation of polar clouds. In particular, one of the types of polar stratospheric clouds is formed at the heterogeneous condensation of nitric acid on the surface of sulfuric acid droplets (*Kondratyev*, 1989).

It is known fact (*Kondratyev et al.*, 1995c) that arctic haze and clouds contain a considerable amount of anthropogenic impurities, including soot, which decreases substantially the albedo of polar regions and reacts against the global effect of atmospheric cooling due to anthropogenic sulfates.

It should be emphasized that heterogenic chemical reactions in the atmosphere related to anthropogenic activity are one of the most important factors of the impact of anthropogenic aerosols on climate. Firstly, these reactions stimulate a faster removal from the atmosphere of a number of gaseous impurities (sulfur dioxide, ozone, hydrocarbons, in particular, methane, nitrogen oxides, hydrochloric acid), thus reducing their lifetimes. Secondly, they influence the evolution of the aerosol particle size spectrum, and consequently, the albedo value. At the same time, photochemical heterogeneous processes can be a sensitive climatic regulator of solar-terrestrial relationships (*Shaw*, 1987).

Aerosols play an important role in the heterogeneous destruction of ozone molecules both in the stratosphere, and the lower atmospheric layers (*Kondratyev*, 1989). Heterogeneous reactions of ozone molecule destruction are mainly due to atmospheric dust particles containing metal oxides, and above all, aluminium oxides. In the presence of shortwave solar radiation ($\lambda > 320$ nm), the destruction of ozone molecules is possible in the process of photochemical oxidation of triplet-exited sulfur dioxide (*Kondratyev* and *Ivlev*, 1995).

4. Unsolved problems

Further studies of atmospheric aerosol properties and their climatic impacts should primarily include:

- Improving standard radiative models of the atmosphere to more adequately simulate the characteristics of various types of aerosols, including low humidity effects, particles size distribution, vertical concentration profiles, etc.
- Obtaining more adequate observational information about the spatial and temporal variability of aerosols on global scales, on the basis of both in situ and remote sensing observations. A special part of the GCOS should be developed to accomplish observations relevant to aerosols and climate problem (*Kondratyev* and *Cracknell*, 1995).
- Developing techniques to identify anthropogenically induced aerosol content and composition on both regional and global scales, with special consideration given to monitoring sulfate dynamics and soot components.
- Studying the dependence of real-aerosol optical properties and their chemical composition and size distribution, accounting for the effects of varying air humidity.
- Comparing special techniques to obtain aerosol characteristics, which includes remote sensing techniques in addition to in situ measurements.
- Undertaking both observational and theoretical studies of the internal aerosol particle structure, considering their multicomponent formation, as well as the role of aerosol particles as condensation nuclei.

References

Ackerman, A.C., *Toon, O.B.* and *Hobbs, P.V.*, 1993: Dissipation of marine stratiform clouds and collapse of the marine boundary layer due to the depletion of cloud condensation nuclei by clouds. *Science 262*, 226–229.

Anderson, T.L., *Wolfe, G.V.* and *Warren, S.G.*, 1992: Biological sulfur, clouds, and climate. *Ency. Earth Syst. Sci. 1*, 363-376.

Andreae, M.O., 1994: Climate effects of changing atmospheric aerosol levels. In *World Survey of Climatology*, Vol. XX. *Future Climate of the World* (ed.: *A. Henderson-Sellers*).

Blanchet, J.-P., 1994: Mechanisms of direct and indirect climate forcing by aerosols. In *Proc. Dahlem Workshop on Aerosol Forcing of Climate*. Berlin, April 1994.

Boers, R., *Ayers, G.P.* and *Gras, J.L.*, 1994: Coherence between seasonal variation in satellite-derived cloud optical depth and boundary layer CCN concentrations at a mid-latitude Southern Hemisphere station. *Tellus 46B*, 123-131.

Box, M.A. and *Trautmann, T.*, 1994: Computation of anthropogenic sulphate aerosol forcing using additive perturbation theory. *Tellus 46B*, 33-39.

Cautenet, G., *Legrand, M.*, *Cautenet, S.*, *Bonnel, B.* and *Brongiez, G.*, 1992: Thermal impact of Saharan dust over land. Part I: Simulation. *J. Appl. Meteorol. 31*, 166-180.

Charlson, R.J. and *Wigley, T.M.L.*, 1994: Sulfate aerosol and climatic change. *Scientific American 270*, 28-35.

Charlson, R.J., Lovelock, J.E., Meinrat, O. and *Warren, S.G.*, 1987: Oceanic phytoplankton, atmospheric sulfur, cloud albedo and climate. *Nature 326*, 655-661.

Charlson, R.J., Langner,J., Rodhe, H., Leovy, C.B. and *Warren, S.G.*, 1991: Perturbation of the Northern Hemisphere radiative balance by backscattering from anthropogenic sulfate aerosols. *Tellus 43A*, 152-163.

Charlson, R.J., Schwartz, S.Z., Hales, J.M., Cess, R.D., Coakley, J.A., Hansen, J.E. and *Hofmann, D.F.*, 1992: Climate forcing by anthropogenic aerosols. *Science 255*, 423-430.

Chylek, P. and *Hallett, J.*, 1992: Enchanced absorption of solar radiation by cloud droplets containing soot particles in their surface. *J. Roy. Meteorol. Soc. 118A*, 167-172.

Coakley, J.A., Jr. and *Cess, R.D.*, 1985: Response of the NCAR community model to the radiative forcing by the naturally occuring tropospheric aerosol. *J. Atmos. Sci. 42*, 1677-1692.

Engardt, M. and *Rodhe, H.*, 1993: A comparison between patterns of temperature trends and sulfate aerosol pollution. *Geophys. Res. Lett. 20*, 117-120.

Falkowski, P.G., Kim, Y., Kodler, Z., Wilson, C., Wirick, C. and *Cess, R.D.*, 1992: Natural versus anthropogenic factors affecting low-level cloud albedo over the North Atlantic. *Science 256*, 1311-1313.

Fouquart, Y. and *Isaka, H.*, 1992: Sulfur emission, CCN, clouds and climate: a review. *Ann. Geophys. 10*, 462-471.

Gates, L.W., Cubasch, U., Meehl, G.A., Mitchell, J.P.B. and *Stouffer, R.J.*, 1993: An intercomparison of selected features of the control climates simulated by coupled ocean-atmosphere general circulation models. World Climate Research Programme. WMO, No. 574, 1-46.

Gore, A., 1993: *Earth in the Balance*. Ecology and the Human Spirit. New York, NY et al., PLUME.

Grassl, H., 1974: Erwarmung und Abkühlung durch atmosphärisches Aerosol. *Ann. Meteorol. Neue Folge 9*, 55-59.

Grassl, H., 1975: Albedo reduction and radiative heating of clouds by absorbing aerosol particles. *Beitr. Phys. Atm. 48*, 199-210.

Grassl, H., 1982: The influence of aerosol particles on radiation parameters of clouds. *Időjárás 86*, 60-75.

Grassl, H., 1988a: What are the radiative and climatic consequences of the changing concentration of atmospheric aerosol particles? In *The Changing Atmosphere* (eds.: *F.S. Rowland* and *I.S.A. Isaksen*). J. Wiley & Sons, Chichester, 187-199.

Grassl, H., 1988b: Radiative effects of atmospheric aerosol particles. In *Aerosols and Climate* (eds.: *P.V. Hobbs* and *M.P. McCormick*). Deepak Publ., Hampton, VA, 241-252.

Hales, J.M., Cess, R.D., Coakley, J.A., Hansen, J.E., Hofmann, D.J., Charlson, R.J. and *Schwartz, S.E.*, 1992: Climate forcing by anthropogenic aerosols. *Science 255*, 423-429.

Hansen, J., Rossow, W. and *Fung, I.* (eds.), 1993: Long-term monitoring of global climate forcing and feedbacks. NASA CP 3234. *Proc. of Workshop held at Goddard Inst. for Space Studies*, New York, Febr. 1992.

Hansen, J., Wilson, H., Sato, M., Ruedy,R., Shah, K. and *Hansen, E.*, 1995: Satellite and surface temperature data at odds? *Clim. Change 30*, 103-107.

Hanson, H.C. and *Svenningson, B.*, 1994: Aerosols and clouds. In *Physico-Chemical Behaviour of Atmospheric Pollutants* (eds.: *G. Angeletti* and *G. Restelli*). Office for Official Publications of the European Communities (Report EUR 15609/2 EN), Brussels-Luxemburg, 2, 837-846.

Harshvardhan, 1993: Aerosol-climate interactions. In *Aerosol-Cloud-Climate Interactions* (ed.: *V. Hobbs*). Academic Press, San Diego et al., 76-96.

Hidy, G.M. and *Wolf, M.*, 1995: Projection of trends in anthropogenic aerosol sources. In *Proc. Dahlem Workshop on Aerosol Forcing of Climate*. Berlin, April 1994 (in press).

Hobbs, P.V., 1993: Aerosol-cloud interactions. In *Aerosol-Cloud-Climate Interactions* (ed.: *P.V. Hobbs*). Academic Press, San Diego et al., 33-75.

Hunter, D.E., Schwartz, S.E., Waggoner, R. and *Berkovitz, C.M.*, 1993: Seasonal, latitudinal, and secular variations in temperature trend: Evidence for influence of anthropogenic sulfate. *Geophys. Res. Lett. 20*, 2455-2458.

IPCC-1990: *Climate Change*. The IPCC Scientific Assessment (eds.: *J.T. Houghton, G.J. Jenkins* and *J.J. Ephraums*). Cambridge Univ. Press, Cambridge.

IPCC-1992: *Climate Change*. The Supplementary Report to the IPCC Scientific Assessment (eds.: *J.T. Houghton, B.A. Callander* and *S.K. Varney*). Cambridge Univ. Press, Cambridge, 200.

Ivlev, L.S., 1982: *Chemical Composition and Size Distribution of Atmospheric Aerosols* (in Russian). Leningrad Univ. Press, Leningrad.

Ivlev, L.S., Kondratyev, K.Ya. and *Korostina, O.M.*, 1992: Numerical simulations of the optical properties of cloud particles of a complex composition. *Optics Atmos. Ocean 5*, 1194-1207.

Jaworowski, Z., Segalstad, T.V. and *Hisdal, V.*, 1992: *Atmospheric CO and Global Warming: A Critical Review*. Second Revised Edition. Norsk Polarinstitutt, Meddelelser Nr.119, Oslo, 76 pp.

Jennings, S.G. (ed.), 1993: *Aerosol Effects on Climate*. Univ. of Arizona Press, 304 pp.

Karl, T.R., Knight, R.W., Kukla, G. and *Gavin, J.*, 1995: Evidence for radiative effects of anthropogenic sulfate aerosols in the observed climate record. In *Aerosol Forcing of Climate* (eds.: *R. Charlson* and *J. Heintzenberg*). John Wiley & Sons, New York (in press).

Kaufman, Y.J. and *Chou, M.-D.*, 1993: Model simulations of the competing climatic effects of SO_2 and CO_2 . *J. Climate 6*, 1241-1252.

Kiehl, J.T. and *Briegleb, B.P.*, 1993: The relative roles of sulphate aerosols and greenhouse gases in climate forcing. *Science 260*, 311-314.

Kiehl, J.T. and *Rodhe, H.*, 1995: Modeling geographical and seasonal forcing due to aerosols. In *Proc. Dahlem Workshop on Aerosol Forsing of Climate*. Berlin, April 1994, (in press).

Kim, Y. and *Cess, R.D.*, 1993: Effect of anthropogenic sulfate aerosols on low-level cloud albedo over oceans. *J. Geophys. Res. 98*, 14883-14886.

Kim, K.-Y. and *Crowley, T.J.*, 1994: Modeling the climate effects of unrestricted greenhouse emission over the next 10 000 years. *Geophys. Res. Lett. 21*, 681-684.

King, M.D., Tsay, S.-C. and *Platnic, S.E.*, 1995: In situ observations of the indirect effects of aerosol on cloud. In *Proc. Dahlem Workshop on Aerosol Forcing of Climate*. Berlin, April 1994, (in press).

Kondratyev, K.Ya., 1972: *The Complete Atmospheric Energetics Experiment*. GARP Publ. Ser., WMO, Geneva, No. 12.

Kondratyev, K.Ya., 1989: *Global Ozone Dynamics* (in Russian). VINITI Publ., Moscow.

Kondratyev, K.Ya. (ed.), 1991: *Aerosols and Climate* (in Russian). Gidrometeoizdat, Leningrad.

Kondratyev, K.Ya., 1992: *Global Climate* (in Russian). NAUKA Publ., St. Petersburg.

Kondratyev, K.Ya., 1993a: *Global Climate Observing System*. Studying the Earth from Space 6 (in Russian), 104-115.

Kondratyev, K.Ya., 1993b: Water cycle and relevant feedbacks in the problem of global climate change (in Russian). *Meteorology and Hydrology 3*, 9-19.

Kondratyev, K.Ya., 1994: *Perspectives of the 'Mission to Planet Earth' and the 'Earth Observing System' Programmes*. Studying the Earth from Space 1 (in Russian), 105-108.

Kondratyev, K.Ya. and *Moskalenko, N.I.*, 1984: *Greenhouse Effect of the Atmosphere and Climate* (in Russian). VINITI Publ., Moscow, 262 pp.

Kondratyev, K.Ya. and *Cracknell, A.P.*, 1995: *Observing Global Climate Change*. Taylor & Francis, London (in press).

Kondratyev, K.Ya. and *Ivlev, L.S.*, 1995: On the aerosol impact on climate (in Russian). *Proc. of Russian Acad. Sci. 340*, 98-99.

Kondratyev, K.Ya., Moskalenko, N.I. and *Pozdnyakov, D.V.*, 1983: *Atmospheric Aerosols* (in Russian). Gidrometeoizdat, Leningrad.

Kondratyev, K.Ya., Buznikov, A.A. and *Pokrovsky, O.M.*, 1995a: *Global Change and Remote Sensing*. WILEY/Praxis, London (in press).

Kondratyev, K.Ya., Asimakopoulos, D.N. and *Varotsos, C.A.*, 1995b: European ecodynamics in the context of global change (in Russian). Studying the Earth from Space 2, 5-19.

Kondratyev, K.Ya., Johannessen, O.M. and *Melentyev, V.V.*, 1995c: *High Latitude Climate and Remote Sensing*. WILEY/Praxis, London (in press).

Langner, J., Rodhe, H., Crutzen, P.J. and *Zimmerman, P.*, 1992: Anthropogenic influence on the distribution of tropospheric sulfate. *Nature 359*, 712-716.

Lawrence, M.G., 1993: An empirical analysis of the strength of the phytoplankton-dimethylsulfide-cloud-climate feedback cycle. *J. Geophys. Res. 98*, 20663-20674.

Leatich, W.R. and *Isaac, G.A.*, 1994: On the relationship between sulfate and cloud droplet number concentration. *J. Climate 7*, 206-212.

Lelieveld, J. and *Heintzenberg, J.*, 1992: Sulfate cooling effect through in-cloud oxidation of anthropogenic SO_2. *Science 258*, 117-120.

Liou, K.-N., 1992: *Radiation and Cloud Processes in the Atmosphere. Theory, Observations and Modelling*. Oxford Univ. Press, New York-Oxford.

Malin, G., Turner, S., Liss, P., Holligan, P. and *Harbour, D.*, 1993: Dimethylsulphide and dimethylsulphoniopropionate in the northeast Atlantic during summer coccolithosphere bloom. *Deep-Sea Res. 40*, 1487-1508.

Manabe, S., Stouffer, R.J. and *Spelman, M.J.*, 1994: Response of a coupled ocean-atmosphere model to increasing atmospheric carbon dioxide. *Ambio 23*, 44-49.

Marchuk, G.I., Kondratyev ,K.Ya., Kozoderov, V.V. and *Khvorostyanov, V.I.*, 1986: *Clouds and Climate* (in Russian). Gidrometeoizdat, Leningrad.

Marchuk, G.I., Kondratyev, K.Ya. and *Kozoderov, V.V.*, 1992: *Earth's Radiation Budget: Key Issues*. Nauka Publ., Moskow.

Mészáros, E., 1981: Atmospheric Chemistry. Fundamental Aspects. Akadémiai Kiadó, Budapest.

Mészáros, E., 1982: On the atmospheric input of sulfur into the ocean. *Tellus 34*, 277-282.

Mészáros, E., 1985: On the climatic effects of radiatively active trace gases and aerosol particles. *Időjárás 89*, 302-308.

Mészáros, E., 1987: Past climatic changes as revealed by recent research in Earth sciences (in Hungarian). *Időjárás 91*, 302-308.

Mészáros, E., 1988: Contemporary variations in atmospheric composition (in Hungarian). *Időjárás 92*, 101-109.

Novakov, T. and *Penner, J.E.*, 1993: Large concentration of organic aerosol to cloud condensation nuclei concentrations: Evidence from a marine site. *Nature 365*, 823-826.

Novakov, T., Rivera-Carpio, C., Penner, J.E. and *Rogers, C.F.*, 1994: The effect of anthropogenic sulfate aerosols on marine cloud droplet concentrations. *Tellus 46B*, 132-141.

Parungo, F., Boatman, J.F., Sievering, H., Wilkinson, S.W. and *Hicks, B.B.*, 1994: Trends in global marine cloudiness and anthropogenic sulphur. *J. Climate 7*, 434-440.

Penner, J.E., Charlson, R.J., Hales, J.M., Laulainen, N.S., Leifer, R., Novakov, T., Ogren, J., Radke, L.F., Schwartz, S.E. and *Travis, L.*, 1994: Quantifying and minimizing uncertainty of climate forcing by anthropogenic aerosols. *Bull. Amer. Meteorol. Soc. 75*, 375-400.

Penner, J., 1995: Organic aerosols. In *Proc. Dahlem Workshop on Aerosol Forcing of Climate*. Berlin, April 1994 (in press).

Platnick, S.E. and *Twomey, S.*, 1994: Determining the susceptibility of cloud albedo to changes in droplet concentration with the Advanced Very High Resolution Radiometer. *J. Appl. Meteorol. 33*, 334-347.

Preining, O., 1991: Aerosol and climate — an overview. *Atmos. Environ. 25A*, 2443-2444.

Putaud, J.-P., Belviso, S., Nguyen, B.C. and *Mihalopoulos, N.*, 1993: Dimethylsulfide, aerosols, and condensation nuclei over the tropical northeastern Atlantic Ocean. *J. Geophys. Res. 98*, 14863-14871.

Raga, G.B. and *Jonas, P.R.*, 1993: On the link between cloud-top radiative properties and subcloud aerosol concentration. *Quart. J. Roy. Meteorol. Soc. 119*, 1419-1425.

Roeckner, E., Siebert, T. and *Feichter, J.*, 1995: Climatic response to anthropogenic sulfate forcing simulated with a general circulation model. In *Proc. Dahlem Workshop on Aerosol Forcing of Climate*. Berlin, April 1994 (in press).

Schlesinger, M.E., Jiang, X. and *Charlson, R.J.*, 1992: Implication on anthropogenic atmospheric sulfate for the sensitivity of the climate system. In *Climate Change and Energy Policy* (eds.: *C. Rosen* and *R. Glasser*). Amer. Inst. of Physics, New York, 75-108.

Schneider, S.H., 1994: Detecting climatic change signals: are there any 'fingerprints'? *Science 263*, 341-347.

Schwartz, S.E., 1994: Climate forcing by gases and aerosols. *Pure and Appl. Chem. 66*, 178-187.

Shaw, G.E., 1987: Aerosol as climate regulators: a climate-biosphere linkage? *Atmos. Environ. 21*, 985-986.

Tanre, D., Geleyn, J.-F. and *Slingo, J.*, 1984: First results of the introduction of an advanced aerosol radiation interaction in the ECMWF low resolution global model. In *Aerosol and Their Climatic Effects* (eds.: *H.E. Gerber* and *A. Deepak*). A. Deepak Publ., Hampton, VA, 133-177.

Taylor, K.E. and *Penner, J.E.*, 1994: Response of the climate system to atmospheric aerosols and greenhouse gases. *Nature 369*, 734-737.

Toon, O.E., Ackerman, A. and *Jensen, J.*, 1994: Interaction between aerosols and clouds. *Proc. Third ARM Science Team Meeting*. March 1993. U.S. Department of Energy, CONF-9303112, UC-402. Washington, DC, 135-158.

Toon, O.B., 1995: Modelling the relationships between aerosol properties: the direct and indirect effects of aerosols on climate. In *Proc. Dahlem Workshop on Aerosol Forcing of Climate*. Berlin, April 1994 (in press).

Twomey, S., 1991: Aerosols, clouds and radiation. *Atmos. Environm. 25A*, 2435-2442.

Washington, W.M., Meehl, G.A., Ver Plank, L. and *Bettge, T.W.*, 1994: A world ocean model for greenhouse sensitivity studies: resolution intercomparison and the role of diagnostic forcing. *Climate Dynamics 9*, 321-344.

IDŐJÁRÁS

Quarterly Journal of the Hungarian Meteorological Service
Vol. 100, No. 1-3, January-September 1996

Recent results on stratospheric ozone depletion

Tibor Bérces

Central Research Institute for Chemistry,
Hungarian Academy of Sciences,
Pusztaszeri u. 59-67, H-1025 Budapest, Hungary

(Manuscript received 3 July 1995; in final form 6 November 1995)

Abstract—Stratospheric ozone protects life on Earth's surface by absorbing harmful UV radiation of the sunlight. All changes which influence the protecting ozone layer may have a negative effect on living organisms. During the last two decades, measurements indicate a decreasing trend in stratospheric ozone concentration at midlatitudes of both hemispheres. In addition, the decrease of ozone level during the Antarctic spring (i.e. the ozone hole) shows a growing tendency. Recent results and observations suggest that stratospheric ozone losses are due to chlorine and bromine compounds, which are largely of anthropogenic origin. The ozone destruction processes are produced by chemical reactions forming catalytic cycles. Three major free radical families are responsible for these reactions: (i) the nitrogen radicals (NO, NO_2); (ii) the odd hydrogen radicals (OH, HO_2); and (ii) the halogen radicals (ClO, BrO). In contrast with former opinions, catalytic cycles that occur with the participation of halogen radicals play the dominant role in stratospheric ozone depletion both at midlatitudes and over Antarctica.

Key-words: ozone destruction, stratospheric ozone depletion, ozone hole, catalytic cycles, nitrogen radicals, odd hydrogen radicals, halogen radicals.

1. Introduction

Most of the atmospheric ozone (about 90%) is found in the stratosphere between 10 and 50 km altitude and the rest of ozone (about 10%) is in the troposphere. The stratospheric and tropospheric ozone has very different effect on living organisms. Stratospheric ozone plays a significant role by absorbing most of the harmful ultraviolet sunlight and hereby protecting life on the Earth's surface. This filter effect is especially important in the UV-B spectral region between 280 and 320 nm. These wavelengths have strong damaging effect on humans and other living systems. In this wavelength range other constituents of the atmosphere hardly absorb. On the other hand, tropospheric ozone has a negative effect at surface level on human health, forests and crop production by its high reactivity which results in damage in tissues of plants and living creatures. This different effect explains the public concern about the increase in surface-level tropospheric ozone and losses of stratospheric ozone.

In this paper we deal with recent important observations and conclusions related to stratospheric ozone depletion. Ozone is formed steadily in the stratosphere where the UV components of sunlight dissociate the oxygen molecules forming reactive (singlet excited) oxygen atoms which subsequently combine with other oxygen molecules to give ozone (*Mészáros,* 1991):

$$O_2 + h\nu \rightarrow O + O,$$

$$O + O_2 \rightarrow O_3.$$

Sunlight can also dissociate ozone by the photolytic reaction

$$O_3 + h\nu \rightarrow O_2 + O,$$

which is the major O_3 consuming process in the stratosphere. In course of time these O_3 forming and consuming reactions led to the establishment of more or less constant stationary ozone concentrations which — apart from temporary small fluctuations — changed only very slowly during a long time period. This was the situation up till about two decades ago when significant amounts of new pollutants from anthropogenic sources began to appear in the stratosphere which caused well observable negative trends in stratospheric ozone concentration due to their O_3 destroying effect.

2. Trends in stratospheric ozone concentration

Measurements made by ground-based and satellite systems have shown significant ozone decreases during the last two decades at midlatitudes (30°– 60°) of both hemispheres (*WMO,* 1994). Decreases in total ozone column are on the average 4–5% per decade at midlatitudes. Depletion is more significant in the Northern Hemisphere and smaller in the Southern Hemisphere. The losses are much larger during winter and spring than during summer and fall. No statistically significant decrease is observed in the tropics (20°S–20°N).

Especially large ozone depletion was observed at midlatitudes in the lower stratosphere in 1992 and 1993. Global-average total-ozone levels were 1–2% below that expected from the long-term trends. It is believed that these dramatic ozone losses in 1992 and 1993 were due, at least in part, to the eruption of Mt. Pinatubo in 1991. The sulfur gases injected in the atmosphere led to a large increase of the stratospheric sulfate aerosol surface area which enhanced heterogeneous reactions and temporary increased ozone loss in the stratosphere.

In the first half of 1994, the aerosol abundance significantly decreased and ozone concentration returned to a level close to that expected from long-term trends.

A special manifestation of loss of stratospheric ozone is the phenomenon known as Antarctic ozone hole. This was first observed in 1985 by the British Antarctic Survey Station at Halley Bay, Antarctica (*Farman* et al., 1985). The phenomenon consists of a sharp decrease in total ozone over Antarctica during the period of Southern Hemisphere spring (i.e. September and October). Available measurements indicate that the decrease of ozone level during the Antarctic spring shows a growing tendency indicating an anthropogenic origin, i.e. the role of halogen containing pollutants. There was a decrease of springtime ozone level over the Antarctica at the time when such pollutants could not cause ozone depletion (which was, however, only 30–40%). This was and is caused by the exceptionally cold temperatures above the Southern Pole. However, recent ozone level decreases go up to 60%. The most severe ozone holes were observed in 1992 and 1993 (after the eruption of Mt. Pinatubo in 1991). Ozone levels as low as 105–108 DU were measured in these years (*Kerr*, 1994), which should be compared with the 280 DU value typical for this time of the year in the late 1970s, before the hole began to form. However, the most disappointing fact is that 102 DU ozone levels were measured in 1994 when the sulfate aerosols produced as a consequence of the Mt. Pinatubo eruption have been swept out of the stratosphere. This is a further evidence that the ozone hole is linked to the increase of anthropogenic pollutants, most likely to human-made chlorine and bromine compounds in the stratosphere.

3. The causes of stratospheric ozone depletion

The problem of stratospheric ozone depletion is a complex one in which meteorological, physical (transport) and chemical elements are involved (*Mészáros*, 1989). Considering the causes of large ozone losses in the stratosphere, the cold temperature at 15–20 km altitudes (where most of the ozone loss occurs) is definitely an important circumstance. The extremely cold temperatures over the Poles may give an answer why the springtime ozone levels are lower and the ozone hole is much deeper over Antarctica compared with Arctic conditions (where the minimum temperature is higher by about 10K). However, meteorology alone is insufficient to explain the downward trends in stratospheric ozone levels observed during the last two decades. Moreover, major volcanic eruptions may have a significant effect in the lower stratosphere on the meteorological conditions and on ozone concentrations through the large increase in sulfate aerosol caused by the eruption. This could be experienced after the Mt. Pinatubo eruption in 1991 which resulted in a transitory rise of 1K in the lower-stratospheric temperature (due to the increased absorption of radiation by the aerosol) and in a severe increase of the Antarctic ozone hole in 1992 and 1993 (due to acceleration of ozone destroying reactions by the aerosol). The volcanic perturbations are temporary, thus the abundance of sulfate aerosol particles decayed and global ozone concentration recovered in 1994, three years after the Mt. Pinatubo eruption (*WMO*, 1994).

The results of observations, laboratory investigations and modelling studies clearly show that anthropogenic pollutants injected from the troposphere in the lower stratosphere are responsible for the long-term global stratospheric ozone depletion. It has been suggested that nitrogen oxides (*Crutzen*, 1971) and certain halogen containing compounds (*Molina* and *Rowland*, 1974) can enhance the rate of ozone decomposition by catalytic cycles (see the discussion of the decomposition mechanism below).

Most of the nitrogen oxides entering the stratosphere is N_2O which originates from microbiological processes in the soil. This N_2O is stable in the troposphere and decomposes only in the stratosphere by photolysis, yielding NO. Only a small part of the NO_x content of the stratosphere originates from anthropogenic sources, mainly from the emission of supersonic aircraft. Previously NO_x was believed to play the dominant role in the chemical destruction of ozone in the midlatitude lower stratosphere. However, recent direct in situ measurements of radical species in the lower stratosphere, coupled with model calculations, have quantitatively shown that the role played by the (largely natural) reactive nitrogen compounds (NO_x) is much smaller than that of the (largely anthropogenic) halogen compounds (*WMO*, 1994).

Recent scientific results and observations suggest that the middle- and high-latitude ozone losses are largely due to anthropogenic chlorine and bromine compounds (*WMO*, 1994). There are three groups of compounds which constitute the most important primary sources of chlorine and bromine entering the stratosphere. These are *chlorofluorocarbons* (CFCs), as for instance CFC-11 ($CFCl_3$), CFC-12 (CF_2Cl_2), CFC-113 ($C_2F_3Cl_3$), CFC-114 ($C_2F_4Cl_2$), CFC-115 (C_2F_5Cl), *other chlorinated hydrocarbons*, as for instance carbon tetrachloride (CCl_4), methyl chloroform ($C_2H_3Cl_3$), chloroform (CH_3Cl), and *halons*, as for instance halon-1211 ($CBrClF_2$), halon 1301 ($CBrF_3$), halon 2402 ($C_2Br_2F_4$). The entirely human made CFC-11, CFC-12, CFC-113, CCl_4 and CH_3Cl_3 provide 80% of the chlorines swept into the stratosphere, while halon 1301 is the most important and most dangerous bromine source (with an ozone depletion potential as high as $ODP = 10$). These compounds (including the entirely human made ones) were detected by measurements made in the stratosphere. The compounds are non-soluble in water and react very slowly in the troposphere, therefore they are characterized by long tropospheric lifetimes which results in a high chance to enter into the stratosphere.

Available data show that the average concentration of chlorine containing compounds in the stratosphere increased during the last 50 years from a 0.6 ppb background level to about 3.5 ppb. If the present tendency continued, the concentration of CFCs and other halogen containing compounds would triple by about 2050, and this high halogen load would result in further serious ozone depletion. The recognition of this situation led to international agreements on the restriction and prohibition of the use of certain halogen containing compounds. The first significant agreement in 1987, known as Montreal Protocol, planned the reduction of the production of certain specially dangerous halogen containing compounds. This was followed by amendments to strengthen the agreement, and finally the Copenhagen Amendment prescribed a ban by 1996 on the production of the most damaging compounds. As a result of these agreements, the concentration of the chlorine and bromine containing compounds in the stratosphere is expected to reach a maximum in a few years, around 1998, and then to decrease slowly. However, it will take a longer time, probably till around the middle of the next century until the ozone layer will recover.

A result of the phase-out of the CFCs is that certain hydrochlorofluorocarbons (HCFCs) and hydrofluorocarbons (HFCs) are being manufactured and used as CFC substitutes. These compounds have reactive hydrogen atoms which result in a relatively short tropospheric lifetime and prevent them from entering into stratosphere.

4. The mechanism of stratospheric ozone depletion

As mentioned already, stratospheric ozone destruction is dominated by catalytic cycles occurring with the participation of free radicals. Three major radical families are responsible for the predominant part of ozone loss in the middle and lower stratosphere: (i) the nitrogen radicals, designated by NO_x and consisting of NO and NO_2; (ii) the odd hydrogen radicals, HO_x, consisting of OH and HO_2; and finally (iii) the halogen radicals ClO and BrO.

For two decades it was believed that nitrogen-radical chemistry dominated the catalytic ozone destruction at midlatitudes. It is only recently that in situ measurements of the concentrations of OH, HO_2, ClO, BrO, NO and NO_2, demonstrated the predominance of odd-hydrogen and halogen free-radical catalysis over nitrogen radical chemistry (*Wennberg et al.*, 1994). On the basis of these measurements it could be estimated that the odd-hydrogen radical cycle accounted for nearly one half of the total O_3 removal, halogen-radical chemistry was responsible for approximately one third of O_3 loss (with about 50–50% of the ClO and BrO contribution), while NO_x catalysis accounted for less than 20% of the O_3 destruction.

The most important ozone destruction cycle in the lower stratosphere (which accounts for 35–50% of ozone depletion) is made up of the following two reactions of odd-hydrogen radical species:

$$\begin{array}{l} OH + O_3 \rightarrow HO_2 + O_2 \\ HO_2 + O_3 \rightarrow OH + 2O_2 \\ \hline \text{Net: } 2O_3 \rightarrow 3O_2. \end{array}$$

The radical which reacts in the first reaction is formed back in the second one thus forming a catalytic cycle. The net result of this cycle is the conversion of two ozone molecules into three oxygen molecules.

The ozone consuming NO_x reactions are different in the lower and middle stratosphere. At higher altitudes, where oxygen atom concentrations are large (due to the high O_2 photolysis rate caused by the strong UV radiation), the dominant cycle is:

$$\begin{array}{l} NO + O_3 \rightarrow NO_2 + O_2 \\ NO_2 + O \rightarrow NO + O_2 \\ \hline \text{Net: } O_3 + O \rightarrow 2O_2. \end{array}$$

In the lower part of the stratosphere ozone destruction by NO_x catalysis occurs via reactions:

$$\begin{array}{l} NO + O_3 \rightarrow NO_2 + O_2 \\ NO_2 + O_3 \rightarrow NO_3 + O_2 \\ NO_3 + h\nu \rightarrow NO + O_2 \\ \hline \text{Net: } 2O_3 \rightarrow 3O_2. \end{array}$$

The two cycles together account for less than 20% of the total O_3 loss.

As a result of the rapid increase of the halogen load of the stratosphere, about one-third of the photochemical ozone loss is due to reactions involving ClO and BrO. The reaction set

$$\begin{array}{l} Cl + O_3 \rightarrow ClO + O_2 \\ ClO + O \rightarrow Cl + O_2 \\ \hline \text{Net: } O_3 + O \rightarrow 2O_2, \end{array}$$

is responsible for 5% of O_3 loss caused by halogen chemistry at 15 km, increasing to 25% at 21 km altitude.

The most important halogen-radical cycle is somewhat more complicated:

$$
\begin{array}{l}
Z + O_3 \rightarrow ZO + O_2 \\
OH + O_3 \rightarrow HO_2 + O_2 \\
HO_2 + ZO \rightarrow HOZ + O_2 \\
HOZ + h\nu \rightarrow OH + Z \\
\hline
\text{Net: } 2O_3 \rightarrow 3O_2,
\end{array}
$$

where Z can be either Cl or Br atom. This cycle accounts for 30% of the halogen-catalyzed ozone loss if Z = Cl, while it accounts for 20–30% if Z = Br.

Finally, both ClO and BrO reactions occur in the other important halogen-radical catalytic cycle:

$$
\begin{array}{l}
Cl + O_3 \rightarrow ClO + O_2 \\
Br + O_3 \rightarrow BrO + O_2 \\
ClO + BrO \rightarrow Cl + Br + O_2 \\
\hline
\text{Net: } 2O_3 \rightarrow 3O_2,
\end{array}
$$

which is responsible for 20–25% of the ozone loss caused by the halogen-radical family.

The mechanism of ozone destruction in the stratosphere above the Poles differs from that at midlatitudes due to the significant differences in meteorology and transport processes (*Zurrer*, 1993). A polar vortex of winds circles the Poles in winter and traps large amounts of air which become very cold during the polar night. The Antarctic vortex is more stable (lasts for five months) and is much colder than the Arctic one which explains that the ozone hole is much deeper and bigger at the South Pole. At these extremely cold temperatures (190–180K), clouds are formed which provide large surfaces where heterogeneous reactions can occur. These heterogeneous reactions play a determining role in the polar ozone depletion, i.e. in the ozone hole formation.

The halogen content in the polar atmosphere is found in the form of different compounds. On the basis of their ozone depletion potential, these compounds are sometimes classified as relatively inert compounds (as for instance HCl and $ClONO_2$) and more reactive compounds (as for instance Cl_2 and HOCl). The heterogeneous reactions which occur on the surface of the cloud particles, convert the inert form of the halogen compounds into the more reactive ones:

$$HCl + ClONO_2 \rightarrow Cl_2 + HNO_3$$

$$H_2O + ClONO_2 \rightarrow HOCl + HNO_3.$$

Among the products, the volatile Cl_2 and HOCl (reactive form) evaporate, while HNO_3 remains adsorbed on the surface of the cloud particles. During the winter, these particles grow in size and sink down to lower altitudes. This process, known as denitrification, removes the HNO_3 far away from the reactive chlorine compounds and hereby prevents the back conversion of the reactive chlorine into the inert one. Therefore, at the end of the polar night, the sunlight photolyses efficiently the reactive chlorine compounds producing Cl atoms which then participate in ozone destruction cycles. The ozone depletion processes take place till the air over Antarctica gets warm enough to break down the polar vortex and air originating from lower latitudes transports nitrogen-compounds which convert active chlorine into inert chlorine compounds.

The circumstances that prevail in the region where polar ozone destruction occurs are such that oxygen atoms are not formed. Therefore, other ozone consuming catalytic cycles occur than at midlatitudes. One of the most important cycle is:

$$2(Cl + O_3 \rightarrow ClO + O_2)$$

$$2ClO \rightarrow Cl_2O_2$$

$$Cl_2O_2 + h\nu \rightarrow Cl + ClO_2$$

$$ClO_2 \rightarrow Cl + O_2$$

$$\text{Net: } 2O_3 \rightarrow 3O_2.$$

The reactions which contribute to the ozone hole formation were given above for chlorine. Bromine can also contribute to the hole formation and the reactions which participate are analogous to those mentioned above.

5. Conclusion

Stratospheric ozone plays a beneficial role by absorbing most of the biologically damaging ultraviolet sunlight called UV-B radiation. During the last two decades stratospheric ozone concentration has decreased by 4–5% per decade at midlatitudes. *In situ* measurements coupled with model calculations have shown that the observed significant ozone losses are mainly due to anthropogenic chlorine and bromine compounds, and occur by catalytic cycles involving ClO or BrO radical reactions. Halogen compounds entering the stratosphere are responsible today for more than one third of the stratospheric ozone depletion. If the increase in the halogen content of the atmosphere continued, the concentration of the halogen compounds would triple by about the year 2050 from which serious ozone depletion could be expected.

In order to stop the decrease of the stratospheric ozone concentration, various international agreements were formulated. As a result, the halogen concentration in the stratosphere is expected to reach a maximum in 1998, however, one has to wait until around the middle of the next century when the ozone layer will completely recover.

References

Crutzen, P.J., 1971: Ozone production rate in an oxygen-hydrogen-nitrogen oxide atmosphere. *J. Geophys. Res. 76,* 7311-7327.

Farman, J.C., Gardiner, B.G. and *Shanklin, J.D.*, 1985: Large losses of total ozone in Antarctica reveal seasonal ClO_x /NO_x interaction. *Nature 315,* 207-210.

Kerr, R.A., 1994: Antarctic ozone hole fails to recover. *Science 217,*

Mészáros, E., 1989: Formation and prevention of atmospheric ozone hole (in Hungarian). *Magyar Tudomány*, 968-973.

Mészáros, E., 1991: The history and significance of atmospheric ozone research (in Hungarian). *Időjárás 95,* 69-76.

Molina, M. and *Rowland, F.S.*, 1974: Stratospheric sink for chlorofluoromethans — chlorine atom catalysed destruction of ozone. N*ature 249*, 810-812.

Wennberg, P.O, Cohen, R.C., Stimpfle, R.M., Koplow, J.P., Anderson, J.G., Salawitch, R.J., Fahey, D.W., Woodbridge, E.L., Keim, E.R., Gao, R.S., Webster, C.R., May, R.D., Toohey, D.W., Avalone, L.M., Proffitt, M.H., Loewenstein, M., Podolske, J.R., Chan, K.R. and *Wolfsy, S.C.*, 1994: Removal of stratospheric O_3 by radicals: In situ measurements of OH, HO_2, NO, NO_2, ClO and BrO. *Science 266,* 398-404.

WMO, 1994: Scientific assessment of ozone depletion: 1994, WMO Global Ozone Research and Monitoring Project — *Report No. 37.*

Zurrer, P.S., 1993: Ozone depletion's recurring surprises challenge atmospheric scientists. *Chem. Eng. News*, 8-18.

IDŐJÁRÁS

Quarterly Journal of the Hungarian Meteorological Service
Vol. 100, No. 1-3, January-September 1996

Large scale distribution of sulfur dioxide results from the TROPOZ II flights

Guido Wolz[1] and **Hans-Walter Georgii**

Institute for Meteorology and Geophysics, University of Frankfurt/Main,
P.O. Box 11 19 32, D-60054 Frankfurt a. M., Germany

(Manuscript received 22 May 1995; in final form 30 November 1995)

Abstract—SO_2 measurements were performed in January-February 1991 on board of research aircraft. The flight route extended from 67°N to 53°S along the European, North American, South American and African continent. The mission enclosed 28 flight tracks with 78 vertical profiles in altitudes between 1-11 km. A chemiluminescent method was used for detection, whereby SO_2 was absorbed on preimpregnated filters. The detection limit was 0.06 ng SO_2/ml, equivalent to a SO_2 mixing ratio of 7 pptv at a sampling volume of 50 l STP or about 3 pptv at 100 l STP.

SO_2 mixing ratios varied between 3 pptv and 5.6 ppbv. Very low and homogeneous values were found in the middle and upper troposphere and the south polar region. In contrast to this, the highest concentrations were measured in the planetary boundary layer over Santiago (Chile).

Key-words: SO_2, filter-chemiluminescent-technique, aircraft measurements, large scale distribution, marine/continental boundary layer, biomass burning.

1. Introduction

Sulfur dioxide is without doubt one of the trace gases widely studied during the last decades. The anthropogenic fraction of the sulfur cycle, is mainly characterized by SO_2 emissions. The global inventory of sulfur emissions of *Spiro et al.* (1992) showed, that about 102 Tg S yr^{-1} was globally emitted in 1980, from which anthropogenic activities account for 76%, while the rest part is produced by such factors as marine biosphere (12%), volcanoes (9%), biomass burning (2%) and the terrestrial biosphere (1%). Comparable to earlier estimates (*Georgii*, 1982; *Warneck*, 1988), they estimated that anthropogenic

---

[1] Now at Deutscher Wetterdienst

sources (fuel combustion and industry) account for 84% of total sulfur emissions in the Northern Hemisphere and for 50% in the Southern Hemisphere. Their calculations showed that biomass burning is the most important source in Central Africa during the dry season. Sulfur emissions by the marine biosphere due to DMS is an important source, especially over the oceans of the Southern Hemisphere during summer. Only few SO_2 measurements of the free troposphere of the Northern and especially of the Southern Hemisphere were carried out up to now (for instance: *Jaeschke et al.*, 1976; *Berresheim*, 1987; *Andreae et al.*, 1988a, b; *Ockelmann*, 1988; *Thornton et al.*, 1990; *Berresheim et al., 1990; Bandy et al., 1993; Thornton et al., 1993*).

In this context, the study by *Ockelmann* (1988) must be pointed out, because he participated in the STRATOZ III experiment. The aim of the STRATOZ III flight mission in June 1984 was to get a better knowledge of the vertical and meridional distribution of trace gases in the upper troposphere and lower stratosphere. Apart from the study of key elements of the ozone chemistry, SO_2 measurements were performed by *Ockelmann* (1988) aboard 'Caravelle'. During both missions a filter chemiluminescent SO_2 technique was used, but with some important improvements during TROPOZ II, as will be discussed later. The flight track in the STRATOZ III and TROPOZ II program were nearly identical. The main difference between STRATOZ III and TROPOZ II is, that TROPOZ II started during the northern winter.

In the TROPOZ II program two meridional cross sections of the SO_2 distribution in the free troposphere between 67°N and 53°S were performed. The data should help to deepen the knowledge of the sulfur cycle and compare the data with the newest results of 3-D sulfur models.

A comparison of the TROPOZ II and STRATOZ III missions should prove if meteorological conditions have an influence on SO_2 vertical distribution with regard to the vertical exchange and transport processes during different seasons. The mission should also answer, how SO_2 distribution is modified in the troposphere by emissions from biomass burning, especially in Central Africa.

2. *Instrumentation*

Before entering into particulars of the measurement technique, some important facts have to be discussed regarding the results of the NASA GTE/CITE 3 airborne instrument intercomparison of the most important sulfur compounds during August and September 1989 at Wallops Island, Virginia and Natal, Brazil (*Gregory et al.*, 1993). One goal of the mission was to test the different SO_2 detection instruments of several groups under laboratory and airborne field conditions. This was realized by an intercomparison of SO_2 calibration standards and airplane measurements. Intercomparison experiments, especially in the range of low SO_2 mixing ratios ($<$ 200 pptv) are very important to test the different techniques, whether they show reliable data of the free troposphere, where 10–200 pptv is a typical value.

The measurement of low SO_2 mixing ratios with high accuracy is very important for estimating the total sulfur budget and to compare SO_2 airborne measurement data with model results. The SO_2 measurement equipment — filter collection employing chemiluminescent analyses — as used by Ockelmann during STRATOZ III in 1984 was tested too at CITE 3. Apart from the overall poor correlation between all measurement techniques at mixing ratios < 200 pptv, the calibration test in laboratory reflected some problems for the filter-chemiluminescent-technique. The filter-chem. showed significantly higher values at around 100 ppt than the NIST Standard (National Institute of Standards and Technology). In comparison with the other methods — GC-FPD, GC-MS and Filter-IC — the filter-chemiluminescent method consistently reported higher SO_2 mixing ratios at < 200 pptv (*Gregory et al.*, 1993).

Before using the SO_2-filter-chemiluminescent-technique on board of the Caravelle, first laboratory experiments showed again *unacceptably high filter blanks*. This problem was dissolved by cleaning the Teflon filter holders in a solution containing potassium-dichromate, which was solved in sulphuric acid (98 %) until reaching saturation. Afterwards the filter holders were washed with distilled water. This successful procedure has to be repeated if discrepancies with filter blanks occur again. Preparing the filter holders in this matter was not applied at CITE 3 (*Beltz*, personal communication, 1994). In our opinion, this is an important fact and helps to explain the problems of the filter-chemiluminescent-technique. The poor results of this technique at CITE 3 might not be transferred to the improved measurement technique used at TROPOZ II.

During TROPOZ II the sampling method was the same as used by *Ockelmann* (1988), but no information was given by *Ockelmann* (1988) whether he treated the filter holders in the same way, as described above.

Ambient air (normally 10–70 l STP) was pumped through a Delbag Microsorban 98-S filter which was previously impregnated 3 times with 5 ml (0.01 molar) TCM (Tetrachlormercurate) solution. SO_2 is stabilized as disulfitomercurate on the filter. To prevent contamination during storage, the filter was immediately analyzed after sampling. It was again rinsed 3 times with 5 ml TCM. 1 ml Cer(IV)-sulfate solution ($pH = 2.3$, 0.1 molar) was injected into a teflon reaction chamber. Then the solution was added. The light yield of the chemiluminescent reaction, which is proportional to SO_2 in the sample, is integrated over 10 s by a photon counter (Model 974, Ortec). *Stauff* and *Jaeschke* (1975) reported, that Cer(IV)-sulfate was also suitable as oxidizing reaction like $KMnO_4$. Experiments with Cer(IV)-sulfate and different molarity of the TCM-solution showed a much better detection limit by using Cer(IV)-sulfate and a 0.01 molar TCM solution instead of $KMnO_4$ and a 0.1 TCM solution as used by *Ockelmann* (1988). The analysis system was calibrated by analysis of standard sulfite solutions which were prepared every day. The detection limit was 0.06 ng SO_2/ml, equivalent to a SO_2 mixing ratio of 7 pptv at a sampling volume of 50 l STP. Filter blanks were determined before and after sampling. The accuracy at SO_2 mixing ratios < 70 pptv is ± 2–7 pptv. This means an error of maximal 100% below 10 pptv. Above mixing ratios of 100 pptv the maximum error is about 10%. The first test flights proved that in contrast to STRATOZ III no difference could be detected between the calibration during flight and at ground level. This result was a great progress because all samples could be analyzed directly during flight, which prevented a contamination of the filters by storage.

Fig. 1 shows the filter sampling in the Caravelle. To prevent absorption of SO_2 in the inlet system, a very short teflon tube (1 m length, 6 mm diameter, no nafion drier) was used. Valves in front of and behind the sample unit prevented a contamination of the impregnated filters. While analyzing one of the two filters, the other one was loaded with a new sample.

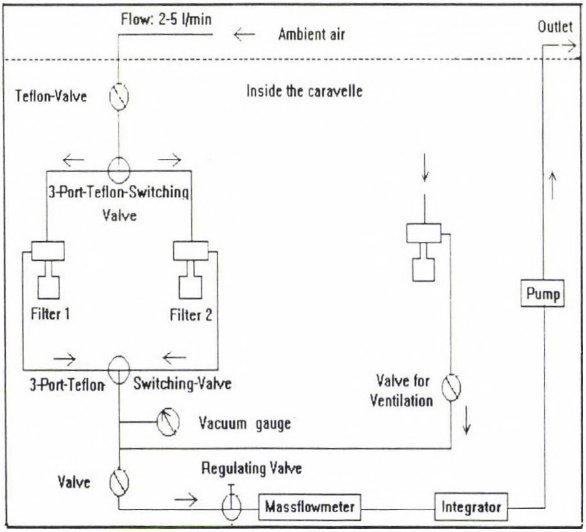

Fig. 1. Sample unit inside the Caravelle.

3. *Results and discussion*

The TROPOZ II mission started on 9 January 1991 in Bretigny sur Orge (France) and ended on 1 February 1991. *Fig. 2* shows the flight tracks. In total, 28 flight legs with 78 vertical profiles were performed. Along the route 246 filter samples were taken.

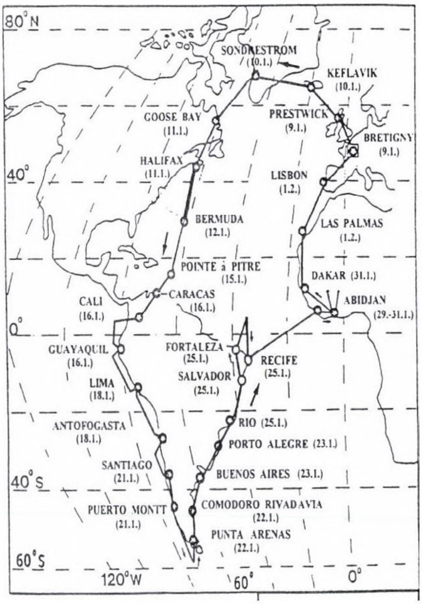

Fig. 2. Flight track during the TROPOZ II campaign in January 1991.

Figs. 3a, b show meridional cross sections along the north-south (Sondrestrom – Punta Arenas) and the south-north (Punta Arenas – Bretigny) cruise track. Comparing the figures, the following results are remarkable:

(1) Both figures show elevated concentrations between 40–60 °N, reflecting the influence of anthropogenic emissions on the SO_2 distribution. This is in agreement with the global sulfur emission inventory for 1980 by *Spiro et al.* (1992), on the assumption that their inventory is still qualitatively true. During TROPOZ II, SO_2 concentrations decreased rapidly with altitude to values below 100 pptv above 3 km and $\leq$ 20 pptv between 6–9 km.

(2) North of 30 °N, SO_2 mixing ratios are approximately homogeneous above an altitude of 3 km. Furthermore, a decrease of SO_2 mixing ratios from temperate latitudes to subtropical and subpolar latitudes was observed in the Northern Hemisphere.

(3) Comparing both figures, a qualitative symmetry near the equator is obvious. Calculations of the vertical wind velocity, derived by the 3-D backward trajectory model of the ECMWF, indicate that SO_2 was transported vertically in this region. We calculated the backward trajectories ourselves at the ECMWF, using the operational working forecast model (see *Kallberg*, 1984; *Roskilly*, 1987).

(4) In the N–S flight pattern (Fig. 3a), it is remarkable that the highest concentrations were measured in the Southern Hemisphere. The analysis of 3-D backward trajectory showed that this was due to an advection of continental air, while the SO_2 maximum over Europe (around 50°N) was sampled from marine air.

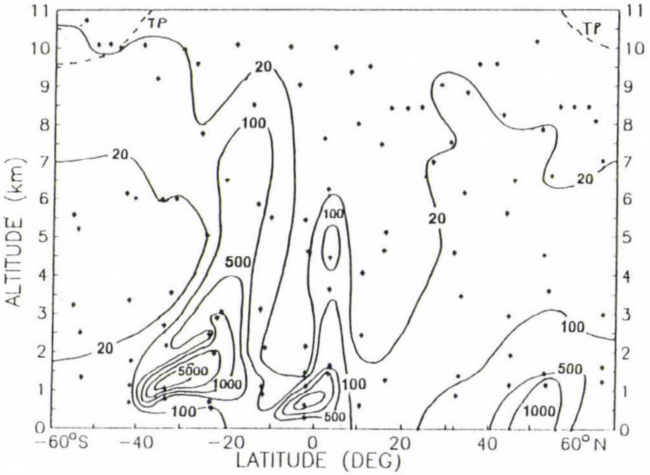

Fig. 3a. SO_2 vertical distribution of the north–south flight pattern from Sondrestrom – Punta Arenas (Flight #1–#15). The asterisks indicate where SO_2 measurements were performed.

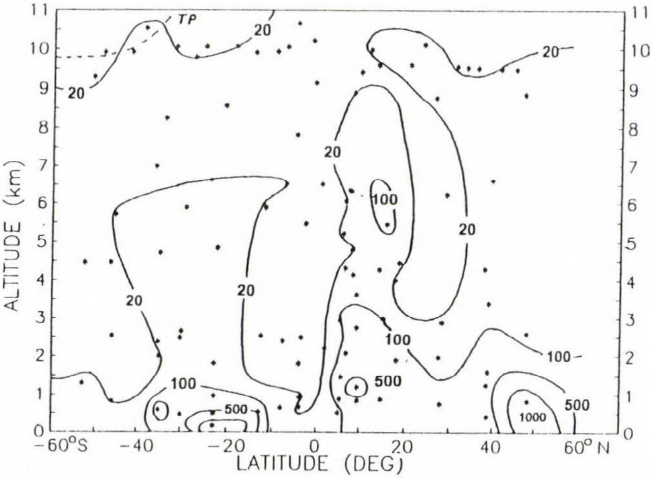

Fig. 3b. SO_2 vertical distribution of the south-north flight pattern from Punta Arenas – Bretigny (Flight #16–#30).

(5) The peak concentrations sampled along the west coast of South America exceeded those on the east coast by an order of magnitude. We conclude that the flight track hit strong regional sources. This is in agreement with the results of the emission inventory by *Spiro et al.* (1992). In this area (e.g. Chile, Peru), they calculated one of the highest sulfur emission fluxes of South America, mainly caused by smelters. A further explanation could be a longer SO_2 residence time, caused by the lack of efficient SO_2 sinks by heterogenous processes. During this period high pressure with dry and stable stratified air persisted.

(6) South of 40°S, very low SO_2 mixing ratios with values $<$ 10–50 pptv were measured. Despite the small number of measurements in subpolar latitudes of the Southern Hemisphere — especially in the planetary boundary layer — it seems that there is only a small increase in SO_2 mixing ratios from the free troposphere towards the boundary layer. This would mean that no efficient sources exist in the planetary boundary layer and true marine background situations were observed. This statement is confirmed by the 3–D backward trajectory analyses, which clearly show an advection of maritime air during the period of the mission.

(7) Relatively high concentrations were recorded in the lower troposphere at 10°N (Ivory Coast), which most likely originated from biomass burning. In this area, biomass burning occurs towards the end of the dry season (Jan/Feb) and bush fires were observed during local flights. The complex meteorological condition at the Ivory Coast favoured the vertical exchange of air together with the advection of continental air from the east in levels between 850–700 hPa.

As mentioned in the previous paragraph, the vertical transport of SO_2 and its precursors may play an important role in the vertical distribution of SO_2 in the middle troposphere. This phenomen was especially described by the so-called 'Staubsauger-Model' of *Chatfield* and *Crutzen* (1984).

To get better information about the influence of vertical transport over the vertical SO_2 distribution, the results of the vertical velocity computations were used from the backward trajectory calculations. The vertical velocities and 3–D backward trajectories were calculated using the archieved ECMWF windfields, which were only available at fixed timesteps, usually every third or sixth hour. To calculate the vertical velocities, a time increment of 30 min was used for linear interpolation. The vertical translation of air parcels was performed in pressure coordinates using the omega equation. The calculation was carried out at a latitude-longitude grid with a resolution of 1.5×1.5 degrees (see *Kallberg*, 1984; *Roskilly*, 1987).

It must be pointed out, that convective processes are only parameterized by the ECMWF trajectory model. For this reason, the figures must be cautiously interpreted. Otherwise, these results allow a rough statement, that qualitative agreement exists between upward and downward motions and the vertical SO_2 distribution.

The following figures (*Figs. 4a, b*) show the vertical velocity (m/s) of both meridional cross sections. Beginning with Fig. 4a, the results are compared with the corresponding cross sections of the vertical SO_2 distribution (Fig. 3a):

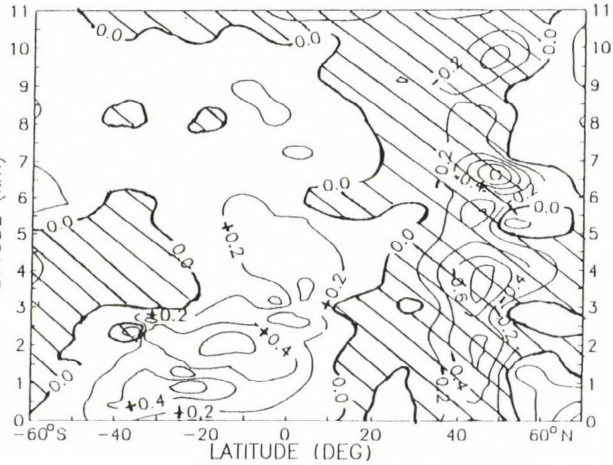

Fig. 4a. Vertical velocity (m/s) for the north-south flight pattern. Positive values indicate updraft and negative values downdraft areas. The vertical velocities were calculated by the 3-D backward trajectories program of the ECMWF.

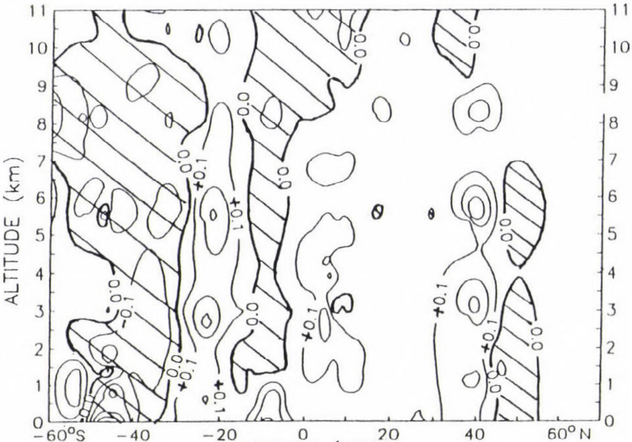

Fig. 4b. Vertical velocity (m/s) for the south-north flight pattern. Positive values indicate updraft and negative values downdraft areas.

(1) Between 40°–60°N (Fig. 4a) subsidence of air dominated in nearly all levels of the troposphere. A comparison with the vertical SO_2 distribution shows, that a strong decrease of the SO_2 mixing ratio was simultaneously observed with altitude.

(2) Subsidence is further prevailing over the subtropics and very low SO_2 mixing ratios were measured in the free troposphere.

(3) Around 0°–5°N and 10°–25°S upward motions correlate well with high SO_2 mixing ratios throughout the free troposphere. Contrary to this, the very low SO_2 mixing ratios between the equator and 10°S cannot be explained by the distribution of the vertical velocities, because upward motions prevailed in this area. A detailed analysis of the backward trajectories showed that horizontal advection of air of different origin was more important than the vertical transport of air.

(4) Between 15°–35°S (Fig. 4b), an area of upward motion dominated, correlated with higher SO_2 values in the troposphere. Much lower SO_2 mixing ratios were observed between 15°–0°S, where a weak subsidence of air was computed by the trajectory model.

(5) During local flights over Ivory Coast (around 10°N), upward motion occurred and relatively high SO_2 mixing ratios were measured in the middle troposphere. This was not only caused by vertical motions but by advection of continental air.

Summarizing these facts it appears, that there is often no disagreement between computed vertical motions and measured SO_2 vertical distributions. An effective vertical SO_2 transportation is possible in areas, where efficient SO_2 sources are present and upward motions occur. The lower the SO_2 emissions, the smaller the influence of vertical motion on SO_2 vertical distribution.

Despite this, it must be added, that vertical SO_2 distribution is influenced not only by vertical processes. Horizontal transportation as well as homogeneous and heterogenous reactions and removal processes by dry and wet deposition also have an important influence on the SO_2 vertical distribution.

In order to study the influence of different sulfur emission source strengths for example in polluted and unpolluted areas on the vertical distribution, average SO_2 mixing ratios were computed for different altitude levels (*Figs. 5a-d*): (1) 0–1.5 km, (2) 1.5–3 km, (3) 3–6 km and (4) > 6 km.

Fig. 5a comprises averaged SO_2 mixing ratios for all TROPOZ II data. One can clearly see the large standard deviations. This is caused by the short SO_2 residence time including great spatial and temporal variations.

In *Fig. 5b*, the very high SO_2 mixing ratios observed along the west coast of South America and at the Ivory Coast, were eliminated because they were characterized by strong local pollution. By comparing the two figures, it is apparent that the average SO_2 mixing values became much smaller below an altitude of 3 km. This is an example that strong emissions are *on average* restricted to *lower* and *middle levels* of the troposphere. Above an altitude of 6 km, SO_2 mixing ratios are comparatively low and show more homogeneous concentrations.

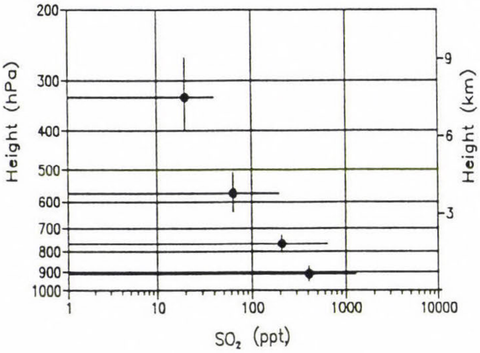

Fig. 5a. Averaged SO_2 vertical profile of all TROPOZ II data: 0–1.5 km: 57 values, 1.5–3.0 km: 45 values, 3.0–6.0 km: 47 values, > 6.0 km: 97 values.

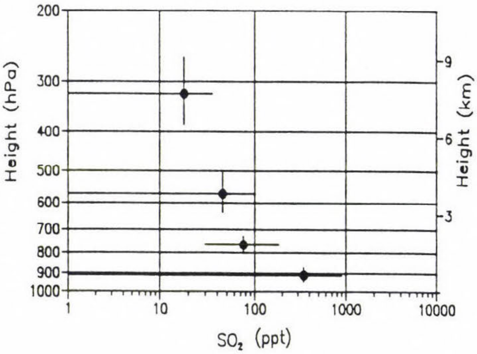

Fig. 5b. Averaged SO_2 vertical profile without the data at the Ivory Coast and Chilean Coast: 0–1.5 km: 41 values, 1.5–3.0 km: 28 values, 3.0–6.0 km: 33 values, > 6.0 km: 82 values.

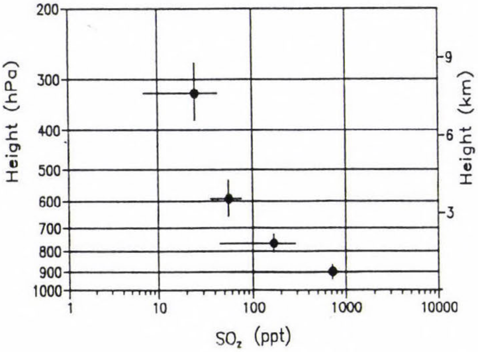

Fig. 5c. Averaged SO_2 vertical profile for 35°–60°N: 0–1.5 km: 6 values, 1.5–3.0 km: 4 values, 3.0–6.0 km: 5 values, > 6.0 km: 17 values.

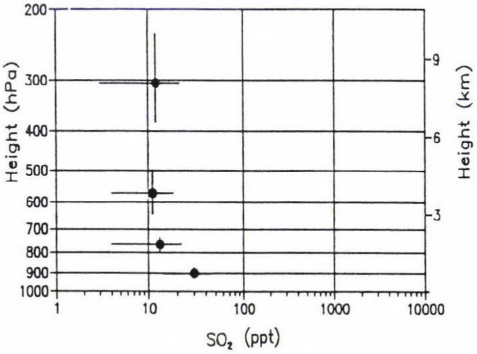

Fig. 5d. Averaged SO_2 vertical profile of all data south of 40°S: 0–1.5 km: 6 values, 1.5–3.0 km: 4 values, 3.0–6.0 km: 7 values, > 6.0 km: 9 values.

In *Fig. 5c*, averaged SO_2 data were calculated for 35°–60°N, where most anthropogenic sulfur is emitted. It can be clearly seen that the average mixing ratios in the planetary boundary layer are higher compared with those in Fig. 5b. In the middle and upper troposphere, the SO_2 values are similar and standard deviations are smaller.

The last figure (*Fig. 5d*) shows the average SO_2 profile of the measurements south of 40°S. Trajectory analysis proved that true background conditions were met. In the planetary boundary layer the average SO_2 mixing ratios were < 30 pptv and thus much lower than in the other areas. Distribution throughout the whole troposphere was very homogeneous.

To draw a conclusion from these results, the figures clearly show that on average, the influence of efficient SO_2 surface source strength on the vertical SO_2 distribution strongly decreases with height. This is in agreement with the short lifetime of SO_2 near surface. For example, SO_2 levels are comparable in the upper troposphere south of 40°S and 35°–60°N, whereas great differences — up to a factor of 30 (!) were observed in the planetary boundary layer between these regions. This is in agreement with the results of the 3-D global sulfur model of *Langner* and *Rodhe* (1991) and qualitatively similar to the flight measurements of *Thornton et al.* (1993) during the CITE 3 mission. Over the Atlantic Ocean, offshore of North and South America, they observed comparable SO_2 mixing ratios above the planetary boundary layer of both hemispheres. Contrary to this, they measured SO_2 concentrations 8 times greater in the northern boundary layer than in the southern boundary layer over the Atlantic Ocean.

4. Individual vertical SO_2 profiles

Some interesting measured SO_2 vertical profiles are presented in *Figs. 6a–d*. Each flight track includes an ascent (symbol: o) and descent SO_2 (symbol: x) profile. The horizontal bars indicate the standard error of the SO_2 mixing ratio and the vertical bars the height interval, where filters were sampled. Backward trajectories were computed for different altitudes of each flight.

The vertical distribution of SO_2 seen on the descent to Bermuda (*Fig. 6a*, Flight #6: Halifax–Bermuda) shows some remarkable facts. In comparison to the ascent profile over Halifax, a higher SO_2 mixing ratio was observed in the middle troposphere. As indicated by backward trajectories analysis, this might be caused by long range transport of polluted air from Central America. The relatively low SO_2 concentrations in the boundary layer over Bermuda were due to the advection of maritime air and a strong inversion which prevented vertical mixing of air. Contrary to this, during their flights over the northwestern Atlantic Ocean (CITE 3) in August–September 1989 *Thornton et al.* (1993) observed that the advection of SO_2 from the continent was limited to the boundary layer in this area, which might be caused by different meteorological conditions.

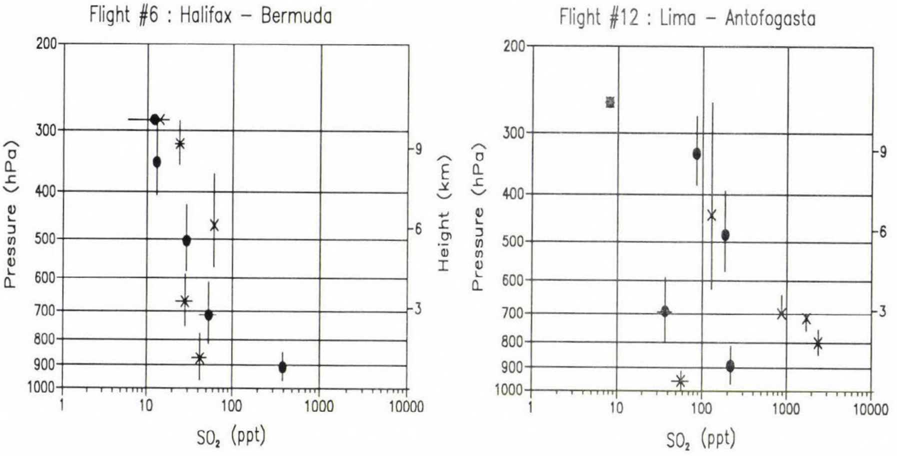

Fig. 6a. SO_2 vertical profiles of Flight #6 (11.01.91): Halifax-Bermuda, Flight #12 (18.01.91): Lima-Antofogasta. Symbol o: ascent, symbol x: descent. Units: pptv.

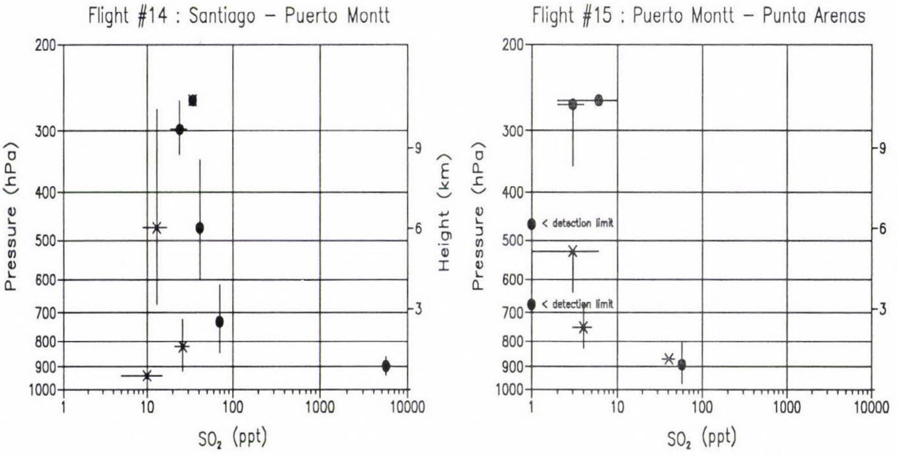

Fig. 6b. SO_2 vertical profiles of Flight #14 (21.01.91): Santiago-Puerto Montt, Flight #15 (21.01.91): Puerto Montt-Punta Arenas, Symbol o: ascent, symbol x: descent. Units: pptv.

Flight #12 from Lima-Antofogasta again revealed some surprising structures. During the descent to Antofogasta, a visible '*brown layer*' could be observed from the airplane, indicating a thin layer of highly polluted air. In agreement with this observation, the visibility decreased and the SO_2 mixing ratio continously increased to 2.4 ppb. Below this layer the SO_2 values sharply decreased again. The measurements of wind direction and relative humidity and the analysis of backward trajectories clearly show that maritime air was advected, which explains the low SO_2 values of nearly 60 pptv.

Flight #14 from Santiago–Puerto Montt (*Fig. 6b*) must be mentioned because the highest SO_2 mixing ratio (5.5 ppb) during the campaign was measured over Santiago. An explanation for this, is the heavy air pollution by emissions of the town in combination with an inversion layer (up to 1800 m), which prevented a vertical mixing. Above this layer, very low SO_2 values were observed because of the advection of maritime air in a westerly flow. The low SO_2 values in the boundary layer over Puerto Montt can be explained by bad weather conditions with deep clouds and rain, most favourable for the removal of SO_2.

The SO_2 vertical profile of Flight #15 from Puerto Montt–Punta Arenas and Flight #16 from Punta Arenas–Comodoro Rivadavia (*Fig. 6c*) are examples of pure undisturbed maritime background conditions in the Southern Hemisphere. The SO_2 values were very low (< 60 pptv) as well as very homogeneous through the whole troposphere in this area.

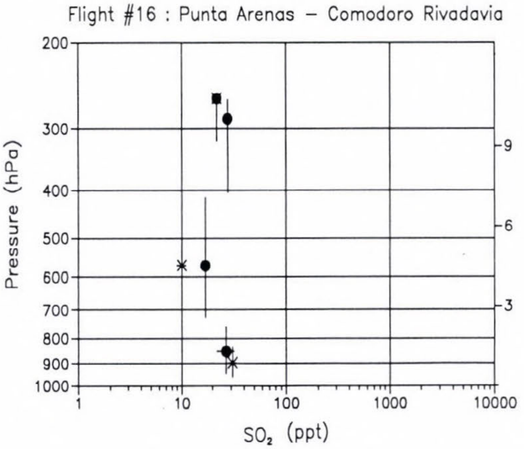

Fig. 6c. SO_2 vertical profiles of Flight #16 (22.01.91): Punta Arenas–Comodoro Rivadavia.

The measurements on 29, 30 January near Abidjan (*Fig. 6d*) should give an indication in which way biomass burning influences the vertical distribution of different trace gases. Special flight patterns were flown. The analysis of the vertical temperature profile showed a great difference between the stratification of air over coast and off coast. In contrast to the vertical temperature profile near the coast, the air was more unstable over land. The analysis of the backward trajectories near coastal region showed an advection of maritime air up to a height of 950 hPa, whereas continental air was advected up to 500 hPa over land. This was also confirmed by the air humidity profiles. As a consequence of this, relatively high SO_2 mixing ratios (150–420 pptv) were measured below an altitude of 4 km. Above this level the SO_2 values strongly decreased to some 10 pptv. Confirmed by both profiles (ascent and desent), the SO_2 concentrations decreased to 60–110 pptv in low levels over coast, which was due to the advection of maritime air. Advection of maritime air above 500 hPa might further be the reason, why the SO_2 values decreased to < 60 pptv. These profiles indicate that the higher SO_2 mixing ratios in the middle troposphere might be caused by the observed biomass burning or by other efficient continental sources.

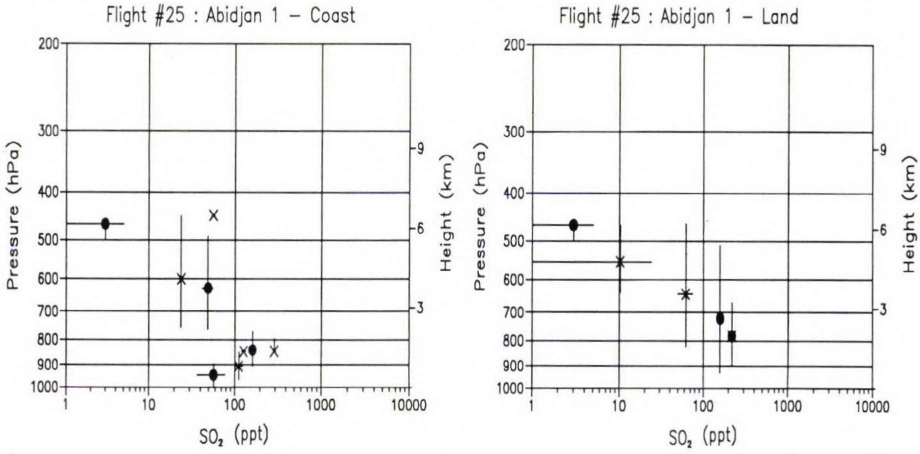
Flight #25 : Abidjan 1 – Coast

Flight #25 : Abidjan 1 – Land

Fig. 6d. SO_2 profiles of Flight #25 (29.01.91): Abidjan–Local 1: near the coast and over land.

5. Comparison with other observations

One advantage of the TROPOZ II mission is the comparability of the results because the SO_2 measurements were performed with very similar equipment by *Ockelmann* (1988) as during STRATOZ III. One important difference is that TROPOZ II took place during the north hemispheric winter and STRATOZ III during the north hemispheric summer.

With some caution, it is possible to prove whether vertical distribution of SO_2 is influenced by different dynamical meteorological conditions during summer and winter. The main results of this comparison are the following:

(1) During both missions high SO_2 mixing ratios were measured between 40°–60°N. The vertical decrease of the SO_2 concentrations varies with season — a better vertical mixing was observed during summer (STRATOZ III) in the Northern Hemisphere.

(2) In the subtropics and the subpolar region the SO_2 values decreased considerably.

(3) During STRATOZ III, a maximum of the SO_2 mixing ratios was measured between 30°–60°S around an altitude of 6–7 km. A similar vertical distribution of SO_2 was not confirmed by the TROPOZ II measurements. These high SO_2 mixing ratios during STRATOZ III are hard to explain because important information by backward trajectories are not available. The relatively high values are possibly due to contamination problems.

(4) It must be emphasized that almost all SO_2 mixing ratios were much lower in the free troposphere during TROPOZ II compared to those of STRATOZ III. It cannot be dismissed, that contamination problems occured during STRATOZ III because the filters had to be stored until post-flight analysis. At TROPOZ II, calibration was performed during the flight tracks and the filters were immediately analyzed after sampling. Sometimes, higher values were partly measured in the boundary layer during TROPOZ II. These elevated values are on the one hand explainable by different source strength, different meterological and chemical conditions during both missions and on the other hand caused by high spatial and temporal variations of the SO_2 mixing ratios in the boundary layer. Furthermore, they might also be the result of shorter time and smaller space resolution during TROPOZ II. Thereby an improved detection of thin levels of polluted air was obtained during the fast flight through in the descending and climbing phase in the planetary boundary layer.

Now, the results of TROPOZ II are compared with former measurements carried out in locations close to the flight route.

Andreae et al. (1990) measured SO_2 on board of an aircraft during the ABLE 2B (Amazon Boundary Layer Experiment) in April/May 1987, using a filter pack with K_2CO_3-impregnated filter. During the wet season, they found SO_2 mixing ratios mostly below 40 ppt in the boundary layer and up to an altitude of 5 km. Averaged SO_2 values were around 25 ppt in the boundary layer and 15 ppt in the free troposphere with no significant differences between the wet and dry season (collected before the impact of biomass burning). Despite the different sample locations, time of season and meteorological conditions, comparatively low SO_2 concentrations (< 10–30 pptv) were measured on the flight track from Fortaleza to 2°N and back to Recife during TROPOZ II.

Luria et al. (1990) have performed SO_2 flight experiments with a fluorescence analyzer. They measured less than 80 pptv over Bermuda. In comparison, 30–60 pptv SO_2 was measured over Bermuda during TROPOZ II.

Thornton et al. (1990) found the highest SO_2 concentrations with < 10–110 pptv near the ITCZ during flight measurements in the central and south Pacific. South of Hawaii they measured mixing ratios < 30 pptv, well in accordance with our figures for marine air from south of 40°S. During CITE 3, *Thornton et al.* (1993) measured SO_2 mixing ratios of nearly 150 pptv in the oceanic boundary layer on the flight track towards Bermuda and 90 pptv in the free troposphere.

The measurements of *Saltzman et al.* (1986) on a ship cruise along the south Peruvian and north Chilean coast are very interesting. They found comparatively high SO_2 levels as in cities, which they explained by the influence of iron sulfid smelters. A comparison with the results of TROPOZ II is very difficult, but very high SO_2 mixing ratios can obviously occur along the west coast of South America. This is confirmed by the model results of *Spiro et al.* (1992), who calculated elevated SO_2 emission fluxes in this area.

Berresheim (1987) measured very low SO_2 mixing ratios (4–17 pptv) — comparable to TROPOZ II — in the Drake Street on a vessel during autumn. In his opinion, SO_2 is formed there by conversion of reduced biogenic sulfur gases. Equivalent low sulfur emission fluxes were calculated by *Spiro et al.* (1992) over subantarctic regions. Their model results confirmed that the main sulfur contributor is the marine biosphere by emissions of DMS.

The aim of an investigation like the TROPOZ II mission should be a comparison of the SO_2 measurements with the results of global 3-D sulfur models. In this context, the results of the 3-D global sulfur model of *Langner* and *Rodhe* (1991) has to be mentioned. Without going into details of the model, the authors computed the *annual* global SO_2 distribution for two different levels: 1000–950 hPa and 600 hPa. First of all, it must be emphasized that a direct comparison between the model results and the measurements during TROPOZ II is limited by the important fact that the SO_2 data are more likely a snapshot of the actual atmospheric condition, whereas the model of *Langner* and *Rodhe* (1991) describes the mean annual state of the troposphere. For this reason, a comparison should be done carefully. Despite this fact, the model results show a good agreement with the measurements. High mean SO_2 mixing ratios of 500–1000 pptv were calculated between 40°–60°N with a sharp vertical decrease of the SO_2 mixing ratio up to 25–50 pptv — depending on the vertical transport of DMS — in the middle troposphere. As during TROPOZ II, the SO_2 mixing ratios decrease to subpolar and subtropical latitudes of the Northern Hemisphere. A very good qualitative and quantitative agreement exists for the subpolar region of the Southern Hemisphere. In this region, a homogeneous vertical distribution with mean SO_2 mixing ratios of 10–25 pptv is calculated by the model.

A great quantitative difference exists between 20°–40°S for South America. Beside the fact that only single measurements were performed, it seems that the SO_2 sources, as well as the vertical transport, are underestimated by the model.

The model calculated a mean annual SO_2 mixing ratio of 250 pptv for the boundary layer and only 10–25 pptv for the middle troposphere over South America, whereas 500–5500 pptv SO_2 in the boundary layer and 20–100 pptv SO_2 in the middle troposhere were measured during TROPOZ II.

Beside the remarkable agreement between this model results and the SO_2 data, further long-term measurements of the SO_2 distribution are needed, especially in the Southern Hemisphere.

6. Conclusion

The results of the TROPOZ II flight mission gained new information on the meriodional SO_2 distribution in the free troposphere and the planetary boundary layer. Particularly informative was the comparison with the results of the STRATOZ III experiment.

In agreement with STRATOZ III, the TROPOZ II mission showed that high SO_2 mixing ratios were measured between 40°-60°N, where the anthropogenic sulfur emissions exceed the sulfur emissions by natural sources. In this region, the SO_2 mixing ratio decreases very rapidly below 20 pptv in the free troposphere and shows a homogeneous spatial distribution in the Northern Hemisphere.

From temperate to higher and lower latitudes a strong decrease of the SO_2 mixing ratio is observed in the Northern Hemisphere. Near the ITCZ, a considerable vertical mass transport of SO_2 by convective processes occurs if there are high SO_2 source strengths at the surface.

Very high SO_2 mixing ratios can also be observed in the Southern Hemisphere, indicating strong local anthropogenic sources. Very low and homogeneous SO_2 mixing ratios with values < 10–50 pptv have been measured throughout the troposphere south of 40°S — typical for the marine background.

The investigation of vertical motions of air upon the SO_2 vertical distribution indicated that the vertical velocity is often in agreement with the vertical transport of SO_2.

This would mean that a seasonal effect upon the SO_2 vertical distribution in the middle latitudes must be expected. A comparison with the results of STRATOZ III shows that this is indeed true. An important topic for future experimental missions and theoretical studies will be to prove this hypothesis.

An aim of further investigations must also be to close the gap in data for the Southern Hemisphere, because there is only a sparse knowledge of sulfur sources and concentrations in the troposphere.

Evaluation of meridional SO_2 distribution revealed that anthropogenic emissions have a massive influence on the sulfur cycle in the atmosphere despite the successful effort in reducing sulfur emissions in Central Europe.

Acknowledgments—The authors thank *A. Marenco*, who organized this flight and the crew of the airplane from the Centre d'Essais en Vol at Bretigny for their assistance during the flight. We also thank the Deutschen Wetterdienst (DWD) for the support to perform backward trajectory calculations at the ECMWF. This work was financially supported by the Bundesministerium für Forschung und Technologie.

References

Andreae, M.O., Berresheim, H., Andreae, T.W., Kritz, M.A., Bates, T.S. and *Merill, J.T.*, 1988a: Vertical distribution of dimethylsulfide, sulfur dioxide, aerosol ions and radon over the northeast Pacific Ocean. *J. Atm. Chem. 6*, 149-173.

Andreae, M.O., Browell, E.V., Garstang, M., Gregory, G.L., Harriss, R.C., Hill, G.F., Jacob, D.J., Pereira, M.C., Sachse, G.W., Setzer, A.W., S. Dias, P.L., Talbot, R.W., Torres, A.L. and *Wofsy, S.C.*, 1988: Biomass - burning emissions and associated haze layers over Amazonia. *J. Geophys. Res. 93*, No. D2, 1509-1527.

Andreae, M.O., Berresheim, H., Bingemer, H., Jacob, D.J., Lewis, B.L., Li, S.-M. and *Talbot, R. W.*, 1990: The atmospheric sulfur cycle over the Amazon Basin, 2. Wet season. *J. Geophys. Res. 95*, No. D10, 16.813-16.824.

Bandy, A.R., Thornton, D.C. and *Driedger III, A.R.*, 1993: Airborne measurements of sulfur dioxide, dimethyl sulfide, carbon disulfide, and carbonyl sulfide by isotope dilution gas chromatography/-mass spectrometry. *J. Geophys. Res. 98*, No. D12, 23.423-23.433.

Berresheim, H., 1987: Biogenic sulfur emissions from the subantarctic and antarctic oceans. *J. Geophys. Res. 92*, No. D11, 13.245-13.262.

Berresheim, H., Andreae, M.O., Ayers, G.P., Gillett, R.W., Merrill, J.T., Davis, V.J. and *Chameides, W.L.*, 1990: Airborne measurements of dimethylsulfide, sulfur dioxide, and aerosol ions over the southern Ocean south of Australia. *J. Atm. Chem. 10*, 341-370.

Chatfiels, R.B. and *Crutzen, P.J.*, 1984: Sulfur dioxide in remote oceanic air: cloud transport of reactive precursors. *J. Geophys. Res. 89,* No. D5, 7111-7132.

Georgii, H.-W., 1982: The atmospheric sulfur-budget. In *Chemistry of the Unpolluted and Polluted Troposphere* (ed.: *H.-W. Georgii* and *W. Jaeschke*). D. Reidel Publishing Company.

Gregory, G.L., Davis, D.D., Beltz, N., Bandy, A.R., Ferek, R.J. and *Thornton, D.C.*, 1993: An intercomparison of aircraft instrumentation for tropospheric measurements of sulfur dioxide. *J. Geophys. Res. 98*, No. D12, 23.325-23.352.

Jaeschke, W., Schmitt, R. and *Georgii, H.-W.*, 1976: Preliminary results of stratospheric SO_2 - measurements. *Geophys. Res. Lett. 3,* 517-519.

Kallberg, P., 1984: Air parcel trajectories from analyzed or forecast windfields. In *Workshop on Simplified Models for Shortrange Forecasting on the Mesoscale.* SMHI R & D notes, No. 37.

Langner, J. and *Rodhe, H.*, 1991: A global three-dimensional model of the tropospheric sulfur cycle. *J. Atm. Chem. 13*, 225-263.

Luria, M., Boatman, J.F., Harris, J., Gunter R.L., Ray, J.D., V. Valin, C.C. and *Chin, J.*, 1990: Atmospheric sulfur gases in the Mid-Pacific region. *Symposium-Abstracts. Commission on Atmospheric Chemistry and Global Pollution.* Chamrousse, France, 5–11 September 1990.

Ockelmann, G., 1988: Großräumige Verteilung des atmosphärischen Schwefeldioxids in der Troposphäre und unteren Stratosphäre — Ergebnisse einer experimentellen Untersuchung. *Berichte d. Inst. f. Met. u. Geophys. d. J. W. Goethe Univ.*, Frankfurt a.M.. Im Eigenverlag des Instituts, Nr. 75.

Roskilly, R., 1987: Data bases for trajectory models. *ECMWF Meteorological Bulletin* M1.1/6.

Saltzman, E.S., Savoie, D.L., Prospero, J.M. and *Zika, R.G.*, 1986: Elevated atmospheric sulfur levels off the Peruvian coast. *J. Geophys. Res. 91*, No. D7, 7913-7918.

Spiro, P.A., Jacob, D.J. and *Logan, J.A.*, 1992: Global inventory of sulfur emissions with 1° x 1° resolution. *J. Geophys. Res. 97*, No. D5, 6023-6036.

Stauff, J. and *Jaeschke, W.*, 1975: A chemiluminescence technique for measuring atmospheric trace concentrations of sulfur dioxide. *Atmos. Environ. 9*, 1038-1039.

Thornton, D.C., Bandy, A.R., Driedger, A.R., Scott, D. and *Ridgeway, R.G.*, 1990: Sulfur gases in the tropical marine atmosphere. *Symposium-Abstracts. Commission on Atmospheric Chemistry and Global Pollution*. Chamrousse, France, 5–11 September 1990.

Thornton, D.C., Bandy, A.R., Beltz N., Driedger III, A.R. and *Ferek, R.*, 1993: Advection of sulfur dioxide over the Western Atlantic Ocean during CITE 3. *J. Geophys. Res. 98,* No. D12, 23.459-23.467.

Warneck, P., 1988: *Chemistry of the Natural Atmosphere*. Int. Geophys. Series, Vol. 41. Academic Press.

IDŐJÁRÁS

Quarterly Journal of the Hungarian Meteorological Service
Vol. 100, No. 1-3, January-September 1996

Long-range transport model estimations on the origin of atmospheric lead and cadmium deposition over Hungary

László Bozó

Hungarian Meteorological Service
H-1675 Budapest P.O. Box 39, Hungary

(Manuscript received 22 May 1995; in final form 13 February 1996)

Abstract—Lead and cadmium concentrations both in the air and precipitation have been monitored since the early 80's under regional background conditions in Hungary. Lead and cadmium are attached to aerosol particles mostly in fine size range. Hence, they can be transported hundreds or more kilometers from their sources before gradually being removed from the atmosphere by dry or wet depositions. The geographical origin — country-to-country budgets — of lead and cadmium deposited in Hungary was estimated by means of a European-scale long-range transport model. It was found that lead and cadmium sources of other European countries provide significant contribution to the total deposition of lead and cadmium over Hungary.

Key-words: lead, cadmium, long-range transport, modeling.

1. Introduction

In recent years there has been an increased interest in trace metals in the atmosphere and the environmental effects of their deposition. This is to large extent because heavy metals can accumulate in the biosphere and may be toxic to living systems. Lead and cadmium are among the most toxic elements in the atmosphere. The rate of contamination can vary from place to place as a function of source densities and intensities of heavy metals flux as well as meteorological conditions. Aerosols containing heavy metals can also be transported far away from their sources before being deposited. It means that a significant part of lead and cadmium emitted in a given country can be removed from the atmosphere beyond its boundaries causing environmental pollution problems over other countries (*Alcamo et al.*, 1992). The aim of this study was to provide a quantitative estimation on the relative contribution from the sources of European countries to the total lead and cadmium deposition over Hungary.

2. Monitoring of Pb and Cd in Hungary

The monitoring of Pb and Cd in atmospheric aerosols and precipitation were begun at the regional background air pollution monitoring station, K-Puszta, in 1981. This station is located on the Hungarian Great Plain (19°33'E, 46°58'N) in central Hungary, about 75 km southeast of Budapest. The nearest city is 25 km southeast (Kecskemét, 100,000 inhabitants).

Aerosol samples are taken every second day by means of Whatman 41 filters. The sampling period is 24 hours and during this time around 20 m^3 of ambient air are pumped over. Lead and cadmium contents in the samples are determined using graphite furnace atomic absorption spectrometry at the Department of Analytical Chemistry of Eötvös Loránd University, Budapest (*Bozó* and *Horváth*, 1992) and from 1993, at the Department of Analytical Chemistry, University of Veszprém. Details on the measurement techniques applied are summarized in *Mészáros* and *Horváth* (1983).

Annual variation of Pb and Cd air concentrations are demonstrated in *Fig.1*. It can be seen that the annual average Pb concentrations were significantly higher in the early 80's than in the second part of the decade and early 90's. The decreasing trend could be caused by the fact that the amount of lead added to a unit volume of gasoline has been continuously decreased (since January, 1993 its value has been below 0.15 g ℓ^{-1} in Hungary) and the use of unleaded gasoline has become more widespread in recent years mostly in Western Europe.

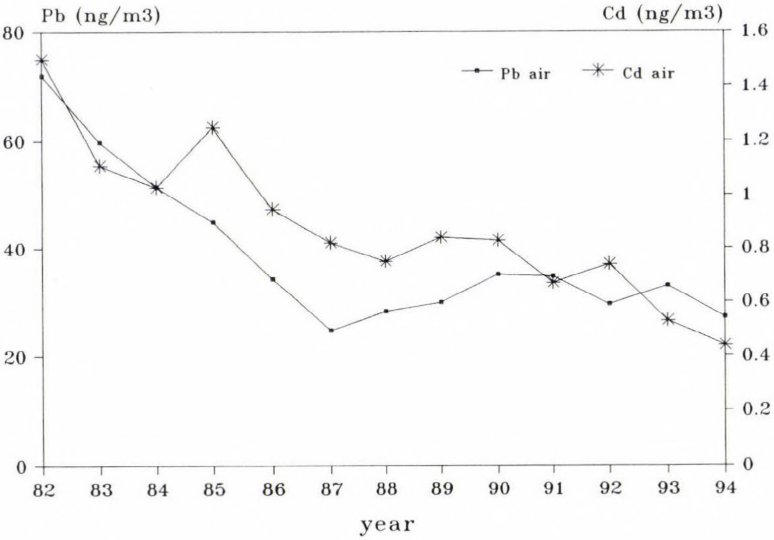

Fig. 1. Multiannual variation of Pb and Cd air concentration at K-puszta.

Concerning the Cd air concentration, higher yearly average values can be seen in the first half (1982–1986) of the monitoring period than in the second one (1987–1994). The decrease may be caused by the development and installation of environmental friendly industrial technologies in the western part of Europe and the economical decline (mostly in the late-80's) in Eastern Europe. The relatively high values for Pb and Cd total depositions in 1987 can be explained by the anomalies in meteorological factors (annual precipitation amount, relative frequency of trajectories from different sectors).

Analyses of Pb and Cd content of precipitation were started in 1983 (Pb) and 1984 (Cd). Wet only collectors are used for precipitation sampling. Monthly average lead and cadmium concentrations are determined by mixing the individual precipitation samples. For the chemical analyses graphite furnace atomic absorption spectrometer is used. Wet deposition are calculated by multiplying the trace metal concentration in precipitation and the precipitation amount.

The results of the measurements are shown in *Fig. 2*. Highest annual lead depositions were calculated for 1983 and 1987. Since 1987 there has been a decreasing trend in wet deposition of lead over Hungary. The highest Cd wet depositions were detected in 1984 and 1985 and the lowest ones in 1989 and 1994. Generally, it can be stated that the annual Cd wet depositions were higher in the period of 1984–1987 than those of between 1988–1994.

The lead and cadmium data measured in Hungary were also applied for the verification of the long-range transport model used for computations.

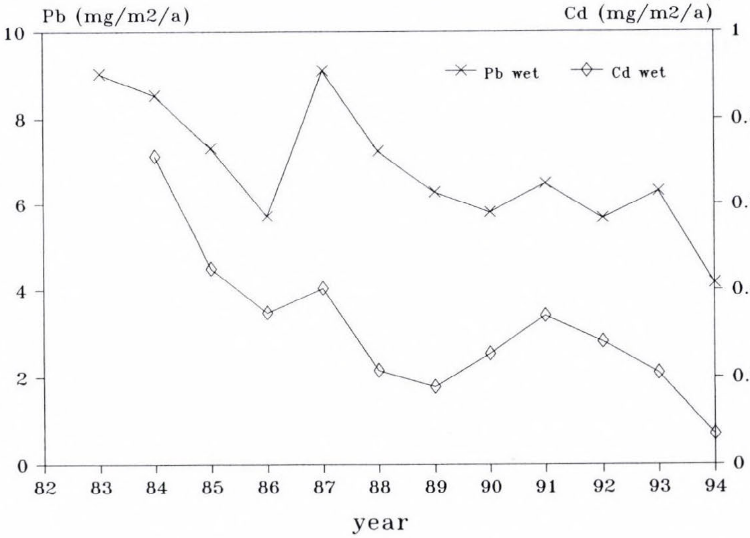

Fig. 2. Multiannual variation of Pb and Cd wet deposition at K-puszta.

3. *Modeling of long-range transport of Pb and Cd*

The TRACE model developed at IIASA, Laxenburg, Austria *Alcamo et al.* (1992) focuses on European-scale emission, transport and deposition of As, Cd, Pb and Zn. An application of this model to the estimation of total deposition and budgets of heavy metals over Eeastern Europe is given in *Bozó et al.* (1992). The model relies on long-term average meteorological data as input, and computes the long-term (annual) average levels of trace metals in the atmosphere. The calculations are based on mid-80's (Cd) and late-80's (Pb) emission inventories with 150 × 150 km^2 grid resolution over Europe. Unfortunately, more recent EMEP-gridded emission inventory (early 90's) for trace metals was not available.

The calculation procedure of this climatological-type model is divided into two steps: first, the loss of pollutant from a parcel of air as it travels from a source to a receptor is represented by a simple loss term. This equation gives the air concentration of a pollutant at a receptor located any distance downwind from a source:

$$c(x_r, y_r; x_e, y_e) = \beta \, E(x_e, y_e) \, R^{-1} \, (1-\alpha) \, e^{-(kd + kw)t}, \tag{1}$$

where c is the concentration of Pb and Cd due to a single emission source; (x_r, y_r) is the receptor position; (x_e, y_e) is the source position; E is the emission at the source; R is the distance between source and receptor; α is the local deposition coefficient (part of Pb and Cd emitted and deposited over the same grid); kd and kw are the first-order loss coefficients, which reflect the loss of Pb and Cd from the air parcel by dry and wet deposition processes, respectively. The factor β is derived by assuming mass conservation i.e. setting the upward flux of metals equal to the downward flux of deposition (for details see *Alcamo et al.*, 1992). The total concentration at the receptor is computed from the sum of contributions coming from all emission sources, weighted according to the frequency of backward trajectories coming from any of 8 sectors.

In the second step of the calculation, wet and dry deposition of the pollutant at the receptor is computed from the air concentration:

$$D_w = c(x_r, y_r) \, \mathrm{WP}, \tag{2}$$

where P is the annual precipitation amount and W is the scavenging ratio. Dry deposition is calculated by:

$$D_d = c(x_r, y_r) \, v_d, \tag{3}$$

where v_d is the dry deposition velocity computed on the basis of the semi-empirical model of *Sehmel* (1980) as a function of particle size, surface roughness and friction velocity.

The model outputs (both air concentrations and depositions) were compared to background measurements carried out at the European monitoring sites including our measurements at K-puszta station. Regarding the Pb, the average of computations and observations referring to air concentration are very close and all computations are within a factor of two of the observations. Calculations of wet deposition are also correlated to the available observations. Cd calculations clearly underestimate observations but are generally within a factor of two of observations. Model calculations of Cd air concentration are correlated with observations. The reason for the underestimation can be the inaccuracy of Cd emission inventory and/or contamination of samples and measurement uncertainty (*Alcamo et al.*, 1992).

4. *The origin of Pb and Cd deposition over Hungary*

The results of model calculations for the estimation of the country-origin of lead and cadmium deposition in Hungary (their total values are 680 t a^{-1} and 16.1 t a^{-1} for Pb and Cd, respectively) are shown in *Fig. 3*. The highest relative Pb contribution was calculated for Hungarian sources (19%). However, the contribution of the former Soviet Union and Poland to the total (dry + wet) lead deposition over Hungary is also significant (18% and 12%, respectively).

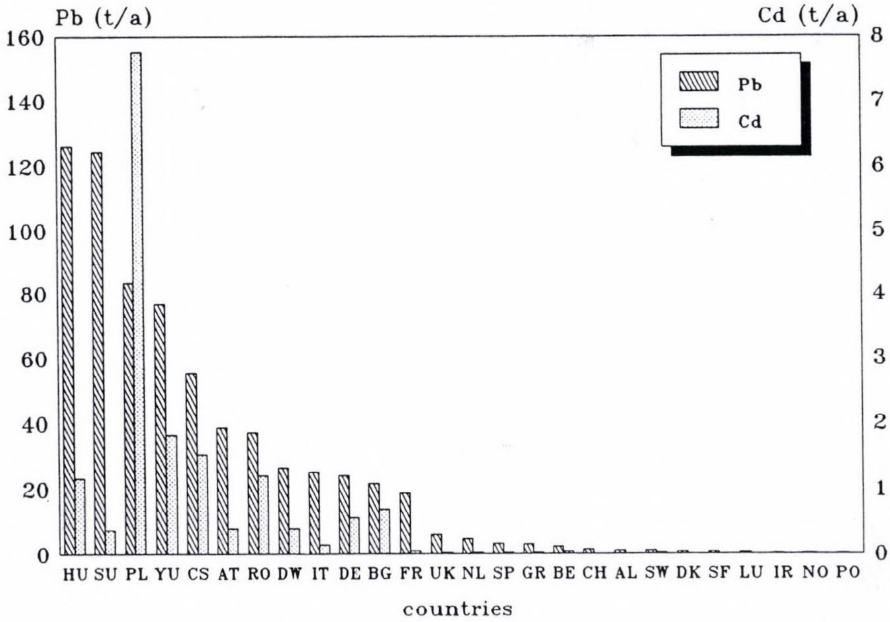

Fig. 3. Country-origin of Pb and Cd total deposition in Hungary.

Concerning the model calculations for Cd — based on a gridded European emission inventory valid for mid-80's — the following conclusions can be drawn. Approximately half the total cadmium deposition over Hungary originates from industrial sources of Poland. On the basis of our model computations even the former Yugoslavian and Czechoslovakian sources provide more cadmium deposited over Hungary (11% and 9%, respectively) than Hungarian emitters do (7%).

As it was mentioned above, lead emission decreased significantly in the Western European countries during the last decade due the introduction of unleaded gasoline and using less lead added to the conventional fuel. Breaking down the contributions to (1) Hungary itself (2) Western European countries and (3) other Eastern European countries the following conclusions can be drawn (*Fig. 4*). The relative contribution of Hungarian sources increased from 16% to 19% during the period of 1982–1989 while that of Western European sources decreased from 33% to 20%. At the same time the percentage contribution of Eastern European sources increased from 51% to 61%. The gridded European emission inventory for lead is valid for 1989–90. It should also be noted, however, that during the recent years the consumption of unleaded gasoline has become more widespread also in Hungary, and the lead content of gasoline has been decreased as well.

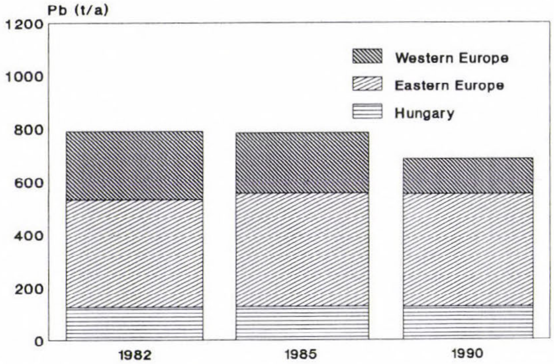

Fig. 4. Contribution of Western and Eastern European as well as Hungarian sources to the Pb total deposition over Hungary.

On the basis of TRACE-model computations the atmospheric Pb and Cd budgets over the Eastern European countries for the mid-80's have also been estimated (*Bozó et al.*, 1992). Concerning lead, an up-dated estimation of the atmospheric budgets valid for 1989–90 is presented in *Fig. 5*. In Bulgaria and Poland the emissions exceed the total deposition. For the other countries the total depositions are higher than the countries' own emissions.

5. Conclusions

It can be concluded from the measurements and model calculations that the atmospheric concentration and deposition of Pb and Cd in rural areas of Hungary are greatly affected by sources hundreds of kilometers far away from the receptor area. In the case of Hungary, it is particularly true for Cd. Emission data over the EMEP-grids for the model calculations were available only for the mid-80's (Cd) and late-80's (Pb). However, up-dated emission inventories are badly needed for the evaluation of the present rates of deposition and atmospheric budgets.

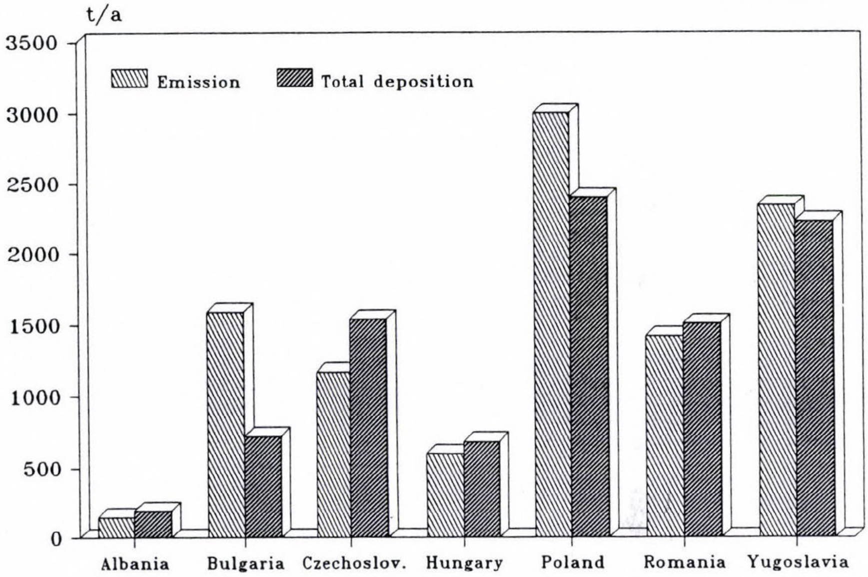

Fig. 5. Atmospheric country budgets for Pb over Eastern Europe.

References

Alcamo, J., Bartnicki, J., Olendrzynski, K. and *Pacyna, J.*, 1992: Computing heavy metals in Europe's atmosphere – I. Model development and testing. *Atmos. Environ. 26A*, 3355-3369.

Bozó, L. and *Horváth, Z.*, 1992: Atmospheric concentration and budget of lead and cadmium over Hungary. *Ambio 21*, 324-326.

Bozó, L., Alcamo, J., Bartnicki, J. and *Olendrzynski, K.*, 1992: Total deposition and budgets of heavy metals over Eastern Europe. *Időjárás 96*, 61-80.

Mészáros, Á. and *Horváth, Zs.*, 1983: Lead and cadmium concentrations in regional background air over Hungary. *Időjárás 87*, 7-13.

Sehmel, G.A., 1980: Particle and gas dry deposition: a review. *Atmos. Environ. 14*, 983-1011.

IDŐJÁRÁS

Quarterly Journal of the Hungarian Meteorological Service
Vol. 100, No. 1–3, January–September 1996

The Henry's law constant of oxalic acid and its partitioning into the atmospheric aerosol

Simon L. Clegg, Peter Brimblecombe and **Ikhtiar Khan**[1]

School of Environmental Sciences, University of East Anglia, Norwich NR4 7TJ, U.K.

(Manuscript received 26 May 1995; in final form 12 October 1995)

Abstract—The Henry's law constant (K_H'/mol kg^{-1} atm^{-1}) of oxalic acid (ethanedioic acid, $C_2O_4H_2$) has been determined from vapour pressures over the solid anhydrous acid, together with its solubility in pure water and aqueous H_2SO_4 solutions. It is given by: $\ln(K_H') = 20.40 - 9.493 \times 10^3 (1/T_r - 1/T) + 22.4(T_r/T - (1 + \ln(T_r/T)))$, where the equilibrium is between the gas phase molecule and undissociated aqueous acid, T (K) is temperature, T_r is equal to 298.15 K. Oxalic acid in the atmosphere will partition almost completely into aqueous aerosols, except under conditions of combined low relative humidity, low aerosol pH and temperatures greater than about 15°C. Simple estimates of wet and dry deposition of oxalic acid suggest that encrustations of calcium oxalates on aged calcareous building stones are not directly attributable to atmospheric sources of oxalate.

Key-words: oxalic acid, Henry's law, aerosols, partitioning, deposition, building stone.

1. Introduction

Oxalic acid (ethanedioic acid, $C_2O_4H_2$) is the most abundant dicarboxylic acid in the atmosphere and is largely derived from a combination of biogenic sources and anthropogenic precursors. Aliphatic dicarboxylic acids have been estimated to make up about 2% of total aerosol carbon (*Kawamura* and *Kaplan*, 1987), but have traditionally received much less attention than monocarboxylic acids in the atmosphere. It has been suggested that the dicarboxylic acids may be involved in aerosol formation and, when sufficiently abundant, increase aerosol acidity and contribute to visibility reduction (*Kawamura* and *Kaplan*, 1987). Oxalate, and other organic anions, are important in the redox chemistry of iron in aerosols and cloud droplets (*Erel et al.*, 1993), and photolysis of oxalato

---

[1] Now at: Department of Chemistry, University of Peshawar, Peshawar, Pakistan

complexes may be a significant sink for atmospheric oxalic acid (*Zuo* and *Hoigne*, 1992). The dicarboxylic acids have a high affinity for calcium, and oxalic acid arising from atmospheric deposition could be associated with deterioration in calcareous building materials (*Del Monte* and *Sabbioni*, 1983; *Jain et al.*, 1991).

The dicarboxylic acids are polar, and have low vapour pressures when compared with the mono-acids, and so should be associated with atmospheric aerosols and other condensed phases (*Kawamura* and *Kaplan*, 1987; *Ludwig* and *Klem*, 1988). However, the thermodynamic properties relevant to the phase partitioning of oxalic acid into water and aqueous solutions are not readily available, which limits our understanding of its atmospheric behaviour. Here, we use existing thermodynamic data to determine the Henry's law constant of oxalic acid as a function of temperature. This information is then used to investigate the partitioning of oxalic acid between the gas phase and aqueous aerosols. Oxalic acid deposition from the atmosphere and its relationship to the oxalate that is sometimes found to accumulate on building stones is briefly discussed.

2. *Sources of oxalic acid in the environment*

Early measurements of oxalic acid (*Norton et al.*, 1983) showed that it was correlated with aerosol nitrate, suggesting an anthropogenic source. Other work (*Kawamura* and *Kaplan*, 1987; *Grosjean*, 1989) has identified motor exhaust and soil as sources, but the ubiquitous occurrence of oxalic acid in photochemically polluted atmospheres suggests that it is largely produced as a secondary pollutant. Oxidation of hydrocarbons readily yields carboxylic acids, and these can be broken down into low molecular weight dicarboxylic acids. For example, succinic acid (butanedioic acid, $HOOCCH_2CH_2COOH$) can be oxidized to malic acid (hydroxybutanedioic acid, $HOOCCH(OH)CH_2COOH$), with further oxidation yielding oxalic and malonic acids (propanedioic acid, $HOOCCH_2COOH$) (*Kawamura* and *Ikushima*, 1993). Malonic acid itself will oxidise readily to oxalic acid. The high relative abundance of oxalic acid can therefore be explained in terms of it being a frequent end product of hydrocarbon oxidation in photochemical smogs. Evidence for a photochemical source comes from the observations of summer and daytime peaks in its concentration (*Satsumabayashi et al.*, 1990; *Kawamura* and *Ikushima*, 1993).

3. *Solubility relationships*

The solubility of gaseous $C_2O_4H_2$ in water and aqueous solutions is described by the following Henry's law equilibrium:

$$C_2O_4H_{2(g)} \rightleftharpoons C_2O_4H_{2(aq)}, \tag{1}$$

$$K_H' = aC_2O_4H_2/pC_2O_4H_2 \equiv mC_2O_4H_2\gamma_{C_2O_4H_2}/pC_2O_4H_2, \tag{2}$$

where K_H' (mol kg^{-1} atm^{-1}) is the Henry's law constant of oxalic acid, $pC_2O_4H_2$ (atm) is its equilibrium partial pressure, prefixes a and m denote aqueous activity and molality (mol per kg of water) respectively, and $\gamma_{C_2O_4H_2}$ is the activity coefficient of $C_2O_4H_2$ in solution. The reference state for the activity coefficient is a solution infinitely dilute with respect to $C_2O_4H_2$ in pure water. In such a solution $\gamma_{C_2O_4H_2}$ is equal to unity at all temperatures.

Aqueous oxalic acid dissociates according to the following equilibria:

$$C_2O_4H_{2(aq)} \rightleftharpoons C_2O_4H^-_{(aq)} + H^+_{(aq)}, \tag{3}$$

$$K_{d1} = aH^+aC_2O_4H^-/aC_2O_4H_2 \equiv mH^+\gamma_H mC_2O_4H^-\gamma_{C_2O_4H}/(mC_2O_4H_2\gamma_{C_2O_4H_2}), \tag{4}$$

$$C_2O_4H^-_{(aq)} \rightleftharpoons C_2O_4^{2-}{}_{(aq)} + H^+_{(aq)}, \tag{5}$$

$$K_{d2} = aH^+aC_2O_4^{2-}/aC_2O_4H^- \equiv mH^+\gamma_H mC_2O_4^{2-}\gamma_{C_2O_4}/(mC_2O_4H^-\gamma_{C_2O_4H}). \tag{6}$$

Here we adopt values of the thermodynamic dissociation constants given by *Kettler et al.* (1991):

$$\log_{10}(K_{d1}) = -626.410 + 35399.5/T + 98.2742\ln(T) - 0.097611T - 2.17087 \times 10^6/T^2, \tag{7}$$

$$\log_{10}(K_{d2}) = -606.206 + 34323.9/T + 94.9734\ln(T) - 0.100249T - 2.17087 \times 10^6/T^2. \tag{8}$$

At 298.15 K, K_{d1} and K_{d2} are equal to 5.29×10^{-2} and 5.33×10^{-5} mol kg^{-1}, respectively. The dissociation of dissolved oxalic acid into oxalate ($C_2O_4^{2-}$) and hydrogen oxalate ($C_2O_4H^-$) ions enhances the overall solubility of the organic acid for a given gas phase partial pressure. In particular, total dissolved oxalate becomes dependent upon pH. For example, in dilute aqueous solution at 15°C and pH 5.5 virtually all oxalate exists as $C_2O_4H^-$ and ($C_2O_4^{2-}$), whereas at pH 1 about 50% of total dissolved oxalate will occur as undissociated $C_2O_4H_2$.

To our knowledge, there are no measurements of equilibrium vapour pressures of oxalic acid above its aqueous solutions from which Henry's law constants can be determined. These must therefore be estimated indirectly. At temperatures below about 190°C pure oxalic acid is a solid, and can exist in both anhydrous form and as a dihydrate ($C_2O_4H_2 \cdot 2H_2O_{(cr)}$) (*Weast*, 1983). There are two crystalline forms of the anhydrous acid, α (orthorhombic) and β (monoclinic). Both can be obtained at room temperature, although α–$C_2O_4H_{2(cr)}$ is the more thermodynamically stable, with the transition point lying above the decomposition temperature (*Bradley* and *Cotson*, 1953).

Solubilities of $C_2O_4H_2 \cdot 2H_2O_{(cr)}$ in pure water are known for a range of temperatures. Saturation with respect to the solid anhydrous acid is only achieved in pure water at temperatures $\geq$98.8°C (*Luk'yanov*, 1953) and, at lower temperatures, in concentrated solutions of strong acids such as H_2SO_4 and HNO_3 where water activities are low. Our approach to estimating the Henry's law constant of oxalic acid is to consider a system in which solid oxalic acid (either the anhydrous or hydrated form) is simultaneously in equilibrium with $C_2O_4H_{2(g)}$ and an aqueous solution containing dissolved $C_2O_4H_2$. A knowledge of the vapour pressure of the pure acid, together with its solubility, allows K_H to be calculated.

Consider the following reactions:

(1) The solubility equilibrium of the dihydrate in aqueous solution,

$$C_2O_4H_2 \cdot 2H_2O_{(cr)} \rightleftharpoons 2H_2O_{(l)} + C_2O_4H_{2(aq)}, \tag{9}$$

$$K_1 = aC_2O_4H_2\, a_w^{\,2} \equiv mC_2O_4H_2\gamma_{C_2O_4H_2}\, a_w^{\,2}, \tag{10}$$

where a_w is the water activity of the solution, and $aC_2O_4H_2$ (mol kg^{-1}) is the activity of undissociated oxalic acid in solution. Note that the activity of the pure solid phase is unity, and therefore does not appear in the denominator of Eq. (10), or in other analogous equations below.

(2) The solubility equilibrium of the anhydrous acid in aqueous solution,

$$C_2O_4H_{2(cr)} \rightleftharpoons C_2O_4H_{2(aq)}, \tag{11}$$

$$K_2 = aC_2O_4H_2 \equiv mC_2O_4H_2\gamma_{C_2O_4H_2}. \tag{12}$$

(3) The dehydration of $C_2O_4H_2 \cdot 2H_2O$,

$$C_2O_4H_2 \cdot 2H_2O_{(cr)} \rightleftharpoons C_2O_4H_{2(cr)} + 2H_2O_{(g)}, \tag{13}$$

$$K_3 = pH_2O^2, \tag{14}$$

where pH_2O (atm) is the equilibrium water vapour pressure.

(4) The vapour pressure of the anhydrous acid (either α or β form),

$$C_2O_4H_{2(cr)} = C_2O_4H_{2(g)}, \tag{15}$$

$$K_4 = pC_2O_4H_2, \tag{16}$$

where $pC_2O_4H_2$ (atm) is the equilibrium vapour pressure of the acid.

It is clear from the above that the Henry's law constant of oxalic acid (Eq. 2) can be calculated from equilibria (2) and (4):

$$K_H' = K_2/K_4. \tag{17}$$

However, while sufficient data are available to define K_4 (see section 4.2 below), K_2 is more difficult to determine. This is because values of the activity coefficient of $C_2O_4H_{2(aq)}$, which are likely to be significantly greater than unity in the concentrated acid solutions which can be saturated with respect to $C_2O_4H_{2(cr)}$, are not known independently. We therefore apply a further constraint, relating K_2 to the solubility of the solid dihydrate in aqueous solution:

$$K_2 = (pH_2O^\circ)^2\, K_1/K_3, \tag{18}$$

where pH_2O° (atm) is the vapour pressure of pure water at the temperature of interest. In the derivation of Eq. (18) we recall that, assuming pressure is equivalent to fugacity for the conditions of interest here, $a_w = pH_2O/pH_2O^\circ$ for a solution in which the liquid and gas phase H_2O are at equilibrium.

In section 4 below the Henry's law constant of oxalic acid is determined as a function of temperature from a knowledge of K_3 and K_4, together with the simultaneous determination of the equilibrium constants for the dissolution of $C_2O_4H_2 \cdot 2H_2O_{(cr)}$ and $C_2O_4H_{2(cr)}$ in aqueous solution (K_1 and K_2), using available literature data. An equation for the Henry's law constant (Eq. 23) is given in subsection 4.4.

4. Determination of the Henry's law constant of oxalic acid

Sources of available thermodynamic data for oxalic acid are listed in *Table 1*. The crystalline form of the acid is indicated for each set of measurements in Table 1, where stated by the authors. However, in many instances this is not given, and we have assumed the thermodynamically stable α–oxalic acid.

Table 1. Availability of thermodynamic data for $C_2O_4H_2$

Data type	t (°C)	Source	Reference
pH_2O $[C_2O_4H_2 \cdot 2H_2O_{(cr)}]^a$	25.0–40.3	1	*Bell* (1940)
pH_2O $[C_2O_4H_2 \cdot 2H_2O_{(cr)}]^b$	0.0–50.0	2	*Baxter* and *Lansing* (1920)
pH_2O $[C_2O_4H_2 \cdot 2H_2O_{(cr)}]$	0.0–50.0	3	*Baxter* and *Cooper* (1924)
pH_2O $[C_2O_4H_2 \cdot 2H_2O_{(cr)}]$	32.7–46.9	4	*Bradley* and *Cotson* (1953)
pH_2O $[C_2O_4H_2 \cdot 2H_2O_{(cr)}]$	-22.24–53.54	5	*de Wit et al.* (1983)
pH_2O $[C_2O_4H_2 \cdot 2H_2O_{(cr)}]$	0.0–50.0	6	*Tagaki* and *Oomi* (1939)
$pC_2O_4H_2$ $[C_2O_4H_{2(cr)}]^c$	59.6–105.28	7	*Noyes* and *Wobbe* (1926)
$pC_2O_4H_2$ $[\alpha\text{-}C_2O_4H_{2(cr)}]^d$	30.0–55.0	8	*de Kruif et al.* (1975)
$pC_2O_4H_2$ $[\alpha\text{-}C_2O_4H_{2(cr)}]^{d,e}$	36.85–61.85[f]	9	*de Wit et al.* (1983)
$pC_2O_4H_2$ $[\alpha,\beta\text{-}C_2O_4H_{2(cr)}]$	37.6–51.9	10	*Bradley* and *Cotson* (1953)
solubility [in pure water]	0.0–80.0	11	*Snethlage* (1950)
solubility [in pure water][g]	0.0–90.0	12	*Snethlage* (1950)
solubility [in pure water]	15.0–25.0	13	*Flottmann* (1928)
solubility [in pure water]	25.0, 60.0	14	*Hill et al.* (1946)
solubility [in pure water][h]	0.0–50.0	15	*Norris* (1951)
solubility [in pure water][i]	0.0–80.0	16	*Chapin* and *Bell* (1931)
solubility [in pure water][j]	30.0	17	*Masson* (1912)
solubility [in pure water]	20.0	18	*Trapp* (1936)
solubility [in pure water]	5.0–65.0	19	*Apelblat* and *Manzurola* (1987)
solubility [in $H_2SO_{4(aq)}$]	25.0, 60.0	20	*Hill et al.* (1946)
solubility [in $H_2SO_{4(aq)}$]	17.0–33.0	21	*Sasaki* (1969)
solubility [in $H_2SO_{4(aq)}]^k$	-0.95–99.5	22	*Luk'yanov* (1953)
solubility [in $H_2SO_{4(aq)}$]	20.0	23	*Trapp* (1936)

(a) – these data rejected when determining the equilibrium constant for dehydration; (b) – the later study of *Bookey* and *Tombs* (1952) (20–49.8°C) confirms the results of *Baxter* and *Lansing*, and the data of *Bookey* and *Tombs* are not included here; (c) – stated by *Bradley* and *Cotson* (1953) that the oxalic acid must be in β form, due to the method of preparation; (d) – values of $pC_2O_4H_2$ were generated from the equation given by the authors; (e) – here assumed to be β-$C_2O_4H_{2(cr)}$ (see section 4.2); (f) – from (presumably) rounded temperatures given in Kelvin; (g) – mean of three earlier studies given in Table 1 of *Snethlage* (1950); (h) – a study of solubilities in the $C_2O_4H_2$-$Na_2(COO)_2$-H_2O system; (i) – a study in which solubilities of $C_2O_4H_2$ in $HCl_{(aq)}$ were determined; (j) – a study in which molar solubilities of $C_2O_4H_2$ in $HCl_{(aq)}$ and $HNO_{3(aq)}$ were also determined; (k) – the data presented by *Luk'yanov* are extensive and, for example, include solubilities of $C_2O_4H_2$ in pure water from -0.95 to 105°C, as well as results for mixtures. Here we use only solubilities measured in aqueous H_2SO_4 at 0 and 25°C.

4.1 The vapour pressure of H_2O over $C_2O_4H_2 \cdot 2H_2O_{(cr)}$ (K_3)

This has been studied by numerous workers (sources 1–6 in Table 1), over a temperature range of -22.24 to 53.54°C. The measurements of *Bradley* and

Cotson (1953) are for $C_2O_4H_2 \cdot 2H_2O_{(cr)}$–($\beta$–$C_2O_4H_{2(cr)}$), the authors stating that they were unable to measure pH_2O over the system including α–$_2O_4H_{2(cr)}$, due to the apparent formation of β–$C_2O_4H_{2(cr)}$ on dehydration. However, no such difficulty was noted by *de Wit et al.* (1983), who state that their data are for the α–dihydrate and note that they were unable to obtain β–$C_2O_4H_2 \cdot 2H_2O_{(cr)}$ in a stable form. No comment is made concerning the crystalline form of the acid by sources 1–3, and 6, and we have assumed the $C_2O_4H_2 \cdot 2H_2O_{(cr)}$–($\alpha$–$C_2O_4H_{2(cr)}$) system.

All data are shown in *Fig. 1*. There is excellent agreement between the different data sets. We note that the *Bradley* and *Cotson* (1953) partial pressures over $C_2O_4H_2 \cdot 2H_2O_{(cr)}$–($\beta$–$C_2O_4H_{2(cr)}$), source 4 in Table 1, are about 7% lower than the values for $C_2O_4H_2 \cdot 2H_2O_{(cr)}$–($\alpha$–$C_2O_4H_{2(cr)}$) from other sources. The equilibrium constant K_3 (atm^2) was determined from the data in Fig. 1 for $C_2O_4H_2 \cdot 2H_2O_{(cr)}$–($\alpha$–$_2O_4H_{2(cr)}$), and is given by:

$$\ln(K_3[T]) = \ln(K_3[T_r]) + (\Delta_r H°/R)(1/T_r - 1/T), \qquad (19)$$

where T (K) is the temperature of interest, T_r is the reference temperature of 298.15 K, $\ln(K_3[T_r])$ is equal to -11.3125 ± 0.009, $\Delta_r H°$ is equal to 112.84 $\pm$ 0.3 kJ mol^{-1}, and R (8.3144 J mol^{-1} K^{-1}) is the gas constant. Finally, we note that $\ln(K_3[T_r])$ equal to -11.47 ± 0.02 is obtained for $C_2O_4H_2 \cdot 2H_2O_{(cr)}$–($\beta$–$C_2O_4H_{2(cr)}$), assuming the same value of $\Delta_r H°$as given above.

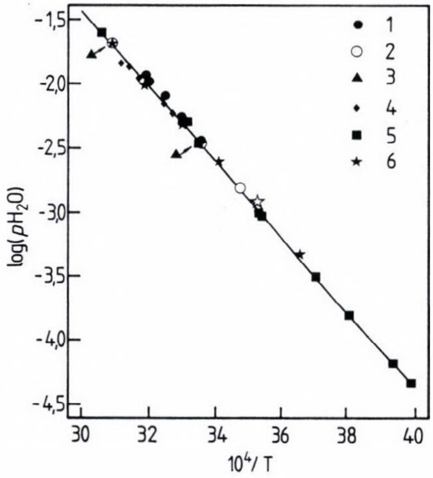

Fig. 1. Equilibrium vapour pressures of water (pH_2O/atm) above $C_2O_4H_2 \cdot 2H_2O_{(cr)}$ as a function of temperature. Symbols – data from numbered sources in Table 1; line – Eq. (19) for $C_2O_4H_2 \cdot 2H_2O_{(cr)}$–($\alpha$–$C_2O_4H_{2(cr)}$). Note that the open star represents a single measurement of *Tagaki* and *Oomi* (1939, source 6) that was excluded from the fit, as were all the data of *Bell* (1940, source 1).

4.2 *The vapour pressure of $C_2O_4H_2$ over α,β-$C_2O_4H_{2(cr)}$ (K_4)*

Measurements from data sources 7–10 are shown in *Fig. 2* for both α and β forms of the acid. *Noyes* and *Wobbe* (1926, source 7) do not state the crystalline form of their acid sample, though *Bradley* and *Cotson* (1953) note that from the method of preparation it is likely to be β-$C_2O_4H_{2(cr)}$. We have assumed this to be the case. The measurements of *Bradley* and *Cotson* (1953, source 10) and *de Kruif et al.* (1975, source 8) for α-$C_2O_4H_{2(cr)}$ are in reasonable agreement. However, the vapour pressures of *de Wit et al.* (1983, source 9) — also stated as being for α-$C_2O_4H_{2(cr)}$ — are considerably higher, and more consistent with the measurements for β-$C_2O_4H_{2(cr)}$. The reason for this is unclear, and *de Wit et al.* (1983) do not comment on the fact that their data are discordant with those of other workers. However, they state that their sample of $C_2O_4H_{2(cr)}$ was prepared by vacuum sublimation, which may have led to the production of the β form as it was also the method used by *Bradley* and *Cotson* (1953). Here we have assumed that the acid samples measured by *Bradley* and *Cotson* (1953) were correctly identified, and that the data of *de Kruif et al.* (1975) are for α-$C_2O_4H_{2(cr)}$ as stated by the authors. The measurements of *Noyes* and *Wobbe* (1926) and *de Wit et al.* (1983) are assumed to be for β-$C_2O_4H_{2(cr)}$. We have fitted values of K_4 (atm) for both α- and β-$C_2O_4H_{2(cr)}$, yielding $\ln(K_4[T_r, \alpha]) = -15.98 \pm 0.02$, $\ln(K_4[T_r, \beta]) = -15.44 + 0.03$, and $\Delta_rH°(\alpha \text{ and } \beta) = 96.85 \pm 0.7$ kJ mol^{-1}.

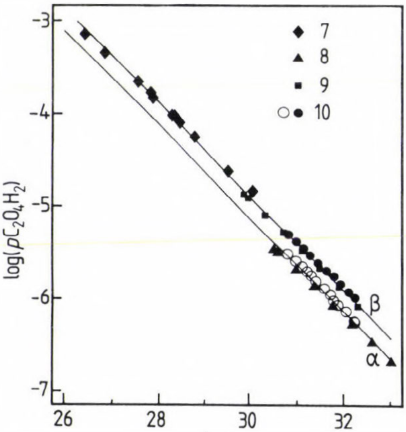

Fig. 2. Equilibrium vapour pressures of oxalic acid ($pC_2O_4H_2$/atm) above α- and β-$C_2O_4H_{2(cr)}$ as a function of temperature. Symbols – data from numbered sources in Table 1; upper line – fitted K_4 (section 4.2) for β-$C_2O_4H_{2(cr)}$, lower line – fitted K_4 (section 4.2) for α-$C_2O_4H_{2(cr)}$. For source 10, open circles are measurements for α-$C_2O_4H_{2(cr)}$, and closed circles are for β-$C_2O_4H_{2(cr)}$.

4.3 *Equilibrium constants for the solubilities of $C_2O_4H_2 \cdot 2H_2O_{(cr)}$ and α–$C_2O_4H_{2(cr)}$ in aqueous solution*

The solubility of $C_2O_4H_2 \cdot 2H_2O_{(cr)}$ in pure water has been obtained in many studies, and the sources (11–19) given in Table 1 are unlikely to form a complete list. Measured solubilities from 0 to 90°C are shown in *Fig. 3*. The large increase in solubility with temperature is due chiefly to the enhanced dissociation (to $C_2O_4H^-$ and $C_2O_4^{2-}$) that occurs at the higher temperatures. We have fitted the solubility of the dihydrate, S_{dh} (total mol of $C_2O_4H_2$ per kg H_2O), with the following empirical equation:

$$\ln(S_{dh}) = -37.30921 + 0.524243T^{0.9} - 0.0136641T^{1.5} + 2.19081 \times 10^{-4}T^2. \quad (20)$$

The fitted line is shown in Fig. 3, with residuals for each data set in.

It is clear from the agreement shown between the different datasets in the figure that oxalic acid solubilities in pure water are quite accurately known. However, the value of the equilibrium constant K_1 is more difficult to determine because, first, the molality of undissociated $C_2O_4H_2$ depends on the equilibria given by Eqs. (4) and (6), where the values of the activity coefficients of $C_2O_4H_2$, H^+, $C_2O_4H^-$ and ($C_2O_4^{2-}$) in aqueous oxalic acid at finite concentrations are not known. Second, the relationship between water activity (a_w) and total oxalic acid concentration also remains to be determined.

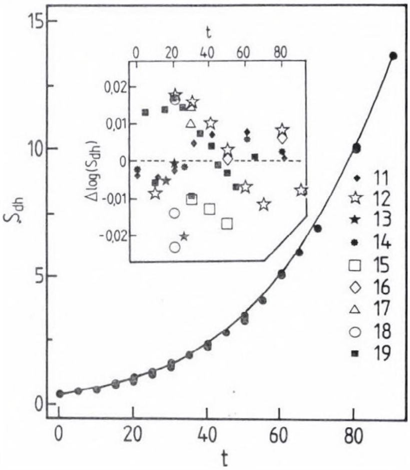

Fig. 3. Equilibrium solubilities of $C_2O_4H_2 \cdot 2H_2O_{(cr)}$ (S_{dh}/mol kg^{-1}) in pure water as a function of temperature (t/°C). Main plot: symbols – all data for sources 11–19 in Table 1; line – Eq. (20). Inset: residuals ($\Delta\log(S_{dh})$) from the fitted equation, for each of the numbered data sources in Table 1.

It is not possible to estimate K_1 without making some quantitative assumptions about the behaviour of the various species in solution and, preferably, introducing further data which provide thermodynamic constraints on the properties of the system. For this, we consider the solubilities of both $C_2O_4H_2 \cdot 2H_2O_{(cr)}$ and α-$C_2O_4H_{2(cr)}$ in aqueous H_2SO_4 to high concentration and over a range of temperatures. The data, from sources 20–23, are shown in *Fig. 4*. At each point where the solution mixture is saturated with respect to either the dihydrate or anhydrate, Eq. (10) or Eq. (12) is satisfied, with the two equilibrium constants related by Eq. (18). An important effect of the H_2SO_4 in solution is to suppress the dissociation of $C_2O_4H_{2(aq)}$, reducing the sensitivity of the results to assumptions concerning the activity coefficients of the oxalate and hydrogen oxalate ions.

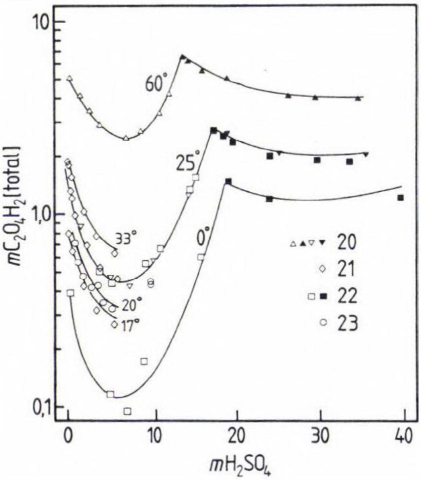

Fig. 4. Equilibrium solubilities of $C_2O_4H_2 \cdot 2H_2O_{(cr)}$ and α-$C_2O_4H_{2(cr)}$ ($mC_2O_4H_2$[total], the stoichiometric molality of oxalic acid) as a function of H_2SO_4 concentration (mH_2SO_4/mol kg^{-1}) at different temperatures. Symbols – data from numbered sources in Table 1 (solid symbols represent saturation with respect to the anhydrate); line – predicted solubilities using the activity coefficient model (section 4.3) and fitted parameters listed in Table 2.

The dissolved species $C_2O_4H_2$, H^+, HSO_4^-, SO_4^{2-}, $C_2O_4H^-$ and $C_2O_4^{2-}$ are present in the aqueous oxalic acid-sulphuric acid mixtures shown in Fig. 4. The thermodynamic properties of pure aqueous H_2SO_4 (i.e., H^+–HSO_4^-–SO_4^{2-}–H_2O) are well established, and are represented from 0–40 mol kg^{-1}, and < 200 to 328 K using the model-fraction-based thermodynamic (activity coefficient) model of *Pitzer, Simonson* and *Clegg* (*Clegg* and *Brimblecombe*, 1995). This model is formulated for an arbitrary number of components, and is not specific to sulphuric acid. It consists of a series of equations for ion and solvent activity coefficients, and other thermodynamic properties, derived from a single expression for the excess Gibbs energy of the solution (*Clegg et al.*, 1992). The equations contain empirical parameters for the interactions between the different components present in solution, whose values are obtained by fitting to thermodynamic data.

We have determined K_1 and K_2 by applying the model to the solubility data shown in Fig. 4. In the model, the parameters for the interactions between H^+, HSO_4^-, SO_4^{2-} and H_2O were set to those given by *Clegg* and *Brimblcombe* (1995) (their Table 4). We note that the small temperature extrapolation from the upper limit of the fitted model to 333.15 K, necessary to incorporate the measurements of *Hill et al.* (1946) at that temperature, is unlikely to introduce any error. The minimum set of additional parameters involving species $C_2O_4H_2$, $C_2O_4H^-$ and $C_2O_4^{2-}$ were then determined that enable the observed solubilities to be represented accurately. In the calculations for each measured point the equilibrium $HSO_4^- \rightleftharpoons H^+ + SO_4^{2-}$, and those represented by K_{d1} and K_{d2}, were solved iteratively. The resulting parameters are given in *Table* 2, and the fitted solubilities shown in Fig. 4. Using the final model, values of K_1 were calculated from 0 to 60°C for the solubilities S_{dh} given by Eq. (20), and then K_2 obtained using Eq. (18) and Eq. (19). These equilibrium constants are given by the following equations:

$$\begin{aligned}\ln(K_1[T]) = {} & (0.03858 \pm 0.002) + ((42.668 \pm 0.07) \times 10^3/R)(1/T_r - 1/T) \\ & + ((265.8 \pm 8)/R)(T_r/T - (1 + \ln(T_r/T))),\end{aligned} \tag{21}$$

$$\begin{aligned}\ln(K_2[T]) = {} & (4.4202 \pm 0.002) + ((17.926 \pm 0.07) \times 10^3/R)(1/T_r - 1/T) \\ & + ((185.7 \pm 8)/R)(T_r/T - (1 + \ln(T_r/T))),\end{aligned} \tag{22}$$

where T_r is the reference temperature of 298.15 K.

Table 2. Fitted activity coefficient model parameters[a]

$w_{1,2} = -5.07655 - 0.0357335(T - 298.15)$

$W_{2,H \cdot HSO_4} = -3.34943 - 1.40166 \times 10^{-4}(T - 298.15)^2$

$W_{2,H \cdot SO_4} = -8.95236 + 0.0499476(T - 298.15)$

Subscripts 1 and 2 represent H_2O and $C_2O_4H_{2(aq)}$, respectively. Parameters relating to H^+-HSO_4^--SO_4^{2-}-H_2O interactions are given by *Clegg* and *Brimblecombe* (1995). All others were set to zero. (a) – see *Clegg et al.* (1992) for a full description of the model.

How sensitive are these results to model assumptions involving the calculation of activity coefficients in the aqueous acid mixtures? Degrees of dissociation of oxalic acid ($(mC_2O_4H^- + mC_2O_4^{2-})/mC_2O_4H_2\{\text{total}\}$) in the mixtures shown in Fig. 4, and derived from the model, are <0.1 for H_2SO_4 molalities greater than 4 mol kg^{-1} at all temperatures. This suggests that even quite large changes in the activity coefficients will not greatly affect the amount of undissociated $C_2O_4H_2$ calculated to be present, and hence the results given in Eq. (21) and Eq. (22). This appears to be confirmed by test calculations in which parameters for $H^+ - C_2O_4H^-$ and $H^+ - C_2O_4^{2-}$ interactions were set to the same values as for $H^+ - HSO_4^-$ and $H^+ - SO_4^{2-}$ respectively. These yield a 20% increase in K_2 at 25°C, and give some indication of the level of uncertainty associated with our estimates of this equilibrium constant. This is comparable to the ~20% difference between the vapour pressures of $C_2O_4H_2$ over $\alpha\text{-}C_2O_4H_{2(cr)}$ obtained by *Bradley* and *Cotson* (1953) and by *de Kruif et al.* (1975).

4.4 The Henry's law constant of $C_2O_4H_2$

The Henry's law constant of oxalic acid is defined by Eq. (2) and Eq. (17), and is given by:

$$\ln(K_H'[T]) = 20.40 - (78.93 \times 10^3/R)\,(1/T_r - 1/T) + (186/R)(T_r/T - (1 + \ln(T_r/T))), \qquad (23)$$

where T_r is the reference temperature of 298.15 K. Henry's law constants calculated from Eq. (23) are listed in *Table 3*. Based on the above comparisons, we estimate that the Henry's law constants given by Eq. (23) are subject to an uncertainty of about ±20%, probably not exceeding ±50%, assuming that there are no significant systematic errors in the data upon which our calculations are based.

Table 3. Henry's law constants of oxalic acid

t (°C)	K_H'	t (°C)	K_H'
-5	2.91×10^{10}	15	2.21×10^9
0	1.46×10^{10}	20	1.25×10^9
5	7.55×10^9	25	7.24×10^8
10	4.03×10^9	30	4.29×10^8

At 25°C, K_H' for oxalic acid is a factor of about 10^5 larger than those for acetic and formic acids (*Khan et al.*, 1995), and with a stronger dependence on temperature ($\Delta_r H°$ equal to –78.93 kJ mol^{-1} compared to –46.86 and –53.51 kJ mol^{-1}, respectively). This very high Henry's law constant indicates that oxalic acid is likely to partition strongly into liquid water in the atmosphere, in all its forms. This is explored below.

5. The partitioning of oxalic acid in the atmosphere

The Henry's law constant for oxalic acid (Eq. 23) is higher than those of most of the lower organic acids found in the atmosphere (*Khan et al.*, 1995) by several orders of magnitude. An effective Henry's law constant ($K_H'^*$) for total oxalic acid of 2.4×10^{11} mol dm^{-3} atm^{-1} at pH 4 (temperature not specified) has been estimated by *Zuo* and *Hoigne* (1992). This can be compared with values calculated from the present study. First, $K_H'^*$ is defined by:

$$K_H'^* = (mC_2O_4H_2 + mC_2O_4H^- + mC_2O_4^{2-})/_pC_2O_4H_2$$

$$= K_H' (1 + K_{d1}/mH^+ + K_{d1}K_{d2}/(mH^+)^2), \qquad (24)$$

where pH (i.e., $-\log_{10}(mH^+)$) is treated as fixed, and all aqueous activity coefficients are assumed to be unity. From Eq. (24) we obtain $K_H'^*$ at pH 4 equal to 1.9×10^{12} and 5.8×10^{11} mol kg^{-1} atm^{-1} at 15 and 25°C, respectively, in moderate agreement with the estimate of *Zuo* and *Hoigne* (1992). We note also that *Gaffney et al.* (1987) quote an effective Henry's law constant of 7×10^6 mol dm^{-3} atm^{-1} for an atmospheric liquid water content of 1 g m^{-3}. This figure implies a much weaker partitioning of oxalic acid into atmospheric liquid phases than does our estimate and that of *Zuo* and *Hoigne* (1992). However, the value given by *Gaffney et al.* (1987) is unlikely to be correct given that the vapour pressure of the pure acid at 15°C is about 10^{-7} atm, and aqueous oxalic acid is almost 99.9% dissociated at pH 4.

The degree to which oxalic acid partitions into liquid water has a major influence on the path (wet or dry deposition) by which it is removed from the atmosphere. The very large values of the Henry's law constant show first of all that oxalic acid will partition completely into the amounts of condensed water typical of clouds and fogs (about 0.05 to 1.0 g m^{-3}). In addition, it is likely to partition into even the small amounts of water associated with hydroscopic aerosol particles. To investigate this, we have calculated the critical pH required to attain, first, equal partitioning between gas and aerosol phases and, second, 90% partitioning into the aqueous phase, as functions of atmospheric liquid water content and temperature. The expression used for this is:

$$(1/V_m)(273.15/T) = F(K'_H/\gamma_{C_2O_4H_2})(1 + K^*_{d1}/mH^+ + K^*_{d1}K^*_{d2}/(mH^+)^2)M_w/10^3, \tag{25}$$

where V_m (m^3 mol^{-1}) is the molar volume of an ideal gas at 273.15 K, M_w (g) is the mass of aerosol liquid water per m^3 of atmosphere, and F is the desired gas/liquid partitioning ratio of oxalic acid.

In our calculations we have assumed that mH^+ is equivalent to 10^{-pH}, and both K^*_{d1} and K^*_{d2} (the stoichiometric dissociation constants) are equal to the thermodynamic values given by Eqs. (7) and (8): that is to say, all the activity coefficients are equal to unity. The results are shown in *Fig. 5*. It is clear, first of all, that partitioning is strongly dependent upon pH and, taking into account typical atmospheric liquid water contents, in all but highly acidic aerosols oxalic acid will partition completely into the liquid phase. In the figure, this partitioning increases downwards (due to the rise in K_H with falling temperature) and to the right (increased atmospheric liquid water content). The areas to the right of the thick solid lines on each plot indicate conditions for which oxalic acid is so soluble that, even where dissociation is completely suppressed, partitioning into the aqueous phase exceeds the specified fractions of 50% and 90%.

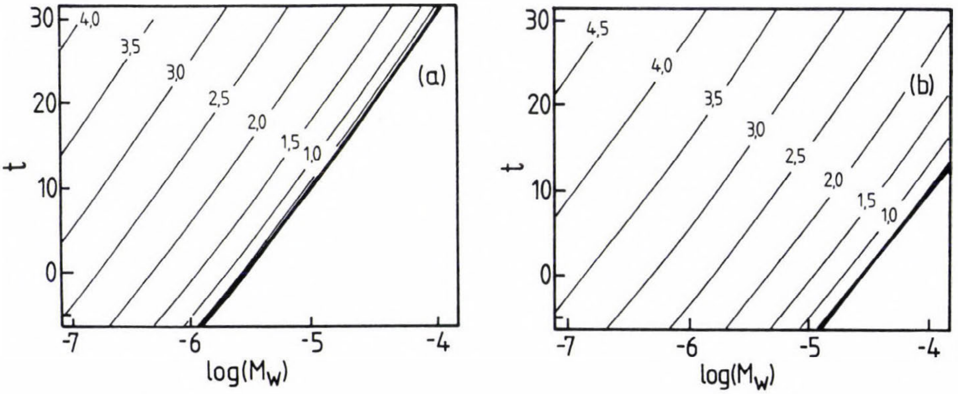

Fig. 5. Part *(a)* – contours of the critical pH required for equal partitioning of oxalic acid between gas and aqueous phases as a function of temperature (t/°C) and atmospheric liquid water content (M_w/g H_2O m^{-3}). Part *(b)* – critical pH for 90% partitioning of oxalic acid into the aqueous phase as a function of t and M_w. In both plots the thick solid line represents the limiting cases for which decreases in pH have no further effect on solubility.

In polluted atmospheres, the concentrations of particulate nitrate plus sulphate typically fall in the range 0.1 to 1.0 μmol m^{-3} (e.g., *Seinfeld*, 1986;

Finlayson-Pitts and *Pitts*, 1986). Assuming that these are the principal anions present in the aerosol, and that the deliquescence curve is approximately that of sulphuric acid, the amounts of liquid water associated with the aerosol (M_w in Fig. 5) can be calculated. For 0.1 μmol m^{-3} M_w ranges from 44 μg H_2O m^{-3} at 90% relative humidity (RH), to 20 μg H_2O m^{-3} and 12.9 μg H_2O m^{-3} at 70% and 50% RH, respectively. *Figure 5a* shows that, unless temperatures exceed about 15°C and RH is 70% or less, partitioning of the oxalic acid into the aqueous aerosol will exceed 50%. At 90% RH, partitioning will be virtually complete under most conditions (*Fig. 5b*). For 1.0 μmol of electrolyte per m^{-3} values of M_w are greater than those given above by a factor of ten. For this case, partitioning of oxalic acid into the aqueous aerosol will always exceed 50%, and will fall below 90% only where the temperature is greater than about 15°C and both relative humidity and aerosol pH are low.

What are the uncertainties associated with these calculations? Where oxalic acid partitioning into the aqueous phase is incomplete, the aerosols will be both highly concentrated with respect to soluble electrolytes, and have a low pH. Under these conditions the degree of dissociation of oxalic acid will be relatively small, so that changes in $\gamma_{C_2O_4H}$, $\gamma_{C_2O_4}$ and $\gamma_{C_2O_4H_2}$ are unlikely to have a major influence. More important is the 'salting-out' of the undissociated $C_2O_4H_2$ molecule (due to an increase in $\gamma_{C_2O_4H_2}$), which will tend to lower the overall solubility. From our model we estimate that $\gamma_{C_2O_4H_2}$ is equal to about 2.5 at 90% RH, 6 at 70% RH, and 9 at 50% RH in a pure aqueous sulphuric acid aerosol. Values of $\gamma_{C_2O_4H_2}$ will vary with aerosol composition, but are always likely to exceed unity. The net effect of these uncertainties, in addition to the ~20% associated with K_H, is likely to be a lowering of oxalic acid solubility in highly concentrated aqueous aerosols. While this implies a broadening of the range of temperature and pH for which partitioning into the aqueous phase is incomplete under low relative humidity conditions, the overall conclusions regarding oxalic acid behaviour are not affected.

6. Removal and deposition

The removal of oxalic acid from the atmosphere potentially involves physical processes, dry deposition and wet removal, as well as chemical reactions. The reaction with OH radical not an important removal mechanism, but photochemical decomposition is comparatively rapid and would be likely to reduce the daytime persistence of gas phase oxalic acid to a few hours (*Grosjean*, 1989). By contrast the aqueous acid appears to be stable. However, the acid forms Fe(III)-oxalate complexes (*Zuo* and *Hoigne*, 1992; *Erel et al.*, 1993), and it has been suggested that their photolysis could be a major sink of atmospheric oxalic acid (*Zuo* and *Hoigne*, 1992).

The comparatively low solubility of the monocarboxylic acids makes dry deposition the main process of removal from the atmosphere (*Grosjean*, 1989). However, the high solubility of oxalic acid and other dicarboxylic acids means that they will be found chiefly within aerosols and other liquid droplets, causing wet deposition to dominate (*Grosjean*, 1989).

The wet and dry deposition fluxes of oxalic acid can be estimated as follows. If we assume in the urban atmosphere an aerosol phase oxalic acid concentration of 6 nmol m^{-3} (e.g., *Kawamura* and *Kaplan*, 1987) and a deposition velocity of 0.01 m s^{-1}, then deposition would be 0.0019 mol m^{-2} a^{-1}. In rainfall, oxalic acid is found at concentrations as high as 20 μmol kg^{-1} (*Kawamura et al.*, 1985; *Steinberg et al.*, 1985), so 100 cm a^{-1} of rain implies a deposition of 0.02 mol m^{-2} a^{-1} — about a factor of ten greater than the dry deposition rate.

It is of some interest to compare these deposition fluxes with the oxalate accumulation on buildings. Although calcium oxalate hydrates on calcareous stones of historical structures are associated with the presence of micro-organisms (*Del Monte* and *Sabbioni*, 1986; *Edwards et al.*, 1992), the balance of sources of oxalate on urban building stones is still a matter of debate. In particular, because lichens are extremely sensitive to air pollutants it is thought that the biological production of oxalates by this route may be limited in urban areas (*Del Monte et al.*, 1987). This has raised interest in the possibility of an atmospheric source of oxalate encrustations. A typical encrusted building might have a 1 mm layer of oxalate (*Del Monte* and *Sabbioni*, 1983) which, assuming a specific gravity of 1.95 and a formula $CaC_2O_2 \cdot 2.5H_2O$ represents 2 kg m^{-2} of deposit. However, even under polluted conditions, combined wet and dry deposition from the atmosphere appears to be slow. The calculations of the paragraph above imply a total deposition of only 0.022 mol m^{-2} a^{-1} of oxalate (3.8 g m^{-2} a^{-1} of $CaC_2O_4 \cdot 2.5H_2O$) which, given the thickness of the encrustations, suggests that biological accumulation is more important.

7. Summary

In this work we have estimated the Henry's law constant of oxalic acid as a function of temperature from vapour pressures over the solid anhydrous acid together with its solubility in pure water and aqueous H_2SO_4 solutions. Gaseous oxalic acid (K_H is equal to 7.2×10^8 mol kg^{-1} atm^{-1} at 25°C) is several orders of magnitude more soluble in aqueous solutions than monocarboxylic acids such as formic and acetic acids which have Henry's law constants of about 5.5×10^3 mol kg^{-1} atm^{-1} at the same temperature.

Our result confirms the commonly held view (based on the low vapour pressure of the pure acid) that oxalic acid in the atmosphere will be chiefly associated with the aerosol phase. However, calculations carried out for a range of aerosol liquid water contents and pH suggest that oxalic acid partitioning into the aqueous phase may be incomplete where the aerosols are highly acidic, relative humidities are low, and temperatures are above about 15°C.

Simple estimates of wet and dry deposition of oxalate in an urban environment suggest that the encrustations of calcium oxalates that are sometimes found on old calcareous building stones are not directly attributable to atmospheric sources of oxalate.

References

Apelblat, A. and *Manzurola, E.*, 1987: Solubility of oxalic, malonic, succinic, adipic, maleic, citric, and tartaric acids in water from 278.15 to 338.15 K. *J. Chem. Thermo. 19*, 317–320.

Baxter, G.P. and *Cooper, W.C. Jr.*, 1924: The aqueous pressure of hydrated crystals. II. Oxalic acid, sodium sulphate, sodium acetate, sodium carbonate, disodium phosphate, barium chloride. *J. Am. Chem. Soc. 46*, 923-933.

Baxter, G.P. and *Lansing, J.E.*, 1920: The aqueous pressure of some hydrated crystals. Oxalic acid, strontium chloride and sodium sulphate. *J. Am. Chem. Soc. 42*, 419-426.

Bell, J., 1940: Salt hydrates and deuterates. Part II. Correlation of heats of dissociation and structure. *J. Chem. Soc.* 72-74.

Bookey, J.B. and *Tombs, N.C.*, 1952: Oxalic acid dihydrate as a source of low water-vapour partial pressure. *J. Iron & Steel Inst. 172*, 86.

Bradley, R.S. and *Cotson, S.*, 1953: The vapour pressure and lattice energy of hydrogen-bonded crystals. Part II. Alpha and beta-anhydrous oxalic acid and tetragonal pentaerythritol. *J. Chem. Soc.* 1684-1688.

Chapin, E.M. and *Bell, J.M.*, 1931: The solubility of oxalic acid in aqueous solutions of hydrochloric acid. *J. Am. Chem. Soc. 53*, 3284-3287.

Clegg, S.L. and *Brimblecombe, P.*, 1995: Application of a multicomponent thermodynamic model to activities and thermal properties of 0-40 mol kg^{-1} aqueous sulphuric acid from <200 K to 328 K. *J. Chem. Eng. Data 40*, 43-64.

Clegg, S.L., *Pitzer, K.S.* and *Brimblecombe, P.*, 1992: Thermodynamics of multicomponent, miscible, ionic solutions. II. Mixtures including unsymmetrical electrolytes. *J. Phys. Chem. 96*, 9470-9479; *98*, 1368; *99*, 6755.

de Kruif, C.G., *van Ginkel, C.H.D.* and *Voogd, J.*, 1975: Torsion-effusion vapour pressure measurements of organic compounds. *Conf. Inter. de Thermo. Chim. (4th) 8*, 11-18.

Del Monte, M. and *Sabbioni, C.*, 1983: Weddellite on limestones in the Venetian environment. *Environ. Sci. and Technol. 17*, 518-522.

Del Monte, M. and *Sabbioni, C.*, 1986: Chemical and biological weathering of an historical building: Reggio Emilia cathedral. *Sci. Total Environ. 50*, 165-182.

Del Monte, M., *Sabbioni, C.* and *Zappia, G.*, 1987: The origin of calcium oxalates on historical buildings, monuments and natural outcrops. *Sci. Total Environ. 67*, 17-39.

de Wit, H.G.M., *Bouwstra, J.A.*, *Blok, J.G.* and *de Kruif, C.G.*, 1983: Vapour pressures and lattice energies of oxalic acid, mesotartaric acid, phloroglucinol, myoinositol, and their hydrates. *J. Chem. Phys. 78*, 1470-1475.

Edwards, H.G.M., *Farwell, D.W.*, *Jenkins, R.* and *Seaward, M.R.D.*, 1992: Vibrational Raman spectroscopic studies of calcium oxalate monohydrate and dihydrate in lichen encrustations on Renaissance frescoes. *J. Raman Spectrosc. 23*, 185-189.

Erel, Y., *Pehkonen, S.O.* and *Hoffmann, M.R.*, 1993: Redox chemistry of iron in fog and stratus clouds. *J. Geophys. Res. 98*, 18423-18434.

Finlayson-Pitts, B.J. and *Pitts, J.N. Jr.*, 1986: *Atmospheric Chemistry: Fundamentals and Experimental Techniques*. Wiley-Interscience, New York.

Flottmann, Fr., 1928: Über Löslichkeitsgleichgewichte. *Z. anal. Chem. 73*, 1-39.

Gaffney, J.S., Strei, G.E., Spall, W.D. and *Hall, J.H.*, 1987: Beyond acid rain. *Environ. Sci. and Technol. 21*, 519-524.

Grosjean, D., 1989: Organic acids in southern California air: ambient concentrations, mobile source emissions, in situ formation and removal processes. *Environ. Sci. and Technol. 23,* 1506-1514.

Hill, L.M., Goulden, T.P. and *Hatton, E.*, 1946: Equilibria in ternary systems containing oxalates. *J. Chem. Soc.*, 78-81.

Jain, K.K., Saxena, V.K. and *Singh, T.*, 1991: Studies of the effects of biogenic acids on stone materials. In *Biodeterioration of Cultural Property* (eds.: *O.P. Agrawal* and *S. Dhawan*). Macmillan, New Delhi, pp. 240-248.

Khan, I., Brimblecombe, P. and *Clegg, S.L.*, 1995: Solubilities of pyruvic acid and the lower (c1-c6) carboxylic acids. Experimental determination of equilibrium vapour pressures above pure aqueous and salt solutions. *J. Atmos. Chem. 22,* 285-302.

Kawamura, K., Steinberg, S. and *Kaplan, I.R.*, 1985: Capillary GC determination of short-chain dicarboxylic acids in rain, fog and mist. *Intern. J. Environ. Anal. Chem. 19*, 175-188.

Kawamura, K. and *Kaplan, I.R.*, 1987: Motor exhaust emissions as a primary source for dicarboxylic acids in Los Angeles ambient air. *Environ. Sci. and Technol. 21*, 105-110.

Kawamura, K. and *Ikushima, K.*, 1993: Seasonal changes in the distribution of dicarboxylic acids in the urban atmosphere. *Environ. Sci. and Technol. 27*, 2227-2235.

Kettler, R.M., Palmer, D.A. and *Wesolowski, D.J.*, 1991: Dissociation quotients of oxalic acid in aqueous sodium chloride media to 175°C. *J. Solution Chem. 20*, 905-927.

Ludwig, J. and *Klem, O.*, 1988: Organic acids in different size classes of atmospheric particulate material. *Tellus 40B*, 340-347.

Luk'yanov, E.I., 1953: Polytherm of solubility of the ternary system H_2SO_4-$H_2C_2O_4$-H_2O. *Izvest. Sekt. Fiz. Khim. Analiza, Inst. Obshchei i Neorg. Khim. 22,* 272-292.

Masson, J.I.O., 1912: The solubility of electrolytes in aqueous solutions. Part III. Solubility of oxalic acid in other acids. *J. Chem. Soc. 101*, 103-108.

Norris, W.H.H., 1951: The system oxalic acid-sodium hydroxide-water. *J. Chem. Soc.* 1708-1715.

Norton, R.B., Roberts, J.M. and *Huebert, B.J.*, 1983: Tropospheric oxalate. *Geophys. Res. Lett. 10,* 517-520.

Noyes, W.A. Jr. and *Wobbe, D.E.*, 1926: The vapour pressure of anhydrous oxalic acid. *J. Am. Chem. Soc. 48*, 1882-1887.

Sasaki, E., 1969: Oxalic acid. III. Solubility of oxalic acid in sulphuric acid. *Kogyo Kagaku Zasshi 72*, 849-851.

Satsumabayashi, H., Kurita, H., Yokouchi, Y. and *Ueda, H.*, 1990: Photochemical formation of particulate dicarboxylic acids under long range transport in central Japan. *Atmos. Environ. 24A,* 1443-1450.

Seinfeld, J.H., 1986: *Atmospheric Chemistry and Physics of Air Pollution.* Wiley-Interscience, New York.

Snethlage, H.C.S., 1950: On the state of oxalic acid dissolved in water. *Rec. trav. chim. Pays-Bas 69*, 5-13.

Steinberg, S., Kawamura, K. and *Kaplan, I.R.*, 1985: The determination of α-keto acids and oxalic acids in rain, fog and mist by HPLC. *Intern. J. Environ. Anal. Chem. 19*, 251-260.

Tagaki, S. and *Oomi, S.*, 1939: Vapour pressure of hydrated crystals of oxalic acid and sodium formate. *J. Soc. Chem. Ind., Japan 42*, 302B-304B.

Trapp, H., 1936: Über die Löslichkeit der Oxalsaure und der Oxalate der alkalischen Erden in Mineralsauren, I. *J. prakt. Chem. 144*, 193-210.

Weast, R.C. (ed.), 1983: *CRC Handbook of Chemistry and Physics*. CRC Press, Boca Raton.

Zuo, Y. and *Hoigne, J.*, 1992: Formation of hydrogen peroxide and depletion of oxalic acid in atmospheric water by photolysis of iron(III)-oxalic complexes. *Environ. Sci. and Technol. 26*, 1014-1022.

IDŐJÁRÁS

Quarterly Journal of the Hungarian Meteorological Service
Vol. 100, No. 1-3, January-September 1996

Speciation of trace elements in the atmosphere

József Hlavay[1], **Klára Polyák**, **Ildikó Bódog** and **Ágnes Molnár**

Department of Analytical Chemistry, University of Veszprém,
8201 Veszprém, P.O. Box 158, Hungary

(Manuscript received 22 May 1995; in final form 19 February 1996)

Abstract—Chemical speciation of trace elements in filter-collected samples of atmospheric aerosols was carried out. Sampling was performed in a moderately polluted city (Veszprém, φ=47°6' N, λ=17°54' E, h = 260 m asl) and in a regional background sampling site (Kabhegy φ=47°5' N, λ=17°36' E, h = 600 m asl). A three-step sequential leaching technique was applied and 12 elements (Al, Fe, Ca, Mg, Mn, Pb, Cd, Cr, Cu, Ni, As and V) were analysed. Distribution of the elements among the (1) environmentally mobile, (2) carbonate and oxide associations and (3) environmentally immobile fractions was determined. In the survey period precipitation samples were also collected in Veszprém by wet-only sampling device. Dry deposition velocities, dry deposition rates, that of for environmentally mobile fractions, wet deposition rates and the total dry and wet depositions for Veszprém were calculated and compared. The data obtained provides information on the source of the metals and on their potential mobility following the deposition of the aerosols to the land surface.

Key-words: chemical speciation, filter-collected aerosols, trace elements, sequential leaching, dry deposition, wet deposition.

1. Introduction

The anthropogenic metals in aerosols can be derived from a number of individual sources: primary non-ferrous metal production, waste incineration, coal combustion, iron and steel production, and oil and gasoline combustion. The processes involve a high temperature treatment of raw materials. The metals can undergo condensation or can be adsorbed onto the surface of the ambient particles as the temperature falls. This process occurs mainly onto *fine particles*. These surface-associated trace metals will be in an *environmentally*

---

[1] Corresponding author

mobile, non-matrix form. Therefore, it is critically important that any chemical treatment designed to identify mobile associations must be able to separate the metals attached to small particles in surface positions.

The low temperature processes do not involve the distribution of volatile elements between matrix and non-matrix components. Instead, they include the generation of aerosols from material formed during crustal weathering and involve the mechanical lifting of surface soils into the atmosphere. The process depends on particle size of aerosols, but the redistribution of elements among different phases of an aerosol is not involved. So, the concentration of the elements in crust-generated aerosols is relatively close to the parent material, i.e. the elements have

$$EF_{crust} = \frac{C_{(i)\,air} / C_{(i)\,soil}}{C_{(Al)\,air} / C_{(Al)\,soil}}$$

values (enrichment factor) among 1 and 10 (*Chester et al.*, 1989).

Nevertheless, from the EF_{crust} values the sources of elements in aerosols can be estimated but to assess the impact that atmospherically-transported trace metals have on the environment, it is necessary to evaluate their subsequent fates in the receiving media; i.e. to understand how they enter into and behave within, for example, the soil or natural waters. The interaction of trace metals in the aerosols with the other receiving partners depends greatly on the solubility of metals under environmental conditions. This measure of environmental mobility is furthermore dependent on how precisely the elements are distributed among the various aerosol components. This information can be obtained by the chemical speciation of the elements in aerosols. *Chester et al.* (1986) have demonstrated that aerosol speciation data can be related to the extent of the solubility of an element in an aqueous medium, with metals in the environmentally mobile form being most soluble, and can provide a framework for assessing the reactivity of the elements once they have been deposited at the surface.

Several atmospheric parameters are controlled by aerosol particles and the human health as well as the life of aquatic and terrestrial ecosystem are also affected by the toxic metal content of particles. *Total concentration* of the elements in the atmospheric aerosol particles can indicate the *sources of the pollutant*, e.g. natural or anthropogenic origin. However, the *chemical speciation* can be used to assess the different *defined species* present *in the aerosol sample*.

The identification of the chemical forms of the trace elements in aerosols is a difficult problem, because relatively high concentrations of the species are required. *Lum et al.* (1982) provided data on the chemical speciation of a number of elements in a pollutant dominated, mainly high temperature generated, aerosol by applying a sequential leaching scheme to samples of an Urban Particulate Matter Standard Reference Material (SRM 1648). For characterisation of the crustal aerosols a five-stage sequential leaching technique was used for soil-sized aerosols (*Chester et al.,* 1986). Comparing the data derived from the two studies reveals that the speciation signatures for some elements differ considerably; aerosols collected at a polluted city contained generally more environmentally mobile fractions concerning Pb, Cr, Zn, Cu, and Cd. The crustal aerosol samples consisted of a higher portion in the stable fractions for the all elements studied. The environmentally mobile/bound to silicates fractions can be interpreted with particle surface/particle matrix associations formed as a result of high temperature anthropogenic processes and low temperature crustal weathering processes.

The environmental mobility means the exchange of metals adsorbed or condensed on the surface of aerosols. For the separation of this fraction of the total metal content of an aerosol, the metals have to be displaced from the substrate by reversing the binding mechanisms without affecting metals held in other associations. The most commonly used reagents are solutions of either 1 M NH_4OAc or $MgCl_2$. The pH needs to be sufficiently high so that protons do not compete, moreover do not react with other phases in the aerosols, but not too high so that hydroxides precipitate. A slightly more acidic solution such as hydroxilamin hydrochloride and acetic acid, is used to decompose carbonates liberating incorporated trace metals, and dissolving any free heavy metal carbonates. This reducing chemical agent can release heavy metals associated with iron and manganese hydrous oxide. After reduction of Mn(III) and Mn(IV) to Mn(II) and Fe(III) to Fe(II), the produced species are soluble, metal ions bound to the oxy-compounds are liberated into solution. Finally, the organic and silicate fractions can be decomposed using a combination of nitric and hydrofluoric acids. Since the SiF_4 is volatile it is lost from the solution, and the metal ions are released from the lattice.

The aim of the work was to apply a well-documented sequential leaching procedure for the determination of the environmentally mobile/stable element ratio in atmospheric aerosols collected on membrane filters. Two sampling sites were chosen, Veszprém and Kabhegy, and the measurement was concentrated for 12 elements.

2. *Experimental*

Aerosol samples were collected in Veszprém city and at a regional background sampling site, Kabhegy, on 5 cm diameter Teflon filters (pore size 5 μm) with a membrane pump of 1.2–1.5 m^3/h air. In the two day periods 55–72 m^3 air was sampled. The moderately polluted Veszprém is situated in the central part of Transdanubia, 15 km from Lake Balaton. It has about 60,000 inhabitants and there is no industrial activities in the surrounding area. The average elevation of the city is 250 m and the sampling has been carried out on the roof of a university building 20 m above the street level. Kabhegy is a part of the Bakony hills with an elevation of 600 m. It is located about 20 km north-west from

Veszprém (*Fig. 1*). The sampling device was placed at 30 m from the ground. Sampling period ranged between August 3, 1993, to February 28, 1994, and 14 samples were collected at both sites.

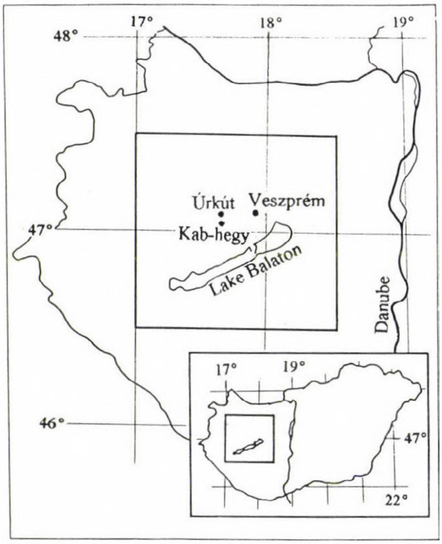

Fig. 1. The map of the sampling sites.

In the same survey period precipitation samples were also collected in Veszprém by wet-only sampling device. The collector consisted of a funnel with a diameter of 23 cm and a beaker of 2 L, both made from polyethylene. The precipitation was transferred to a polyethylene bottle, acidified by nitric acid to pH = 2, and kept in refrigerator. The sampling apparatus was placed onto the top of a university building, close to the aerosol sampler. In 1994, 513 mm precipitation was observed in Hungary on average.

A 3-stage sequential leaching procedure was applied to establish the distribution of metals between environmentally mobile (1), bound to carbonates and oxides (2), and environmentally immobile, bound to silicates (3) fractions. The details of the leaching experiments are published elsewhere (*Hlavay et al.*, 1996).

Elements were determined by atomic absorption spectrometry (Perkin Elmer 5100). Distribution of Al, Fe, Mn, Ca, Mg, Cu, Cr, V, As, Ni, Pb and Cd was investigated. Standards were prepared from ultra pure chemicals. Analytical blanks were performed on filters from the same batch. The blank obtained is a reagent + filter blank. Certified reference materials, BCR No. 38, *Fly ash from pulverised coal* and No. 176, *City waste incineration ash* were used for evaluation of the procedure.

3. Results and discussion

The commonly used method of relating an element in an aerosol to its source is to calculate enrichment factors (EF) by employing a source marker or indicator element. For crustal aerosol Al is normally used as the indicator element. Those elements that have EF_{crust} values < 10 are usually termed the crustal, or non-enriched elements (NEE) (*Rahn,* 1989). Elements of EF_{crust} values in the range 10–5000 are generally emitted by anthropogenic sources and termed the anomalously enriched elements (AEE). The factors were calculated to Al, the crustal reference element, for the comparison of data from different sources (*Rahn,* 1989; *Molnár et al.*, 1993; *Adams et al.*, 1983) and summarized in *Table 1*. Along with EF values calculated for the mean concentration of each element in aerosol samples, the percentage of non-crustal fractions is also tabulated.

Table 1. Enrichment factors (EF) and non-crustal factions (nc) in aerosol particles in Veszprém (Vp) and in Kabhegy (Kab) (mobile is the environmentally mobile fraction). K-puszta is the Hungarian background station

Elements	$(C_i/C_{Al})_{crust}$ *	EF Vp	nc %	EF Vp mobile	EF Kab	nc %	EF Kab mobile	K-puszta	Budapest
Al	1	1	0	1	1	0	1	1	1
Fe	0.518	3.65	69	0.06	2.53	50	0.09	2.86	5.05
Mg	0.257	19.8	95	1	6.8	85	0.3		
Mn	$8.3*10^{-3}$	108	99	9.8	76	99	11.3	3.1	5.9
Pb	$9.6*10^{-5}$	1685	100	1206	1028	100	578	824	7710
Cd	$2.4*10^{-6}$	4665	100	241	2404	100	356		
Cr	$622*10^{-6}$	24.2	96	12.4	20.	95	8.9	59.4	57.7
Cu	$4.97*10^{-4}$	59.8	98	10.0	38.7	97	4.3	68.0	158
Ni	$5.44*10^{-4}$	312	99	84	414	100	78.3	26.1	40.9
As	$1.24*10^{-5}$	809	99	57.2	655	100	68.7	2265	6443
V	$7.8*10^{-4}$	34.7	97	19.8	23.	96	8.7	19.3	28.5

$*(C_i/C_{Al})_{crust}$ data from *Molnár et al.* (1993)

Iron is a crust-dominated element and 50–70% of it originates from non-crustal fractions. Magnesium shows a crustal character at Kabhegy, EF = 6.8 and higher value (EF = 19.8) at Veszprém. Manganese is largely non-crustal, emitted from an open-mine. There is an active open-mine producing manganese ores at Úrkút, which is located just about between Ajka and Kabhegy. Ajka, with a major industry, is situated 25 km north-west from Veszprém and 8 km from Kabhegy. EF values of Ca and Mn are considerably higher than those of Budapest and Kabhegy.

EF values and percentage of non-crustal fractions show that Pb, Cd, Cr, Cu, Ni, As, and V are emitted from anthropogenic sources. No major differences have been found among the values calculated for different sampling sites in Hungary. The total quantity of Cd, for example, is emitted from anthropogenic sources, EF ranges between 4665 (Veszprém) and 2404 (Kabhegy) (see Table 1). The cadmium species in aerosols are probably Cd, CdS, CdO, $Cd(OH)_2$ and mixed oxides with copper and zinc (*Pacyna,* 1987; *Nriagu,* 1980). Cadmium is reported to be more concentrated on the surface of particles produced by combustion (*Nriagu,* 1980).

EF values of Cr and Cu indicate that these elements are also emitted by anthropogenic sources, however, the factors are somewhat lower than which have been calculated to Budapest and K-puszta (a regional background monitoring station) (*Molnár et al.,* 1993). Ni shows much higher EF value at these two sampling sites than that in other parts of Hungary. This suggests that there has been a strong anthropogenic source nearby. However, any local source (sampling head, sampling device, or surroundings of samplers) should also be taken into consideration. High proportions of Ni and Cu were identified in soluble and/or exchangeable forms and those of Cr in residual fraction in urban particulate matter analysed by sequential extraction procedure (*Lum et al.,* 1982).

EF values of As are much less than those of K-puszta and Budapest indicating only a weak emission source in this area. Somewhat lower concentrations of As were found in the aerosol samples collected at Kabhegy and Veszprém as compared to the other monitoring stations in Hungary and to some major cities (*Molnár et al.*, 1993; *Hlavay et al.,* 1995; *Salomons,* 1986). This is entirely consistent with its urban sources from which it is released during high temperature volatilisation processes and subsequently becomes bound to particle surfaces or is incorporated into individual compounds. The major chemical species of arsenic are As, As_2O_3, As_2S_3 and organoarsenic compounds from combustion and metallurgical technologies (*Pacyna,* 1987). EF values of vanadium were similar to those at other stations. Vanadium is predominantly non-crustal in character, and it has been probably derived from oil combustion. The concentration ranges agree well with other findings measured at different domestic stations (*Molnár et al.,* 1993).

If the EF values are calculated for the environmentally mobile fractions the two sampling sites show a similar picture. Values of Fe, Ca, Mg, Cr, and Cu are less than 10, so a certain part of the total element content of aerosols can be considered as crustal origin. It is assumed that with sequential leaching the crustal and non-crustal fractions can be approximately estimated. Other elements (Pb, Cd, Ni, As, V) have much higher EF values, i. e. the total amount originates from anthropogenic emission sources.

Dry deposition at Kabhegy

The dry deposition rates were calculated by means of the dry deposition velocities (*Table 2*). Dry deposition velocities were calculated by *Molnár et al.* (1995) using the size distributions of metals measured with a cascade impactor at Veszprém. For the environmentally mobile fractions the dry deposition velocities were also calculated. Three-stage sequential leaching procedure was applied for the 8 particle size fractions collected by the cascade impactor. The ratio of the mobile/total fractions for 9 elements is tabulated in the Table 2.

Table 2. Dry deposition velocities (v), geometric mean concentration of elements in aerosols collected in Kabhegy (c_{tot}), geometric standard deviation (S. D.), dry deposition rates (D_{dry}), total dry deposition (10^3 g yr^{-1}) and those of the environmentally mobile fractions

Elements	v_{total} cm/s	c_{total} ng/m^3	S.D.	D_{drytot} mg/m^2 yr	v_{mobile} cm/s	c_{mobile} ng/m^3	$D_{drymobile}$ mg/m^2 yr	$\frac{D_{drymobile}}{D_{drytot}}$ %
Al	0.950	234	3.4	70.0	0.914	37	10.65	15.2
Fe	0.926	243	3.6	70.9	0.181	10	0.57	0.8
Mn	0.680	148	3.6	31.7	1.180	22	8.18	25.9
Pb	0.114	23.1	2.1	0.83	0.075	13	0.31	36.9
Cd	0.096	1.35	4.7	0.04	0.140	0.22	0.01	24.2
Cu	0.092	4.5	4.0	0.13	0.069	0.50	0.011	8.4
Ni	0.220	52.7	2.9	3.65	0.132	10	0.416	11.4
Cr	0.067	2.9	2.0	0.061	0.052	1.30	0.021	34.4
As	0.235	1.9	7.8	0.14	0.906	0.2	0.06	42.8
V	0.139	4.2	2.0	0.18	0.076	1.6	0.038	20.9

It can be seen that Pb, Cr, and As have been found in the environmentally mobile fraction at least 34–43% of the total concentration. During deposition and mixing of aerosol with aqueous solutions they are the anthropogenic elements that are preferentially released. They have, potentially, the most harmful impact on the biological community. Nickel behaves differently, the dry deposition rates are higher at Kabhegy than at a city. These findings need further investigations but only 11% of the total Ni is environmentally mobile, the other part is in stable form.

Dry and wet depositions at Veszprém

For evaluation of the atmospheric budget for a city and the environmental effects of trace metals on biosphere the calculation of the dry and wet depositions is of vast importance. The dry deposition rates and the total dry deposition were calculated by means of the dry deposition velocities for the area of Veszprém (19.1 km^2) (*Table 3*).

Table 3. Geometric mean concentration of elements in aerosols collected in Veszprém (c_{tot}), geometric standard deviation (S. D.), dry deposition rates (D_{dry}), total dry deposition and those of the environmentally mobile fractions

Elements	c_{tot}	S.D.	D_{drytot}	c_{mobile}	$D_{drymobile}$	Total dry	Total dry-mobile	$\frac{D_{drymobile}}{D_{drytot}}$
	ng/m^3		mg/m^2 yr	ng/m^3	mg/m^2 yr	10^3 g/yr	10^3 g/yr	%
Al	259	2.4	77.5	13	3.74	1474	71.4	4.8
Fe	433	3.0	125.3	9	0.51	2393	9.7	0.4
Mn	232	1.9	49.8	21	7.81	951	149	15
Pb	41.9	1.9	1.51	30	0.71	29	13.6	47
Cd	2.9	6.8	0.088	0.15	0.007	1.7	0.13	8
Cu	7.7	2.6	0.22	1.3	0.028	4.25	0.53	13
Ni	44	2.3	3.1	11.9	0.49	59.2	9.4	16
V	5.2	2.5	0.23	3	0.072	4.4	1.4	31

The dry deposition rates obtained for the two sampling sites show, except Ni, always lower values at Kabhegy (local background site) than at Veszprém (see Tables 2 and 3). Along with the total dry deposition rates, those of calculated by the ratio of the environmentally mobile/total fractions are also tabulated. As it was pointed out earlier, the deposition of Mn is extremely high in this area, either at Kabhegy or at Veszprém, as compared to other part of Hungary, due to the close mining activities (*Molnár et al.,* 1995). Deposition of Pb, Cd, Cu, Cr and V does not significantly differ from the other values published (*Alcamo et al.,* 1992; *Milford* and *Davidson*, 1985) based on a different approach. However, taking into account the data derived for the environmentally mobile fractions, 0.71 mg m^{-2} yr^{-1} of Pb, a completely non-crustal element, is directly available to the biosphere. For Veszprém it means a 13.6 kg dry deposition annually. However, the half of this Pb pollution is in an environmentally mobile form and it can be harmful for the biosphere.

Atmospheric removal occurs either by dry deposition of aerosol particles to water, soil, buildings or plants, or by wet deposition of aerosol particles and gases in rain, fog, hail and snow. The relative importance of the two depositional processes varies with location and is primarily a function of the rainfall intensity in that area. Wet deposition has been shown to be a very important removal process for those elements associated with small particles. These elements are also of predominantly anthropogenic origin. Wet deposition rates are based upon the concentration of trace metals in precipitation samples collected by a wet-only sampler in Veszprém. Weighed mean concentrations were calculated by taking into account the volume of precipitation collected at each case, and the annual precipitation amounts. Results are shown in *Table 4.*

Table 4. Concentration of elements in precipitation collected in Veszprém (c_{prec}), wet deposition rates (D_{wet}), total wet deposition, dry deposition rates (D_{dry}), and those of the environmentally mobile fractions

Ele-ments	c_{prec} mg/L	D_{wet} mg/m^2 yr	Total wet 10^3 g/yr	D_{drytot} mg/m^2 yr	$\frac{D_{wet}}{D_{dry}}$	$D_{drymobile}$ mg/m^2 yr	$\frac{D_{wet}}{D_{drymobile}}$
Fe	11.8	6.05	115.6	125.3	0.05	0.51	11.9
Mn	3.41	1.75	33.44	49.8	0.035	7.81	0.22
Pb	2.8	1.43	27.3	1.51	0.94	0.71	2.0
Cd	0.11	0.05	0.95	0.088	0.56	0.007	7.3
Cu	2.1	1.08	20.6	0.22	4.84	0.028	38.9
Ni	0.6	0.31	5.9	3.1	0.10	0.49	0.63
V	2.2	1.12	19.1	0.23	4.34	0.072	13.6

Wet deposition data are usually lower than they have been published for Hungary and other areas like marine, rural and urban (*Kasahara et al.,* 1992; *Salamons,* 1986). Most information available is on lead and the deposition levels range from < 5 mg m^{-2} yr^{-1} in remote areas to 25-330 mg m^{-2} yr^{-1} in urban areas and much higher close to the lead based industries, and roads busy with traffic (*Nriagu,* 1980). A number of factors influence the level of deposition in any area, such as the locality i.e. remote, rural, urban or industrial. Wet deposition depends on the existence of rain or snow, the amount, its duration and intensity. The concentration of Pb in precipitation decreases with increasing intensity of the rain (*Nriagu,* 1980). So, the comparison of data derived from different sources is very difficult, and sometimes no any relevance has been noticed.

The comparison of wet and dry depositions shows a very exciting picture. It has been published recently (*Kasahara et al.,* 1992) that the D_{wet}/D_{dry} ratio is significant in particular for Pd and Zn and usually higher for the others (V, Cr, Ni, Cu, As). In our case it has been found that for elements like Fe, Mn, Pb, Cd and Ni the ratio of the two depositions gives an opposite appearance; namely, the dry deposition plays an important role in the pollution of the environment. On the other hand, the $D_{wet}/D_{drymobil}$ ratios entirely indicate that, except Mn and Ni, the environmentally mobile fractions of other elements are much smaller than the soluble part in rain water. Wet deposition provides a mechanism by which the metals in aerosol particles can be solubilised.

The aim of collecting precipitation and aerosol samples in the same place at the same time was to determine the distribution of elements in the two phases. Nevertheless, calculations are affected by the dry deposition velocities and some emission sources along with the air trajectory can also influence the deposition. Further investigations are necessary to confirm these data; other sampling sites have to be selected and more samples should be collected and analysed.

Acknowledgements—The research was supported by OTKA 16315.

References

Adams, F., Van Espen, P. and *Maenhaut, W.*, 1983: Aerosol composition at Chacaltaya, Bolivia, as determined by size-fractioned sampling. *Atmospheric Environment 17,* 1521-1536.

Alcamo, J., Bartnicki, J., Olendrzynski, K. and *Pacyna, J.* 1992: Computing heavy metals in Europe's atmosphere–I. Model development and testing. *Atmospheric Environ. 26A,* 3355-3369.

Chester, R., Lin, F.J. and *Murphy, K.J.T.*, 1989: A three stage sequential leaching scheme for the characterization of the sources and environmental mobility of trace metals in the marine aerosol, *Environ. Tech. Letters, 10,* 887-900.

Chester, R. Murphy, K.J.T., Towner, J. and *Thomas, A.*, 1986: The partitioning of elements in crust-dominated marine aerosols. *Chem. Geol. 54,* 1-15.

Hlavay, J., Polyák, K., Bódog, I., Molnár, Á. and *Mészáros, E.* 1996: Distribution of trace elements in filter-collected aerosol samples. *Fresenius J. of Analytical Chemistry 354,* 227-232.

Kasahara, M., Takahashi, K., Hitzenberger, R. and *Preining, O.* 1992: Intercomparison of trace metal in atmospheric aerosol collected in Kioto and Vienna. *J. Aerosol Sci. 23,* S1003-S1006.

Lum, K.R., Betteridge, J.S. and *Mcdonald, R.R.*, 1982: The potential availability of P, Al, Cd, Co, Cr, Fe, Mn, Ni, Pb and Zn in urban particulate matter. *Environ. Technol. Letters 3,* 57-62.

Milford, J.B. and *Davidson, C.I.* 1985: The sizes of particulate trace elements in the atmosphere - a review. *J. Air. Pollut. Control Ass. 35,* 1249-1260.

Molnár, Á., Mészáros, E., Bozó, L., Borbély-Kiss, I., Koltay, E. and *Szabó, Gy.*, 1993: Elemental composition of atmospheric aerosol particles under different conditions in Hungary. *Atmospheric Environment 27A,* 2457-2461.

Molnár, Á., Mészáros, E., Polyák, K., Borbély-Kiss, I., Koltay, E., Szabó, Gy. and *Horváth, Zs.*, 1995: Atmospheric budget of different elements in aerosol particles over Hungary. *Atmospheric Environment 29,* 1821-1828.

Nriagu, J.O. 1980: Cadmium in the atmosphere and precipitation. In *Cadmium in the Environment, Part I Ecological Cycling* (ed.: *J. O. Nriagu*). Wiley, New York, Tokyo, Amsterdam, 71-114.

Pacyna, J. M. 1987: Atmospheric emissions of arsenic, cadmium, lead, and mercury from high temperature processes in power generation and industry. In *Lead, Mercury, Cadmium and Arsenic in the Environment* (eds.: *T. C. Hutchinson* and *K. M. Meema*). Wiley, New York, Tokyo, Amsterdam, SCOPE, 69-87.

Rahn, K.A., 1989: The chemical composition of the atmospheric aerosol. Graduate School of Oceanography, Univ. of Rhode Island, Kingston, R. I., *Tech. Rep., 226.*

Salamons, W., 1986: Impact of atmospheric inputs on the hydrospheric trace metal cycle. In *Toxic Metals in the Atmosphere* (eds.: *J. O. Nriagu* and *C. I. Davidson*). Wiley, New York, Tokyo, Amsterdam, 409-466.

IDŐJÁRÁS
Quarterly Journal of the Hungarian Meteorological Service
Vol. 100, No. 1–3, January–September 1996

Retrieval of the aerosol size distribution function from spectral solar radiation measurements

J. Lukáč[1] and **M. Kocifaj**[2]

[1] *Geophysical Institute, Slovak Academy of Sciences,*
Dúbravská cesta 9, SK-84228 Bratislava, Slovak Republic
[2] *Astronomical Institute, Slovak Academy of Sciences,*
Dúbravská cesta 9, SK-84228 Bratislava, Slovak Republic

(Manuscript received 18 May 1995; in final form 15 August 1995)

Abstract—The contribution deals with the estimation of the aerosol size distribution function. This function is calculated by means of the inverse tasks from the direct or diffuse spectral solar radiation. The aerosol size distribution function is chosen in the form of a modified gamma function. Three examples of the retrieval of the aerosol size distribution function from the spectral solar radiation measurements (two from the direct solar radiation and one from the sky radiance) show the utilized procedures. The presented results show that the measurements of the spectral direct solar radiation or the spectral sky radiance are suitable means to achieve this goal.

Key-words: atmospheric aerosols, solar radiation, aerosol distribution function, aerosol optical thickness, aerosol scattering function.

1. Introduction

Aerosols have the potential to change the radiative balance of the Earth, both directly, by scattering solar radiation back into the space, and indirectly, by acting as cloud condensation nuclei and changing the radiative properties of the clouds (*Hobbs*, 1994). The evaluation of aerosol influence on solar radiation is connected with the knowledge of aerosol properties like the aerosol quantity expressed by the aerosol optical thickness, the aerosol structure expressed by the aerosol size distribution function and the aerosol quality expressed by the complex aerosol refractive index. All introduced characteristics can be estimated by two methods: directly, by the collection of the aerosols from atmosphere and by the determination of the aerosol characteristics in laboratory or indirectly, e.g. from spectral characteristics of the radiation field by the solution of the inverse tasks.

The authors are interested in the second method of the aerosol characteristics estimation in this contribution. The own radiation measurements are the basis for the retrieval of the aerosol size distribution function in the urban atmosphere. A great attention is given to the various procedures of the inverse tasks solution at present time. Many of them are described in the *Lenoble's* (1985) monography or in other publications. The inverse problems in atmospheric remote sensing can be in many cases formulated in terms of a Fredholm's integral equation of the first kind. Methods of its solution for light scattering and extinction problems are known. The technique how to determine the aerosol size distribution function from the measured data of the aerosol optical thickness is described by e.g. *Shifrin* and *Perelman* (1963, 1964), *Box et al.* (1992), *Schnablegger* and *Glatter* (1993), *Dellago* and *Horvath* (1993, 1993a), *Amato et al.* (1994) and *Kaufman et al.* (1994). *Jones et al.* (1994, 1994a) describe a new method of the Fredholm's equation solution, where the aerosol size distribution function is expanded as a linear combination of a set of orthonormal basic functions. The inversion is a classic ill-posed problem. The way from the measurements of the aerosol optical thickness to the aerosol size distribution function estimation is far from smooth.

2. *Theoretical assumptions*

2.1 Direct radiation and aerosol

The changes in the direct solar radiation during the transfer through the Earth's atmosphere can be written as follows:

$$I(\lambda) = I_0(\lambda) \exp\{-\tau(\lambda) M\}, \tag{1}$$

where $I(\lambda)$ and $I_0(\lambda)$ are the measured direct solar radiation flux density and the spectral solar constant, respectively, $\tau(\lambda)$ is the atmospheric spectral optical thickness and M is the optical air mass.

Atmospheric spectral optical thickness is the sum of the spectral optical thicknesses of the individual atmospheric components. We can write:

$$\tau(\lambda) = \tau_R(\lambda) + \tau_\omega(\lambda) + \tau_w(\lambda) + \tau_A(\lambda), \tag{2}$$

where $\tau_R(\lambda)$, $\tau_\omega(\lambda)$, $\tau_w(\lambda)$ and $\tau_A(\lambda)$ are the spectral optical thickness values of the pure atmosphere, the ozone, the water vapour and the aerosol, respectively.

Aerosol spectral optical thickness can be expressed according to *Mc Cartney* (1979):

$$\tau_A(\lambda,m) = \pi \int_0^{\infty} Q(\rho,m)\, r^2 f(r)\, dr, \tag{3}$$

where $Q(\rho,m)$ is the extinction efficiency factor, r is the particle radius, $f(r)$ is the column aerosol size distribution function ($\mu\mathrm{m}^{-3}$), m is the complex refractive index, $\rho = 4\pi(m - 1)r/\lambda$. Thus, Eq. (3) specifies the relation between the aerosol spectral optical thickness and aerosol size distribution function.

The aerosol/solar radiation interaction is the most intense in the shortwave spectrum range. In this range the radiation scattering is higher by several orders than the radiation absorption (*d'Almeida et al.*, 1991; *Xu et al.*, 1992 personal communication). Therefore, we use scattering coefficients instead of the extinction ones in the considerations. The scattering efficiency factor $Q(\rho,m)$ in the Eq. (3) is a complex function of the wavelength, of the particle radius and of the refractive index, and can be calculated with the help of the Mie's functions (*Mie*, 1908).

There are several possible ways how to solve the Eq. (3). Some of them are given by *Shifrin* and *Perelman* (1963, 1964), *Bakushinskij* and *Goncharskij* (1989) and *Imanaliev* (1981). These publications describe either a classical solution of the integral Eq. (3) or an approximate solution using the optimization methods. The solution accuracy depends which of two methods is used on. *Kocifaj* and *Lukáč* (1994) calculated the aerosol size distribution function $f(r)$ from the Eq. (3) firstly, applying the Mellin's transformation and secondly, using the optimization method. The first method is applicable only if $K(x,y) = K(xy)$, where K is the kernel of the integral equation (*Schneider*, 1955). The second method resides in the minimization of the difference between the measured and calculated aerosol optical thickness.

The aerosol size distribution function was chosen in the form of a sum of the modified gamma functions (*McCartney*, 1979; *Podzimek*, 1992 personal communication; *Lukáč* and *Kocifaj*, 1994):

$$f(r) = r \sum_{n=1}^{N} a_n \exp(-b_n r), \tag{4}$$

where a_n and b_n are the unknown coefficients.

2.2 *Diffuse radiation and aerosol*

The atmospheric aerosol has the property to scatter the solar radiation. Scattering coefficient and scattering function are two characteristics quantifying the scattering process. The first one is the volume characteristics and the second one is the direction characteristics of the scattering.

In the case of the single scattering the relationship between the sky radiance and the scattering function can be written according to *Kocifaj* (1994) as follows:

$$i_1(h_1,\xi_0,\xi,\alpha) = \mu(\xi)\int_0^\infty \Gamma(h,0^+) I_h(\xi_0) I_{h1,h}(\xi)\, dh\,, \tag{5}$$

where

$$I_h(\xi_0) = I_0 \exp\{-\mu(\xi_0)\int_0^\infty [\beta_A(z) + \beta_R(z) + \beta_w(z)]\, dz\}\,, \tag{6}$$

$$I_{h1,h}(\xi) = \exp\{-\mu(\xi)\int_{h1}^{h} [\beta_A(z) + \beta_R(z) + \beta_\omega(z)]\, dz\} \tag{7}$$

and

$$\Gamma(h,0^+) = \frac{P_R(\theta^+)}{4\pi}\beta_R(h) + \frac{P_A(\theta^+)}{4\pi}\beta_A(h)\,. \tag{8}$$

In these relations $i_1(h_1,\xi_0,\xi,\alpha)$ is the sky radiance component at h_1 height for single scattering; I_0 is the spectral solar constant; $\beta_A(z)$ and $\beta_R(z)$ are the scattering coefficients of the aerosol and pure atmosphere, respectively; $\beta_\omega(z)$ is the ozone absorption coefficient; $P_A(\theta^+)$ and $P_R(\theta^+)$ are the phase functions of the aerosol and the pure atmosphere, respectively; $\mu(\xi_0)$ and $\mu(\xi)$ are the optical air mass of the Sun and of the observed point in the sky, respectively and θ^+ is the scattering angle.

The relations for the higher order scattering are in detail described by *Kocifaj* (1994). The numerical calculation in that paper was done up to second scattering order.

In the real cloudless atmosphere, the total sky radiance is expressed by the sum:

$$i(h_1,\xi_0,\xi,\alpha) = \sum_{n=1}^{\infty} i_n(h_1,\xi_0,\xi,\alpha)\,, \tag{9}$$

where $i_n(h_1,\xi_0,\xi,\alpha)$ is the n-th component of the sky radiance belonging to the n-th order of scattering.

Eqs. (5) to (9) allow to obtain the scattering function and the aerosol size distribution function from the measured sky radiance.

The aerosol size distribution function was chosen in the form of a modified gamma function according to *McCartney* (1979):

$$f(r) = A r^{a} \exp(-br), \tag{10}$$

where A, a, b are the unknown coefficients. We solve this problem by means of the optimization of the aerosol parameters in order that the deviations between the measured and calculated sky radiance values may be minimal.

3. Experimental results

The applicability of the first introduced procedure is illustrated on the radiation characteristics obtained from the measurements in Bratislava (Slovak Republic) realized since 1991. The measurements of the spectral direct solar radiation are made with the multiwavelength solar spectral photometer model SPM 1040. The instrument operates with six narrow band filters. The effective wavelengths of the individual filters are: 377, 406, 520, 599, 749 and 857 nm. The measurements in single days are utilized for the calibration of the instrument. The Smithsonian long method for the determination of the solar constant is employed (*Liou*, 1980). All measurements are made in the spectral bands without the water vapour influence. The ozone amount is taken from *Keating et al.* (1989). The applied spectral interval is sufficient to determine the aerosol size distribution function in the particle radius range from $r_1 \approx 0.3$ μm to $r_2 \approx 1.5$ μm (*Kocifaj* and *Lukáč*, 1994).

Aerosol spectral optical thickness was calculated from the measured spectral density of the direct solar radiation according to the following relationship:

$$\tau_A(\lambda) = \frac{1}{M} \ln [I_0(\lambda) / I(\lambda)] - \tau_R(\lambda) - \tau_\omega(\lambda). \tag{11}$$

The aerosol optical thickness values obtained in this way were used as the input data by the solution of the Eq. (3). The solution accuracy and thus the reality of the aerosol size distribution function is proved by the reverse calculation of the aerosol spectral optical thickness and by comparing it with the original measured data. The function *f(r)* is found in the Hilbert space of the quadratically integrable and continuous functions L_2. The negative part of integral of function $f(r)$ in the limits from r_1 to r_2 must be smaller than in advance estimated value ϵ.

The results of calculations are documented on two examples for the day with low turbidity (September 9, 1993) and the day with high turbidity (April 22, 1994). *Fig. 1* presents the measured and recalculated aerosol spectral optical thicknesses for low and high turbidities.

The introduced results show good coincidence between the measured and recalculated aerosol optical thicknesses with the mean deviations of 7.3% in the case of low turbidity and of 2.6% in the case of high turbidity. *Fig. 2* shows corresponding aerosol size distribution functions obtained firstly, solving the Fredholm's integral equation of the first kind using the Mellin's transformations (dashed curves) and secondly, applying our optimization method (solid curves).

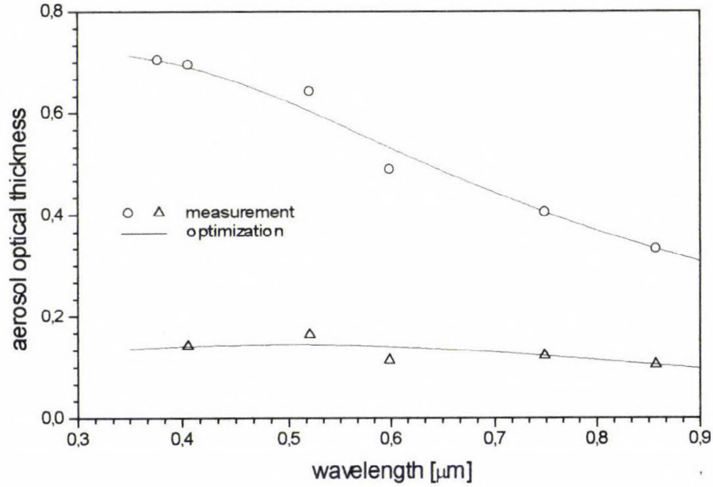

Fig. 1. Aerosol optical thicknesses in day with low turbidity (September 9, 1993) and in day with high turbidity (April 22, 1994).

The differences between both functions depend on the number of the terms (N) in the Eq. (4). In our case $N = 2$. The optimization method is so suitable for the description of the aerosol size distribution function near the main modal particle radius. The parameters of the aerosol size distribution functions (Eq. 4) are in *Table 1*.

The applicability of the second introduced procedure is illustrated on the spectral sky radiance measurements in the urban atmosphere of Bratislava in October 22, 1990. The measurements of the spectral sky radiance are made with the multiwavelength sky radiance scanner (*Foitzik* and *Zschaeck*, 1961). The instrument operates with three narrow band filters. The effective wavelengths of the individual filters are: 450, 550 and 650 nm. The instrument is calibrated in the laboratory by the calibrating set with known radiance. The influence of the ozone and water vapour on the recalculated data is taken into account similar as in the case of the direct solar radiation. The measuring procedure consists of the measurement of the sky radiance in some points in the solar vertical circle and in some horizontal circles (including the solar horizontal circle) (*Foitzik et al.,* 1970).

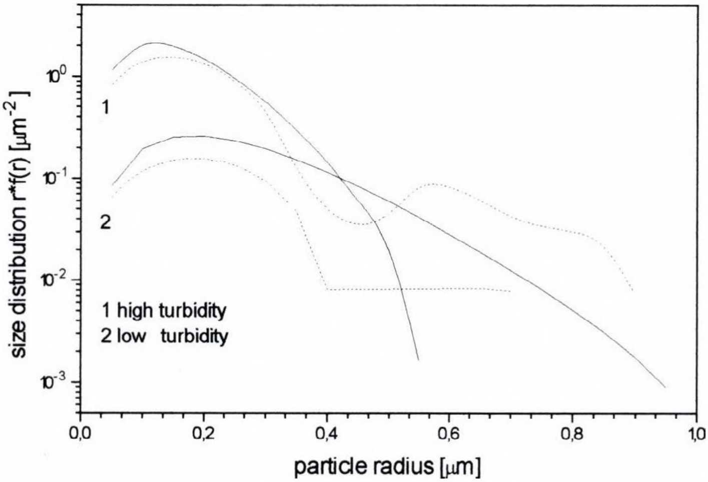

Fig. 2. Aerosol size distribution function $r^*f(r)$ obtained by Mellin's transformation (dashed curves) and by optimization method (solid curves).

Table 1. Parameters of the calculated aerosol size distribution function for refractive index $m = 1.5$

Date	N	Coefficient a (μm^{-4})	Coefficient b (μm^{-1})
September 9, 1993	1	a1 = 58.5	b1 = 12.5
	2	a1 = -0.0018	b1 = 1.0
		a2 = 58.6	b2 = 11.0
April 22, 1994	1	a1 = 1612.6	b1 = 19.0
	2	a1 = -1402.3	b1 = 14.0
		a2 = 2450.9	b2 = 15.0

Fig. 3 presents the comparison between the measured and recalculated spectral sky radiances on solar almucantar for three filters. The data are given in relative values corresponding to throw of pointer. The mean deviation

between the measured and recalculated spectral sky radiance for all three filters was 12.2% (15.7% for 450 nm, 15.4% for 550 nm and 5.6% for 650 nm). The parameters of the aerosol size distribution function (Eq. 10) are: $A=940\ \mu m^{-4}$, $a=1$, $b=28\ \mu m^{-1}$.

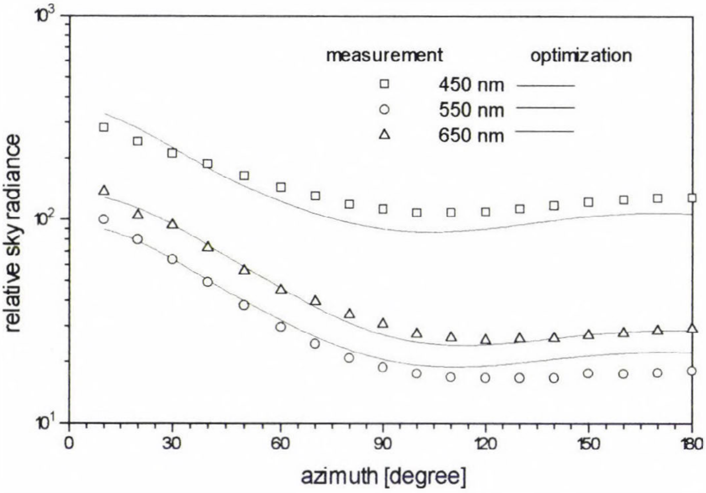

Fig. 3. Relative sky radiance in Bratislava (October 22, 1990).

4. Conclusions

Knowledge about the aerosol structure in the Earth's atmosphere is an important from the viewpoint of the radiation processes. We have shown that it is suitable to use the data about the Earth's atmosphere radiation field in order to determine the aerosol structure. Two examples from the direct solar radiation and one example from the sky radiance measurements were the pattern of the convenience of the applied procedure on the determination of the aerosol size distribution functions.

The investigation of the aerosol properties directed like this will contribute to improvement our knowledge about aerosol temporal and spatial changes and can contribute to the climatic research programs.

References

d'Almeida, G.A., Koepke, P. and *Shattle, E.P.*, 1991: Atmospheric aerosols. In *Global Climatology and Radiative Characteristics*. A Deepak Publishing, Hampton.

Amato, U., DiBello, D., Esposito, F., Romano, F. and *Serio, C.*, 1994: Intercomparing parametric and nonparametric inversion methods to retrieve aerosol size distribution. In *Proc. of the*

International Specialty Conference: Aerosols and Atmospheric Optics: Radiative Balance and Visual Air Quality. Vol. A. Air & Waste Management Association, Pittsburg, 277-292.

Bakushinskij, A.B. and *Goncharskij, A.V.*, 1989: *Ill-posed Tasks. Numerical Methods and Examples* (in Russian). Moscow University Publishing, Moscow .

Box, G.P., Sealey, K.M. and *Box, M.A.*, 1992: Inversion of Mie extinction measurements using analytic eigenfunction theory. *J. Atmos. Sci. 49*, 2074-2081.

McCartney, E. J., 1979: *Optics of the Atmosphere* (in Russian). Mir, Moscow.

Dellago, C. and *Horvath, H.*, 1993: On the accuracy of the size distribution information obtained from light extinction and scattering measurements - I. Basic considerations and models. *J. Aerosol Sci. 24*, 129-141.

Dellago, C. and *Horvath, H.*, 1993a: On the accuracy of the size distribution information obtained from light extinction and scattering measurements - II. Case studies. *J. Aerosol Sci. 24*, 143-154.

Foitzik, L. and *Zschaeck, H.*, 1961: Messungen der spektralen Strahldichte und der Polarisation des wolkenlosen Himmels. *Gerl. Baitr. Geophys. 70*, 350-372.

Foitzik, L., Lukáč, J. and *Unger, E.*, 1970: Messungen der Himmelsstrahlung und ihrer Polarisation auf der Lomnitzer Spitze (CSSR). *Gerl. Baitr. Geophys. 79*, 50-66.

Hobbs, P.V., 1994: Recent field studies of aerosol and cloud processes relevant to climate. In *Cloud - Radiation Interactions and Their Parameterization in Climate Models. WCRP - 86, WMO/TD - No. 648*, Geneve, 75.

Imanaliev, M.I., 1981: *Generalizing of First Kind Integral Equation Solutions* (in Russian). Ilim Publishing, Frunze.

Jones, M.R., Curry, B.P., Brewster, M.Q. and *Leong, K.H.*, 1994: Inversion of light-scattering for particle size and optical constants: theoretical study - I. *Appl. Opt. 33*, 4025-4034.

Jones, M.R., Curry, B.P., Brewster, M.Q. and *Leong, K.H.*, 1994a: Inversion of light-scattering for particle size and optical constants: theoretical study - II. *Appl. Opt. 33*, 4035-4041.

Kaufman, Y.J., Holben, B.M., Remer, L., Gitelson, A., Karnieli, A. and *Nakajima, T.*, 1994: Measurements of the ambient aerosol size distribution, scattering phase function and backscattering fraction. In *Proc. of the International Specialty Conference: Aerosols and Atmospheric Optics: Radiative Balance and Visual Air Quality. Vol. A.* Air and Waste Management Association, Pittsburg, 349-359.

Keating, G.M., Pits, M.C. and *Young, D.F.*, 1989: Ozone reference models for the middle atmosphere (New CIRA). In *MAP Handbook 31*, Geneve, 1-36.

Kocifaj, M., 1994: Diffusion of radiation in planetary atmospheres - I. The Earth's atmosphere: A model. *Earth, Moon and Planets, 65*, 21-29.

Kocifaj, M. and *Lukáč, J.*, 1994: Relation between the structure of particles of the dispersion layer and its spectral optical thickness in an optically thin environment. *Stud. Geoph. Geod. 38*, 399-415.

Lenoble, J., 1985: *Radiative Transfer in Scattering and Absorbing Atmospheres: Standard Computational Procedures*. A. Deepak Publishing, Hampton.

Liou, K.N., 1980: *An Introduction to Atmospheric Radiation.* Academic Press, New York, London, Toronto, Sydney and San Francisco.

Lukáč, J. and *Kocifaj, M.*, 1994: Utilization of inverse methods in atmospheric optics. *Contr. GI SAS,14*, 45-56.

Mie, G., 1908: Beiträge zur Optik trüben Medien, speziell kolloidaler Metal-lösungen. *Annalen der Physik 25*, 377-445.

Schnablegger, H. and *Glatter, O.*, 1993: Simultaneous determination of size distribution and refractive index of colloidal particles from static light-scattering experiments. *J. Colloid and Interface Sci. 158*, 228-242.

Schneider, W., 1955: *Integralgleichungen mit Anwendungen in Physik und Technik.* A. V. Geest & Portig K.-G., Leipzig.

Shifrin, K.S. and *Perelman, A.Y.*, 1963: Determination of particle size distribution in disperse medium using its transparency data - I (in Russian). *Optika i Spektroskopija 15*, 533-542.

Shifrin, K.S. and *Perelman, A.Y.*, 1964: Determination of particle size distribution in disperse medium using its transparency data - II (in Russian). Optika i Spektroskopija 16, 117-128.

IDŐJÁRÁS

Quarterly Journal of the Hungarian Meteorological Service
Vol. 100, No. 1-3, January-September 1996

Radon and natural indoor radioactive aerosol

A. Renoux

Laboratoire de Physique des Aérosols et de Transfert des Contaminations,
Université Paris XII, Avenue du Général de Gaulle, 94000 Créteil, France

(Manuscript received 3 July 1995; in final form 20 November 1995)

Abstract—An outline is given of the origin and nature of the natural atmospheric radioactivity due to radon (^{222}Rn) and thoron (^{220}Rn), and the relevant units and parameters are defined. Attention is then focused on the problem of radon and its short-lived daughters in residential structures. Values are given for the measured concentrations, potential alpha energy and equilibrium factor. Some details concerning different devices used in this area are given (CEA alpha dosimeter, SDI 2000). The different methods used for the measurement of the unattached fraction are recalled and some results obtained in different conditions are summarized. We also indicate the effective dose equivalents due to inhalation of the decay products of ^{222}Rn and ^{220}Rn. Finally, models of the behaviour in dwellings of radon and its daughters are discussed.

Key-words: radon, radioactive aerosol, indoor radioactivity, models.

1. Natural atmospheric radioactivity

The Earth has always been subject to natural radioactivity, which was first demonstrated by *Elster* and *Geitel* (1901). *Rutherford* in 1900, *Dorn* in 1900 and *Giesel* in 1902 (see e.g. *Frisch*, 1958) discovered thoron (^{220}Rn), radon (^{222}Rn) and actinon (^{219}Rn), respectively, which are isotopes of the same inert gas, radon ($z = 86$). *Table 1* (from *Gouronnec*, 1995) shows that it was not until 1908 that a molecular weight for ^{222}Rn close to the value accepted today was determined.

We now know that natural atmospheric radioactivity arises in particular from ^{222}Rn (of the ^{238}U decay series) and, in a lesser way, from ^{220}Rn (thoron, of the ^{232}Th decay series), both of which are noble and radioactive alpha-emitter gases originating from the soil. Their short-lived daughters, like Po (RaA, ThA), Pb (RaB, ThB) and Bi (RaC, ThC), are generally attached to atmospheric aerosols and make up the natural atmospheric radioactive aerosol. *Fig. 1* (*COGEMA*, 1994) shows the radioactive decay chains of radon and thoron. Atmospheric levels of actinon (^{219}Rn) are too low to be taken into account.

We shall not deal here with radioactive aerosols or atmospheric radon, which have been discussed elsewhere (*Renoux*, 1986, 1992).

Table 1. History of the radon 222 molecular weight

Author	Year	Molecular weight
Rutherford and Brooks	1901	40 to 100
Curie and Danne	1903	40 to 100
Bumstead and Wheeler	1904	180
Makower	1905	85.5 to 97
Perkins	1908	235

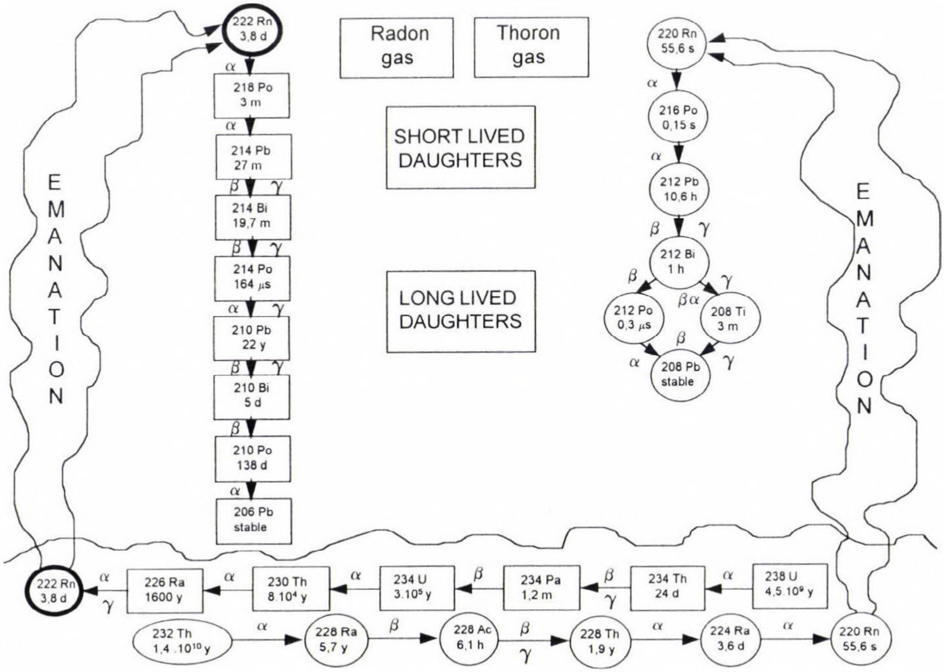

Fig. 1. Radioactive decay chains of radon and thoron.

2. *Some definitions*

The risk for an individual exposed to a radioactive gas in the atmosphere can be calculated by means of the potential alpha energy (PAE) of the air expressed in joules m^{-3} ($J\ m^{-3}$). By definition, the PAE is the sum of the energies delivered by the alpha particles which are emitted upon disintegration of all the short-lived decay products (whatever their proportions) present at a given time in a certain volume of air (chosen as the units, generally m^3). Hence, 1 pCi ℓ^{-1} of ^{222}Rn at radioactive equilibrium with its daughters corresponds to 0.208×10^{-6} J m^{-3}.

A very important notion in atmospheric radioactivity is that of radioactive equilibrium. If the radioactive body A (number of atoms at time t: N_A; radioactive decay constant λ_A) gives rise to a body B which is also radioactive (N_B, λ_B),

$$dN_B = \lambda_A N_A - \lambda_B N_B \tag{1}$$

atoms of B will appear during the period dt. Radioactive equilibrium is reached when $dN_B = 0$: equal amounts of B are created and disappear. So, $\lambda_A N_A = \lambda_B N_B$, i.e. the activities of A and B are identical.

The equilibrium factor ($0 < F < 1$) is defined by $F = \mathrm{PAE}/mA_0$, where

$$m = 34630 \text{ MeV Bq}^{-1} \text{ for } {}^{222}\text{Rn}$$
$$m = 471833 \text{ MeV Bq}^{-1} \text{ for } {}^{220}\text{Rn}$$

A_0 being the activity per unit volume of ^{222}Rn or ^{220}Rn.

The equilibrium factor F is the ratio between the PAE of a mixture of radon daughters and the PAE relative to the mixture if it was in equilibrium with the parent.

3. *Radon and its short-lived daughters in dwellings*

In France, the subject of radiation toxicity of radon was investigated from 1904 onwards, following the work of *Bouchard* and *Balthazard*. In 1924, it was hypothesised that the high mortality due to lung cancer observed among the uranium mineworkers of Schneeberg in Germany and Joachmisthal in Czechoslovakia could be due to radon. This is why, particularly in France, numerous studies were devoted to radon and its daughters in uranium mines (*Pradel*, 1955; *Renoux et al.*, 1978).

In fact, radon appeared as the principal radiological risk to which each individual is exposed: the dose due to inhalation of short-lived daughters of ^{220}Rn and ^{222}Rn represents almost half of the radiological exposure of populations (see *Fig. 2*) (*UNSCEAR*, 1982; *Renoux*, 1986).

Pradel (1978) pointed out that because of the very high concentrations of radon in certain dwellings, some exceeding 3000 Bq m^{-3}, the resulting exposure can reach considerable values. Indeed, it should not be forgotten that the annual exposure levels can be three to four times those in uranium mines. And the people are, of course, exposed throughout their lives. Because of the world energy crisis, substantial efforts were made in the 1970s and 80s, in particular in Western countries, to improve the thermal insulation of dwellings and buildings. The consequence of all these was to confine buildings, thus accentuating their internal pollution and hence radon risk. From 1980, various countries, including France, therefore examined the problem of radon and its daughters in dwellings, and found that the concentrations of radon and its daughters are generally much higher indoors than outdoors (*Rannou*, 1987; *Porstendörfer*, 1994; *Gouronnec*, 1995).

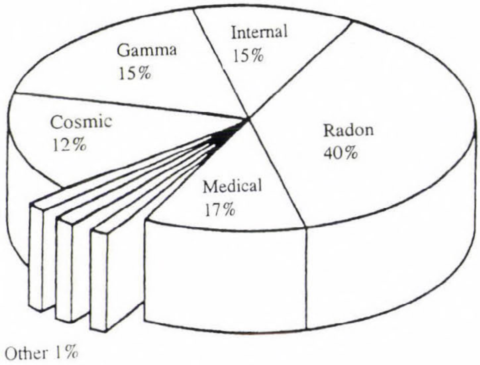

Fig. 2. Map of the universal dose.

The exhalation is greater if the building materials and floor are porous and radium-rich. *Table 2* (*Rannou*, 1989) indicates the radium contents and exhalation rates of ^{222}Rn (radon) for various building materials. Worldwide, the estimated value of the radon flux (E) is 1.6×10^{-2} Bq m^{-2} s^{-1} (*Wilkening et al.*, 1972).

Note that the exhalation rate per surface area E (Bq m^{-2} s^{-1}) is given by the equation

$$E = \lambda_{Rn} R \, Cs \, \rho \, L_{Rn}, \tag{2}$$

where λ_{Rn} (s^{-1}) is the radioactive decay constant of ^{222}Rn, R is the exhalation coefficient, Cs (Bq kg^{-1}) is the specific activity of the environment in ^{226}Ra, ρ (kg m^{-3}) is the specific mass of the environment, L_{Rn} (m) is the diffusion length of radon.

Table 2. ^{226}Ra rate and ^{222}Rn emission rate of different building materials (typical values in brackets)

Building material	^{226}Ra amount ($\mathrm{Bq\ kg^{-1}}$)	^{222}Rn emanation rate ($\mathrm{10^{-3}\ Bq\ kg^{-1}\ s^{-1}}$)
Concrete	9 - 141 (25)	2.9 - 20 (10)
Bricks	7 - 69 (50)	0.17 - 3.9 (2)
Gypsum		
(USA)	12	6.3
(Denmark)		0.23
Phosphogipsum		
(Poland)	580 - 740	
(Belgium)	333 - 848	
Alunifer shist		
Sweden, before 1975	620 - 2100 (1500)	

Table 3 (*Gouronnec*, 1995) gives the radon concentrations in dwellings in various countries. Note that on a global scale, the radon activity per unit volume in the atmosphere is 6 Bq m^{-3}.

In most countries, the geometric mean ranges between 20 Bq m^{-3} and 70 Bq m^{-3} and is close to the authentic mean. But in certain dwellings, and in particular in basements, the value may reach several thousand Bq m^{-3} (for example, 8,000 Bq m^{-3} in a cellar in Brittany).

Fewer measurements have been made of radon decay products: their activities range from 1 to 50 Bq m^{-3}, and the equilibrium factor F ranges between 0.4 and 0.5. This corresponds to PAE values between 10^{-2} and 10^{-1} μJ m^{-3} (*Gouronnec*, 1995).

These results naturally vary within a given country, and between countries. *Fig. 3* shows the distribution of radon concentrations in the dwellings of the Swiss commune Cadro. The mean (110 Bq m^{-3}) is almost twice that of the Swiss median (60 Bq m^{-3}) given in Table 2.

More than 10% of dwellings have radon concentrations above 400 Bq m^{-3}, and 2% above 1,000 Bq m^{-3} (*OFSSP*, 1993).

At the end of the 1970s in France, the CEA developed an alpha dosimeter (*Duport et al.*, 1978) for measurement of alpha radioactivity due to short-lived daughters of ^{222}Rn. This is illustrated in *Fig. 4*. The air to be analyzed is sucked through three 1.4 mm cylindrical orifices arranged at 120° in the lateral wall of the apparatus. Aerosols present in the air are captured by means of a membrane placed 6 mm upstream from the inlets. A small electric vane pump provides an aspiration flow rate of 5 ℓ/h. Alpha radiation is detected by means of solid state nuclear track detectors. The detector is a cellulose acetate film

Table 3. Radon concentrations indoor in different countries

Country	Concentrations law distribution	Radon 222 concentration			Range or maximum	Method	Measurements number
		Arithmetic mean (Bq m^{-2})	Geometric mean or median (Bq m^{-2})	Geometric standard deviation σ_g			
Turkey (Istanbul)	normal log	50			10–260	ATD, 6 months 2 times	
USA	normal log	46.3	24.8	3.11	0.2–350 0.06% >740	ATD, 1 year	5600 houses
	normal log	47.7	27.4	2.92	0.05% >740	ATD, 1 year	13,400 persons
Poland (Lublin)	normal log		26	1.6	12–75	Scintillating cell	80
Cyprus	normal log	6.58	6.75	2.6	0–78	ATD, 5 months (winter)	89
Greece (north)	normal log	32	~26	?	8–185	ATD, 2 months	?
Japan	normal log	19–57	23	1.6	?	KfK (passive german dosimeter)	6300
China	normal log	23.5+/-10	16.7	1.7	?	Method of 2 filters	8220
Estonia	?	148	52.6	?	4.5% >800	Flasks of Lucas ATD ?	400
Sweden	normal log	108	56	?	3904	ATD, 3 months	1360
India (Aligarth)	?	31.9+/-1	?	?	18–51	ATD, 1 month 12 times	3 sites
Norway	normal log	110				Active coal between 5 and 7 days	1500
	normal log		225		70–1500	ATD ?	47
India	normal log	?	63.2	2.02	8.7–198.2	ATD, between 40 and 60 days	76 (25 sites)
Algeria	?	32+/-3			2–137	ATD, 1 or 2 months	50
Croatia (Osijek)	?	50 47 43.7				Scintillating flasks Radhome ATD	
Canada	normal log		15.2	?	36% >37 3% >185 2775	Flasks of Lucas	9999
Switzerland	normal log	60+/-6	47	?	15–3604 1% >204	ATD, 120 days	400
Spain	normal log		41.1	3	15402	Cells of Lucas, 1 liter	1555 homes
Belgium	?	66.5				Active coal	730 homes
France	?	40			4600		

placed 22 mm in front of the filter. It is preceded by mylar screens and then by four collimators 13 mm in length and 6 mm in diameter. The thicknesses of the screen are calculated such that the portions of the film of cellulose nitrate are only sensitive to the alpha radiation of ^{218}Po (RaA, 6 MeV), ^{214}Po (RaC', 7.68 MeV), ^{212}Po (ThC', 8.77 MeV) and ^{222}Rn. The traces produced by the alpha radiation are revealed by alkaline treatment which transforms them into conical holes having a few μm in diameter visible in the optical microscope. This dosimeter has, of course, been tested in the laboratory (*Mouden et al.*, 1980). The dosimeter, initially used in uranium mines, has been adapted to measurements in dwellings.

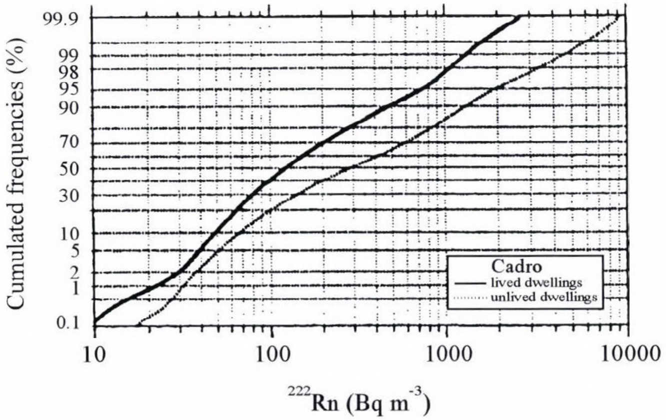

Fig. 3. Distribution of radon concentrations in the dwellings of the Swiss commune CADRO.

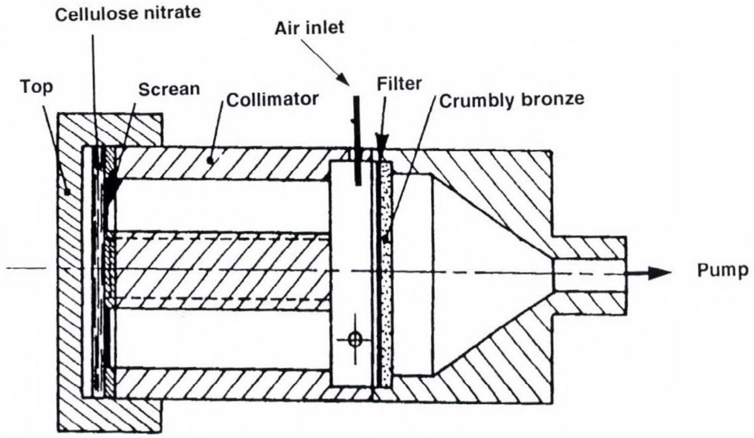

Fig. 4. The CEA α dosimeter.

Table 4 shows the results obtained (in Bq m^{-3}) in various French administrative departments.

Table 4. Indoor radon concentrations (Bq m^{-3}) in various French departments

Department	Year	Nb of points	Mean
Aisne	1992	200	62
Alpes-Maritimes	1982-83	32	35
Ardennes	1992	180	91
Ariège	1983	24	80
Bouches-du-Rhône	1981-82	28	14
Corrèze	1988	102	171
Côte-d'Or	1984	47	75
Côtes-d'Armor	1989	92	122
Creuse	1988	71	198
Dordogne	1986	232	75
Doubs	1983-84	40	110
Drôme	1984	44	35
Finistère	1987-88	220	150
Garonne (Haute)	1983-84	23	30
Gers	1984	47	50
Hauts-de-Seine	1991-92	73	34
Hérault	1982-83	43	30
Jura	1984-85	81	85
Loir-et-cher	1986-87	85	70
Loire	1983	47	175
Loire-Atlantique	1989-90	159	66
Loiret	1987	113	55
Maine-et-Loire	1989-90	132	50
Manche	1986	43	70
Marne (Haute)	1984	26	60
Mayenne	1988	184	97
Meurthe-et-Moselle	1985-86	103	60
Morbihan	1986-87-88	438	140
Moselle	1985	82	50
Pyrénées (Hautes)	1984	23	75
Pyrénées-Orient.	1983	28	50
Rhin (Bas)	1987	81	35
Rhin (Haut)	1985	71	55
Saône (Haute)	1984	12	100
Saône-et-Loire	1984	47	85
Sarthe	1988-89	229	41
Savoie (Haute)	1983	42	30
Seine St Denis	1991-92	79	34
Tarn	1982	21	50
Tarn-et-Garonne	1983	46	35
Val de Marne	1992	55	46
Var	1983-84	20	70
Vienne (Haute)	1984-85-86	289	238
Vosges	1985-86	75	135
Yvelines	1992	73	30
Paris et Région Parisienne	1987-1991	29	20
TOTAL: 46 Dpts		4211 points	

According to the most recent studies, there are three ranges of particle sizes of radon decay products in dwellings:

- approximately 10^{-3} μm, corresponding to the unattached fraction,
- 0.1 μm – 0.5 μm, corresponding to the attached fraction,
- 3.10^{-3} μm – 8.10^{-2} μm, the intermediate fraction.

According to *Reinecking* and *Porstendörfer* (1990), ^{214}Pb (RaB) and ^{214}Bi (RaC) have the same particle size distribution, unlike ^{218}Po (RaA).

Recently, *Tymen et al.* (1992) have used the SDI 2000 instrument developed by *Diouri* (1987), which couples an Andersen impactor and bead beds, to determine the particle size distribution of radon daughters in different dwellings in Brittany in which there were high radon concentrations. The main results are summarised in *Table 5*.

Table 5. ^{222}Radon mean concentrations in the houses of 46 French departments

Equilibrium factor F	$0.10 < F < 0.48$	$F = 0.26$
Unattached fraction	$0.008 < f < 0.49$	$f = 0.086$
Attached fraction	0.11 μm < total AMD < 0.2 μm 0.07 μm < ^{214}Pb < AMD < 0.13 μm 0.10 μm < ^{214}Bi < AMD < 0.23 μm	

The mean value $f = 0.086$ of the unattached fraction is close to that measured by *Reineking* and *Porstendörfer* (1990), and the value of 0.03 generally used in dosimetry models must therefore be reconsidered.

The particle size distribution of radon daughters is frequently determined by means of a diffusion battery with 4 or 5 screens arranged in series or in parallel, each screen comprising a different number of juxtaposed metal grids defined by a known penetration curve (*Tymen et al.*, 1992). In this way, *Reineking* and *Porstendörfer* (1990) have developed a high-volume, screen diffusion battery, which is shown in *Fig. 5*. The alpha energy of radon daughters is measured by means of suitable detectors placed downstream from the screens. Numerical data reduction yields the particle size distribution of the radon daughters.

As we have seen, it is also possible to use the SDI 2000 instrument, which combines aerosol capture by impaction (Andersen impactor) and by diffusion (granular bed) and defines the particle size distribution of aerosols in the 7 to 15 μm range (*Fig. 6*).

The filters collect particles which have crossed the glass bead bed. This instrument has been used in field measurements in Brittany (*Tymen et al.*, 1992).

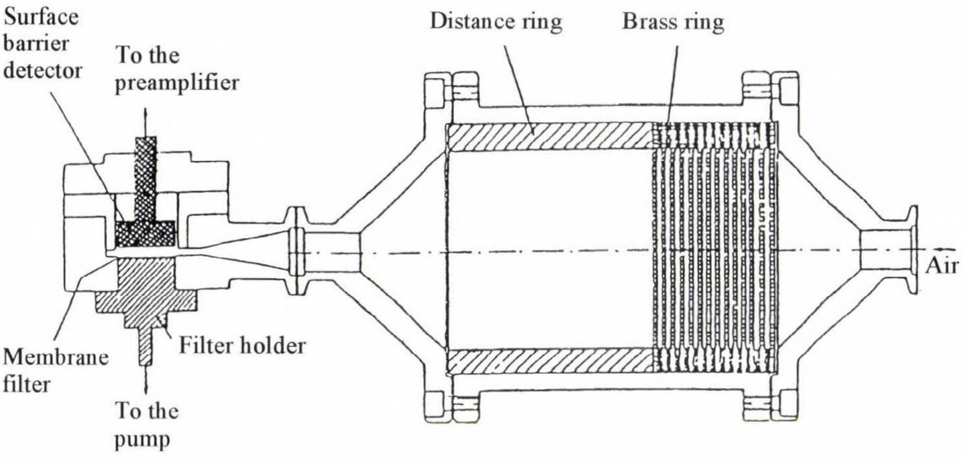

Fig. 5. Diagram showing the high volume screens diffusion battery of *Reineking* and *Porstendorfer* (1990).

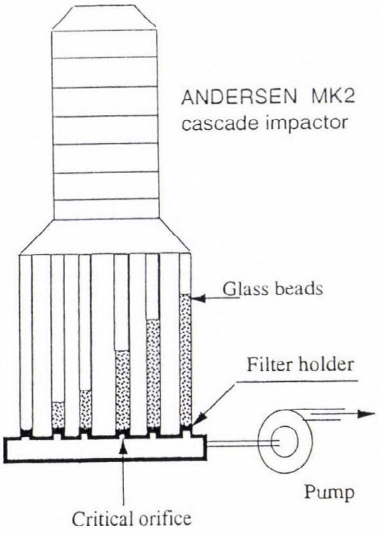

Fig. 6. Diagram showing the SDI 2000.

The measurement of the unattached fraction of radon daughters has been widely studied since the early 1970s. Because of its very high coefficient of diffusion, the unattached fraction is likely to be extensively deposited in the respiratory system. This is why the activity median diameter of the attached radioactive aerosol and the unattached fraction of ^{218}Po (RaA) are vital parameters in all lung dosimetry models used to estimate radiation doses from inhaled radon daughters (*Hopke*, 1990). As most of the ^{218}Po^{+} ions initially formed (*Renoux*, 1965) will be rapidly neutralised in the atmosphere (*Chu* and *Hopke*, 1988), the electrostatic collection underestimates the unattached fraction and should not therefore be used. This is why the first measurements were made using diffusion through cylindrical tubes. This technique has been principally used in uranium mines (*Chamberlain* and *Dyson*, 1956; *Fusamura et al.*, 1967), and recently for measurements in dwellings (*Malet et al.*, 1995).

The unattached radon daughter fraction is now most commonly estimated by means of wire mesh screens (*George*, 1972; *Bigu*, 1985; *Reineking et al.*, 1988), which have been used for measurements in dwellings (*Porstendörfer*, 1987; *Van Marke et al.*, 1989; *Kojima* and *Abe*, 1988; *Gouronnec*, 1995). *Gouronnec* (1995) has also used a battery of 300 identical, fine cylindrical tubes.

In dwellings, the unattached fraction of ^{218}Po (RaA) is generally higher than that of ^{214}Pb, that of ^{214}Bi being virtually nil. The unattached fraction is higher at lower aerosol concentrations.

Table 6 (*UNSCEAR*, 1984) gives the mean values for the indoor and outdoor exposures to ^{222}Rn and ^{220}Rn in France, in terms of concentration (Bq m^{-3}) and mean potential alpha energy (J m^{-3}).

Table 6. Internal exposures indoor and outdoor in France

		Indoor	Outdoor
Rn 222 series	CO (Bq m^{-3})	41	6
	PAE (x 10^{-8} J m^{-3})	9.8	1.3
Rn 220 series	Co (Bq m^{-3})	18	0.2
	PAE (x 10^{-8} J m^{-3})	4.1	0.6

Note that the PAE due to ^{220}Rn decay products represents about 30% of the total PAE of ^{222}Rn and ^{220}Rn. As an indication, *Table 7* (*Rannou*, 1987) gives the same parameters measured in the granite-rich region Finistère, in France.

Table 7. The different mechanisms involved in the behaviour of radon and its daughters in a dwelling

		Indoor	Outdoor
Rn 222 series	CO (Bq m^{-3})	78	11
	PAE (x 10^{-8} J m^{-3})	17.2	2.4
Rn 220 series	Co (Bq m^{-3})	31	0.3
	PAE (x 10^{-8} J m^{-3})	7.0	1.0

From these results, it is possible to calculate the effective dose equivalents due to inhalation of the decay products of ^{222}Rn and^{220}Rn (UNSCEAR, 1984). These are indicated in *Table 8*, together with the outdoor exposure.

The values given in Table 7 indicate an indoor ^{222}Rn value of 1.93 mSv year^{-1} and an outdoor value of 0.126 mSv year^{-1}. The respective values for ^{220}Rn are 0.275 mSv year^{-1} and 0.010 mSv year^{-1}, which indicate an annual dose equivalent of 2.43 mSv (243 mrems).

If an individual spends two thirds of his day in houses or offices, his total annual exposure will be 1.80 mSv instead of 1.97 mSv, and will drop to 1.60 mSv if he spends only half of his time there. The doses received are therefore highly dependent on the lifestyle of the individual.

Table 8. Diagram of the PRADDO model

Annual exposure (msv)	Indoor	Outdoor	Total
External exposure	0.510	0.120	0.63
Internal exposure (^{222} Rn series)	1.099	0.068	1.17
Internal exposure (^{222} Rn series)	0.161	0.007	0.17
Total	1.77	0.20	1.97

4. Modelling of the behaviour of radon and its daughters in dwellings

Jacobi (1972) was the first to publish a mathematical model designed to predict the behaviour of radon and its daughters in uranium mine air, and more particularly the possible relations between the PAE, the equilibrium factor F, the unattached fraction of daughters f_E, the ambient aerosol, the ventilation in the mine gallery, and the geometry of the gallery. This model remains the reference for describing the behaviour of radon and its daughters in a defined volume.

Porstendörfer et al. (1978) adapted Jacobi's model by, in particular, slightly modifying the calculation of the radon activity. In this way he developed a 'room model' which is able to describe the air inside dwellings. *Fig. 7* (*Gouronnec*, 1995) outlines the mechanisms involved in the behaviour of radon and its daughters in a dwelling.

At time t, the rate of variation of the concentration C_i of element i is given by the difference between the sources and the sinks of i, i.e.

$$dC_i(t)/dt = S_i(t) - P_i(t), \tag{3}$$

where $i = 0$ for ^{222}Rn or ^{220}Rn, and $i = 1, 2$ or 3 for Po (218 or 216), Pb (214 or 212) and Bi (214 or 212). $C_i(t)$ is expressed in Bq m^{-3}. $S_i(t)$ is the sum of the sources of i (Bq m^{-3} s^{-1}) and $P_i(t)$, the sum of the sinks of concentration of i (Bq m^{-3} s^{-1}).

Tymen et al. (1989) developed a model describing the dynamics of the variation in the particle size distribution of ^{222}Rn daughters in a closed space. The variation depends greatly on the size distribution of the ambient aerosol, on the rate of production of ^{218}Po (RaA) linked to the activity of ^{222}Rn, on the rate of deposition of radioactive aerosols on the walls of the chamber, and on the electric charge of the unattached fraction.

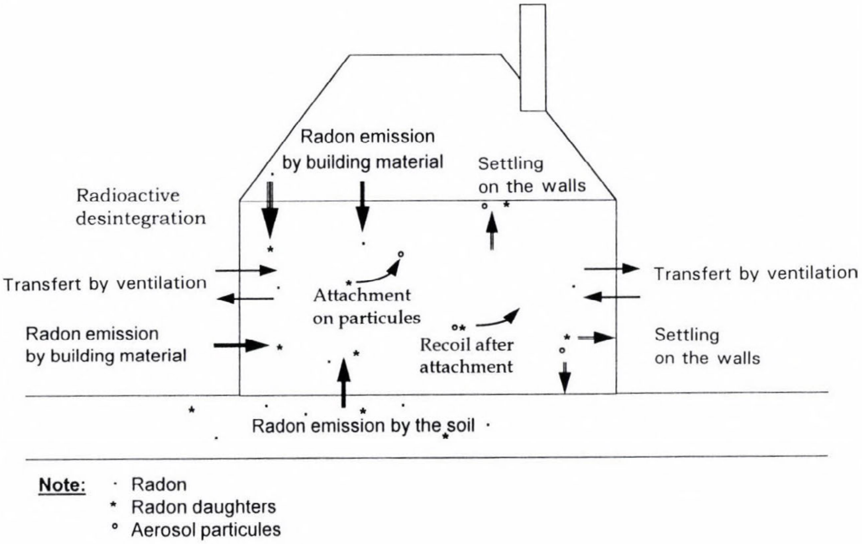

Fig. 7. The different mechanisms involved in the behaviour of radon and its daughters in a dwelling.

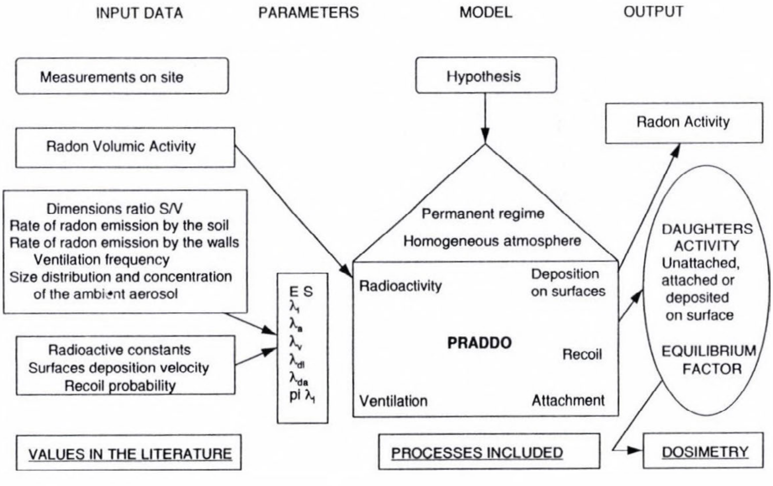

Fig. 8. Diagram of the PRADDO model.

Recently, *Gouronnec* (1995) used the 'room model' to develop an original model called PRADDO (*Physique du RAdon et de ses Descendants dans des atmosphères DOmestiques*: physics of radon and its daughters in home atmospheres). *Fig. 8* summarizes the input parameters of this model, which can be used to calculate the activities of radon and its daughters (unattached, attached, or deposited on surfaces), the PAE, and the equilibrium factor F.

Gouronnec (1995) realised that a single-chamber model is unable to provide a full description of events occurring throughout a room, and therefore considered the air inside buildings to develop a model with NX chambers. This model has NX elementary individual equations, each describing a chamber. Likewise, the expression giving the rate of variation in the concentration C_k of radon or of one of its daughters in the chamber k is written as follows:

$$\frac{dC_k}{dt} = \underset{\text{in the chamber } k}{\overset{\text{source terms}}{I}} + \Sigma_j\, t_{jk}\, C_j - \underset{\text{in the chamber } k}{\overset{\text{sink terms}}{I}} - \Sigma_j\, t_{kj}\, C_k,$$

where j designates the adjacent chambers, C_j is the concentration of the nuclide (radon or daughters) in the chamber j, t_{jk} is the rate of transfer in the chamber j towards k (s^{-1}), and t_{kj} is the rate of transfer of k towards j.

Gouronnec (1995) tested the model in the laboratory using the ICARE measurement set-up of the CEA, and then applied it in field measurements in the cellar of a house in Brittany.

Fig. 9 compares the activity per unit volume of ^{214}Bi (RaC) calculated and measured at different points in the cellar. The mean deviation between calculated and measured values was 13%. *Fig. 10* compares the PAE values measured and calculated at the same points.

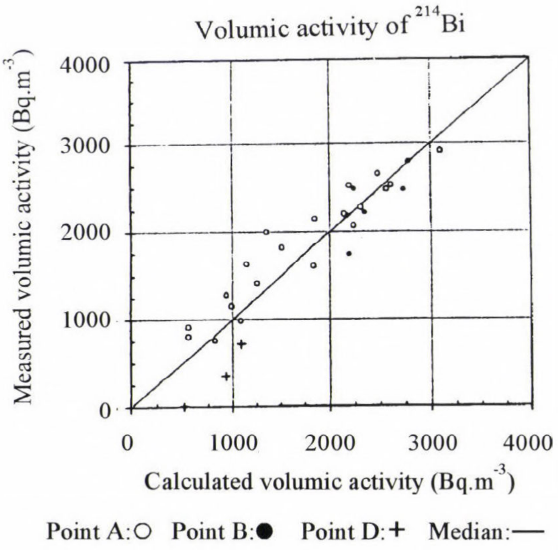

Fig. 9. Volumic activity measured and calculated of ^{214}Bi (RaC).

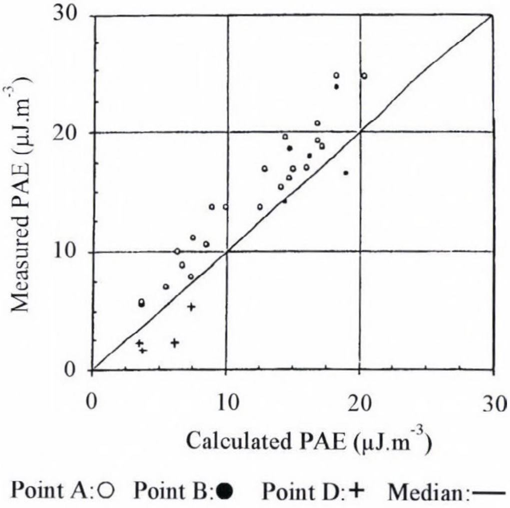

Fig. 10. PAE measured and calculated.

It can be seen that the predictions of the PRADDO model are excellent and therefore allow description of the behaviour of radon and its daughters in the aerosol-rich atmospheres found in most dwellings. However, the PRADDO model does not yet allow modelling of the unattached fraction.

5. Conclusions

Studies of radon, thoron and natural radioactive aerosols developed significantly in the early 1980s, after the relatively unproductive 1970s. The aim has been to evaluate pollution in dwellings in terms of the comfort and well-being of the residents, and as a consequence research into indoor radioactivity has burgeoned in all major industrialised countries. In France, *Tymen et al.* (1992) has made routine measurements in Brittany in cooperation with different teams of the CEA (*Robe et al.*, 1993). Modelling has also been improved, and our group CEA-IPSN at the University of Paris XII, and others, have compared theory and practice in the laboratory and in residential structures. There is now a need to improve measurements of the unattached fraction of Rn and to increase precision in determination of the rate of deposition of radon daughters on the walls of chambers.

Je suis très honoré d'avoir été choisi pour faire un article célébrant les deux fois 30 ans du Professeur E. Mészáros, Membre de l'Académie des Sciences de Hongrie à qui je souhaite tout le bonheur possible.

References

Bigu, J., 1985: Radon daughter and thoron daughter deposition velocity and unattached fraction under laboratory conditions in underground uranium mines. *J. Aerosol Sci. 16*, 157-165.

Chamberlain, A.C. and *Dyson, E.D.* 1956: The dose to the trachea and bronchi from the decay products of radon and thoron. *Brit. J. Radiol. 29*, 317-325.

Chu, K.D. and *Hopke, P.K.*, 1988: Neutralization kinetics for Polonium 218. *Environ. Sci. Technol. 22*, 711-717.

COGEMA, 1994: *Radon*. Villacoublay.

Diouri, M., 1987: Contribution à l'étude du comportement aérodynamique des aérosols: le SDI 2000 - *Thèse* PARIS XII, Rapport CEA R 5412.

Duport, P., *Chapuis, A.M.* and *Pradel, J.*, 1978: Appareil individuel pour la dosimétrie des descendants du radon. IAEA - Colloque international sur les progrès du contrôle radiologiques aux fins de radioprotection.

Elster, J. and *Geitel, H.*, 1901: Weitere Versuche über die Elektrizitätszerstreuung in abgschlossenen Luftmengen. *Phys. Z.*, 560-563.

Frisch, O.R., 1958: *The Nuclear Handbook*. G. Newnes Ltd., London.

Fusamara, N., *Kurosawa, R.* and *Maruyama, M.*, 1967: Determination of f. value in uranium mine air. In *Symposium on Instruments and Techniques for the Assessment of Airborne Radioactivity in Nuclear Operation*. IAEA, Vienna, 213-227.

George, A.C., 1972: Measurement of the uncombined fraction of radon danghters with wire screens. *Health Phys. 23*, 390-392.

Gouronnec, A.M., 1995: Modélisation et étude expérimentale du comportement du radon et de ses descendants dans une enceinte confinée. Application à une habitation; *Thèse* - Paris XII.

Hopke, P., 1990: A critical review of measurements of the unattached fraction of radon decay products U.S. Department of Energy.

Jacobi, W., 1972: Activity and potential alpha energy of Radon 222 and Radon 220 daughters in different air atmospheres. *Health Physics 22*, 441-450.

Kojima, H. and *Abe, S.*, 1988: Measurement of the total and unattached radon daughters in a house. *Radioat. Prot. Dosim. 24*, 241-244.

Malet, J., *Montassier, N.*, *Boulaud, D.* and *Renoux, A.*, 1995: Diffusion of radon daughters in laminar tube flow. European Aerosol Conference - Helsinki. *J. Aerosol Sci. 26* Suppls, S 325-326.

Mouden, A., *Renoux A.* and *Madelaine G.*, 1980: Étude expérimentale du comportement d'un dosimètre α vis-à-vis de certains types d'aérosols. In *Solid State Nuclear Track Detectors*. Pergamon Press, 633-637.

OFSSP (Office fédéral suisse de santé publique), 1993: Radioactivité de l'environnement et sources de radioactivité en Suisse. Fribourg.

Porstendörfer, J., 1987: Free-fractions, attachment rates, and plate-out rates of radon daughters in houses. In *Radon and its Decay Products* (ed.: *P. K. Hopke*), Symposium Series 331. American Chemical Society, Washington D.C., 285-300.

Porstendörfer, J., 1994: Properties and behaviour of radon and thoron and their decay products in the air. *J. Aerosol Sci. 25*, 219-263.

Porstendörfer, J., *Wicke, A.* and *Schraub, A.*, 1978: The influence of exhalation, ventilation, and deposition processes upon the concentration of radon and thoron and their decay products in room air. *Health Phys. 34*, 465-473.

Pradel, J., 1955: La radioactivité dans les mines d'uranium. Conférence CEA n°13, Rapport CEA - Saclay.

Pradel J., 1978: Le radon et les risques associés. Séminaire OCDE - AEN, Paris.

Rannou, A., 1987: Contribution à l'étude du risque lié à la présence du radon 220 et du radon 222 dans l'atmosphère des habitations. Thèse BREST, Rapport CEA R 5378.

Rannou, A., 1989: Le radon. *Clefs CEA*, 13, 18-27.

Reineking, A. and *Porstendörfer, J.*, 1990: Unattached fraction of short lived Rn decay products in indoor and outdoor environments. *Health Physics 58,* 715-727.

Reineking, A., Becker, K.H. and *Porstendörfer, J.*, 1988: Measurement of activity size distribution of the short-lived radon daughters in the indoor and outdoor environment. *Radioact. Prot. Dosim. 24*, 245-250.

Renoux, A., 1965: Étude des ions radioactifs de l'atmosphère. *Thèse*, Paris, *Rapport CEA*; R 2771.

Renoux. A., 1986: La radioactivité naturelle. *Pollution Atmosphérique 112*, 240-248.

Renoux, A., 1992: The radon and the natural atmospheric radioactive aerosol. *Időjárás 96,* 51–60.

Renoux, A., Barzic, J.Y., Madelaine, G. and *Zetwoog, P.*, 1978: Quelques caractéristiques de l'air d'une mine d'uranium. *Nuclear Technology 37,* 313-327.

Robe, M.C., Rannou,A., Tymen, G. and *Le Bronec, J.*, 1993: Radon diagnosis based on investigation of radon sources and radon entry in houses. *Radiation Protection Dosimetry 45,* 319-322.

Tymen, G., El Moussaoui, B. and *Renoux, A.*, 1989: Dynamics of Rn 222 daughter size distribution evolution: modelling and experimental aspects. *J. Aerosol Sci. 20*, 1413-1416.

Tymen, G., Robe, M.C. and *Rannou, A.*, 1992: Measurement of aerosol and radon daughters in five radon houses. *Radiation Protection Dosimetry 45,* 319-322.

UNSCEAR, 1982: Ionising Radiations: Sources and Biological Effects. New York, United Nations.

UNSCEAR, 1984: Exposures from Natural Sources of Radiation. New York, United Nations.

Van Marke, H., Berkvens, P. and *Poffijn*, 1989: Radon versus radon daughters. *Health Physics 56,* 229-231.

Wilkening, M.H., Clements, W.E. and *Stanley, R.D.* 1972: Radon 222, flux measurements in widely separated regions. Natural radiation environment II, CONF. 720905, 717-730.

IDŐJÁRÁS

Quarterly Journal of the Hungarian Meteorological Service
Vol. 100, No. 1-3, January-September 1996

Historical and recent data on sulfate and other water soluble particles in the atmosphere over Hungary

Ágnes Molnár[1] and **Bettina Mihályi**[2]

[1] *Department of Analytical Chemistry, University of Veszprém, P.O. Box 158, H-8201 Veszprém, Hungary*
[2] *Technical University of Wien, Getreidemarkt 9, A-1060 Austria*

(Manuscript received 1 June 1995; in final form 21 September 1995)

Abstract—The determination of the size distribution of inorganic ions in atmospheric aerosol particles is of interest for many problems in atmospheric studies. In this work we summarize the results obtained by Ernő Mészáros and other scientists in Hungary and we compare them with our recent data. It contains the discussion of size distribution of inorganic cations (ammonium, sodium, potassium, calcium) and anions (sulfate, nitrate, chloride) analyzed by capillary electrophoresis and dry deposition velocities determined from size distributions.

Key-words: water soluble ions, capillary electrophoresis, size distribution, dry deposition velocity, ion balance.

1. Introduction

Year to year large amount (100 Tg yr^{-1} as an order of magnitude) of sulfur enters the atmosphere from both natural and anthropogenic sources (*Möller*, 1984). Over more than 30 years many efforts have been done to determine the physical and chemical properties of atmospheric sulfur (*Mészáros*, 1991 and 1993). By now, our knowledge is more complete about the conversion of gaseous sulfur to sulfate in gas phase, in fog and cloud droplets, on the surface of other aerosol particles, and their cycle in the atmosphere.

Our interest on the acidic, mostly sulfate containing atmospheric particles was focused at the first time in the end of the fifties and sixties (see, e.g. *Mészáros*, 1977; *Warneck*, 1988). The reason was a relatively recently recognized ecological effect, that is the degradation of the vegetation and water ecosystems caused by acid deposition. Many studies were made to look for the relationship between rainwater composition (air pollution) and the ecological problems found (*Radojević* and *Harrison*, 1992). It is well known that acidic compounds of anthropogenic origin can increase the hydrogen ion concentration with 1–2 orders of magnitude. It has serious direct and indirect effects both in terrestrial and aquatic ecosystems mainly in the more sensitive ones.

Recently, investigation of sulfate became again a very interesting task. The reason is that the increasing atmospheric aerosol particle concentration has negative effect on global warming (*Charlson et al.*, 1992; *Horvath*, 1992). From model calculations it is thought that the rate of cooling due to aerosol particles is comparable to the effect of greenhouse gases, at least in the highly polluted regions, like Europe (*Taylor* and *Penner*, 1994). The aerosol particles causing this effect are of sulfate and other water soluble compounds that can be found in the fine size range.

Our aim in this paper is to overview the research of Hungarian workers carried out to understand the physical and chemical behavior of sulfate and other water soluble particles. We also intend to present the results of our recent measurements and compare them with earlier information.

2. Historical investigation of sulfate and other water soluble ions in Hungary

Sulfate measurements have already begun in the first part of the sixties. The investigation of atmospheric sulfur in Hungary is certainly connected to the name of Ernő Mészáros, who started this research field and directed the attention of his co-workers to the sulfur problem. He already in 1968 reported about the size distribution of water soluble ions (ammonium, sulfate and chloride) obtained by means of a Casella cascade impactor (*Mészáros*, 1968). The 4-stage impactor had cut-off radii of 3.8, 1.2 and 0.14 μm. For the chemical analysis colorimetric and nephelometric analytical methods were used. Mészáros found that the majority of NH_4 was in the range of particles with radius less than 0.14 μm (stage 4), while the highest sulfate concentration was observed in the size range of $1.2 > r > 0.14$ μm (stage 3) in agreement with the results of similar measurements carried out at that time in the USA (e.g. *Ludwig* and *Robinson*, 1965). Good inverse relationship was found between sulfate fraction in stage 4 ($r < 0.14$ μm) and the relative humidity. In this way he could directly point out the effect of atmospheric water vapor on the size of sulfate particles. A question was also arised why excess ammonium was found on the very small aerosol particles. He concluded that around 60% of ammonium could be found as ammonium sulfate, while the other part was connected to other anions. He also stated that the major part of water soluble particles were in the $0.1 < r < 0.3$ μm size range.

In an other work *Mészáros* (1970) summarized the result of a more complete sampling campaign (200 samples) carried out from March 1967 to February 1969. In this paper the seasonal variation found in the size distribution of sulfate particles was also discussed. A Casella cascade impactor with 5 stages (cut-off radii: 3.6, 1.2, 0.46, 0.14 μm) was used during the sampling, and nephelometric method was applied in the chemical analysis. In winter sulfate particles were found to be two times larger than in summer (mass median radii were in winter and summer 0.24 and 0.11 μm, respectively). In this paper Mészáros tried to demonstrate directly the role of photochemical reactions in sulfate formation, but without success because of very long sampling time.

However, he was able to show the role of photochemical conversion of sulfur dioxide to sulfate particles in a later work (*Mészáros*, 1973) based on sampling made solely during daylight. In this series of observations, along with aerosol samplings (bulk samples, total number concentration, number concentration of large and giant particles), trace gases (SO_2, NO_x, NH_4) and meteorological parameters (surface temperature, relative humidity, wind speed and direction, vertical temperature gradient, intensity of solar radiation with wavelength of 0.29–0.50 μm, etc.) were also measured. The results obtained on 48 sampling days in the summer half year indicated a significant correlation between logarithmic mole ratios of SO_4^{2-}/SO_2 and temperature; relative humidity; and solar radiation. This was a direct proof of sulfate formation by photochemical reactions followed by thermal processes.

The results on the size distribution of calcium, ammonium and chloride were published at the first time in the beginning of seventies (*Mészáros*, 1971) along with a review on sulfate and nitrate. Summarizing the data in the summer half year, the majority of water soluble materials were found in the Aitken size range, while only about 20% of the total mass were in this size interval. As a conclusion this finding showed that with decreasing size the relative quantity of water soluble substances increased. An interesting thing in this paper that calcium was found to have very small mass median radius ($r = 0.15$ μm). In contrast to calcium, mass median radius of chloride was larger ($r = 0.44$ μm). In the winter half year calcium and sulfate particles were larger, while ammonium particles were smaller than in summer. In different size ranges stoichiometric ratio of ammonium and sulfate showed that in the winter half year the large sulfate particles were composed of ammonium sulfate. In this paper Mészáros calculated the extinction coefficient of sulfate particles by means of visibility observed. The calculation showed the particularly important role of particles of 0.1–0.3 μm dry radius.

A lot of attention was paid to the determination of the vertical profile of sulfate and the other ions in the aerosol particles. First, *Mészáros* and *Mészáros* (1970) attempted to determine it with taking samples at a mountain station (Kékestető) on the highest point of Hungary (1014 m). During the winter half year of 1973 already aircraft measurements were carried out (*Mészáros*, 1974). In addition to surface sampling, samples were obtained at elevations of 500, 1000 and 2000 m. The results gained showed that in the giant size range sulfate concentration decreased significantly with height. On the other hand, below

1000 m there were practically no changes in the concentration of large and Aitken particles. Later, *Várhelyi* (1978) published information on the vertical profile of sulfur compounds on the basis of 20 aircraft measurements taken over Hungary in 1975–76. She determined not only the vertical distribution of sulfate but that of sulfur dioxide. Her conclusions were that SO_2 concentration decreased by 90% in the lowest 1000 m layer, while for sulfate the concentration decrease was 50% in the same layer. These numbers show that SO_2 decreases significantly with height, but the decrease is not very important for sulfate particles. This pattern can be well interpreted by the conversion of sulfur dioxide into sulfate particles.

From the beginning of the eighties the concentration of sulfate has been regularly measured at K-puszta which is a background air pollution monitoring station operated by the Institute for Atmospheric Physics. The bulk samples have been analyzed by several analytical methods including nephelometry, isotope dilution method and recently by ion chromatography. *Mészáros* and *Horváth* (1984) reported about the first sulfate, nitrate and ammonium measurements (1982–83). Confirming the results in the literature they found summer minimum and winter maximum concentrations for these ions. From their size distribution they determined the dry deposition velocity (0.024, 0.03, 0.022 cm s^{-1} for sulfate, nitrate and ammonium, respectively). Since 1981, in addition to wet chemistry, we also determined the elemental composition of atmospheric aerosol particles using PIXE (Proton Induced X-ray Emission) method (*Molnár et al.*, 1993). While in 1982–83 both PIXE and wet chemistry methods indicated sulfate concentration around 8 $\mu g\ m^{-3}$ (*Mészáros* and *Horváth*, 1984; *A. Mészáros et al.*, 1984), for 1991 the average sulfate concentration measured by PIXE was only 2.7 $\mu g\ m^{-3}$ (*Molnár et al.*, 1993).

In this paper we would like to make a contribution to this more than 30-year series of observations by measuring the size distribution of sulfate and other water soluble anions and cations by means of a low pressure cascade impactor and a new analytical method.

3. Sampling and analysis

Our cascade impactor measurements were taken in Veszprém in a relatively small town near to Lake Balaton. This town is the center of one of the counties in western Hungary with a population of 60,000. It is assumed, but not proved, that information gained from this site can be compared to earlier size distribution data measured in suburban Budapest. The sampling site was on the roof of the students' dormitory at the University of Veszprém. Nine samples were taken from January to March 1994 by means of a Berner-type low pressure cascade impactor. The duration of each sampling was 48 hours with a sampling rate of 31.3 $\ell\ min^{-1}$. We used aluminium foils without coating to impact the particles.

The parameter of this impactor is shown in *Table 1*. From these samples the concentration distribution of several metals was also determined as discussed elsewhere (*Molnár et al.*, 1995). Because of this fact we used only about 10% of each sample for determining the water soluble compounds. Unfortunately it was not possible to preserve any part of stage 8 for our analysis and this stage — with the coarser particles — is missing from our data.

Table 1: Physical parameters of Berner impactor with 9 stages

Stages	Cut-off diameter (mm)	Geometric mean diameter (μm)
9	16.0	–
8	8.0	11.3
7	4.0	5.66
6	2.0	2.83
5	1.0	1.41
4	0.5	0.71
3	0.25	0.354
2	0.125	0.177
1	0.0625	0.088

Capillary zone electrophoresis (CZE) is a relatively new analytical method in environmental studies. Despite the relatively high detection limit compared to e.g. ion chromatography, this method avoids several problems of other techniques arising from the fact that the amount of the samples is sometimes too small and the concentrations are low. CZE has a very useful advantage, because it needs only some nanoliters of the sample and for the analysis only some minutes are necessary. Because of its small sample demand, the preparation of some mL solution from the aerosol samples is enough. This property can significantly decrease the disadvantage coming from the high detection limit. It should also be noted that the detection limit highly depends on the detector used in the instrument (in our case it is an indirect UV detector) and for a given detector it can also be improved by e.g. applying different injection mode. (This analytical method is based on the different mobility of the ions due to their mass and charge. The separation in the capillary is carried out under high voltage.)

During the sample preparation we leached the samples with 5 mL of high quality deionised water (MilliQ-water) for 15 minutes in ultrasonic bath. After leaching we filtered the samples on filter of 0.45 μm pore size. The analyses were carried out by means of Quanta 4000 Capillary Electrophoresis Instrument (manufactured by Waters). The details of the measurements are summarized by *Mihályi* (1995), while the detection limits of different ions are given in *Table 2*.

Table 2. Detection limits of different ions in mg ℓ^{-1}

Cations		Anions	
ammonium	0.152	chloride	0.073
potassium	0.239	sulfate	0.101
calcium	0.211	nitrate	0.149
sodium	0.132		

5. *Results*

On the basis of our analyses we determined the size distribution of sulfate, nitrate, chloride, ammonium, potassium, calcium and sodium in the aerosol particles (*Fig. 1*). The size distributions were calculated by averaging the concentrations of each size interval and the cumulative distribution were determined on the basis of these calculations.

The distribution of sulfate and ammonium is similar concerning their occurrence and mass median diameter (0.6 and 0.53 μm for sulfate and ammonium, respectively). It can be seen that both ions are composed of two independent distributions, one in range of $d < 2$ μm, the other above this size. Comparing the distributions of this paper and the former ones (*Mészáros*, 1970 and 1971), we can state that the shapes of the curves are very similar excluding the coarsest particles. Earlier only one distribution was found for these ions. Our second distribution shows other formation processes that could be a result of a small source (for both ions 5% of total sulfate and ammonium) closed to the sampling site. For sulfate we obtained 1.25 times larger mass median diameter than *Mészáros* (1970) gave for the winter half year of 1969. This indicates that during the last 25 years practically no changes occurred in the sulfate distribution. In spite of this fact the dry deposition velocities obtained by *Mészáros* and *Horváth* (1984) are rather different from ours. They gave a 0.024 and 0.022 cm s^{-1} dry deposition velocities for sulfate and ammonium, respectively, which are 2–3 times smaller than ours (see in *Table 3*). The differences are probably due to fact that for dry deposition calculations *Mészáros* and *Horváth* (1984) used simply the mass median diameters and we applied the detailed distribution curves. This means that for each impactor stage we determined separately the deposition velocities and the average deposition of all particles was calculated by weighting with the concentration. The deposition velocities for a certain particle size, as in the case of work by Mészáros and Horváth, was taken from the Chamberlain's curve (e.g. *Beilke* and *Gravenhorst*, 1987) giving the relationship between particle size and deposition velocity.

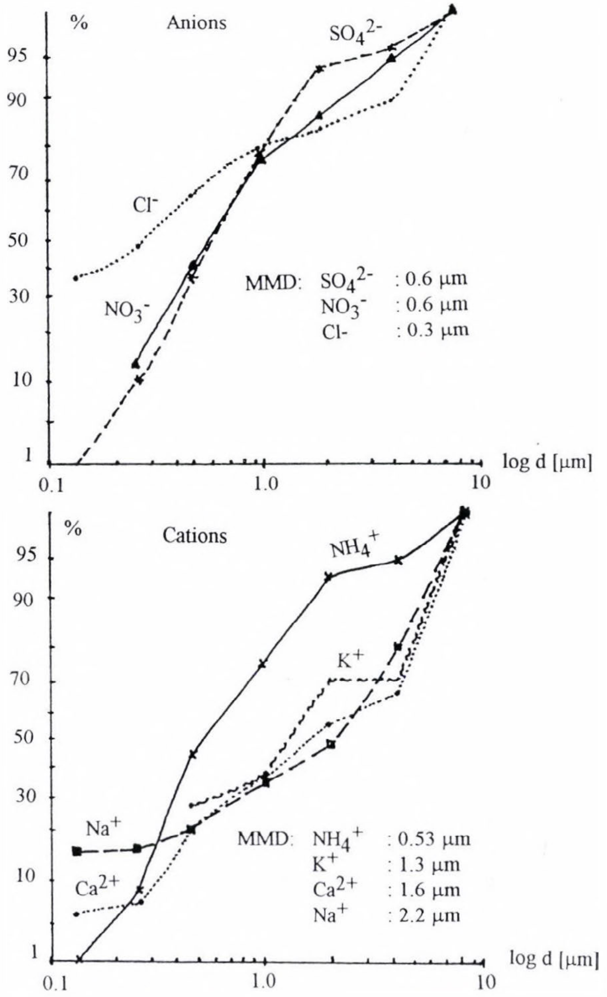

Fig. 1. Logarithmic normal size distribution of different water soluble ions in the aerosol particles. (MMD denotes the aerodinamic mass median diameter)

Nitrate shows only one distribution that can be the result of the condensation of nitric acid and this is consistent to the results of *Mészáros* (1971). Even the mass median diameters given by him and us are the same ($d = 0.6$ μm). The comparison of the dry deposition velocities shows 2–3 times differences again (Table 3). The chloride distribution in the recent measurements differs significantly from that published by *Mészáros* (1971). According to our data it can be seen that at least during the measurements the majority of this ion was found on very small particles that could refer to anthropogenic effects. In contrast to this Mészáros found the majority of chloride in the accumulation mode and in the coarse size range that resulted in a much larger mass median diameter (d = 0.88 μm) than ours (d = 0.3 μm). The dry deposition velocity for chloride does not indicate this very small MMD. An important fraction (more than 20%) of chloride was found on coarse particles which significantly determines the value of the dry deposition velocity.

Table 3. Dry deposition velocities of different water soluble ions

	Dry deposition velocity (cm s^{-1})	
Ions	This paper	*Mészáros* and *Horváth*, (1984)
Sulfate	0.04 - 0.08	0.024
Nitrate	0.06 - 0.10	0.030
Chloride	0.08 - 0.13	–
Ammonium	0.06 - 0.09	0.022
Potassium	0.15 - 0.23	–
Sodium	0.14 - 0.26	–
Calcium	0.18 - 0.28	–

As expected, potassium and sodium were found on the coarse particles confirming the crustal origin of these species. The majority of calcium was in the coarse particle size range that is in contrast to the size distribution published by *Mészáros* (1971). In the recent measurements we determined mass median diameter of 1.6 μm that is about 3 times larger than that is in the referred publication. It was explained with a large portion of calcium from anthropogenic sources but our results show that calcium is mostly of crustal origin.

Calculating the ion balance for 1–7 size ranges (*Table 4*) one can state that significant anion excess was found in the 0.5–1.0 μm range, while cation surplus appeared in the largest size range (4.0–8.0 μm). In the other size ranges anions and cation are practically balanced. Taking into account the total balance calculated on the basis of all stages, one can see that it is important and negative (-14.5 neq/m^3). This negative balance is due to the particles in the range of 0.5 μm < d < 1.0 μm. It should be noted, however, that this result should be confirmed by measuring the acidity/alkalinity of each impactor stage.

As it is well known (e.g. *Mészáros*, 1992) acidic particles of the size interval where the most important negative balance was measured cause the majority of acid deposition on background and remote areas owing to their transport processes. On the other hand particles in this size range are also very important in aerosol climate forcing since they scatter significantly solar radiation (*Mészáros*, 1971; *Horvath*, 1992). For this reason we will continue this research to determine the relationship between the concentration and size distribution of water soluble particles as well as their scattering properties.

Table 4. Ion composition of the aerosol particles in different size ranges (neq/m^3)

	Cut-off diameter of the impactor stages (μm)						
	0.0625	0.125	0.250	0.50	1.0	2.0	4.0
Ions:							
Chloride	1.5	0.5	0.7	0.6	0.2	0.3	0.5
Sulfate	1.7	11.2	32.9	55.4	20.5	4.5	5.2
Nitrate	0.1	4.3	10.5	13.5	2.9	3.9	2.4
Ammonium	1.4	8.9	38.4	37.3	20.0	3.1	7.5
Potassium	–	–	1.1	0.5	1.4	–	1.2
Calcium	1.7	0.4	3.7	5.2	4.0	4.4	10.0
Sodium	1.3	–	0.2	1.1	1.3	2.8	1.7
Anions	-3.3	-16.0	-44.1	-69.5	-23.4	-8.7	-8.1
Cations	+4.4	+9.3	+43.4	+44.1	+26.7	+10.3	+20.4
Total	+1.1	-6.7	-0.7	-25.4	+3.3	+1.6	+12.3

References

Beilke, S. and *Gravenhorst, G.*, 1987: Deposition. In *Evaluation of Atmospheric Processes Leading to Acid Deposition in Europe. Air Pollution Report 10*, Commission of the European Communities, Brussels, 113-135.

Charlson, R.J., Schwartz, S.E., Hales, J.M., Cess, R.D., Coakley, J.A. Jr., Hansen, J.E. and *Hofmann, D.J.*, 1992: Climate forcing by anthropogenic Aerosols. *Science 255*, 423-430.

Horvath, H., 1992: Effects on visibility, weather and climate. In *Atmospheric Acidity* (eds.: *M. Radojevic* and *R. M. Harrison*), Elsevier Applied Science, London, New York, 435-466.

Ludwig, F.L. and *Robinson, E.*, 1965: Size distribution of sulfur-containing compounds in urban aerosols. *J. Colloid. Sci. 20*, 571-584.

Mészáros, A., Haszpra, L., Kiss, I., Koltay, E., László, S. and *Szabó, Gy.*, 1984: Trace element concentrations in atmospheric aerosol over Hungary. *Proc. 11th International Conference on Atmospheric Aerosols, Condensation and Ice Nuclei.* Pre-print volume I, 113-117.

Mészáros, E., 1968: On the size distribution of water soluble particles in the atmosphere. *Tellus 20*, 443-448.

Mészáros, E. and *Mészáros, A.*, 1970: On the properties of active condensation nuclei (in Russian). *Proc. 8th National Conference on Cloud Physics and Cloud Modification.* Gidrometeoizdat, Leningrad, 77-83.

Mészáros, E., 1970: Seasonal and diurnal variations of the size distribution of atmospheric sulfate particles. *Tellus 22*, 236-238.

Mészáros, E., 1971: The size distribution of water soluble particles in the atmosphere (in Hungarian). *Időjárás 75*, 308-314.

Mészáros, E.,1973: Evidence of the role of indirect photochemical processes in the formation of atmospheric sulphate particulate. *J. Aerosol Sci. 4*, 429-434.

Mészáros, E., 1974: Aircraft measurements of the concentration and size distribution of atmospheric sulfate particles. In *Special Environmental Report; Observation and Measurement of Atmospheric Pollution*. WMO, Geneva, 276-280.

Mészáros, E., 1977: *Atmospheric Chemistry: Fundamental Aspects* (in Hungarian). Akadémiai Kiadó, Budapest.

Mészáros, E., 1991: The atmospheric aerosol. In *Atmospheric Particles and Nuclei* (eds.: *G. Götz, E. Mészáros* and *G. Vali*). Akadémiai Kiadó, Budapest, 17-84.

Mészáros, E., 1992: Occurence of atmospheric acidity. In *Atmospheric Acidity* (eds.: *M. Radojevic* and *R. M. Harrison*). Elsevier Applied Science, London, New York, 1-38.

Mészáros, E., 1993: *Global and Regional Changes in Atmospheric Composition*. Lewis Publ., Boca Raton, Ann Arbor, London, Tokyo.

Mészáros, E. and *Horváth, L.*, 1984: Concentration and dry deposition of atmospheric sulfur and nitrogen compounds in Hungary. *Atmospheric Environment 18*, 1725-1730.

Mihályi, B., 1995: The relationship between the chemical composition of aerosol particles and their optical properties. *Diploma Thesis,* Technical University of Wien, Austria.

Molnár, A., Mészáros, E., Bozó, L., Borbély-Kiss, I., Koltay, E. and *Szabó, Gy.*, 1993: Elemental composition of atmospheric aerosol particles under different conditions in Hungary. *Atmospheric Environment 27A*, 2457-2461.

Molnár A., Mészáros, E., Polyák, K., Borbély-Kiss, I., Koltay, E., Szabó, Gy. and *Horváth, Zs.*, 1995: Atmospheric budget of different elements in aerosol particles over Hungary. *Atmospheric Environment 29*, 1821-1828.

Möller, D., 1984: On the global natural sulfur emission. *Atmospheric Environment 18*, 29-39.

Radojević, M. and *Harrison, R.M.* (eds.), 1992: *Atmospheric Acidity*. Elsevier Applied Science, London, New York.

Taylor, K.E. and *Penner, J.E.*, 1994: Response of the climate system to atmospheric aerosols and greenhouse gases. *Nature 369*, 734-737.

Várhelyi, G., 1978: On the vertical distribution of sulfur compounds in the lower troposphere. *Tellus 30*, 542-545.

Warneck, P., 1988: *Chemistry of the Natural Atmosphere*. Academic Press, Inc., San Diego, New York, Berkeley, Boston, London, Sydney, Tokyo, Toronto.

IDŐJÁRÁS
Quarterly Journal of the Hungarian Meteorological Service
Vol. 100, No. 1–3, January–September 1996

Precipitation and cloud chemistry in the Neue Bundesländer of Germany in the background of changing emissions

D. Möller[1], K. Acker[1], W. Marquardt[2] and
E. Brüggemann[2]

[1] *Brandenburg Technical University Cottbus, Faculty 4,*
P.O. Box 10 13 44, D-03013 Cottbus, Germany

[2] *Institute for Tropospheric Research, Leipzig,*
Permoserstr. 15, D-04303 Leipzig, Germany

Abstract—This paper presents precipitation chemistry data from a continuous record since 1983 at Seehausen, Germany (Neue Bundesländer or former GDR) showing the influence of changing emissions, caused by industrial collapse after German unification, on the chemical composition of the atmosphere. This activity is a part of a joint research project, called by 'SANA'. Another SANA activity, started in 1992 is the monitoring of air pollutants and sampling of cloud water at Mt. Brocken station. The recorded changes in the chemical composition of rainwater, especially when using sectoral data based on backward trajectory calculations, clearly show the source-receptor relationship. The most important result is the decrease of atmospheric neutralizing capacity. By the results of the first continuous cloud chemistry monitoring station in Europe, Mt. Brocken, we also found a strong increase in cloud water acidity. This monitoring program in the background of highly decreasing emissions is a unique opportunity to study atmospheric chemical processes. As an example the continental sea-salt contribution hypothesis is also supported by the result of stations.

Key-words: air pollution, cloud chemistry, emission, sea-salt, trends, precipitation chemistry.

1. Introduction

Since the German unification in 1990 a dramatic decrease in air pollutant emission and consequently lower atmospheric concentration has been forecasted and observed. The decrease of the 'classical' pollutant emission like sulfur dioxide and alkaline flue ash from lignite-fired power stations is most likely accompanied with an increase of the emission of photo-oxidant precursors NO_x and VOC. To investigate this problem a national scientific program of recovery of the atmosphere (SANA) was started in 1991 funded by the Ministry for Education and Science of Germany. More than 40 German groups are involved within this joint research project. The program is subdivided into five main projects: distribution, transformation, modeling, and impact. In this contribution we report results from the 'transformation' project.

A precipitation network consisting of 15 stations using wet-only collectors was established (*Brüggemann et al.,* 1993). In this paper we use the results from the Seehausen station, having been in operation since 1983. Another SANA activity is the Mt. Brocken Cloud Chemistry Program, based on the first continuously operating cloud chemistry station in Europe (*Möller et al.,* 1994a, b). We started the sampling program in 1992 and it will be continued till 1995. Our preliminary results strongly support the need of the long-term cloud chemistry climatology monitoring. Clouds play an important role in transport and transformation of atmospheric trace species. They redistribute gas phase species, especially through vertical mixing and may also influence the photochemical processes. Clouds capture aerosols by nucleation and absorb gaseous species by scavenging from gas phase into cloud water. Chemical processes in cloud water are often more effective than in gas phase and must be therefore included in any atmospheric budget of trace species. Finally, precipitating clouds remove trace species from the atmosphere via wet deposition. Clouds have important indirect effect on climate forcing. Moreover, there could be feedback mechanisms through aerosols and chemical processes that can change the physical properties of clouds. From the point of view of the climate studies it leads to an increasing interest in aerosol-cloud processes and cloud chemistry.

2. Experiment

The wet deposition network consists of 15 stations, using wet-only collectors. These home-made collectors were tested during different international campaigns (*Marquardt* and *Ihle*, 1988). Two stations have already had a long-term record (Seehausen from 1983 and Greifswald from 1984). The Wiesenburg station has been established in 1988 whereas all others started in 1991 as the part of the SANA network. To show the effect of the dramatically changed emission after 1990, we present data only from the long-term station Seehausen. The sampling procedure takes four hours. Samples are continuously cooled while stored and transported and they are analyzed in Leipzig, within 10 days. Former investigations of stability of samples (*Brüggemann et al.,* 1991) were adopted in the quality assurance/quality control (QA/QC) program. Before 1991 spectrophotometric and atomic spectroscopy methods were used for anions and cations, respectively, since then both methods have been replaced by ion chromatography (Metrohm type). Sector analysis of incoming air masses have been done by backward trajectory analysis. For the sampling site

Seehausen we defined 6 fixed sectors for air masses. For example sector 'H' (106–208°) covers the industrial areas in Eastern Germany, while 'I' (209–239°) and 'J' (240–259°) sectors are in the direction of West Germany (e.g., Ruhr industrial area). Since 1993 the transport analysis is based on a 3D-model of the Meteorological Institute of the Free University Berlin (*Reimer* and *Scherer*, 1992).

At Mt. Brocken (1142 m a.s.l.), which is located in the Harz-Mountains at the former border between Eastern and Western Germany, cloud water is collected by 1 hour sampling period (before 1993 on event basis) using a Mohnen-type string collector, installed in combination with an automatic wet-only sampling unit. The 1 hour samples are stored in a cooled collector unit and analyzed by ion chromatography within 10 days in our laboratory in Berlin. The stability of the samples has been studied before adoption of the sampling procedure. Liquid water content (LWC) of clouds has been continuously measured using a PVM-100 based on forward scattering of laser beam. Meteorological standard parameters (wind direction and velocity, temperature and humidity, global radiation) are measured by commercial instruments (Thies company). Mixing ratio of trace gases are monitored with instruments from Thermo-environments (SO_2), Ecophysics (NO/NO_2), Dasibi (O_3) and Aerolaser (H_2O_2). All data are recorded by two independent systems: (a) 30-sec averages by commercial data acquisition system (Labtech notebook) and (b) by x-y-recorders for on-line registration. For more experimental details see *Möller et al.* (1996). Beside the standard monitoring activity we have carried out some measurement campaigns with an extended program.

Laboratory work of both groups (Leipzig and Berlin) is regularly checked by inter-laboratory calibrations with standard reference samples, organized by U.S. EPA within the network of the World Meteorological Organization. The field measurements are under quality control within the SANA joint research program using operation plans adopted from the EPA.

3. Results

3.1 Precipitation network

The main problem in the estimation of a trend in the chemical composition of precipitation, as a consequence of a change in anthropogenic emission, is the natural variation from event to event and consequently from period to period (e.g. from year to year). Periods could be different in parameters determining precipitation (frequency, duration, intensity), cloud (type, liquid water content, cloud base height, etc.), and air mass characteristics (geographical origin, trajectory). Moreover, there are fluctuations in natural emissions resulting in fluctuation of trace gas and aerosol concentration distribution. This is the basic (natural) level for an assessment of a changing chemical composition of the troposphere, caused by man-made activities. Therefore, it is very useful to study natural variations at negligible or constant anthropogenic influence.

Trends, that have been found for precipitation composition in Europe are based on the (Western) European precipitation network (around 120 stations) and generally are in agreement with the emission trends. Between 1955/59 and 1970/72 sulfate, nitrate and ammonium in precipitation increased in Central Europe and Scandinavia by 40–60%, whereas between 1972 and 1984 sulfate decreased in Scandinavia by 30% and no changes have been observed for nitrate and ammonium (*Rodhe* and *Granat*, 1984; *Rodhe* and *Rood*, 1986). *Jost* and *Beilke* (1983) published an increase of nitrate between 1956 and 1976 in Western Europe by 120%. *Hedin et al.* (1994) found that sulfate decreased also in the period after 1970, by 30% between 1978 and 1989 in the Netherlands and by 30% between 1971 and 1989 in Sweden. These authors also found a strong decrease of base cations (Ca^{2+}, Mg^{2+}, K^+, Na^+) in the order of 50–70% in the same period.

Only very few data are available from Eastern Europe. It seems that precipitation composition reflects generally the same tendency. In Hungary, between 1968/70 and 1979/80 no increase in nitrate and ammonium was observed (*Horváth* and *Mészáros*, 1984); the increase between 1979/80 and 1989/90 was small (15% for NO_3^-), whereas between 1989/90 and 1993/94 nitrogen increased significantly (20% for NO_3^- and 42% for NH_4^+ after *Horváth,* 1995 personal communication). *Moldan et al.* (1987) reported that sulfate decreased in Czechoslovakia in the period of 1976–1984 (no figure is given).

Precipitation chemistry data from former East Germany are available since 1958 (*Möller* and *Lux*, 1992) but only episodically, and because of different sampling techniques they can be used for trend analysis only with caution. It seems that in the period up to 1989 no trend in any rain water components has been observed. The only stations with continuous sampling are Seehausen (since 1983), Greifswald (since 1984), and Wiesenburg (since 1988) covering the period before and after 1989/90.

Fig. 1 shows a comparison between trends of the lignite consumption in the former GDR (or lately in Neue Bundesländer) and the concentrations of sulfate and calcium in rainwater. The figure suggests a relationship between the decrease in sulfate and calcium and the decreasing coal consumption. This is in agreement with the changing emissions after 1990 (*Fig. 2*). After 1992, however, there seems to be a tendency for different slopes in sulfate and calcium: Ca decreases like before 1990 whereas sulfate is stagnant; note that emission data since 1993 are not yet available. This different concentrations development explains the high increase in rain water acidity in precipitation derived from 'eastern' sectors (see below). The mean acidity in precipitation derived from all sectors (*Fig. 3*) shows no trend. The different curves in Fig. 3 representing ratios between 'acidic' and 'alkaline' ions, emphasize the importance of single species in the acidity balance. It is obvious that ammonium indicates mostly the neutralizing capacity. The data in *Table 1* reflect, however, that ammonium also decreases due to drastic structural changes in the agriculture after German unification (Fig. 2). Such drastic ammonia emission decrease in other European countries has never been observed. Decrease of sulfate and calcium was already observed before 1989, reflecting the general trend in Europe.

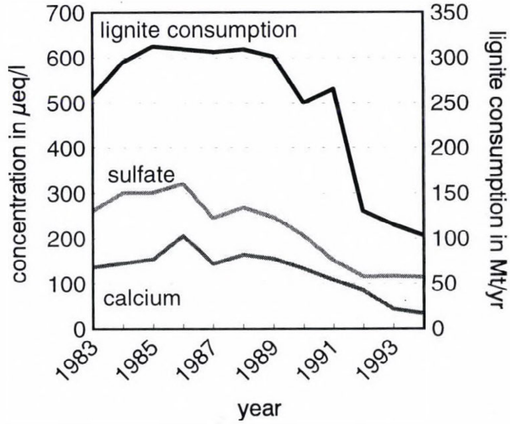

Fig. 1. Yearly variation of sulfate and calcium in precipitation at Seehausen from sector H ('east') in µeq ℓ^{-1} (precipitation-weigthed) and coal consumption within former GDR and Neue Bundesländer, respectively (in Mt yr^{-1}).

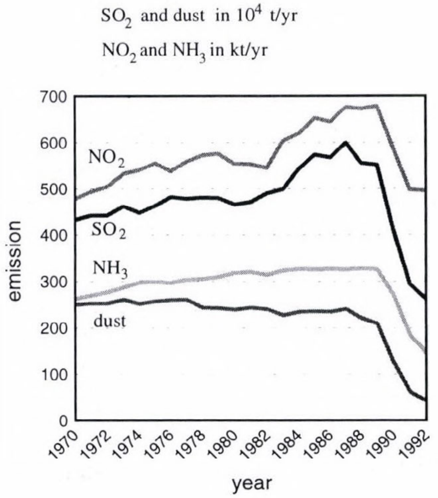

Fig. 2. Yearly variation of emissions in former GDR and Neue Bundesländer (after *Friedrich,* 1995).

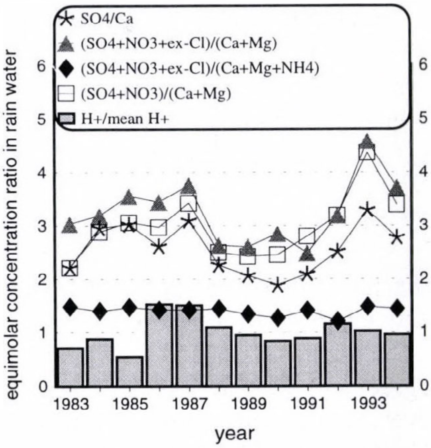

Fig. 3. Yearly variation of different concentration ratios and deviation of hydrogen ion concentration from the period average in rainwater at Seehausen.

Table 1. Averaged precipitation-weighted rain water composition in Seehausen before and after 1990 (in μeq ℓ^{-1}); decrease (in %) between the periods

	SO_4^{2-}	Ca^{2+}	Mg^{2+}	Cl^-	NH_4^+	Na^+	NO_3^-	K^+
1983–89	150±17	59±12	12±2	63±18	85±11	33±9	45±9	6±2
1991–94	72±11	28±9	7±1	39±6	52±5	31±7	44±4	6±2
Decrease in %	52	53	42	38	39	–	–	–

Table 1 shows that from 1990 a dramatic decrease in concentrations of sulfate, calcium, magnesium, chloride and ammonium has been observed (*Brüggemann* and *Rolle*, 1994). This is caused mainly by the collapse of the industrial and agricultural structure of the new states of Germany. The sulfate to nitrate ratio has decreased continuously since 1983 in rainwater (*Fig. 4*). No significant change of nitrate in rainwater has been observed since 1983, after 1990 nitrate increased in rainwater from 'east' sectors at all SANA sites between 10 and 20%. The averaged figures are (in μeq/ℓ): 43±7 for sector I+J ('west') and 73±11 for sector H ('east'). Note that rainwater nitrate loading is higher from eastern sectors than that from western one, despite of higher NO emission densities in west. This may be a consequence of different emission structures between former Western and Eastern Germany: in East Germany 60% of total NO was emitted by power plants with high stacks, traffic contributed to about 25%, whereas in West Germany percentage of traffic was about 45% and the height of stacks here is generally lower. It follows that NO is emitted into different atmospheric layers and, consequently, because NO is practically not deposited by either wet or dry deposition it results in different ratios between dry deposition and wet removal after NO oxidation to nitrogen dioxide and nitric acid.

Despite of the large annual fluctuation, the 'east-to-west' ratio for nitrate and sulfate (*Fig. 5*) suggests a general increase. In the period 1990–1992 (the time period of extremely changing emissions in the Neue Bundesländer) these curves are in agreement with the emission pattern: decreasing SO_2 (therefore sulfate) and increasing NO (therefore nitrate). After 1992 the following tendency appeared: increase of sulfate with no change of nitrate. We need future monitoring to assess these changes in the context of changing emissions. Fig. 5 shows clearly that the ratio for calcium decreased significantly between 1991 and 1993 (by more than 50%). Trend analysis shows that over the whole measurement period the slope is positive for sulfate ($b = 0.07$ y^{-1}) and nitrate ($b = 0.05$ y^{-1}) and negative for calcium ($b = -0.09$ y^{-1}).

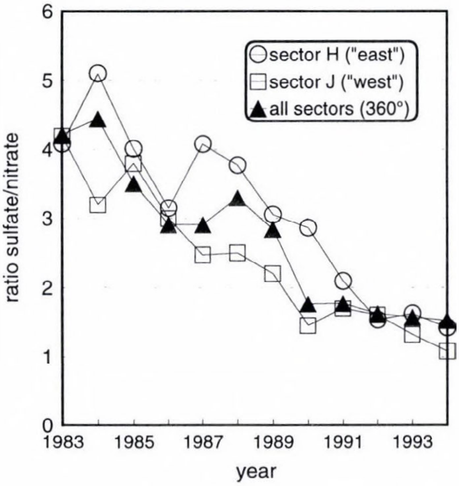

Fig. 4. Trend of concentration ratio sulfate to nitrate in rainwater at Seehausen for different sectors.

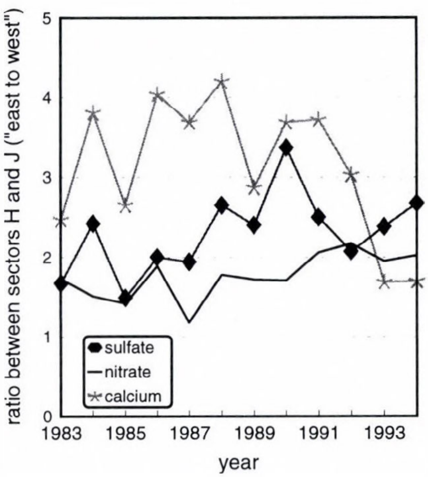

Fig. 5. Trend of rainwater concentration ratio of sectors 'east' to 'west' for sulfate, nitrate and calcium.

Finally, these different tendencies are in agreement with the most important result we found, that the acidity increased in 'eastern' rain water after 1992 (*Fig. 6* and cf. Fig. 1 and discussion above). The acidity here, in 1994, is higher by a factor of three than in rainwater from sector I+J ('west').

In the period 1983–1992 no difference was observed: 41 ± 16 and 41 ± 16 μeq H^+ ℓ^{-1} for 'east' and 'west', respectively (average from all sectors are: 43.1 ± 11.8 μeq ℓ^{-1}) see Fig. 6. Note that the sectoral acidity contributes to the averaged (precipitation-weighted) H^+ concentration taking into account the percentage of precipitation. From Fig. 6 it follows that this percentage can extremely vary from year to year: in the period of 1983–88 small variations (11–16%) have been observed, whereas in the period 1989–94 the variation is larger (3–36%). The very similar acidity in rainwaters coming from 'eastern' or 'western' sectors can be interpreted by a similar ratio of sulfate plus nitrate to calcium plus ammonium, despite of the fact that the absolute figure for denominator (acid species) and numerator (basic species) is quite larger in rain water from 'eastern' sectors (cf. Fig. 5). We identify the reason of very recently observed acidity increase in 'eastern' sectoral rainwater as a consequence of reduced neutralizing capacity by alkaline calcium compounds and ammonia.

On the other hand, the data listed in Table 1, reflecting the average precipitation composition before and after 1990, show that concentrations of 'acid' components decreased more than that of 'alkaline' components. The difference (sulfate plus nitrate plus chloride) minus (calcium plus magnesium plus sodium plus ammonium) before 1989 amounts 63 and after 1989 it is 31 $\mu eq\ \ell^{-1}$, respectively. Assuming that these figures represent the acidity, we must conclude that the average acidity of precipitation became smaller. However, in view of the variations of the average H^+ concentration (Fig. 6) it is very speculative to say that H^+ decrease is significant since 1992. The only significant change of acidity can be observed between sector H ('east') and I+J ('west'), see Fig. 6, because of the contrary development.

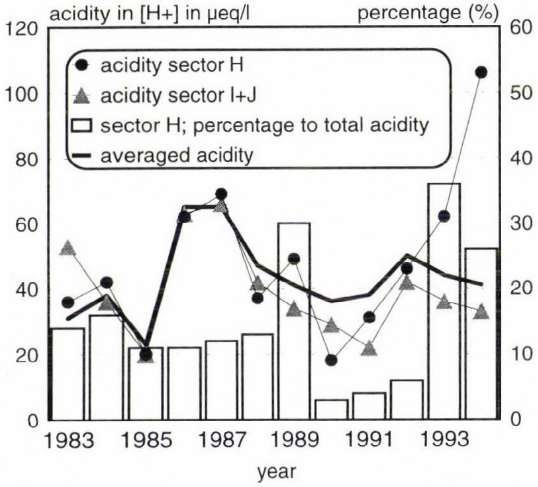

Fig. 6. Trend of acidity in rain water at Seehausen.

3.2 The ratio between sea-salt and excess chloride

Excess-chloride (non sea-salt Cl^-) contributed significantly to the atmospheric acidity before 1990, see Fig. 3. Excess-chloride has been calculated on the basis of a widely accepted molar ratio $(Na^+/Cl^-) = R_{sea} = R_{bulk} = 0.86$ ('sea' indicates rain water sea-salt contribution and 'bulk' represents the ratio in seawater) for sea-salt contribution, assuming that no other sources for sodium in precipitation are significant:

$$Cl^-_{excess} = Cl^-_{sea}\,(R_{sea}/R - 1), \qquad (1)$$

where $R = (Na^+/Cl^-)_{sample}$. After 1990 total chloride decreases as Table 1 reflects. Change in Na^+ before and after 1990 is not significant, suggesting that most of Na^+ is of sea-salt origin (it is not excluded that there is a negligible Na^+ contribution by flue ash emission). Therefore, it is evidently that only excess-Cl^- decreased. Main source of excess-Cl^- has been identified as HCl emission from lignite-fired power stations (*Möller,* 1990). It was about 95 kt yr^{-1} in 1985. Waste incineration was negligible in the former GDR.

The above mentioned ratio (figure $R_{sea} = 0.86$) is not valid ($R_{sea} > R_{bulk}$) for sea-salt contribution to rain water above continents. *Möller* (1990) suggested a hypothesis to change Na^+ to Cl^- ratio due to the difference in efficiency of the removal processes for these species while air mass transported from sea to the continent. A figure of $R_{sea} = 1.16$ was suggested to be more reliable for Northern Europe. In the evaluation of the excess chloride trend we use this latter figure.

Using $R_{sea} = 0.86$, excess-Cl^- decreases from 25 to 3 μeq ℓ^{-1} (*Table 2*), i.e., the decrease amounts to 88%, a figure, which is not probable. However, using the referenced ratio $R_{sea} = 1.16$, excess-Cl^- drops only by 65% (from 35 to 12 μeq ℓ^{-1}), which is more likely figure. This decrease is somewhat larger than the decrease for sulfate and calcium (52 and 53%, respectively) and could be explained by the fact that after unification in the Neue Bundesländer salty coal combustion and potash industry stopped. We would like to emphasize that this is an interesting example for an air chemistry interpretation based on monitoring under changing emissions.

Table 2. Calculation of excess-Cl in rain water in Seehausen (in μeq ℓ^{-1}) based on different R_{sea}

Period	$[Na^+]$	$[Cl^-]$	$R = [Na]/[Cl]$	Cl_{excess} based on	
				$R_{sea} = 0.86$	$R_{sea} = 1.16$
1983–89	33±9	63±18	0.52±0.11	25	35
1990–94	31±7	39±6	0.79±0.15	3	12

3.3 Cloud chemistry measurements at Brocken

Numerous investigators have reported data on cloud acidity and chemistry of cloud water collected at mountain sites (*Okita,* 1968; *Falconer* and *Falconer*, 1980; *Weathers et al.*, 1995; *Fuzzi,* 1995 and many others). A Mountain Cloud Chemistry Program (MCCP) was created in eastern North America for an assessment of atmospheric exposure and deposition to high elevation forests because ion deposition may be 2 to 5 times the deposition received due to precipitation (*Mohnen* and *Kadlecek*, 1989; *Saxena et al.*, 1989; *DeFelice* and *Saxena,* 1991 and others). Within the MCCP there were found different mean liquid water contents of clouds at the measurement stations and it was concluded that the observed LWC values at any site were mostly a function of site elevation relative to the cloud base height as well as synoptic meteorological conditions. The European cloud chemistry research was mostly focused on cloud processes, especially activation of cloud condensation nuclei as well as liquid phase chemistry (e.g. S(IV) oxidation in clouds and fog); see, e.g. *Fuzzi* (1995). We started a cloud chemistry program at Mt. Brocken (the first continuously program in Europe) to study the role of clouds in the atmospheric budget of air pollutants, especially to establish a cloud chemistry climatology. We adopted experiences from the MCCP (*Saxena* and *Lin*, 1990; *Mohnen* and *Vong*, 1993). The aim of this section is to present results on different influences on the chemical composition of cloud water to reflect possible changes due to emissions; details concerning LWC variations are given elsewhere (*Wieprecht et al.*, 1995; *Möller et al.*, 1996).

We found much larger differences in the chemical composition of cloud water from event to event (*Table 3*), than it is usual for precipitation water.

Table 3. Mean chemical composition including standard deviation as well as minima and maxima of cloud water collected at Mt. Brocken (in μeq ℓ^{-1})

Year	n[1]	SO_4^{2-}	NO_3^-	Cl^-	NH_4^+	Na^+	Ca^{2+}	Mg^{2+}	H^+
1992	37	331	387	127	391	156	147	40	39
		(±286)	(±374)	(±123)	(±354)	(±191)	(±237)	(±44)	(±67)
		41	21	6	9	<1	10	1	<0.1
		1194	1071	579	1007	854	1311	212	339
1993	1054	265	280	68	410	60	54	26	83
		(±380)	(±445)	(±136)	(±581)	(±141)	(±147)	(±50)	(±138)
		4	0.5	0.3	2	2	3	5	<0.1
		4169	5946	2401	8083	2444	2245	693	1500
1994	1261	293	351	130	435	126	121	39	146
		(±384)	(±512)	(±223)	(±684)	(±236)	(±332)	(±66)	(±246)
		1	0.5	0.3	2	2	3	5	<0.1
		3922	3803	2101	6815	2744	4859	679	2884

[1] number of events (sampling time resolution in 1992) and 1-hour samples since 1993

In principle, there are three different reasons for these variations: (a) differences in the air pollution situation, (b) large scale transport characteristics and (c) dynamic and microphysical characteristics of clouds. For an assessment and understanding the role of clouds in atmospheric chemistry and air pollution it is important to separate between the different reasons that are responsible for the chemical composition of cloud water.

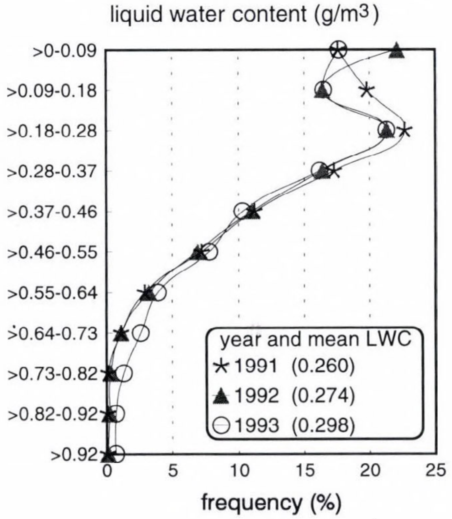

Fig. 7. Frequency of LWC classes of cloud water at the Brocken site.

Fig. 7 shows the frequency distribution of LWC classes for every year since the beginning of the mountain cloud chemistry program. Variations in distribution and in yearly average of LWC are small. The variation of LWC with time during cloud events, however, could be significant. We found different 'types' of LWC behavior: sharp decrease or increase of LWC showing an ending or beginning of the cloud event, small LWC variation within a cloud event, and high LWC fluctuation nearby the cloud base. The chemical composition of samples, representing these 'types', is quite different. We discussed this behavior as an indication for a general physical relationship between LWC and the total ionic content (TIC) of cloud water (*Möller et al.,* 1996).

In *Fig. 8* we show the possible relation between TIC and LWC based on all 1-hour samples of cloud water from non precipitating clouds, neglecting any event connection; TIC represents the sum of liquid phase concentrations of SO_4^{2-}, NO_3^-, Cl^-, NH_4^+, Ca^{2+}, Mg^{2+}, Na^+ and K^+. The best approximation of the relationship ($r = 0.52$) is given by a power function:

$$\mathrm{TIC} = 48599 \times \mathrm{LWC}^{-0.72}, \tag{2}$$

where TIC in μeq ℓ^{-1} and LWC in mg m^{-3}. This phenomenological relation between ionic content of cloud water and liquid water content of the air parcel, discussed here, is one (microphysical) reason for fluctuation of chemical composition. Other reasons, already mentioned above, could be the different air mass characteristics (large-scale transport processes and air pollution situation) and dynamic reasons (cloud type characteristics). Therefore, it should be necessary to classify the cloud chemistry data set not only according to LWC and height of cloud base but also by transport characteristics (3D backward trajectory calculation for each sample or event; first results see in *Acker et al.,* 1995 and *Wieprecht et al.,* 1995) and cloud type. In the next section we show examples for the influence of air pollution characteristics on TIC.

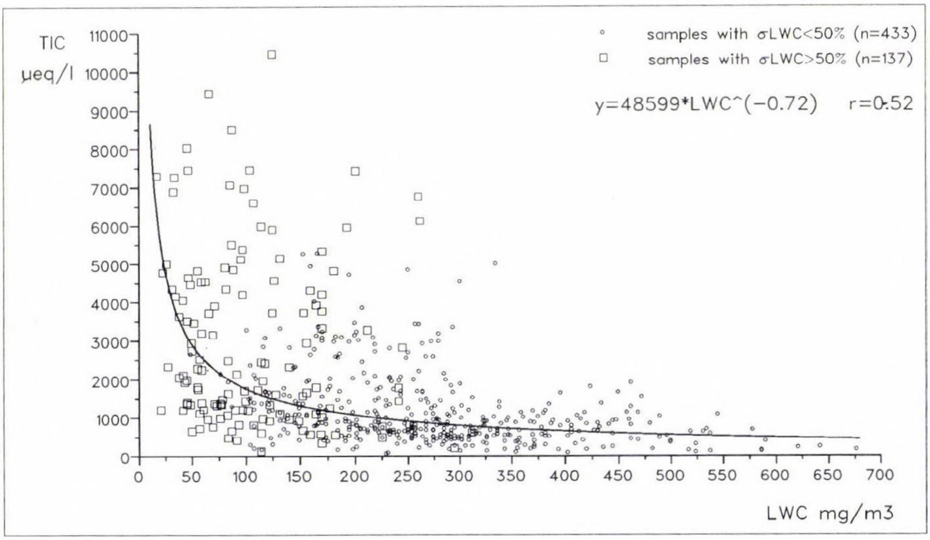

Fig. 8. Relationship between total ionic content (TIC) and LWC for all 1-hour samples collected in 1993 from non-precipitating clouds (n = 570) subdivided into classes of different LWC standard deviation σ.

Table 4 shows the chemical composition of cloud water, TIC and LWC for selected events with different air mass characteristics. It is evident that LWC and the air pollution situation determine the chemical composition in terms of TIC. The events listed in Table 4 are used to present the TIC-LWC relationships for selected cloud events (*Fig. 9*) to explain the scattering of points in

Fig. 8. In principle, the power curve is valid for each single event. The dependence of the liquid water content on time for the cloud event from 30 Sep to 1 Oct 1993 is presented in *Fig. 10.* The sample numbers correspond to points in Fig. 9. Samples from start and end of the cloud event lie in the TIC-LWC diagram at the upper left-hand side. Samples taken during the middle of the cloud event are represented by points in the lower part of the TIC-LWC diagram. The positions of the power curves in Fig. 9, representing different single events however, are different. Neglecting the event connection, it is obvious that the points are scattered around the 'averaged' power curve (cf. Fig. 8).

Table 4. Mean chemical composition (in μeq ℓ^{-1}) and LWC (in mg m^{-3}) for selected events in 1993 with different air mass characteristics

	30.09.-1.10.	21.08.	09.10.	11.10.	05.10.
n	13	9	6	11	10
Cl^-	52±36	36±33	281±282	24±34	27±26
NO_3^-	1038±381	561±329	455±224	110±73	183±146
SO_4^{2-}	1508±564	468±346	450±242	96±91	193±190
NH_4	1596±539	902±771	858±490	150±165	217±267
Na^+	37±25	15±14	324±350	21±29	11±18
Ca^{2+}	423±328	14±17	55±40	9±7	60±86
Mg^{2+}	86±54	3±5	76±79	8±9	11±8
H^+	289±286	236±173	40±78	50±33	97±40
TIC	5036±1851	2477±1417	2540±1642	470±389	858±725
LWC	162±70	274±100	160±147	350±389	166±128
	extreme polluted cloud; origin from Bohemia	typical for prevailing wind directions (270°) crossing industrial areas	example for a typical air mass from western directions with significant maritime influence (high sea salt contribution)	slightly polluted event with air masses from south-western directions	south-western directions; ending period (07.00 to 14.00 MEZ on October 5) of an extreme long cloud event (started 10.00 MEZ on October 3); precipitation before October 5

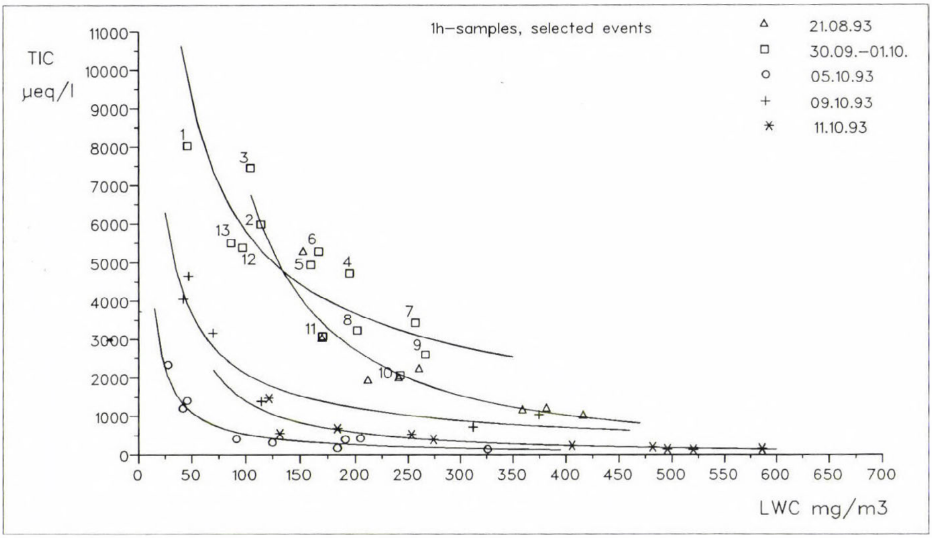

Fig. 9. Relationship between TIC and LWC for selected cloud events (cf. Table 4).

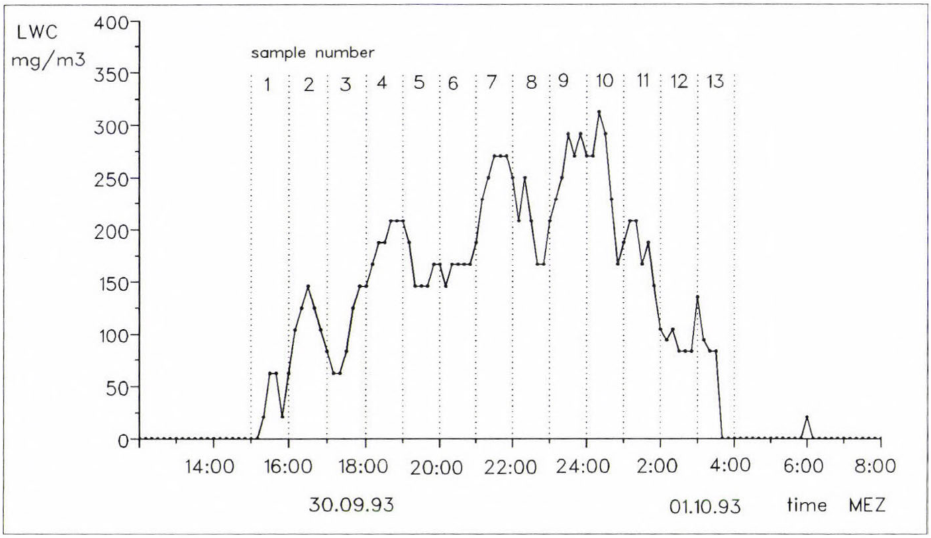

Fig. 10. Time dependent LWC for the cloud event from 30 September to 1 October 1993; sampling time and number of collected samples are marked.

A very important finding is the increase of the yearly average of cloud water acidity at Mt. Brocken, from 1992 until now (Table 3). This is in coherence with the acidification of rainwater, found within the SANA precipitation network (cf. Chapter 3.1). Another interesting result is the bimodal pH distribution of cloud water, see *Fig. 11*. In *Table 5* the main chemical composition of cloud water samples is presented for both pH maximum classes. Reflecting only a part of the whole data set, the largest difference between them can be recognized in the case of calcium, which could be a result of different neutralizing effect of alkaline calcium compounds, e.g., alkaline flue ash from lignite based power plants. No difference can be seen for nitrate for both years. In 1993 the sulfate concentration is significantly higher, however, it seems that sulfate is balanced by ammonium.

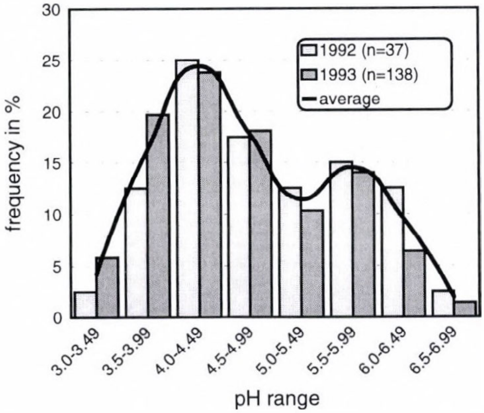

Fig. 11. pH distribution of cloud events.

Table 5. Mean chemical composition of two classes of pH's

Species	pH 4.0 … 4.5		pH 5.5 … 6.0	
	1992 (n = 10)	1993 (n = 44)	1992 (n = 6)	1993 (n = 20)
Cl^-	73	42	77	169
NO_3^-	227	195	294	287
SO_4^{2-}	211	190	200	309
Na^+	93	38	142	157
NH_4^+	267	270	297	462
Ca^{2+}	48	36	107	110
Mg^{2+}	23	18	22	52

4. Conclusions

We have concluded from the results of the SANA precipitation chemistry and the Mt. Brocken cloud chemistry measurement program that long-term sampling is necessary to separate different microphysical, dynamic and air pollution influences on the cloud and rainwater quality. A comparison of the chemical composition of cloud water samples is impossible without information on physical parameters of cloud. We found a relationship between liquid water content (LWC) and the total ionic content (TIC) in clouds, approached by a power function, to be valid for all main chemical species. It appears it is necessary to classify any cloud chemical data set into classes, according to 'LWC type' (σ–LWC < or > 50%), sampling height above cloud-base, cloud type and air mass characteristics.

Because of present and future political and economic changes in Eastern Germany and in Eastern European countries as well, the emission and consequently the concentration are also changing. The yearly magnitude of 'pollution change' (emission-concentration-deposition) amounts more than 10% yr^{-1}, a figure that is much higher than observed anywhere in the world in this short time-scale. We tried to take the advantage of this opportunity within SANA as 'natural simulation experiment' in studying the air chemical processes. Despite of the end of the joint research program SANA in 1995 we strongly feel that scientific monitoring programs in Eastern Europe, using well-equipped and regionally representative stations, would be extremely helpful in the investigation of air pollution and air chemistry problems.

One of the most important findings from the 'atmospheric research part' of SANA is the high increase in atmospheric acidity by about 100% yr^{-1}. It is obvious that this rate, which has never been observed in any other part of the world, could have significant impact on ecosystems. Because of the high complexity of atmospheric chemistry and non-linear relationships between most of trace species, air pollution politics must be changed to consider the emission decrease not only for selected components.

Acknowledgements—This work is a part of the joint research project SANA (Scientific Program on Recovery of the Atmosphere) funded by the *German Ministry for Education and Science* (BMBF). Some results of the present work have been done within the EUROTRAC subproject GCE, also funded by the BMBF. We would like to thank for the financial support.

References

Acker, K., Wieprecht, W., Möller, D. and *Mauersberger, G.*, 1995: Evidence for ozone destruction in clouds. *Naturwissenschaften 82*, 86-89.

Brüggemann, E., Gnauck, Th. and *Rolle, W.*, 1991: Stabilitätsverhalten von ausgewählten anorganischen Spurenstoffen in Niederschlagsproben. *Umweltwiss. und Schadstoff-Forschung 5*, 260-265.

Brüggemann, E. and *Rolle, W.*, 1995: Trends of some components of wet deposition in East

Germany after unification. In *Acid Rain Research: Do we have enough answers?* (eds.: *G. J. Heij* and *J. W. Erisman*). Elsevier Sci. Publ., Amsterdam , 403-406.

DeFelice, T.P. and *Saxena, V.K.*, 1991: The characterization of extreme episodes of wet and dry deposition of pollutants on an above cloud-base forest during its growing season. *J. Appl. Meteor. 30*, 1548-1561.

Falconer, R.E. and *Falconer, P.D.*, 1980: Determination of cloud water acidity at a mountain observatory in the Adirondack Mountains of New York State. *J. Geophys. Res. 85C*, 7465-7470.

Friedrich, R., 1995: *SANA Report on Emissions*. Universität Stuttgart.

Fuzzi, S. (ed.), 1995: *The Kleiner Feldberg Cloud Experiment 1990*. Kluwer Academic Publ., Dordrecht.

Jost, D. and *Beilke, S.*, 1983: Trend saurer Depositionen. *VDI-Berichte 500*, 135-140.

Hedin, L.O., Granat, L., Likens, G.L. Buishand, T.A., Galloway, J.N., Butler, T.J. and *Rodhe, H.*, 1994: Steep decline in atmospheric base cations in regions of Europe and North America. *Nature 367*, 352-354.

Horváth, L. and *Mészáros, E.*, 1984: The composition and acidity of precipitation in Hungary. *Atmos. Environ. 18*, 1843-1847.

Marquardt, W. and *Ihle, P.*, 1988: Acidic and alkaline precipitation components in the mesoscale range under the aspect of meteorological factors and the emission. *Atmos. Environ. 22*, 2707-2713.

Mohnen, V.A. and *Kadlecek, J.A.*, 1989: Cloud chemistry research at Whiteface Mountain. *Tellus 41B*, 79-91.

Mohnen, V.A. and *Vong, R.J.*, 1993: A climatology of cloud chemistry for the eastern United States derived from the cloud chemistry project. *Environ. Rev. 1*, 38-54.

Moldan, B., Veseley, M. and *Bartonova, A.*, 1987: Chemical composition of atmospheric precipitation in Czechoslovakia, 1976-1984 - 1. Monthly samples. *Atmos. Environ. 21*, 2383-2395.

Möller, D., 1990: The Na/Cl ratio in rainwater and the seasalt chloride cycle. *Tellus 42B*, 254-262.

Möller, D. and *Lux, H.* (eds.), 1992: Deposition atmosphärischer Spurenstoffe in der ehemaligen DDR bis 1990. Methoden und Ergebnisse. Band 18 *Schriftenreihe Kommission Reinhaltung der Luft*, Düsseldorf, 1992.

Möller, D., Acker, K. and *Wieprecht, W.*, 1994a: Cloud chemistry at the Brocken in the Harz mountains, Germany. *EUROTRAC Newsletter 12*, 24-29.

Möller, D., Acker, K. and *Wieprecht, W.*, 1994b: Cloud chemistry at Mt. Brocken/Harz. In *Physico-Chemical Behavior of Air Pollutants* (eds.: *G. Angeletti* and *G. Restelli*), Report EUR 15609/2 EN, Brussel 1994, 968-974.

Möller, D., Acker, K. and *Wieprecht, W.*, 1996: A relationship between liquid water content and chemical composition in clouds. *J. Atmos. Res.* (in press).

Okita, T.J., 1968: Concentration of sulfate and other inorganic materials in fog and cloud water and in aerosol. *J. Meteor. Soc. Japan 46*, 120-126.

Reimer, E. and *Scherer, B.*, 1992: An operational meteorological diagnostic system for regional air pollution and long term modeling. In *Air Pollut. Mod. and its Appl.* (eds.: *H. van Dop* and *G. Kallos*), NATO Challanges of Modern Society, *Vol. 17*. Plenum Press, New York, London, 565-572.

Rodhe, H. and *Granat, L.*, 1984: An evaluation of sulfate in European precipitation 1955-1982. *Atmos. Environ. 18*, 2627-2639.

Rodhe, H. and *Rood, M.J.*, 1986: Temporal evolution of nitrogen compounds in Swedish precipitation since 1955. *Nature 321*, 762-764.

Saxena, V.K., Stogner, R.E., Hendler, A.H., DeFelice, T.P., Yeh, R.J.-Y. and *Lin, N.H.*, 1989: Monitoring the chemical climate of the Mt Mitchell State Park for evaluation of its impact on forest decline. *Tellus 41B*, 92-109.

Saxena, V.K. and *Lin, N.H.*, 1990: Cloud chemistry measurements and estimates of acidic deposition on an above cloud base coniferous forest. *Atmos. Environ. 24A*, 329-352.

Weathers, K.C., Lovett, G.M. and *Likens, G.E.*, 1995: Cloud deposition to a spruce forest edge. *Atmos. Environ. 29*, 665-672.

Wieprecht, W., Möller, D., Acker, K. and *Naumann, S.*, 1995: Influence of cloud physical parameters on chemical composition of clouds. In *Air Pollution III*, Vol. 2: *Engineering and Management* (eds.: *H. Power, N. Moussiopoulos* and *C. A. Brebbia*), Comput. Mech. Publ., Southhampton, 199-205.

IDŐJÁRÁS

Quarterly Journal of the Hungarian Meteorological Service
Vol. 100, No. 1–3, January–September 1996

Investigation on polycyclic aromatic hydrocarbons in precipitation over Hungary

Gyula Kiss[1], **Zita Varga-Puchony**[1], **József Hlavay**[2,*] and **Joyce Harris**[3]

[1] *Air Chemistry Group of the Hungarian Academy of Sciences at University of Veszprém,*
P.O. Box 158, H-8201 Veszprém, Hungary
[2] *Department of Analytical Chemistry, University of Veszprém,*
P.O. Box 158, H-8201 Veszprém, Hungary
[3] *NOAA Environmental Research Laboratories,*
325 Broadway, Boulder, CO 80304 USA

(Manuscript received 4 July 1995; in final form 26 January 1996)

Abstract—Concentration of the polycyclic aromatic hydrocarbons (PAHs) was investigated in precipitation samples over Hungary. Naphthalene, phenanthrene, fluoranthene and pyrene were found in the highest concentration (close to or over 100 ng/ℓ) in both rain and snow samples. The phase distribution of the aromatic compounds (vapour phase and particle phase) was studied by analysing filtered precipitation samples and filter extracts. The ratio of the PAHs extracted from the filter (i.e. compounds adsorbed on particles) increased with increasing ring number. The concentration profile of the aromatic hydrocarbons was similar in the precipitation samples. Relationship between concentration of the PAHs and isentropic trajectories was also studied.

Key-words: polycyclic aromatic hydrocarbons (PAHs), precipitation, isentropic trajectories.

1. Introduction

Weather can play an important role in the transport of environmental pollutants. Compounds emitted into the atmosphere may pollute remote areas. This is particularly true for the compounds adsorbed on fine particles that can have atmospheric residence time of 10 days in the absence of wet deposition (*Götz et al.*, 1991). Recently, pollutants of this kind have been used as tracers of anthropogenic activities in a study of long range transport (*Jaffrezo et al.*, 1993).

Polycyclic aromatic hydrocarbons (PAHs) are carcinogenic and/or mutagenic pollutants of anthropogenic origin. They are emitted into the

---

[*] Corresponding author

atmosphere as gases during combustion processes. The non-volatile PAHs (consisting of 4 or more rings) are rapidly condensed or adsorbed onto particles, predominantly onto soot particles having aerodynamic diameter less than 3 μm (*Vo-Dinh,* 1989). The fine particles are removed by wet and, to a lesser extent, dry deposition. The more volatile 2- and 3-ring compounds exist longer in the gas phase before they are washed out by precipitation. Determination of the concentration of the PAHs in precipitation can help to estimate the amount removed by wet deposition.

The concentration of the PAHs in the atmosphere changes periodically over the year as a consequence of the varying emission. In winter rain 2–3 times higher concentration values were observed by *Levsen et al.* (1991) in Hannover than in summer. *Leuenberger et al.* (1988) found 2–10 times higher concentration of PAHs in snow compared to summer rain.

Results of rain and snow analysis in Hungary are discussed in this paper. Relationship between the concentration of the PAHs and isentropic trajectories was also studied.

2. Sampling site

Precipitation was collected at the centre of Veszprém, a town located in the west part of Hungary with approximately 60,000 inhabitants. Both the town and the region are free from major industrial sources, only traffic and heating give the local contribution. Sampling of rain and snow was performed by an automatic wet-only sampler. Precipitation samples were analysed within a few hours after the rain or snow events. Sample preparation by solid phase extraction and liquid chromatographic separation of the PAHs are detailed elsewhere (*Kiss et al.,* 1996).

3. Results and discussion

Several snow and rain samples were analysed in winter of 1994/95 and spring of 1995. During the sample preparation of the first sample the solid phase extraction cartridge became plugged. Therefore the next samples were filtered through a glass fibre filter (cut-off: 2.7 μm) before sample preparation. Results are summarized in *Table 1*. The concentration of the PAHs in the filtered precipitation samples ranged from 2 ng/ℓ to 830 ng/ℓ. Naphthalene was present in the highest concentration (470 ng/ℓ to 830 ng/ℓ) what can be explained with its relatively high volatility and water solubility. The concentration of phenanthrene, fluoranthene and pyrene was found close to or over 100 ng/ℓ, while the concentration of the other 3–6-ring compounds was usually less than 20 ng/ℓ. It can also be observed that the concentration of a given compound was similar in the precipitation samples. The comparable concentration profile of the PAHs refers to their similar origin (mainly heating and traffic).

Table 1. Concentration of PAHs in filtered rain and snow samples in winter (ng/ℓ)

Date	01.18.95.	01.19.95.		01.27.95.	02.17.95.		03.02.95.	
		morning	afternoon		filtered water	filter extract	filtered water	filter extract
Type of sample	snow	snow	snow	rain	rain	rain	rain	rain
	1	2	3	4	5	6	7	8
naphthalene	610	470	830	n.q.	590	n.d.	670	n.q.
fluorene	20	31	23	23	21	n.q.	22	n.q.
phenanthrene	100	130	120	90	120	10	100	8.6
anthracene	4.3	6.3	4.3	6.7	3.7	n.q.	2.0	n.q.
fluoranthene	100	150	78	44	210	20	72	18
pyrene	120	89	62	n.q.	140	50	77	25
benzo[*a*]anthracene	n.q.	n.q.	n.q.	n.q.	n.q.	n.q.	n.q.	n.q.
chrysene	12	10	10	6.1	12	12	6.7	5.0
benzo[*b*]fluoranthene	30	15	11	11	11	13	7.8	3.5
benzo[*k*]fluoranthene	11	3.5	n.q.	2.4	3.4	4.6	2.0	1.1
benzo[*a*]pyrene	10	10	6.0	7.5	2.2	2.5	5.3	1.3
dibenz[*a,h*]anthracene	7.1	3.5	n.q.	3.6	5.3	6.0	n.q.	n.q.
benzo[*g,h,i*]perylene	20	15	12	16	26	19	15	4.4

n.q. = detected but not quantitated

n.d. = not detected

The heavy snowfall on 19 February made two analyses possible. Lower concentration values were found in the snow sample collected in the afternoon (column 3) than in the the sample collected in the morning (column 4). This results from the partial cleaning of the air by the continuous snowfall.

In case of the samples collected on 17 February and 2 March the extraction of the filters (columns 6 and 8) was performed in addition to the analysis of the filtered rain samples (columns 5 and 7) to get information about the phase distribution of the PAHs (solution phase and particle phase). Due to their low vapour pressure, low polarity and low water solubility, the PAHs exhibit a strong adsorption affinity on airborne particles. In winter naphthalene and fluorene are present in vapour phase, the other PAHs can be found in both vapour phase and adsorbed on particles. This tendency can be observed if the results of analyses of filtered rain water and filter extract are compared. The ratio of the PAHs extracted from the filter (i.e. compounds adsorbed on particles) increases with increasing ring number. E.g., while naphthalene could be detected only in solution, more than half of dibenz[*a,h*]anthracene was found in the filter extract.

After these experiments the precipitation samples were analysed without filtration. Results are shown in *Table 2*. The concentration of the PAHs in unfiltered samples ranged from 2 ng/ℓ to 1200 ng/ℓ. Since the compounds adsorbed on particles were not filtered out in this case, somewhat higher values were obtained. Similar results were obtained in Dübendorf, Switzerland (*Leuenberger et al.*, 1988). The concentration of the individual PAHs in the precipitation samples usually varied in a narrow range except some events (e.g. concentration of benzo[*g,h,i*]perylene ranged from 14 ng/ℓ to 37 ng/ℓ except 15 March when it was significantly higher). The outlying results can be explained with the different origin of the air masses. The transport of aerosols in the atmosphere can be traced by isentropic trajectories. The trajectories to K-puszta (KPO — situated approximately 100 km far from Veszprém) were available, therefore these data were used for the interpretation of the analytical results.

The trajectories to K-puszta on 6 March and 15 March in 1995 are depicted in *Fig. 1* and *Fig. 2*, respectively. These trajectories were chosen because of the significantly different PAH content of the precipitation samples. Numbers on the lines in Fig. 1 show that the air masses advanced over the Mediterranean Sea 2–4 days earlier and arrived in Hungary from the south. The heavy rains over the Mediterranean Sea washed out most of the pollutants. This is reflected in the low concentration values found in the rain sample on 6 March.

On the contrary, the highest concentrations of the 4–6-ring PAHs were detected in the snow sample of 15 March. The trajectories in Fig. 2 show that these air masses arrived from the east, transporting pollutants of anthropogenic origin. The high level of pollution can be explained with both the high surface of the snowflakes and the lack of precipitation along the trajectory.

Table 2. Concentration of PAHs in unfiltered rain and snow samples in winter (ng/ℓ)

Date	02.19.95.	02.23.95.	02.26.95.	03.06.95.	03.15.95.	03.16.95.	03.18.95.	03.21.95.	03.27.95.
Type of sample	rain	rain	rain	rain	snow	snow	rain	rain	rain
	1	2	3	4	5	6	7	8	9
naphthalene	980	730	530	570	1100	700	1200	560	600
fluorene	67	20	34	26	35	20	35	58	31
phenanthrene	460	130	210	140	110	91	130	160	100
anthracene	3.9	2.7	4.9	3.0	6.3	2.7	3.6	6.3	3.6
fluoranthene	270	130	180	72	140	100	73	120	120
pyrene	180	230	200	76	200	140	130	170	140
benzo[*a*]anthracene	n.q.	n.q.	2.5	n.q.	2.8	n.q.	n.q.	n.q.	n.q.
chrysene	22	50	32	8.4	73	22	14	32	29
benzo[*b*]fluoranthene	9.5	40	17	8.7	59	23	15	32	21
benzo[*k*]fluoranthene	2.3	14	6.1	2.1	19	7.0	4.9	10	7.3
benzo[*a*]pyrene	2.0	7.5	4.5	2.4	8.0	5.0	8.6	6.4	7.4
dibenz[*a*,*h*]anthracene	7.3	n.q.	n.q.	n.q.	n.q.	n.q.	n.q.	n.q.	n.q.
benzo[*g*,*h*,*i*]perylene	23	37	14	n.q.	79	18	15	26	23

n.q. = detected but not quantitated

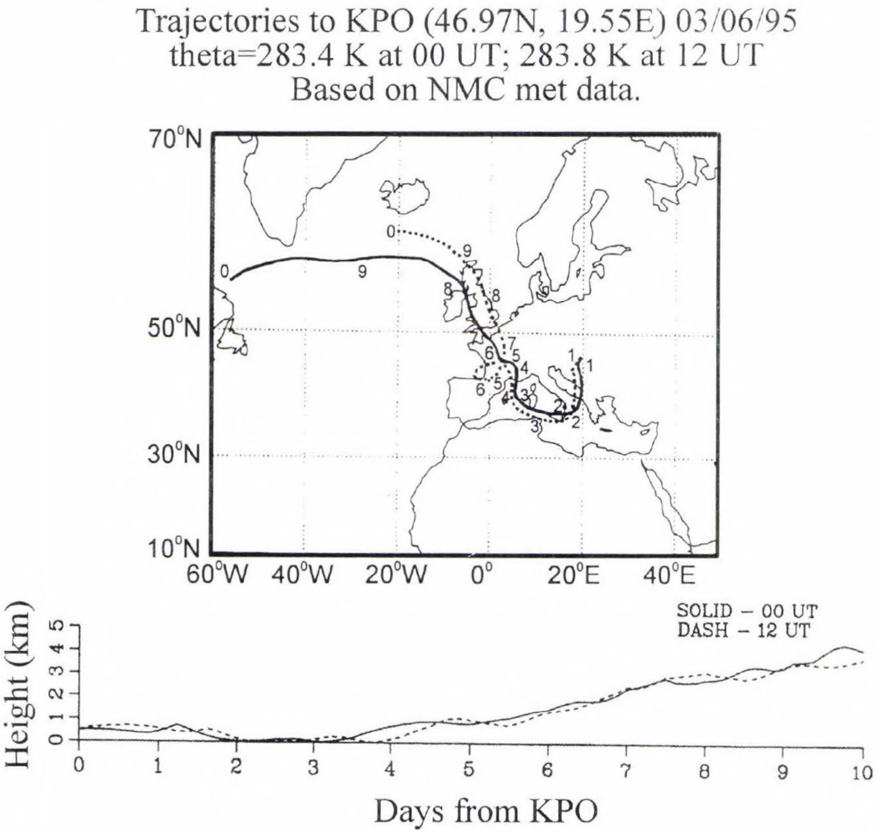

00 UT

Day	km	hPa	°C
0	0.5	944	6
1	0.4	955	9
2	0.0	1009	14
3	0.0	1024	14
4	0.7	933	3
5	0.8	926	4
6	1.5	858	-2
7	2.4	757	-11
8	2.8	704	-17
9	3.3	649	-23
10	4.1	583	-30

12 UT

Day	km	hPa	°C
0	0.5	944	6
1	0.6	937	5
2	0.1	995	14
3	0.1	1001	14
4	0.1	1006	12
5	1.0	903	3
6	1.4	873	0
7	2.5	753	-11
8	3.1	676	-19
9	3.4	640	-23
10	3.7	612	-27

Fig. 1. Trajectories to K-puszta on 6 March, 1995.

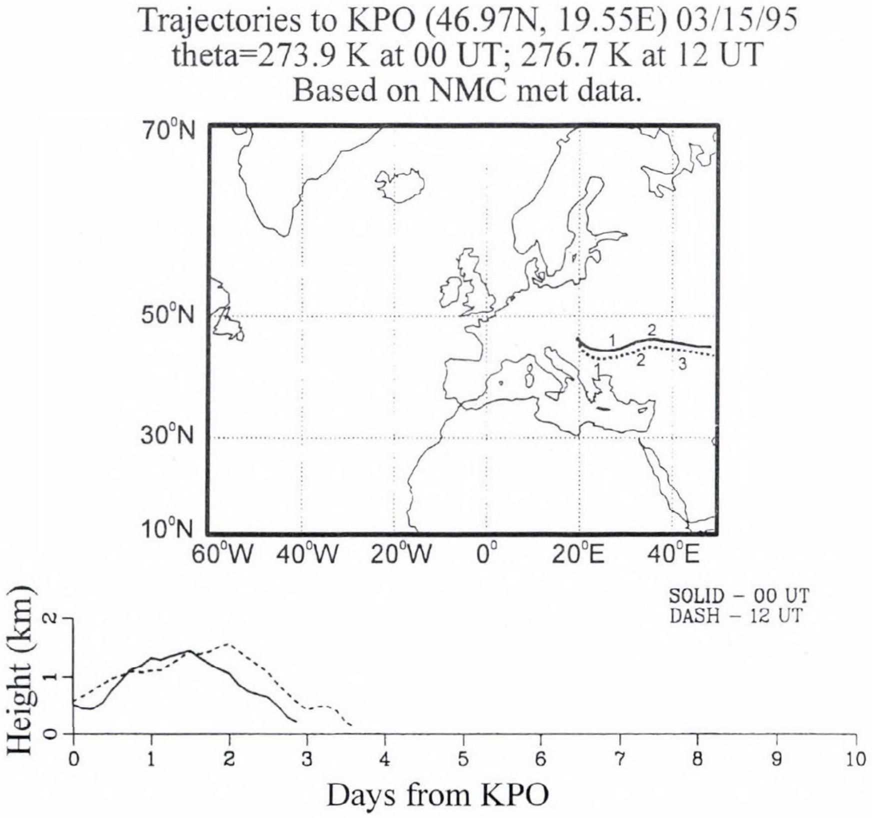

00 UT

Day	km	hPa	°C
0	0.5	949	-4
1	1.3	871	-10
2	1.1	899	-8

12 UT

Day	km	hPa	°C
0	0.6	940	-1
1	1.1	886	-6
2	1.6	842	-10
3	0.4	969	1

Fig. 2. Trajectories to K-puszta on 15 March, 1995.

4. Conclusion

Analysis of rain and snow samples showed that the concentration of polycyclic aromatic hydrocarbons ranged from 2 ng/ℓ to 1200 ng/ℓ in precipitation over Hungary. Compounds with higher water solubility (e.g. naphthalene, phenanthrene, fluoranthene and pyrene) were found in concentration close to or over 100 ng/ℓ while the concentration of the other aromatic compounds was usually less than 20 ng/ℓ. Good agreement was found between the concentration of PAHs and meteorological data. The concentration profile of the PAHs in the precipitation samples did not change substantially in the observed period. This is caused by the similar origin of the pollutants and the mixing processes in the atmosphere. Since PAHs may reach atmospheric residence time of ten days, the pollutants can be transported over thousands of kilometres. During this time polluted air masses can be diluted or originally clean air may become polluted. As a consequence, the concentrations of PAHs determined in precipitation are similar in most cases. This is reflected by the fact that the concentration of the PAHs in precipitation samples over Hungary was similar to the values measured elsewhere in Europe.

This study will be extended to other factors such as the intensity and location of precipitation along the trajectory to identify the main factors influencing the concentration of PAHs in precipitation.

Acknowledgements—The financial supports of the World Bank for the HPLC instrument and the Hungarian National Science Foundation, OTKA 16315 and F 16262 are gratefully acknowledged.

References

Götz, G., Mészáros, E. and *Vali, G.*, 1991: *Atmospheric Particles and Nuclei.* Akadémiai Kiadó, Budapest.

Jaffrezo, J.-L., Masclet, P., Clain, M.P., Wortham, H., Beyne, S. and *Cachier, H.*, 1993: Transfer function of polycyclic aromatic hydrocarbons from the atmosphere to the polar ice I. *Atmospheric Environment 27A,* 2781-2789.

Kiss, Gy., Varga-Puchony, Z. and *Hlavay, J.* 1996: Determination of polycyclic aromatic hydrocarbons in precipitation using solid phase extraction and column liquid chromatography. *J. Chromatogr. 725,* 261-272.

Leuenberger, C., Czuczwa, J., Heyerdahl E. and *Giger, W.*, 1988: Aliphatic and polycyclic aromatic hydrocarbons in urban rain, snow and fog. *Atmospheric Environment 22*, 695-700.

Levsen, K., Behnert, S. and *Winkler, H.D.*, 1991: Organic compounds in precipitation. *Fresenius J. Anal. Chem. 340,* 665-671.

Vo-Dinh, T., 1989: *Chemical Analysis of Polycyclic Aromatic Compounds.* John Wiley & Sons, New York.

IDŐJÁRÁS
Quarterly Journal of the Hungarian Meteorological Service
Vol. 100, No. 1-3, January-September 1996

Sulfur in the Siberian atmosphere

A. Ryaboshapko, S. Gromov and **S. Paramonov**

Institute of Global Climate and Ecology,
20-b, Glebovskaya, Moscow, 107258, Russia

(Manuscript received 6 June 1995; in final form 6 November 1995)

Abstract—A significant part of anthropogenic sulfur emitted into the atmosphere of European industrial regions is transported to the Asian part of Russia. On the other hand, there are a lot of anthropogenic sulfur sources in Siberia itself, and emissions here tend to rise. By 1990s the total sulfur emission here was 3.4 Tg/year. The emission field is very uneven. Only one point source of sulfur dioxide provides annual emission of 1.1 Tg sulfur. So, Siberia can be not only the sink but also the source of atmospheric sulfur for the north-western Pacific region. Generalization of monitoring data for last years shows that about 8 Tg of sulfur are removed from the atmosphere over Siberia annually. Main part of this sulfur is removed by wet deposition. The highest sulfur concentrations in air and precipitation are characteristic for industrialized areas of south-western Siberia. At the same time unpredictable high concentrations of excess sulfur in precipitation are observed over Pacific coast areas. The lowest sulfur concentrations can be found in the north-eastern regions of Siberia. Seasonal and long-term variations of atmospheric sulfur in Siberia are discussed.

Key-words: sulfur, emission, concentrations, deposition, long-term variations.

1. Introduction

For the purposes of the present work, the term 'Siberia' refers to Russian Siberia proper, the whole of Kazakhstan, and Russian Far East. Siberia is vital for the atmospheric budgets of various substances as a sink and source of atmospheric constituents, however, from the viewpoint of atmospheric chemistry it is still a virtual blank space on the globe. Siberia is especially important for understanding the fate of anthropogenic substances emitted into the European atmosphere since they are mainly transported eastward by air flows. Besides, Siberia is interesting as a source of pollutant input to the Pacific Ocean. Knowledge of sulfur sources into the Siberian atmosphere, of its content in ambient air and precipitation is necessary to construct global climate models (*Langner et al.*, 1993).

The selection of sulfur can be accounted for by two factors: (1) sulfur compounds are believed to be a major reason for acidification; (2) it is the sulfur on that we have accumulated the largest amount of reliable information in this part of the world. The contribution of marine sulfur to the continental atmosphere is rather small. Besides, the Siberian atmosphere contains significant amounts of sodium, calcium and nonmarine chloride, therefore a conventional method for calculating 'excess' sulfur is loaded with significant mistakes. So, we use here 'total sulfur' in the atmosphere and precipitation.

2. Sulfur sources into Siberian atmosphere

Volcanic phenomena in the eastern edge of the region (Kamchatka Peninsula, Kurils), release of reduced (DMS-type) compounds from soils, transport of sea salt sulfate from the marine atmosphere (especially in the east), and aeolian emission of soil sulfate are probably the most important natural sources of sulfur into the Siberian atmosphere. The volcanic impact is likely to be insignificant since active volcanoes are not numerous and continuously released fumarole gases are mainly transported to the Pacific Ocean. However, rather rare volcanic eruptions can result in sulfur emissions in excess of 1 Tg within a few days (*Abramovsky et al.*, 1977). Assuming the reduced sulfur input into the Earth's continental atmosphere of 20 Tg/yr (*Brimblecombe* and *Lein*, 1989) and a similar emission intensity in all terrestrial zones (except Antarctica), the input to the Siberian atmosphere should be about 2 Tg S/yr as reduced compounds. Taking into account the global atmosphere circulation pattern, it can be assumed that the transport to Siberia does not exceed 2 per cent of 20 Tg/yr of sea salt sulfur globally transported from the marine atmosphere to the continent (*Brimblecombe* and *Lein*, 1989), i.e. it is no more than 0.4 Tg/yr. Aeolian emission of soil sulfate is practically unquantifiable though it can be stated a priori that for South-west Siberia (arid zones in Kazakhstan) the contribution of the source is quite significant.

Anthropogenic sulfur can be injected into the Siberian atmosphere both from the adjacent industrialized regions (mostly from Europe) due to advection and from Siberian sources. EMEP's models (*Afinogenova et al.,* 1992) estimate the annual sulfur transport from Europe as 0.76 Tg (mean estimate for 1987-1991). Import from sources over the Ural region cannot exceed 0.5 Tg S/yr. The global atmosphere circulation pattern allows to assume that advection from Mongolia, China, Korea and Japan is quite insignificant.

The distribution of anthropogenic sulfur emissions over Siberia is rather inhomogeneous (*Fig. 1*). Most sources are concentrated between 50° and 55°N. The most intensive point source not only for Siberia, but for the whole world (1.12 Tg/yr) is located in the city of Norilsk (69°N, 88°E). The atmospheric sulfur emission in Siberia is growing rather rapidly: at the beginning of the 20th century it was 0.016 Tg/yr; before World War II it amounted to 0.13 Tg/yr; by the early 1990s it exceeded 3 Tg/yr. It can be assumed that the rapid emission growth will continue in the next decade since the resource base and industrial potential of the region are growing steadily.

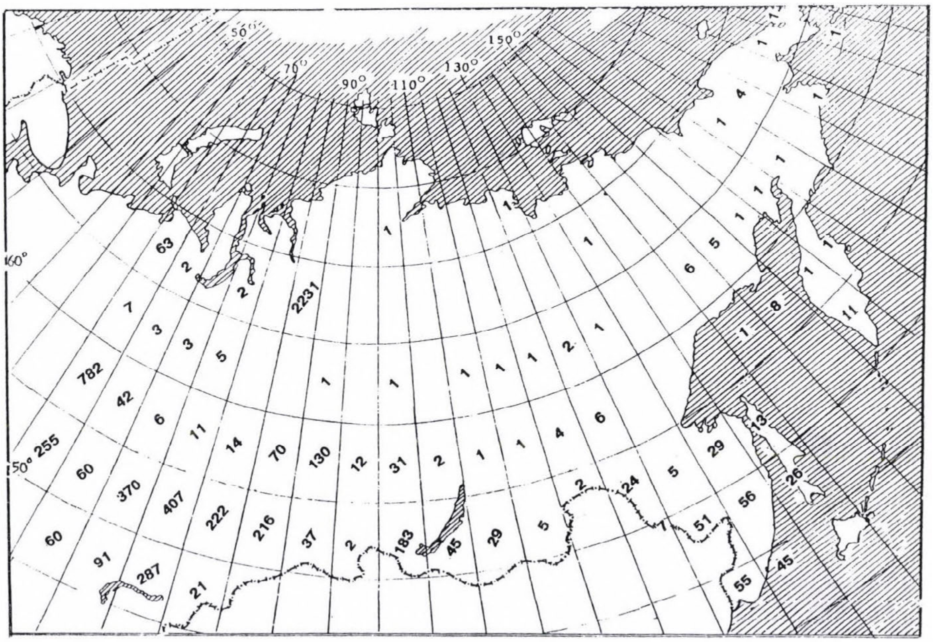

Fig. 1. The distribution of anthropogenic sulfur emissions over Siberia for 1990, in kT (SO_2)/yr.

3. *Monitoring stations and programmes*

Systematic precipitation chemistry observations were initiated in Lake Baikal region in the 1950s. By the early 1990s, the number of regular precipitation sampling sites in the given area amounted to a hundred, however, their distribution is rather nonuniform (*Fig. 2*). Most of them are located in the southern part of Asian Russia and North-eastern Kazakhstan while the vast area of Kazakh semi-deserts and North-eastern Siberia are not covered by observations at all. In addition, only one-third of the stations can be referred to background sites. Precipitation samples are collected either on a monthly or on a 10-day basis. Only two stations whose location is shown in Fig. 2 conduct regular (in general every day) observations of the atmospheric concentrations of sulfur dioxide and particulate sulfate.

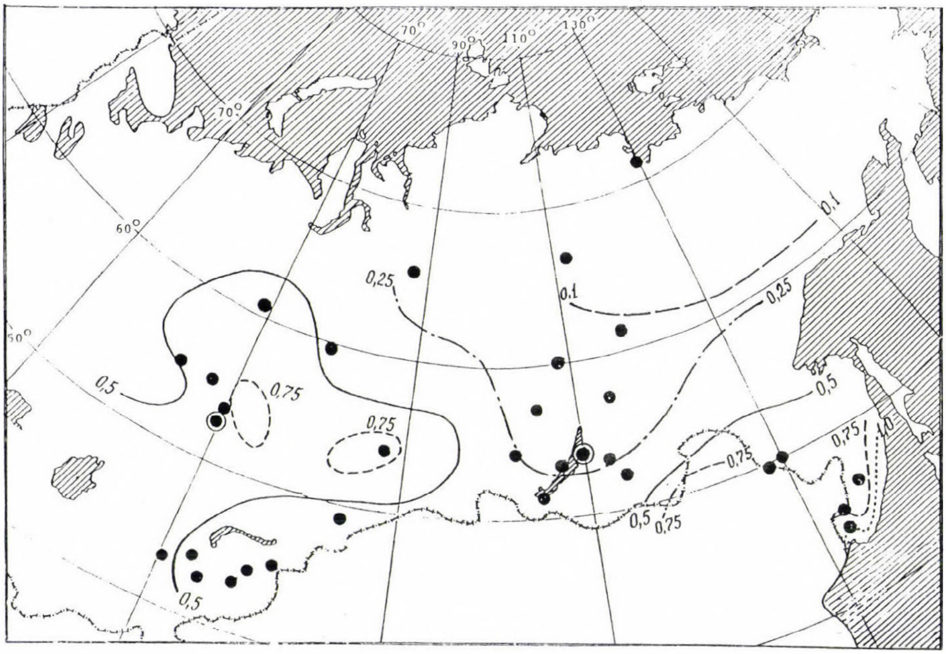

Fig. 2. Monitoring network and spatial distribution of wet sulfur deposition, g S/m^2/yr; ● precipitation chemistry, ◉ air and precipitation chemistry.

4. Sulfur in precipitation

Variability of sulfur concentrations observed at individual, even nearby stations is rather high depending on both the degree of anthropogenic impact on atmospheric chemistry and physico-geographical conditions. For instance, with concentrations over Siberia as a whole varying between 0.5 and 2 mg S/ℓ, the mean annual value in the city of Norilsk was 51 mg S/ℓ in 1990. Nevertheless, some regional peculiarities of sulfur deposition with precipitation can be identified.

The highest mean sulfur concentrations in precipitation are observed over Kazakhstan which can be accounted for by an intensive aeolian weathering of sulfur-bearing solonchak soils, on the one hand, and relatively little precipitation, on the other. The lowest concentration and deposition levels are typical for North-east of Siberia where natural and anthropogenic sulfur sources into the atmosphere are practically absent. It is impossible to explain rather high concentration and deposition values in the Far East as affected by the Pacific Ocean. There are no significant anthropogenic sources here, the contribution of the sea salt (in terms of sodium and chlorine) does not exceed 15%, and however sulfur concentrations in precipitation are unexpectedly high. Sizeable wet precipitation, especially in the period of marine air mass arrival, results in a relatively large sulfur deposition with precipitation.

The spatial distribution of wet sulfur deposition for 1990 is shown in Fig. 2. We estimate total sulfur deposition over Siberia as 8.6 ± 3.5 Tg/yr.

Nonuniform anthropogenic emissions during the yearly and seasonal changes in cloud formation conditions cause a significant seasonal variability of sulfur concentrations and deposition with precipitation. Continental areas in Siberia are characterized by a spring concentration maximum (the Turukhansk station, *Fig. 3*). The situation in the Pacific coast areas is drastically different: a marked winter concentration maximum and summer deposition minimum. Let us note that it is in summer that most precipitation events occur here when wet oceanic air masses are transported to the continent.

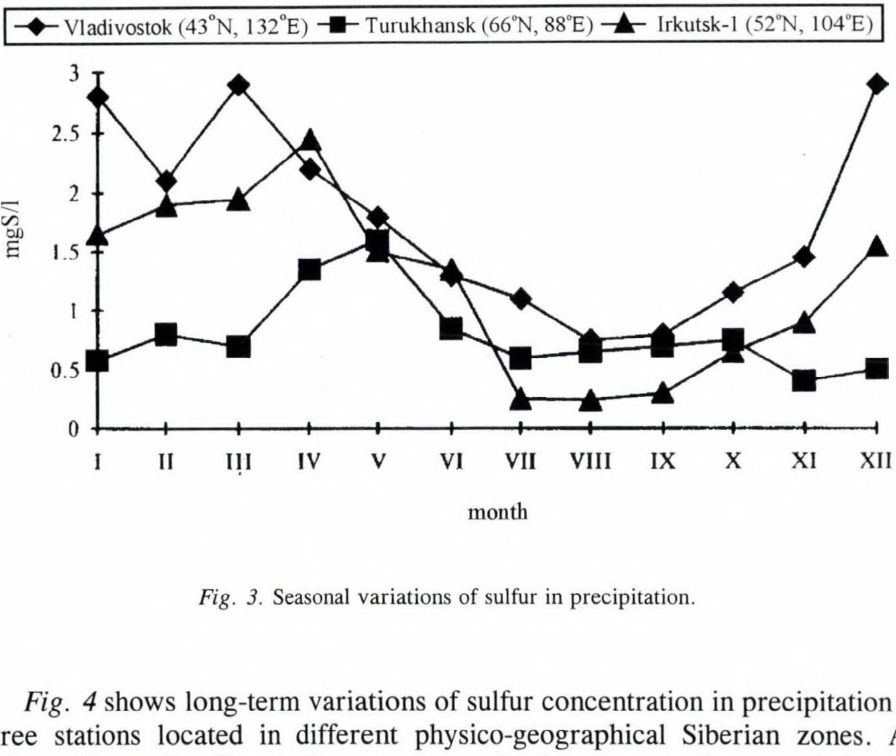

Fig. 3. Seasonal variations of sulfur in precipitation.

Fig. 4 shows long-term variations of sulfur concentration in precipitation at three stations located in different physico-geographical Siberian zones. As follows from the figure, long-term trends do not reveal any relation to anthropogenic emission growth in the USSR in the 1960s–1970s.

Data from *Svistov* and *Zaitsev* (1991) indicate that precipitation over the greater part of Siberia is either neutral or weakly alkaline. Mean annual pH varies from 5.5 in the north-west to 6.5 in the central and eastern areas. Arid zones in Kazakhstan are characterized by markedly alkaline precipitation, mean pH ranging from 6 to 7. Thus, it can be definitely stated that there is no large scale precipitation acidification over Siberia in spite of relatively high sulfur concentrations in precipitation.

Atmospheric sulfur concentrations in terms of sulfur dioxide and particulate sulfate were systematically measured only at two Siberian stations: Borovoe (53°N, 70°E) and Barguzin (54°N, 109°E). *Table 1* presents mean concentrations over the whole observation period (1980–1992).

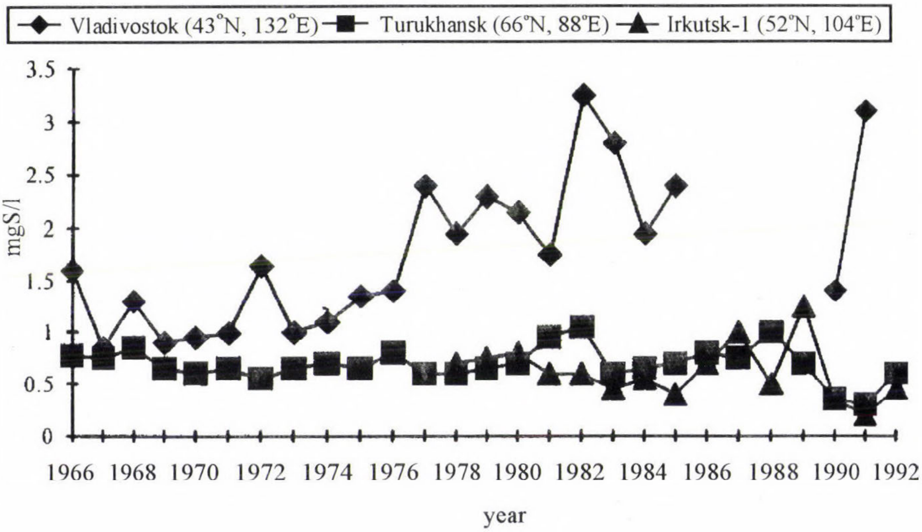

Fig. 4. Long-term variations of sulfur in precipitation.

It follows from Table 1 that atmospheric sulfur concentrations in western Siberia exposed to polluted air mass advection from Europe are noticeably higher than in central Siberia.

Table 1. Air sulfur concentrations over Siberia, 1980–1992; $\mu gS/m^3$

Station	SO_2			SO_4		
	Mean	Median	Geom.mean	Mean	Median	Geom.mean
Borovoe	1.94	0.70	0.83	1.15	0.89	0.80
Barguzin	0.33	0.04	0.05	0.48	0.37	0.31

The concentrations of sulfur dioxide and sulfate have strong seasonal variations (see *Fig. 5*). Sulfur dioxide is characterized by a December-February concentration maximum whereas the concentration maximum for sulfate is shifted to early spring.

Assuming roughly that concentrations observed at Borovoe are typical for western Siberia and those observed at Barguzin are typical for eastern Siberia and taking that the mean annual rate of dry uptake is 0.005 m/s for sulfur dioxide and 0.002 m/s for sulfate, dry sulfur deposition over Siberia would be 3.6 Tg/yr. It is a very rough estimate and to make it more accurate one should establish at least ten stations in Siberia.

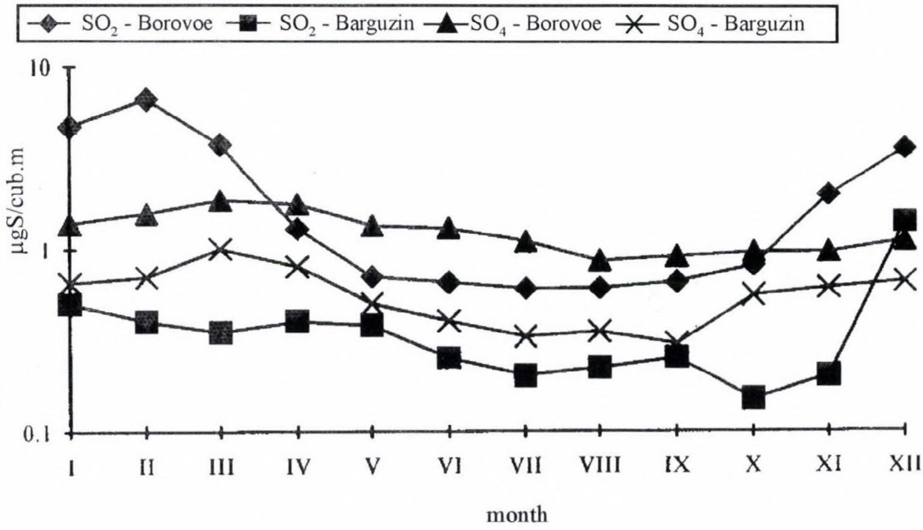

Fig. 5. Seasonal variations of SO_2 and SO_4^{2-} in air.

5. *Conclusions*

Conclusions can be presented as *Table 2* which shows our knowledge and gaps with respect to major sulfur budget items in Siberia.

As follows from Table 2, total atmospheric sulfur sinks in the region exceed 12 Tg/yr. Total known sources are much less. It means that there should be an additional sulfur input to the Siberian atmosphere of about 7 Tg/yr from so far unquantified sources.

Table 2. Atmospheric sulfur budget elements in Siberia, Tg/yr

Sources:	
- natural (reduced sulfur)	2
- volcanic activity	?
- aeolian emission of soil sulphate	?
- marine sulphate sulfur input	0.4
- anthropogenic activity in Siberia	3.1
- anthropogenic sulfur advection from the west	1.3
- advection from the south, north and east	?
Sinks:	
- wet deposition	8.6
- dry deposition	3.6
- advection beyond Siberia	?

References

Abramovsky, B., Alimov, V., Ionov, V., Nazarov, I., Patrakeev, S., Fedotov, S. and *Chirkov, V.*, 1977: Atmospheric emission of gaseous and aerosol eruption products from the Tolbachek Volcano (Kamchatka) (in Russian). *Doklady akademii nauk 37*, 1479-1482.

Afinogenova, O., Dedkova, I., Galperin, M., Grigoryan, S. and *Subbotin, S.*, 1992: *Transboundary transport of airborne sulphur and nitrogen compounds in Europe 1987, 1988, 1989, 1990, 1991. EMEP/MSC-E, Report 1/92*, Moscow.

Brimblecombe, P. and *Lein, A.*, 1989: *Evolution of the Global Biogeochemical Sulfur Cycle. SCOPE-39*. J. Wiley and Sons, Chichester.

Langner, J., Bates, T.S., Charlson, R.J., Clarce, A.D., Durkee, P.A., Gras, J., Heintzenberg, J., Hofmann, D.J., Huebert, B., Leck, C., Lelieveld, J., Ogren, J.A., Prospero, J., Quinn, P.K., Rodhe, H. and *Ryaboshapko, A.G.*, 1993: The global atmospheric sulphur cycle: An evaluation of model predictions and observations. *Report CM-81*. Department of Meteorology, Stockholm University. International Meteorological Institute in Stockholm.

Svistov, P. and *Zaitsev, A.* (eds.), 1991: *Acidity of Atmospheric Precipitation over the USSR Territory* (in Russian). Main Geophysical Observatory, St. Petersburg.

IDŐJÁRÁS

Quarterly Journal of the Hungarian Meteorological Service
Vol. 100, No. 1–3, January–September 1996

Contribution of car exhaust to the non-methane hydrocarbon burden of the air in Budapest

László Haszpra

Institute for Atmospheric Physics,
H-1675 Budapest, P.O. Box 39, Hungary

(Manuscript received 7 June 1995; in final form 13 December 1995)

Abstract—The maximum potential contribution of car exhaust to the non-methane hydrocarbon burden of the air in Budapest is estimated on the basis of direct atmospheric and exhaust gas measurements using a version of the chemical mass balance source reconciliation technique. The maximum potential contribution of this source was found 37–39wt%. Attention is called to the relatively high, non exhaust originated ethene and ethane content of the air, the sources of which should be identified by further research.

Key-words: vehicle emission, non-methane hydrocarbon, air quality.

1. Introduction

Summer measuring campaigns carried out in 1987–1989 indicated that the non-methane hydrocarbon (NMHC) burden of the air in Budapest is rather high (*Haszpra et al.*, 1991). There are at least two reasons why their concentrations and sources must be studied: (i) some of them are noxious (e.g. benzene); (ii) they play a key role in the photochemical oxidant formation in the troposphere, which seriously endangers the environment and human health.

For the elaboration of an efficient NMHC control strategy, their sources have to be known well. At the time of the preparation of the present paper a detailed NMHC emission inventory was not available for Budapest (*Bozó* and *Baranka*, 1994), while the accessible unpublished inventories were contradictory. In addition, during the compilation of an emission inventory the emission factors (specific emission expressed as mass of pollutant emitted per kilometre driven, per mass of fuel burned, per amount of energy produced, per mass of product produced, etc.) taken from the international literature have to be considered with caution. They may not be representative of Budapest having, for example, a car fleet different from that of those cities for which the emission factors have been determined (*Haszpra* and *Szilágyi*, 1994a; *Haszpra* and *Szilágyi*, 1994b).

As in most industrialized countries, the vehicular related emission is one of the largest anthropogenic sources of NMHC in Hungary (*Molnár*, 1990; *Veldt*, 1991). The vehicular related emission involves the direct tailpipe emission (exhaust gas), the hot soak emission and the NMHC release during gasoline distribution, and refuelling (headspace emission, gasoline spillage). Each kind of emissions requires different control techniques. In the present paper the maximum potential contribution of the direct tailpipe emission to the total NMHC emission for Budapest is estimated. In this context the maximum potential contribution means a theoretical upper limit for the contribution of the direct tailpipe emission to the total NMHC emission of the city. The estimation is based on direct atmospheric measurements carried out in Budapest and on the chemical mass balance source reconciliation technique. The results show the maximum possible improvement in the NMHC pollution of the air in Budapest which might be achieved if 100% of the car fleet used three-way catalytic converters, and they were 100% efficient, which is an obvious overestimation. The results may be useful as input data for a model estimating the potential improvement in the photochemical oxidant formation in the city and in the urban plume.

2. Database for the estimation

In summer 1987, 1988 and 1989, in the context of a photochemical air pollution study, the Institute for Atmospheric Physics and the Central Research Institute for Chemistry, both in Budapest, measured the atmospheric concentration of non-methane hydrocarbons. Two stationary measuring sites were set up for the study: Site 1 at the border of the downtown area, approximately 3 km away from the centre of the city, and Site 2 directly downtown (operational only in 1988) (*Fig. 1*). Both measuring platforms were located at roof-top (approx. 20 m above the street level), above the top of the neighbouring buildings to increase the spatial representativeness of the measurements. As the investigation of photochemical air pollution was the primary aim of the study, all the samples were taken on calm, sunny working days in the morning hours. The samples were analyzed for C_2–C_8 hydrocarbon species.

During the periods of 17 August–2 September, 1987, 5 July–18 August, 1988, as well as 10–25 July, 1989, 118 spot samples were taken at Site 1 and 62 samples at Site 2 (operational only in 1988). The measuring program, its primary results and the analytical technique applied are described in details by *Haszpra et al.* (1991). For the present study the 20 most abundant species have been chosen. The averaged NMHC composition of these species is presented in *Fig. 2*. The speciation is given in the figure in weight percentage (wt%) of the total weight of the 20 species considered. On average, total concentrations of the species considered are 135 $\mu g/m^3$ and 164 $\mu g/m^3$, respectively.

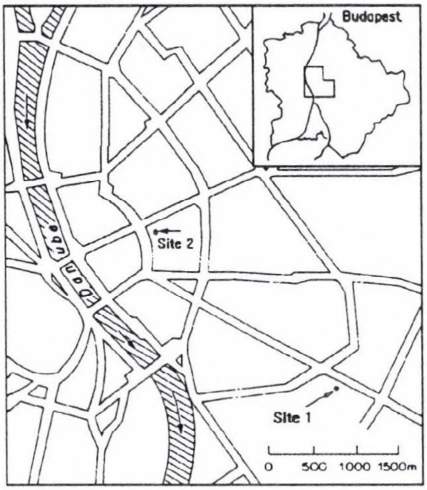

Fig. 1. The location of the sampling sites.

The averaged tailpipe NMHC emission profile (*Fig. 3*) was determined during a one-day roadway tunnel experiment in Budapest in 1991 (*Haszpra* and *Szilágyi*, 1994b). The sampling and analytical technique were identical in both projects.

As the tailpipe emission depends on the ambient temperature (*Stump et al.*, 1989; *Stump et al.*, 1992) it should be emphasised that both projects were performed in summertime.

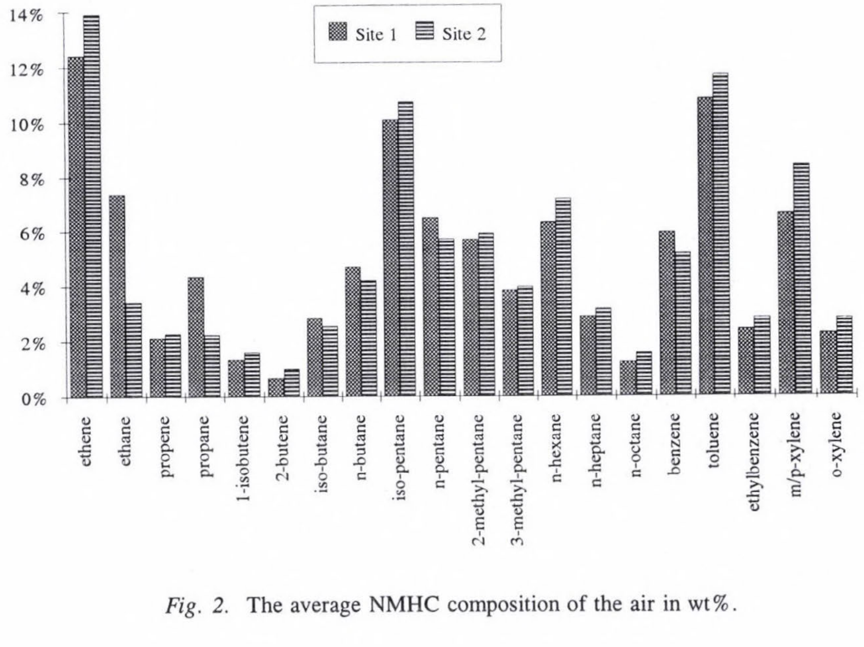

Fig. 2. The average NMHC composition of the air in wt%.

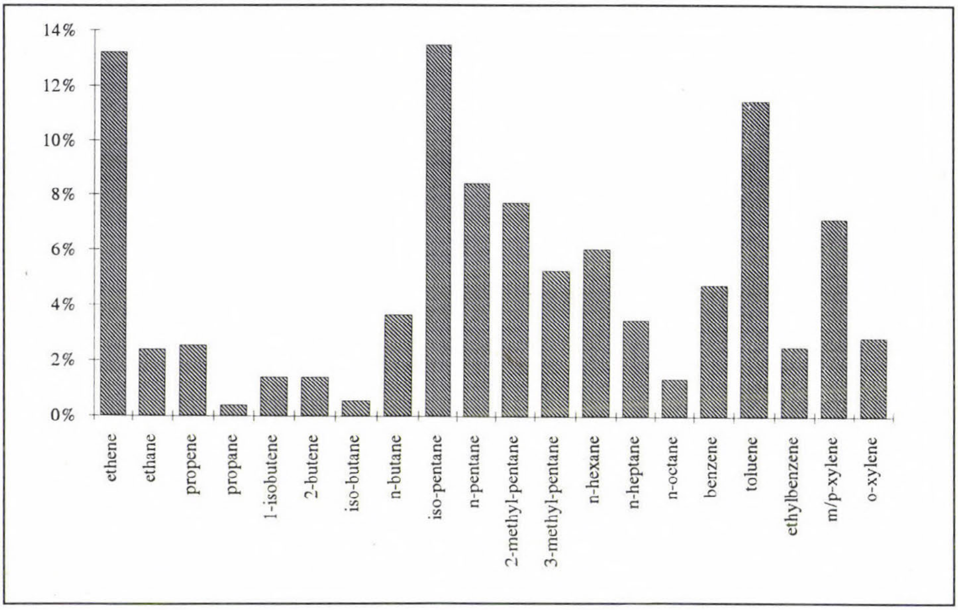

Fig. 3. Tailpipe emission source profile measured in Budapest during a roadway tunnel experiment (wt%).

3. *Mathematical method*

Different variants of the chemical mass balance source reconciliation technique have been widely used for two decades (e.g. *Friedlander*, 1973; *Mayrsohn* and *Crabtree*, 1976; *Nelson et al.*, 1983; *Wadden et al.*, 1986; *O'Shea* and *Scheff*, 1988; *Aronian et al.*, 1989; *Li* and *Kamens*, 1993; *Lewis*, 1994). Here the procedure applied by *Nelson et al.* (1983) is used, which employs *Hanna*'s (1971) model for atmospheric dispersion.

Hanna's model gives the ground level concentration, c, in the following form:

$$c = kQ/u, \tag{1}$$

where Q is the area source emission, u is the wind speed, while k is a dimensionless parameter. The parameter k is a function of atmospheric stability and the pollutant species being considered.

Hydrocarbon species with atmospheric concentrations of c_i are emitted by a number of sources with emission rates of Q_j. The values of k and u are assumed to be the same for the various sources. The weight fraction of hydrocarbon i in the jth source is taken to be a_{ij}. Then

$$c_i = \sum_{j=1}^{N} a_{ij} (kQ_j/u), \qquad [i = 1,\dots,n] \tag{2}$$

where N is the number of sources and n is the number of species considered. For simplicity Q_j' will be introduced instead of kQ_j/u in the equations. Q_j' is known as the effective source strength.

The source profile is only known for the tailpipe emission, therefore only two sources can be distinguished in the model: 'tailpipe emission', denoted by Q_1', and 'other sources', denoted by Q_2'. The tailpipe emission profile presented in *Fig. 3* is given by a_{i1}, while the unknown profile of the 'other sources' is described by a_{i2}.

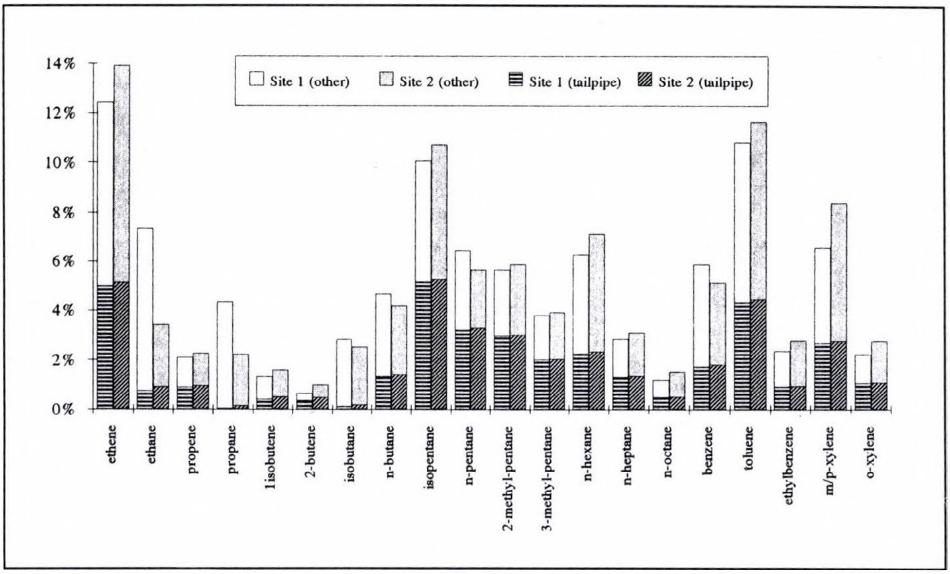

Fig. 4. Contribution of tailpipe emission to the non-methane hydrocarbon pollution of the air at two sites in Budapest (wt%).

For the system of Eq. (2) no unique solution can be found because the number of the unknown parameters is greater than the number of the equations. Therefore, only the maximum possible source strength, the maximum potential contribution of the tailpipe emission can be determined. For this purpose Q_2' is assumed zero and each equation of (2) is solved for Q_1'. Each equation gives a different Q_1' value but only the least one satisfies all of the equations simultaneously (Q_2' and a_{i2} [i = 1,...,n] are ≥ 0). It implies that one of the species in each sample is assumed to originate exclusively from tailpipe emission. For this reason Q_1' is the maximum possible effective source strength for tailpipe emission.

4. Results

By means of the mathematical method described above the maximum potential contribution of the tailpipe emission to the atmospheric NMHC burden was determined for each air sample separately. In more than half of the cases propene and 2-butene determined the maximum potential contribution at both sites. Averaging the results it was found that the maximum potential contribution of tailpipe emission to the NMHC pollution of the atmosphere was 37% at Site 1 and 39% at Site 2. The standard deviations were 17% and 20%, respectively, indicating that the maximum potential contribution varied significantly from sample to sample. One of the reasons for the high variability may be the short sampling time (1–2 minutes).

For 34 samples of the total 180 the maximum potential contribution was less than 20%. In 31 cases of the 34 propene and 2-butene determined the maximum potential contribution. In most of these samples the concentration of at least one of these species was very low, in a few cases even below the detection limit. However, a few samples, especially at Site 2, had unusual NMHC composition which resulted in a low tailpipe contribution. Some samples could be identified as xylene-rich, propane-rich and C_4–C_5 rich (gasoline vapour?). As Site 2 was located on the territory of Eötvös Loránd University solvent and commercial gas release from the laboratories might have contaminated certain samples.

The maximum potential contribution of tailpipe emission and the minimum potential contribution of the other sources are presented in *Fig. 4* for each site, species by species. Contribution of the tailpipe emission to the propane and isobutane contents of the atmosphere is low in accordance with the literature (*Mayrsohn et al.*, 1977; *Nelson et al.*, 1983). The contribution is the highest for 2-butene and for the pentane and methyl-pentane components. Maximum 30wt% (Site 1) and 36% (Site 2), respectively, of benzene (qualified as carcinogenic substance) in the air originate from car exhaust.

In most cities ethene is believed almost exclusively of tailpipe origin with some minor contribution of natural gas and (petrol)chemical industry (*Mayrsohn et al.*, 1977; *Nelson et al.*, 1983; *Aronian et al.*, 1989; *Doskey et al.*, 1992; *Lewis et al.*, 1993; *Henry et al.*, 1994). However, in this study only about 40% of the ethene content of the air can be attributed to this source. As the same sampling and analytical technique, and the same analytical device were used in both projects producing our database (*Haszpra et al.*, 1991; *Haszpra* and *Szilágyi*, 1994b), the analytical problems can be excluded as a probable source. Although there are chemical laboratories around Site 2 and medical laboratories as well as industrial plants around Site 1 which may also release ethene, such a high amount is not probable. The question should be studied further.

Another interesting feature is the highly different ethane contribution to the total non-methane hydrocarbon pollution of the air at the two sampling sites. Ethane has two basic sources: exhaust gas of the cars and commercial gas (*Mayrsohn et al.*, 1977; *Nelson et al.*, 1983; *Lewis et al.*, 1993). Assuming only these two sources to be present, the contribution of the commercial gas release to the NMHC content of the air can be estimated. At Site 1 7.36wt% of the NMHC content of the air is ethane, 10.3% of which can be attributed to the car exhaust. It means that at least 6.6wt% of the total NMHC content of the air is of commercial gas originated. As the commercial gas also contains a certain amount of propane and butane the contribution may exceed 8wt%. The value estimated in the similar way is only 3wt% for Site 2 while the NMHC pollution of the air is only about 20% higher here. It should be noted that refineries may also emit ethane (e.g. *Aronian et al.*, 1989), but there are no refineries in the vicinity of the sampling sites.

5. *Conclusions*

In this paper the potential maximum contribution of the tailpipe emission to the NMHC pollution of the air in Budapest is estimated using only direct, on site atmospheric measurements. In this way the errors introduced by the application of potentially non-adequate emission factors can be avoided. It is found that at most 37–39wt% of the NMHC content of the air in Budapest can be attributed to this source. It indicates the maximum improvement which can be achieved by the over-all introduction of emission control devices like three-way catalysts on the cars. Questions arose about the origin of the high amount of ethene at both sampling sites and that of ethane at Site 1.

Since the time of these measurements slow changes have started in the composition of the Hungarian car fleet, the number of cars equipped with exhaust catalysts has increased, and the structure of the industry has also changed due to the economical decline. All these changes would make it highly desirable to repeat this study on a more recent database. The measuring program should be extended to at least ethyne which would allow a more detailed source reconciliation through, for example, the GRACE/SAFER method (*Henry et al.*, 1994).

Acknowledgements—The author expresses his appreciation to *István Szilágyi* (Central Research Institute for Chemistry, Budapest) who developed the sampling and analytical techniques as well as performed the NMHC analyses used in this study. This study was supported by the European Union as an EUROTRAC/TOR contribution (contract PHARE ACCORD H9112-0400), while the projects providing the database were partially or fully supported by the Ministry for Environmental Protection and Water Management (11-01007-K/87/15/A) and by the National Committee for Technological Development (Mec-92-0007).

References

Aronian, P.F., Scheff, P.A. and *Wadden, R.A.*, 1989: Wintertime source reconciliation of ambient organics. *Atmospheric Environment 23*, 911-920.

Bozó, L. and *Baranka, Gy.*, 1994: Model simulation of ozone formation in an urban plume. *Proc. of EUROTRAC '94 Symposium*, 10-14 April, 1994, Garmisch-Partenkirchen.

Doskey, P.V., Porter, J.A. and *Scheff, P.A.*, 1992: Source fingerprints for volatile non-methane hydrocarbons. *J. Air & Waste Management Assoc. 42*, 1437-1445.

Friedlander, S. K., 1973: Chemical element balances and identification of air pollution sources. *Environmental Science & Technology 7*, 235-240.

Hanna, S.R., 1971: A simple method of calculating dispersion from urban area sources. *J. Air Pollution Control Assoc. 21*, 774-777.

Haszpra, L., Demeter, A., Szilágyi, I., Turányi, T. and *Bérces, T.*, 1991: Hydrocarbon and aldehyde measurements in Budapest. *Atmospheric Environment 25A*, 2103-2110.

Haszpra, L. and *Szilágyi, I.*, 1994a: Non-methane hydrocarbon measurements in a road tunnel in Budapest. *Proc. of NATO Advanced Research Workshop on Monitoring and Control Strategies for Urban Air Pollution*. 9-14 October, 1994, Erice, Italy.

Haszpra, L. and *Szilágyi, I.*, 1994b: Non-methane hydrocarbon composition of car exhaust in Hungary. *Atmospheric Environment 28*, 2609-2614.

Henry, R.C., Lewis, C.W. and *Collins, J.F.*, 1994: Vehicle-related hydrocarbon source compositions from ambient data: The GRACE/SAFER method. *Environmental Science & Technology 28*, 823-832.

Lewis, C.W., 1994: Receptor methods for VOC source apportionment in urban environments. *Proc. of NATO Workshop on Monitoring and Control Strategies for Urban Air Pollution*. October 10-14, 1994, Erice, Italy.

Lewis, C.W., Conner, T.L., Stevens, R.K., Collins, J.F. and *Henry, R.C.*, 1993: Receptor modeling of volatile hydrocarbons measured in the 1990 Atlanta Ozone Precursor Study. *Proc. of the 86th Annual Meeting of Air & Waste Management Assoc.* June 14-19, 1993, Denver.

Li, C.K. and *Kamens, R.M.*, 1993: The use of polycyclic aromatic hydrocarbons as source signatures in receptor modeling. *Atmospheric Environment 27*, 523-532.

Mayrsohn, H. and *Crabtree, J.H.*, 1976: Source reconciliation of atmospheric hydrocarbons. *Atmospheric Environment 10*, 137-143.

Mayrsohn, H., Crabtree, J.H., Kuramoto, M., Sothern, R.D. and *Mano, S.H.*, 1977: Source reconciliation of atmospheric hydrocarbons 1974. *Atmospheric Environment 11*, 189-192.

Molnár, Á., 1990: Estimation of volatile organic compounds (VOC) emissions for Hungary. *Atmospheric Environment 24*, 2855-2860.

Nelson, P.F., Quigley, S.M. and *Smith, M.Y.*, 1983: Sources of atmospheric hydrocarbons in Sydney: A quantitative determination using a source reconciliation technique. *Atmospheric Environment 17*, 439-449.

O'Shea, W.J. and *Scheff, P.A.*, 1988: A chemical mass balance for volatile organics in Chicago. *J. of Air Pollution Control Assoc. 38*, 1020-1026.

Stump, F., Tejada, S., Ray, W., Dropkin, D., Black, F., Creus, W., Snow, R., Siudak, P., Davis, C.O., Baker, L. and *Perry, N.*, 1989: The influence of ambient temperature on tailpipe emission from 1984-1987 model year light-duty gasoline motor vehicles. *Atmospheric Environment 23*, 307-320.

Stump, F.D., Knapp, K.T., Ray, W.D., Snow, R. and *Endy, L.*, 1992: The composition of motor vehicle organic emission under elevated temperature summer driving conditions (75 to 105 °F). *J. Air & Waste Management Assoc. 42*, 1328-1335.

Veldt, C., 1991: Emissions of SO_x, NO_x, VOC and CO from East European countries. *Atmospheric Environment 25*, 2683-2700.

Wadden, R.A., Uno, I. and *Wakamatsu, S.*, 1986: Source discrimination of short-term hydrocarbon samples measured aloft. *Environmental Science & Technology 20*, 473-480.

IDŐJÁRÁS
Quarterly Journal of the Hungarian Meteorological Service
Vol. 100, No. 1-3, January-September 1996

A high density network for wet only precipitation chemistry sampling in Austria

M. F. Kalina and **H. Puxbaum**[1]

Institute for Analytical Chemistry,
Vienna University of Technology,
Getreidemarkt 9/151, A-1060 Vienna, Austria

(Manuscript received 7 June 1995; in final form 6 October 1995)

Abstract—To estimate wet deposition loads of major ions and determine trends in the composition of wet only precipitation in Austria 33 sampling sites have been operated in the 9 Austrian countries. In this study the annual data for the year 1992 are presented to give an overview of the spatial distribution of concentrations and wet deposition loads for the ions sulfate, nitrate, chloride, ammonium, sodium, potassium, calcium and magnesium. Average deposition loads were determined to be 6.3 kg/ha for SO_4^{2-}–S, 3.6 kg/ha for NO_3^-–N and 5.5 kg/ha for NH_4^+–N, respectively. Two spatial gradients were found, increasing concentrations from the West to the East and decreasing concentrations from the North to the South leading to by a factor of 4 higher concentrations of SO_4^{2-}–S and NO_3^-–N in the eastern part of Austria. Because of the respectable precipitation amount at high elevated sites with up to 2064 mm in 1992 and the observed ionic concentrations, critical loads for sensitive ecosystems were exceeded in the Austrian Alps. The highest wet deposition loads of all analysed components were determined for Ca^{2+} and Cl^- with values from 12.1 to 51.2 kg/ha Ca^{2+} and from 15.8 to 82.6 kg/ha Cl^- at different sampling sites. The physiological relevance of high deposition loads of chloride has not been discussed until now. Our studies demonstrate that more research concerning the atmospheric behaviour of chloride is needed.

Key-words: acid deposition, wet fluxes, precipitation chemistry, sulfate, nitrate, ammonium, calcium, chloride.

1. Introduction

Systematic studies of the composition of wet precipitation in Austria were started in 1957 at a station in Retz being part of the European Air Chemistry Network (EACN) and of the WMO Background Air Pollution Monitoring Network (BAPMON). The samples in these networks were taken by bulk

---

[1] Corresponding author

collectors on a monthly basis. Despite of considerable shortcomings of the EACN data (*Granat*, 1978) an increasing trend of the sulfate concentration in wet precipitation in Central Europe from the late 1950's to the early 1970's could be documented (*Rhode* and *Granat*, 1984). The increase at the continental European sites was found to range from 40 to 60%. Uncorrected data from Retz indicate that the increase in Northeastern Austria was likely on the upper end of the range (*Cehak* and *Chalupa*, 1985). A decline of the sulfate concentrations was observed for the Central European sites starting in the early 1970' s (*Rhode* and *Granat*, 1984), for the Austrian site 'Retz' in the year 1978. An even stronger increase than for sulfate could be found at Retz for the nitrate concentration in precipitation. From the late 1950's to the early 1970's the nitrate concentration increased by 140% at the Austrian station and remained constant until the early 1980's.

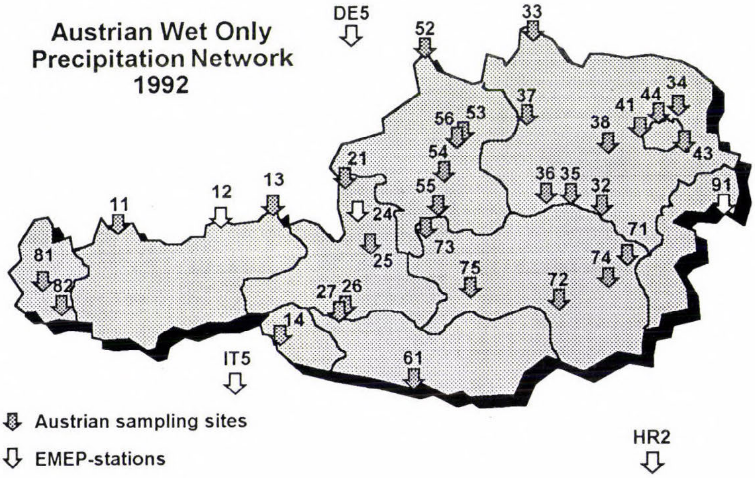

Fig. 1. Austrian precipitation chemistry network, location of the sampling sites, 1992.

In 1982 a framework for a national precipitation sampling network was established in Austria based on daily sampling by means of wet only collectors (*BMGU*, 1984). The network comprises at present 33 stations, three of which are also part of the EMEP-network (Co-operative programme for monitoring and evaluation of the long range transmission of air pollutants in Europe). *Fig. 1* shows a map of the Austrian sampling sites together with the EMEP-stations in the neighbouring countries located near the Austrian border. The code in Fig. 1 is related to a short description of the sampling sites in *Table 1*. The stations are operated by the environmental authorities of the local governments of the 9 countries of Austria except for the EMEP sites in Austria which are operated by the Federal Environmental Authority. The network started in 1983 with 7

Table 1. Austrian precipitation chemistry network, characteristics of the sampling sites, 1992

Country Code	Station	Longitude E	Latitude N	Altitude (m a.s.l.)	Period (MM/JJ)	Laboratory
Tyrol						
11	Reutte	10°40′54″	47°29′11″	930	11/83–	IAC
12	Achenkirch	11°38′25″	47°34′55″	840	11/83–	UBA
13	Kufstein	12°13′38″	47°39′47″	680	11/83–	IAC
14	Innervillgraten	12°21′10″	46°49′06″	1730	8/84–	IAC
Salzburg						
21	Haunsberg	13°01′00″	47°57′23″	520	10/83–	IAC
24	St. Koloman	13°14′00″	47°39′03″	1020	10/83–	UBA
25	Werfenweng	13°15′12″	47°25′18″	940	10/83–	IAC
26	Kolm Saigurn	12°59′04″	47°04′05″	1600	10/89–	IAC
27	Sonnblick	12°57′32″	47°03′15″	3106	10/87–	IAC
Lower Austria						
32	Naßwald	15°42′26″	47°46′04″	600	5/88–	IAC
33	Litschau	15°02′20″	48°57′20″	560	10/89–	IAC
34	Wolkersdorf	16°31′22″	48°23′02″	180	10/89–	IAC
35	Josefsberg	15°18′56″	47°50′42″	1010	11/89–	IAC
36	Lunz	15°04′07″	47°51′18″	618	4/90–	IAC
37	Ostrong	15°05′02″	48°13′15″	575	4/91–	IAC
38	Kl-Leopoldsdorf	15°59′56″	48°05′20″	400	7/91–	IAC
Vienna						
41	Lainz	16°14′02″	48°12′02″	230	4/86–	IAC
43	Lobau	16°30′54″	48°11′15″	155	4/86–	IAC
44	Bisamberg	16°22′49″	48°18′49″	310	4/90–	IAC
Upper Austria						
52	Schöneben	13°57′02″	48°42′43″	920	1/84–	LR-OÖ
53	Steyregg	14°21′16″	48°17′23″	335	1/84–	LR-OÖ
54	Kremsmünster	14°07′49″	48°03′21″	384	1/86–	LR-OÖ
55	Grünau	13°57′22″	47°46′22″	591	1/87–	LR-OÖ
56	Linz-ORF	14°18′09″	48°17′52″	263	5/90–	LR-OÖ
Carynthia						
61	Naßfeld	13°16′33″	46°33′37″	1530	11/89–	IAC
Styria						
71	Masenberg	15°52′56″	47°20′53″	1137	3/90–	IAC/FZS
72	Hochgößnitz	15°01′00″	47°03′33″	900	3/90–	IAC/FZS
73	Grundlsee	13°47′48″	47°37′50″	954	3/90–	IAC/FZS
74	Weiz	15°37′49″	47°13′03″	456	4/90–9/92	IAC/FZS
75	Stolzalpe	14°12′10″	47°07′50″	1302	12/91–	FZS
Vorarlberg						
81	Thüringerberg	09°47′05″	47°13′05″	960	4/90–3/92	IAC
82	Gaschurn	10°01′30″	46°59′30″	960	4/92–3/94	IAC
Burgenland						
91	Illmitz	16°46′08″	47°46′12″	117	8/83–	UBA

FZS	Research Center Seibersdorf
IAC	Institute for Analytical Chemistry, Vienna University of Technology
LR-OÖ	Laboratory of the Environmental Authority of Upper Austria
UBA	Umweltbundesamt

sampling sites in Tyrol, Salzburg and Burgenland followed by the other countries as to be seen in Table 1. Due to the complex terrain in Austria the number of sampling sites is justified. The altitudes of the sampling sites reach from 155 m a.s.l. in the East to 3106 m a.s.l. at high elevation sites in the Central Alps, the annual precipitation amounts range from 260 mm to 2100 mm. The purpose of the Austrian network is to estimate the wet deposition loads of major ions and determine the trends in the composition of wet precipitation for Austria. The dataset serves as important databasis for estimations of the development of soil conditions in Austria concerning discussions of critical loads and levels (*Schulze et al.*, 1990), for the investigations of mechanistic processes in the atmosphere (*Puxbaum et al.*, 1991) as well as for the validation of air chemistry models (*Sandnes,* 1993).

In this study the data for the 9 Austrian countries are summarized for the year 1992 to present an overview of the spatial distribution of concentrations and deposition loads for the Austrian territory compared to data of foreign sampling sites near the Austrian border. The year 1992 is chosen to continue the series of overview studies concerning the Austrian wet precipitation network (*Puxbaum, et al.*, 1988; *Puxbaum, et al.*, 1991; *Kovar* and *Puxbaum*, 1992; *Kalina* and *Puxbaum*, 1994).

2. *Analysis*

The Austrian precipitation sampling network is equipped with the WADOS ('Wet and dry only precipitation sampler', *Winkler et al.*, 1989). A slightly heated resistance sensor coupled to a lid ensures the collection of wet only precipitation samples. The daily control of the samples is carried out by local observers usually in the morning hours. The collection procedure follows the recommendation of the Austrian Ministry of Health and Environment (*BMGU*, 1984). The samples are stored in polyethylene bottles at 0–4 °C, transported in biweekly intervals to the central laboratories and analysed generally within 1–4 weeks after receipt. The samples of most of the stations are analysed at the Institute for Analytical Chemistry of the Vienna University of Technology, the samples of the stations in Upper Austria are analysed at the laboratory of the local government, the samples of Styria at the Research Center Seibersdorf and the samples of the EMEP-stations at the Federal Environmental Authority (Table 1).

The samples are analysed for the anions sulfate, nitrate and chloride and the monovalent cations ammonium, sodium and potassium by ion chromatography (IC). Parameters of the IC-systems are listed in *Table 2*. The divalent cations calcium and magnesium are determined by Atomic Absorption Spectroscopy (Perkin Elmer 403, flame atomizer, PM detector), pH and conductivity in the low ionic strength samples are determined electrometrically (*BMGU*, 1984). The detection limits calculated according to 3 S.D. of the blank values were

0.01 mg/ℓ for ammonium, chloride, magnesium, potassium and sodium, 0.02 mg/ℓ for calcium and 0.03 mg/ℓ for nitrate and sulfate, respectively. Quality control of the analytical data is performed by comparing calculated vs. measured conductivities and by the cation vs. anion balances of the individual samples. The results for the data of 1992 show a good correlation of calculated and measured conductivities, the correlation coefficientes for the individual sampling sites range between 0.92 and 0.98. The correlation coefficientes for the ionic balances range between 0.75 and 0.95. The weaker correlations are caused by a relatively high cation excess at some of the stations explained by anions that are not determined in the routine analysis like HCO_3^- and organic anions (*Puxbaum et al.*, 1991).

Table 2. Parameters of the IC-systems

	Cation-IC	Anion-IC
System:	Dionex-Qic Analyzer	Dionex GPM-2
Column:	Dionex Ion Pac CS12	Dionex Ion Pac AS4A-SC
Precolumn:	Dionex Ion Pac CG12	Dionex Ion Pac AG4A-SC
Eluent:	17 mM MSA	1,8 mM Na_2CO_3 + 1,7 mM $NaHCO_3$
Flow:	1 mℓ/min	1 mℓ/min
Suppressor:	Dionex CSRS I – 4mm (electrochemical)	ASRS I – 4mm (electrochemical)
Sample loop:	20 $\mu\ell$	30 $\mu\ell$
Detection:	conductivity	conductivity
Sensitivity:	10 μS	5 - 30 μS

3. Results and discussion

The precipitation weighted annual mean concentrations of the main ionic constituents for the Austrian stations are listed in *Table 3a* together with the data from the EMEP-stations Brotjacklriegel (Germany, DE5 in Fig. 1), Arabba (Italy, IT5 in Fig. 1) and Puntijarka (Croatia, HR2 in Fig. 1) (*Kalina* and *Puxbaum*, 1995; *Schaug et al.*, 1994). Wet deposition data yielded by multiplication of the concentration value and the precipitation amount of each station are listed in *Table 3b*.

The spatial distributions of the concentrations of SO_4^{2-}–S, NO_3^-–N and NH_4^+–N over Austria for 1992 are presented in *Fig. 2a–c*. Two gradients are to be seen, increasing concentrations from the West to the East and decreasing concentrations from the North to the South. These gradients are reported by

Table 3a. Ionic concentrations, Austrian precipitation chemistry network and neighbouring EMEP-stations, 1992

Station	Code	Precip. [mm]	pH	H^+	NH_4^+-N	Na^+	K^+	Ca^{2+} [mg/ℓ]	Mg^{2+}	Cl^-	NO_3^--N	SO_4^{2-}-S
Reutte	11	1468	5.2	0.006	0.5	0.1	0.1	0.6	0.1	0.5	0.2	0.3
Achenkirch	12	780	4.8	0.016	0.3	0.1	0.0	0.3	0.1	0.3	0.4	0.4
Kufstein	13	979	4.8	0.017	0.6	0.1	0.0	0.3	0.0	0.2	0.4	0.5
Innervillgraten	14	475	5.0	0.010	0.6	0.1	0.1	0.4	0.1	0.4	0.3	0.5
Haunsberg	21	912	4.9	0.013	1.0	0.3	0.1	0.6	0.1	0.7	0.5	0.6
St. Koloman	24	1106	5.0	0.010	0.5	0.1	0.0	4.6	0.2	7.5	0.4	0.6
Werfenweng	25	968	5.3	0.006	0.5	0.3	0.2	0.7	0.1	0.3	0.3	0.4
Kolm Saigurn	26	674	4.9	0.014	0.3	0.1	0.0	0.3	0.0	0.1	0.3	0.4
Sonnblick	27	1506	5.0	0.009	0.3	0.1	0.0	0.6	0.0	0.4	0.2	0.4
Naßwald	32	1082	4.9	0.013	0.4	0.1	0.1	1.1	0.1	1.5	0.3	0.7
Litschau	33	650	4.6	0.025	1.1	0.1	0.1	0.5	0.1	0.6	0.6	1.0
Wolkersdorf	34	347	4.9	0.013	1.3	0.2	0.2	1.5	0.2	0.8	0.8	1.4
Josefsberg	35	851	4.6	0.027	0.6	0.1	0.1	0.4	0.1	0.2	0.4	0.7
Lunz	36	1271	4.5	0.029	0.5	0.1	0.0	0.3	0.1	0.3	0.4	0.6
Ostrong	37	614	4.7	0.018	1.0	0.2	0.1	0.3	0.1	0.4	0.5	0.8
KI-Leopoldsdorf	38	643	4.7	0.019	0.9	0.1	0.1	0.5	0.1	0.4	0.6	0.9
Lainz	41	559	4.8	0.017	0.6	0.2	0.1	0.8	0.1	0.5	0.5	0.9
Lobau	43	405	5.4	0.004	0.7	0.2	0.6	1.5	0.4	0.4	0.6	1.1
Bisamberg	44	258	5.1	0.008	1.0	0.2	0.1	1.5	0.2	1.0	0.6	1.3
Schöneben	52	619	5.0	0.010	1.2	0.3	0.1	7.1	0.2	6.1	0.7	1.3
Steyregg	53	348	5.9	0.001	4.7	1.1	0.6	2.8	0.5	3.7	1.2	2.5
Kremsmünster	54	1401	6.2	0.001	0.7	0.3	0.1	1.4	0.9	1.2	0.7	1.2
Grünau	55	1565	5.0	0.010	0.4	0.2	0.1	1.2	0.1	1.2	0.6	0.6
Linz-ORF	56	675	5.2	0.006	1.3	0.3	0.2	1.6	0.2	0.6	0.8	1.3
Naßfeld	61	2064	4.9	0.014	0.4	0.3	0.0	0.7	0.1	0.7	0.3	0.6
Masenberg	71	676	5.0	0.010	0.9	0.3	0.2	1.3	0.1	0.7	0.3	1.3
Hochgößnitz	72	827	4.8	0.018	0.9	0.2	0.2	0.9	0.1	0.4	0.3	1.0
Grundlsee	73	882	5.1	0.007	1.4	0.3	0.2	0.4	0.0	0.6	0.4	0.7
Weiz	74	463	4.9	0.012	0.9	0.2	0.3	0.8	0.1	0.4	0.4	1.4
Stolzalpe	75	646	5.0	0.009	0.5	1.2	0.4	2.4	0.8	0.8	0.2	1.0
Gaschurn	82	750	5.4	0.004	0.4	0.1	0.1	0.6	0.1	0.3	0.2	0.3
Illmitz	91	390	5.6	0.003	0.9	0.4	0.2	3.5	0.6	1.1	0.7	1.5
Brotjacklriegel	DE5	805	4.6	0.024	0.7	0.2	0.1	0.3	0.1	0.3	0.6	0.8
Arabba	IT5	695	4.9	0.013	0.5	0.1	0.1	0.6	0.1	0.3	0.4	0.6
Puntijarka	HR2	1136	4.9	0.013	1.1	0.8	2.3	1.1	0.4	1.1	0.6	1.3

Table 3b. Wet deposition loads, Austrian precipitation chemistry network and neighbouring EMEP-stations, 1992

Station	Code	H^+	NH_4^+-N	Na^+	K^+	Ca^{2+} [kg/ha]	Mg^{2+}	Cl^-	NO_3^--N	SO_4^{2-}-S
Reutte	11	0.1	6.9	1.7	1.0	9.0	1.2	6.7	3.6	5.1
Achenkirch	12	0.1	2.6	1.0	0.3	2.5	0.4	2.3	3.0	3.5
Kufstein	13	0.2	6.1	0.7	0.3	3.1	0.5	2.2	4.0	5.3
Innervillgraten	14	0.0	2.6	0.4	0.4	2.1	0.4	1.7	1.4	2.5
Haunsberg	21	0.1	8.8	3.1	1.2	5.1	0.6	6.7	4.8	5.9
St.Koloman	24	0.1	5.8	1.2	0.4	51.2	1.7	82.6	4.5	6.3
Werfenweng	25	0.1	4.9	2.5	1.9	7.0	1.2	2.9	3.1	3.8
Kolm Saigurn	26	0.1	1.8	0.7	0.2	2.3	0.2	0.9	1.8	2.4
Sonnblick	27	0.1	4.2	1.6	0.6	8.8	0.7	5.4	3.3	5.9
Naßwald	32	0.1	4.5	1.6	1.1	12.1	1.1	15.8	3.5	7.1
Litschau	33	0.2	6.9	0.8	0.4	3.1	0.3	4.2	3.6	6.2
Wolkersdorf	34	0.0	4.4	0.7	0.6	5.2	0.7	2.9	2.6	4.9
Josefsberg	35	0.2	5.0	1.1	0.9	3.4	0.8	2.1	3.6	6.3
Lunz	36	0.4	6.8	1.6	0.5	4.2	0.7	3.3	5.7	7.2
Ostrong	37	0.1	5.9	1.4	0.4	1.8	0.3	2.5	3.2	5.0
KI-Leopoldsdorf	38	0.1	5.6	0.9	0.5	3.2	0.5	2.4	3.8	5.8
Lainz	41	0.1	3.3	1.1	0.4	4.4	0.6	2.5	2.6	4.9
Lobau	43	0.0	2.7	0.9	2.3	6.1	1.5	1.6	2.4	4.3
Bisamberg	44	0.0	2.5	0.5	0.4	3.8	0.5	2.5	1.7	3.3
Schöneben	52	0.1	7.4	1.8	0.8	44.2	1.5	37.8	4.3	8.0
Steyregg	53	0.0	16.4	3.7	2.1	9.8	1.8	12.9	4.2	8.7
Kremsmünster	54	0.0	9.8	4.1	1.7	20.1	12.1	16.8	9.8	16.8
Grünau	55	0.2	6.3	3.7	1.9	18.3	1.2	18.8	9.4	9.4
Linz-ORF	56	0.0	8.8	2.3	1.5	10.5	1.3	4.1	5.4	8.8
Naßfeld	61	0.3	7.4	5.5	0.7	13.6	1.4	14.0	5.4	11.8
Masenberg	71	0.1	6.0	2.0	1.5	9.1	0.5	4.7	2.2	8.7
Hochgößnitz	72	0.1	7.1	1.5	1.5	7.3	0.5	3.5	2.5	8.6
Grundlsee	73	0.1	12.2	2.2	2.1	3.5	0.3	5.2	3.8	6.6
Weiz	74	0.1	4.3	0.9	1.5	3.6	0.4	2.0	1.8	6.4
Stolzalpe	75	0.1	3.1	8.0	2.4	15.3	5.2	5.2	1.4	6.2
Gaschurn	82	0.0	2.6	0.6	0.8	4.8	0.5	2.4	1.6	2.6
Illmitz	91	0.0	3.4	1.7	0.7	13.5	2.3	4.3	2.6	6.0
Brotjackliegel	DE5	0.2	6.0	1.4	0.7	2.4	0.4	2.4	4.7	6.2
Arabba	IT5	0.1	3.1	0.9	0.6	4.0	0.6	2.2	2.4	4.4
Puntijarka	HR2	0.1	12.2	9.2	26.3	12.0	4.8	12.3	6.9	14.4

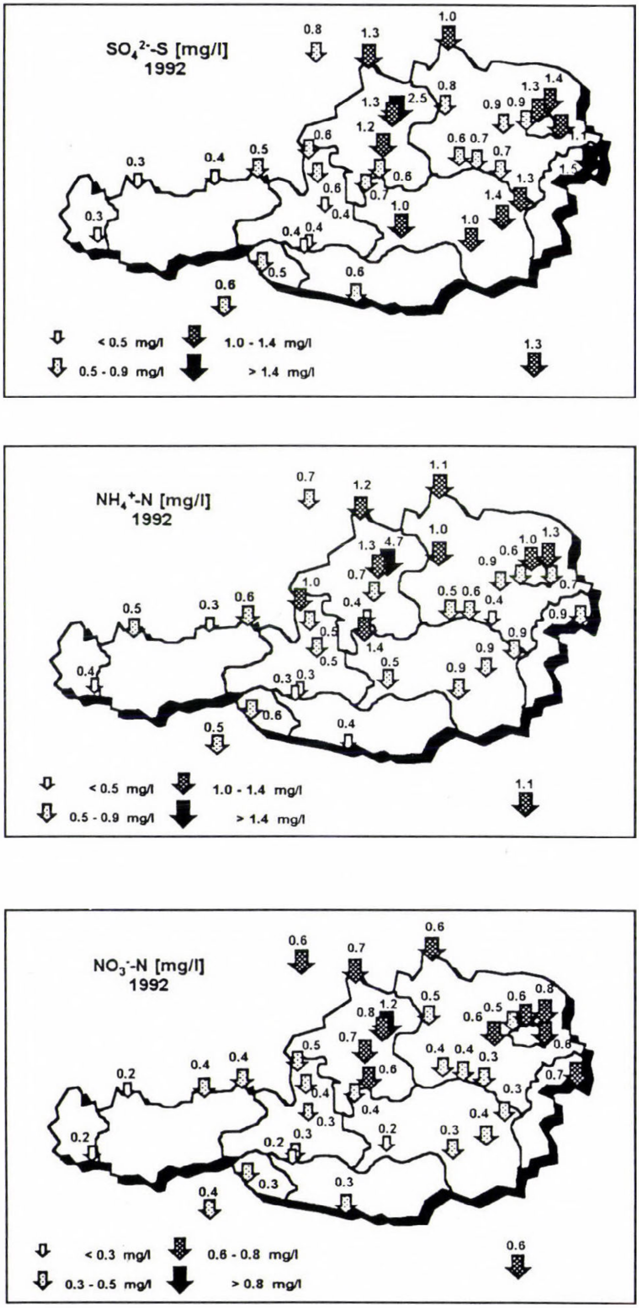

Fig. 2a–c. Spatial distribution of SO$_4^{2-}$–S (*a*), NO$_3^-$–N (*b*) and NH$_4^+$–N (*c*) concentrations over Austria, 1992.

Puxbaum et al. (1991) examining four sampling sites (Reutte, Kufstein, St. Koloman and Haunsberg) with data from an earlier observation period (1987/88 to 1988/89) and can be verified in this study with the data for the complete Austrian precipitation network and the comparison with the neighbouring EMEP-stations from Germany, Italy and Croatia. Since Austria is a small country (83900 km²) the major fraction of the deposition of sulfur and nitrate-nitrogen is imported (*Umweltbundesamt*, 1993). For SO_2 and the estimated imported fraction is about 90% of the total sulfur deposition in Austria. Thus a reduction of the deposition loads depends on the reductions of the emissions of SO_2 and NO_x in the neighbouring countries. The strong influence of the former Eastern European countries on the sulfate gradient (Fig. 2a) can be seen very well comparing the concentrations in Vorarlberg and Tyrol with the concentrations in the Vienna area yielding by a factor of 4 higher values in the eastern part of Austria (0.3 mg/ℓ compared to 1.3 mg/ℓ SO_4^{2-}–S). This factor of 4 is also reflected in the NO_3^-–N concentrations with 0.2 mg/ℓ in the West compared to 0.8 mg/ℓ in the East (Fig. 2b). The local influence at the city sampling site Linz-Steyregg is clearly shown in the NH_4^+–N concentration with a factor of 4 higher values than at the surrounding sampling sites (Fig. 2c). Therefore this dataset is excluded when calculating deposition rates over the whole country. The concentration levels at inneralpine sites are in general lower than outside of the Alps, but no significant dependence on altitude for the ionic concentrations as presented by *Fowler et al.* (1988), discussing an increase in concentrations between 250 and 847 m a.s.l. at Great Dun Fell for wet deposition from orographic clouds, or *Rihm* (1994), assuming a linear decrease of concentrations above 1000 m altitude by 25% per kilometer for 3 stations in Switzerland, could be found for the Austrian sampling sites. *Fig. 3* for example shows the sulfate concentration vs. altitude with a correlation coefficient of -0.52. For the other ionic species either correlation coefficients of similar value (-0.49 for ammonium and -0.60 for nitrate), or negligible correlation coefficients from -0.04 for potassium up to -0.22 for magnesium were calculated.

Wet deposition loads are not only influenced by the ionic concentrations in precipitation but also by the precipitation amount. Due to the complex terrain precipitation amounts at the Austrian sampling sites show large fluctuations. For the year 1992 the precipitation amount varies between 258 mm and 2064 mm (see Table 3a). Because of the respectable precipitation amount at high elevated sites and the observed ionic concentrations the wet deposition loads are considerably high in that regions (*Puxbaum et al.*, 1991). A good example is given by comparing the two sampling sites Sonnblick (3106 m a.s.l.) and Kolm Saigurn (1600 m a.s.l.). The Sonnblick Observatory is located in the main ridge of the Austrian Alps. In the Northeast of the observatory a steep wall descends to the Kolm Saigurn sampling site. The concentrations of the main constituents of wet precipitation (Fig. 2a-c) show comparable values at the two stations while the wet deposition loads are featured by a factor of about 2 higher values at the Sonnblick sampling site (Table 3b). This factor is to be explaned by the higher precipitation amount at the Sonnblick Observatory (1506 mm) compared to 674 mm observed at Kolm Saigurn for 1992. Thus critical loads for sensitive ecosystems (*Schulze et al.*, 1990) are exceeded at high alpine sites in Austria. On the other hand, sampling sites which show the highest concentration levels for SO_4^{2-}-S, NO_3^--N and NH_4^+-N like Wolkersdorf and the stations in Vienna are below the Austrian average for wet deposition in 1992 (6.3 kg/ha for SO_4^{2-}-S, 3.6 kg/ha for NO_3^--N and 5.5 kg/ha for NH_4^+-N) caused by low precipitation amounts in the east part of Austria (258–559 mm for 1992).

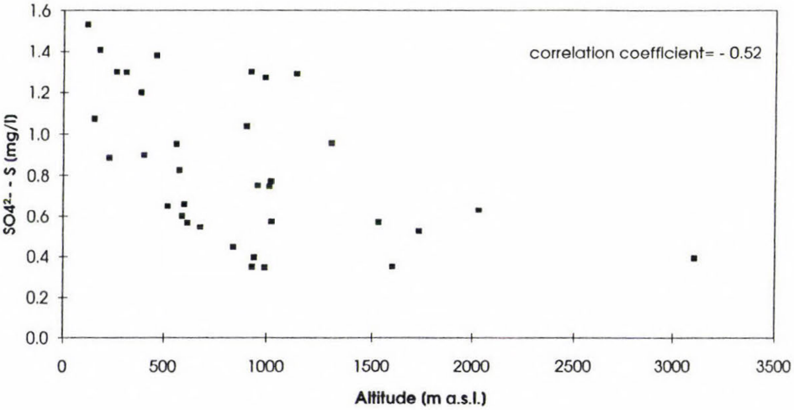

Fig. 3. SO_4^{2-}-S concentrations versus altitude, Austria, 1992.

In *Table 4* a cross correlation matrix calculated by using the annual averages for the Austrian sampling sites is presented. At the Austrian sites SO_4^{2-}-S is highest correlated with NH_4^+-N, followed by NO_3^--N. NO_3^--N is highest correlated with NH_4^+-N, too. This emphasizes results from event studies at Mount Sonnblick (*Brantner et al.*, 1994; *Kasper*, 1994) or Achenkirch (*Kalina et al.*, 1995) that acid aerosol is mainly neutralised by ammonia. The good Ca^{2+}/Mg^{2+} correlation pointed out by *Puxbaum et al.* (1991) for the western stations Reutte, Kufstein, St. Koloman and Haunsberg could not be found using the data for all sampling sites of Austria, because only the western part of Austria is dominated by limestone. On the other hand a correlation between Mg^{2+} and Na^+ can be seen examining the 1992 data set that could not be explained at present time. A correlation with Cl^- is found neither for Mg^{2+} nor for Na^+.Thus an origin from seasalt aerosol as described by *Ruijgrok* and *Römer* (1993) or *Yamaguchi et al.* (1991) is to be excluded. Due to the small absolute amount of these ions in wet precipitation this result is not so important as the highly correlated Ca^{2+}/Cl^- values observed. Both ions occured in considerably high concentrations at different sampling sites as St. Koloman in Salzburg, Naßwald in Lower Austria, Schöneben, Kremsmünster and Grünau in Upper Austria with values between 1.1 and 7.1 mg/ℓ for Ca^{2+} and between 1.2 and 7.5 mg/ℓ for Cl^- (Table 3a), yielding wet deposition loads from 12.1 to 51.2 kg/ha Ca^{2+} and from 15.8 to 82.6 kg/ha Cl^-, respectively (Table 3b). These are the highest wet deposition loads of all analysed components and must be mentioned as relevant for air chemistry considerations, although their origin is not completely clear until now. Also a physiological relevance of high deposition loads of chloride has not been discussed until now. Our studies demonstrate that more research concerning the atmospheric behaviour of chloride is needed.

Table 4. Cross correlation matrix based on annual concentration averages for the Austrian sampling sites, 1992.

	H^+	NH_4^+-N	Na^+	K^+	Ca^{2+}	Mg^{2+}	Cl^-	NO_3^--N	SO_4^{2-}-S
H^+	1.00	−0.03	−0.22	−0.11	−0.33	−0.47	−0.17	−0.04	−0.17
NH_4^+-N		1.00	0.18	0.28	0.25	0.10	0.13	**0.69**	**0.73**
Na^+			1.00	0.56	0.25	**0.70**	0.03	0.08	0.38
K^+				1.00	0.03	0.33	−0.01	0.20	0.35
Ca^{2+}					1.00	0.40	**0.87**	0.33	0.42
Mg^{2+}						1.00	0.15	0.32	0.50
Cl^-							1.00	0.20	0.14
NO_3^--N								1.00	**0.68**
SO_4^{2-}-S									1.00

References

Brantner, B., Fierlinger, H., Berner, A. and *Puxbaum, H.*, 1994: Cloudwater chemistry in the subcooled droplet regime at Mount Sonnblick (Austrian Alps). *Water, Air and Soil Pollution 74*, 1-24.

BMGU, 1984: *Richtlinie 11, Immissionsmessung des nassen Niederschlags und des sedimentierten Staubes, Luftverunreinigung - Immissionsmessung*. Bundesministerium für Gesundheit und Umweltschutz, Vienna, Austria.

Cehak, K. and *Chalupa, K.*, 1985: Observations of various chemical contaminants of the precipitation at a BAPMoN station in the Eastern Pre-Alpine Region. *Arch. Met. Geophys. Bioclimat. B35*, 307-322.

Fowler, D., Cape, J.N., Leith, I.D., Choularton, T.W., Gay, M.J. and *Jones, A.*, 1988: Wet deposition and altitude: The role of orographic cloud. In *Acid Deposition at High Elevation Sites* (eds.: *M.H. Unsworth* and *D. Fowler*). Kluwer, Dordrecht, 231-257.

Granat, L., 1978: Sulfate in precipitation as observed by the European Atmospheric Chemistry Network. *Atmos. Environ. 12*, 413-424.

Kalina, M.F. and *Puxbaum, H.*, 1994: Verteilung der nassen Deposition von Schwefel- und Stickstoffverbindungen in Österreich. Dokumentation der Daten für 1991, Bericht 9/94, Institute for Analytical Chemistry, Vienna University of Technology, Austria.

Kalina, M.F. and *Puxbaum, H.*, 1995: Verteilung der nassen Deposition von Niederschlagsinhaltstoffen in Österreich. Dokumentation der Daten für 1992. *Bericht 3/95,* Institute for Analytical Chemistry, Vienna University of Technology, Austria.

Kalina, M.F., *Zambo, E.* and *Puxbaum, H.*, 1995: 1. Zwischenbericht Okkulte Deposition in Achenkirch. *Bericht 2/95*, Institute for Analytical Chemistry, Vienna University of Technology, Austria.

Kasper, A., 1994: Saisonale Trends atmosphärischer Spurenstoffe sowie deren Auswaschverhalten an der Hintergrundmeßstelle Hoher Sonnblick. *Dissertation*. Institut für Analytische Chemie, TU Wien.

Kovar, A. and *Puxbaum, H.*, 1992: Nasse Deposition im Ostalpenraum. *Bericht 14/92,* Institute for Analytical Chemistry, Vienna University of Technology, Austria.

Puxbaum, H., *Vitovec, W.* and *Kovar, A.*, 1988: Chemical composition of wet deposition in the Eastern Alpine region. In *Acid Deposition at High Elevation Sites* (eds.: *M.N. Unsworth* and *D. Flower*). Kluwer, 419-430.

Puxbaum, H., *Kovar, A.* and *Kalina, M.*, 1991: *Chemical Composition and Fluxes of Wet Deposition at Elevated Sites (700-3105 m a.s.l.) in the Eastern Alps (Austria).* NATO ASI Series, Vol. G28, Seasonal Snowpacks (ed.: *T.D. Davies et al.*). Verlag Springer Berlin, Heidelberg, 273-297.

Rhode, H. and *Granat, L.*, 1984: An evaluation of sulfate in European precipitation 1955-1982. *Atmos. Environ. 18*, 2627-2639.

Rihm, B., 1994: Critical loads of acidity for forest soils and alpine lakes. *Environmental Series Report No. 234.* Federal Office of Environment, Forests and Landscape, Bern, Switzerland.

Ruijgrok, W. and *Römer, F.G.*, 1993: Aspects of wet, acidifying deposition in Arnheim: source regions, correlations and trends.

Sandnes, H., 1993: Calculated budgets for airborne acidifying components in Europe, 1985 1987, 1988, 1989, 1990, 1991, and 1992. *EMEP Report 1/93,* MSC-W, Norway.

Schaug, J., *Pedersen, U.*, *Skjelmoen, J.E.*, *Arnesen, K.* and *Bartanova, A.*, 1994: EMEP data report 1992. Part 1: Annual summaries. *EMEP Report 4/94,* Norwegian Institute for Air Research, Norway.

Schulze, E.D., *de Vries, W.*, *Hauhs, M.*, *Rosen, K.*, *Rasmussen, L.*, *Tamm, C.O.* and *Nilsson, J.* 1990: Critical loads for nitrogen deposition on forest ecosystems. *Water Air and Soil Pollution 48*, 451-456.

Umweltbundesamt, 1993: *Umweltkontrollbericht – Teil A.* State of the Environment in Austria (ed.: *J. Mayer*). Umweltbundesamt, Wien.

Winkler, P., *Jobst, S.* and *Harder, C.*, 1989: Meteorologische Prüfung und Beurteilung von Sammelgeräten für die nasse Deposition. *BPT-Bericht 1/89*, GSF München, Germany, 1989.

Yamaguchi, K., *Tatano, T.*, *Tanaka, F.*, *Nakao, M.*, *Gomyoda, M.* and *Hara, H.*, 1991: An analysis of precipitation chemistry measurements in Shimane, Japan. *Atmos. Environ. 25A*, 285-291.

IDŐJÁRÁS

Quarterly Journal of the Hungarian Meteorological Service
Vol. 100, No. 1-3, January-September 1996

CCN determination, comparing counters with single-drop-counting and photometric detectors, at Mace Head Ireland

J. L. Gras[1], **S. G. Jennings**[2] and **M. Geever**[2]

[1] *CSIRO Division of Atmospheric Research,*
PMB 1, Aspendale, Vic., 3195, Australia

[2] *Department of Experimental Physics, University College Galway,*
University Road, Galway, Ireland

(Manuscript received 1 June 1995; in final form 12 February 1996)

Abstract—Two static thermal-gradient cloud condensation nucleus (CCN) counters utilising different detection methods were operated over a three week period during May 1994, at Mace Head on the west coast of Ireland. One was a DH Associates model (MI), the other was custom built at the CSIRO Division of Atmospheric Research. Concentrations of CCN at a supersaturation of 0.5% were determined during this period for artificial NaCl aerosol particles and for ambient particles in clean maritime westerly, and continental easterly conditions. No significant differences were found between the relative performance of the counters with artificial NaCl particles and ambient particles, and no statistically significant differences in response were observed between maritime and continental conditions. Overall agreement between the two counters, for concentrations less than 1000 cm^{-3} was better than 15%.

Key-words: cloud condensation nuclei, aerosol, condensation coefficient, Mace Head.

1. Introduction

The period of the 1960s and 1970s saw a substantial progress in understanding the physical processes of cloud production and generation of precipitation. These advances resulted in part from extensive field work and accompanying developments in cloud physics instrumentation. Instruments for determination of the concentration of aerosol capable of nucleating water droplets, so called cloud condensation nucleus or CCN counters were part of this development and during the period 1967 to 1980 these instruments alone were the subject of three international workshops. These were held at Lannemezan France 1967, Fort Collins Colorado USA 1970 and Reno, Nevada USA in 1980 (*Kocmond et al.*, 1981; *Jiusto et al.*, 1981).

During the period since the last major international workshop the potential importance of CCN to the radiative properties of cloud and hence to global climate, which has been recognised within the cloud physics community for several decades, (for example *SMIC*, 1971; *Twomey,* 1974), has found support in the wider research community that is now involved in understanding and predicting global climate change (for example *Charlson et al.,* 1987; *Jonas et al.,* 1995). Unfortunately, the momentum that was present during the 1970s in developing CCN instrumentation was not translated during subsequent years into CCN climatologies that would be useful for addressing climate change questions. Indeed, only one long-term measurement series of CCN concentration has so far resulted from the understanding of the climatic importance of CCN reported in the 1970s; it is part of the Australian Baseline Program at Cape Grim Tasmania. This program, which also comprises the major Australian contribution to the WMO GAW program, has included measurement of CCN in clean Southern Ocean air from 1980 to the present (see for example *Gras,* 1995).

This paucity of regionally-representative CCN data should not be interpreted as indicating that interesting developments have not taken place, they certainly have. Several new instrument designs for CCN counters have emerged, including sophisticated continuous counters such as that reported by *Hudson* (1989). Developments on the static thermal gradient instruments have allowed real-time electronic imaging and image processing for count determination and instruments using these procedures have been commercially produced. Other instruments, particularly the mobility classifiers and single-particle condensation nucleus (CN) counters, which are now commercially available, offer alternative calibration possibilities even for older style static counters. The now widely acknowledged climate role of CCN has also seen a call for globally representative CCN determinations and the design of new measurement programs, particularly the WMO Global Atmosphere Watch aerosol program (*WMO*, 1991). One thing that is still lacking though is a truly representative network of stations measuring CCN concentrations and determining the mix of local, regional and global factors maintaining CCN concentration. The commercial production of automated static CCN counters has seen some new climatologies, such as at Mace Head Ireland, begun however protocols for the WMO GAW aerosol program are still in development and the type of close intercomparisons necessary for a cohesive network of CCN counters are certainly not in place yet.

A first step towards comparing the performance of two such CCN counters in the still embryonic GAW 'global network' is reported here. In May 1994 an automated static thermal gradient counter, of the type used at Cape Grim Tasmania, and a commercially-produced automated image-processing type CCN counter (DH Associates, Twomey design) that has been operating at Mace Head (53°19'N, 9°51'W) on the west coast of Ireland since 1993 were run on both artificial NaCl and ambient particles at Mace Head, see *Fig. 1*. This was by design a limited experiment at a single supersaturation, however it is the first such comparison reported. Over the two week period of the comparison there was a significant change in air mass. This afforded an opportunity to look not only at relative differences in calibration using well-defined artificial particles but also for differences between the single particle counting and the photometric techniques for determining CCN concentration with ambient particles. These might arise for example from differences in condensation coefficient of the nucleating aerosol in maritime and anthropogenically influenced continental air masses.

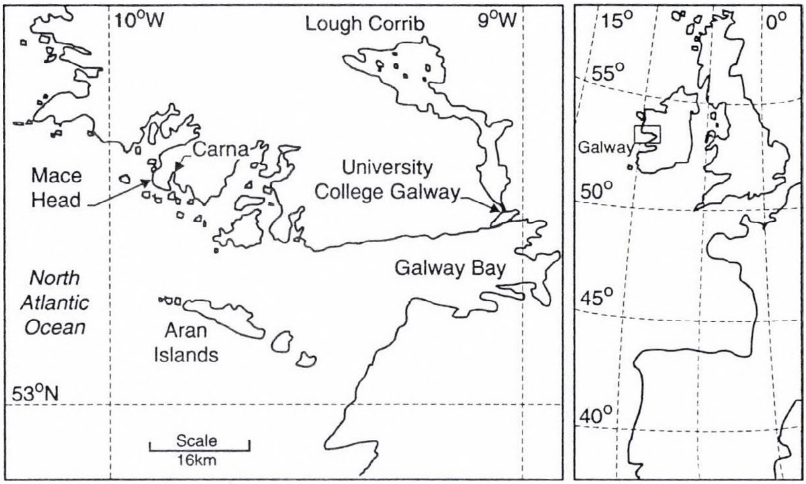

Fig. 1. Map showing location of Mace Head observatory on the west coast of Ireland.

2. *Instrumentation and study details*

2.1 *University College Galway CCN counter — description*

The cloud condensation nucleus counter used by the University College Galway is manufactured by DH Associates (model MI). It consists of a 75 mm diameter glass walled static thermal diffusion chamber illuminated by a laser and viewed by a small CCD camera. The two parallel wetted surfaces separated by a distance of slightly under 10 mm are maintained at different temperatures and a thermocooler controls the temperature of the lower plate of the chamber. The temperature of each plate is monitored separately by means of a thermocouple, the output of which is amplified by a cold-junction compensated amplifier. This is a modification to the manufacturers' arrangement whereby the temperature difference between the plates was measured. An additional modification is the incorporation of a feedback control to maintain a constant controllable supersaturation within the chamber. The resulting supersaturation allows particles to grow into droplets which are made visible by the illuminating laser beam. Digitised video images of activated droplets are used to determine the CCN number concentration. The sampled volume is approximately 6.6 mm^3 and is outlined on the video monitor picture.

A sampling frequency of 30 seconds is used and it requires about 15 samples to complete a 0.1 cm^{-3} count. The cloud chamber contains some 25 cm^3 of air and is flushed at a sampling flow rate of about 1.5 ℓ min^{-1} for 5 seconds for each measurement. The disposition of the inlet and outlet ports in the chamber is somewhat less than ideal however the equivalent of five volume changes should ensure an adequate air exchange. Step changes in concentration, for example connection of a sample storage bag containing aerosol, were certainly registered immediately in this comparison. To obtain a sample representing 1 cm^3 of air requires approximately 75 minutes operation.

The determination of the presence of a drop in the sensing volume is made on the basis the coincidence of illumination in groups of pixels in the scanned field, the processing software for this is proprietary. The tight coincidence and redundancy procedures used are necessary to determine legitimate drops, so that for operation in cleaner environments when either ones or zeros are encountered, there is confidence that electrical or optical glitches are rejected (*Twomey* 1992, personal communication).

2.2 CSIRO automated CCN counter — description

The CSIRO automated CCN counter utilises a static thermal gradient chamber with an internal diameter of 75 mm, a plate spacing of 12.5 mm and a sample volume of 90 mm^3. It has an insulating light-tight spacing ring lined with a thin stainless steel inner surface to minimise edge effects on the thermal gradient. This chamber is identical to that used on the manually operated counter that was intercompared at the 1980 Reno workshop (*Kocmond et al.,* 1981; *Bartlett* and *Ayers*, 1981) and which has operated at Cape Grim since 1981. Upper and lower plate temperatures are sensed using solid state sensors and differential temperature is actively controlled to provide constant supersaturation within the chamber by thermoelectrically cooling the lower plate. The upper and lower plates are covered with black filter papers which act as water reservoirs. The detection system comprises a well-defined, focused, white light from a quartz-halogen illuminator, a reference detector and 45° forward scattering detector. Voltages from the reference and signal detectors are amplified and logged before and for 60 seconds during the cloud formation. The peak scattering signal is used for determination of CCN concentration. This forward scatter system was developed and reported by *Lala* and *Jiusto* (1977) who have also shown theoretically the basis for a linear relationship between peak scattered signal and CCN concentration. The flow system on the CSIRO counter allows for a flush cycle of 20 s at a flow rate of around 2 ℓ m^{-1} and an inbuilt filter zero cycle. As it was operated here it takes about 15 minutes to achieve a sample representing 1 cm^3 although this can be reduced to about 10 minutes.

2.3 University College Galway CCN counter — calibration

This instrument is operated as an 'absolute' counter in the sense that droplets are registered individually by the video processing system from a volume of the illuminating laser beam, defined by the intersection of the laser beam and the video scanning system. This sensing volume is determined from the beam and video system geometry and inevitably has some uncertainty. In order to be counted as a single drop the processing software requires illumination within a set range of adjacent pixels to avoid both spurious counts and to allow for the presence of adjacent droplets. Although the resulting volume is small (6.6 mm^3) the sampling logic accumulates counts to a point where they represent a statistically significant value.

2.4 CSIRO CCN counter — calibration

The CSIRO counter has a photometric output which, based on the work of *Lala* and *Jiusto* (1977), is expected to be linear with CCN concentration. Early calibration of the CSIRO counter as used for the 1980 Reno Intercomparison Workshop and at Cape Grim were based on photography of the resulting cloud. This was used to derive the voltage response by counting cloud droplets in a well-defined volume and confirmed the linear response. Subsequent calibrations of the CSIRO counters have utilised monodisperse soluble particles (NaCl and $(NH_4)_2SO_4$) with a radius of 0.1 μm, classified using a TSI 3760 electrostatic classifier and counted with a TSI 3020 continuous CN counter. The flow rate of the CN counter is independently calibrated to within 1% using a bubble flow meter (Gillibrator Corp.). Because of the single count limitation of the TSI 3020 this calibration is only carried out for CCN concentrations less than 1000 cm^{-3}, however for the normal application this is an adequate range. For the present intercomparison, the automated CCN counter was calibrated about eight months before shipping to Mace Head Ireland and again one month after return shipping to Cape Grim. Calibrations agreed to within 7% and a mean of the calibration factors from before and after shipping has been applied for this work.

2.5 CCN measurement program

The study ran from May 2 through to May 19, although not continuously. Usually operation was limited to periods were the instruments were attended and operated semi-automatically. Both counters employ static thermal gradient chambers which were operated with a peak (centre of chamber) supersaturation of 0.5%. In both cases this was maintained automatically by controlled cooling of the lower plates.

3. Comparison data

In the initial part of the study, artificial particles were used to provide a controlled comparison; this was followed by other longer periods using the ambient aerosol. Polydisperse artificial aerosols of sodium chloride were generated from 0.1% w/v aqueous solution using a #40 de Vilbiss nebuliser and subsequently stored in conductive plastic (3M Velostat) bags. Natural aerosol was sampled, without storage using a common inlet system which brought ambient air into the laboratory. In both cases the counters were operated side-by-side, in a temperature-controlled laboratory, using a shared sample line.

During the comparison the CSIRO CCN counter was operated with manual watering. In retrospect this was a disadvantage because of the limited duration of only several hours before watering becomes necessary. Consequently, periods where the counter water sensing circuitry indicated that the counter was not wet enough or data were missing for any other reason have been edited from the data set. The remaining valid data periods have been concatenated leaving small gaps between the periods with valid data. CCN concentrations plotted on this reduced time scale are given *Fig. 2* and include all of the coincident ambient data. Both counters consistently show the same broad features; the fine detail of the ratio of the concentrations will be discussed later. One problem with the DH counter became evident during the comparison, requiring revision of the output data. Counts in the 0.1 cm^3 accumulations, derived by the instrument processor from the corrected single frame counts showed a quantisation due to the incorrect reading of an internal BCD register, this also increased the output counts slightly. All DH Associates counter data presented here have been corrected.

Fig. 3 shows the observed relationship between the concentration of CCN determined using the CSIRO counter and those on the DH counter for all particles with concentrations less than 1000 cm^{-3} using coincident, unaveraged samples. The upper limit of 1000 cm^{-3} was selected because this is the normal upper range of calibration of the CSIRO counter. The response of both counters is linear and so differences in calibration can be best treated as a scale factor or ratio; zeros were checked using filtered air and for the CSIRO counter these have been corrected. Mean ratios, for a variety of conditions including both artificial and ambient particles are included in *Table 1*. These were derived for all valid data periods on the DH counter where there were corresponding readings on the CSIRO counter. Other data in Table 1 are standard deviation and number of samples for the different comparison regimes.

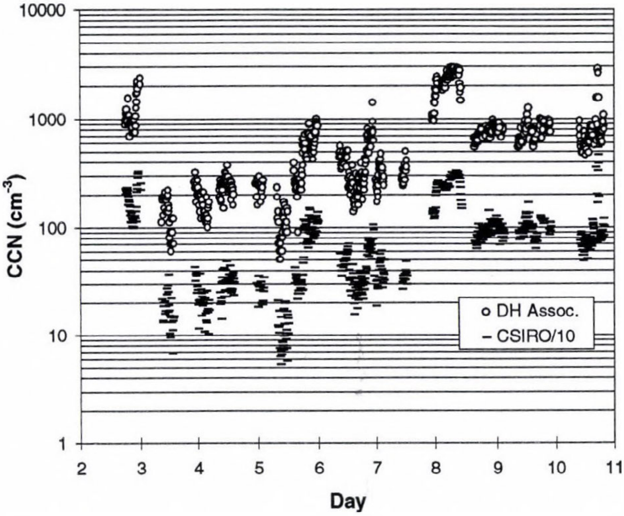

Fig. 2. The concentration of CCN active at 0.5% supersaturation for all simultaneous ambient samples obtained during the study. Concentrations obtained from the CSIRO counter have been scaled by a factor of 10 to prevent overlap. See text for details on the time scale.

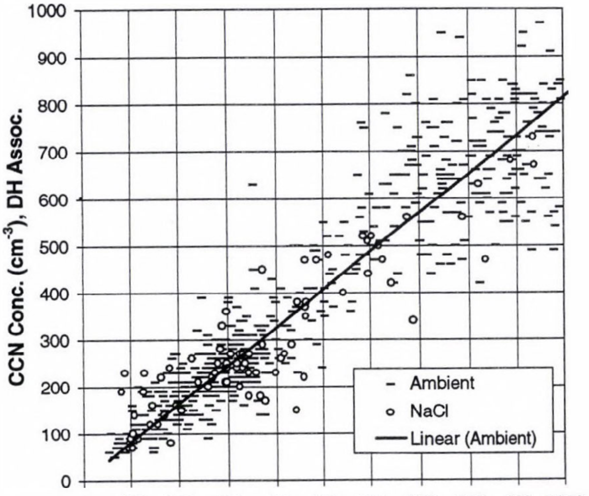

Fig. 3. Comparison of CCN concentration derived using CSIRO and DH Associates counters for all particles with concentrations less than 1000 cm^{-3}.

Table 1. CCN concentration ratio means (for DH Associates/CSIRO), standard deviations and number of cases for different comparison regimes

	$N < 1000$ cm^{-3}			All N		
	Ratio	σ	n	Ratio	σ	n
Artificial NaCl particles	0.88	0.37	79	0.80	0.36	103
Ambient, west sector days 3.4–5.7	0.86	0.26	181	0.86	0.26	181
Ambient, east sector days < 3 & 5.8–11	0.86	0.17	333	0.82	0.17	552

There is a small difference for artificial aerosol for all concentrations and those less than 1000 cm^{-3} although the difference is only marginally significant (t test significant at around the 0.15 level). This included a number of samples at the start of the comparison which appear atypical. The ratio of the two counter outputs (DH Associates) for ambient particles is given in *Fig. 4* as a function of time using the concatenated time scale; wind direction is also plotted (values shown are individual samples representing volumes of approximately 0.1 cm^3). During the period between days 3.4 and 5.7, wind direction was consistently from the westerly sector, subsequently backing to become easterly for the remaining period. Reference to Fig. 2 shows that corresponding CCN concentrations were typically around 200–400 cm^{-3} during the westerly period increasing to around 1000 cm^{-3} in the later part of the study where the winds had an easterly component. Although the ratios as plotted in Fig. 4 are noisy because of the small sample volumes in the two counters, the average ratio for the different sample periods does not show any consistent variation corresponding to wind direction change from westerly through to easterly. The immediate origin of the air in this latter case was from over Ireland. Greater variance in the ratio CSIRO/DH Assoc. is also evident during westerly conditions; this can be expected because of the significantly lower concentrations during these conditions. The periods of the westerly and easterly regimes can reasonably be considered separately as broadly representing maritime (possibly anthropogenically modified) and continental air. Concentrations of CN during the period where winds had a westerly component were generally less than 600 cm^{-3} although there was one period where over about eight hours concentrations rose to around 1100 cm^{-3} and then returned to the lower levels. Table 1 gives the mean ratios of concentration on the DH counter and CSIRO counter for both wind regimes with differentiation between CCN concentrations less than 1000 cm^{-3} and all values (all cases had CCN $<$ 1000 cm^{-3} for the westerly sector).

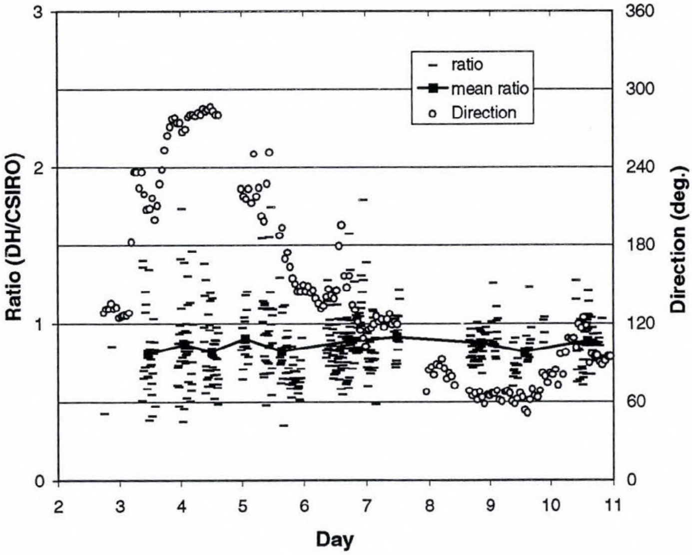

Fig. 4. Individual CCN concentration ratios (DH Assoc./CSIRO) for coincident ambient samples with CCN concentration less than 1000 cm^{-3}. Mean ratios for each group of (joined by straight line segments) are also included as are hourly mean wind directions.

For CCN $< 1000\ cm^{-3}$ the mean CCN concentration ratios given in Table 1 show no statistically significant differences between artificial NaCl aerosol and ambient particles for either the westerly maritime period or easterly period, (*t* test significant at > 0.6 level). Also, on average there is no difference between the relative response in easterly and westerly sectors. For both sectors this result is consistent with the aerosol in the CCN size range being comprised principally of soluble species. By examining aerosol volatility, *Jennings and O'Dowd* (1990) determined that in westerly conditions around 85–95% of the size fraction, by volume, with radii $< 0.2\ \mu m$ were ammonium sulfate or bisulfate. For the radius range 0.3 to 1.5 μm around 80% consisted of salt.

There is some difference in the relative response of the two counters when CCN concentrations greater than 1000 cm^{-3} are included, although these comparisons extended only to around 3000 cm^{-3}. Ratios of DH Assoc./CSIRO given in Table 1 for all values, using artificial NaCl show a systematic but not strongly significant difference (significant at around the 15% probability level). On the other hand, for the case of natural particles observed during easterly conditions, a similar change in ratio as that for artificial NaCl particles is observed by including the larger concentrations. In this case the difference is statistically significant (at around the 0.1% level), indicating a relative shift in the response of the two counters at larger concentrations.

4. Aerosol condensation coefficient

The DH and CSIRO counters use static thermal gradient chambers of similar geometry to supersaturate a sample of air but the method of detecting the nucleated droplets is different. The DH counter is a true counter in the sense that individual drops in an illuminated sensing volume are counted whereas the output from the CSIRO counter is a scattered light signal.

To some degree both counters are subject to uncertainty in concentration because of the condensation coefficient of the growing droplet. Strictly, it is only a problem for aerosol of unknown composition, where the particles detected may differ from that of a pure salt 'calibration' aerosol. The CSIRO counter is probably more sensitive because it operates in a photometric mode. With the DH counter the condensation coefficient potentially could influence the sensing volume (around edges), and possibly some drops may not reach a detection threshold in the wait period (20 sec) if the condensation coefficient is very small. For the CSIRO counter, where the output is a function of drop number and final size, the condensation coefficient could influence the final droplet size and hence the apparent concentration.

The absence of any statistically observable difference between the ratios of the two counters for westerly and easterly conditions, and the similarity also for artificial and ambient particles is an indication that effects of unknown condensation coefficient are relatively minor compared to other noise sources. Whilst no difference was observed on average, for the observed variance in the ratios and number of observations, a 4% difference in ratio for example would have been significant at the 5% probability level.

This estimation of a lower bound for the effects of condensation coefficient is of interest for CCN counters with photometric detectors in general, since there are few data available. Such effects could be particularly important where these counters are used in climatologies that include anthropogenically impacted air. The present work suggests that this is not a major concern.

5. Conclusions

Two static thermal gradient CCN counters that use quite different detection schemes have been shown to give good agreement using artificial NaCl particles and ambient particles in a short comparison experiment on the west coast of Ireland. For the NaCl particles and ambient aerosol the agreement averaged better than about 14% at concentrations less than 1000 cm^{-3} with some systematic shift in relative response at larger concentrations. No significant differences were observed in the response of the two counters in maritime (westerly) or easterly (continental) conditions although for the particular experimental conditions, any shift in response greater than about 4% would have been statistically significant (at the 95% confidence level). This allows an estimate of the upper bound for the likely effects of the condensation coefficient on response of CCN counters with photometric detectors at less than this value. Overall agreement between the two CCN counters, particularly in the CCN < 1000 cm^{-3} calibration range of the CSIRO counter is within 15% which is good when seen in the light of previous comparison workshops.

This direct comparison of two CCN counters might serve as a useful model for further comparisons of such counters in the WMO GAW aerosol program. Where counters are operating on different principles, or as here just employing different detection schemes, it is important to use not only well defined artificial aerosol types but to include a range of compositions and particularly ambient particles.

References

Bartlett, B.M. and Ayers, G.P., 1981: Static diffusion cloud chamber. *J. Rech. Atmos. 15*, 231-233.

Charlson R.J., Lovelock, J.E., Andreae, M.O. and *Warren, S.G.*, 1987: Oceanic phytoplankton, atmospheric sulphur, cloud albedo and climate. *Nature 326*, 655-661.

Gras, J.L., 1995: CN, CCN and particle size in Southern Ocean air at Cape Grim. *Atmos. Res. 35*, 233-251.

Hudson J.G., 1989: An instantaneous CCN spectrometer. *J. Atmos. Ocean Technol. 6*, 1055-1065.

Jennings, S.G. and *O'Dowd, C.D.*, 1990: Volatility of aerosol at Mace Head, on the west coast of Ireland. *J. Geophys. Res. 95*, 13937-13948.

Jiusto J.E., Ruskin, R.E. and *Gagin, A.*, 1981: CCN comparisons of static diffusion chambers. *J. Rech. Atmos. 15*, 291-302.

Jonas P., Charlson, R.J. and *Rodhe, H.* (eds.), 1995: *Aerosols, in Climate Change 1994, Radiative Forcing of Climate Change and an Evaluation of the IPCC IS92 Emission Scenarios.* Intergovernmental Panel on Climate Change, Cambridge University Press, 127-162.

Kocmond, W.C., Rogers, C.F. and *Rea, S.W.*, 1981: *The Third International Cloud Condensation Nuclei Workshop*. NASA Conference Publication, No. 2212.

Lala, G.G. and *Jiusto, J.E.*, 1977: An automated light scattering CCN counter. *J. Appl. Meteor. 16*, 413-418.

SMIC, 1971: *Study of Man's Impact on Climate*. MIT press, Cambridge, Massachusetts.

Twomey S., 1974: Pollution and the planetary albedo. *Atmos. Environ. 8*, 1251-1256.

WMO, 1991: Report of the WMO meeting of experts to consider the aerosol component of GAW. Boulder, CO., *WMO Report 79*, WMO/TD-NO, 485.

IDŐJÁRÁS

Quarterly Journal of the Hungarian Meteorological Service
Vol. 100, No. 1–3, January–September 1996

Statistical analysis of the pollutant levels in Budapest

Györgyi Baranka

Institute for Atmospheric Physics,
H-1675 Budapest, P.O. Box 39, Hungary

(Manuscript received 7 June 1995; in final form 18 August 1995)

Abstract—Urban air quality has been monitored by a new network system in Budapest since 1991. Statistical analysis of the data shows which are the most polluted sites in the city. Cumulative frequency distributions in the data set indicate the percentage exceedence of threshold values during the monitoring period. The average seasonal variations of the air pollutants have been investigated as well. Some possible temporal and spatial features of air pollutants have also been considered. Generally, the trend in NO_2 and CO concentration is decreasing, while TSP and SO_2 levels are similar during the period of 1991–1994.

Key-words: urban air quality, cumulative frequency distribution, threshold values.

1. Introduction

Emission of air pollutants, climate and geographical situation determine the air quality in cities. In Budapest these factors are not favourable for pollutant dispersion. The geographical obstacle of the Carpathian mountains around Hungary moderates the air flow in the surface layer. Budapest is divided into two parts, Buda (on the westside) and Pest (on the eastside of the Danube). Buda is characterized by hilly terrain and Pest by flat terrain.

Approximately one fifth of the population of Hungary lives in Budapest. This report provides a summary of the air pollution situation in the capital. The recent situation and temporal variations of air quality are investigated using air quality thresholds. A general overview and statistical evaluation of air quality in Budapest has not been carried out before. This is the first report that attempts to show which pollutants still cause the urban air pollution, and points to areas where high concentrations are frequent.

Similar surveys have been carried out for several towns in UK by *Bower et al.* (1991), *Hewitt* (1991) and *Eggleston et al.* (1992). The measurement results for all air pollutants and some other aspects of urban air quality in UK are summarized by the Quality of Urban Air Review Group (*Harrison,* 1993).

2. *Emissions*

The present general air pollution conditions in Budapest (more than 2 million inhabitants over 525 km^2) are mostly determined by the emission from mobile sources (road traffic). The form of the emissions has changed significantly over the last 15–20 years in Budapest due to the 'natural gas program'. As a result, the emission of sulfur and nitrogen oxides from the industry as well as district and domestic heating, has decreased a lot. The nature of urban air pollution has changed over recent decades. Motor vehicles are now the dominant source.

The annual anthropogenic emissions of CO, VOCs (volatile organic compounds), NO_x and SO_2 — based on a survey (*M. Szilágyi*, 1991) referring to 1990 — for different source categories are summarized in *Table 1*.

Table 1. Annual anthropogenic emissions in Budapest (kt yr^{-1})

	CO	VOCs	NO_x	SO_2
Mobile sources	111,500	14,000	7,712	1,663
Industry and energy production	24,949	2,177	8,705	9,095
District and domestic heating	10,236	2,794	2,516	12,125
Total	146,685	18,971	18,933	22,883

It should be noted, however that the emission rate of particulate matter is also giving a significant contribution to the air pollution over Budapest. Its estimated annual total is around 9 thousand tons.

The number of cars is seven times higher than it was 20 years ago. Although the number of western type cars keeps growing a large part of them is yet equipped with out-of-date engines without catalytic converters. The average age of the car fleet is over 10 years. The improvement of road infrastructure is far behind the rapid development of mobilization: the total length of public roads is only 50% more compared to the conditions in the 70's. It can be seen from Table 1 that mobile sources are responsible for the majority of CO (76%) and VOC (74%) emissions in Budapest.

3. *Monitoring of air quality*

Air quality monitoring has increased in recent years both in terms of the number of pollutants monitored and the number of sites. However, coverage of urban areas is still limited.

The Institute of the Government Service for Public Health, Budapest, has been operating an air pollution monitoring network in Budapest consisting of 8 stations (*Fig. 1*) for the measurement of SO_2, NO_x, CO and TSP (total suspended particulate) concentrations since 1991. There is also O_3, and TNMHC monitoring at two of these stations (No. 1 and No. 4).

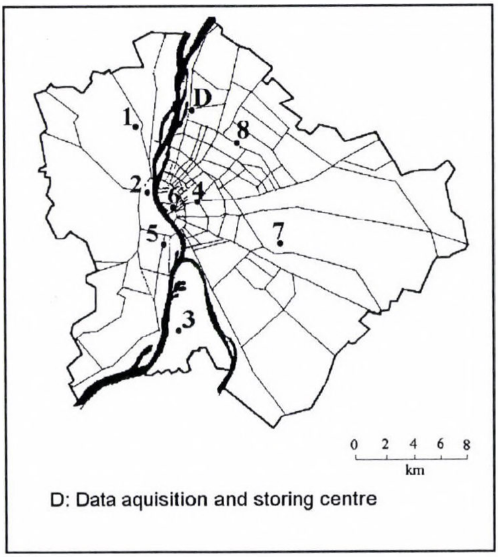

D: Data aquisition and storing centre

Fig. 1. Locations of urban air quality monitoring sites in Budapest.

The type of air quality monitoring equipment is different according to pollutant. SO_2 is measured by pulsed fluorescence, NO_x by chemiluminescence with molybdenum converter, CO by IR detection with gasfilter correlation, TSP by β-ray emission, and O_3 by UV absorption type of monitors. All the substantial meteorological information (wind speed and direction, temperature and humidity) are measured by meteorological sensors. Monitors are connected with a telemetric system.

A central data acquisition system collects and stores the data coming from the stations. There are two public display systems in Budapest at two underground stations to inform the inhabitants of the actual air pollution conditions in the downtown area.

The location of monitoring stations is an important consideration in any air quality monitoring network. The stations should cover the industrial, roadside, urban background and suburban areas of the city. It is sometimes difficult to classify a site into one of these categories, but the basic features and circumstances of monitoring sites in Budapest are described in *Table 2*.

For the general investigation the stations are divided into two groups. One type consists of the four monitoring sites in the downtown area, they are sites No. 2, No. 4, No. 5 and No. 6. The other group involves the remained four stations in suburb, namely No. 1, No. 3, No. 7 and No. 8 (see Fig. 1).

Table 2. Urban monitoring network, site information

Number of station	Site	General surroundings
1	Laborc utca	Sparsely built-up residential area in the suburbs with detached houses, quiet back streets, close to the forestry area
2	Széna tér	Residential area affected by car traffic and industrial sources in the centre of the town
3	Déli utca	In a open area belonging to a factory
4	Baross tér	Next to a main road with a high traffic density in the downtown area
5	Kosztolányi tér	Densely built-up residential area affected by road traffic in the downtown area
6	Erzsébet tér	Business, office and residential area in the centre of the town
7	Gergely utca	In an area strongly influenced by industrial pollution on the outskirts
8	Ilosvay utca	Residential area on the outskirts of the town, bounded on all sides by streets

The non-realtime analysis of the data collected by the monitoring network is carried out in the Institute for Atmospheric Physics. Daily and seasonal variations of the concentrations as well as the characteristics of the actual meteorological situations, are considered together.

Operational period of the new monitoring system in Budapest started in 1991 April. Investigation presented here involves data from this date to December 1994.

4. Cumulative frequency distribution of daily averages

Concentration measurements of chemicals in the atmosphere often exhibit a log-normal distribution. When the distribution are transposed to cumulative frequencies plotted on log-probability paper, they become straight lines with the slope proportional to the variance and the lines intersecting at the median (cumulative probability of the 50 percentile). Generally, the cumulative distribution shows how many percentiles of the data set (horizontal scale) are under given value (vertical scale).

Similar frequency distribution analysis have been carried out for each station and pollutant. To view the distributions the station data have been grouped into several categories. Two examples of lognormal cumulative frequency distribution plots are illustrated in *Fig. 2a* and *Fig. 2b* for NO, NO_2 and CO. In Budapest pollutants, which have very high concentrations (NO, NO_2 and CO), originate from traffic sources. Nitrogen monoxide and carbon monoxide are primary pollutants, nitrogen dioxide is a secondary pollutant, because it is formed from nitrogen monoxide by different chemical reactions in the air. Emissions play a great role in determining primary pollutant levels, whilst chemical reactions and meteorology dominate the formation of the secondary pollutant concentrations. These effects are seen in the frequency distributions, namely the cumulative distribution of secondary pollutants less closely approximates a lognormal distribution.

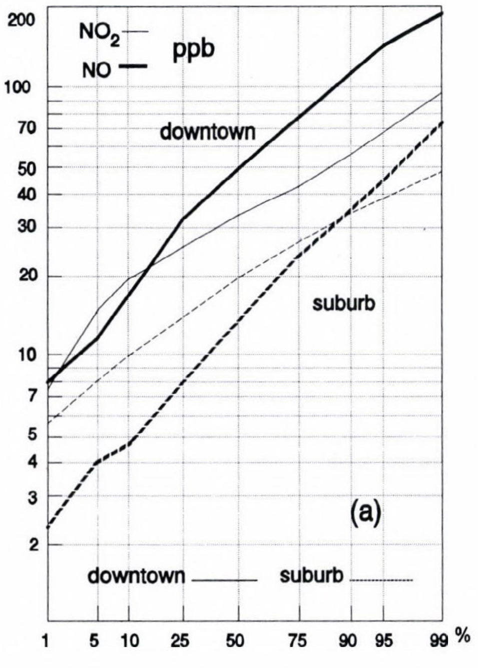

Fig. 2a. Cumulative distribution of NO and NO_2 daily averages during 1991–1994.

In *Fig. 2a* NO and NO_2 distributions are shown for downtown and suburban sites (see above the categories of the stations). The steeper slopes of NO indicate a greater temporal variability. High variability is generally due to pronounced seasonal changes in the concentrations of the pollutants (see Fig. 3 below). The curves of suburban values are below the curves of downtown data, since their concentration values are generally lower.

Another example, showing how the unusual source emissions and meteorological conditions can affect the cumulative frequency distribution, is the data set from the city-centre commercial site in Budapest. Most of the daily CO concentrations are very well approximated by straight line log-normal plots, illustrated in *Fig. 2b*. For CO the stations have been divided into three groups. The first one includes stations under high traffic influences (No. 4, No. 5), the second one is far from roads (No. 7, No. 8), and the third one is moderately polluted by CO (No. 1, No. 2, No. 3 and No. 6).

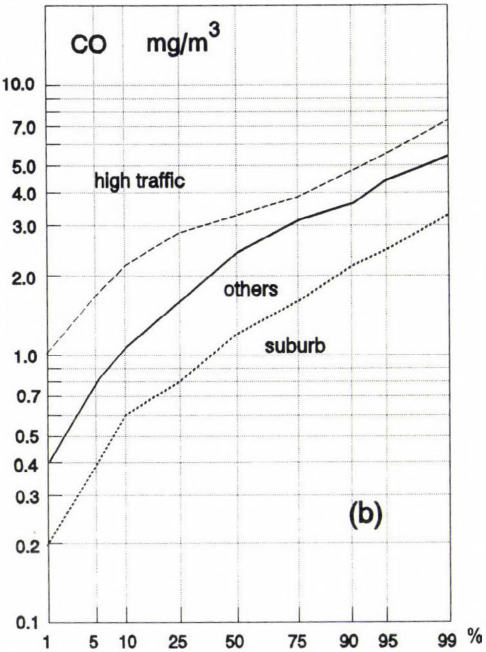

Fig. 2b. Cumulative distribution of CO daily averages during 1991–1994.

Study of the cumulative frequency distributions are very useful, because the threshold and guide values of air pollutants and the general exposure of the population to air pollution are decided on the basis of the data distribution over several measuring periods. To evaluate air quality, the threshold values for the long and short-term periods are given. The long-term threshold value is the yearly average, or the 50th percentile of the daily data set, which is generally somewhat lower. The 98th percentile (P_{98}) values presented in Fig. 2 are representative of the maximum daily concentrations. In particular, the P_{98} value corresponds to the concentration that is not exceeded for more than 7 days during the year. Nowadays the following threshold values (see *Table 3*) are valid in Budapest.

Table 3. Air concentration threshold values in Budapest

Elements	Threshold values in Budapest	
	24 h	half-hour
NO_2 ($\mu g/m^3$)	85	100
SO_2 ($\mu g/m^3$)	150	250
CO (mg/m^3)	5	10
TSP ($\mu g/m^3$)	100	200
O_3 ($\mu g/m^3$)	100	110

5. The seasonal variation of air pollutants

The average seasonal variations of the air pollutants for the period of 1991–1994 are shown in the *Fig. 3*. It can be seen that SO_2, NO and CO concentrations have similar seasonal variations with summer minima and winter

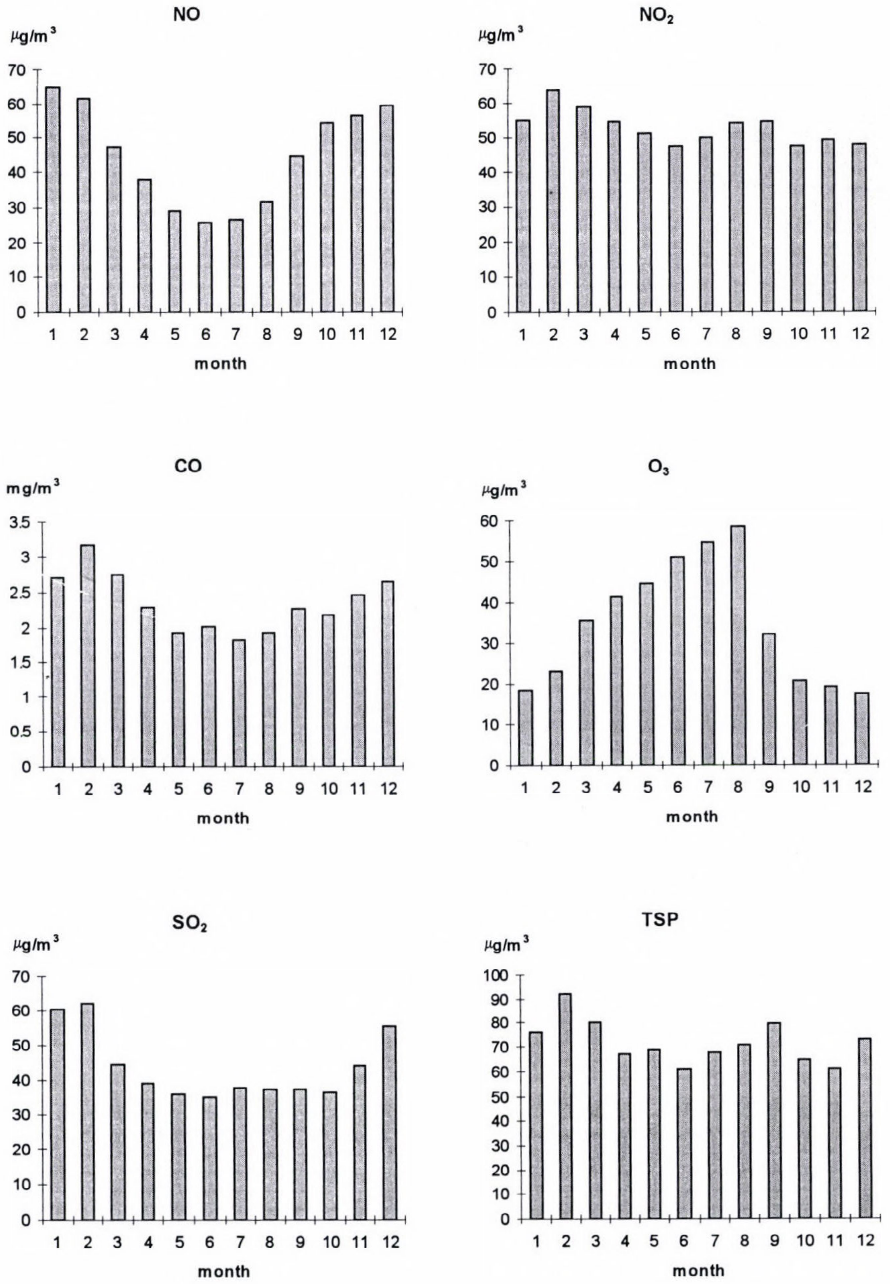

Fig. 3. Annual variation of air pollutants during the period of 1991–1994.

maxima. NO and CO are the primary pollutants with strong dependence on meteorological conditions, while the cause of the winter high level of SO_2 is the increased domestic emission. Due to the photochemical formation the ozone peaks can be detected in summer. The seasonal variations of NO_2 and TSP are not strongly marked.

It can be seen that the multiyear average concentrations of NO_2, CO, SO_2 and TSP are highest in February. The reason is that in general the yearly absolute maxima occur in February at most of the stations, especially in 1993, when the peaks of above mentioned pollutants were found at every station in February.

6. Temporal variation of air pollutant

Average annual variations of SO_2, NO_2, NO, CO, TSP and O_3 for the period of 1991–1994 (the operational period of the new monitoring system in Budapest) do not show a significant trend. It is obvious that all the pollutants have significant spatial variation in the city. For these reasons we can try to consider some possible temporal and spatial feature of air pollutants.

In the recent period (1991–1994) the temporal variation of air quality in Budapest is characterized by changes in the exceedence of threshold values. NO is missing from the evaluation because no threshold value for NO exists. In the case of SO_2 and O_3 there are no exceedences in these years. The relative frequency of the exceedences of threshold values for other pollutants are shown in the *Fig. 4*. It is indicated that the number of exceedences has decreased in the case of NO_2 since 1991; there was less stations and smaller percentages of exceedence in 1994 than in earlier years. Generally, the tendency of CO level is decreasing, but at the station No. 5 a significant increase was observed. The frequency of TSP threshold values is similar in the two years with high relative percentage exceedences in the downtown area.

7. Conclusions

Earlier, in the 70's years the important air pollutants were SO_2 and NO_2 originated from industrial and district/domestic heating. Now, the traffic is the main contributor to poor urban air quality. Emissions from traffic are near groundlevel and thus have a greater impact on local air quality emissions from industrial sources, released at a higher level.

Spatial distribution of the most important air pollutants (NO_2 and CO) are shown in Fig. 2. In the downtown area only a few percentiles of the daily average NO_2 concentration exceed the threshold value, while in suburban area there are always below the threshold value. About 10 percent of CO concentrations measured at stations closed to roads with the high traffic in the downtown area are above the threshold value during the monitoring period.

On the basis of our investigations it can be stated that the daily sulfur dioxide and ozone concentration is not high, but the town are strongly polluted by TSP. Pollutants (NO_2, CO) originating from mobile sources have generally decreased over the period of 1991–1994 but the monitoring period is too short to draw firm conclusion. This means that motor vehicles are now the dominant source in Budapest.

Trends of NO_2 and CO concentration are decreasing, while TSP and SO_2 levels are similar during the period of 1991–1994. The most polluted areas in Budapest are the main roads full of motor traffic in downtown area.

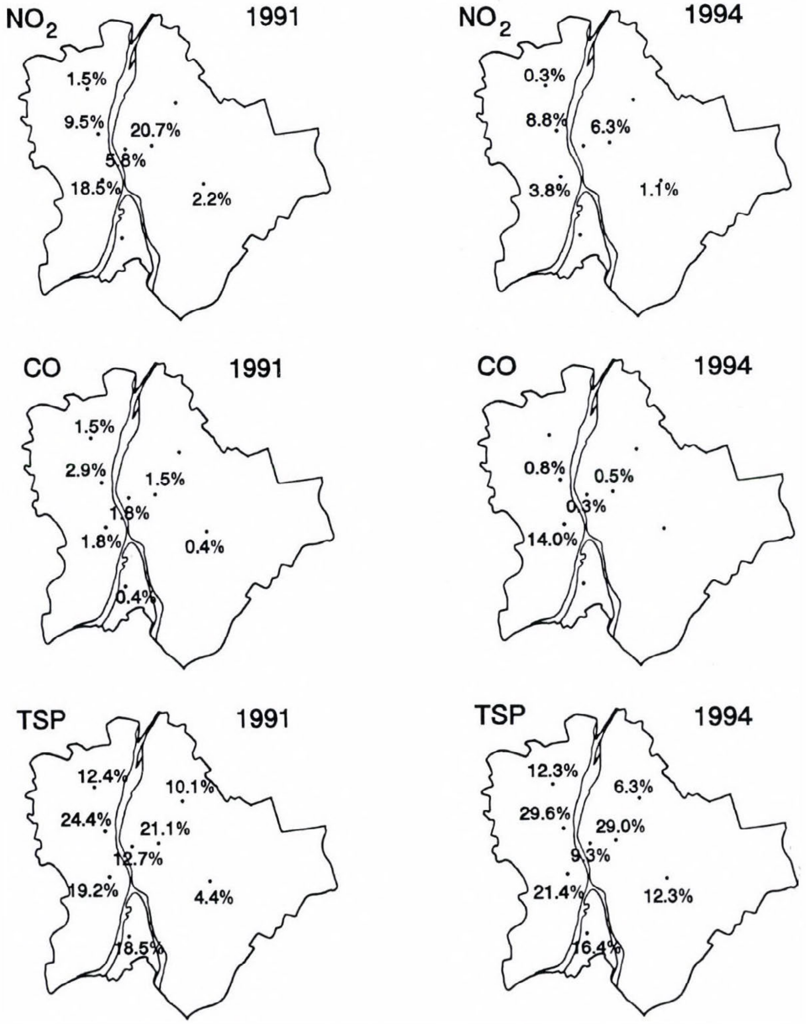

Fig. 4. Relative frequency of the exceedences of threshold values.

References

Bower, J.S., Broughton, G.F.J., Dando, M.T., Lees, A.J., Stevenson, K.J., Lambert, J.E., Sweeny, B.P., Parker, V.J., Driver, G.S, Laight, S.E. and *Waddon, C.J.*, 1991: Urban NO_2 concentrations in the UK in 1987. *Atmospheric Environment 25B*, 267-284.

Eggleston, S., Hackman, M.P., Heyes, C.A., Irwin, J.G., Timmis, R.J. and *Williams, M.L.*, 1992: Trends in urban air pollution in the United Kingdom during recent decades. *Atmospheric Environment 26B*, 227-239.

Hewitt, C.N., 1991: Spatial variations in nitrogen dioxide concentrations in an urban area. *Atmospheric Environment 25B*, 429-434.

Harrison, R.M. (ed.), 1993: *Urban Air Quality in the United Kingdom.* Published by Air Quality Division Department of the Environment, London.

M. Szilágyi, K. (ed.), 1991: Report on air pollution of Budapest (in Hungarian). Published by Air Quality Protection Ltd., Budapest.

IDŐJÁRÁS

Quarterly Journal of the Hungarian Meteorological Service
Vol. 100, No. 1-3, January-September 1996

Climate and water in plant ecology

Emánuel Antal[1] and **Károly Szesztay**[2]

[1]*Péterhalmi u. 3/a, H-1181 Budapest, Hungary*
[2]*Kőrózsa u. 21, H-1028 Budapest, Hungary*

(Manuscript received 22 May 1995; in final form 16 August 1995)

Abstract—Fluctuation and change of climate are the major driving force of changes and shifts within plant ecological zones with important feed-backs on local climate and with cycles of water as the fundamental tool and vehicle of this interaction. In coping with pressure of increasing energy prices and the demand of long term sustainability crop production has foreseeably to come rather soon considerably closer to its ecological and environmental conditions. The fundamental processes of plant growth can be best identified and analyzed at the plant ecological scale (Fig. 1) within which plant communities have powerful capabilities for interacting with their physical environment through finely tuned water use strategies (Fig. 2). The water systems framework embraces and brings into interaction the terrestrial, the aquatic and the littoral ecosystems (Fig. 3) and being continuously shaped and reshaped under the combined influences of geology and climate (Fig. 4), it introduces the features of *local diversity* as one of the natural characteristics and stability factors of plant ecology. These patterns of local diversity are supplemented by patterns of *regional and global coherence and interaction* through the climate driven cycles of water which also provides the major pathways for the biogeochemical cycles (Fig. 5 and 6). Crop productivity systems could and should be brought closer to these natural patterns of plant ecology through several means and levels of planning and policies for which water balance simulation at the plant ecological scale is one of the basic tools (Fig. 7, 8 and 9).

Key-words: climate change, evapotranspiration, irrigation water requirement, soil moisture simulation, water balance simulation.

1. Plant ecological scale and interactions among climate, soil and vegetation

When looking at the systems of crop production from the viewpoint of the *natural sciences* it becomes clear that the terms *'Environment'* and *'Resources'* applied in planning and evaluating such systems within their institutional and technological context hide essentially another system which comprises the factors and processes of *plant physiology* based on the interactions among climate, soil and vegetation as mediated by the infiltrating and exfiltrating water fluxes of the root zone (boxes 1.a, 1.b and 1.c of *Fig. 1*). This natural unit of plant communities under practically uniform conditions of climate, soil and vegetation becomes also important constituent of its broader regional and global environment through the fluxes of energy, water and biogeochemical materials cycling within the fluvial systems and the atmosphere (boxes 2 and 3).

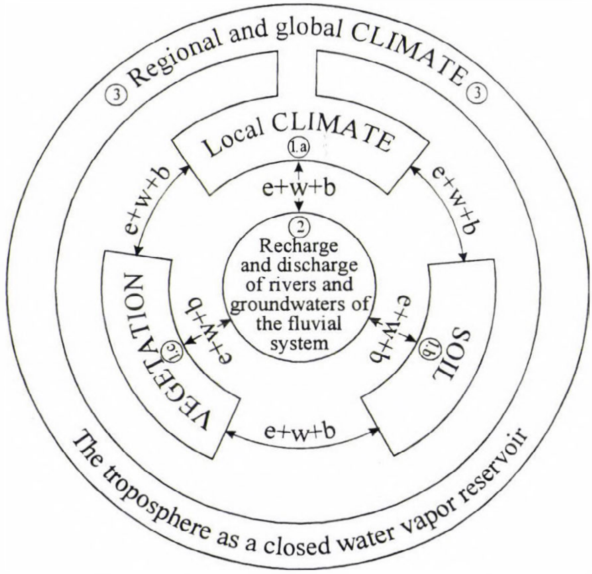

Fig. 1. Internal and external flow of energy (*e*), water (*w*) and biogeochemical elements (*b*) within and among the plant ecological units.

Vegetation is the leading component in these interactions for several reasons. It is the only living component of the interacting systems. It is, therefore, capable, by its very nature, of responding to information flows from outside by structural changes. In this way the vegetation cover has developed and maintained two distinct features at all scales and modalities of the geosphere-biosphere interaction:

- it is capable of adapting itself, by evolutionary changes, to virtually all types of land environments and its unceasing modifications;
- at the same time it is also capable of powerfully influencing and modifying its physical environment with definite and consequent evolutionary strategies. This twofold ability of the vegetation species introduces the capability of self-organization and pattern making/using into plant ecological systems of all types and scales.

One of the reasons why vegetation cover could occupy all the available continental lands and can successfully survive and evolve even within the severest environments (such as the coast and mountains of Alaska with more than 300 rainy days a year, or the semideserts with one or two occasional showers a year) lies in the extreme flexibility of plant water use strategies and the great diversity of plant physiological solutions for the regulation of water storage and transpiration. At the *micro-level* of individual plants and their small size communities these diversities and flexibilities can be described (*Eagleson,* 1982) as variations of the indices

$$M_o = A_v : A \tag{1}$$

and

$$k_{vo} = ET_v : E_{so} \tag{2}$$

according to the exfiltration index (see *Fig. 2*)

$$E = T_{hko} : T_{hk}, \tag{3}$$

where M_o is the *canopy density* (the shaded fraction of the surface) defined by the ratio of the vertical projection area of the canopies A_v to the total surface A; k_{vo} is the species-dependent *plant water use coefficient* defined as the ratio of the unstressed rate of plant transpiration ET_v to the potential rate of bare soil evaporation E_{so}; E the *exfiltration index* is a composite and residual representation of 21 climatic and soil physical factors specifying the rate of the exfiltration process which takes place during the periods between two successive rainfalls. Eq. (3) is a simplified description and approximate solution for quantifying the value of E as the ratio of the period T_{hko} (during which bare soil exfiltration proceeds at its potential rate, i.e. the rate of moisture supply from the deeper layers does not limit surface evaporation) to T_{hk} the average time period between two successive rainfalls. Under *dry conditions*, when the value of E is smaller than one (section B_1–B_2 in Fig. 2) the vegetation cover acts as saver and preserver of moisture and under extreme dryness of desertic conditions (E around 0.01), it performs these functions very efficiently (with a value of k_{vo} around 0.4) but at a very low canopy density (M_o around 0.2). When the environmental water stress loosens (the index E gradually rises) both k_{vo} and M_o are increasing indicating that the vegetation cover consumes greater and greater part of the available soil moisture. At point D of Fig. 2 (at value of E between 2 and 3) the environmental water stress virtually ceases and plant physiology changes its evolutionary trends from *water controlled strategy* (aiming at capturing greater and greater part of the environmental water supply) toward a *heat controlled strategy* (aiming at absorbing more and more photosynthetic radiation and heat for increasing biomass and yield production) with the consequence of decreasing values of k_{vo} and increasing values of M_o.

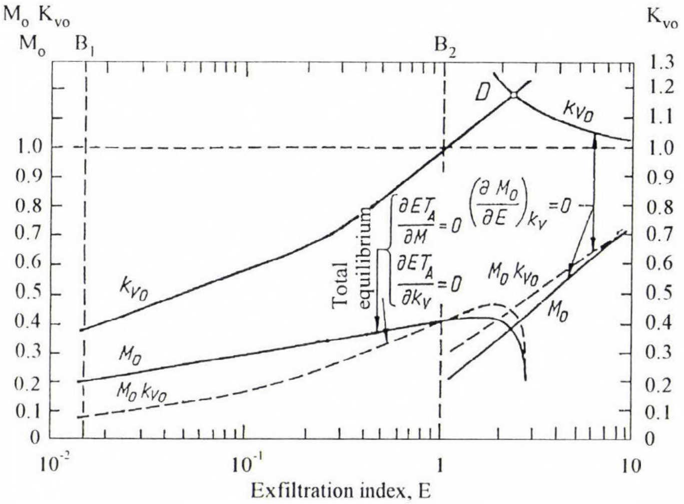

Fig. 2. Variation of the canopy density index (M_o) and the plant water use coefficient (k_{vo}) according to the exfiltration index (E) under equilibrium conditions (*Eagleson,* 1982).

2. *Water systems framework*

Within the great majority of continental lands plant ecology is structured according to sets of smaller and larger river basins with different local climate and soils conditions. When looking at the scheme of climate-soil-vegetation interaction of Fig. 1 from viewpoints of the fluvial basin framework the conceptual representation needs extension in three major directions (*Orlóci et al.,* 1993):

- beside the terrestrial ecosystems land areas hold and nourish also aquatic and littoral ecosystems;
- the three types of ecosystems are contained and interlinked within smaller and larger pieces of landscape which have ecological, local climatic and hydrological characteristics and rules of their own;
- in terms of geobiophysical processes forming the topography, the soils, as well as the surface and groundwater systems of the fluvial basin the scheme of Fig. 1 has to be completed to include crustal movement and rock formation processes. This altered and extended scheme (*Fig. 3*) is, of course, also permeated and integrated by the continuous flow of water, biogeochemicals and climatic energy from among which the flow and storage of water through and within the river network and the groundwater aquifer system are the most decisive unity-forming process of the fluvial basin. The formation of river basins is a slow and delicate

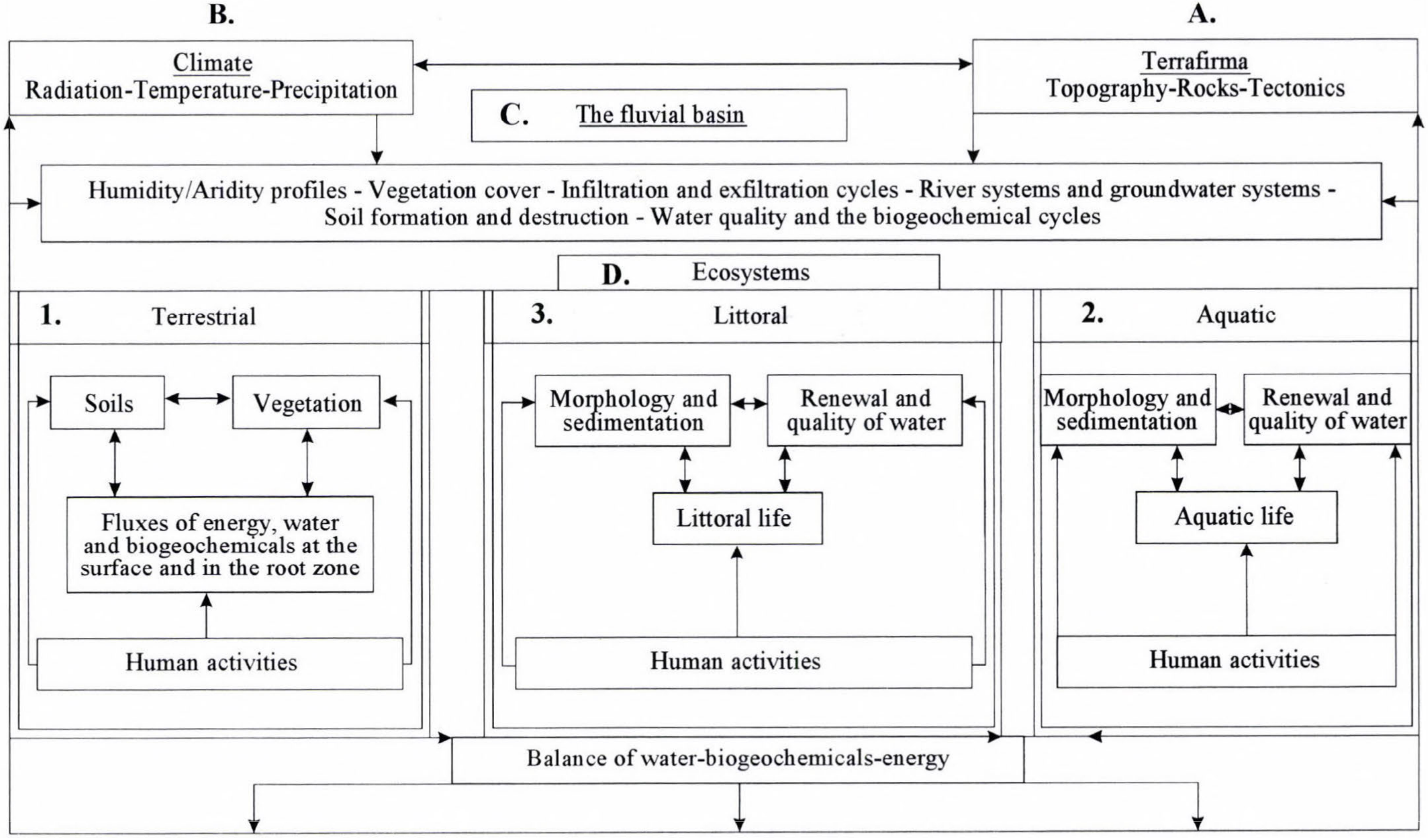

Fig. 3. Major physical and ecological factors and processes in the formation and evolution of the fluvial basins.

process of sedimentary rock formation governed by the interplay of climate change cycles and variation of the intensity of crustal sinking and lifting in time and in space (*Fig. 4*).

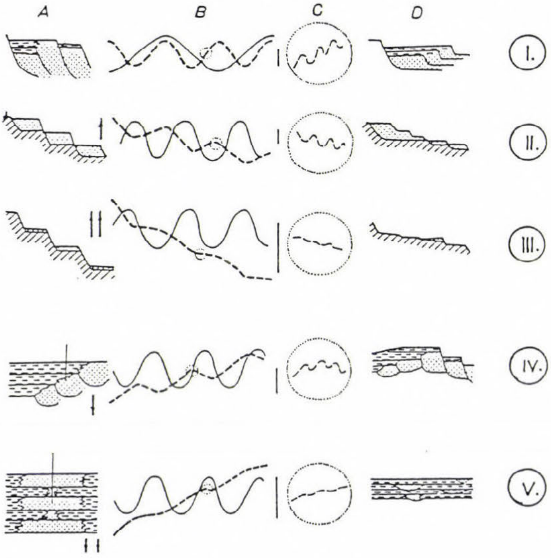

Fig. 4. Climatic and tectonic factors coinciding in the fluvial response (*Starkel*, 1990). I. climate change cycles in tectonically stable areas; II. in conditions of slight tectonic uplift, II. in conditions of intense tectonic uplift; III. in conditions of slight tectonic subsidence; V. in conditions of intense tectonic subsidence. The column B shows the overlapping of climate cycle (continuous line) and variations between erosion (down) and aggradation (up-broken line); the column A shows typical sequences of terrace bodies for glacial-interglacial cycles (dots-channel deposits, dashes-overbank deposits, diagonals-bedrock); the column C gives the enlarged fragments of curve (from B) with second-order rhythmic climate variations and column D their reflection in alluvial sequencies.

From point of view of system theory the formation and evolution of river basins, depicted very schematically on Fig. 3 and 4, are a strikingly clear example how the different compartments of the Earth system hierarchically interact within planetary evolution. This evolution process seems to bear all the typical features of self-organizing and pattern making/using active systems that are characterized by a strategy oriented interaction between the processes of system formation (i.e. structural and quantitative changes of the system's 'hardware') and the rules and algorithms of system functioning (i.e. the software of the system directing the flows and transformations of energies and materials processed through the system). In fact, the fluvial basins are hardware products of the rock formation systems (functioning in time scales of million years and directed ultimately by the Earth's internal radioactive heating) and at the same time these basins are important software components of ecology defining the partitioning rules and the flow patterns of the terrestrial water cycles (functioning in time scales from hours to years and providing the major mechanism for the interactions among climate, soil and vegetation).

3. Planetary dimension of the climate formation

The evolutionary strategy of this planet seems to be tied rather closely and directly to the genesis, extension and diversification of plant and animal life forms leading to the emergence of man during the last few million years. This strategy required the combination and harmonization of seemingly contradictory tendencies, such as stability and variability of climate; and microscale diversity supplemented by macroscale and global coherence of the water cycle with closely interacting similar features of plant ecology as fundament of the biosphere. All these features were essentially achieved and maintained through interactions and feedbacks among the various constituents of crustal movements and rock formation processes guiding the constitution of the planet's secondary atmosphere with a mass and chemical composition properly and timely establishing the life-supporting patterns of climate and the global water cycle as its basic constituents (*Mészáros*, 1981).

The formation of vegetation cover on the continents about 500 million years ago is a relatively recent event within the roundly 4 billion year evolution of the biosphere. The fact, that major vegetational zones of the recent age can be identified rather closely by mean temperature and precipitation, seems to suggest that climate was the major determinant of ecological conditions also in the geological past. One of the striking feature of the planetary-scale evolution is the tendency of climate to remain within the surprisingly narrow range of about 15 °C in terms of the global mean temperature while its two fundamental determinants, the solar radiation and the CO_2 content of the planetary atmosphere varied very significantly, but almost exactly compensatingly. Within this narrow range, however, the Earth's surface mean temperature was in unceasing rise and fall (see e.g. *Fig. 5* for million year scale fluctuations), thus becoming a major spur for ecological change and biotic evolution. The survey of *Budyko, Ronow* and *Yansin* (1985), referred to in Fig. 5 also indicates how powerful information might be obtained by rock formation data if the many linkages within and between the various geospheric and biospheric processes are properly revealed. This holds particularly for the relation between vegetation and climate, for which atmospheric CO_2 content is an important common causative and impact-transmitting factor. Through photosynthesis of vegetation there is a major regulator of the significant seasonal CO_2 variations in its fast

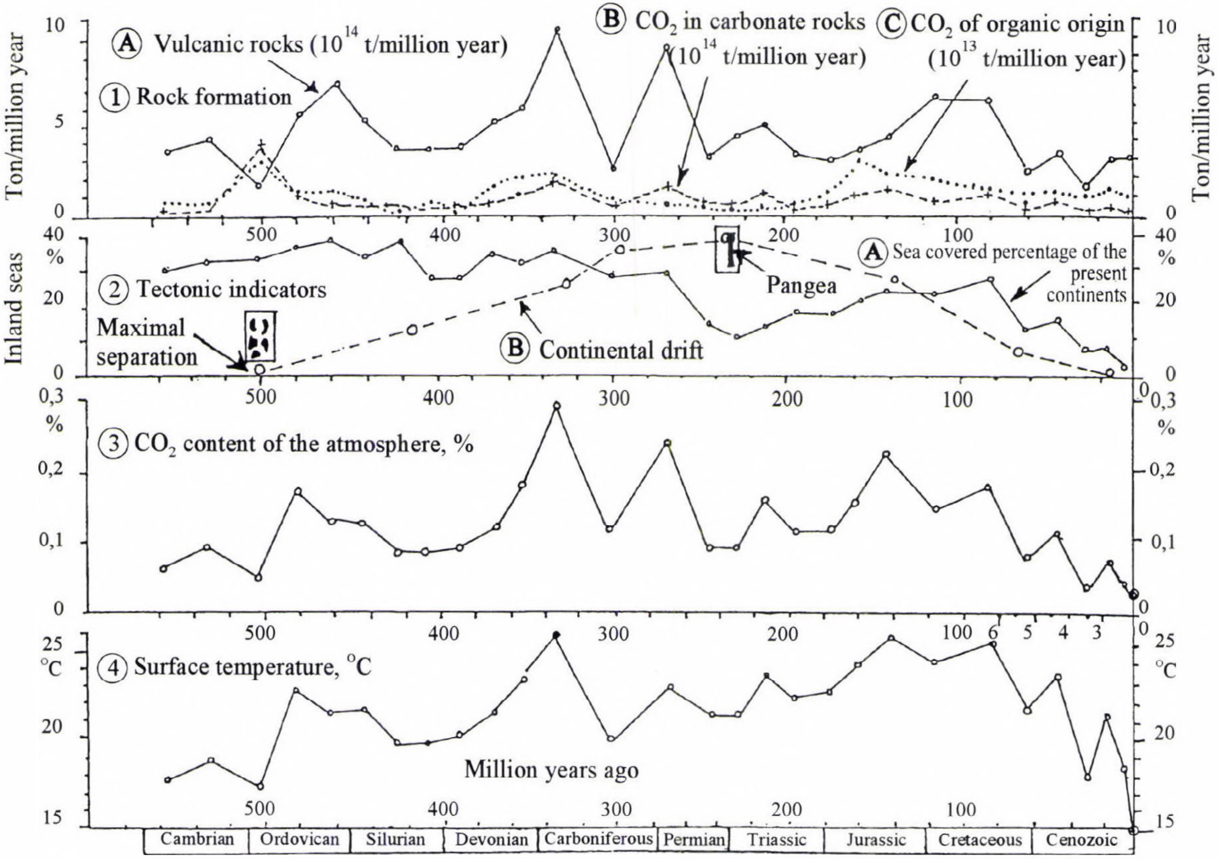

Fig. 5. Tentative data on volcanic and sedimentary rock formation, as well as on atmospheric CO_2 and surface temperature during the last 570 million years (based on *Budyko et al.,* 1985, data 2.B from *Szabó,* 1989).

cycle. At the same time vegetation also participates in the much slower geochemical cycle of CO_2 (see Fig. 5, 1C) and it affects the climate through changes in surface albedo and in humidity regime as well. The responsiveness of the continental vegetation to climate and atmospheric CO_2 concentration change is remarkably written into geological history in the form of the coal deposits of the Carboniferous age when, some 340 million years ago, the temperature was some 10 centigrades higher and the atmosphere was some 10 times richer in CO_2 concentration than today. The manybranched and multiple way feedback mechanism of climate formation (depicted in a highly simplified version in *Fig. 6*) hides also probably the explanation for the striking twofold character of climate formation: its surprising stability at the scale of planetary evolution and its high variability at all other scales.

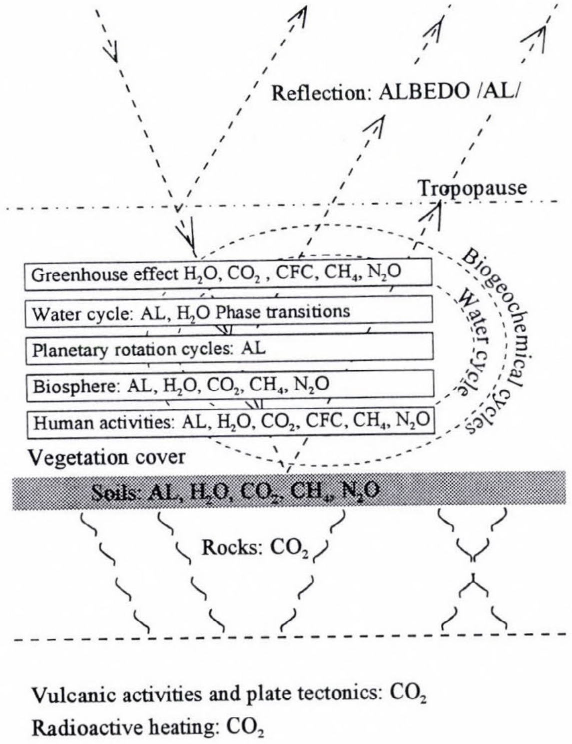

Fig. 6. Major factors and processes affecting climate formation.

However, the atmospheric CO_2 content participates in the climate formation not only by oneself, but jointly with other greenhouse gases deriving from the human activities. Nowadays, it is commonly accepted and generally recognized that about half the radiative forcing is caused by concentration changes of non-CO_2 greenhouse gases. With respect to the preindustrial time, about two centuries ago, radiative forcing of CH_4 and ozone (O_3) averaged globally, amounted to about 30 % of the total radiative forcing, almost equally shared by CH_4 and O_3 (*Beck et al.,* 1994). Over Europe the share of O_3 locally is expected to be even larger due to the relatively large increase of tropospheric O_3 concentrations in the European countries. The scheme of Fig. 6 also visualizes the rapidly increasing significance of human activities in climate formation, as well the difficulties of integrating human impacts with natural trends in the climate predictions.

4. Implications on crop production

Crop production — lying at the heart of agriculture and food supply of growing population — can be looked upon in two ways:

- as the greatest success story of mankind removing the ecological barrier of population size and holding the promise of Paradise for all;
- it can also be seen, however, as the largest human intervention into nature's functioning lying at the heart of the present global environmental crisis.

Both visions are valid and might become our common future pending on motivations, attitudes and decisions of individuals and governments during the years and decades to come.

The invention of crop production and its widespread introduction some ten thousand years ago was a central event in the human occupation of our planet. It made possible a hundredfold multiplication of the *population number* within a relatively very short span of time and it marks a significant and rapid increase in the scale of *social organization.*

A climate and water-centric investigation of theoretical and practical questions arising in the context of crop production usually leads sooner or later to a comprehensive analysis of the heat and water balance processes taking place within the roote zone and canopy. Understanding and quantifications resulting from this analysis should be firm and detailed enough to allow the formulation of a *water balance and crop production simulation model and procedure* as a basic methodological tool for answering the great number and variety of questions asked by agriculturists or land use planners.

The needs for and the possibilities of water balance and crop production simulation come from the experimentally and theoretically well documented notion that for given climate and soil conditions plant communities tend to evolve according to well defined margins of deficiencies and excesses of heat and water whereby the extent and frequency of this limiting extremes vary from species to species (*Fig. 7*) and also according to the phenological phases of plant development (*Fig. 8*; *Antal*, 1966, 1972, 1975a; *Parry,* 1986).

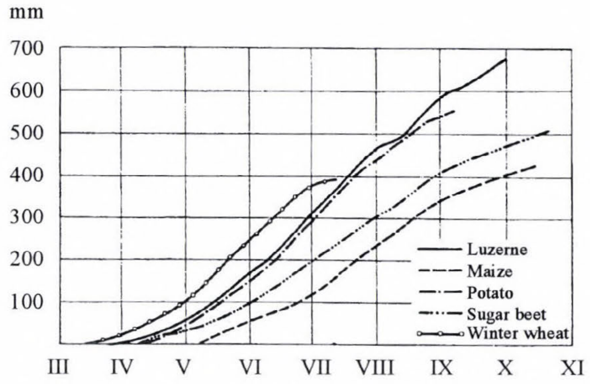

Fig. 7. Summarized evapotranspiration of different crops in 1966 (Szarvas, Hungary, meadow clay, varieties: alfalfa Szarvasi kékvirágú; maize MV-1; potatoes Kisvárdai rózsa; sugar-beet beta-poly 2; winter-wheat Besostaya).

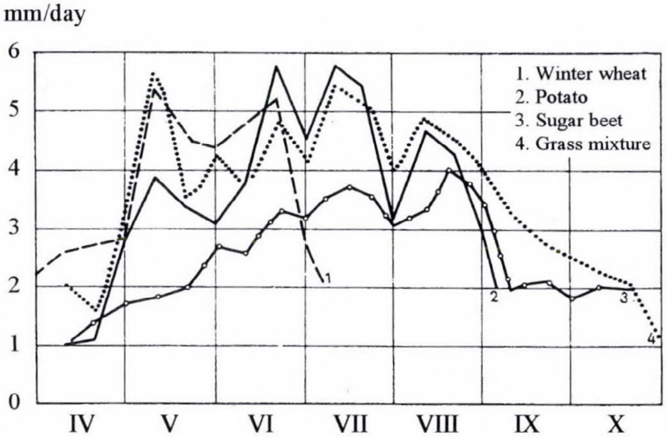

Fig. 8. Changes in the daily water use of different crops during the growing season in 1966 (Szarvas, Hungary, medow clay, varieties: winter-wheat Bezostaya; potatoes Kisvárdai rózsa; sugar-beet beta-poly 2; grass mixture).

Fig. 7 shows the summarized curves of the evapotranspiration of different plant species with optimum water supply (*Antal*, 1966). It is worthwhile pointing out several features. The most conspicuous feature is the difference in the summarized consumptive use. Since all plant species were grown under identical soil-, nutrient-, and water supply and even weather conditions, it was obvious that differences in water requirement were due to differing biological and physiological properties of plant species. What have been told above are even more confirmed by the curves of Fig. 8, which represent the daily evapotranspiration of various plant species in the phenological phases of plant development. It is clearly seen that besides the meteorological factors the plant species and the phenological phases also play a decisive role in determining the trend of water requirement and water use within the growing season. The maximum value of daily water requirement is different in each plant culture and its time coincides with the critical period of plant growth. It can be established further, that the character of dynamics of water requirement in the individual plant species is determined primarily by their growth rate, while daily evapotranspiration decisively by the meteorological factors. Breaks seen on the curves of the figure are caused by the rapid daily changes of weather rather than by changes occurring in the growth of plants.

With regard to possibilities and ways of quantifying evapotranspiration as the key element of the soil moisture balance equation there seem to be important differences between the water-stress controlled and the heat controlled strategy of plant growth discussed briefly in relation to Fig. 2. When the soil moisture is unlimited and the system maximizes the biomass production under given radiation and heat supply the use of water in the form of evapotranspiration can be well estimated for a given plant species and a given phase of phenological evolution through atmospheric data alone (*Antal,* 1966, 1972). The possibility of such approximation is probably a reflection of the coincidence of factors and mechanism guiding stomatal regulation of evapotranspiration with those promoting maximal biomass production. The acceptability of such approximation seems to be supported by the great number of empirical irrigation water requirement formulae applied all around the world and quantified for the conditions of Hungary by *S. Szalóki* of the Irrigation Research Institute in Szarvas on the basis of a nation-wide system of agrometeorological research stations initiated some three decades ago by *E. Antal* (*Antal* and *Takács,* 1964; *Antal,* 1966, 1975b).

The simulation procedure is based on a step by step compilation of the soil moisture balance equation of the root zone for continuous ten day periods (*OVK,* 1984; *Orlóci et al.,* 1993). Wherever the soil moisture content drops below the level of unrestricted water availability — which varies widely according to crop type and species properties and the phases of plant growth — the root zone is hypothetically filled up to field capacity. The amount of irrigation water needed to this effect is registered in the simulation procedure as a measure of climatic water deficit event whereby the accumulated amounts of the hypothetical irrigations provide a quantitative measure of the dry weather events corresponding to the actual local conditions (*Antal,* 1988).

For the purposes of a National Water Policy for Hungary some 2000 computerized soil moisture simulations have been made for the country's farmlands according to 13 crop varieties, 7 soil types, 4 categories of groundwater depth and 3 levels of farming technologies. This plant ecology oriented water balance simulation — initiated and co-ordinated by *I. Orlóci* and *A. Pintér* — is based on the 1928–1977 data of 23 meteorological stations characterizing climatic differences in the country. The major results were summarized in the form of maps quantifying deficiencies and excesses of the soil moisture content according to major crop types for selected characteristic period. One strongly simplified example of such maps is given in *Fig. 9*. Water shortages belonging to risk factors other than those indicated on the maps (given for 80% as the probability that the actual shortage will be smaller than that shown on the map) are specified by tables or graphs obtainable directly from the simulation results.

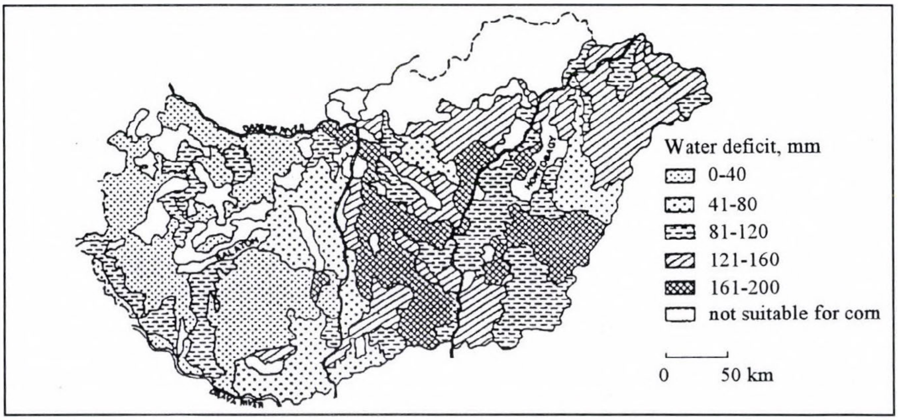

Fig. 9. Summarized water deficit within the root zone of corn during the growing season with a 80% probability of occurrence as derived from the 1928–1977 data of 23 climate stations (*OVK*, 1984).

These risk factors (climate water deficite, irrigation water demand) presumably will be modified according to the global and regional changes. For instance due to Hungary's being situated in the center of Carpathian-Basin, while determines its natural-ecological conditions, the global warming-up will presumably manifest itself in a specific way due to the country's position in the climatic buffer zone of this basin. As for the water resources, when elaborating the water management strategies of agriculture not only a decrease of the total precipitation must be reckoned with, but also a decrease of the amount of water coming to Hungary by the rivers (since water balance is likely to worsen also in the watershed areas of our rivers), as well as a worsening of the quality of water (since the decrease of the water output, along with the stagnation or even increase of the pollution, results in the increase of the concentration of the latter). *Antal* and *Szesztay* (1994) concluded from the above statements that, whatever the presumable or probable future of the country's climate may be, an analysis of the consequences of climatic change is an indispensable part of any study aimed at evaluating and preparing perspectives of Hungarian agriculture and water management.

References

Antal, E. und *Takács, L.*, 1964: Wasser- und Wärmehaushaltmessungen in Interesse der Bewässerung. *Wiss. Zeitschrift*, K.M. Universität Leipzig. 13 Jahrgang, Math. Naturwiss. Rehe Heft, 4, 789-791.

Antal, E., 1966: Potential evapotranspiration from some agricultural plant species (in Hungarian). *Öntözéses Gazdálkodás 4,* No. 1, 69-86.

Antal, E., 1972: Is plant growth determined by internal water balance and turgor in the cells or by external factors? *Acta Agronomica.* Academiae Scientiarum Hungaricae, Tomus 21, 458-468.

Antal, E., 1975a: The climatic potential in Hungary determining the upper limits of plant growth. *XVII. Georgikon Napok*, Keszthely, Hungary, 109-124.

Antal, E., 1975b: Ein neues agrometeorologisches Modell zur Vorhersage bei der Bewässerung. *Práce a Studie 14*, 200-217 (Nitra, Czechoslovakia).

Antal, E., 1988: Comparative analysis of the irrigation water requirement and aridity conditions. In *Identifying and Coping with Extreme Meteorological Events* (eds.: *E. Antal* and *M.H. Glantz*). Hungarian Meteorological Service, Budapest, 205-254.

Antal, E. and *Szesztay, K.*, 1994: Interactions between the prospective climatic changes and the environment (in Hungarian). *'AGRO-21' Füzetek - Az agrárgazdaság jövőképe,* No. 1, Budapest, 8-40.

Beck, J., *Builtjes, P.* and *Roemer, M.*, 1994: Tropospheric ozone - a major component of global change. *Change* (Research and Policy Newsletter on global change from the Netherlands, 19/April, 1-3.

Budyko, M.I., *Ronow, A.B.* and *Jansin, A.L.*, 1985: *History of Atmosphere* (in Russian). Gidrometeoizdat, Leningrad.

Eagleson, P.S., 1982: Ecological optimality in water limited natural soil-vegetation systems. *Water Resources Research 18,* No. 2.

Hillel D. and *Rosenzweig, C.*,1989: The greenhouse effect and its implications regarding global agriculture. *Research Bulletin*, No. 724. University of Massachusetts at Amherst.

Mészáros, E., 1981: *Atmospheric Chemistry: Fundamental Aspects.* Akadémiai Kiadó, Budapest, and Elsevier Sci. Publ. Co., Amsterdam.

Orlóci, I., Pintér, A., Szalóki, S. and Szesztay, K., 1993: Hydroecological equilibrium and risk analysis for crop production in Hungary. *TEMPUS EWA Ring Postgraduate Seminar*, Lecture Notes. April 1993, Gödöllő, Hungary, 19-23.

OVK, 1984: National plan and policy analysis for water management in Hungary (in Hungarian). Országos Vízügyi Hivatal, Budapest, Hungary.

Parry, M., 1986: Some implications of climatic change for human development. In *Sustainable Development of the Biosphere* (eds.: *W.C. Clark* and *R.E. Munn*). Published for IIASA, by the University of Cambridge Press, USA.

Starkel, L., 1990: Fluvial environment as an expression of geological changes. *Z. Geomorph.* N.F., Suppl.-Bd. 79, Berlin-Stuttgart.

Szabó, J., 1989: *Geography of Europe* (in Hungarian). Móra Kiadó, Budapest.

IDŐJÁRÁS

Quarterly Journal of the Hungarian Meteorological Service
Vol. 100, No. 1–3, January–September 1996

Agroclimatological analysis of natural periods and growing seasons

Z. Varga–Haszonits, A. Porpáczy and **R. Schmidt**

Pannon Agricultural University,
H–9200 Mosonmagyaróvár, Vár 2, Hungary

(Manuscript received 22 May 1995; in final form 30 January 1996)

Abstract—For agroclimatological purposes the authors determined the beginning, the end and the length of natural periods on the basis of 40 year data. The natural periods are very important time spells for agricultural production. The warming up period (a period of temperatures between 5 and 15°C) plays in turn an important role in determining the sowing time. All these periods can be determined by using climatological data.

Knowing the length of growing seasons the effect of meteorological factors during the vegetation period on the plant productivity can be investigated. Firstly a general index was calculated as a ratio of actual crop yields and trend values. Since trend values express the influence of technology on yield, the ratio of actual yield and trend value can be considered as a complex weather index. The values of complex weather indices show how many percent of yield variation can be caused by meteorological factors.

Lastly the efficiency of the radiation under the vegetation period was calculated.

Key-words: natural period, growing season, plant productivity, complex meteorological effects, radiation efficiency.

1. Introduction

Climatology investigates the meteorological conditions of the most important calendar periods, including the annual course of the climatic elements. Considering the demand of agricultural production, however, also the natural and vegetation periods have to be taken into account. Therefore, firstly the beginning and ending date of these periods must be determined. It is generally assumed that the length of the vegetation period can be simply calculated, since it ranges from sowing to ripening. Unfortunately, the date of sowing and the date of ripening during a long time period are not exactly registered, so they must be ordinarily calculated. There is a similar situation in determining the natural periods. Consequently, the agricultural climatology has two important tasks: one is to determine the beginning and the end of natural periods and vegetation periods, and the other is to investigate the meteorological conditions of these two mentioned periods.

In our country there are three different growing seasons for cultivated plants. For winter cereals the vegetation period ranges from the first half of October to the first half of July. For annual crops the growing season is the time spell from the beginning of April to the end of October. Finally, this period for the fruit trees and grapes lasts from the beginning of November to the end of next October.

One of the most significant tasks of agroclimatology is to determine these periods on the basis of meteorological data and to analyse their meteorological conditions.

2. *Natural periods*

The natural periods can be determined in different ways. In present days they are not defined exactly. For determining these periods we use the monthly temperature, precipitation and evaporation data which show the annual course. The natural periods will be calculated for Hungary on the basis of a 40 year data series (1951–1990) of 22 meteorological stations.

2.1 Period above 5°C

The date, when the daily mean temperatures transcend the 5°C strongly varies from year to year. Therefore, an approximate date for this event has to be calculated by using of 10 days or monthly mean temperature data. Assuming that the mean values of temperature are connected to the 15th day of months and the days are numbered from the 1st of January, the first day of the period above 5°C can be calculated by the following formula (*Varga-Haszonits,* 1983):

$$D_S = D_L + \frac{t_0 - t_L}{t_H - t_L} \cdot d_L , \qquad (1)$$

where D_S is the date of the beginning of the period in spring, D_L is the date of the middle day of month with the nearest lower temperature than 5°C, t_0 is the threshold temperature which is 5°C in this case, t_L is the mean temperature of the month which has the nearest lower temperature than 5°C, t_H is the mean temperature of the month which has the nearest higher temperature than 5°C and d_L is the number of days in the month with the nearest lower temperature than 5°C.

The last day of the period can be similarly determined, but according to the annual course of temperature the monthly values fall down after July, so that the highest values precede the date of 5°C, that is

$$D_A = D_M + \frac{t_M - t_0}{t_M - t_L} \cdot d_M, \tag{2}$$

where D_A is the date of the last day of the period in autumn, D_M is the date of the middle day of month with the nearest higher temperature than 5°C, d_M is the number of days in the month with the nearest higher temperature than 5°C and all other values have the same meaning as in Eq. (1).

Knowing the first and last day of the period its length can be calculated in the following way:

$$LVP_T = D_A - D_S, \tag{3}$$

where LVP_T is the length of vegetation period determined by temperature, i.e. LVP_T may be designated as temperature defined growing season.

These calculated values play an important role in the agroclimatology. For example having the monthly mean values of temperature and the base temperature we are able to determine the possibility of production of a crop in a given area. The criterium is the following:

$$LVP_T > LVP_A, \tag{4}$$

where LVP_A is the actual vegetation period (in days) which ranges from the sowing to the ripening. This means that the length of the growing season determined by temperature must be longer than the actual vegetation period if we want to produce a crop in an area.

In addition the value of D_S can be considered as the possible earliest date of the sowing or planting if the value of t_0 is the base temperature of a given crop i.e. D_S may be designated as temperature defined sowing date. To calculate D_S the monthly (or 10 days) values of temperature and the base temperature of the investigated crop must be known. Generally, the temperature is measured in the meteorological stations and since the temperature is a continuous element, it varies only slowly especially in the plain agricultural areas, thus the data of the meteorological station nearest to the agricultural field can be used. The base temperature of various crops is given in the agricultural and horticultural literature. *Table 1* contains the most important crops growing in our country (*Varga-Haszonits,* 1987). So the necessary data for solving Eq.

(1) are available and the possible earliest date of sowing can be computed. The computation was made by using 40 years data series for 22 meteorological stations, so both spatial and temporal changes in sowing date may be analysed.

Table 1. Base temperature of important crops

Below 5°C			
Winter wheat	1–5	Garden sorrel	2–3
Winter barley	1–5	Red clover	2–3
Rye	1–5	Poppy	3–5
Oat	1–5	Flax	3–5
Pea	1–5	Lucerne	3–6
Lentil	1–5	Spinach	4–5
Radish	2–3	Onion	4–5
Cabbage–lettuce	2–3	Carrot	4–6
Between 5 and 10°C			
Horse–bean	5–9	Millet	8–10
Sugar beet	5–8	Bean	8–10
Mangel–wurzel	6–8	Sunflower	8–10
Hemp	6–8	Potato	8–10
Between 10 and 15°C			
Cauliflower	10–12	Squash	12–14
Tobacco	10–12	Cabbage	12–14
Maize	12–14	Kohlrabi	12–14
Rice	12–14	Tomato	12–16
Soyabean	12–14	Water melon	14–16
Cucumber	12–14	Musk–melon	14–16

Firstly we want to investigate the spatial distribution of the temperature defined sowing date (D_S). A possible way to determine the spatial variations of the sowing date is to calaculate the statistical values for all meteorological stations of the country and to compare them. The results of these calculations are displayed in *Table 2.*

As we can see in Table 2, there is a noticeable deviation in the statistical values and in the frequency distribution of the onset of the period between the western and central, north-eastern part of the country. The earliest date of the onset of the period can be generally expected with the values below 50 (before 20 of February) and in the north-eastern part of the country with the values above 50 (after 20 of February). The mean values and the maximum values show very similar spatial distributions. If we look at the frequency values, they prove the mentioned spatial distributions since again the latest date occurs most frequently in Northern Hungary.

Table 2. The beginning of the period above 5°C temperature
(in serial numbers from 1st of January)

	Statistical values			Frequency values in %						
County	Min	Avr	Max	31-40	41-50	51-60	61-70	71-80	81-90	91-100
Transdanubia										
Győr-Moson-Sopron	41	70	91	-	10	10	22	28	28	2
Vas	43	70	94	-	2	10	15	28	35	10
Zala	42	72	93	-	7	10	22	28	28	5
Somogy	37	67	91	2	10	13	25	28	20	2
Veszprém	39	70	92	2	8	10	28	22	28	2
Komárom-Esztergom	39	69	90	2	5	18	20	30	23	2
Fejér	44	72	91	-	5	12	23	25	33	2
Tolna	40	70	89	-	7	10	28	20	35	-
Baranya	38	68	90	2	13	8	20	30	25	2
Great Plain										
Bács-Kiskun	42	70	90	-	7	13	22	28	28	2
Pest	43	69	90	-	7	13	30	23	25	2
Jász-Nagykun-Szolnok	45	70	90	-	8	10	25	30	25	2
Csongrád	43	69	89	-	12	10	20	35	23	-
Békés	44	69	89	-	10	10	25	32	23	-
Hajdú-Bihar	46	72	91	-	2	13	25	30	28	2
Szabolcs-Szatmár-Bereg	52	75	93	-	-	7	23	35	30	5
Northern Hungary										
Borsod-Abaúj-Zemplén	56	76	91	-	-	5	25	25	40	5
Heves	51	73	90	-	-	10	30	22	33	5
Nógrád	44	75	97	-	2	5	28	25	35	5

2.2 Warming up period

We can see from Table 1 that the base temperature of the plants grown in Hungary varies between 5 and 15°C. Since the monthly average temperature rises from January to July and decreases from July to January we can easily calculate the period when the temperature reaches these values. This is the period when we have to prepare the soil and to sow the plants that we want to grow at a certain farm. For the calculation of this period we have to know the date when the temperature reaches the threshold mentioned. These dates can be calculated by using Eq. (1) and at the same time we can calculate the length of the period also according to the following formula:

$$HP = D_{15} - D_5, \tag{5}$$

where HP is the length of the warming up period, D_{15} and D_5 is the date when the temperature reaches the 15 and 5°C, respectively.

The results calculated by Eq. (5) are summarised in *Table 3*. The data clearly show that in the Transdanubian counties even the lowest average value is higher than the highest value in the counties of the Great Plain and of Northern Hungary. It means that the warming up is slower and the warming up period is longer than in the other parts of the country. From agricultural point of view it has two consequences:

- one of the consequences is that in Transdanubia we have a longer period available to sow the plants than in the other parts of the country;
- the other is that development of the emerged plants is slower in Transdanubia than in other areas.

Table 3. Length of warming up period, 1951–1990

Counties	Minimum	Average	Maximum
Transdanubia			
Győr–Moson–Sopron	40	64	101
Vas	36	66	105
Zala	29	66	105
Somogy	27	64	104
Veszprém	29	65	102
Komárom–Esztergom	31	62	104
Fejér	38	61	94
Tolna	29	62	95
Baranya	28	63	104
Great Plain			
Bács–Kiskun	37	59	93
Pest	35	60	96
Jász–Nagykun–Szolnok	39	59	95
Csongrád	34	59	97
Békés	38	60	103
Hajdú–Bihar	30	58	102
Szabolcs–Szatmár–Bereg	36	58	95
Northern Hungary			
Borsod–Abaúj–Zemplén	38	59	96
Heves	37	59	98
Nógrád	40	60	98

If we look at the extreme values we realise that there are areas and years where and when the length of the warming up period can be reduced and can be shorter than one month. It is an interesting fact that this seems to occur in Transdanubia where the warming up period is generally long. On the contrary the table also shows that sometimes the warming up period can be longer than three months.

We can conclude that the sowing period of the crops grown in Hungary varies between 27 and 105 days and it is generally longer in Transdanubia than in the other parts of the country.

2.3 Warm period

Basically we can call warm period that part of the year when the average temperature is higher than 15°C. The duration of this time can be calculated also by using the Eqs. (1) to (3).

Table 4. Length of period over 15°C, 1951–1990

Counties	Minimum	Average	Maximum
Transdanubia			
Győr–Moson–Sopron	106	129	156
Vas	96	117	163
Zala	97	120	153
Somogy	110	133	176
Veszprém	104	127	168
Komárom–Esztergom	105	132	177
Fejér	109	131	172
Tolna	108	132	173
Baranya	114	136	173
Great Plain			
Bács–Kiskun	106	135	179
Pest	113	136	179
Jász–Nagykun–Szolnok	112	136	153
Csongrád	110	138	173
Békés	106	136	154
Hajdú–Bihar	103	132	151
Szabolcs–Szatmár–Bereg	100	128	145
Northern Hungary			
Borsod–Abaúj–Zemplén	93	124	142
Heves	102	131	149
Nógrád	99	123	144

The results can be found in *Table 4*. In Hungary the period when the average daily temperature is higher than 15°C is between the middle of May and the middle of September. In accordance with this the average length of the warm period is between 117 and 138 days. We can see from Table 1 that the base temperature of plants requiring warm is approximately about 15°C therefore the possible growing period for them coincides with the warm period. The table also shows that this period is the longest in the counties situated in eastern Transdanubia and in the Great Plain. During the warm period the coolest part of the country is western Transdanubia, where the length of the warm period is only 120 days in the average. The warm period is also short in the northern counties.

Regarding the extreme values the length of the warm period is over 100 days on the majority of the area of the country in the past 40 years except the counties mentioned in south-western Transdanubia and in Northern Hungary. The maximum values are over 140 days everywhere and over 170 days in the eastern part of Transdanubia and in the central part of the country between the rivers Danube and the Tisza.

The warm period — as we already mentioned — generally terminates in the second part of September. After this time a cooling down period starts that lasts approximately till the middle of November. In this period the temperature falls below 5°C and a cold period starts that generally lasts till the middle of March.

3. The productivity of plants

In our country the growing season of plants generally includes three major types. The first one is the vegetation period that lasts from October to the October of the next year. This vegetation period is important for fruit trees and for grapes. These plants are exposed to the effects of both the periods below and above 5°C. The second type is the vegetation period of winter cereals that lasts from the sowing date of these plants in the autumn till their harvest that occurs at the beginning of the summer. These plants are also exposed to the unfavourable effects of the period below 5°C, but they are harvested before the hottest part of the summer. Finally, we should mention the growing period of the spring plants that are sown generally after the time when the temperature passed the 5°C threshold value and they are harvested before the time when the temperature falls below the 5°C in the autumn.

As a result of the situation described we can conclude that the plants grown in our region live their life under different meteorological conditions even in the same year and therefore are exposed to different effects and they have to tolerate the different meteorological conditions at different phenological state. This is the reason why the effect of meteorological conditions on the plants should be analysed separately though according to the same general methodological considerations.

From methodological point of view our starting point is that the important physiological and economical quantities of the plants (Y) are regulated and modified by both internal (F_i) and external (F_0) factors, so we can state that at a certain time

$$Y(t) = f(F_i, F_0)\,. \tag{6}$$

We want to analyse only the meteorological elements, therefore the internal factors and the non-meteorological external factors should be fixed in some way. There are two possible methods of doing this:

1. We consider the internal factors and the non-meteorological external factors to be constant, in other words we grow the same cultivar by using the same technology;
2. We consider the internal and the non meteorological factors to be such ones that are slowly changing from year to year, as in time new cultivars, hybrids and technologies are introduced in larger and larger areas. Therefore the effects of these factors can be described by a trend function.

In our present study we follow the second method. The object of this study is yield, supposing that a certain yield is formed by the common effect of the technology and the meteorological conditions in a process where the meteorological factors modify, increase or decrease the effect of the technology (hybrids, fertiliser, plant protection, etc.) according to the following equation:

$$Y(t) = f(t) \cdot f(m), \tag{7}$$

where $f(t)$ is the trend function and $f(m)$ is the function expressing the effect of meteorological factors. From Eq. (7) we can calculate the common effect of the meteorological elements:

$$f(m) = \frac{Y(t)}{f(t)}. \tag{8}$$

We can see from the equation that the complex meteorological effects can be expressed by the trend ratio (*Varga-Haszonits* and *Harnos*, 1988). If we calculate these values for the plants grown in the different vegetation periods between 1971 and 1990 we get the figures summarised in *Table 5*. The values in the table are the average yields in the country calculated from the yields achieved in the individual counties by using a fourth power trend ratio function.

According to the figures the yield of winter wheat, maize and cabbage exceeded the technological level by 16% in 1984, by 15% in 1982, by 14% in 1984, respectively. The yield of grape was also 32% higher than the country average in 1982. At the same time the unfavourable meteorological effects decreased the yield of winter wheat by 20% in 1979 and the yield of maize by 17% in 1973 (we should mention that the 22% decrease registered in 1990 was not the result of meteorological factors). The yield of cabbage decreased by 15% in 1983 and the yield of grapes was also reduced by 14% in 1974 and in 1987 compared to the technological level. It means that there was a significant fluctuation in the average yield registered in the country due to meteorological factors. The table also displays that meteorological factors raised the yields over the technological level in 12, 10, 9 and 7 years in terms of wheat, grapes, cabbage and maize, respectively. It is worth mentioning that in the case of cabbage there were 6 years in a series between 1973 and 1978 when the countrywide average yields exceeded the technological levels.

Table 5. Averages of complex weather indices for Hungary

Years	Wheat	Maize	Cabbage	Grape
1971	1.05	0.93	0.92	0.96
1972	0.99	1.05	0.95	1.01
1973	1.07	0.99	1.09	1.14
1974	1.12	0.98	1.05	0.76
1975	0.90	1.12	1.05	0.82
1976	1.05	0.83	1.04	0.93
1977	1.04	0.92	1.07	1.03
1978	1.08	0.97	1.11	0.95
1979	0.80	0.99	0.88	1.00
1980	1.13	0.94	0.97	1.10
1981	0.91	1.00	0.96	0.84
1982	0.98	1.15	0.88	1.32
1983	0.98	0.92	0.85	1.31
1984	1.16	0.96	1.14	1.08
1985	1.01	1.04	1.10	0.64
1986	0.89	1.03	0.98	1.09
1987	0.90	1.05	1.00	0.76
1988	1.09	1.00	0.97	1.06
1989	1.03	1.18	1.06	0.82
1990	0.99	0.78	0.95	1.20

Naturally we can analyse not only the complex meteorological effects but we can also study the rate of responsibility of certain meteorological factors for the changes in the yields. For yield formation one of the most important factors is the radiation that supplies energy for the production of organic materials. Therefore, when we study the significance of meteorological elements one of the most important questions is to what extent the plants are able to utilise the radiation energy. For analysing this question we have to consider the following facts:

If we know the amount of photosynthetically active radiation (Q_{PhAR}) that reaches the surface of plants' canopy and we know the amount of energy necessary for the production of 1 kg biomass (Q_0=17,000 kJ) then we can determine the amount of biomass (Y_{MAX}) that would be produced in a unit area (1 ha) if all the energy was used for biomass production. The maximum possible amount of biomass can be calculated according to the following:

$$Y_{MAX} = \frac{Q_{PhAR}}{Q_0} . \tag{9}$$

It is obvious that such amount of biomass can not be formed since the radiation energy that reaches the surface is first of all used for heating up the soil and the air and for evaporation. The plants utilise only a certain proportion of the energy (ϵ), so the amount of energy used for biomass production (Y_{BIO}) is:

$$Y_{BIO} = \epsilon \frac{Q_{PhAR}}{Q_0} . \tag{10}$$

If we know the value of Y_{BIO} we can determine ϵ from Eq. (10) that is called efficiency coefficient. The difficulty in doing this is that in agriculture generally the economically utilised parts are measured and not the total amount of biomass. Therefore, we need a conversion factor for the calculation of total biomass. Perhaps the most suitable formula is the so called harvest index (HI) that is widely used in agricultural research:

$$HI = \frac{Y_{ECO}}{Y_{BIO}} . \tag{11}$$

Using Eq. (11) we easily make the conversion, so if we have the yield data by the means of Eqs. (10) and (11) we can determine the rate of radiation utilisation:

$$\epsilon = \frac{Y_{ECO} \cdot \dfrac{1}{HI} \cdot Q_0}{Q_{PhAR}} . \tag{12}$$

Eq. (12) expresses what rate of radiation is utilised by plants compared to the total amount of radiation reaching the surface. If the right side of Eq. (12) is multiplied by 100 we get the value of radiation efficiency in per cent.

In *Table 6* the radiation efficiency values are shown, calculated using Eq. (12) for the whole area of the country on the basis of the average county yields between 1971 and 1990. The figures display that winter wheat, maize, cabbage and grapes utilised only 0.85–1.53%, 0.68–1.40%, 1.66–2.79%, 0.70–1.39% of photosynthetically active radiation, respectively. According to *Burgos*

(1986), theoretically plants would be able to utilise maximum 22–24% of the photosynthetically active radiation. If it is true we can conclude that our cultivated plants produce the present yields by utilising less than tenth of the highest possible amount of radiation.

Table 6. Averages of radiation efficiencies for Hungary

Years	Wheat	Maize	Cabbage	Grape
1971	0.85	0.68	1.68	0.70
1972	0.86	0.90	1.94	0.87
1973	0.94	0.81	1.95	0.92
1974	1.06	0.91	2.02	0.70
1975	0.87	1.04	1.91	0.74
1976	1.00	0.80	1.90	0.84
1977	1.07	0.94	1.96	0.97
1978	1.20	1.07	2.16	0.98
1979	0.88	1.07	1.66	0.97
1980	1.37	1.12	2.04	1.15
1981	1.05	1.19	2.00	0.86
1982	1.18	1.40	1.96	1.39
1983	1.22	1.11	1.91	1.27
1984	1.53	1.24	2.74	1.13
1985	1.33	1.25	2.56	0.63
1986	1.15	1.18	2.31	1.02
1987	1.18	1.23	2.47	0.78
1988	1.49	1.11	2.39	1.08
1989	1.42	1.33	2.79	0.92
1990	1.30	0.76	2.26	1.28

References

Burgos, J.J., 1986: Equilibrium and extreme climatic conditions of the world's biomass and agrosystems. In *Land Use and Agrosystem Management under Severe Climatic Conditions*. WMO Technical Note No. 184, 12–56.

Varga-Haszonits, Z., 1983: *Agroclimatology and Agrometeorological Forecasting*. Lecture notes for international course of meteorology. Orsz. Meteorológiai Szolgálat, Budapest.

Varga-Haszonits, Z., 1987: Agrometeorological information and its use (in Hungarian). Mezőgazdasági Kiadó, Budapest.

Varga-Haszonits, Z. and *Harnos, Zs.*, 1988: Effect of climate variability and drought on wheat and maize production. In *Identifying and Coping with Extreme Meteorological Events* (eds.: *E. Antal* and *M.H. Glantz*). Orsz. Meteorológiai Szolgálat, Budapest, 138–166.

IDŐJÁRÁS

Quarterly Journal of the Hungarian Meteorological Service
Vol. 100, No. 1–3, January–September 1996

Effect of potential air temperature and precipitation change on the flow regime of the Danube

B. Gauzer and **Ö. Starosolszky**

Water Resources Research Centre Plc. (VITUKI),
Kvassay Jenő út 1, H-1095 Budapest, Hungary

(Manuscript received 22 May 1995; in final form 16 August 1995)

Abstract—Potential climate change influences runoff. Water Resources Research Centre studied the impact on hydrological and water quality parameters on the basis of a research grant of the National Scientific Research Foundation (OTKA–716/90). Special emphasis was given to the change of flow regime of the Danube. Simulation of flow time-series was made by a numerical model applied for different scenarios: temperature change by 1 and 3 °C, and annual precipitation change by 10% and seasonally ±20%. Daily flows output was received for the stream gauging station at Nagymaros, and an average, a wet and a dry year data were used for the simulation and for comparison. Conclusions, particularly for winter and spring flows due to snowmelt runoff, could be derived.

Key-words: climate change, temperature, precipitation, runoff, flow, modelling, simulation, annual flow data series, impact on flow, seasonal change of the mean discharges, climate scenarios.

1. Introduction

Both the IPCC reports and the special studies (*Kuusisto et al.*, 1994) have demonstrated that potential climate change may considerably influence the runoff conditions of the rivers. From the point of view of the Hungarian water management the flow regime of the Danube is extremely important. In 1991 a study was launched by the National Research Foundation (OTKA–716/90) and the project was executed by the Water Resources Research Centre (*VITUKI,* 1994a), which covered several aspects of the climate change impact on hydrological and water quality parameters. Within this project special emphasis was given to the change of the flow regime of the Danube. The results related to the Danube were also reported to IIASA (*VITUKI,* 1994b).

In this paper an attempt is made to introduce a part of the studies, namely, the study of the Danube flow regime with regard to potential change of air temperature and/or rainfall. In the OTKA and IIASA report the effect of air temperature change was only simulated. In this paper the effect of precipitation change is, in addition, also included.

The simulation of runoff was carried out for selected scenarios (see later) and the results received have been analyzed. The following questions have been tackled:

- seasonal and monthly distribution of runoff;
- changes in the winter low-flow period;
- changes in the peak discharges of floods during the winter;
- changes in the peak discharges of the spring snowmelt induced floods.

2. *Scenarios*

For references three periods based on the 10 years data set have been chosen. The periods start and end with snowless conditions:

- an average period, from 1 September 1991 to 31 August 1992, annual mean discharge: cca. 2000 m^3/s;
- a wet period, from 1 September 1987 to 31 August 1988, annual mean discharge: cca. 2300 m^3/s;
- a dry period, from 1 September 1990 to 31 August 1991, annual mean discharge: cca. 1600 m^3/s.

Three scenarios for the daily temperatures have been analyzed for only temperature changes

(1) Temperatures are distributed according to the observed values;

(2) Temperatures are 1 °C higher than the observed ones for the stated period throughout the year;

(3) Temperatures are 3 °C higher than the observed ones for the stated period throughout the year;

(4) Annual average plus 3 °C temperature, annual average –10% precipitation;

(5) Average plus 3 °C temperature, average –20% precipitation in summer, and average plus 20% precipitation in winter.

These (4) and (5) scenarios were intercompared with scenarios (1) and (3), respectively. Scenarios are not related to GCM results, they are oversimplified and hypothetical.

3. *Data available*

The actual simulation tackled the system of River Danube and its nine tributaries altogether including 28 cross-sections, 13 on the Danube and 15 on the 9 main tributaries.

Observations of discharge at 12-hour time steps have been used. To estimate snowmelt and rainfall-runoff processes data from 32 meteorological stations over the catchment have been used, namely observations of precipitation and air temperature at 12-hour time steps including daily minima and maxima of air temperatures. As a first step time series of active precipitation and soil frost are estimated for each meteorological observation site. Consequently areal means of active precipitation and soil frost are calculated for each of the drainage basins belonging to individual cross-sections, serving as input for the GAPI (Gamma Antecedent Precipitation Index) rainfall-runoff model. Runoff time series produced by GAPI are routed with the use of DLCM (Discrete Linear Cascade Model). The above procedure has been carried out with the set of optimized parameters used in the operational forecasting practice.

4. Methods of simulation

For the simulation of flow time series a model set developed in VITUKI with one component from the National Meteorological Service was used. It contains four models:

- Quantitative precipitation model (of the National Meteorological Service);
- Snowmelt processes model;
- Rainfall-runoff model (GAPI);
- Coupled structural stochastic model based on the unsteady flow equations (DLCM), including a stochastic submodel.

By these models the daily flow time series for the Nagymaros streamflow gauging station were calculated for each scenarios for an average, a wet and a dry year selected from the data base of the Hungarian Hydrological Forecasting Service (*Fig. 1*). The calculations resulted in runoff data for other stream-gauging stations (e.g. for Pfelling on Danube and Wasserburg on Inn), but in our study the flow time series of Nagymaros were only discussed.

5. Results of the studies

5.1 Air-temperature changes only

Flow conditions of the Danube were analyzed in connection with the change of air-temperatures in the drainage basin, with a special emphasis on snowmelt induced runoff.

The average values and standard deviations for the three selected years, each of those characterized for three temperature scenarios have been calculated and given in *Table 1*.

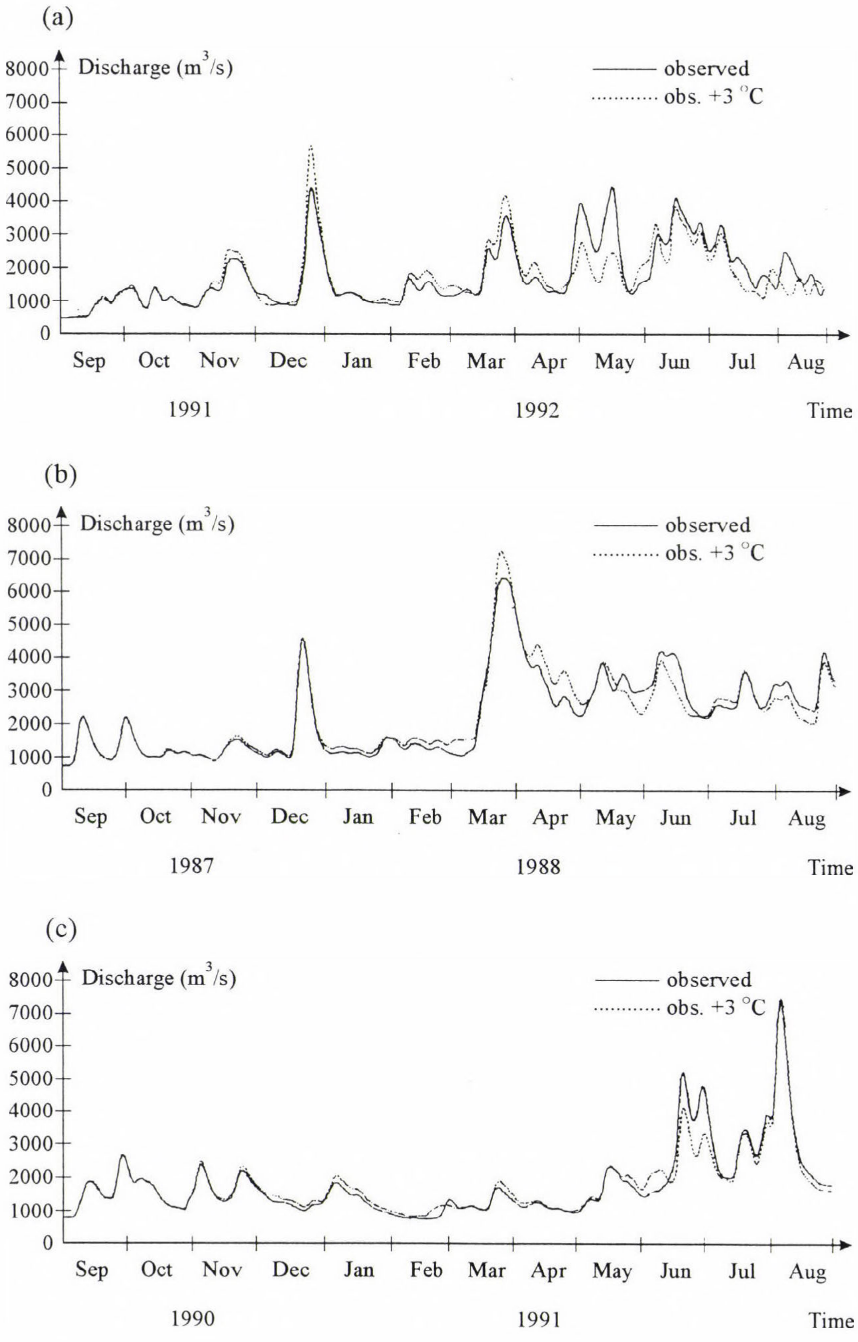

Fig. 1. Simulated annual flow time-series for the Nagymaros gauging station on the Danube at an average temperature rise of 3°C [scenario (3)].

Table 1. Average values (x) and standard deviations of the discharge hydrographs

	Average period			Wet period			Dry period		
Scenario	$T = T_o$	$T=T_o+1\,°C$	$T=T_o+3\,°C$	$T=T_o$	$T=T_o+1\,°C$	$T=T_o+3\,°C$	$T=T_o$	$T=T_o+1\,°C$	$T=T_o+3\,°C$
x m³/s	1984	1970	1928	2267	2285	2302	1827	1826	1813
σ m³/s	892	870	824	1236	1229	1234	1076	1058	1061

Since minimum discharges generally appear during spring, the effect of rise of temperatures remained insignificant.

The higher snowmelt induced winter flood wave occurs, the larger increase in the ratio of the volume of winter runoff to the annual volume can be expected. If no winter flood wave passes on the river, the changes remain insignificant (i.e. under 1–2%).

Changes of a winter flood wave depend on the role of snowmelt. If a winter flood wave induced by liquid precipitation passes on the river increase of peak discharge remains insignificant (see December flood wave in the wet period). In the case of mostly snowmelt induced winter flood waves peak discharges rise significantly (15–30%, see December flood wave in the average period in Fig. 3a).

In the case of several spring and early summer snowmelt induced flood waves the rise of temperature results in increasing peak discharge for the first flood wave, while consecutive flood waves in such a period pass on the river with decreasing peak discharges (see flood waves in the dry and average period in *Fig. 2a* and *c*). Peak discharge of a single major snowmelt induced flood wave shows increasing tendency (see spring flood in the wet period in *Fig. 2b*).

From the modular flow forecasting system precipitation patterns, snowmelt and evaporation process, runoff simulations by rainfall-runoff models, and runoff transformation calculations were derived with an output of simulated daily flows for three selected years.

Monthly and seasonal sums of active precipitations were simulated for the Pfelling streamgauging section of the Danube and the Wasserburg streamgauging section of the River Inn besides those of the Nagymaros streamgauging section. In this way flows at two upstream streamgauging stations were simulated.

The average values and standard deviations do not show a great variety depending on the temperature scenario (precipitation change was not

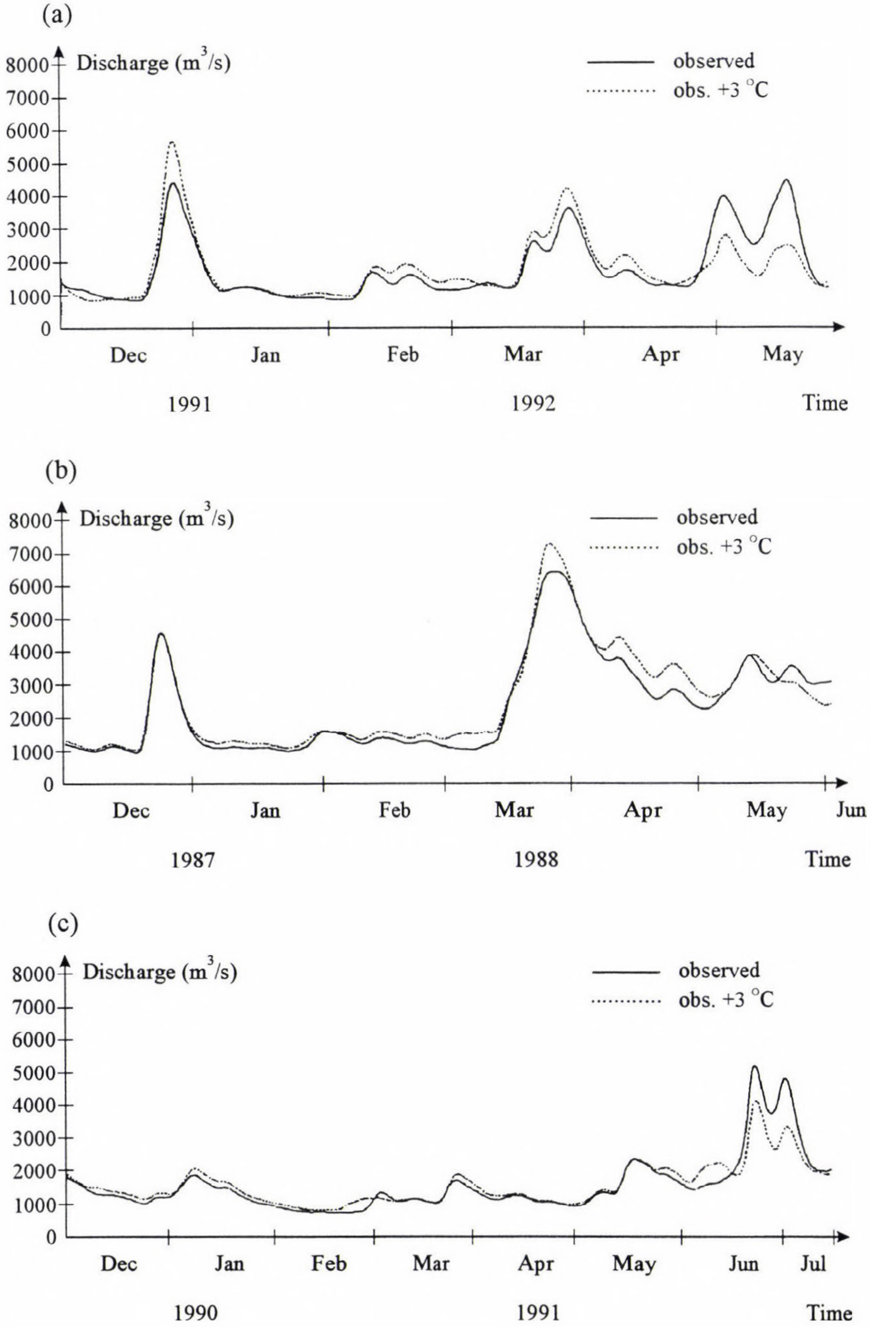

Fig. 2. Simulated flow time series for the winter–spring period, Danube, Nagymaros.

considered, only temperature change), thus temperature change independently may cause almost negligible change in the annual average values.

On the other hand the higher snowmelt induced flood wave occurs, the larger increase in the ratio of the winter runoff volume can be expected.

Changes of a winter flood were depending on the role of the snowmelt. Winter flood waves peak discharges rise significantly (15–30%). In the case of several spring and early summer snowmelt induced flood waves, the rise of temperature results in increasing peak discharge for the first flood wave, while consecutive flood waves decrease.

5.2 Air-temperature and precipitation changes

The simulated flow time series for the scenario (4) are plotted in *Fig. 3*.

In the three investigated periods the distribution of the seasonal flows is demonstrated by the *Table 2*.

The following conclusions can be derived

- The 10% precipitation reduction causes less effect than 10% for the runoff, due to the fact that the base flow is rather independent of the actual precipitation conditions (at least for shorter periods).
- If average, or more precipitation is observed the winter precipitation increase and the summer precipitation decrease can result in a gain in the annual volume.
- In the late autumn-winter low water periods the 10% precipitation decrease does not cause considerable flow reduction, due to the fact that the base flow is originating from subsurface waters. The 20% precipitation increase has also little effect on the minimum flows, due to similar reasons.
- In two cases of the winter periods considerable flood waves occurred generated by rainfall. Due to the 10% precipitation decrease, the discharge reduction shows similar values. On the other hand the 20% precipitation increase caused a higher influence, because the rainfall increases the snowmelt intensity.
- It can be concluded that the 3°C temperature rise and the 10% precipitation decrease in the Upper Danube catchment of Pfelling can counterbalance each other. On the other hand, in the Inn catchment of Wasserburg the effect of the temperature rise is more definitive due to the stored snow volume.
- For the runoff conditions during the spring period it can be characteristic that the increase of the winter precipitation can influence the period of the smaller precipitation up to the middle of the summer.

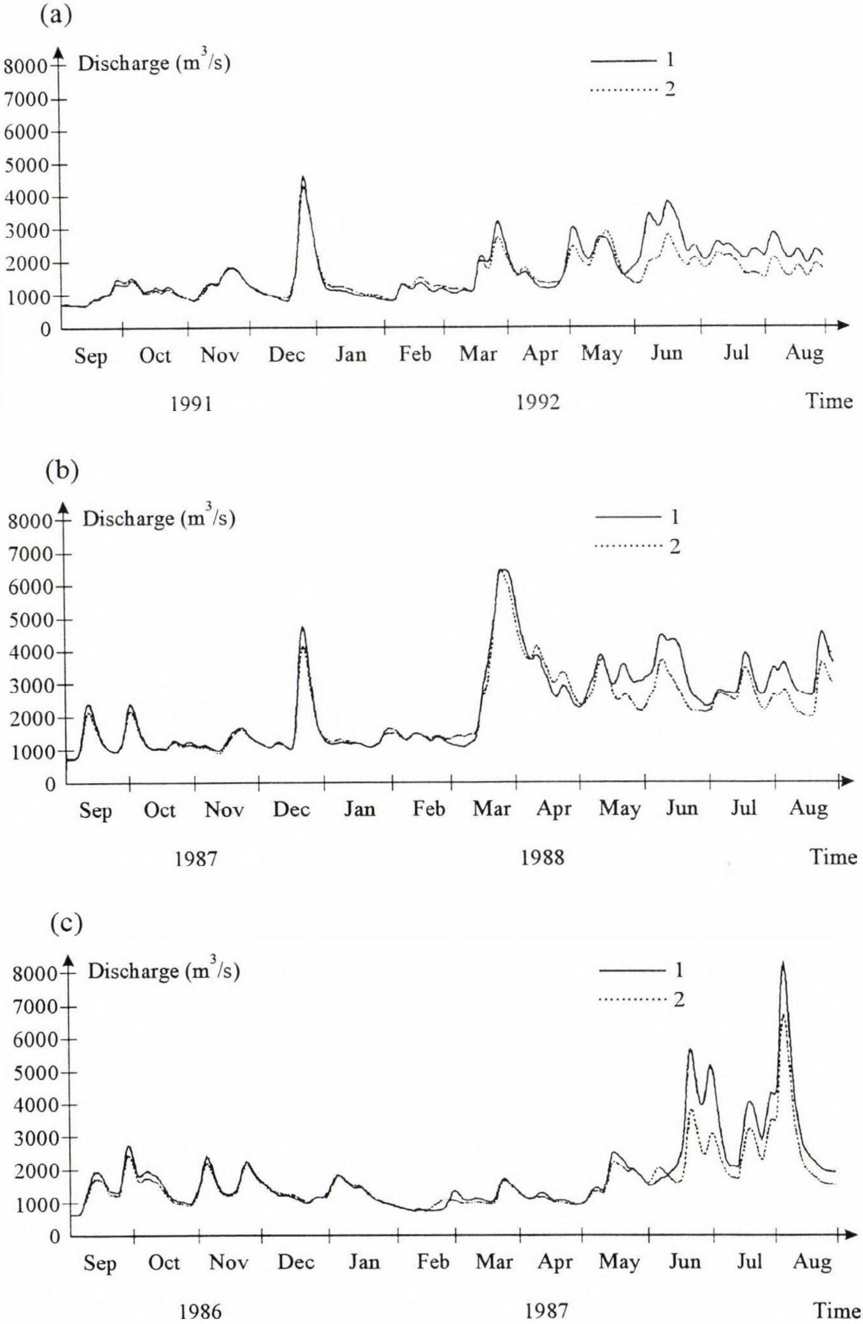

Fig. 3. Simulated annual flow time-series in the scenario (4): temperature rise +3°C, and annual precipitation decrease 10% Danube, Nagymaros

Table 2. The seasonal change of the mean discharges

	Average period			Wet period			Dry period		
	(3)	(4)	(5)	(3)	(4)	(5)	(3)	(4)	(5)
Q	1770 100%	1597 90%	1835 104%	2370 100%	2162 91%	2573 108%	1806 100%	1683 93%	1778 98%
Q_{winter}	1566 44%	1436 45%	1776 48%	1891 40%	1710 40%	2119 41%	1438 40%	1329 39%	1601 45%
Q_{summer}	1974 56%	1758 55%	1893 52%	2848 60%	2614 60%	3027 59%	2174 60%	2038 61%	1956 55%

6. Future studies

The selected scenarios oversimplified the natural conditions to be caused by the potential climate change and the selection of the investigated periods was arbitrarily made due to the pragmatic reason of the available data base for the Danube catchment.

Thus, both the basic time series and the scenarios should be more carefully selected. The characterization of the simulated time series with different statistical analysis (like distribution curves) may better represent the impact of the climate change on the flow time-series of the Danube.

Since the simulation covers the upper catchments as well, the results can be interesting for other countries, particularly for Bavaria, Austria and Slovakia.

Therefore, a closer co-operation in the studies would be useful for all of the riparian countries, including exchange of hydrometeorological data, studies for the climate change scenarios and numerical simulations of the resulted change in the flow regime.

References

VITUKI, 1994a: Effect of climate change on hydrological and water quality parameters (in Hungarian) OTKA No. 716/90, VITUKI Report 59. Budapest.

VITUKI, 1994b: Climate change impacts on the water resources of Hungary including the Upper Danube basin report for IIASA, Contract No. 94-115, Budapest.

Kuusisto, E., Lemmelä, R., Liebscher, H. and *Nobilis, F.*, 1994: Climate and water in Europe; some recent issues. WMO Technical Report. WG on Hydrology, RA VI.

IDŐJÁRÁS

Quarterly Journal of the Hungarian Meteorological Service
Vol. 100, No. 1–3, January–September 1996

On the possibilities of forecasting forecast skill

G. Götz

Lupény utca 6–8, H–1026 Budapest, Hungary

(Manuscript received 22 May 1995; in final form 15 November 1995)

Abstract—The accuracy of numerical weather predictions varies from day to day and from region to region, depending strongly on the state of the atmosphere. For this reason, the practical usefulness of a forecast can be greatly enhanced if supplemented by a skillful estimate of reliability. The purpose of this paper is to review the results of methods developed to predict the skill of dynamical forecasts.

On short- and medium-range time scales, the forecast skill is mainly influenced by the sensitive dependence of the predicted atmospheric flow on inevitable errors in the specification of initial conditions; model imperfections become crutial beyond the 10-day forecast period. Attempts to predict the quality of a forecast are therefore based on analysing the flow-dependent effects of initial uncertainties in a perfect-model environment, and differ from each other in the way these uncertainties are identified and handled.

Ensemble-prediction techniques — the most advanced methods introduced to forecast the forecast skill — utilize the results of stability theorem, and transform the deterministic forecasting problem into a probabilistic framework. Issues connected with the costliness of preparing ensemble predictions as well as with the adequate presentation of output products are currently exciting topics of debate in operational meteorology.

Key-words: predictability, error-growth dynamics, stochastic-dynamic forecasts, ensemble forecasts.

1. Introduction

In addition to his active and creative involvement in the promotion of our knowledge of cloud physics and atmospheric chemistry, *Prof. Ernő Mészáros* has always paid a particular attention to new achievements of the universal science that might help solving special problems arising in meteorology. During the 1980s, when we were working together at the Institute for Atmospheric Physics in Budapest, he decided to organize a series of lectures in order to survey the latest developments in atmospheric sciences, and he occasionally invited experts of related disciplines to give a talk on how they saw the biological and chemical aspects of the deteriorating atmospheric environment.

That was the time when the global environmental change due to inadvertent anthropogenic influences became one of the most important issues of internationally coordinated multidisciplinary research, and at our Institute, on the initiative of Professor Mészáros, an ambitious long-term research plan was set up, based on the collaboration of a group of enthusiastic and talented young scientists. The plan was supported by the Hungarian Academy of Sciences, and aimed at evaluating and interpreting the modifications of air quality as well as modelling numerically the possible regional characteristics of a global climatic change.

On the other hand, the 1980s were the years when implications of the discovery of seemingly random, *chaotic* behaviour of nonlinear deterministic systems became more and more evident in virtually every scientific discipline. The recognition of sensitive dependence of chaotic systems on initial conditions had eliminated the viewpoint that deterministic systems were predictable for all time, and had given birth to a new field of research called *nonlinear dynamics*. The most passionate advocates of this rapidly developing branch of investigations went so far as to say that twentieth-century science would be remembered for just three things: relativity, quantum mechanics and chaos (*Gleick,* 1988). As the chaotic behaviour of a deterministic system had been first recognized by *Lorenz* (1963) some twenty years previously in the context of a meteorological problem, namely the temporal evolution of the Rayleigh-Bénard convection, it seemed obvious that the results of nonlinear systems research should have a major impact on the methodology which we might use for an enhanced understanding of atmospheric processes. Therefore I mentioned to Professor Mészáros that I would be willing to deliver a set of lectures on *Chaos and order in the atmosphere*. In retrospect, I am not sure that I could really convince the audience of the fact that the discovery of chaos was not merely a bad news for weather forecasters; instead, nonlinear dynamics would offer a new and promising way of looking at complexity in nature.

Since those days many years have gone. In the meantime, the theory of dynamical systems has further shaped our way of investigating the weather and its prediction. *Lorenz*'s (1995) book provides a fascinating account of chaos, and the application of the science of chaos to meteorology, leading — among others — to the possibility of producing a reliable quality evaluation of a forecast along with the forecast itself (*Götz,* 1994, 1995).

2. Error sources of forecasts

Broadly speaking, one can distinguish two sources of forecast error. First, it has long been recognized that the atmosphere cannot be perfectly and completely observed at any instant. Thus, there is always some uncertainty in the specification of the initial conditions that are used to start the integration of a numerical weather prediction model. *Internal errors* are associated with the self-amplification of these inevitable uncertainties in initial data due to the intrinsic flow-dependent instabilities and nonlinearity of the atmospheric circulation. This process leads unavoidably to unpredictable random behaviour, and could be thought of as 'God given' (*Palmer* and *Tibaldi*, 1988). Second, the loss of forecast skill can be associated with analysis errors, with the tendency of models to drift towards their own climates, with the inability of models to describe all atmospheric regime types in their observed frequencies, and with the inability of models to predict realistic regime transitions beyond a few days. The random growth of these *external errors* is thus related to deficiencies in the way we choose to observe and simulate the real atmosphere; they are essentially 'man made'. In practice, the observed variability of forecast skill is influenced by interactions between these two categories of forecast errors (*Reynolds et al.*, 1994). For instance, the propagation and amplification of errors in the initial conditions depend strongly on the structure and stability of the large-scale flow. Similarly, the way in which systematic deficiencies in model formulation influence forecast skill will depend on the detailed structure of the flow. Therefore, the study of these interactions on different time scales constitutes an important research area.

On the other hand, it is usually assumed that much of the observed variability in current short- and medium-range forecast skill is associated with the flow-dependent internal error growth. According to *Palmer* and *Tibaldi* (1988), there is every indication that for the shorter ranges the forecast-error amplification by baroclinic wave growth is dominant; they argue that the influence of external error growth becomes crutial only beyond the 10-day forecast period, when the quality of extended-range prediction is mainly influenced by model systematic errors. Certainly, the formulation of numerical models will continue to be improved, and the accuracy of the initial state will also be increased. However, even when the effects of model imperfections are truly negligible, and when the state of the whole atmosphere can be measured with high and uniform accuracy, variability in forecast skill associated with the amplification of the remaining uncertainties in the initial state by dynamical instabilities will be sufficiently large to restrict the useful range of the forecast.

The recognition that flow-dependent estimates of the amplification of inevitable uncertainties in the initial conditions would be an important additional component of the weather forecast, giving an *a priori* assessment of its reliability, has aroused interest in investigating the possibilities connected with the task of forecasting the forecast skill. In producing useful skill prediction, it is necessary to understand in detail the dynamics of internal error growth, as outlined in Section 3. Objective methods for predicting the accuracy of forecasts may be categorized as either statistic-dynamical or ensemble predictions; they will be described in Section 4. Recently, ensemble forecasting has become the most advanced method to provide reasonable probabilistic predictions.

However, ensemble forecasting is a computationally expensive technique. Therefore, despite the continuous increase in computer power, a conflict might arise between the need of improving the resolution and sophistication of the operational model, and the need to generate ensembles which are large enough to produce realistic probabilistic estimates. This issue, together with the possible methods for disseminating ensemble information to forecasters and to users, will be discussed along with the conclusions in Section 5.

3. The theory of internal error growth

Let $\mathbf{x}(t)$ be the state vector at time t in the phase space of a finite n-dimensional dynamical system. The primitive equations that describe the nonlinear time evolution of the system can be formally written as

$$d\mathbf{x}/dt = \mathbf{f}(\mathbf{x}), \tag{1}$$

where the model operator $\mathbf{f}$ includes the nonlinearity of the resolved dynamics as well as the nonlinearities in the physical parametrizations. Let us consider a small perturbation (error) $\mathbf{y}(t_o)$ superimposed on the initial state $\mathbf{x}(t_o)$, and let us study its evolution. For sufficiently short time intervals and small initial amplitudes, the problem can be described in the context of linear stability theorem (*Ott*, 1993; *Thompson* and *Stewart*, 1993), i.e. the evolution of $\mathbf{y}$ is approximately governed by the linearized equation

$$d\mathbf{y}/dt = \boldsymbol{G}(t)\mathbf{y}, \tag{2}$$

where the linear evolution operator $\boldsymbol{G}$ is a Jacobian matrix whose elements $G_{ij} = \partial f_i/\partial x_j$ $(i,j = 1,2,\dots,n)$ are time dependent, and corresponds to the model operator $\mathbf{f}$ relative to the phase-space trajectory of the nonlinear basic flow $\mathbf{x}(t)$. The solution of the tangent linear system (2) can be obtained by numerically integrating it between times t_o and t_1, and can be represented by

$$\mathbf{y}(t_1) = \boldsymbol{A}(t_o,t_1)\mathbf{y}(t_o). \tag{3}$$

Here the linear operator $\boldsymbol{A}$ is the matrix solution of the equation $d\boldsymbol{A}/dt = \boldsymbol{GA}$ subject to the initial condition $\boldsymbol{A}(\mathbf{x}(t_o),t_o) = \boldsymbol{I}$ ($\boldsymbol{I}$ denoting the $n \times n$ identity matrix). Due to the asymmetry of the Jacobian $\boldsymbol{G}$, which is always the case for realistic basic-state flows, the operator $\boldsymbol{A}$ is not a normal matrix. It is usually referred to as the forward tangent propagator: $\boldsymbol{A}$ maps small perturbations along the nonlinear trajectory $\mathbf{x}(t)$ from an initial time t_o to some future time t_1.

For the evaluation of amplifying initial perturbations, an error measure needs to be defined. Using the expression $< \mathbf{y},\mathbf{y} >$ as a fixed norm, where

$< , >$ denotes the Euclidean inner product, from Eq. (3) the perturbation norm at time t_1 is given by

$$< \mathbf{y}(t_1), \mathbf{y}(\mathrm{t}_1) > \; \equiv \; |\mathbf{y}(t_1)|^2 \; = \; < \mathbf{y}(t_o), \boldsymbol{A}^*\boldsymbol{A}\boldsymbol{y}(t_o) > , \tag{4}$$

where $\boldsymbol{A}^*$ is the adjoint of the operator $\boldsymbol{A}$ with respect to the perturbation norm; that is, for any two state vectors $\mathbf{x}$ and $\mathbf{y}$, $< \boldsymbol{A}\mathbf{x}, \mathbf{y} > \; = \; < \mathbf{x}, \boldsymbol{A}^*\mathbf{y} >$. Whilst in general $\boldsymbol{A}$ itself is not a symmetric matrix, by construction the product operator $\boldsymbol{A}^*\boldsymbol{A}$ is. Hence its eigenvectors $\mathbf{u}_i(t_o)$ can be chosen to form a complete orthonormal basis in the n-dimensional tangent space of linear perturbations with real eigenvalues $\gamma_i^2 \geq 0$; that is

$$(\boldsymbol{A}^*\boldsymbol{A})\mathbf{u}_i(t_o) = \gamma_i^2 \; \mathbf{u}_i(t_o). \tag{5}$$

At a future time t_1, these eigenvectors evolve to

$$\mathbf{u}_i(t_1) \; = \; \boldsymbol{A}\mathbf{u}_i(t_o), \tag{6}$$

which in turn satisfy the eigenvector equation

$$(\boldsymbol{A}\boldsymbol{A}^*)\mathbf{u}_i(t_1) = \gamma_i^2 \; \mathbf{u}_i(t_1). \tag{7}$$

From Eqs. (4) and (7) it follows that

$$|\mathbf{u}_i(t_1)|^2 \; = \; < \mathbf{u}_i(t_o) \; , \boldsymbol{A}^*\boldsymbol{A}\mathbf{u}_i(t_o) > \; = \; \gamma_i^2 . \tag{8}$$

The square roots γ_i of the eigenvalues of the product operator $\boldsymbol{A}^*\boldsymbol{A}$, with their magnitudes arranged in descending order, are called the singular values of the operator $\boldsymbol{A}$, and the vectors $\mathbf{u}_i(t)$ are called the singular vectors of $\boldsymbol{A}$. Since any $\mathbf{y}(t_1)/|\mathbf{y}(t_o)|$ can be expressed as a linear combination of the set $\mathbf{u}_i(t_1)$, it follows that if $\mathbf{y}(t_o) \neq 0$, then

$$\max \; [|\mathbf{y}(t_1)|/|\mathbf{y}(t_o)|] \; = \; \gamma_1 \, .$$

Maximum perturbation (error) growth over the time interval $t_1 - t_o$ is therefore associated with the dominant singular vector: $\mathbf{u}_1(t_o)$ at initial time and $\mathbf{u}_1(t_1)$ at some final time. In order to identify $\mathbf{u}_1(t_o)$, it suffices to integrate the adjoint equation of Eq. (2) backwards in time from time t_1 to time t_o. For a more detailed description of the adjoint technique, see *Barkmeijer* (1992), *Buizza* (1992, 1994), *Vukicevic* (1993), and *Buizza* and *Palmer* (1995).

The limits

$$\lambda_i = \lim_{t\to\infty} \frac{\ln \gamma_i}{t - t_0} = \lim_{t\to\infty} \frac{1}{t - t_0} \ln \frac{y_i(t)}{y_i(t_0)} \tag{9}$$

define the Lyapunov exponents of the system. The corresponding set of singular vectors, obtained by replacing limits in Eq. (9) by limits as $t_0 \to -\infty$ while t remains fixed, are called the local Lyapunov vectors of the system at $\mathbf{x}(t)$ (*Lorenz*, 1984).

From (9) it follows that

$$y_i(t) \sim y_i(t_0) \exp[\lambda_i(t - t_0)]\,. \tag{10}$$

The Lyapunov exponents represent the *average* exponential rate at which initially close trajectories diverge or converge asymptotically in the phase space of the system. The positive exponents represent diverging trajectories, whereas the negative ones are related to converging trajectories. A dynamical system that possesses one or more positive Lyapunov exponents is called chaotic, and exhibits sensitive dependence on initial conditions. Note that although the Lyapunov exponents are themselves *global* quantities, the Lyapunov vectors are still defined *locally,* and thus vary with position in the phase space and hence with time. As the analyses of the simplest chaotic models show, the degree of divergence of *finite segments* of initially nearby trajectories depends considerably on the position of the starting points in the attractor set (*Nese*, 1989; *Abarbanel et al.,* 1991; *Mukougawa et al.*, 1991). On the other hand, local Lyapunov vectors exhibit a peculiar phase-spatial organization (*Ziehmann-Schlumbohm et al.,* 1995). This underlying structure permits the identification of regions in phase space of high and low predictability and, in some cases, it permits an estimate of predictability to be assigned to the predictability variable itself.

As the initially infinitesimal errors continue to grow, while they are still small, they must eventually cease to be small, whereupon the linearized equation (2) governing them will no longer hold. The errors have then left the linear phase of growth and entered the nonlinear, irregular phase of growth. During this second phase the growth rate must eventually subside, since ultimately the errors will become only as large as the difference between two randomly chosen states of the system (*Lorenz,* 1965; *Nicolis* and *Nicolis,* 1991; *Savijarvi,* 1995). The degree of chaos and the dominant Lyapunov exponent show considerable variation with change in the control parameters of the system, which implies that the time variation in the external forcing can also introduce a variable character to predictability (*Nicolis* and *Nicolis*, 1991; *Krishnamurthy,* 1993).

By observing the divergence between initially analogous weather situations, *Lorenz* (1969) suggested that the self-growth of the initially small rms error E could be modelled by the simple one-dimensional quadratic logistic equation

$$dE/dt = \lambda\, E(1 - E/E_s) \tag{11}$$

as the leading nonlinear terms in the governing equations of the atmosphere are quadratic. According to (11), small initial errors grow exponentially with a growth rate λ (now known as the first Lyapunov exponent of the system), their e-folding time being $1/\lambda$. After the errors have grown large, they are governed by the quadratic nonlinearities and asymptote toward a saturation value E_s, which is the rms difference between randomly picked flow states. If E_0 is the initial error at time t_0, then Eq. (11) gives the error E at a later time t as

$$\frac{E\,(1 - E_0/E_s)}{E_0(1 - E/E_s)} = \exp[\lambda(t - t_0)]\,. \tag{12}$$

Eq. (11) should be considered as a 'perfect model' approach, i.e. systematic modelling errors do not overwhelm internal errors that grow from initial data uncertainties. In a related extension, *Dalcher* and *Kalnay* (1987) modified Eq. (11) to include the effects of external error growth due to different model imperfections. These appear in the equation as an additional forcing term m:

$$dE/dt = (\lambda E + m)(1 - E/E_s). \tag{13}$$

It can be shown that in extended-range forecasts, systematic model errors become as important as errors due to uncertainties in the initial data set (*Barker,* 1991).

For sufficiently large initial errors, comparable to real observational errors, the exponential phase of growth can be shown to be absent, indicating that the linear theory of the growth of small errors is not applicable at all, and the growth is governed completely by *nonlinear* error dynamics. During a part of the initial growth phase, the growth rate can be higher than the largest Lyapunov exponent (*Nicolis* and *Nicolis*, 1993). Therefore, the use of Lyapunov exponents to estimate error-growth rate and predictability is valid only for initially small errors and, as *Krishnamurthy* (1993) concludes, it is unlikely that the errors in numerical weather prediction models, at the current level of exactness of the observed data, can be interpreted in terms of the Lyapunov exponents.

In recent literature, particular attention has been devoted to the transient short-range evolution of initially small errors controlled by rapidly growing perturbations that are *not* of normal-mode form (*Lacarra* and *Talagrand*, 1988; *Farrell*, 1990; *Nicolis et al.*, 1995). The phenomenon of *superexponential error* *growth* is a direct consequence of two principal mechanisms which have, so far, been proposed in the literature. The first mechanism is the variability of the local Lyapunov vectors in the phase space, reflecting the highly inhomogeneous character of chaotic attractors. This variability is manifested by appreciable fluctuations of the local Lyapunov exponents around their global values. The second mechanism is the non-orthogonality of the eigenvectors of the forward tangent propagator $\boldsymbol{A}$ in Eq. (3), which enables superposition of several normal-mode perturbations to grow faster than the most unstable normal-mode amplification for a short time. Consequently, error-growth rates inferred from the singular values of $\boldsymbol{A}$ (i.e. the eigenvalues of the symmetric product operator $\boldsymbol{A}^*\boldsymbol{A}$) can be very much larger than those inferred from the eigenvalues of $\boldsymbol{A}$ (that is, by the growth rates of the normal modes), and therefore the predictability estimates made from the maximum normal-mode growth rate can be erroneously optimistic.

Singular vectors with the largest singular values are usually referred to as *optimal*, in the sense that they maximize linear disturbance growth over a chosen integration period, and insofar as the optimal singular vectors describe an amplifying disturbance ($\gamma_i^2 > 1$), the growth associated with them is called *finite-time instability*. In recent years, optimal singular vectors have been calculated for a number of idealized basic states e.g. by *Borges* and *Hartmann* (1992), *Yoden* and *Nomura* (1993), *Trevisan* (1993), and *Trevisan* and *Legnani* (1995).

Finally, it should be emphasized once again that *internal instability* appears to be the most fundamental property of a chaotic dynamical system, and may be considered the cause of both its *irregular (aperiodic) behaviour* and its *sensitive dependence on initial conditions*. The atmosphere is a geophysical fluid in which these two manifestations of chaos could be clearly demonstrated. Therefore, it is currently believed that the tendency of the extended-range weather forecasts to become progressively worse is mainly due to the intrinsic instability of the atmosphere. Instability is created by nonlinear interactions in the atmospheric dynamics, and due to the inherent nonlinearity of the governing equations, the unavoidable inaccuracy of the initial data will tend to amplify with time even if the prediction model is somehow made perfect. This fact prompted *Tennekes et al.* (1987) to assert that 'no forecast is complete without a forecast of forecast skill'.

4. Techniques for predicting the forecast skill

The problem of producing a precise *a priori* quality evaluation of the skill of a prediction has been addressed in various ways at theoretical level and on operational basis.

4.1 Stochastic-dynamic predictions

The stochastic-dynamic prediction method is based on the assumption that the laws governing atmospheric behaviour are entirely deterministic, but seeks solutions corresponding to probabilistic statements of the initial conditions, thus recognizing the impossibility of exact observations. A complete stochastic-dynamic prediction procedure would provide the probability distribution of possible atmospheric states at a desired forecast time. The method, described by *Epstein* (1969), is a simplified version of such an exceedingly complex task being well beyond present computational resources.

Deterministic procedures follow the assumption that the changing state of the atmosphere is represented by Eq. (1), i.e. the predicted state $\mathbf{x}(t)$ at some time $t > t_0$ can be symbolically written as

$$\mathbf{x}(t) = \mathbf{x}(t_0) + \int_{t_0}^{t} \mathbf{f}(\mathbf{x}(t))dt. \tag{14}$$

Here $\mathbf{x}(t_0)$ is a *single* 'best' initial condition which is chosen somehow on the basis of the available observations. Now, *Epstein* (1969) has argued that a more reasonable interpretation of the observations is that they imply a probability density function $\varphi(\mathbf{x},t_0)$ defined over the entire n-dimensional phase space, where φ must have the properties that $\varphi \geq 0$ for all $\mathbf{x}$ and t, and the total probability is, by definition, one:

$$\int\int \cdots \int \varphi(\mathbf{x},t)\, dx_1\, dx_2 \ldots dx_n = 1 .$$

In place of $\mathbf{x}(t_0)$, then, one must consider an analysis of the observations which accomplishes this. Moreover, if $\mathbf{x}(t_0)$ is modified, so also must a substitute be found for Eq. (14); it is necessary to describe an algorithm by which $\varphi(\mathbf{x},t)$, $t > t_0$, can be determined, once $\varphi(\mathbf{x},t_0)$ is known. For this purpose the continuity equation for probability is extended to the n-dimensional case and written as

$$\partial\varphi/\partial t + \nabla_n(\varphi d\mathbf{x}/dt) = 0, \tag{15}$$

where ∇_n is the del-operator in the n-dimensional phase space. Eq. (15) is based on the principle that the total amount of probability must always be one, i.e. no ensemble members may be created or destroyed.

Given appropriate boundary conditions and the initial value $\varphi(\mathbf{x},t_0)$, the direct integration of (15) to obtain $\varphi(\mathbf{x},t)$, $t > t_0$, offers no mathematical difficulties, and the likelihood of skill of the forecast can then be estimated from the variance of the probability distribution. Practically, however, any calculation of φ by direct numerical integration of Eq. (15) would be a most ambitious undertaking. If one wishes to evaluate φ at d incremental values of each of the components of the state vector, this corresponds to n^d points, for each of which it is necessary to store and update the numerical value at each time step. $n = 10$, $d = 100$ would be a realistic meteorological problem, but it would create formidable computational requirements. Therefore, *Epstein* (1969) proposed an approach where only the first and second moments of the probability distribution are predicted by making closure assumptions about the higher-order moments in Eq. (15).

Even with this simplified approach, very expensive numerical computations are necessary. Practical applications of the stochastic-dynamic prediction technique have thus proven to be unfeasible, except for the simplest models and approximate solutions to Eq. (15).

4.2 Ensemble predictions

Another technique for estimating predictability is to construct an ensemble of possible initial states at t_0. As each member of the ensemble is, *a priori*, equally likely to be the true state, the ensemble provides a fair representation of the uncertainty of the initial conditions. The deterministic numerical weather prediction model can then be run from each initial state, producing an ensemble of forecasts for $t > t_0$. Thus, the ensemble forecast method trades the closure problem of stochastic-dynamic prediction for a sampling problem.

The ensemble-mean forecast (i.e. the first moment of the probability distribution of the predicted states) is an improvement over a single forecast since some of the errors in the individual forecasts cancel when averaged. The second moment of the probability distribution (often called ‘spread’) contains information that may be useful for predicting the forecast skill in advance. The spread is a measure of dispersion of the ensemble, indicating whether or not the uncertainties in the initial state are having a detrimental effect on forecast quality: high spread of solutions across the ensemble provides an indication of low confidence in the prediction, while a lower spread indicating limited sensitivity to errors in initial conditions and therefore higher confidence in the prediction. It is important to emphasize that the ensemble technique reveals forecast deficiencies that are due to *internal error growth,* i.e. this approach may only be applied in an ideal sense given a perfect atmospheric model.

The idea of ensemble prediction is illustrated schematically in *Fig. 1*, where individual forecast trajectories starting from a set of slightly perturbed initial conditions, representing the uncertainty in specification of the initial state, may end after some time within a much larger range of possible states. As the figure suggests, the forecasting problem can be considered *deterministic* for the shorter ranges, since the trajectories remain close to each other, but beyond a certain time, one cannot ignore the fact that the forecasting problem assumes a *stochastic nature*. The forecasts may cluster into just a few groups of similar trajectories, and it may be possible to assign probabilities to the differing scenarios based on the number of forecasts in each cluster, denoted A and B in the figure.

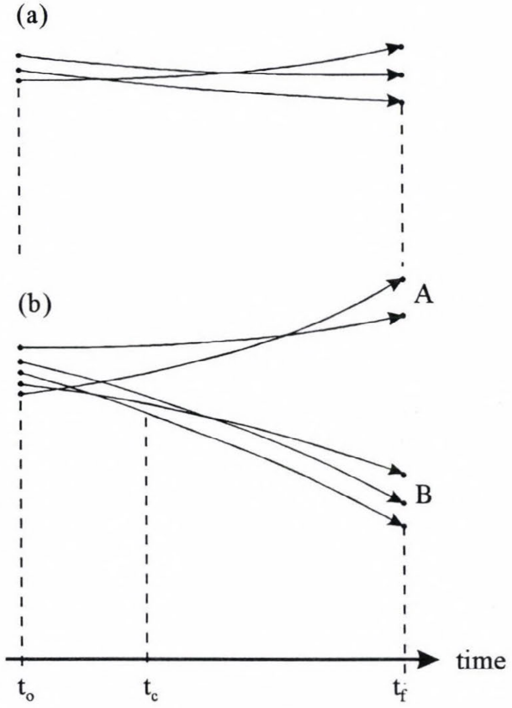

Fig. 1. Schematic illustration of the temporal evolution of initially close states in the phase space. (*a*) Predicted trajectories diverge slowly, categorical statements for t_f are possible. (*b*) Predicted trajectories diverge rapidly; beyond t_c forecasts should be expressed in a probabilistic form. Note that the predicted states for t_f may cluster into groups denoted by A and B.

A fundamental difficulty with ensemble forecasting is that the number of balanced degrees of freedom in current numerical weather prediction models (on the order of 10^6) greatly exceeds the maximum practicable size of an ensemble (say between 10 and 100). Various types of ensemble predictions differ from each other in *sampling strategy*, i.e. in the way the initial ensemble is constructed.

Monte Carlo forecasts — The concept of ensemble forecasting procedure was introduced by *Leith* (1974), in order to avoid the shortcomings of the stochastic-dynamic predictions. As we have seen, the stochastic-dynamic forecasting scheme is based on a moment expansion technique, and the approximation involved is a moment closure that gives equations for the evolution of the mean and covariance directly. On the other hand, the Monte Carlo forecasting scheme is based on a sampling approximation in which the forecast ensemble mean and covariance are estimated from a finite sample of initial phase-space points, determined by computing q trajectories in the phase space. In this context, a conventional single prediction can, of course, be considered as a special case of a Monte Carlo forecast with sample size $q = 1$.

Let the true but unknown state of the atmosphere be $\mathbf{x}$, and let $\hat{\mathbf{x}}$ represent some estimate of $\mathbf{x}$. We assume that $\hat{\mathbf{x}}$ is an unbiased estimate of $\mathbf{x}$ in the sense that for an ensemble of many estimation trials $< \mathbf{x} - \hat{\mathbf{x}} > = 0$, where the brackets $< >$ denote here an average over the ensemble. A conventional single forecast takes $\hat{\mathbf{x}}$ as *the* initial state. In order to generate an initial sample for a Monte Carlo forecast, we choose a finite set of state vectors $\mathbf{x}_i(t_0) = \hat{\mathbf{x}} + \mathbf{y}_i$ $(i = 1,2,\ldots,q)$ with $\mathbf{y}_i$ being normal random vectors such that $< \mathbf{y}_i > = 0$. Using a simple two-dimensional homogeneous isotropic turbulence model, *Leith* (1974) concluded that such a Monte Carlo forecasting procedure represents a practical, computable approximation to the stochastic-dynamic forecasts proposed by *Epstein* (1969), and adequate accuracy can be obtained for the best mean estimate of the forecast field with sample sizes as small as $q = 8$.

The complexity of the current forecast models would, however, greatly obstruct the operational use of the Monte Carlo technique. Moreover, recent experiments have clearly revealed that the addition of spatially uncorrelated, *truly random* noise (closest to the original meaning of the Monte Carlo method) is inpracticable for numerical weather prediction models, because some of the random perturbations to a chosen initial state could be in meteorologically irrelevant directions of the phase space. These perturbations will be largely removed by initialization, or they will project onto non-meteorological modes and will be dissipated in the model as the initial states are integrated forward in time. Thus, the spread of the initial ensemble may start to decrease, and the eventual delayed dispersion of the ensemble can lead to an overestimate of the predictability (*Palmer et al.*, 1990). However, meteorological relevance is not in itself a sufficiently strong constraint to determine the structure of viable perturbations. The number of degrees of freedom required to explain most of the variance of the synoptic-scale flow is on the order of 10 to 100. Therefore, it is very unlikely that $q = 10$ to 100 *randomly* chosen perturbations from the 10^6 degrees of freedom of the forecast model will have any significant projection onto the 10 to 100 synoptic degrees of freedom (*Mureau et al.*, 1993).

The recognition of these facts has motivated the interest in looking for techniques that generate initial perturbations which are energetically active and affect the evolution of the large-scale atmospheric circulation whose prediction is the goal of the weather forecast.

Lagged-average forecasts — A feasible way of ensemble prediction is the method of lagged-average forecasting proposed by *Hoffman* and *Kalnay* (1983). Here the ensemble of forecasts at a particular forecast time $t_f > t_0$ consists of the latest operational numerical weather prediction started from the initial conditions at t_0 together with forecasts based on previous analyses at $t_0 - \tau$, $t_0 - 2\tau$, ... (τ being a 6- or 12-hour time interval) but with the same verification time t_f. Since the perturbations obtained by this way are short-range forecast errors, it can be assumed that they represent realistic, actively growing error modes corresponding to the flow at time t_0 which is being predicted. A disadvantage of the method, compared to Monte Carlo forecasting, is that the perturbations are not similar in size. The 'older' forecasts have larger perturbations and, therefore, tend to be less skillful than the later or 'younger' forecasts. This problem can be alleviated by a careful statistical weighting the different members of the ensemble as a function of the relative skill of the newer versus older predictions.

In an application of the method to operational forecasts, *Dalcher* and *Kalnay* (1987) found that the success in predicting individual forecast skill was only minimal. They attributed this lack of success to the use of *global* verifications, which could have possibly masked regional variations in skill. Indeed, when the method was used to predict *regional* forecast skill, *Kalnay* and *Dalcher* (1987) were quite well able to predict the quality of individual forecasts. When the verification area was enlarged to the whole Northern Hemisphere, a deterioration of the forecast-skill prediction was observed.

Ensemble predictions using dynamically conditioned initial perturbations — A new era in operational numerical weather prediction, particularly as it relates to medium- and extended-range forecasting, began in December 1992 when two of the major meteorological centres started performing regularly (now daily) ensemble predictions. Though the techniques adopted at the two centres to select the ensemble of initial conditions differ from each other, both procedures are based on the theory of internal error growth, and are designed to concentrate perturbations around the fastest-growing instabilities in the current atmospheric circulation. Thus, perturbations are superimposed on the basic state mainly in regions where integrations are sensitive to errors in initial conditions; over other regions only minor, or even no, perturbations are added.

At the European Centre for Medium-range Weather Forecasts (ECMWF) in Reading, the method is built upon the selection of optimal non-modal singular vectors, i.e. initial perturbations that grow fastest over a finite time interval (*Buizza et al.*, 1993; *Mureau et al.*, 1993; *Palmer et al.*, 1994; *Buizza* and *Palmer*, 1995). The dominant 35 singular vectors of the atmospheric general circulation are routinely calculated from a primitive equation model, using an iterative Lanczos algorithm with 36-hour trajectories to solve the eigenvalue problem of the product operator $\boldsymbol{A}^*\boldsymbol{A}$. The initial perturbations are constructed from 16 of the dominant singular vectors. An individual ensemble perturbation is a linear combination of these singular vectors, weighted by the analysis error variance estimated from an optimal interpolation scheme. The ensemble prediction system consists of 34 ten-day forecasts: the high-resolution operational forecast, and an ensemble of 32 + 1 (control) integrations of a medium-resolution nonlinear deterministic model.

The ensemble forecast configuration implemented at the U.S. National Meteorological Center (NMC) in Washington provides 14 independent medium-range predictions every day valid for a ten-day period (recently, the ensemble size has been increased to 38). The construction of the forecast ensemble is made up of a combination of time lagging (*Hoffman* and *Kalnay*, 1983) and a new method called breeding of the growing modes (*Toth* and *Kalnay*, 1993; *Tracton* and *Kalnay*, 1993; *Wobus* and *Kalnay*, 1995). Kalnay and her collaborators argue that fast-growing perturbations naturally develop in a regular analysis cycle. Based on this observation, the technique consists of the following steps: (a) a small random perturbation is added to the atmospheric analysis; (b) the prediction model is integrated for 6 hours from both the unperturbed (control) and the perturbed initial condition; (c) the 6-hour control forecast is subtracted from the perturbed forecast; and (d) this difference field is scaled down such that it has the same size (in an rms sense) as the initial perturbation. This process is then repeated forward in time. By construction, the method selects ('breeds') the perturbations that have grown most rapidly during some period prior to the analysis and are likely to continue to grow after the analysis. In a perfect-model environment, this method would be equivalent to identifying the local Lyapunov vectors in the phase space.

As we can see, the 'optimal' modes technique to generate errors gives the largest error at a prespecified *forecast* time, while the 'bred' modes are obtained from perturbations that have developed *prior* to the analysis. The relative benefits of these two methods, and the advisability of concentrating perturbations only in the regions of highest sensitivities to small initial errors, are currently topics of active debate (*Harrison*, 1994; *Houtekamer* and *Derome*, 1995).

5. Concluding remarks

In addition to the principal methods shortly described in Section 4, several other techniques have been proposed for the prediction of forecast reliability. For example, *Palmer* and *Tibaldi* (1988) have considered four possible sets which, given the present data, could be used as predictors of forecast skill: the spread between today's day-k forecast and yesterday's day-$(k + 1)$ forecast; the synoptic features of flow pattern associated with the forecast height field; the rms skill of the yesterday's day - 1 forecasts; and the rms difference between the forecast 500-hPa height and the initial 500-hPa height (the use of this predictor was motivated by diagnostic studies showing relationships between interannual variability of forecast scores and interannual variability of persistence errors). They concluded that using these types of predictors, some aspects of the low-frequency component of forecast-skill variability can be satisfactorily predicted, though significant high-frequency variability remains unpredicted. Some later modifications of this real-time scheme are described in the paper by *Molteni* and *Palmer* (1991). *Chen* (1989) has proposed an approach which does not require at all an ensemble of forecasts. He shows evidence that the degree of persistence of the model atmosphere is in itself an effective predictor of the quality of the forecast: the correlation between this simple predictor and the forecast skill is significant for the entire medium range, both over limited regions and over the Northern Hemisphere. Motivated by the earlier results, *Leslie* and *Holland* (1991) developed a procedure using a statistical regression scheme, a persistence measure and the spread between forecasts of different weather centres as predictors. In predicting the skill of the 36-hour forecasts, they were able to obtain a high correlation between the predictor set and the forecast error. Some additional, more sophisticated techniques, based on statistical as well as on dynamical considerations, are presented by *ECMWF* (1992).

The statistical techniques mentioned above are examples of the ones which are sometimes referred to as 'poor man's methods' of forecasting the forecast skill. Indeed, ensemble forecasts prepared at ECMWF and NMC apply ensemble sizes of about 35, and to cover all possible instabilities in the initial conditions, ensemble sizes of 50, perhaps 100, are currently thought to be necessary. However, the run of larger forecast ensembles to bracket the range of uncertainty is just one line of attack for improving weather predictions; improving the estimates of initial conditions, and improving the models, presumably through increased resolution with enhanced dynamical processes and physical parametrization, are also directions towards a better prediction system. Four-dimensional variational data assimilation, the most advanced analysis technique yet proposed, is estimated to demand a tenfold increase over present computing requirements. Plans for incorporating the oceans into forecast models, introducing more advanced parametrization schemes and improving model resolution will also place greater demands on computer resources. Therefore, despite the promising development in computing technology as the result of the maturation of massively-parallel-processor architecture, a conflict will arise between the computing requirements of the three approximations to prediction-system development mentioned above. Analysis and model improvement currently take centre stage because of the traditional deterministic approach of constructing the most accurate single prediction. In this connection it is worth-while to quote *Harrison*'s (1994) view: 'However sophisticated observing and assimilating techniques become, there will always be errors in initial fields of magnitudes that are sufficient to perturb individual model predictions away from reality. Improvements in analysis techniques are not sufficient, by themselves, to solve the prediction problem. Ensembles provide an approach through which the uncertainties resulting from errors in initial conditions may be objectively assessed.'

Ensemble predictions transform what, given a single objective, deterministic forecast, can be expressed only as *categorical statements* into a more useful *probabilistic framework,* i.e. estimates of chances for realizing several possible scenarios. Such a change in philosophy may not easily come about everywhere in the face of traditional practices. Therefore, high priority should be given in the future to the problem of considering the vast amounts of information from ensembles into a coherent form, and presenting the products in a readily assimilable, user-friendly format to both forecasters and recipients of forecasts. Early steps towards adequate information presentation have been already made at the major meteorological centres of the world. Products disseminated by the ECMWF include probability forecasts ('plumes') at a point throughout the forecast range, a cluster analysis of the 500-hPa height flow to determine the principal ensemble flow types, and probability fields of precipitation, low-level temperature and wind speed. Output products of the NMC include the display of each prediction of the ensemble, ensemble mean, spread charts (displaying the geographical distribution of the variability within the ensemble), 'clustering' of similar forecasts, and explicit estimates of the probability of some event or distribution of a given parameter.

With the demand of forecasting the forecast skill and with the operational implementation of ensemble predictions, meteorologists explicitly recognize that weather forecasts, especially for the medium range (and beyond), are *inherently stochastic,* that is, *probabilistic in nature.* There is no unique solution, only an array of possibilities, which ensemble forecasting attempts to sample. Education concerning the practical efficacy of probabilistic prediction, research evidence of the value of ensembles, and improved information presentation will in the coming years change the view even of those who received their training in the spirit of traditional deterministic attitude.

References

Abarbanel, H.D.I., Brown, R. and *Kennel, M.B.*, 1991: Variation of Lyapunov exponents on a strange attractor. *J. Nonlinear Sci. 1,* 175-199.

Barker, T.W., 1991: The relationship between spread and forecast error in extended-range forecasts. *J. Climate 4,* 733-742.

Barkmeijer, J., 1992: Local error growth in a barotropic model. *Tellus 44A*, 314-323.

Borges, M.D. and *Hartmann, D.L.,* 1992: Barotropic instability and optimal perturbations of observed zonal flows. *J. Atmos. Sci. 49*, 335-354.

Buizza, R., 1992: Unstable perturbations computed using the adjoint technique. *ECMWF Research Department Technical Memorandum,* No. 189.

Buizza, R., 1994: Sensitivity of optimal unstable structures. *Quart. J. Roy. Meteor. Soc. 120*, 429-451.

Buizza, R. and *Palmer, T.N.*, 1995: The singular-vector structure of the atmospheric global circulation. *J. Atmos. Sci. 52*, 1434-1456.

Buizza, R., Tribbia, J., Molteni, F. and *Palmer, T.*, 1993: Computation of optimal unstable structures for a numerical weather prediction model. *Tellus 45A*, 388-407.

Chen, W.Y., 1989: Another approach to forecasting forecast skill. *Mon. Wea. Rev. 117*, 427-435.

Dalcher, A. and *Kalnay, E.*, 1987: Error growth and predictability in operational ECMWF forecasts. *Tellus 39A*, 474-491.

ECMWF, 1992: *New Developments in Predictability*. Proc. workshop held at ECMWF, 13-15 November 1991.

Epstein, E.S., 1969: Stochastic dynamic prediction. *Tellus 21*, 739-759.

Farrell, B.F., 1990: Small error dynamics and the predictability of atmospheric flows. *J. Atmos. Sci. 47*, 2409-2416.

Gleick, J., 1988: *Chaos: Making a New Science*. Heinemann, London, 354 pp.

Götz, G., 1994: Application of nonlinear dynamics in atmospheric sciences. Part II. Some examples. *Időjárás 98*, 65-86.

Götz, G., 1995: Predictability of nonlinear dynamical systems. *Időjárás 99*, 1-32.

Harrison, M.S.J., 1994: Ensembles, higher-resolution models and future computing power - A personal view. *Weather 49*, 398-406.

Hoffman, R.N. and *Kalnay, E.*, 1983: Lagged average forecasting, an alternative to Monte Carlo forecasting. *Tellus 35A*, 100-118.

Houtekamer, P.L. and *Derome, J.*, 1995: Methods for ensemble prediction. *Mon. Wea. Rev. 123*, 2181-2196.

Kalnay, E. and *Dalcher, A.*, 1987: Forecasting forecast skill. *Mon. Wea. Rev. 115*, 349-356.

Krishnamurthy, V., 1993: A predictability study of Lorenz's 28-variable model as a dynamical system. *J. Atmos. Sci. 50*, 2215-2229.

Lacarra, J.-F. and *Talagrand, G.*, 1988: Short-range evolution of small perturbations in a barotropic model. *Tellus 40A*, 81-95.

Leith, C.E., 1974: Theoretical skill of Monte Carlo forecasts. *Mon. Wea. Rev. 102*, 409-418.

Leslie, L.M. and *Holland, G.J.*, 1991: Predicting regional forecast skill using single and ensemble forecast techniques. *Mon. Wea. Rev. 119*, 425-435.

Lorenz, E.N., 1963: Deterministic nonperiodic flow. *J. Atmos. Sci. 20*, 130-141.

Lorenz, E.N., 1965: A study of the predictability of a 28-variable atmospheric model. *Tellus 17*, 321-333.

Lorenz, E.N., 1969: Atmospheric predictability as revealed by naturally occurring analogues. *J. Atmos. Sci. 26*, 636-646.

Lorenz, E.N., 1984: The local structure of a chaotic attractor in four dimensions. *Physica 13D*, 90-104.

Lorenz, E.N., 1995: *The Essence of Chaos*. UCL Press, London, 227 pp.

Molteni, F. and *Palmer, T.N.*, 1991: A real-time scheme for the prediction of forecast skill. *Mon. Wea. Rev. 119*, 1088-1097.

Mukougawa, H., Kimoto, M. and *Yoden, S.*, 1991: A relationship between local error growth and quasi-stationary states: Case study in the Lorenz system. *J. Atmos. Sci. 48*, 1231-1237.

Mureau, R., Molteni, F. and *Palmer, T.N.*, 1993: Ensemble prediction using dynamically conditioned perturbations. *Quart. J. Roy. Meteor. Soc. 119, 299-323.*

Nese, J.M., 1989: Quantifying local predictability in phase space. *Physica D35*, 237-250.

Nicolis, C. and *Nicolis, G.*, 1991: Dynamics of error growth in unstable systems. *Phys. Rev. A43*, 5720-5723.

Nicolis, C. and *Nicolis, G.*, 1993: Finite time behavior of small errors in deterministic chaos and Lyapunov exponents. *Int. J. Bifurcation and Chaos 3*, 1339-1342.

Nicolis, C., Vannitsem, S. and *Royer, J.-F.*, 1995: Short-range predictability of the atmosphere: Mechanism for superexponential error growth. *Quart. J. Roy. Meteor. Soc. 121*, 705-722.

Ott, E., 1993: *Chaos in Dynamical Systems*. Cambridge University Press, Cambridge, 385 pp.

Palmer, T.N., Buizza, R., Molteni, F. and *Mureau, R.*, 1994: The ECMWF ensemble prediction system. In *Research Activities in Atmospheric and Oceanic Modelling*, Report No. 19 (ed.: *G.J. Boer*). WMO/TD-No. 592, pp. 6.16-6.17.

Palmer, T.N., Mureau, R. and *Molteni, F.*, 1990: The Monte Carlo forecast. *Weather 45*, 198-207.

Palmer, T.N. and *Tibaldi, S.*, 1988: On the prediction of forecast skill. *Mon. Wea. Rev. 116,* 2453-2480.

Reynolds, C.A., Webster, P.J. and *Kalnay, E.*, 1994: Random error growth in NMC's global forecasts. *Mon. Wea. Rev. 122,* 1281-1305.

Savijarvi, H., 1995: Error growth in a large numerical forecast system. *Mon. Wea. Rev. 123,* 212-221.

Tennekes, H., Baede, A.P.M. and *Opsteegh, J.D.*, 1987: Forecasting forecast skill. In *Proc. ECMWF Workshop on Predictability in the Medium and Extended Range, June 1986.* ECMWF, Shinfield Park, Reading, pp. 277-302.

Thompson, J.M.T. and *Stewart, H.B.*, 1993: *Nonlinear Dynamics and Chaos*. John Wiley and Sons, Chichester, 376 pp.

Toth, Z. and *Kalnay, E.*, 1993: Ensemble forecasting at NMC: The generation of perturbations. *Bull. Amer. Meteor. Soc. 74,* 2317-2330.

Tracton, M.S. and *Kalnay, E.*, 1993: Operational ensemble prediction at the National Meteorological Center: Practical aspects. *Wea. Forecasting 8,* 379-398.

Trevisan, A., 1993: Impact of transient error growth on global average predictability measures. *J. Atmos. Sci. 50,* 1016-1028.

Trevisan, A. and *Legnani, R.*, 1995: Transient error growth and local predictability: A study in the Lorenz system. *Tellus 47A,* 103-117.

Vukicevic, T., 1993: Possibility of skill forecast based on the finite-time dominant linear solutions for a primitive equation regional forecast model. *J. Atmos. Sci. 50,* 1777-1791.

Wobus, R.L. and *Kalnay, E.*, 1995: Three years of operational prediction of forecast skill at NMC. *Mon. Wea. Rev. 123,* 2132-2148.

Yoden, S. and *Nomura, M.*, 1993: Finite-time Lyapunov stability analysis and its application to atmospheric predictability. *J. Atmos. Sci. 50,* 1531-1543.

Ziehmann-Schlumbohm, C., Fraedrich, K. and *Smith, L.A.*, 1995: Ein internes Vorhersagbarkeitsexperiment im Lorenz-Modell. *Meteor. Zeitschrift N. F. 4,* 16-21.

IDŐJÁRÁS

Quarterly Journal of the Hungarian Meteorological Service
Vol. 100, No. 1–3, January–September 1996

Climate ensemble forecasts: how to create them?

Zoltan Toth[1] and **Eugenia Kalnay**

Environmental Modeling Center,
National Centers for Environmental Prediction
5200 Auth Rd., Rm. 204, Camp Springs, MD 20746, USA

(Manuscript received 2 June 1995; in final form 22 November 1995)

Abstract—In this paper we discuss the construction of ensemble predictions for anomalies associated with El-Niño/Southern Oscillations (ENSOs), which depend on the coupling of the atmosphere and ocean. First we distinguish between two types of ensembles. In the boundary forcing ensembles, which have been used so far in seasonal to interannual predictions/simulations, the ensemble approach is applied only on the atmosphere; the boundary SST is assumed to be known (or 'perfectly' predicted). In the forecasts no information is retained from the atmospheric initial state; the system is driven by the anomalous boundary forcing only. In the initial value ensemble that we propose for the coupled ocean-atmosphere system on the ENSO time scales, an ensemble of possible oceanic initial conditions are integrated forward, coupled with the atmosphere. The atmospheric initial conditions are still 'forgotten' in this approach, but the oceanic predictions can be improved due to the nonlinear filtering process that the ensemble offers.

We propose the use of the breeding method, successfully applied in atmospheric ensemble predictions, for generating the flow dependent, growing type of errors present in oceanic analyses. The bred growing vectors represent an extension into nonlinear systems of the leading local Lyapunov vectors that describe maximum sustainable growth in a linear sense. We argue that the breeding method can not only offer a good description of initial uncertainty but can also serve as a new diagnostic tool, describing the leading instabilities associated with different ENSO episodes.

Key-words: climate prediction, ensemble forecasting, coupled ocean-atmosphere modeling, ENSO, local Lyapunov vectors.

1. Introduction

In a series of by now classical papers *Lorenz* (1963; 1965; 1969a) showed that the atmosphere is a chaotic system. It follows that unless the initial state (and the dynamics) of the system is perfectly known, atmospheric predictability is lost after a finite period of time. Though the loss of predictability is unavoidable we can try

---

[1] Corresponding author

to describe the way this loss occurs. For this end we need to know the dynamics of the system in question and we need to estimate the initial uncertainty present in our analysis of the state of the system. When these two conditions are combined with adequate computer resources one can run a set of model integrations from possible analyses beyond that from the control analysis (*Leith*, 1974) and follow these forecasts to evaluate how the initial uncertainty spreads with increasing lead time till all information about the state of the system is lost (*see Fig. 1*).

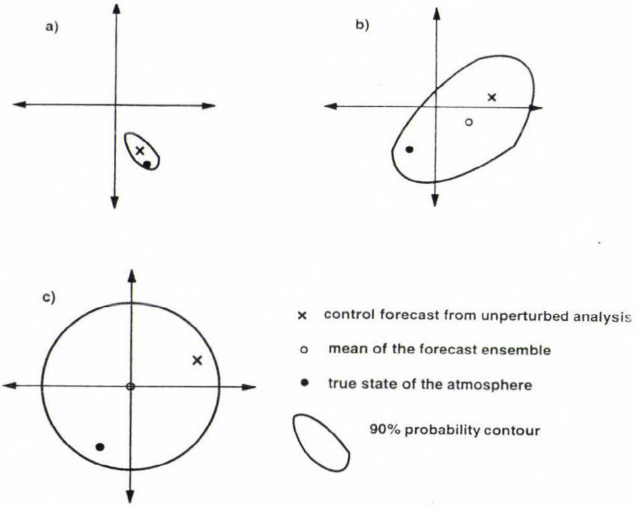

Fig. 1. Schematic illustrating the loss of predictability with increasing lead time (*a-c*) in a nonlinear dynamical system with constant forcing. (*a*) Estimated initial uncertainty; (*b*) Initial value ensemble stage: Part of the information about the state of the system is still preserved; (*c*) Boundary forcing ensemble: All information given on the state of the system at initial time is lost. At this forecast lead time it is solely the external forcing that determines the possible states (conditional climate) of the system.

Such ensemble forecast systems are by now operational for atmospheric predictions (*Tracton* and *Kalnay*, 1993; *Molteni et al.*, 1995). Experience shows that the spread among the ensemble members can provide case dependent information on how long a forecast is reliable. In addition, the ensemble provides alternate scenarios that are as likely as that associated with the control forecast. And most importantly, the ensemble average, due to nonlinear filtering of unpredictable components from the forecasts, can provide a better estimate of the future state of the system than a single control, extending the span of useful skill by a considerable amount (*Toth* and *Kalnay*, 1996). In this paper we draw upon the experience accumulated in the area of atmospheric ensembles to explore the possibility of creating ensemble forecasts for the ocean-atmosphere coupled system for climate predictions on the ENSO time scales.

2. *Two types of climate ensembles*

In recent years, thanks to the increasing computer power available to researchers, there has been an outburst of activity in the application of the ensemble approach in climate studies (see, e.g., *Fennessy* and *Shukla*, 1991; *Ferranti et al.*, 1994; *Barnett*, 1995; *Kumar* and *Hoerling*, 1995; *Stern* and *Miyakoda*, 1995). These studies, however, use the ensemble approach to describe the *atmosphere's response to specified boundary forcing* (e.g., the impact of observed or predicted SST on atmospheric circulation). Note that since the time range of these ensemble integrations are on the order of seasons or years, the scope of these studies is beyond the range of atmospheric predictability. All information given in the *atmospheric initial condition* is lost after two-three weeks (*Lorenz*, 1969b); the atmosphere is in a full nonlinear saturation (see Fig. 1c and *Fig. 2*). It follows that the initial atmospheric conditions play no role in these integrations (see, e.g., *Barnett*, 1995) and can be chosen randomly. In a broad sense, these studies are searching for an equilibrium solution: Given the forcing, what are the *possible states* the atmosphere can assume? We can call this kind of approach a 'boundary forcing' ensemble, for the *specification of the conditional climatology*.

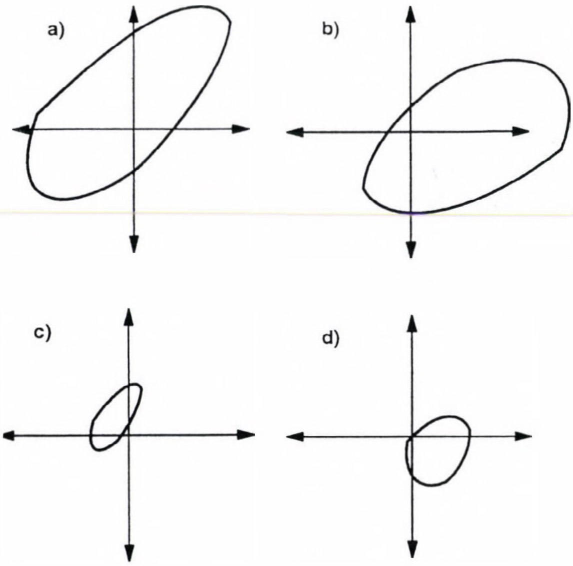

Fig. 2. As Fig. 1c except assuming different anomalous external forcing patterns. (*a*) Conditional climate of extratropical atmospheric circulation given cold phase of ENSO boundary conditions; (*b*) As in (a) except for warm phase of ENSO; (*c*) and (*d*) As in (a) and (b) except for tropical circulation. Note that the effect of different boundary conditions is much more pronounced in the tropics.

The ensemble application that we consider in this paper is different from the above case where an equiliblrium response is sought in a nonlinearly fully saturated system. Instead of assuming a known forcing for the atmosphere, we are interested in *forecasting* the ocean-atmosphere coupled system before the full nonlinear saturation of the *coupled system* occurs, within the time period in which part of the information given in the initial state is still preserved (see Fig. 1b) It is evident that randomly chosen initial conditions for the coupled system in this second, 'initial value' ensemble approach are not useful. Without a realistic description of the initial uncertainty present in our analysis of the coupled system (see Fig. 1a) this endeavor offers no hope.

3. Describing initial uncertainty

The most important aspect of the initial value ensemble approach is the determination of the initial perturbations that are applied onto the control analysis. This is equivalent to describing the uncertainty in the control analysis. *Toth* and *Kalnay* (1993) suggested that in analysis schemes in which short-range dynamical forecasts are blended with observations an important component of the analysis error lies in the direction of fast growing modes. This is because in a short range forecast initial errors projecting onto decaying modes (i.e., phase space directions in which perturbations decay) will tend to disappear with increasing lead time while those projecting onto growing modes will amplify (see also *Kalnay* and *Toth*, 1994). In areas where observations are scarce, the successive application of the forecast model in the analysis cycle will lead to the emergence of fast growing errors in the analysis. Note also that it is the fast growing errors that will play the major role in error development when extended range forecasts are considered. And since the ocean analysis relies heavily on dynamical forecasts due to the lack of adequate data coverage, it follows that a good description of possible and relevant ocean analysis errors would be the subspace of the growing modes in the phase space of the coupled ocean-atmosphere system.

4. Lyapunov characteristics

In a linear tangent framework the perturbations that are associated with the fastest sustainable growth in a dynamical system are the leading local Lyapunov vectors (LLVs). If we follow the evolution of initially equally lengthed perturbations in all phase space directions, the initial 'hypersphere' of errors will develop into a 'hyperellipsoid'. The LLVs are defined as the principal axes of this hyperellipsoid, after infinite time evolution. We note that the directions in which maximum growth occurs strongly depend on the state of the system in the phase space. The global Lyapunov exponents can be defined as the integral of the instantaneous growth rates over the whole attractor. The presence of only one positive exponent (i.e., instability at least in one direction over the long run) turns the behavior of the system chaotic. Further details can be found, for example, in *Wolf et al.* (1985). For a practical comparison of the Lyapunov characteristics with finite time instabilities (optimal or singular vectors) see, e.g., *Szunyogh et al.* (1996).

The LLVs give a good conceptual framework when considering ensemble perturbations. However, they offer no practical solution for such complex nonlinear systems as the atmosphere or the coupled ocean-atmosphere system. In these real life systems a multitude of physical processes operate at different spatial and time scales, which all have different maximum growth rates and different saturation levels (see *Fig. 3*). In this situation, the linearly calculated LLVs may turn out to be irrelevant: the highest attainable growth may be associated with a process that saturates at a perturbation level below that of the estimated level of analysis errors. In reality, the linear LLV may actually *decay* in the nonlinear system at amplitudes representative of analysis errors.

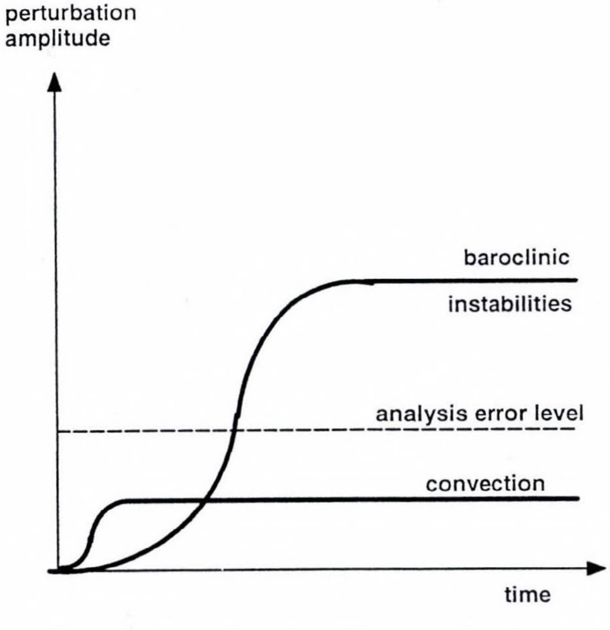

Fig. 3. Schematic illustrating the growth rates of convective and baroclinic modes. Note that convection has much faster growth but saturates at a much lower energy level. If analysis errors have an energy level *above* the saturation of convective modes, convective systems cannot attain an energy that could dominate an analysis error field. Consequently, the initial uncertainty in the analysis will be associated with baroclinic modes.

5. *Breeding of growing modes*

Toth and *Kalnay* (1993) extended the notion of LLVs into the nonlinear domain. They introduced a simple technique called 'breeding of the growing vectors' (BGV, see *Fig. 4*). The BGV method amounts to running a nonlinear perturbation model with amplitudes comparable to the level of analysis errors. An arbitrary perturbation introduced at initial time is carried over in time as a difference between a control and a pertrurbed forecast. The perturbation is periodically rescaled and reintroduced onto successive new analysis fields. After a finite period of time which is a characteristic of the system, all the decaying components of the perturbations disappear and only the fast growing perturbations remain. These perturbations are a combination of vectors that could be called in a loose sense the leading LLVs of the system for the nonlinear perturbation amplitude range considered. Note that once a breeding cycle is started with an arbitrary perturbation, it evolves on a strictly dynamical basis, without any stochastic influence. And the only free parameter of the breeding method is the perturbation amplitude.

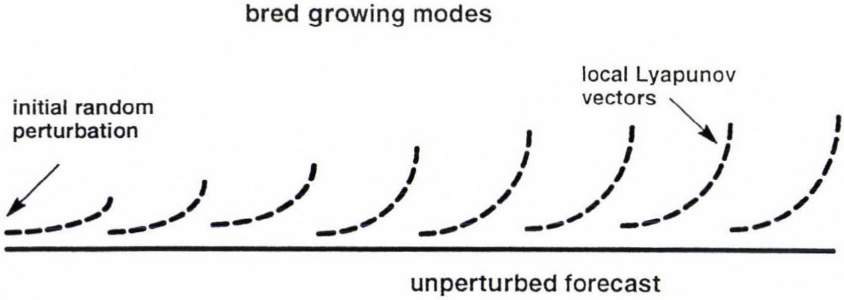

Fig. 4. Schematic of the breeding of growing vectors method. Note that after a random perturbation is initially introduced upon an analysis, the breeding process (rescaling and reintroducing the difference between two model runs) is purely dynamical, avoiding any further stochastic element. As a result, the perturbation field becomes dominated by the modes that grow fastest upon the trajectory of analysis fields, given the range of perturbation amplitudes chosen.

6. *Application to the ocean-atmosphere coupled system*

As we discussed earlier, in coupled ocean-atmosphere forecasts on the time scale of the ENSO, the atmosphere has already lost all information present in its initial condition. It is in full nonlinear saturation (and its behavior differs from climatology only due to anomalous oceanic conditions). Information regarding the state of the coupled system is primarily in the ocean, which has not reached nonlinear saturation in its phase space. When applying the BGV method onto the coupled ocean-atmosphere system one then has to focus his/her attention on the ocean. It is this part of the coupled system that has to reproduce perturbations at amplitudes that are characteristic of the errors in the analysis.

It follows that the breeding cycle of an ocean-atmosphere model could be started with a random perturbation upon the ocean part of the coupled system. The initial perturbation should have a magnitude equivalent to the estimated ocean analysis error. After integrating the coupled model from both the control and perturbed initial conditions, the difference between the two runs has to be rescaled to its original magnitude based on perturbation growth *in the ocean*. The rescaled perturbation then has to be reintroduced onto the successive analysis. The renormalization frequency could be on the order of a month.

In this setup, the atmosphere in the perturbed run would develop a nonlinearly fully saturated perturbation with respect to the control run. The relatively small rescaling based on oceanic growth (~ 2/month) would have virtually no impact on the atmospheric perturbation (that would have a growth rate of 1.5/day with smaller perturbation magnitudes corresponding to atmospheric analysis errors). The perturbation for the atmospheric part of the coupled system could be evaluated by computing differences between the control and perturbed integrations for monthly or longer time averages.

The very different roles the ocean and atmosphere plays in the above described coupled breeding cycle could be compared to the role of large scale dynamics vs. convection in a breeding cycle applied on the (uncoupled) atmosphere (see Fig. 3). In this system with perturbation amplitudes characteristic of atmospheric analysis errors, the largest growth is associated with baroclinic instabilities. We know, however, that much faster growth is occuring at smaller amplitudes, associated with convection. The behavior of convection in the perturbations, however, could be evaluated only in a time mean fashion, on the time scales of baroclinic processes.

7. Conclusions

In a wide range of climate prediction and simulation studies an ensmeble of atmospheric integrations have been used to describe possible atmospheric response to observed (or predicted) sea surface temperature (SST) conditions. Especially in the extratropics, one integration would give little information since on the ENSO time scales the atmosphere is in its nonlinearly fully saturated state. What is searched by these studies is the conditional climatology of the atmosphere, given the observed (or predicted) SST (boundary forcing ensemble).

In contrast to the above described, *'specification'* type of approach, we propose to use an ensemble to *predict* the state of the coupled ocean-atmosphere system. Since the 'memory' of this system lies in the ocean, we focus our attention on that part of the system. In particular, we propose that a breeding cycle, where regularly rescaled perturbations are carried over between two nonlinear forecasts, initiating around successive oceanic analyses, be used to generate initial ensemble perturbations for the coupled system. These perturbations are related to the local Lyapunov vectors of the coupled system and represent directions in which the nonlinear system exhibits maximum sustainable growth. Since the atmosphere is in a nonlinearly saturated state on the long ENSO forecast time scales, the atmospheric perturbations can be used in a time average sense to evaluate the preferred atmospheric pattern and/or variability associated with the state of the coupled system.

Based on available computer resources a number of perturbed forecasts, each started with a perturbation from independently run breeding cycles, could be run in addition to the control ENSO forecast. *Toth* and *Kalnay* (1996) found that it is advantageous to have the perturbations paired (i.e., the same initial perturbations are both added and subtracted from the control analysis). In case the ensemble forecasts are regularly run, say once a month, the bred modes can be created based on the differences between those forecasts at one month lead time, without additional model runs (see *Fig. 5*).

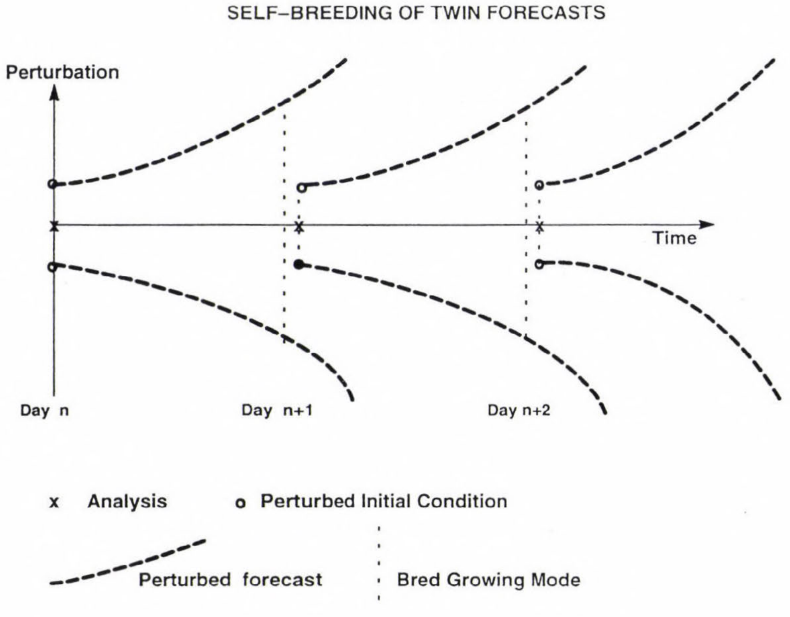

Fig. 5. Schematic of a self contained breeding pair of ensemble forecasts. Note that breeding is part of the extended ensemble forecasts and that the creation of efficient initial ensemble perturbations requires no additional computing resources beyond that needed to run the forecasts themselves (from *Toth* and *Kalnay*, 1996).

The average of the ensemble of forecasts should provide a prediction that is, in a statistical sense, superior to any individual forecast, including the control. In addition, the ensemble can provide valuable information on the reliability of the forecasts: high spread among the members in the time and spatial domain may indicate lower skill. In an operational environment, additional perturbed forecasts could be generated for such strongly unstable situations to increase the skill. And the individual runs, or groups of them may provide possible forecast scenarios that are alternatives to the single control forecast.

We expect that a breeding cycle applied on the ocean-atmosphere coupled system would not only provide efficient perturbations for initial value climate ensemble forecasting but would also give a new tool in the analysis of ENSO itself. Different realizations or 'flavors' of ENSO could be associated with different oceanic LLVs, pointing to leading instabilities that differ from one realization of ENSO to another. At the Environmental Modeling Center of the National Centers for Environmental Prediction (formerly NMC) we plan to test these ideas in the near future, using the coupled ocean-atmosphere model (*Ji et al.*, 1994) developed in the Climate Modeling Branch.

References

Barnett, T.P., 1995: Monte Carlo climate forecasting. *J. Climate 8*, 1005-1022.

Fennessy, M.J. and *Shukla, J.*, 1991: Comparison of the impact of the 1982/83 and 1986/87 Pacific SST anomalies on time-mean predictions of atmospheric circulation. *J. Climate 4*, 407-423.

Ferranti, L., Molteni, F. and *Palmer, T.N.*, 1994: Impact of localized tropical and extratropical SST anomalies in ensembles of seasonal GCM integrations. *Q. J. R. Meteorol. Soc. 120*, 1613-1646.

Ji, M., Kumar, A. and *Leetmaa, A.*, 1994: An experimental coupled forecast system at the National Meteorological Center. Some early results. *Tellus*, *46A*, 398-418.

Kalnay, E. and *Toth, Z.*, 1994: Removing growing errors in the analysis. *Proceedings of the Tenth Conference on Numerical Weather Prediction*. July 18-22, 1994, Portland, OR. AMS, 212-215.

Kumar, A. and *Hoerling, M.P.*, 1995: Prospects and limitations of seasonal atmospheric GCM predictions. *Bull. Amer. Meteorol. Soc. 76*, 335-345.

Leith, C.E., 1974: Theoretical skill of Monte Carlo forecasts. *Mon. Wea. Rev. 102*, 409-418.

Lorenz, E.N., 1963: Deterministic non-periodic flow. *J. Atmos. Sci. 20*, 130-141.

Lorenz, E.N., 1965: A study of the predictability of a 28-variable atmospheric model. *Tellus 17*, 321-333.

Lorenz, E.N., 1969a: The predictability of a flow which possesses many scales of motion. *Tellus 21*, 289-307.

Lorenz, E.N., 1969b: Three approaches to atmospheric predictability. *Bull. Amer. Meteorol. Soc. 50*, 345-349.

Molteni, F., Buizza, R., Palmer, T.N. and *Petroliagis, T.*, 1996: The ECMWF ensemble system: Methodology and validation. *Q. J. R. Meteorol. Soc.* 122, 73-119.

Stern, W. and *Miyakoda, K.*, 1995: The feasibility of seasonal forecasts inferred from multiple GCM simulations. *J. Climate 8*, 1071-1085.

Szunyogh, I., Kalnay, E. and *Toth, Z.*, 1996: A comparison of Lyapunov vectors and optimal vectors in a low resolution GCM. *Tellus*, under review.

Toth, Z. and *Kalnay, E.*, 1993: Ensemble Forecasting at the NMC: The generation of perturbations. *Bull. Amer. Meteorol. Soc. 74*, 2317-2330.335-345.

Toth, Z. and *Kalnay, E.*, 1996: Ensemble forecasting at NCEP and the breeding method. *Mon. Wea. Rev.*, under review.

Tracton, M.S. and *Kalnay, E.* 1993: Ensemble forecasting at NMC: Operational implementation. *Wea. Forecasting 8*, 379-398.

Wolf, A., *Swift, J.B.*, *Swinney, H.L.* and *Vastano, J.A.*, 1985: Determining Lyapunov exponents from a time series. *Physica 16D*, 285-317.

IDŐJÁRÁS

Quarterly Journal of the Hungarian Meteorological Service
Vol. 100, No. 1-3, January-September 1996

Diagnosis of vertical heat fluxes in near coastal water

M. Stoyanova and **E. Donev**

Department of Meteorology and Geophysics, Faculty of Physics,
University of Sofia,
5, J. Bourchier Blvd, BG—1126 Sofia, Bulgaria

(Manuscript received 22 May 1995; in final form 27 December 1995)

Abstract—Diagnosis of vertical heat and radiation fluxes in shallow water and in the underlying sand is made with a 1-D model. A feature of the model is that it accounts for the influence of the bottom as solar radiation reaches it and warms it directly. The model uses near coastal measurements of water and air temperatures, humidity, total solar radiation and wind. The governing processes are the air-water and water-sand interaction. The model can be used as a boundary condition to atmospheric boundary layer models.

Key-words: sea, surface layer, vertical heat flux, coastal zone, shallow water.

1. Introduction

Surface layer modelling and air-water interaction in coastal areas and in shallow water basins have persistently been drawing attention in recent years. Uncertainties still exist in understanding the thermal structure with even one-dimensional approaches, yet they need to be resolved before two-dimensional or fully three-dimensional modelling efforts can be confidently used.

The 1-D models for surface layer in water can be classified into three main groups: integral models (e.g. *Kraus* and *Turner*, 1967), diffusion models (e.g. *Mellor* and *Yamada*, 1974) and transilient models (e.g. *Stull* and *Kraus*, 1987). As *McPhee* (1987), *Martin* (1985) and *Garwood* (1979) show, the more complicated the model is, the more details it gives about the surface homogeneous layer (SHL), but the before-hand tuning of a model with field data from the modelled site appears to be of greatest importance for receiving good model results.

The above mentioned models use the heat fluxes at the air-water interface as a boundary condition and concentrate on predicting SHL deepening or stratification. A further investigation of heat fluxes formation and distribution in water could lead to better understanding of air-water interaction, to better micro- and mesoscale modelling of atmospheric processes. A useful approach in this direction could be the development of a diagnostic model for the analysis of sophisticated interaction processes.

This model uses data from an experiment that was held in September 1990, near Shkorpilovtsy on the Black Sea coast. There the beach is straight, the depth gradually increases off the beach line, the bottom is sandy, and the sand is terrigenous. A pier built there goes 200 m into the sea, there is an 18 m high mast at its edge and the water depth is 4.5 m. Our instruments were distributed along that mast.

Measurements were taken every 100 s. Temperature at three levels in water at 0.3, 1.3 and 2.5 m depth, temperature and humidity at 3.0 and 6.0 m height in the air, wind at the top of the mast (18 m) and total solar radiation at the water surface were recorded.

The data series from September 24, 1990 is used in this study. The weather was calm and sunny with well developed breeze circulation. There was no swell during that day.

The governing equations of the model are presented in Section 2; the results are analyzed in Section 3, and the conclusions are summarized in Section 4.

2. *Model description*

A three-layer model was developed: air-water-sand (*Fig. 1*), as the water depth at the point of the experiment is only 4.5 m, and the bottom influences heat and radiation fluxes in water.

2.1 Heat balance equations

The heat budget within the water column is governed by the heat balance equations at the air-water and water-sand interfaces:

$$\begin{aligned} L_{w0}\downarrow - L_{w0}\uparrow &= H + LE + G_1, \\ S_{ws} + L_w\downarrow - L_w\uparrow &= G_b + G_s, \end{aligned} \tag{1}$$

where the longwave radiation at the air-water interface is

$$L_{w0}\downarrow = \sigma\, T_{ref}^4, \tag{2}$$

σ is the Stephan-Boltzmann constant, and T_{ref} is a reference temperature for the atmospheric longwave radiation. Efforts have been made towards determining the reference temperature as a function of distribution of temperature and humidity with height, but good results are obtained only for climatic calculations. In our model T_{ref} is determined after *Bortkovskii et al.* (1974).

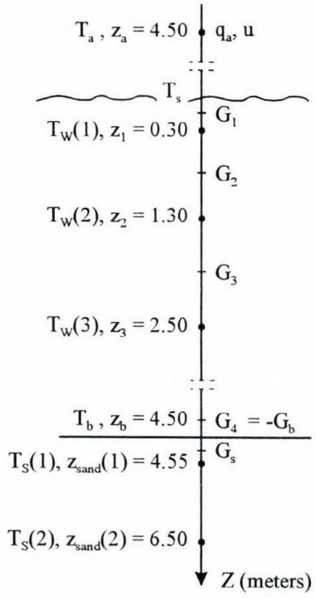

Fig. 1. Vertical grid.

The longwave radiation of water is:

$$L_{w0}\uparrow = \epsilon_w \sigma T_s^4, \tag{3}$$

where ϵ_w is the longwave emissivity of sea water. It depends on sea surface state and ranges between 0.90 and 1.00.

The longwave radiation at the sand-water interface is given by

$$\begin{aligned} L_w\downarrow &= \epsilon_w \epsilon_s \sigma T_{w,ref}^4, \\ L_w\uparrow &= \epsilon_s \sigma T_b^4, \end{aligned} \tag{4}$$

where $T_{w,ref}$ is a reference water temperature for longwave radiation, T_b is the bottom temperature, and ϵ_s is the emissivity of sand.

The longwave radiation component is substantial for the air-water surface and reaches only up to 10% of the heat balance at the bottom.

The shortwave radiation is included only in the heat balance equation for the sand-water interface, as the part of it that reaches the bottom $Q_R(z_b)$ is absorbed in the uppermost millimetre in the sand:

$$S_{ws} = (1 - a_s)\, Q_R\,(z_b)\,, \tag{5}$$

where a_s is the wet sand albedo. On the contrary, the solar radiation in the band 300–2500 nm penetrates into the water, acting as a dispersed energy source for the water layer and thus influences its dynamics. The radiation profile in the first meter depends mainly on pure water absorption properties. For greater depths and shorter wavelengths, absorption and scattering by suspended matter appears to be the main reason for attenuation of the radiation flux.

The shortwave radiation S_w (total solar radiation) is measured and we assume constant albedo $a_w = 0.07$. Then

$$Q_R(0) = (1 - a_w)\, S_w\,. \tag{6}$$

Radiation with wavelength $\lambda \geq 800$ nm is almost fully absorbed down to 1 m depth (*Jerlov,* 1976). A one-exponential decay term is incapable of describing the radiation attenuation in the uppermost meter of water. A two-exponential decay term model is usually used (*Krauss*, 1972, *Paulson* and *Simpson*, 1977) which allows the near-surface irradiance to be attenuated very rapidly:

$$Q_R(z) = S_w(1 - a_w)[\alpha e^{-\beta_1 z} + (1 - \alpha)\, e^{-\beta_2 z}]\,, \tag{7}$$

where α, β_1 and β_2 are parameters. The latter expression employs one-exponential decay term for an upper layer where absorption of longwave radiation is important and a second term for greater depths where the radiation which is attenuated is in the blue-green region.

We tested the three parameter model for light propagation in water column — that of *Zeneveld* and *Spinrad* (1980):

$$Q_R(z) = S_w(1 - a_w) e^{-K_1 z}\,(1 - K_2\,\mathrm{arctg}\,K_3 z)\,. \tag{8}$$

According to the authors the two-exponential model does not allow for rapid radiation attenuation in the first meter. But through varying the three parameters in Eq. (7) we managed to achieve proper description of solar radiation attenuation in all water types in Jerlov's classification and to fit the three data sets from *Zeneveld* and *Spinrad* (1980).

The values of the coefficients α, β_1 and β_2 in Eq. (7) that we use were determined by *Dera et al.* (1983) particularly for our experimental site during the experiment 'Kamchia'79':

$$\alpha = 0.45, \quad \beta_1 = 0.15 \text{ m}^{-1}, \quad \beta_2 = 30.0 \text{ m}^{-1}. \tag{9}$$

A part of the solar radiation that reaches the bottom is reflected back, and we can finally write for each level:

$$\begin{aligned} Q_R(z) = Q_{R1}(z) + Q_{R2}(z) = S_w(1 - a_w)[\alpha e^{-\beta_1 z} + (1 - \alpha) e^{-\beta_2 z}] + \\ Q_R(z_b) a_s [\alpha e^{-\beta_1 (2z_b - z)} + (1 - \alpha) e^{-\beta_2 (2z_b - z)}], \end{aligned} \tag{10}$$

where the solar radiation that reaches the bottom is:

$$Q_R(z_b) = S_w(1 - a_w)[\alpha e^{-\beta_1 z_b} + (1 - \alpha) e^{-\beta_2 z_b}]. \tag{11}$$

Sensible and latent heat fluxes are parameterized by bulk-formulae:

$$\begin{aligned} H &= \rho c_p C_H (T_s - \theta_a) u, \\ LE &= \rho L C_E (q_s - q_a) u, \end{aligned} \tag{12}$$

where C_H and C_E are the bulk transfer coefficients for sensible and latent heat, respectively, q_s and q_a are the specific humidity at the water surface and at a specified level in the air, θ_a is the potential temperature on the same level, T_s is the sea surface temperature (SST).

Determination of the bulk transfer coefficients is not trivial as they depend on wind speed directly and indirectly through the roughness length z_0 , which on the other hand depends not only on wind speed but on fetch and duration of wind too.

Roughness length and bulk transfer coefficients depend on air stratification and many schemes for their determination have been proposed (*Smith*, 1980; *Wu*, 1980; *Large* and *Ponds*, 1981; *Garrat* and *Hyson*, 1975; *Amorocho* and *DeVries*, 1990). Though all of them are based on the similarity theory, the results reported by their authors as those reported by authors who compared them, are quite controversial. Testing ten different schemes with more than 2600 data series from ship observations at the ocean station C, *Blanc* (1985) found discrepancies between parameters in the different parameterization schemes as follows: for z_0 – 250 times, for sensible heat H – 100%, and for latent heat LE – 120%.

We use the scheme from OSU 1-D PBL Model by *Ek* and *Mahrt* (1991) with contributions by *A. A. M. Holtslag, H. L. Pan, P. Ruscher, J. Kim, N. N. K. Gamage, W. Gibson* and others; based on the simple 1-D PBL Model by *Troen* and *Mahrt* (1986), which for stable stratification follows *Mahrt* (1987), and for unstable — *Louis* (1979) (with modifications by *Holtslag* and *Beljaars,* 1989):

$$C_H = C_E = \frac{\kappa^2}{R}\,\frac{F(z, z_0, z_{0H}, Ri_B)}{\ln(z/z_0)\ln(z/z_{0H})}\,, \tag{13}$$

where κ is the von Kármán constant (0.4), R is the ratio of bulk transfer coefficients of momentum and heat at neutral stratification and is taken from *Businger et al.* (1971) with modification by *Holtslag* and *Beljaars* (1989). Ri_B is the bulk Richardson number for the layer from the water surface to z — the layer at which temperature, humidity and wind are taken:

$$Ri_B = \frac{gz(\theta_{av} - \theta_{sv})}{\theta_{av}u^2}\,, \tag{14}$$

where u is wind speed at height z, and θ_{av} and θ_{sv} are virtual potential temperatures at z and on water surface (z_{0H}), respectively. The function F is given by

$$F = \begin{cases} \exp(-Ri_B) & \text{, stable} \\ 1 - \dfrac{15\,Ri_B}{1 + 7.5\,\dfrac{10\,\kappa^2}{\ln(z/z_0)\ln(z/z_{0H})}\left[-Ri_B(z/z_0)\right]} & \text{, unstable} \end{cases} \tag{15}$$

The roughness length is determined after Charnock's law with $a = 0.0375$, and the wind measured at 18 m height is reduced to wind at 4.5 m using the logarithmic law.

The sensible and latent heat fluxes H, LE and the diffusive heat flux just below the water surface G_1 are positive when they are diverging from the surface, i.e. when they take heat off the surface. Similarly, the turbulent heat flux G_b from water and the diffusive G_s from sand at the sand-water interface are positive when they are diverging from the surface (*Fig. 2*).

2.2 Sea surface temperature

A stable cold skin layer is formed at wind speed not exceeding 10 m s^{-1} during a sunny day. The reasons for that are: first, that millimetre layer emits the longwave radiation towards the atmosphere, evaporation and contact heat exchange take energy exactly from it; second, the solar radiation (the heat source) is absorbed in a thicker water layer thus raising the temperature below the surface layer; and third, the heat exchange into the latter is molecular.

We have data for the temperature at 30 cm depth $T_w(1)$ and we use two parameterizations of the difference $\Delta T = T_s - T_w(1)$ to determine the sea surface temperature T_s. We take into account the influence of the different heat fluxes at the air-water interface on skin layer formation. The scheme of *Schluessel et. al.* (1990) for a night skin layer (Sch-n) and the one from *Bortkovskii et al.* (1974) (B-B) are:

$$\begin{aligned} \Delta T &= b_0 + b_1 u\,(T_s - T_a) + b_2 u\,(q_s - q_a) + b_3 L, && \text{(Sch–n)},\\ \Delta T &= C_h\,(H + LE - L_{w0}), && \text{(B–B)}, \end{aligned} \qquad (16)$$

where $b_0 = -0.285$ K, $b_1 = 0.0115$ s m^{-1}, $b_2 = 37.255$ K, $b_3 = -0.00212$ km^2 W^{-1}, $C_h = 0.01286$ W K m^{-1}.

Having determined ΔT and then T_s, it is easy to find $L_{w0}\uparrow$, H and LE from Eqs. (3) to (12) and to find G_1 from Eq. (1). The flux G_1 is needed as a boundary condition for finding heat fluxes in water.

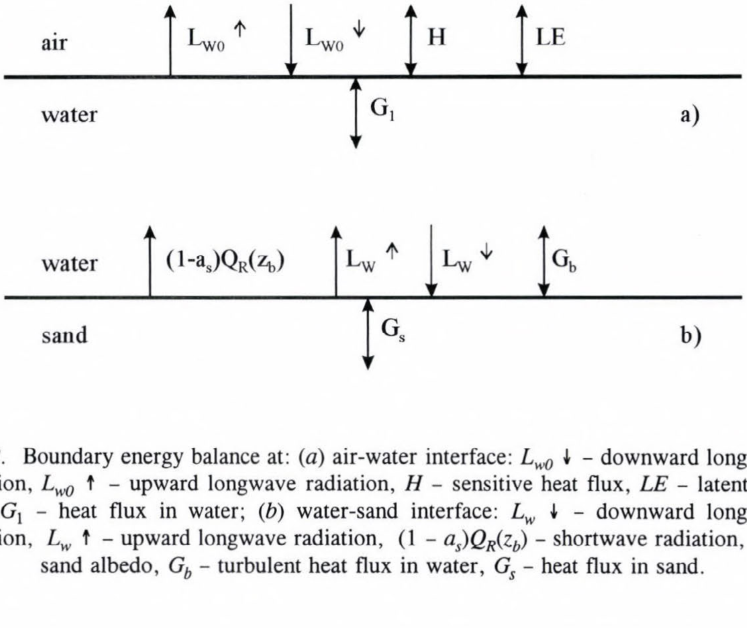

Fig. 2. Boundary energy balance at: (*a*) air-water interface: $L_{w0}\downarrow$ – downward longwave radiation, $L_{w0}\uparrow$ – upward longwave radiation, H – sensitive heat flux, LE – latent heat flux, G_1 – heat flux in water; (*b*) water-sand interface: $L_w\downarrow$ – downward longwave radiation, $L_w\uparrow$ – upward longwave radiation, $(1 - a_s)Q_R(z_b)$ – shortwave radiation, a_s – sand albedo, G_b – turbulent heat flux in water, G_s – heat flux in sand.

2.3 *Heat distribution into the water and into the sand*

Solar radiation and turbulent vertical heat flux — these are the only factors changing water temperature at a certain point under idealized conditions we use:

$$\rho_w C_{pw} \frac{\partial T}{\partial t} = - \frac{\partial G}{\partial z} - \frac{\partial Q_R}{\partial z}, \tag{17}$$

where C_{pw} is the specific water heat capacity at constant pressure, T is its temperature, G is the vertical turbulent heat flux, and Q_R is the radiation flux at that level.

Sand heat regime is modelled by a prognostic equation:

$$\rho_s C_{ps} \frac{\partial T}{\partial t} = \frac{\partial}{\partial z} K_s \frac{\partial T}{\partial z}, \tag{18}$$

where K_s is the thermal diffusivity for the sandy bottom. The specific heat C_{ps} and the density ρ_s refer to saturated terrigenous sand.

We used direct numerical integration for Eq. (17), as $\partial T/\partial t$ and $\partial Q_R/\partial z$ were known from the spline approximation of the data and the solar radiation attenuation parameterization, respectively. To determine the heat flux into the sand (Eq. 18) we used the Crank-Nickolson time integration scheme.

2.4 *Vertical grid*

The vertical grid is shown in Fig. 1. Vertical stepping is irregular, temperatures are referred to the z-levels and heat fluxes G_i relate to the layers between them. The heat flux G_b is assumed equal to $-G_4$.

The two vertical steps in sand are quite different. The first is a small one and we can approximately accept that $G_s = G_{sand}$ (1) in Eq. (1). As there is no available data in the sand, we can only make an assumption that there is a level in the sand z_{sand} (2) from which downward temperature remains unchanged during one day ($T(z_{sand}$ (2)) = const). We have chosen that level to be two meters beneath the bottom, as we are sure that day and night temperature variations do not reach that level.

The bottom boundary condition is the already mentioned unchanging temperature $T_s(2)$ during 24 hour period. Its value was chosen to be higher than the measured ones, because it had been formed during summer, the measurements were at the end of September and the temperature of the sand had to be still higher than that of the water.

3. *Results and discussion*

There were no large scale events such as swell or passage of a front on Sept 24, 1990. The measured solar radiation shows that the day was sunny and cloudless. The wind direction during the day changed at about 1^{30} (late turn of the breeze for the previous day), 10^{30} and 22 hours; its speed was higher during the daytime (up to 12 m s^{-1}) while there was intensive solar radiation and hence unstable air stratification. During night-time the wind speed reached about 6 m s^{-1}.

The water temperature at the lowest level remained higher and its variances were greater than those of the two upper ones during the whole period of the experiment. This shows that the bottom and the deeper water mass were warmer than the water at higher levels, except for the hours of intensive sunshine, and they had accumulated heat during the summer. The most intensive heating of water was between 10 and 13 hours when wind speed rose rapidly and solar radiation increased. The three water temperatures became almost equal at about 14 hours due to intensive turbulent mixing. Water stratification was unstable all the time but during daytime it became almost neutral. This corresponds to solar radiation absorption mainly in the first meter of the water column.

Smoothing of data series was necessary before applying the model. The degree of smoothing of the spline approximation method we used was regulated by a number for each data point, which corresponded to the standard deviation of that peculiar measurement, and by one common (for the whole series) parameter, which controlled the closeness of the smoothed line to the data points. The main reason for which we chose this method was that it gave us the temperature derivatives with time, which were a term in Eq. (17). We chose such a degree of smoothing that events with duration less than about an hour be eliminated (*Fig. 3*).

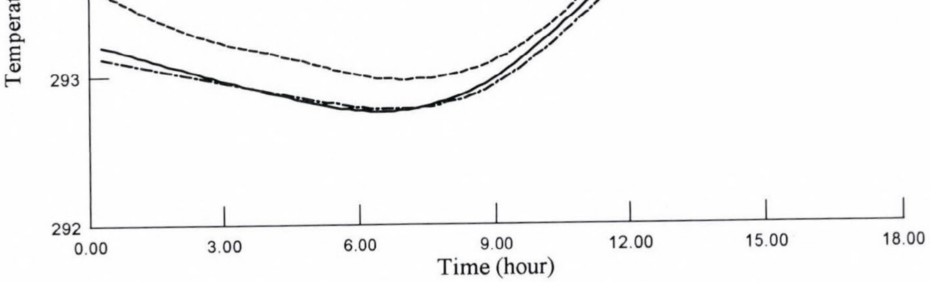

Fig. 3. Smoothed water temperatures on September 24, 1990: T_i — same as in Fig. 1.

The sea surface temperature was determined as a boundary condition following the two mentioned schemes—Sch-n and B-B. They gave similar diurnal results: the temperature difference during the night was greater than during the day, and only when wind speed changed sharply the results diverged (about 1^{30}, 10^{30} and 22 h). When wind speed decreases, sensible and latent heat fluxes decrease too what reduces cooling as well. *Fig. 4* shows the results obtained by using the Sch-n scheme.

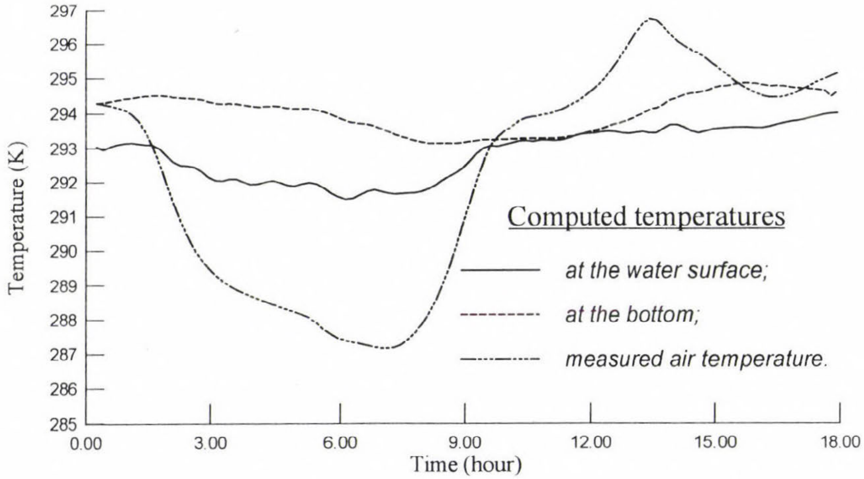

Fig. 4. Parameterized sea surface temperature following the Sch-n scheme (*Schluessel et al.*, 1990), calculated bottom temperature and measured air temperature on September 24, 1990.

Our measurements were taken at about 200 m off the shore. During the sunny early autumn day, when solar radiation is still high, and the nights are longer than in summer, the difference between land and water surfaces is well marked. The well developed sea breeze circulation is a consequence of this difference. Another consequence is the night air-water temperature difference (Fig. 3), which is responsible for the relatively high sensible heat flux in the morning. The sensible heat flux H changes its sign (*Fig. 5*): it is directed from water to air during the night and oppositely during the day. It reaches its maximum night value before sunrise at 6 hours. This value is determined mainly by the air-water temperature difference, as dry and cold air from the land comes over the warmer water. The maximum of H during daytime is reached at 13^{50} hours. This maximum is determined mainly by the wind speed which at that time is about 12 m s^{-1}. These values are relatively high for sensible heat flux in open ocean, where air-water temperature differences are small. When air with different characteristics is situated over warm water, the sensible heat flux rises significantly. *Shay* and *Gregg* (1986) report of measured sensible heat flux reaching a two-hour average value of 350 W m^{-2} during a cold air outbreak near the Bahamas after the passage of a front, when cold air was situated over the experimental site and the winds were still strong. Close to the sea-shore meteorological situation in our experiment is the experiment, reported by *Bill et al.* (1980). Eddy-correlation measurements were taken over Ontario Lake, Florida. The water is shallow and air-water temperature difference, wind speed, sensible and latent heat fluxes are consistent with the values obtained with the parameterization we used. Unfortunately, there is no data reported in that paper for the day period of significant water heating, when though the air-water temperature difference suggests stable stratification, the sea-breeze circulation leads to a considerable wind driven convection and hence strong heat exchange between air and water.

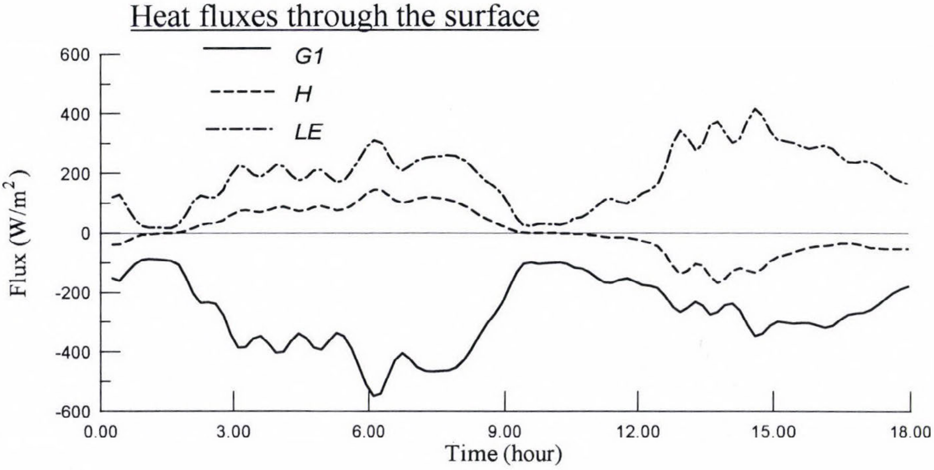

Fig. 5. Sensible *H* and latent *LE* heat fluxes and diffusive heat flux G_1at the air-water interface.

The sign of G_1 is determined by the latent heat flux *LE* , which is at certain moments by an order of magnitude higher than *H* and is directed all the time from the water surface upward. The resulting heat flux through the air-water interface is given by the sum of G_1 and the shortwave radiation flux $Q_R(0)$. This sum changes its sign and from about an hour after sunrise to an hour before sunset it is directed to water. That is the period when water gathers energy and that period coincides with the reported data by *Lombardo* and *Gregg* (1989) and *Schluessel et al.* (1990), which means that the used parameterization of *H* and *LE* (z_0, z_{0H} and C_H, respectively) gives proper results.

As the solar radiation is not absorbed at the surface, it warms the underlying water layer. Consequently, the heat flux G changes sign with depth. The surface flux G_1 (Fig. 5) remains negative during day and night, while the rest three turbulent heat fluxes G_2, G_3 and G_4 change sign with succession of day and night (*Fig. 6*). From about 2 hours until about 8 hours all fluxes are negative, which means that they are directed upward from the bottom to the water surface.

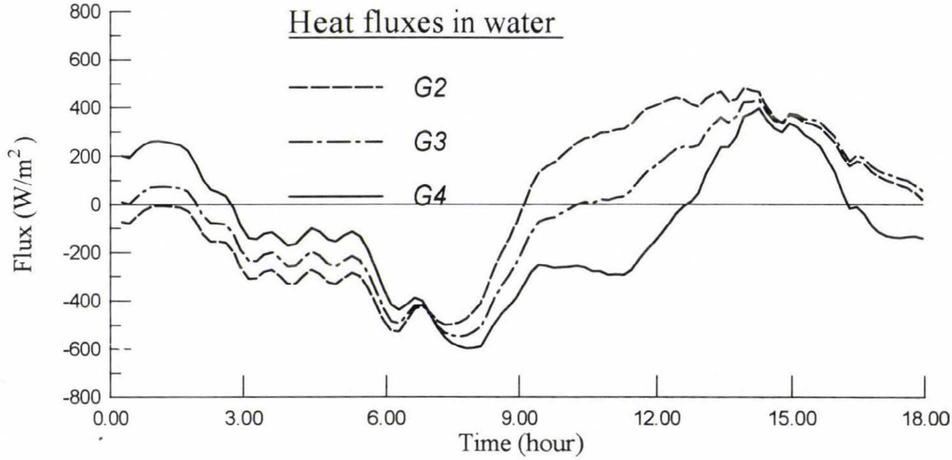

Fig. 6. Heat fluxes in water on September 24, 1990: G_i — same as in Fig. 1.

All the temperatures — the surface temperature, the three measured ones and the predicted bottom temperature – decrease during that period, T_3 remaining higher than T_1 and T_2 (Fig. 3). As the Sun rises and the solar radiation increases, the three turbulent heat fluxes gradually change sign one by one. Beneath the water surface solar radiation acts as a distributed heat source, and G_2 substantially exceeds G_1 because of the strong absorption of radiation in the uppermost water meter. The depth at which the heat flux changes sign is about 0.5 m which corresponds well to that reported by *Protassov* and *Protassova* (1976). Water temperatures increase after sunrise. The bottom temperature T_b follows the water temperature with a retardation. The bottom turbulent heat flux becomes positive (downward) at about noon time and at about 14 hours the turbulent heat flux becomes uniform through the water column. As sufficient solar radiation reaches the bottom, sand temperature rises and reaches its maximum value at about 15 hours (Fig. 4). About an hour before sunset all heat fluxes become negative (upward), which again coincides with the reported data.

4. Summary and conclusions

The presented three-layer model (air-water-bottom) includes, for the first time, the influence of a shallow-lying bottom on the heat distribution through the water column and hence on the air-water heat exchange. The three layers interact strongly and the bottom cannot be regarded only as a mechanical factor, as it is usually treated. It turns to be a heat accumulator, thus becoming an additional (to water) softening factor for the temperature variations and its thermal regime should be modelled when shallow basins are focused and in the coastal areas.

Our model gives a consistent description of diurnal changes of heat fluxes in water and of air-water-sand radiation and thermal energy exchange, though non-linear effects are not included. This model can be used as a surface boundary condition for planetary boundary layer models.

One possible step toward explanation of short-period events could be the adding of non-linear terms to the system of equations.

Acknowledgements—The authors gratefully acknowledge *Prof. S. Panchev* for his valuable comments on the drafts of this paper.

References

Amorocho, J. and *DeVries,J. J.*, 1990: A new evaluation of the wind stress coefficient over water surface. *J. Geophys. Res. 85*, 433–442.

Bill, Jr., R. G., Cook, A. F., Allen, Jr., L. H. and *Bartholic, J.F.*, 1980: Predicting fluxes of latent and sensible heat of lakes from surface water temperatures. *J. Geophys. Res. 85*, 507–512.

Blanc, T. V., 1985: Variation of bulk-derived surface flux, stability, and roughness results due to the use of different transfer coefficient schemes. *J. Phys. Oceanogr. 15*, 650–669.

Bortkovskii, R. S., Butner, E. K., Malevskii-Malevich, S. P. and *Preobrajenskii, L. Y.*, 1974: *Transfer Processes in the Ocean-Atmosphere Interface* (in Russian). Leningrad, Gidrometeoizdat.

Businger, J. A., Wyngaard, J. C., Izumi, Y. and *Bradley, E. F.*, 1971: Flux-profile relationships in the atmospheric surface layer. *J. Atmos. Sci. 28*, 181–189.

Dera, E., Sudbin, A. I. and *Chishek, V.*, 1983: Solar radiation absorption in surface water layers. *Interaction of Atmosphere, Hydrosphere and Lithosphere in Coastal Sea Area* (in Russian), Sofia, BAS, 101–110.

Ek, M. and *Mahrt, L.*, 1991: *A One-Dimensional Planetary Boundary Layer Model with Interactive Soil Layers and Plant Canopy—User's Guide.* Oregon State University.

Garrat, J.R. and *Hyson, P.*, 1975: Vertical fluxes of momentum, sensible heat and water vapour during the Air Mass Transformation Experiment (AMTEX) 1974. *J. Meteorol. Soc. Japan 53,* 149-160.

Garwood, R. W., Jr., 1979: Air-sea interaction and dynamics of the surface mixed layer. *Rev. Geophys. and Space Phys. 17*, 1509–1524.

Holtslag, A.A.M. and *Beljaars, A.C.M.*, 1989: Surface flux parameterization schemes: developments and experiences at KNMI. *Proc. of* the 1988 ECMWF Workshop on Parameterization of Fluxes over Land Surface. European Center for Medium-Range Weather Forecasts, Reading, England, 121-147.

Jerlov, N. G., 1976: *Marine Optics.* Elsevier, New York.

Krauss, E. B. and *Turner, J. S.*, 1967: A one dimentional model of the seasonal thermocline. *Tellus 19,* 98–105.

Krauss, E. B., 1972: *Atmosphere Ocean Interaction*. Oxford University Press, New York.

Large, W. G. and *Pond, S.*, 1981: Open ocean momentum flux measurements in moderate to strong winds. *J. Phys. Oceanogr. 11*, 324–336.

Lombardo, C. P. and *Gregg, M. C.*, 1989: Similarity scaling of viscous and thermal dissipation in a convecting surface boundary layer. *J. Geophys. Res. 94*, 6273–6284.

Louis, J.-F., 1979: A parametric model of vertical eddy fluxes in the atmosphere. *Boundary Layer Meteorol. 17*, 187–202.

Mahrt, L., 1987: Grid-averaged surface fluxes. *Mon. Wea. Rev. 115*, 1550–1560.

Martin, P. J., 1985: Simulation of the mixed layer at OWS November and Papa with several models. *J. Geophys. Res. 90*, 903–916.

McPhee, M. G., 1987: A time-dependent model for turbulent transfer in a stratified oceanic boundary layer. *J. Geophys. Res. 92*, 6977–6986.

Mellor, G. L. and *Yamada, T.*, 1974: A hierarchy of turbulence closure models for planetary boundary layers. *J. Atmos. Sci. 31*, 1791–1806.

Paulson, C. A. and *Simpson, J. J.*, 1977: Irradiance measurements in the upper ocean. *J. Phys. Oceanogr. 7*, 953–956.

Protasov, S. N. and *Protasova, G. G.*, 1976: About the day-and-night temperature variances in the air and water surface layers (in Russian). *Meteorologia i Gidrologia 9*, 53–59.

Schluessel, P., Emery, W. J., Grassel, H. and *Mammen, Th.*, 1990: On the bulk-skin temperature difference and its impact on satellite remote sensing on sea surface temperature. *J. Geophys. Res. 95,* 13341–13356.

Shay, T. J. and *Gregg, M. C.*, 1986: Convectively driven turbulent mixing in the upper ocean. *J. Phys. Oceanogr. 16*, 1777–1798.

Smith, S. D., 1980: Wind stress and heat flux over the ocean in gale force winds. *J. Phys. Oceanogr. 10,* 709–726.

Stull, R. B. and *Krauss, E. B.*, 1987: The transilient model of the upper ocean. *J. Geophys. Res. 92*, 10745–10755.

Troen, I. and *Mahrt, L.*, 1986: A simple model for the atmospheric boundary layer; sensitivity to surface evaporation. *Boundary Layer Meteorology 37*, 129-148.

Wu, Jin, 1980: Wind stress coefficients over sea surface near neutral conditions—a revisit. *J. Phys. Oceanogr. 10*, 727–740.

Zeneveld, J.R.V. and *Spinrad, R.W.*, 1980: An arc tangent model of irradiance at sea. *J. Geophys. Res. 85,* 4919–4922.

BOOK REVIEW

Charlson, R. J. and *Heintzenberg, J.* (eds.): **Aerosol Forcing and Climate**. John Wiley and Sons, 1995, Chichester, New York, Brisbane, Toronto, Singapore. pp. 416, price (hardback) 80 US $.

It is well-known that human activities modify the composition of the Earth's atmosphere on different scales depending on the residence time of the pollutants emitted. Since greenhouse gases have a long residence time, several years or decades, their effect impacts the atmosphere as a whole, called global warming. During the last twenty years tremendous papers were published on this subject. In the major part of these papers the authors tried to model the possible increase in temperature in the future as a function of predicted greenhouse gas emisions. Due to this effort one estimates presently a *climate forcing* (change in heat balance of a tropospheric air column) of 2.5 Wm^{-2}. The uncertainty of such a global estimation is less than about 15%. This means that the problem seems to be well solved.

However, very few papers have been devoted in the past to climatic effect of anthropogenic aerosol particles formed in the air by the chemical conversion and/or by the condensation of gaseous precursors. Thus, one assumed that the sulfur dioxide released during the combustion of fossil is essential in the acidification of the environment, but nobody, or very few scientists (e.g. *Bolin* and *Charlson*) recognized the importance of sulfate particles in climate control on regional and continental scale (the residence time of sulfur species is much less than that of greenhouse gases: only some days or a week). Further, organic compounds were considered in tropospheric gas phase chemistry (e.g. smog formation), but it was only recently suggested that organic aerosol particles can play a role even in climate forcing. This situation was due, at least partly, to the fact that aerosol particles are much more complicated entities than gaseous molecules. Their size, form and composition can vary considerably as a function of the strength and nature of formation, dynamic and removal processes. Consequently, their observation and modeling are much more complicated than in the case of pollutant gases. In addition to this, atmospheric aerosol particles influence not only directly the solar radiation transfer in the air, but, as cloud condensation nuclei, they control the structure and finally the albedo of clouds. This makes the estimation of their effects on the climate even more difficult.

Fortunately, during the last years the role of aerosol particles has become an important subject of research in the field of climatic variations. Among other things, this is proved by the fact that a *Dahlem conference* (a series of conferences held regularly in Berlin, Germany) in 1994 dealt with this problem. The present volume contains the materials of this conference in the form of review papers and expert group reports. The content of the book is divided into five great parts. The first section presents the general background papers, while in the remaining part of the book the papers are distributed according to the themes of four working groups. These chapters are closed by the group reports. The four working groups addressed the following subjects:

(1) What factors influence atmospheric aerosols, how have they changed in the past, and how might they change in the future (Rapporteur: *D. J. Jacob*, U.S.A.),
(2) Connection between aerosol properties and forcing of climate (Rapporteur: *S. E. Schwartz,* U.S.A.),
(3) Magnitudes and geographical variations and uncertainties of properties of tropospheric and stratospheric aerosols and their forcing (Rapporteur: *J. Lelieveld,* The Netherlands),
(4) What are the observed and anticipated meteorological and climatic responses to aerosol forcing? (Rapporteur: *V. Ramaswamy,* U.S.A.).

Since the conference was attended by excellent scientists, the volume is also excellent and can be proposed to all persons interested in the physics and chemistry of atmospheric aerosol particles, solar radiation transfer and climate variations.

The content of the book, that is the main suggestions and conclusions of the participants are summarized in an introductory chapter written by the editors. They state, among other things, that global anthropogenic aerosol forcing, due to the direct scattering of solar radiation by the particles, is equal to about -1 W m^{-2}. This causes probably a global cooling of 1–1.5 K. However, over industrial regions the climate forcing can be as large as -10 W m^{-2}. Anthropogenic effects are revealed by satellite observations. They show that over the Northern Hemisphere the aerosol extinction is three times more at summer mid-latitudes than over the Southern Hemisphere. On the other hand, meteorological observations in the Southern Hemisphere indicate a higher temperature increase during the last century than measurements, being carried out in the Northern Hemisphere do.

Concerning the indirect aerosol forcing thru the modification of cloud structure, the uncertainty is even higher than the value estimated for direct effects (a factor of two). Model calculations suggest a figure between -1.3 and -2.5 W m^{-2} for the Northern Hemisphere.

After reading this interesting volume, the reviewer has such an impression that during the last years an important step has been made for understanding the relationship between atmospheric composition and climate. However, it is clearly indicated in the volume that further efforts are needed in the future. This means that research of aerosol forcing of climate will certainly be a fascinating area for the scientific community in a number of years to come.

E. Mészáros

NEWS

Iván Csiszár won WMO Research Award

On 6 July 1995 *Professor G. O. P. Obasi*, Secretary-General of the World Meteorological Organization, wrote to *Mr. Iván Csiszár*:

> «Dear Mr. Csiszár,
>
> It is a great pleasure for me to inform you that the forty-seventh session of the WMO Executive Council (June 1995) has selected you as the winner of the 1995 WMO Research Award for Young Scientists. This award has been granted in recognition of your outstanding research entitled *The effect of the droplet size distribution on the reflectivity of boundary layer clouds*.
>
> I am very pleased to convey to you the warm congratulations of the President of WMO and of the members of the Executive Council, as well as my own personal congratulations on your success.
>
> The award consists of a citation and a sum of US $ 1000 that will be presented to you at a ceremony which will be arranged in consultation with the Permanent Representative of Hungary with WMO who nominated you for the award. You will receive further information concerning the ceremony in due course.»

Iván Csiszár has been working for the Hungarian Meteorological Service since 1988. His main research area is the satellite sounding of the atmosphere. In 1994 he won one of the COSPAR's Zeldovich Award for young scientists.

The ceremony of presentation occurred on 11 March 1996 in the Headquarters of the Hungarian Meteorological Service, Budapest, in the presence of *Minister Ferenc Baja* and several other guests. Mr. Csiszár summarized the essence of his paper that had appeared in *Időjárás 98*, pp. 107–117.

Using this occasion, Professor Obasi visited each department of the Hungarian Meteorological Service.

G. Major

International conference on Climatology and Air Pollution Mendoza, Argentina, August 14-21, 1995

The Commission on Climatology (COC) of the International Geographical Union (IGU) has been initiative in organizing a series of international meetings on climatology in recent years. Among others in 1994 there was held a Conference on Contemporary Climatology in Brno, Czech Republic; Climate, Environment and Planning in Tel-Aviv, Israel, 1993; the 13th Congress of the International Society of Biometeorology in Calgary, Canada, 1993; International Symposium on Climate and Life in the Asia-Pacific Region in Brunei Darussalem, April, 1995. The *Climate Digest*, Quarterly Bulletin of COC, edited by *Lawrence Nkemdirim* of Calgary, Canada, gives news of such events.

The International Conference on Climatology and Air Pollution, Mendoza, Argentina, August 14–21, 1995 was also sponsored partly by COC and other institutions. The conference was held in Universidad Nacional de Cuyo, Facultad de Filosofia y Letras and organized by *Professor Raul Mikkan*, with active collaborations of *Dr. W. Endlicher* of Marburg, *Dr. E. Schultz* of Freiburg, both from Germany, *Dr. H. Wanner* of Bern from Switzerland, *Dr. R. Capitanelli* and *Professor Alessandro* from Argentina, and *Professor L. Nkemdirim* from Canada.

On behalf of Department of Climatology, József Attila University, Szeged, Hungary two researchers took part in the conference: *Professor G. Koppány* and *Dr. J. Unger* with a paper and a poster, respectively. Namely: *Teleconnection method for drought prediction in five regions of Great Hungarian Plain* by *G. Koppány, J. Unger* and *L. Csikász*, and *Some aspects of the human bioclimate of a medium-sized town and its surroundings* (poster) by *J. Unger*.

Altogether about 40 papers were presented either in English or in Spanish with synchronous interpretations. Both languages are officially used in the United Nations and in WMO. Besides the sessions several workshops contributed to understanding of observation and classification of air pollutants by presentations of balloon soundings, city cross section measurements and microscopic samples of different types of aerosols. Approximately 60 participants gathered from Argentina, Brasilia, Chile and from Europe, mostly Germany, Austria and Switzerland, but people came also from France, Poland, Portugal, Rumania, Hungary, Canada, New Zealand and Israel. Proceedings of this conference consists of about 400 pages.

For European people, like us, it was quite unusual the late winter snowing in August, and seeing palm trees covered with snow. We took part in an exciting one-day excursion to the slope of Aconcagua, the highest point of the Western Hemisphere (6959 m a.s.l.), driving along the Valley of Mendoza River. A visit was also organized to Santa Anas Winnery, Asado near Mendoza city. The readiness to help of Argentineans has been much more, than customary in any other country. The same must be said upon the hospitality of our landlords. The cleanliness of Mendoza city has been extraordinary. The city is called oasis one, because it obtains water support exclusively from Mendoza River in an extremely arid surroundings. Thus Mendoza County suffers from drought even more than Hungarian Plain does.

Finally, the 13,000 km long trip and the 13 hour unceasingly flight over the Atlantic Ocean from Frankfurt to Buenos Aires was an unparalleled experience.

G. Koppány

NOTES TO CONTRIBUTORS

The purpose of *Időjárás* is to publish papers in the field of theoretical and applied meteorology. These may be reports on new results of scientific investigations, critical review articles summarizing current problems in certain subject, or shorter contributions dealing with a specific question. Authors may be of any nationality but papers are published only in English.

Papers will be subjected to constructive criticism by unidentified referees.

* * *

The manuscript should meet the following formal requirements:

Title should contain the title of the paper, the names(s) of the author(s) with indication of the name and address of employment.

The title should be followed by an *abstract* containing the aim, method and conclusions of the scientific investigation. After the abstract, the *key-words* of the content of the paper must be given.

Three copies of the manuscript, typed with double space, should be sent to the Editor-in-Chief: *P.O. Box 39, H-1675 Budapest,* Hungary.

References: The text citation should contain the name(s) of the author(s) in Italic letter or underlined and the year of publication. In case of one author: *Miller* (1989), or if the name of the author cannot be fitted into the text: *(Miller,* 1989); in the case of two authors: *Gamov* and *Cleveland* (1973); if there are more than two authors: *Smith et al.* (1990). When referring to several papers published in the same year by the same author, the year of publication should be followed by letters a,b etc. At the end of the paper the list of references should be arranged alphabetically. For an article: the name(s) of author(s) in Italics or underlined, year, title of article, name of journal, volume number (the latter two in Italics or underlined) and pages. E.g. *Nathan, K. K.,* 1986: A note on the relationship between photosynthetically active radiation and cloud amount. *Időjárás 90,* 10-13. For a book: the name(s) of author(s), year, title of the book (all in Italics or underlined with except of the year), publisher and place of publication. E.g. *Junge, C. E.,* 1963: *Air Chemistry and Radioactivity.* Academic Press, New York and London.

Figures should be prepared entirely in black India ink upon transparent paper or copied by a good quality copier. A series of figures should be attached to each copy of the manuscript. The legends of figures should be given on a separate sheet. Photographs of good quality may be provided in black and white.

Tables should be marked by Arabic numbers and provided on separate sheets together with relevant captions. In one table the column number is maximum 13 if possible. One column should not contain more than five characters.

Mathematical formulas and *symbols:* non-Latin letters and hand-written marks should be explained by making marginal notes in pencil.

The final text should be submitted both in manuscript form and on *diskette.* Use standard 3.5" or 5.25" DOS formatted diskettes for this purpose. The following word processors are supported: WordPerfect 5.1, WordPerfect for Windows 5.1, Microsoft Word 5.5, Microsoft Word 6.0. In all other cases the preferred text format is ASCII.

* * *

Authors receive 30 *reprints* free of charge. Additional reprints may be ordered at the authors' expense when sending back the proofs to the Editorial Office.

Published by the Hungarian Meteorological Service

Budapest, Hungary

INDEX: 26 361

HU ISSN 0324-6329

IDŐJÁRÁS

QUARTERLY JOURNAL
OF THE HUNGARIAN METEOROLOGICAL SERVICE

CONTENTS

VOL. 100 * NO. 4 * OCTOBER–DECEMBER 1996

IDŐJÁRÁS

Quarterly Journal of the Hungarian Meteorological Service

Editor-in-Chief
G. MAJOR

Executive Editor
Ms. M. ANTAL

Editorial Office: P.O. Box 39, H-1675 Budapest, Hungary or
Gilice tér 39, H-1181 Budapest, Hungary
E-mail: gmajor@met.hu; Fax: (36-1) 290-7387
antal@met.hu

Subscription from customers in Hungary should be sent to the
Financial Department of the Hungarian Meteorological Service,
Kitaibel Pál u. 1, H-1024 Budapest

Abroad the journal can be purchased from the distributor:
KULTURA, P.O. Box 149, H-1389 Budapest

IDŐJÁRÁS

Quarterly Journal of the Hungarian Meteorological Service
Vol. 100, No. 4, October–December 1996

ARPEGE/ALADIN: A numerical weather prediction model for Central-Europe with the participation of the Hungarian Meteorological Service

A. Horányi, I. Ihász and **G. Radnóti**

Hungarian Meteorological Service,
H-1525 Budapest, P.O. Box 38, Hungary

(Manuscript received 19 June 1995; in final form 10 October 1995)

Abstract—This paper intends to give a general description of the limited area numerical weather prediction model ARPEGE/ALADIN developed by a collaboration between Météo-France and some Central- and Eastern-European meteorological services (and also Morocco) including the Hungarian Meteorological Service (HMS). The model is a hydrostatic, spectral limited area model for dynamical adaptation at the limit of the hydrostatic approximation. The main characteristics of the model are discussed like the preparation of initial and lateral boundary conditions, the initialization method, the representation of the meteorological fields, the dynamics, the physics and the post-processing. The first experiences at HMS are discussed in the light of the one year quasi-operational application of the model. Finally, the possible future utilization for nowcasting purposes is mentioned.

Key-words: numerical weather prediction, spectral limited area model, dynamical adaptation, coupling, double-periodicization.

1. Introduction

The aim of this paper is to describe a new limited area model which is developed in collaboration with other Central- and Eastern-European countries and Morocco as well with French leadership. Nowadays in the operational numerical weather prediction practice two main intentions can be identified. The first is the improvement of the initial data for the models, using more measurements and more exact data assimilation methods. Due to the chaotic behaviour of the atmosphere without exact initial conditions, even a 'perfect' model could not provide a good forecast, therefore the improvement of the quantity (new type of data as Doppler radars, windprofilers etc.) and quality of initial data is of great importance. The second tendency is the improvement of the models by enhancing their resolution and especially their physical parameterization package in order to have better models for the prediction of local weather phenomena. During the last 20 years, beside the global models, more meteorological services started to use limited area models for operational purposes (following the latter tendency), which are specialized for high resolution short range numerical weather prediction. Recently the Hungarian Meteorological Service (HMS) also applies operationally a limited area model adapted from the Swedish Meteorological and Hydrological Institute (*Dévényi et al.,* 1992). This model uses a resolution of 0.9 × 0.9 degrees with 12 vertical levels. The implementation of this model was a major milestone in the field of predicting local meteorological events for the Carpathian basin. However, the resolution of this model is still not satisfactory, especially if the ECMWF (European Centre for Medium Range Weather Forecasting) products (getting full ECMWF products became possible with the status of associated membership) are kept in mind with their similar resolution. The Hungarian Meteorological Service has realized the necessity to have a modern high resolution limited area model, so in 1990 an offer of Météo-France was accepted to participate in an international collaboration in the field of numerical weather prediction. The other countries joining the collaboration until now are Austria, Bulgaria, Croatia, Czech Republic, Morocco, Poland, Romania, Slovakia and Slovenia. The main purpose of this project was the development of the limited area counterpart of the global French numerical weather prediction model (ARPEGE). The main development phase of the project was finished at the end of 1992. For the entire 1993 the model was mainly used for research studies and after getting new financial fundings the model was quasi-operationally implemented in Toulouse starting from 31 May, 1994. This paper intends to give a detailed description of this model, which is developed with the participation of HMS and also to mention its potential future applications for numerical weather prediction purposes for our region.

2. Projects for model developments

The project ARPEGE/IFS is a collaboration between Météo-France and ECMWF in numerical weather prediction. The main goals of this collaboration were to develop efficient data assimilation tools (variational assimilation) and also to have numerical weather prediction models at every spatial and time scale (*Courtier et al.,* 1991). These ambitious goals were covered by one model family which is called IFS (Integrated Forecasting System) at ECMWF and ARPEGE (Action de Recherche Petite Echelle Grande Echelle — research at small and large scale) in France. The models are spectral hydrostatic global models (*Courtier* and *Geleyn*, 1988) with the corresponding initializations and preparations of initial fields. The French acronym indicates one of the most important feature of the models to have variable resolution using the idea of *Schmidt* (1977). This means that the resolution changes over the whole sphere according to a stretching factor. In France the original idea was to use the ARPEGE global model for both synoptic and mesoscale purposes with the relevant choice of the stretching factor. The main advantage of this solution is to avoid the negative effect of the lateral boundary conditions between a high resolution domain and the coarser resolution area. However, stretching can't be increased infinitely to increase the resolution in a given area (and decrease it on the other side of the Earth), due to the fact that the spectral characteristics are broken after a limit stretching value. This statement means that for very high resolutions (near to meso-β scale) this solution can't be applied (*Caian* and *Geleyn*, 1995).

Hereafter the main elements of the ARPEGE/IFS model system are introduced. These elements can be activated by a properly chosen configuration number and they are as follows:

- 3D forecast model using the primitive equations of the atmosphere,
- variational assimilation (3D variational analysis and different options of 4D variational analysis),
- 2D forecast models (shallow water model, vorticity equation model, linear gravity wave model),
- Kalman filter and predictability studies,
- test of the adjoint models,
- test of the tangent linear models,
- calculation of eigenvalues and eigenvectors,
- objective analysis using optimal interpolation,
- sensitivity studies,
- geometrical transformations for the preparation of initial conditions of the models.

In 1990 Météo-France launched an initiative in order to start a collaboration with Central- and Eastern-European countries in numerical weather prediction. The proposal was directed towards the development of the limited area counterpart of the global spectral ARPEGE/IFS model system. The main objective of the project to be fulfilled was to develop a limited area model in the framework of the existing ARPEGE/IFS code for dynamical adaptation at the limit of the hydrostatic approximation. The ALADIN model is intended to be a version of the ARPEGE/IFS code system using as much as it is possible the already existing code and creating new modules only if it is unavoidable. From a practical point of view it means that the main part of the model existed even before the development was started. It is especially true for the main scientific part of the model (the grid-point calculations) which is so general and independent of any metric or geometry that it can be used without any modifications also for limited area purposes. Dynamical adaptation stands for a system, where independent objective analysis isn't carried out for producing initial and lateral boundary conditions, only simple interpolation is performed starting from global ARPEGE fields. The target resolution is at around the limit of the hydrostatic approximation. Hereafter the main points (where the original system had to be modified) to be considered in the development of the model are reviewed:

- The consideration of the meteorological processes evolving outside the domain using coupling. The coupling is achieved by a relaxation technique, which ensures continuous transition between the internal and external part of the model domain.
- The geometric transformation of the spherical geometry onto the limited area in order to prepare the initial and lateral boundary conditions.
- The modification of the horizontal representation of the fields from spherical harmonics to full harmonic functions and taking into account all of its consequences (e.g. derivative calculations, spectral space computations).
- The development of digital filter dynamical initialization method.

The solution of these basic tasks allowed to create the limited area spectral model called ALADIN (Aire Limitee Adaptation Dynamique Developpement International — international development of a limited area model for dynamical adaptation) or ARPEGE/ALADIN referring to the mother system ARPEGE. After the development and refinement of the basic parts of the model some research topics were defined such as the application of the tangent linear and adjoint versions for sensitivity studies or the development of a non-hydrostatic version.

3. The general description of the model system ARPEGE/ALADIN

As it was mentioned before, ARPEGE/ALADIN is a hydrostatic, spectral limited area model. Recently for global numerical modelling spectral methods are generally used because of having certain advantages with respect to the traditional grid-point methods. Mostly these advantages are preserved in the case of limited area applications and they are summarized below:

- the possible simple and more accurate calculation of derivative fields,
- good description of the phase and amplitude of the meteorological fields,
- the horizontal and vertical dimensions are well separated allowing simplified conservation properties,
- easy and cheap implementation of semi-implicit time integration schemes,

- simple unaliasing condition due to the spectral truncation,
- the technique can be easily extended to variational developments,
- less disk space requirements due to the data storage in the form of spectral coefficients.

Taking into account these advantages *Machenhauer* and *Haugen* (1987) proposed the full harmonic expansion of the meteorological fields (which means that the fields must be double-periodic) in the case of spectral limited area applications. This solution was implemented for the ARPEGE/ALADIN model.

As far as the execution of the model system is concerned it is decomposed into three main steps. The first two preparatory steps provide climatological fields and initial and lateral boundary conditions over the limited area for the model integration. During the preparation of climatological fields using global climatological fields and the definition of the domain interpolation is carried out onto the limited area. The results of this operation are monthly average climatological fields for the given domain (*Cordoneanu,* personal communication). In the second phase similar interpolation is performed in order to obtain the initial and lateral boundary conditions for the limited area model. During this operation the analyses and the forecasts of the global model are interpolated to the target grid. The climatological fields, the initial and lateral boundary conditions are already double-periodic. This fact prevents further double-periodicization during the time integration of the model. After these preparations the heart of the model system, the integration of the non-linear hydrostatic model takes place. The main aspects of the integration are the dynamical initialization of the initial fields (using digital filters), the calculation of dynamical and physical tendencies using Eulerian or semi-Lagrangian semi-implicit time integration scheme, consideration of lateral boundary conditions through coupling, the creation of post-processed fields using internal post-processing.

In the following sections these major steps will be reviewed with special emphasis on the model part.

3.1 The preparation of initial and lateral boundary data

The double-periodic initial and lateral boundary conditions of model ALADIN are obtained by interpolation from global ARPEGE analyses and forecasts. The following sequence of operations (the order is of great importance) are performed: the transformation of global spectral fields from spherical harmonics to the collocation grid, horizontal interpolation, double-periodicization and afterwards vertical interpolations to the target geometry and finally transformation of the grid-point fields into full harmonics. The horizontal interpolation is done with the possibility to use a bilinear or a 12-point interpolation with cubic Lagrangian polynomials. The most important option running the horizontal interpolations is the capability of using departures between the climatological mean values and the surface prognostic fields. This option ensures to have small scale details in the interpolated data. For the vertical interpolation a displacement of the planetary boundary layer (PBL) has been implemented in order to keep its structure as much as it is possible. For this method first an intermediate vertical system is created which is defined by a special combination of the characteristics of the input and target systems. The next step is the vertical interpolation from the input and intermediate systems to the target one using a weight function varying between zero and one and which ensures smooth transition in the PBL transition layer. Below this transition zone the results of the intermediate system are taken alone and above it only the original one is considered (*Bubnová et al.,* 1993).

Concerning the double-periodicization, it is an operation which makes the meteorological fields double-periodic (periodic in both direction of the plane). This operation is essential in order to be capable for performing Fourier transformations for the calculation of derivatives. The double-periodicization operator should also take care not to introduce undesirable numerical noises in the area of meteorological interest. As double-periodicization operator, cubic spline functions are used with subsequent Laplacian transversal smoothing with the following desirable features: continuous derivatives up to second order, isotropy and no unrealistic overshooting (*Batka,* personal communication).

Finally, after the double-periodicization and the direct spectral transformations all the necessary information is available (in the form of spectral coefficients) for the integration of the model. These are the three dimensional state variables of the model like temperature, wind components and specific humidity and two dimensional variables like surface pressure and orography. The necessary surface fields are surface and deep soil temperature, surface and deep soil relative moisture contents, snow cover, albedo, emissivity, land-sea mask, proportion of vegetation, roughness length, standard deviation, anisotropy and orientation of subgrid-scale orography.

3.2 Digital filter initialization

Due to the finer orography used by ALADIN and the noise unavoidably introduced by the interpolation from the global to limited area geometry, dynamical initialization of the prognostic fields is desirable even if the original information came from an initialized state. Therefore the time integration is preceeded by the dynamical initialization of the initial fields.

For ALADIN it was decided to implement the digital filter initialization method (*Lynch* and *Huang*, 1992) instead of adapting the non-linear normal mode initialization from the global model. The main purpose of the initialization is the removal of those fast propagating inertia-gravity waves from the initial conditions which would cause numerical instability at the beginning of the integration. For the digital filters the main idea is filtering out the high frequency noises by considering the temporal Fourier series of the fields of interest and setting to zero the Fourier coefficients corresponding to high frequency waves and recompute the fields again. Then these fields will not contain high frequency spurious waves any more. It can be seen that the method is very simple, its coding is based on a very simple algorithm. On top of that the method is not sensitive to the formulation and the changes of the model and there are no convergence problems as for normal modes. The success of the utilisation of digital filters (with its various variants as recursive or non-recursive, diabatic or adiabatic, incremental or non-incremental filters) inspired its potential application also for the ARPEGE global system (*Ivanovici,* personal communication).

3.3 The vertical representation of the meteorological fields

The vertical coordinate to be used is the pressure based hybrid coordinate η following the orography as described by *Simmons* and *Burridge* (1981). The main feature of this coordinate is that at the bottom of the model it is terrain following and at the top it is pressure type coordinate. The vertical coordinate is defined by the following implicit relationship:

$$p(x,y,\eta,t) = A(\eta) + B(\eta)\,\pi(x,y,t)\,, \tag{1}$$

where η is the vertical coordinate, p is the pressure, π is the surface pressure and A and B are constants depending on the vertical levels. The η vertical coordinate varies between 0 and 1 (0 at the top and 1 at the bottom) and the following conditions are fulfilled:

$$A(1) = 0;\quad B(1) = 1;\quad B(0) = 0 \;\text{ and }\; \frac{\partial \eta}{\partial p} > 0\,. \tag{2}$$

Therefore the vertical coordinate is defined by the constants A and B. This coordinate with a properly chosen vertical discretisation ensures the conservation of energy and angular momentum of the system (*Simmons* and *Burridge*, 1981). This main constraint was kept in mind while designing the vertical discretisation scheme. The model is vertically discretised into L layers. Between model levels layer boundaries ($L + 1$) are also defined. The model variables are naturally defined at model levels and fluxes and advecting vertical velocity at half levels. It is mentioned here that the Eq. (1) for the definition of the vertical coordinate is valid for half levels and the pressure values of the main levels can be computed from the half level values. The vertical discretisation is of great importance for the hydrostatic equation through its vertical integration.

3.4 The horizontal representation of the meteorological fields

The horizontal domain of ALADIN is decomposed into three regions which are shown in *Fig. 1*. These are as follows:

- Inner zone, which is in fact the domain of meteorological interest for adapting the larger scale forecast to a smaller scale orography or surface conditions. It is labelled by C as central zone.
- Intermediate zone (denoted by I), where the large scale solution is mixed together with the central zone solution. This zone is also called coupling zone or relaxation zone.
- Extension zone, which is considered for the spectral expansion. In this zone the fields are extended in agreement with the chosen basis function (these are the full harmonic functions). It is labelled with E.

The fields are geographically meaningful over the C and I zone, for the E zone those are expanded as a result of a purely mathematical operation.

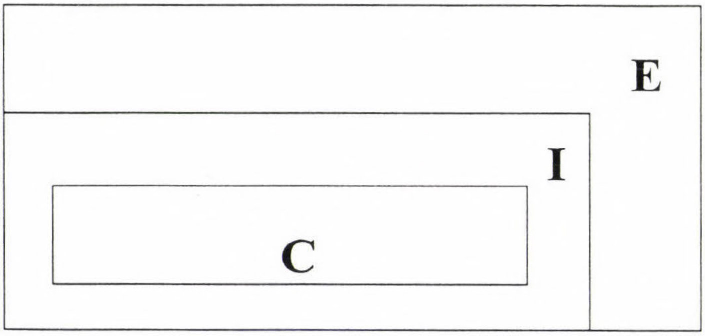

Fig. 1. The horizontal domain of ARPEGE/ALADIN. The C zone is the inner domain, the domain of meteorological interest. The I zone is the relaxation zone, where the coupling term is considered. The E zone is the extension zone, the region for double-periodicization.

Following the idea of *Machenhauer* and *Haugen* (1987) and considering an arbitrary X field its full harmonic expansion reads as:

$$X(x,y,\eta,t) = \sum_{m=-M}^{M} \sum_{n=-N}^{N} X_m^n(\eta,t)\, e^{im(2\pi/L_x)x}\, e^{in(2\pi/L_y)y}, \tag{3}$$

where L_x and L_y are the horizontal wavelengths and X_m^n-s are the spectral coefficients corresponding to the given waves. The field X is expressed by the combination of different waves with different wavenumbers. This formulation directly gives the truncated form, but from mathematical point of view the summation is of course infinite. It can be seen that the largest wavenumber considered in x direction is $M(2\pi/L_x)$ and in y direction it is $N(2\pi/L_y)$. It is clear from Eq. (3) that the calculation of the derivatives of X is rather simple knowing the spectral coefficients. These spectral coefficients can be calculated from the continuous form as:

$$X_m^n(\eta, t) = \frac{1}{JK} \sum_{j=0}^{J-1} \sum_{k=0}^{K-1} X(j,k,\eta,t)\, e^{-im(2\pi/J)j}\, e^{-in(2\pi/K)k}, \tag{4}$$

where J is the number of points along x and K is the number of points along y.

Eqs. (3) and (4) define the direct and inverse Fourier transformation between spectral and physical spaces. Inverse transforms are performed while going from spectral space to physical space and direct ones in the other direction. The transformations are decomposed into two steps for the two horizontal directions. The double-Fourier inverse transforms create the set of spectral coefficients and for every pair of waves there are four real coefficients. For the calculation of the coefficients in order to keep the isotropy the following constraint is considered:

$$\frac{n^2}{N^2} + \frac{m^2}{M^2} \leq 1, \tag{5}$$

where M and N are the maximum wavenumbers (these are chosen according to the size of the domain in the x and y direction, respectively). This expression defines the elliptic truncation, which has the same properties on the Cartesian plane as the triangular truncation of spherical harmonics on the sphere.

Another big advantage of the application of Fourier series is the fact that there exists a computationally efficient algorithm for transforming real fields. This algorithm is the Fast Fourier Transform (FFT) and utilizes the optimization possibilities of the trigonometrical functions (*Temperton*, 1979). In spectral models the existence of efficient spectral transformations is of great importance due to the fact that these transforms are performed at each timestep of the model.

Eqs. (3) and (4) involve $2M + 1$ and $2N + 1$ modes in spectral space and J and K points in physical space. Obviously, the number of waves and the number of points aren't independent parameters. Let us consider a field of a physical quantity, which is characterized by M modes in spectral or $2M$ points in physical space. When products of such fields are considered in physical space, information on wavenumber larger than M is created, i.e. if Eq. (4) is performed on the same $2M$ points the M waves aren't sufficient for describing the given quantity due to the so called aliasing errors which might lead to nonlinear instability. Therefore in order to avoid aliasing, more points need to be defined for a given number of modes. The number of points depends on the highest order of product to be considered for solving the physical problem. In the case of ALADIN, the relationship between the number of points and waves is:

$$J \geq 3M + 1 \quad \text{and} \quad K \geq 3N + 1\,. \tag{6}$$

Concerning the number of points to be chosen, there are also some constraints because of the optimal performance of FFT-s.

3.5 The equations of the nonlinear, hydrostatic model

The horizontal momentum equations on the sphere for ARPEGE (*Courtier et al.*, 1991) can be expressed as the acceleration of the individual particle is equal to the accelerations due to pressure gradient force, Coriolis force and due to diffusion and different parameterization processes. The physical parameterization package for the ALADIN model is kept the same as it is used for its global counterpart:

- complete and cheap radiation scheme (*Geleyn* and *Hollingsworth*, 1979; *Ritter* and *Geleyn*, 1992),
- vertical exchange calculations taking into account a planetary boundary layer and a surface layer based on the Louis scheme (*Louis et al.*, 1982),
- shallow convection parameterization (*Geleyn*, 1987),
- gravity wave drag based on the scheme of Boer (*Boer et al.*, 1984),
- Bougeault-type deep convection scheme (*Bougeault*, 1985),
- simplified Kessler-type scheme for the large scale precipitation,
- force-restore method for the soil hydrology.

Concerning the horizontal momentum equations over a limited area, ARPEGE/ALADIN is capable for integrating the primitive equations over an arbitrarily chosen limited area (the domain can be in any part of the Earth with well defined position), with the smoothest and most regular possible distribution of grid points. The traditional system of latitudes and longitudes provides such a regularity only in the vicinity of the equator or if it is conveniently projected on a plane. In the latter case the optimal projection highly depends on the location of the domain. By taking into account the above mentioned aspects during the preparatory phase of the model integration the rotation of the spherical coordinates or the three basic conformal projections (polar stereographic, Lambert, Mercator) or the combination of rotation and projection is available.

Concerning the rotation of the latitude-longitude coordinates, the goal of this operation is to roughly center the domain of interest over the new equator. This kind of transformation is also used for the HIRLAM model (*Gustafsson*, 1993). After investigating this option it turns out that a rotation of the Equator to the domain of interest followed by the Mercator projection is the only coherent way to handle the spherical metric of a portion of a sphere. The above mentioned three conformal projections can be merged into one using their map factor function and a constant parameter (K). When $K = 1$, then the polar stereographic projection is considered. For the Lambert projection K varies between 0 and 1 and for the Mercator one it is 0. Using the above mentioned projections the fundamental scalars (e.g. vorticity and divergence) and pseudo-scalars (e.g. kinetic energy) can be defined in the framework of the Cartesian geometry.

When projecting the momentum equations from the sphere to the plane, some terms containing the characteristics of the projections occur. These terms (curvature terms) can be expressed explicitly in terms of map factor function and kinetic energy.

The other equations to be considered are the hydrostatic equation, the thermodynamic equation and the continuity equation. All the governing equations used by ALADIN can be found in the Appendix.

3.6 The semi-implicit semi-Lagrangian time integration scheme

The time integration of the model includes a semi-implicit correction for fast-propagating processes independently of the application of semi-Lagrangian scheme. The semi-implicit correction allows a bigger timestep due to the removal of some fast-propagating waves taking into account the Courants-Friedrichs-Levy condition. For the Eulerian version the explicit leap-frog scheme reads as:

$$\frac{e^{+}-e^{-}}{2\Delta t} = D(e), \tag{7}$$

where e is the given variable at time t, e^{+} is at $t + dt$ and e^{-} is at $t - dt$. D refers to the expressions on the right hand side of the differential equation. The operator D describes different processes e.g. energy conversions, advection, wave propagation etc. Some of the processes are linear or well approximated by a linear (L) operator and excluding them from the operator D gives

$$\frac{e^{+}-e^{-}}{2\Delta t} = D(e) + \beta L\left[\frac{1}{2}(e^{+}+e^{-})-e\right], \tag{8}$$

where β is the semi-implicit coefficient. Utilizing the linearity of L, Eq. (8) can be rewritten as

$$(I - \beta \Delta t L) e^{+} = \overset{+}{e}_{explicit} + \beta \Delta t L (e^{-} - 2e) . \tag{9}$$

It can be seen that the price for the increase of the timestep with the removal of some fast waves is the inversion of the matrix on the left hand side. It is remarked that the terms occurring on the right hand side are generally called as the explicit part of the semi-implicit correction and these operations are performed in the grid-point space. The matrix inversion of the left hand side is computed in spectral space, because it involves the inversion of a Laplacian operator. This latter operation is called the implicit part of the semi-implicit correction.

It was decided for ALADIN to implement the semi-Lagrangian scheme for the further increase of the timestep with the removal of some fast-propagating waves. The applied scheme for the model is originated from the existing semi-Lagrangian scheme of ARPEGE, only some adjustment was done to the plane geometry and the limited area character was kept in mind. The main characteristics of the scheme are as follows (*Janousek,* personal communication):

- three dimensional semi-Lagrangian advection,
- 3-time level scheme with second order accuracy,
- fully interpolating version, with provision for future implementation of vertically non-interpolating version,
- upstream trajectories,
- wind-component based approach to the solution of momentum equations,
- approximation of trajectories by stream lines, using trilinear interpolation of wind components for trajectory construction,
- 32-point interpolation of the terms in the trajectory points,
- off-centering technique in order to avoid spurious resonant wave generation.

The application of semi-Lagrangian scheme and the necessity of grid-point calculations over the extension zone have a special interaction due to the treatment of the trajectories coming form the extension zone. If calculations are needed over the extension zone (when coupling is performed before the grid-point calculations) the computation of the trajectories at the edge of the $C + I$ zone is rather complicated, because taking into account the double-periodicity information about the top and bottom of the integration area is needed at the same time. This can be solved only in a very complicated manner due to the special organization of grid-point calculations. At the same time these calculations would be very superfluous, because of the unnecessary computations over the extension zone. If such a coupling strategy is chosen (and it is the case for ALADIN), where there is no need for calculation over the E

zone, the solution for the semi-Lagrangian scheme is much simpler. In that case the treatment of the external boundary of *I* zone (where trajectories might come from the extension zone) is based on the assumption that values of variables in extension zone are constant along the line perpendicular to the boundaries. According to the experiences, the errors occurring due to this assumption can be controlled with a proper choice of the width of the relaxation zone.

3.7 The coupling

The purpose of coupling is to impose the larger scale solution on a part of the domain taking into account the processes evolving outside the limited area. The coupling is also responsible for removing the artificial reflection and transmission of small scale waves on the boundaries of the domain of interest (*C* zone). Within the coupling zone (*I*) there is a smooth transition between the fields produced by the global model and those of ALADIN. This method is also considered as relaxation and can be described by the following formula (*Davies*, 1976):

$$X^{c} = (1 - \alpha) X^{bc} + \alpha X^{ls}, \tag{10}$$

where X^{bc} refers to values before coupling, X^{ls} refers to large scale values at the external edge of *I* zone and X^{c} corresponds to the values after the coupling. α is the relaxation coefficient, its value is 0 for the *C* zone, varies between 0 and 1 for the *I* zone and 1 for the *E* zone. The relaxation coefficients for the *I* zone are deduced from some special differentiable functions (*Janiskova,* 1994). Some specific aspects of the chosen coupling strategy are mentioned in *Radnóti* (1995).

3.8 The post-processing

During the model integration in specified time intervals some post-processed fields are created, which are as follows: post-processed prognostic variables, instantaneous fluxes (surface fluxes) and cumulated fluxes (precipitation fluxes). The normal post-processed file contains the albedo, deep soil temperature, emissivity, geopotential, land-sea mask, mean sea level pressure, orography, orography deviation, relative humidity, relaxation temperature, relaxation water, roughness, skin water, snow depth, soil moisture, specific humidity, surface temperature, temperature, vegetation, vertical velocity and wind fields. The three dimensional fields are generally represented on pressure levels, although there is an option to keep the original η levels. The instantaneous fluxes file contains the 2 m relative humidity, 2 m specific humidity, 2 m temperature, 10 m wind, total cloud cover, 2 m minimum and maximum temperature. The cumulated fluxes file contains the convective precipitation, stratiform precipitation, radiative fluxes, surface fluxes, gravity wave drag momentum fluxes and turbulent momentum fluxes.

4. The quasi-operational model and its results

ARPEGE/ALADIN is quasi-operationally applied in Toulouse (at the forecast center of Météo-France on a CRAY-90 computer) for a domain over Europe. The orography of the domain can be seen in *Fig. 2*.

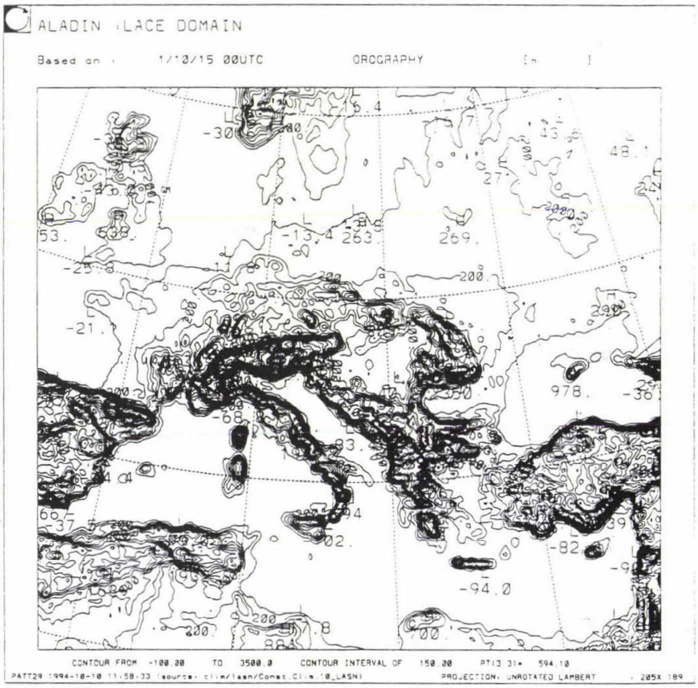

Fig. 2. The domain and the orography of the quasi-operational version of ARPEGE/ALADIN.

The main characteristics of the model are as follows:

- digital filter initialization,
- semi-implicit semi-Langrangian integration scheme with Asselin time filter,
- 432 seconds of timestep,
- circ. 18 km of horizontal resolution using 205 × 189 collocation grid points on Lambert projection,

- the domain size is around 3800 × 3400 km,
- 24 vertical levels (the lowest level is at 17 m and the highest is at 10 hPa),
- the boundary values are specified from ARPEGE and linearly interpolated with a 6 hour interval,
- the computational cost is around 4400 seconds CPU time for CRAY-98 (it roughly means 12 minutes execution time with 8 processors) for a 36 hours forecast.

The quasi-operational model is launched every day for 36 hours, starting from 00 UTC data and creates post-processed output fields every 6 hours. Some post-processed fields are disseminated to the participating countries in chart form via satellite. These charts are available for the bench-forecasters every day at around 04 UTC, so they can use them for operational purposes. The traditional meteorological forecast variables are available on pressure levels as geopotential, temperature, relative humidity, wind vector and also mean sea level pressure. In addition to this information, 10 m wind, wet bulb potential temperature, vertical velocity and precipitation forecasts are displayed on the disseminated maps.

5. Application of ALADIN products at HMS

The disseminated products of ALADIN (some examples can be seen in *Fig. 3*) are used in the daily operational suite at HMS. The receipt of these products are solved by MATRA satellite receivers. These machines were obtained from Météo-France in order to make possible the reception of numerical weather prediction products used in France. These are analyses and forecasts of French models (e.g. ARPEGE) and some alphanumeric telegrams used for aviation meteorology (like METAR or TAF messages). The data received by the MATRA station serve as a complement to the GTS information and these are particularly useful for aeronautical meteorological purposes, because it is able to complete automatically some flight plans and files for a predefined time. The application of this equipment was natural while the dissemination of ALADIN products was concerned. This device is able to decode the Tektronix files coming from Toulouse in order to produce meteorological charts. The charts can be visualized either on the screen or on the paper, however the ALADIN products are automatically plotted for the use of the forecaster on shift. As far as the application of the products is concerned three main fields can be identified: general forecast, aviation forecast and storm forecast. The general forecast provides predictions for the media and also some guidelines for the specialized forecasts and mostly uses the 12–36 hours ALADIN forecasts. The aviation and storm forecasts obviously utilizes shorter range forecasts due to their nowcasting character. It is especially true for the storm forecast system at Lake Balaton (a MATRA receiver is also installed there), where up to date storm warnings have to be issued. In this field the possible further application of ALADIN products opens a new perspective with respect the dangerous quickly evolving small scale systems.

(a)

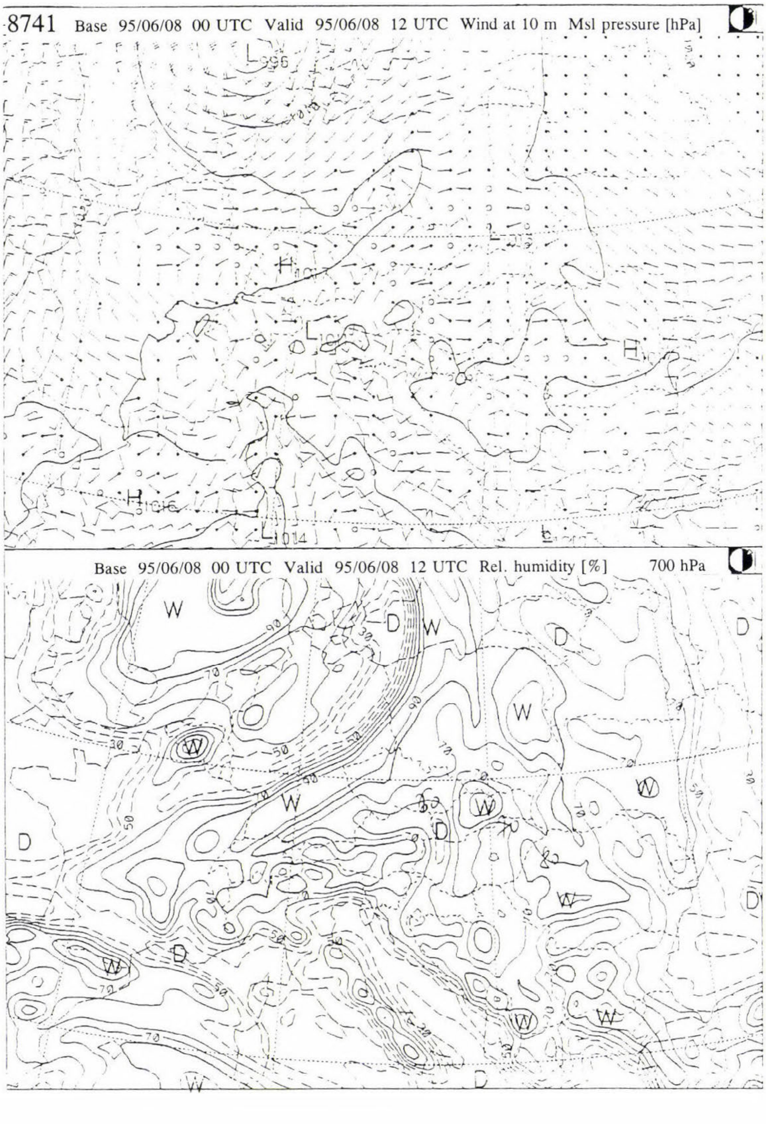

Fig. 3. A 12 hours forecast starting from 00 UTC, 08 June, 1995. (*a*) 10 m wind vector with mean sea level pressure (hPa) and relative humidity (%) at 700 hPa; (*b*) geopotential height (dam) with temperature (°C) at 500 hPa and vertical velocity (Pa/s) at 700 hPa.

Continued Fig. 3.

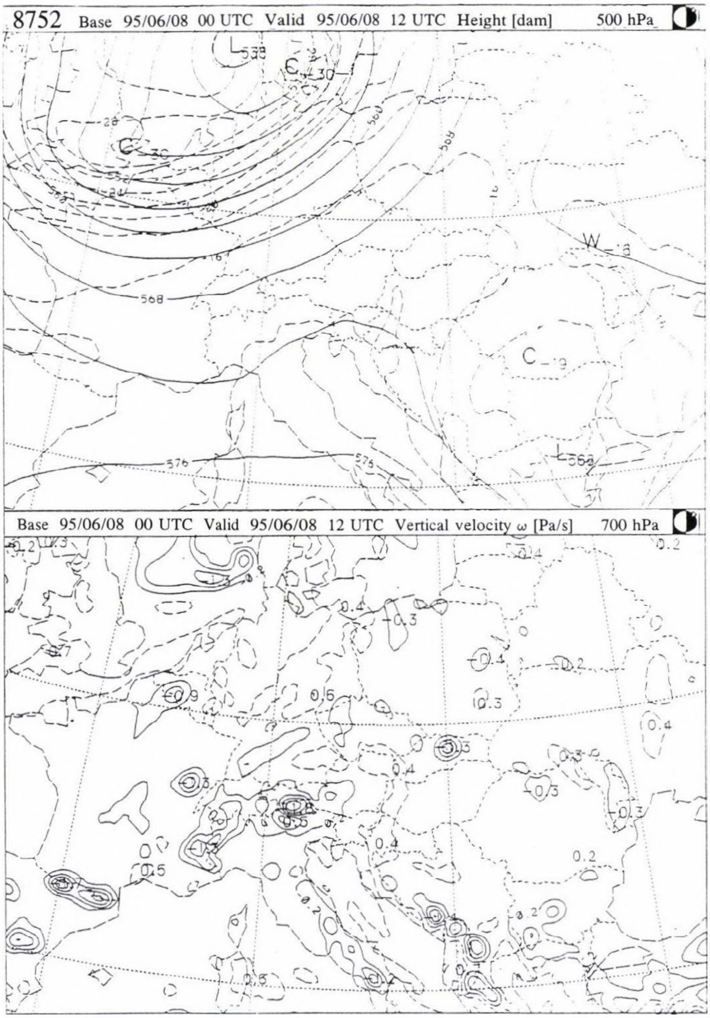

(b)

However at the moment, the technical facilities of the satellite dissemination do not make it possible to get the full meteorological information provided by the model (this fact is illustrated in *Fig. 4*), so further efforts are needed to get alphanumerical messages in order to benefit from the full horizontal and vertical resolution of the model. The first step towards this longer range goal is the receipt of electronic mail messages containing some vertical profiles in predefined stations of interest (Szombathely, Győr, Siófok, Pécs, Budapest, Szeged, Debrecen and Miskolc) over Hungary. These ‘pseudo-TEMP’ forecasts are displayed on workstations in traditional emagram form (see *Fig. 5*) and those are especially useful for aviation meteorological purposes. In the near future it is planned to prepare the receipt of GRIB telegrams, which will allow us to utilize the full post-processed products of ARPEGE/ALADIN.

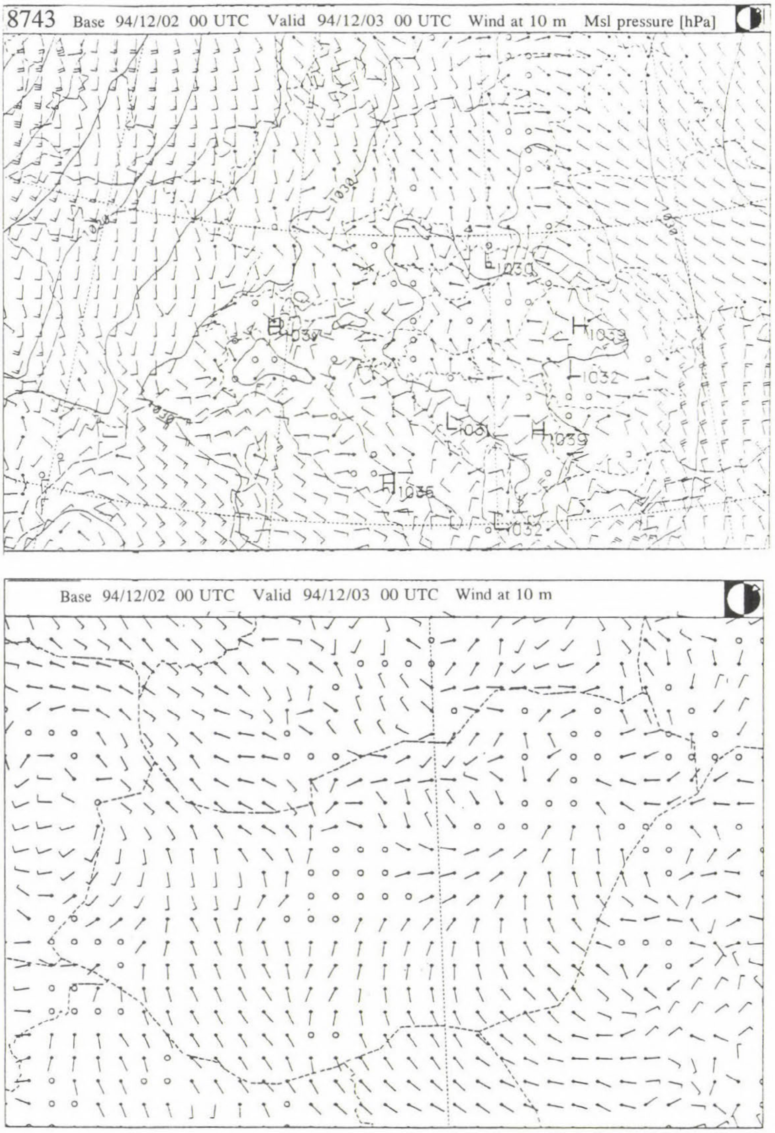

Fig. 4. Comparisons of 24 hours 10 m wind forecasts (based on 2 of December, 1994) in m/s over Hungary. (*a*) The traditional chart form used in the daily operational regime (every fourth gridpoints are displayed); (*b*) A zoom over Hungary displaying all gridpoints of the model.

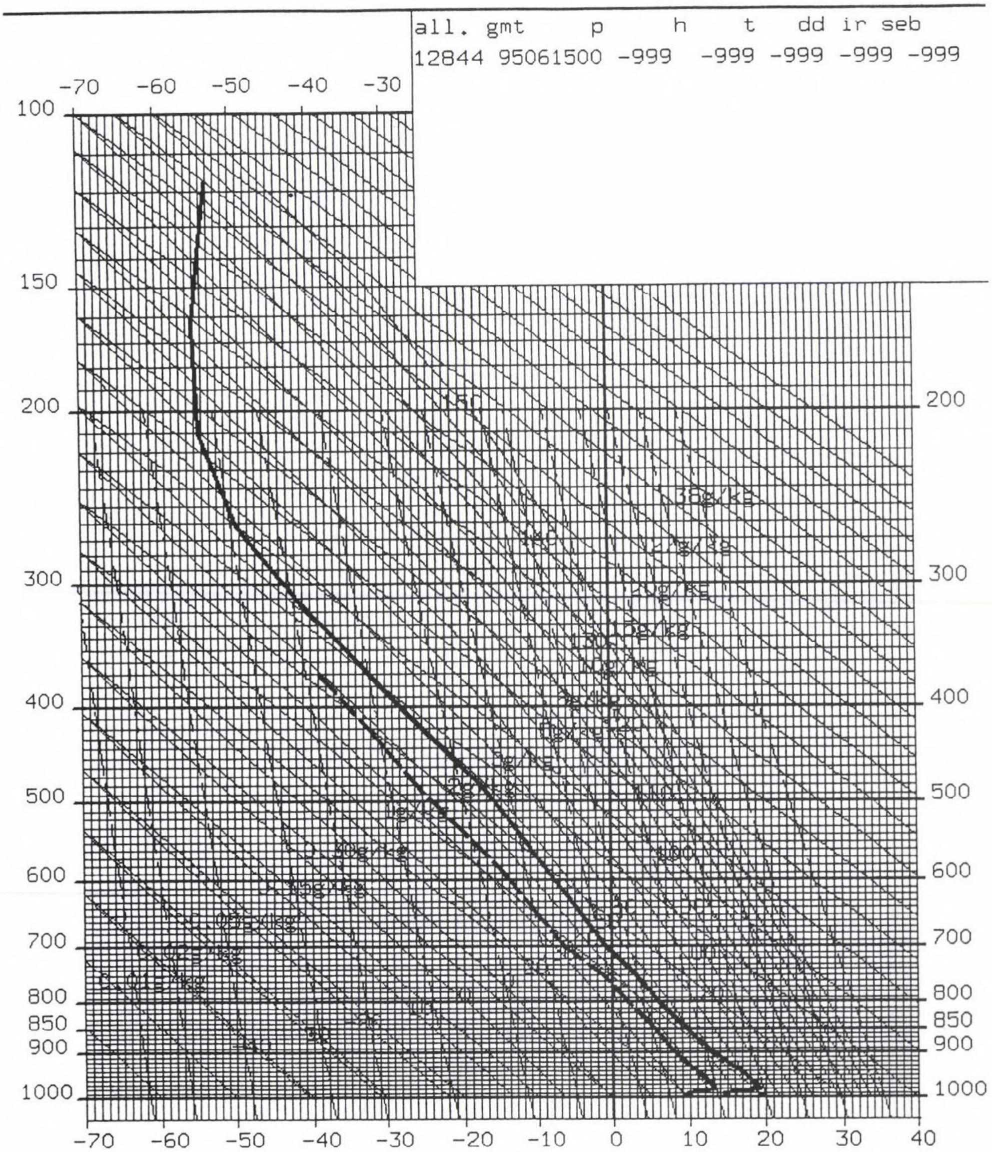

Fig. 5. An emagram prepared using 'pseudo-TEMP' message of ALADIN. A vertical profile of a 24 hours ALADIN forecast starting from 14 of June, 1995 over Budapest.

Concerning the evaluation of the ALADIN products, both objective and subjective verification is carried out. Before the quasi-operational start the basic validation of the model was performed by Czech, Polish and Hungarian forecasters. In Toulouse the experts of Météo-France compute monthly verification scores (mean forecast error, standard deviation and root mean square error) with respect to SYNOP and TEMP observations and also comparison is done to the results of operational ARPEGE. The main conclusions of the objective verification are that ALADIN usually gave slightly worse scores than ARPEGE when it was compared to SYNOP observations for wind and slightly better for temperature fields. While ALADIN results are compared to TEMP observations for the lower part of the atmosphere the same conclusion can be drawn. These results are rather surprising according to the expectations. This weakness is probably linked to the exaggerated amount of surface and upper air drag in ALADIN with respect to ARPEGE. Ways to cure it are tested to find the best balance between the several factors contributing to the low level drag of the model.

In Budapest monthly subjective verifications over Hungary based on the disseminated charts are performed. Below some of the experiences will be summarized with respect to the one year utilization of ALADIN products in Hungary. Detailed case studies are out of scope of this paper, they are planned to be presented in another paper. Generally it can be said that the configuration of the meteorological objects (their mean sea level pressure, geopotential and temperature) is very well represented by ALADIN. It is especially useful in the case of mesoscale systems due to the fact that other models applied at HMS (e.g. UKMO or DWD models) have coarse resolution for predicting these regional events. Nevertheless, also sometimes weaknesses can be detected like the underestimation of 2 m temperature and the wind speed at 10 m. For the latter quantity it is interesting to note that practically overestimation never occurs even in the cases of very strong wind the model gives moderate values (see *Table 1*). For the temperature fields time by time overestimation can be noticed at 850 hPa and underestimation for the 500 hPa pressure levels. The mean sea level pattern is sometimes overestimated.

Table 1. Subjective evaluation of the 10 m wind speeds for September. The values are in percentage.

Time (hr)	Prediction		
	exact	high	low
06	70	-	30
12	17	-	83
18	53	-	47
24	77	-	23
30	59	-	41
36	15	-	85

One of the most important parameter to be considered is the precipitation. This variable caused most of the difficulty for the forecasters as far as its occurrence and quantity are concerned. At the first months the convective precipitation was strongly overestimated and due to this fact the frontal precipitation zones were hidden into the convective patterns. After the identification of this serious problem a modification of the convective precipitation parameterization scheme was implemented, which improved the results dramatically (*Table 2*). Recently the precipitation forecasts are much better (less overestimation and more correct forecasts), however this variable is still the most problematic one.

Table 2. Subjective verification of precipitation forecasts of ALADIN before (July) and after (September) the modification of the convection scheme. The values are in percentage.

The right forecast (first column) means those cases, when the position and the quantity of the forecast were correct. Second column: precipitation was forecasted, but didn't occur; third column: precipitation wasn't forecasted, but occurred; fourth column: precipitation was forecasted but to wrong place; fifth column: the position of the forecast was correct, but it was overestimated; sixth column: the position of the forecast was correct, but underestimated.

Time (hr)	Occurrence								Quantity			
	right		forec.: yes real: no		forec.: no real: yes		wrong place		over-estimation		under-estimation	
	Jul	Sep	Jul	Sep	Jul	Sep	Jul	Sep	Jul	Sep	Jul	Sep
06	35	40	24	7	32	27	4	10	-	-	5	17
12	22	57	35	13	8	10	16	10	5	3	14	7
18	24	53	27	13	-	7	13	20	14	-	22	7
24	18	70	50	7	-	3	9	7	18	7	5	7
30	37	57	32	57	18	27	7	3	3	-	3	13
36	16	54	43	4	-	23	9	8	14	8	18	4

6. Plans for the future

Concerning the future, the first objective is the full validation of the model in order to be capable for using it in operational way. To this end a systematic evaluation of the subjective and objective verifications will take place in order to discover the possibly existing weaknesses of the model.

Regarding the further development of the model there are ambitious objectives in that respect. Concerning the objective analysis and data assimilation recently the objective analysis scheme based on optimal interpolation is adapted from the ARPEGE system to ALADIN (in the framework of the French-Moroccan collaboration), however its full validation is not yet finished.

In the long term the implementation of variational assimilation schemes is planned. The first step towards this goal is the development of the tangent linear and adjoint versions of the model. The already existing adjoint version of the doubly-periodic version is used for sensitivity studies for the better understanding of the dynamics of frontal waves (*Horányi* and *Joly*, 1994). Regarding the dynamics of the model the improvement of the semi-Lagrangian scheme is of great importance. First of all a two-time level scheme is under implementation and later a more exact CUD-5 (compact upwind differencing) interpolation will be applied (*Tolstykh,* 1994, 1995). Another essential development is the creation of the non-hydrostatic version of the model. This work is based on the idea of *Laprise* (1992) introducing the hydrostatic pressure as vertical coordinate. This idea made it possible to transform the hydrostatic model into the non-hydrostatic one without deeply changing its basic structure (*Bubnová et al.*, 1995). The first results of the non-hydrostatic model are encouraging, which give a hope of its longer range operational applications. The climate version of the model is also under development and it is intended to participate in climate research projects by running ALADIN in climate mode.

Finally, it has to be mentioned that there is an international collaboration between Central-European countries (the participants are Austria, Croatia, Czech Republic, Hungary, Slovakia, and Slovenia) in order to establish a computer center where ALADIN can be launched operationally for the short range weather prediction purposes of the participating countries. This project is strongly supported by Météo-France, who made it possible to participate in the ALADIN project and allowed to use their computer power in the quasi-operational application of the model as well.

Acknowledgements—We would like to thank the whole staff of Météo-France in Toulouse for their hospitality and supports during the authors' stays in Toulouse. We are particularly grateful to the project leaders *Jean-Francois Geleyn*, *Alain Joly* and *Joel Hoffman* and also to *Emmanuel Legrand*. We also thank all ALADIN members for their contributions to the common work and among them *Sylvie Malardel*, who helped especially in practical questions. Furthermore, we would like to thank all Hungarian forecasters, who contributed to the work in some extent: *Imre Bonta, Szilvia Jenki* and *Ágnes Takács*. We are grateful for the support of the direction of HMS concerning the ALADIN project and it is a great pleasure to acknowledge the generous support of *Dr. Dezső Dévényi* and his particularly useful comments on the manuscript of the paper.

The ALADIN project was supported by different funds like the MICECO program, by the European Community, by the French Ministere de l' Enseignement Superieur et de la Recherche and also by the bilateral program called Balaton.

References

Boer, G.J., Mc Farlane, N.A., Laprise, R., Henderson, J.D. and *Blanchet, J.P.*, 1984: The Canadian Climate Centre spectral atmospheric general circulation model. *Atmos. Ocean 22,* 397-429.

Bougeault, Ph., 1985: Parameterization of cumulus convection for GATE. A diagnostic and semi-prognostic study. *Mon. Wea. Rev. 113,* 2108-2121.

Bubnová R., Horányi, A. and *Malardel, S.* 1993: International project ARPEGE/ALADIN. *EWGLAM Newsletter* 22, 117-130.

Bubnová, R., Hello, G., Benard, P. and *Geleyn, J.-F.*, 1995: Integration of the fully elastic equations cast in the hydrostatic pressure terrain-following coordinate in the framework of the ARPEGE/ALADIN NWP system. *Mon. Wea. Rev. 123,* 515-535.

Caian, M. and *Geleyn, J.-F.*, 1995: Some limits to the variable mesh solution and comparison with the nested LAM one. Submitted to *Quart. J. Roy. Meteorol. Soc.*

Courtier, Ph., Freydier, C., Geleyn, J.-F., Rabier, F. and *Rochas, M.*, 1991: The Arpege project at Météo-France. *Note de travail interne 'ARPEGE'.*

Courtier, Ph. and *Geleyn, J.-F.*, 1988: A global numerical weather prediction model with variable resolution: Application to shallow-water equations. *Quart. J. Roy. Meteorol. Soc. 114,* 1321-1346.

Davies, H.C., 1976: A lateral boundary formulation for multi-level prediction models. *Quart. J. Roy. Meteorol. Soc. 102,* 405-418.

Dévényi, D., Horányi, A., Ihász, I. and *Radnóti, G.*, 1992: Recent limited area modelling activities in Hungary. *EWGLAM Newsletter, 1992,* 47-50.

Geleyn, J.-F. and *Hollingsworth, A.*, 1979: An economical analytical method for the computation of the interaction between scattering and line absorption of radiation. *Beitr. Phys. Atmosph. 52,* 1-16.

Geleyn, J.-F., 1987: Use of a modified Richardson number for parameterizing the effect of shallow convection. *J. Meteor. Soc. Japan, Special NWP symposium issue,* 141-159.

Gustafsson, N. (ed.), 1993: HIRLAM 2 final report. *Technical report, c/o SMHI, S-601 76 Norrkoping, Sweden,* No. 9.

Horányi, A. and *Joly, A.*, 1994: Sensitivity studies using the doubly-periodic version of ARPEGE/ALADIN. *Abstract to the Second Workshop on Adjoint Applications in Dynamic Meteorology, 2-6 May, 1994, Visegrád, Hungary.*

Janiskova, M. 1994: Study of coupling problem. *Note ALADIN,* No. 1.

Laprise, R., 1992: The Euler equations of motion with hydrostatic pressure as an independent variable. *Mon. Wea. Rev. 120,* 197-207.

Louis, J.-F., Tiedke, M. and *Geleyn, J.-F.*, 1982: A short history of the PBL parametrization at ECMWF. *Proc. of the ECMWF workshop on planetary boundary layer parametrization, Reading, 25-27 Nov, 1981,* 59-80.

Lynch, P. and *Huang, X.Y.*, 1992: Initialization of the HIRLAM model using a digital filter. *Mon. Wea. Rev. 120,* 1019-1034.

Machenhauer, B. and *Haugen, J.E.*, 1987: Test of a spectral limited area shallow water model with time-dependent lateral boundary conditions and combined normal mode/semi-Lagrangian time integration schemes. In *Workshop Proceedings: Techniques for horizontal discretization in numerical weather prediction models; ECMWF, 2-4 November 1987,* 361-377.

Radnóti, G., 1995: Comments on: A spectral limited-area formulation with time-dependent boundary conditions applied to the shallow-water equations. *Mon. Wea. Rev. 123,* 3122-3123.

Ritter, B. and *Geleyn, J.-F.*, 1991: A comprehensive radiation scheme for numerical wether prediction models with potential applications in climate simulations. *Mon. Wea. Rev. 120,* 303-325.

Schmidt, F., 1977: Variable fine mesh in spectral global model. *Beitr. Phys. Atmos. 50,* 211-217.

Simmons, A. and *Burridge, D.*, 1981: An energy and angular momentum conserving vertical finite-difference scheme and hybrid vertical coordinates. *Mon. Wea. Rev. 109,* 2003-2012.

Temperton, C., 1979: Fast Fourier Transforms on Cray-1. *ECMWF internal report, 21.*

Tolstykh, M.A., 1994: Application of fifth-order compact upwind differencing to moisture transport equation in atmosphere. *J. Comput. Phys. 112,* 394-403.

Tolstykh, M.A., 1995: The response of the variable resolution semi-Lagrangian NWP model to the change of horizontal interpolation. Submitted to *Quart. J. Roy. Meteorol. Soc.*

APPENDIX

The governing equations of the model

According to the possible projections used by the model the horizontal momentum equations over the plane reads as follows:

$$\frac{\partial u}{\partial t} = \nu\varsigma - \nu\nabla^{u}\nu - u\nabla^{u}u - (u^2 + \nu^2)\, C_u(\varphi, \lambda) - \dot{\eta}\frac{\partial u}{\partial \eta} + f\nu - RT\,\nabla^{u}\ln p - \nabla^{u}\Phi - F^{u}$$

and

$$\frac{\partial \nu}{\partial t} = -\nu D - u\nabla^{u}\nu + \nu\nabla^{u}u - (u^2 + \nu^2)\, C_\nu(\varphi, \lambda) - \dot{\eta}\frac{\partial \nu}{\partial \eta} - fu - RT\,\nabla^{\nu}\ln p - \nabla^{n}\Phi - F^{\nu},$$

(A.1)

where u and ν are the wind components, R is the gas constant, T is the temperature, f is the Coriolis parameter, Φ is the geopotential and ∇^u and ∇^ν denote the physical component of the gradient of a given field. D and ς are the divergence and vorticity, C_u and C_ν are the curvature terms and F^u and F^ν represent the forcing terms or in other words all the terms which are described by the physical processes of the model. The most important physical processes are the vertical turbulent diffusion, vertical exchange of momentum due to convection, vertical transport of momentum due to unresolved gravity waves generated by the small scale changes of the orography, the tendency resulting from momentum transport by falling precipitation, radiative budget, heating or cooling due to condensation of rain in stratified or convective clouds, evaporation of rain and all processes described by considering two or three phases of water.

The hydrostatic equation reads as:

$$\frac{\partial \Phi}{\partial \eta} = -\frac{RT}{p}\frac{\partial p}{\partial \eta}. \qquad \text{(A.2)}$$

The mass conservation is expressed by the continuity equation, although for ARPEGE there is a possibility for the mass not to be conserved. In the latter case the mass changes are controlled by the precipitation-evaporation budget. Nevertheless, considering the total mass conservation (when the precipitating rain is replaced by air) the continuity equation reads as

$$\frac{\partial}{\partial t}\left[\frac{\partial p}{\partial \eta}\right] = -\nabla\left[V\frac{\partial p}{\partial \eta}\right] - \frac{\partial}{\partial \eta}\left[\dot{\eta}\frac{\partial p}{\partial \eta}\right], \qquad \text{(A.3)}$$

where V denotes the horizontal wind vector.

If this equation is vertically integrated over the whole depth of the model atmosphere and suitable boundary conditions are taken into account, the evolution equation of the surface pressure can be obtained:

$$\frac{\partial \pi}{\partial t} = -\int_0^1 \nabla \left[V \frac{\partial p}{\partial \eta} \right] d\eta . \qquad \text{(A.4)}$$

At an arbitrary η level using the definition of the vertical coordinate

$$\frac{\partial}{\partial t} \left[\frac{\partial p}{\partial \eta} \right] = \frac{dB(\eta)}{d\eta} \frac{\partial \pi}{\partial t} \qquad \text{(A.5)}$$

can be deduced and integrating it from the top of the model atmosphere down to level η, one gets the advecting vertical velocity

$$\left[\dot{\eta} \frac{\partial p}{\partial \eta} \right] = -B(\eta) \frac{\partial \pi}{\partial t} - \int_0^\eta \nabla \left[V \frac{\partial p}{\partial \eta} \right] d\eta . \qquad \text{(A.6)}$$

Finally by using the previous equations the pressure vertical velocity can also be expressed:

$$\omega = \frac{\partial p}{\partial t} + (V\nabla)p + \left[\dot{\eta} \frac{\partial p}{\partial \eta} \right] = B(\eta) V \nabla \pi - \int_0^\eta \nabla \left[V \frac{\partial p}{\partial \eta} \right] d\eta . \qquad \text{(A.7)}$$

The thermodynamical energy equation can be written as:

$$\frac{\partial T}{\partial t} = -V \nabla T - \dot{\eta} \frac{\partial T}{\partial \eta} + \frac{RT}{c_p} \frac{\omega}{p} . \qquad \text{(A.8)}$$

It is noted that for the calculation of gas constant and specific heat the humidity content of the atmosphere must also be considered.

IDŐJÁRÁS

Quarterly Journal of the Hungarian Meteorological Service
Vol. 100, No. 4, October–December 1996

A statistical model based on multiple regression applied to the prediction of air particle concentrations in the atmosphere

A. Boix[1], **J. Mateu**[2], **M. M. Jordán**[1] and **T. Sanfeliu**[1]

[1]*Departement de Ciencies Experimentals, Universitat Jaume I, Campus de Borriol,*
12080 Castellón, Spain.
[2]*Departament de Matematiques, Universitat Jaume I, Campus de Penyeta Roja,*
12071 Castellón, Spain.

(Manuscript received 15 May 1995; in final form 14 September 1995)

Abstract—A study of the statistical correlation was carried out between the air particle concentrations collected at two strategic points in the area of Castellón, using local weather parameters (wind speed, direction and air temperature). One of the stations was situated in Grao of Castellón, on the coast in the vicinity of an important industrial complex which houses an electricity generating plant, a petro-chemical plant and various auxilliary industries. The second station was installed in the city centre, where it is subject to diverse emissions of an urban nature (domestic heating systems, vehicles, construction work, infrastructural factors, etc.)

This paper intends to establish the most determinant variables of the air particle concentrations from each of the sample stations by means of the application of linear regression models. The independent variables of the first model are the normalized temperature, wind speed and direction data.

Differences were observed between the sample stations. At Grao station, the most influential meteorological parameter on air particle concentrations was wind direction, whilst wind speed and temperature were of secondary importance. However, in the case of the city centre station, the most important variable is undoubtedly the wind speed.

The second model consists of the previous model plus the SO_2 concentration level measured at the sample station itself. The importance of SO_2 as an independent variable was clearly seen at the city centre station (Herrero), since the multiple regression coefficient calculated for this second model, was larger. Therefore, after wind speed, SO_2 is seen to be the second determining factor in the air particle concentrations measured at Herrero station.

However, the SO_2 measured at the station located in Grao is not at all decisive for the proposed linear regression equation, being of much lesser importance than local meteorological parameters.

Key-words: statistical model, particle concentration, Spain, multiple regression.

1. Introduction

Within the study of atmospheric pollution, air pollution by air particles deserves a special mention for various reasons: it increases atmospheric opacity and reduces visibility, it enters the respiratory system, and it can act synergetically by increasing the toxic effects of other pollutants, etc.

The main anthropogenic sources of air particles are the manufacture of inorganic materials for use in the building industry (the production of cement, plaster, building materials, ceramics, etc.), extraction industries (mines and quarries) and public works. Other sources include combustion processes, residues proceeding from industries involving polishing or grinding of surfaces or the petrochemical industry. The true composition depends on the origin of the air particles. Air particles of an edaphic nature are principally composed of calcium, aluminium and silicate, elements which are common to mineral soils. Additionally, the smoke emanating from any combustion process gives rise to large quantities of suspended air particles. Secondary air particles are formed in the atmosphere from chemical compositions such as ammoniac salts, sulphates and nitrates.

Experimental evidence demonstrates that there exists a pronounced relationship between wind and the presence of solids in suspension in the atmosphere, be it in an urban or rural environment. *Boix* (1992), in a study carried out in the area of Castellón, noted that wind speed has a directly influence on the concentrations of air particles. In a study carried out in Brussels, *Hallez et al.* (1984) show a marked exponential relationship between wind and the presence of particles in suspension. Air particles can cause a wide range of material damage. *Matyniak* (1989) calculated the distribution of SO_2 concentrations in the air over Poland. Physical aspects of the atmospheric aerosol were described by *Jaenicke* (1984) in relation with some climatic effects. *Horvath et al.* (1989) determined, at up to eleven location in the town of Vienna, the mass size distribution of the aerosol. Many authors have undertaken studies of these effects, such as Graedel's study (*Graedel* and *Mcgill*, 1986) of the degradation of buildings and Del Monte and Leysen's specific study (*Del Monte*, 1987; *Leysen*, 1989) of their effect on monuments. Air particles accelerate the process of corrosion, especially in the case of compositions containing sulphur. The effects of air particles on plant life have been studied by Harrison (*Harrison et al.*, 1989), principally the decrease in photosynthesis caused by impeding the penetration of the necessary quantities of sunlight, and therefore inhibiting growth. Studies have also appeared dealing with the influence of air particles on public health (see *Rondia* and *Closset,* 1985; *Liu et al.*, 1988). Air particles enter the human body almost exclusively through the respiratory system, and it is this which is most readily affected. *Lipnick* (1991) defined a mathematical relationship between chemical structure and toxicity using statistical models.

Castellón, a Spanish town situated on the Mediterranean coast, has two important nuclei of inhabitants, the Grao area situated at the coast and the town proper situated some 3 km inland to the west. The town centre is little affected by emissions into the atmosphere from the large industrial centres. Pollution there is ostensibly the product of vehicle and domestic heating emissions, as well as particle emissions caused by urban construction and works.

Without question, the Grao of Castellón is one of the most important industrial areas situated locally. It includes a petrochemical complex and power station. Other important industrial areas in the province are Almazora, Villarreal, Nules, Alcora and Onda, which together constitute one of the most important concentrations of ceramic tile industry in the world.

Two sampling sites were established in the following colleges: Herrero (in the center of the city) and Grao de Castellón. The geographic location of these sites can be found on the map accompanying this study (*Fig. 1*). In each of these sampling sites daily readings of sulphur dioxide and particle concentration levels were taken throughout 1993. Measurements were taken every 24 hours. Furthermore, data relating to direction and speed of wind and air temperature was collected at a site located in El Mijares Industrial Estate (see map).

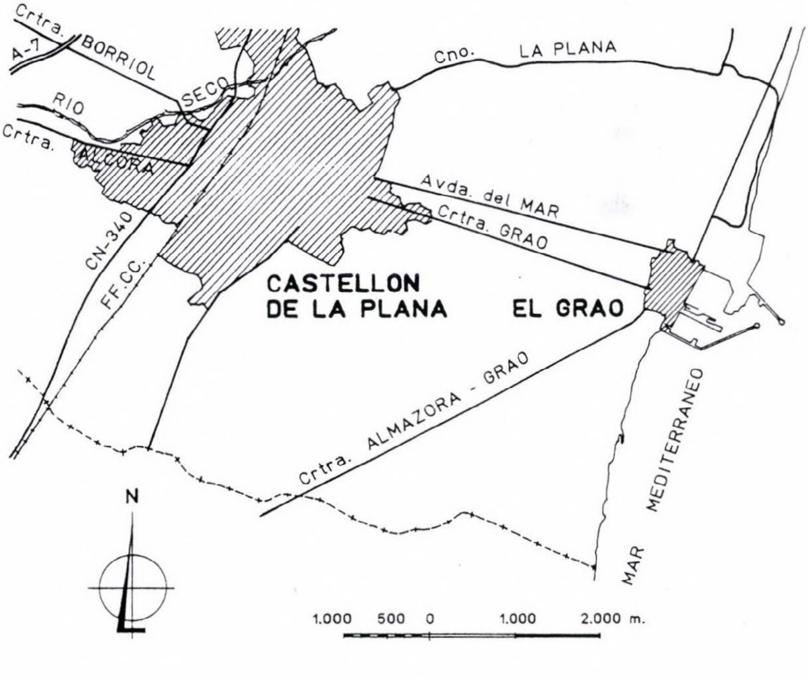

Fig. 1. Geographic location of the sampling sites.

2. *Experimental*

The samples taken provide data representing atmospheric pollution by SO_2 and particles in suspension. They were gathered using an MCV low volume detector of the type CPV-8 D/A, a model designed to detect sulphur dioxide and smoke (particle size < 11 μm), and with eight separate sampling periods. Samples were taken at the rate of 3 m^3/minute, and the filter papers were of 7 cm diametre Whatman No. 1. Sampling was done over a 24 hour period.

The technique used in determing the levels of emission of particles in suspension was that known as high volume sampling. SO_2 emission levels were determined using Thorina technical analysis.

The hourly data for wind speed and direction were obtained using a Fuess 90z-22E anemocinemograph which permitted the permanent register of wind data, its intensity and direction. The sensory devices of the anemocinemograph include a wind direction vane and an anemometre housing for measuring intensity. Measurements can be transmitted electrically. The range of wind intensity readings is between 0–40 m/s. The corresponding inscription needle responds electronically in one second.

3. *Statistics*

3.1 Multiple regression models

Multiple linear regression extends bivariate regression by incorporating multiple independent variables. The model can be expressed as:

$$Y_i = \beta_0 + \beta_1 X_{1i} + \beta_2 X_{2i} + \ldots + \beta_p X_{pi} + e_i \, .$$

The notation X_{pi} indicates the value of the pth independent variable for case i. The β terms are unknown parameters and the e_i terms are independent random variables that are normally distributed with mean 0 and constant variance σ^2. The model assumes that there is a normal distribution of the dependent variable for every combination of the values of the independent variables in the model (*Anderson*, 1984; *Draper* and *Smith*, 1981).

When working with several independent variables, it is important to calculate a correlation matrix for all variables. Remember that the correlation coefficient is a measure of the linear association between two variables. Particularly note that any large intercorrelations between the independent variables can substantially affect the results of multiple regression analysis (*Hoskuldsson*, 1988).

The F test associated with the analysis of variance table is a test of the null hypothesis that $\beta_1 = \beta_2 = \ldots = \beta_p = 0$. In other words, it is a test of whether there is a linear relationship between the dependent variable and the entire set of independent variables. In multiple regression, the coefficients labeled B are called *partial regression coefficients* since the coefficient for a particular variable is adjusted for other independent variables in the equation.

It is also inappropriate to interpret the B's as indicators of the relative importance of variables. The actual magnitude of the coefficients depends on the units in which the variables are measured. Only if all independent variables are measured in the same units are their coefficients directly comparable. When variables differ substantially in units of measurement, the sheer magnitude of their coefficients does not reveal anything about relative importance. One way to make regression coefficients somewhat more comparable is to calculate *Beta weights*, which are the coefficients of the independent variables when all variables are expressed in standardized (Z-score) form. The Beta coefficients can be calculated directly from the regression coefficients using

$$BETA_k = B_k \left(\frac{S_k}{S_y} \right) ,$$

where S_k is the standard deviation of the kth independent variable.

Another way of assessing the relative importance of independent variables is to consider the increase in R^2 when a variable is entered into an equation that already contains the other independent variables. This increase is $R^2_{change} = R^2 - R^2_{(i)}$, where $R^2_{(i)}$ is the square of the multiple correlation coefficient when all independent variables except the ith are in the equation. A large change in R^2 indicates that a variable provides unique information about the dependent variable that is not available from the other independent variables in the equation. The signed square root of the increase is called the *part correlation coefficient*. It is the correlation between Y and X_i when the linear effects of the other independent variables have been removed from X_i. If all independent variables are uncorrelated, the change in R^2 when a variable is entered into the equation is simply the square of the correlation coefficient between that variable and the dependent variable. The square of the part coefficient tells only how much R^2 increases when a variable is added to the regression equation. It does not indicate what proportion of the unexplained variation this increase constitutes. If most of the variation had been explained by the other variables, a small part correlation is all that is possible for the remaining variable. It may therefore be difficult to compare part coefficients.

A coefficient that measures the proportional reduction in variation is

$$P_{\eta^2} = \frac{R^2 - R^2_{(i)}}{1 - R^2_{(i)}} .$$

The numerator is the square of the part coefficient; the denominator is the proportion of unexplained variation when all but the *i*th variable are in the equation. The signed square root of P_{η^2} is the *partial correlation coefficient*. It can be interpreted as the correlation between the *i*th independent variable and the dependent variable when the linear effects of the other independent variables have been removed from both X_i and Y. Since the denominator of P_{η^2} is always less than or equal to 1, the part correlation coefficient is never larger in absolute value than the partial correlation coefficient.

The null hypothesis that the true population value for the change in R^2 is 0 can be tested using

$$F_{change} = \frac{R_{change}{}^2\,(N - p - 1)}{q(1 - R^2)},$$

where N is the number of cases in the equation, p is the total number of independent variables in the equation, and q is the number of variables entered at this step. Sometimes, this is referred to as a partial F test. Under the hypothesis that the true change is 0, the significance of the value labeled F_{change} can be obtained from the F distribution with q and N-p-1 degrees of freedom.

The hypothesis that the real change in R^2 is 0 can also be formulated in terms of the β parameters. When only the *i*th variable is added in a step, the hypothesis that the change in R^2 is 0 is equivalent to the hypothesis that β_i is 0. The F value printed for the change in R^2 is the square of the t value displayed for the test of the coefficient. When q independent variables are centered in a single step, the test that R^2 is 0 is equivalent to the simultaneous test that the coefficients of all q variables are 0.

When highly intercorrelated independent variables are included in a regression equation, results may appear anomalous. The overall regression may be significant while none of the individual coefficients are significant. High correlations between independent variables inflate the variances of the estimates, making individual coefficients quite unreliable.

Including irrelevant variables to the equation increases the standard errors of all estimates without improving prediction. On the other hand, it is important not to exclude potentially relevant independent variables. It is needed to use a procedure for selecting variables. The most commonly procedures used are: *forward selection*, *backward elimination* and *stepwise regression*. None of these variable selection procedures is 'best' in any absolute sense. We shall focus on stepwise selection.

Stepwise selection of independent variables is really a combination of backward and forward procedures and is probably the most commonly used method. The first variable considered for entry into the equation is the one with the largest positive or negative correlation with the dependent variable. The F test for the hypothesis that the coefficient of the entered variable is 0 is then calculated. To determine whether this variable is entered, the F value is compared to an established criterion. One criterion is the minimum value of the F statistic that a variable must achieve in order to enter, called *F-to-enter* (FIN). The other criterion is the probability associated with the F statistic, called *probability F-to-enter* (PIN). If the variable fails to meet entry requirements, the procedure terminates with no independent variables in the equation. If it passes the criterion, the second variable is selected based on the highest partial correlation. If it passes entry criteria, it also enters the equation.

After the first variable is entered, it is examined to see whether it should be removed according to the removal criterion. Two removal criteria may be considered. The first is the minimum F value (FOUT) that a variable must have in order to remain in the equation. Variables with F values less than this *F-to-remove* are eligible to removal. The second criterion is the maximum probability of *F-to-remove* (POUT) a variable can have.

In the next step, variables not in the equation are examined for entry. After each step, variables already in the equation are examined for removal. Vyariables are removed until none remain that meet the removal criterion. To prevent the same variable from being repeatedly entered and removed, PIN must be less than POUT (or FIN greater than FOUT). Variable selection terminates when no more variables meet entry and removal criteria.

3.2 Searching for violations of assumptions

It is don't known in advance whether a regression model is appropriate. Therefore, it is necessary to conduct a search focused on residuals to look for evidence that the necessary assumptions are violated.

3.2.1. Independence of error

Whenever the data are collected and recorded sequentially, you should plot residuals against the sequence variable. Even if time is not considered a variable in the model, it could influence the residuals. If sequence and residual are independent, a discernible pattern should not be seen.

The Durbin-Watson statistic, a test for sequential correlation of adjacent error terms, is defined as

$$D = \frac{\sum_{t=2}^{N} (E_t - E_{t-1})^2}{\sum_{t=1}^{N} E_t^2} .$$

Small values of D indicate positive correlation and large values of D indicate negative correlation. Values of D about 2 indicate absence of correlation.

3.2.2. Linearity and equality of variance

It is convenient to plot the residuals against the predicted values. If the assumptions of linearity and homogeneity of variance are met, there should be no relationship between the predicted and residual values. Residuals can also be plotted against individual independent variables. Again, if the assumptions are met you should see a horizontal band of residuals.

The previously described plots can also be used to check for violations of the equality of variance assumption. If the spread of the residuals increases or decreases with values of the independent variables or with predicted values, you should question the assumption of constant variance of Y for all values of X.

3.2.3. Normality

One of the most important assumptions for a regression model is the normality of all the variables, dependent and independent, and the normality of the residuals (e_i). In advance, several transformations of variables to achieve normality has been conducted (see which are the variables used and their transformations). Once the variables used in the model are normal, we have to look at the residuals.

The distribution of residuals may not appear to be normal for reasons other than actual non-normality: misspecification of the model, nonconstant variance, a small number of residuals actually available for analysis, etc. One line of investigation is to construct a histogram of the residuals.

3.2.4. Looking for influential points

Before interpreting the results of a regression analysis, it is a good idea to find out whether the data contain observations that violate important assumptions. When there are several independent variables, one or more multivariate outliers may distort the analysis. To identify these unusual observations different diagnostic statistics need to be considered. The diagnostics fall roughly into three groups:

(a) *Residual statistics* identify potential outliers in the dependent variable (Y).

(b) *Leverage statistics* identify potential outliers in the independent variables.

(c) *Influence statistics* combine the effects of leverage and residuals to identify influential cases.

Observations having either extreme leverage or large residuals are said to be potentially influential. Influence statistics confirm whether or not the potentially influential cases exert undue force on the regression.

3.2.4.1 *Leverage measures*

Hatdiag Diagonal elements of the 'hat', or projection, matrix (h_{ii}). The h_{ii} vary between $1/n$ and 1, with an average value of p/n. X is the ($n \times p$) matrix of centered independent variables; x^t_i is the ith row of X:

$$(1/n) + x_i^t (X^t X)^{-1} x_i .$$

Mahal Mahalanobis distance: the distance of each case to the mean of all cases used in the regression equation. Computed using only the independent variables:

$$(n - 1) \left[h_{ii} - \frac{1}{n} \right] .$$

3.2.4.2 *Residual measures*

Residual The usual residual $e_i = y_i - \hat{y}_i$.

Stresid The standardized residual, $r_i = \dfrac{e_i}{\hat{\sigma} \sqrt{1 - h_{ii}}}$, is the usual residual divided by an estimate of its standard error.

3.2.4.3 *Influence measures*

Cook Cook's distance is a measure of the influence of the ith case on the estimated regression coefficients:

$$\frac{e_{(i)}{}^2 h_{ii}}{p \hat{\sigma}^2} .$$

3.2.5. *Measures of co-linearity*

Co-linearity refers to the situation in which there is a high multiple correlation when one of the independent variables is regressed on the others. The tolerance of a variable is a commonly used measure of co-linearity. The tolerance (TOL) of variable i is defined as $1 - R^2_i$, where R_i is the multiple correlation coefficient when the ith variable is predicted from the other independent variables. If the tolerance of a variable is small, it is almost a linear combination of the other independent variables.

4. Original and transformed variables used in the models

The original variables considered in this study are: *Partgrao* (Particle concentration for Grao sampling site), *Partherr* (Particle concentration for Herrero sampling site); SO_2grao (SO_2 concentration for Grao sampling site), SO_2her (SO_2 concentration for Herrero sampling site); *Direc* (wind direction), *Tempseco* (air temperature) and *Veloc* (wind speed) as meteorological parameters.

Different tests of normality have been conducted to conclude that the only normal variable is Tempseco.

Following different methods of transformations of variables to achieve normality, the normal transformed variables are:

$$rpargra = \sqrt{Partgrao} \qquad rparher = \sqrt{Partherr} \qquad rSO_2gra = \sqrt{SO_2grao}$$

$$rSO_2her = \sqrt{SO_2\,her} \qquad tddirec = \frac{(Direc)^2 - 1}{2} \qquad \mathrm{ln}tdvel = \ln(2\sqrt{Veloc + 2}\ .$$

Finally, needless to say that the models have been worked out using the transformed variables.

5. Results and discussion

The correlation matrix between the variables is shown in *Table 1.*

Table 1. Correlation matrix

Correlation	tddirec	lntdvel	tempseco	rparher	rpargra	rSO_2her	rSO_2gra
tddirec	1	0.013	- 0.176	0.175	0.336	0.064	0.016
lntdvel		1	0.328	-0.372	-0.285	-0.044	-0.051
tempseco			1	-0.285	-0.336	-0.147	-0.142
rparher				1	0.594	0.263	0.021
rpargra					1	0.185	0.004
rSO_2her						1	0.467
rSO_2gra							1

The low level of linear relationship between the independent or explicative variables can be seen, thus avoiding possible problems of multico-linearity.

Here are the two models of linear regression:

Model 1: Air particle concentration = f (meteorological parameters),
Model 2: Air particle concentration = f (meteorological parameters, SO$_2$ concentration).

Using the stepwise method, the regression parameters are seen in *Table 2*.

Table 2. Linear regression models

	Linear equation	Multiple R
Model 1	rparher = –0.324 lntdvel + 0.149 tddirec – 0.152 tempseco	0.4353
	rpargra = 0.302 tddirec – 0.22 lntdvel – 0.21 tempseco	0.4846
Model 2	rparher = –0.324 lntdvel + 0.228 rSO$_2$her + 0.14 tddirec – 0.12 tempseco	0.4902
	rpargra = 0.302 tddirec – 0.22 lntdvel – 0.21 tempseco	0.4846

5.1 Model 1

(a) Model 1.1 (Herrero station)

The results given by Model 1 for Herrero station are presented in *Table 3*.

Table 3. Results for Model 1.1

	Variables entered on step number		
Model 1.1	1. lntdvel	2. tddirec	3. tempseco
Multiple R	0.372	0.412	0.435
F(Sig. F)	57.398(0.0)	36.372(0.0)	27.678(0.0)
Coefficient B	–2.135(b_1) 9.196(b_0)	–2.148(b_1) 0.003(b_2) 8.492(b_0)	–1.859(b_1) 0.002(b_2) –0.045(b_3) 8.979(b_0)
Coefficient Beta	–0.372(Beta1)	–0.374(Beta1) 0.176(Beta2)	–0.324(Beta1) 0.149(Beta2) –0.152(Beta3)
T(Sig. T)	b_1 –7.576(0.0) b_0 24.027(0.0)	b_1 –7.753(0.0) b_2 3.655(0.0) b_0 20.08(0.0)	b_1 –6.389(0.0) b_2 3.062(0.003) b_3 –2.952(0.004) b_0 19.969(0.0)

The first independent variable, lntdvel, selected is the one which shows the greatest correlation with rparher, explaining 37.2% of the variability of the latter. The correlation is statistically significant (F = 57.398, Sig. F = 0.00). The linear model with this single variable turns out in the following way.

The coefficient B1 = –2.135 is statistically significant, that is, different from zero (T = –7.576, Sig. T = 0.0).

The second variable which enters into the model is tddirec, which together with lntdvel explains 41.2% of the variability of rparher. The multiple model with these two variables is significant (F = 36.37, Sig. F = 0.0) as are the respective beta coefficients. The co-linearity diagnostics indicate the low level of linear dependence between the two independent variables.

Finally, the variable tempseco enters into the model. The linear regression equations, described in Tables 2 and *3*, are significant and the independence requirements.

We may consider the independence of the errors since the Durbin Watson test provides a value of 1.4121. On the other hand, randomness can be seen in the different graphs for the study of linearity and equality of variables which confirms this hypothesis (see *Fig. 2*). The fundamental prerequisite of normality is fulfilled, and is confirmed by both the histogram graph for the residues and the Kolmogorov-Smirnov test (K-S Z = 0.858, 2-tailed P = 0.454), see *Fig. 3*. Different outliers are detected, both by Mahalanobis' distance and Cook's, but none are significant enough to distort the results.

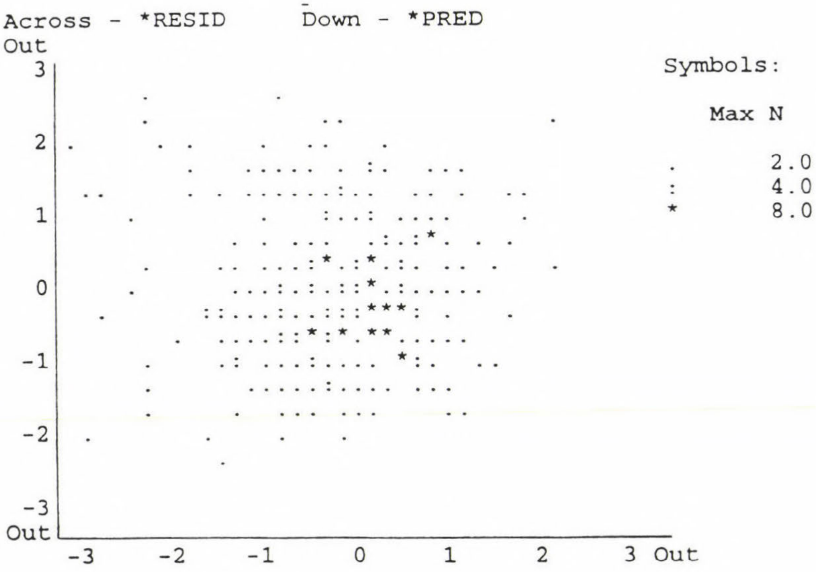

Fig. 2. Model 1.1 Standardized scatterplot.

```
 N Exp N        (* = 1 Cases,     . : = Normal Curve)
 2   .28   Out **
 0   .55  3.00 .
 0  1.40  2.67 .
 2  3.20  2.33 **.
 6  6.55  2.00 ******.
 5 12.00  1.67 *****      .
15 19.70  1.33 ***************    .
32 28.96  1.00 ****************************:***
45 38.13   .67 *************************************:*******
61 44.98   .33 ********************************************:****************
48 47.52   .00 ***********************************************:
42 44.98  -.33 ******************************************  .
37 38.13  -.67 *************************************.
24 28.96 -1.00 ************************    .
19 19.70 -1.33 *******************.
 6 12.00 -1.67 ******     .
 3  6.55 -2.00 ***   .
 6  3.20 -2.33 **:***
 3  1.40 -2.67 :**
 2   .55 -3.00 :*
 1   .28   Out *
```

Fig. 3. Model 1.1 Histogram-standardized residual.

(b) Model 1.2 (Grao station)

The results given by Model 1 for Grao station are presented in *Table 4*.

Table 4. Results for Model 1.2

Model 1.2	Variables entered on step number 1. tddirec	2. lntdvel	3. tempseco
Multiple R	0.336	0.443	0.484
F(Sig. F)	45.412(0.0)	43.639(0.0)	36.317(0.0)
Coefficient B	$0.004(b_1)$ $2.946(b_0)$	$0.004(b_1)$ $-1.363(b_2)$ $4.734(b_0)$	$0.004(b_1)$ $-1.036(b_2)$ $-0.051(b_3)$ $5.286(b_0)$
Coefficient Beta	0.336(Beta1)	0.339(Beta1) -0.289(Beta2)	0.3027(Beta1) -0.2204(Beta2) -0.2101(Beta3)
T(Sig. T)	b_1 6.739(0.0) b_0 16.146(0.0)	b_1 7.152(0.0) b_2 -6.104(0.0) b_0 13.8960.0)	b_1 6.38(0.0) b_2 -4.472(0.0) b_3 -4.195(0.0) b_0 14.764(0.0)

In this case the variable which has the greatest correlation with rpargra is tddirec and as such occupies first place by explaining 33.59% of the variability of the dependent variable. The regression equation is significant (F = 45.41, Sig. F = 0.0) as is the coefficient B1. The next variable which enters into the model, and independently of tddirec, is lntdvel, and this, together with tddirec, explains 44.37%. The regression is once again significant. Last of all comes tempseco to give the full equation for Table 2. All the coefficients are statistically different from zero, producing a significant model for the explanation of rpargra.

There is no serial correlation for the errors (Durbin Watson = 1.382). In the corresponding graphs we can see the existence of linearity in the model as well as the equality of variances. The outliers that are found are not significant and do not influence the significance of the model. Finally, the normality of the residues is supported by the Kolmogorov-Smirnov test (K-S Z = 0.939, 2-tailed P = 0.341) and is shown by the histogram of the residues (*Fig. 4*).

```
 N Exp N         (* = 1 Cases,      . : = Normal Curve)
 1   .28   Out *
 1   .55  3.00 :
 0  1.40  2.67 .
 2  3.20  2.33 **.
 6  6.55  2.00 ******.
10 12.00  1.67 ********** .
19 19.70  1.33 *******************.
27 28.96  1.00 ***************************  .
41 38.13   .67 **************************************:***
57 44.98   .33 *********************************************:************
49 47.52   .00 ************************************************:*
48 44.98  -.33 *********************************************:***
32 38.13  -.67 ********************************      .
28 28.96 -1.00 ****************************.
11 19.70 -1.33 ***********         .
12 12.00 -1.67 ************:
 7  6.55 -2.00 ******:
 4  3.20 -2.33 **:*
 0  1.40 -2.67 .
 3   .55 -3.00 :**
 1   .28   Out *
```

Fig. 4. Model 1.2. Histogram-standardized residual.

(c) Model 1 — Conclusion

Both models are significantly statistical and validated by their residues. The variability explained by independent variables is based on a linear relationship. The rest could be explained by other kinds of non-linear relationships, such as quadratics or cubic relationships. The relationship between air particle concentration and wind direction is direct (positive) while its relationship with wind speed and temperature variables is inverse (negative).

The goodness of fit of Model 1 is expressed by the coincidence between the recorded and expected values in the Normal Probability Plot graph (*Fig. 5*).

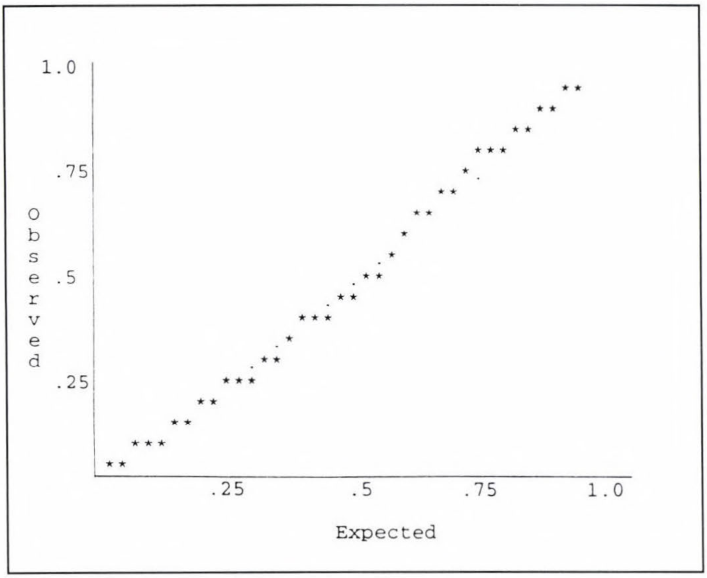

Fig. 5. Model 1.2. Normal probability plot.

5.2 Model 2

(a) Model 2.1 (Herrero station)

In spite of considering the influence of SO_2 in air particle concentrations at Herrero, wind speed remains, as in Model 1, the most important variable for the prediction of rparher. It accounts for 37.21% of the variability of this dependent variable. In second place comes the SO_2 variable, explaining, between the first two variables, 44.99% — more than the three atmospheric parameters explained in Model 1. Afterwards come the temperature and wind direction variables which give the linear equation of Table 2 and a percentage of overall explanation of 49.02%. This equation is significant (F = 27.99, Sig. F = 0.0) and the four explicative variables show a degree of linear independence between each of them (see *Table 5*).

Analysis of the residues shows that this proposed regression model is statistically valid. There is no serial correlation for the residues since the Durbin-Watson test gives a reading of 1.398. Equality of variances and linearity have been achieved. Normality is shown by means of the Kolmogorov-Smirnov test which gives readings of K-S Z = 1.013 and 2-tailed P = 0.256 and is expressed graphically by the histogram (*Fig. 6*). The outliers found are not significant.

Table 5. Results for Model 2.1

Model 2.1	Variables entered on step number			
	1. lntdvel	2. rSO_2her	3. tddirec	4. tempseco
Multiple R	0.372	0.449	0.478	0.49
F(Sig. F)	57.397(0.0)	45.19(0.0)	34.993(0.0)	27.99(0.0)
Coeff. B	$-2.135(b_1)$ $9.1958(b_0)$	$-2.071(b_1)$ $0.279(b_2)$ $7.961(b_0)$	$-2.085(b_1)$ $0.267(b_2)$ $0.002(b_3)$ $7.371(b_0)$	$-1.862(b_1)$ $0.252(b_2)$ $0.002(b_3)$ $-0.035(b_4)$ $7.823(b_0)$
Coeff. Beta	-0.372(Beta1)	-0.361(Beta1) 0.253(Beta2)	-0.364(Beta1) 0.243(Beta2) 0.161(Beta3)	-0.325(Beta1) 0.228(Beta2) 0.141(Beta3) -0.119(Beta4)
T(Sig. T)	b_1 -7.576(0.0) b_0 24.027(0.0)	b_1 -7.617(0.0) b_2 5.343(0.0) b_0 18.29(0.0)	b_1 -7.786(0.0) b_2 5.19(0.0) b_3 3.442(0.001) b_0 15.961(0.0)	b_1 -6.598(0.0) b_2 4.864(0.0) b_3 2.967(0.003) b_4 -2.37(0.018) b_0 15.75(0.0)

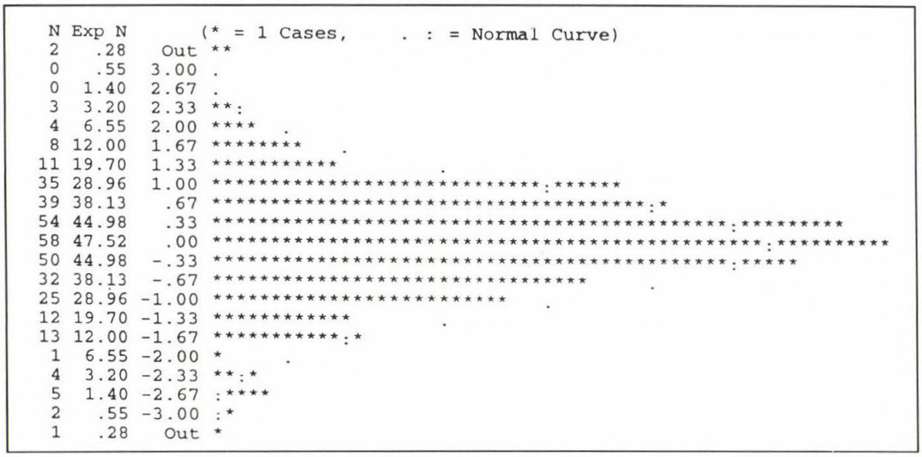

```
 N Exp N        (* = 1 Cases,     . : = Normal Curve)
 2   .28   Out **
 0   .55  3.00 .
 0  1.40  2.67 .
 3  3.20  2.33 **:
 4  6.55  2.00 ****  .
 8 12.00  1.67 ********   .
11 19.70  1.33 ***********        .
35 28.96  1.00 ****************************:******
39 38.13   .67 *************************************:*
54 44.98   .33 ********************************************:*********
58 47.52   .00 ***********************************************:**********
50 44.98  -.33 ********************************************:*****
32 38.13  -.67 ********************************     .
25 28.96 -1.00 *************************   .
12 19.70 -1.33 ************       .
13 12.00 -1.67 ***********:*
 1  6.55 -2.00 *     .
 4  3.20 -2.33 **:*
 5  1.40 -2.67 :****
 2   .55 -3.00 :*
 1   .28   Out *
```

Fig. 6. Model 2.1. Histogram-standardized residual.

(b) *Model 2.2 (Grao station)*

This model does not require any discussion as it matches exactly with the Model 1.2 described above.

(c) Model 2 – Conclusion

Model 2 is a statistically significant model, in that a substantial part of the variation of the dependent variable can be explained by the independent variables by means of a linear relationship. It is likely that if we introduced some other explicative variable such as atmospheric pressure, we would make a more accurate prediction of air particle concentration.

This model is validated by the residue analysis. Observe that the SO_2 concentration variable is of greater importance when predicting rparher than the meteorological parameters of wind direction and temperature. This, however, is not the case when predicting rpargra — the three meteorological parameters are more influential than SO_2.

The goodness of fit of Model 2 can be studied by observing the Normal Probability Plot graph (*Fig. 7*) in which the ideal case is where the values observed and expected are superimposed on the diagonal line of the rectangle.

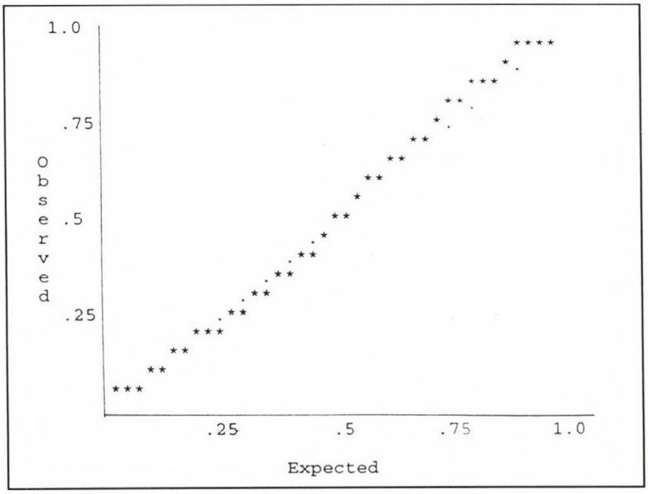

Fig. 7. Model 2.1. Normal probability plot.

5.3. Analysis of bivariate relationships for Grao station

1 [rpargra = f(lntdvel)]

On studying the evolution of air particle concentration in relation to wind speed (*Fig. 8*), it is seen that, at temperatures of below 18°C, there is a slight increase in air particle concentration until the threshold wind speed value of around 8.2 km/h is reached. At higher speeds air particle concentrations decrease for the whole range of wind directions, but less so for W, NW and N winds.

At temperatures of above 18 °C, asymptotic behaviour is seen between air particle concentrations and wind speed, reaching a relationship of independence between the two variables.

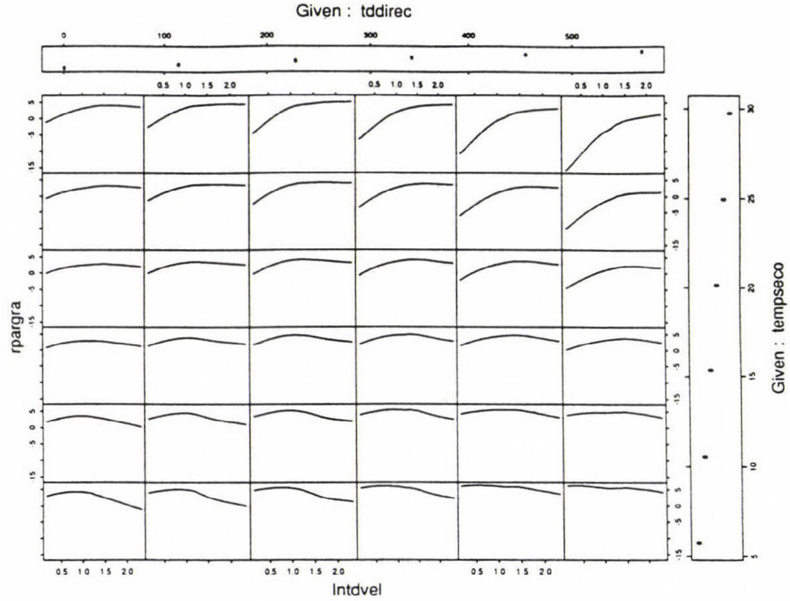

Fig. 8. Multiple linear regression of rpargra compared with lntdvel for tempseco and tddirec values.

2 [rpargra = f(tddirec)]

By studying the variation between air particle concentration and wind direction, we can observe three types of behaviour in relation to temperature, but without appreciable differences in its relationship with wind speed.

At temperatures below 14 °C, a slight increase in air particle concentration is noted in the presence of N and NW winds.

In the temperature range of 14–18 °C, air particle concentration remains stable, independently of wind direction.

At temperatures above 18 °C, a slight decrease in air particle concentration is observed when there is a change from winds of the first quadrant to those of the fourth. This is clearly seen when the evolution of air particle concentration is observed in the light of wind direction. At constant temperatures with wind speed rising progressively, it can be seen how wind direction becomes less decisive and wind speed gains importance.

3 [rpargra = f(tempseco)]

When we study the influence of temperature on the determination of air particle concentrations with different wind speeds and directions, a marked decrease in air particle temperatures is seen when there is an increase in temperature in the presence of W-NW and NW-N winds.

There is an increase in air particle concentrations as temperature increases when there are N-NE, NE-E and E-SE winds, throughout the whole range of wind speeds.

5.4 Analysis of bivariate relationships for Herrero station

1 [rparher = f(lntdvel)]

At temperatures of above 14°C with N-NW, NW-E, E-SE, SE-S and S-SW winds, a slight increase can be seen (*Fig. 9*) in the air particle concentration until wind speeds of between 6.5 and 10 km/h are reached. At this point, at speeds of over 10 km/h, a marked decrease in air particle concentration begins. At temperatures below 14°C with N-NW, NW-E, E-SE, SE-S and S-SW winds, the trend is similar to the previous case, although the decrease is less marked.

For W-NW and NW-N winds at temperatures of above 14°C, the curve develops two definite inflexion points — the first for wind speeds of 10 km/h and the second for 16 km/h. There is an initial stage (v = 3.24–10 km/h) with a decrease in contamination. At the second stage (v = 10–16 km/h) there is an increase in air particle concentration which later decreases during the third stage (v = 16–26.74 km/h). This same pattern is observed for NW-N winds at temperatures of below 14°C.

2 [rparher = f(tddirec)]

A slight increase in air particle concentration was seen with N-NE, NE-E, E-SE, SE-S and S-SW winds and slight decline with SW-W, W-NW and NW-N. These curves are slightly concave (*Fig. 10*).

At wind speeds below 6 km/h and at temperatures above 18°C, air particle concentrations remain constant in the presence of N-NE, NE-E, E-SE, SE-S and S-SW winds, but increase significantly when winds are SW-W, W-NW and NW-N.

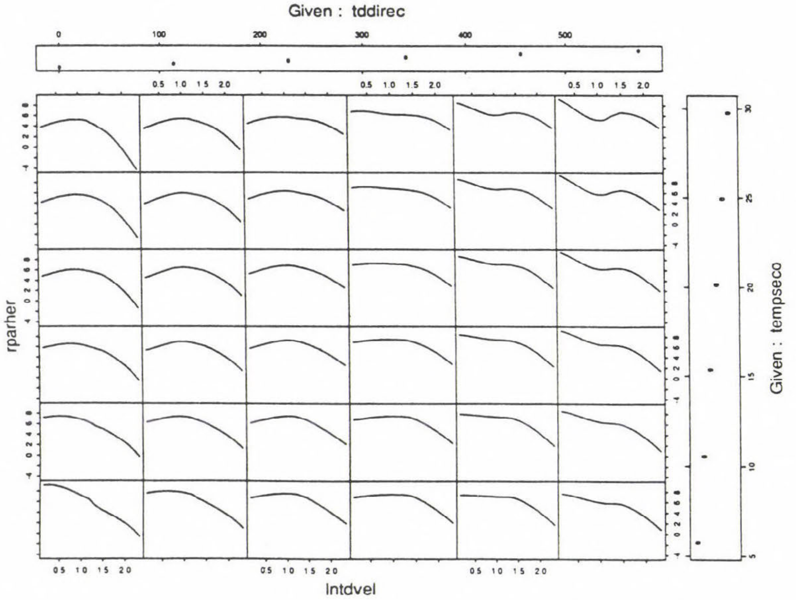

Fig. 9. Multiple linear regression of rparher compared with lntdvel for tempseco and lntdvel values.

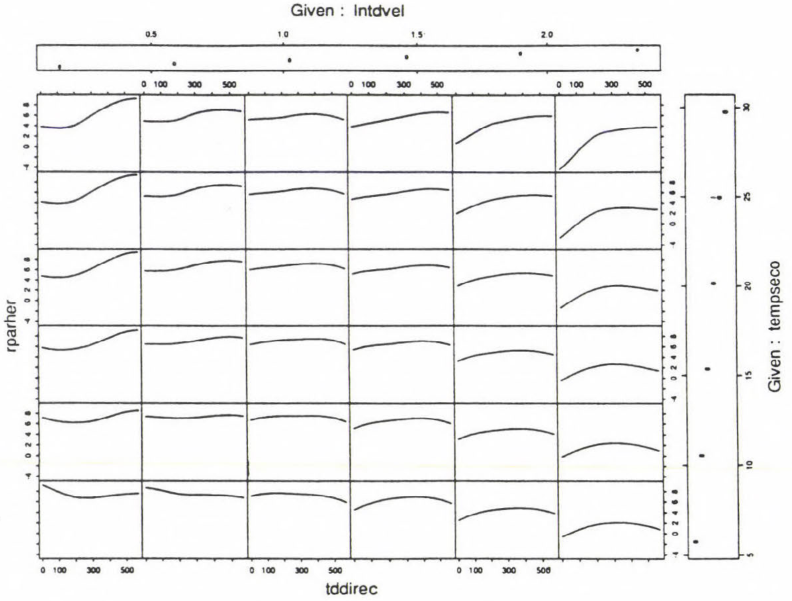

Fig. 10. Multiple linear regression of rparher compared with tddirec for tempseco and lntdvel values.

3 [rparher = f(tempseco)]

Generally speaking, a small decrease in air particle concentrations is noted when temperatures rise. As wind speed increases, we see a progressive decrease in air particle concentrations, also reflected in a lower vertical axis value as temperature rises.

4 [rparher = f(rSO_2her)]

(*a*) *Calm conditions*

The pattern of air particle concentrations with respect to SO_2 concentrations is of a convex nature, and this concavity increases with rises in temperature.

Initially, there is an increase in air particle concentration which rises alongside the increase in SO_2 concentrations until the maximum value for sulphur dioxide is reached. From then on, it starts to decrease (*Fig. 11*).

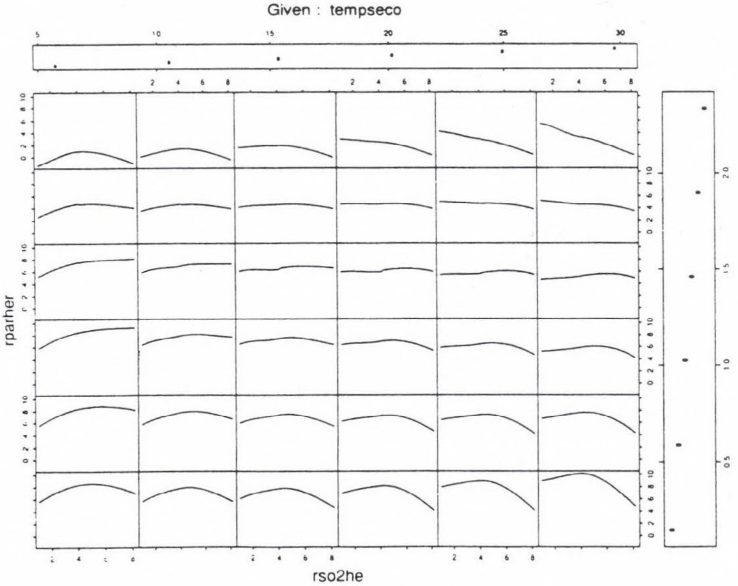

Fig. 11. Multiple linear regression of rparher compared with rSO_2her for lntdvel and tempseco values.

(*b*) *Medium-intensity wind conditions*

Air particle concentrations remain constant at a wide range of temperatures. In the case of T < 10°C, there is an increase in air particle concentrations when the SO_2 is rising, but these remain constant on reaching the maximum value.

(*c*) *Gusts of strong wind*

There is a marked decline in air particle concentrations when the SO_2 values increase.

5 [SO_2her = f(direc)]

SO_2 concentrations reach their maximum values when S, W and NW winds are blowing. Minimum SO_2 values are registered when E and SW winds are blowing. With other wind directions, SO_2 values vary irregularly.

4. Remarks

Model 1

(*a*) *Herrero*

For the proposed multiple regression equation, wind speed is a determining factor in the prediction of air particle concentrations in a linear model. Increases in wind speed are associated with a decline in air particle concentrations in the atmosphere. The atmosphere's ability to disperse pollutants is fundamentally connected to wind speed and to the presence of atmospheric turbulence which helps in their dispersion. Wind is the most important meteorological parameter given its ability to disperse pollutants and to keep air particles in suspension. Other less important climatic factors are temperature and wind direction. With this first model, a clear relationship between wind and the presence of air particles in suspension in the atmosphere was shown experimentally.

(*b*) *Grao*

In the multiple regression equation, it is clearly shown that wind direction is of fundamental importance for the prediction of air particle concentrations in a linear model. The local wind conditions operating in the area can explain the higher or lower levels of air particle concentrations recorded at any time. The remainder of the climatic factors analysed — wind speed and thermal gradient — are of lesser importance at this sampling station.

Model 2

(*a*) *Herrero*

For this model we have proposed a multiple linear regression equation in which we have included the sulphur dioxide concentration measured at this station as a variable. It has been established that sulphur dioxide concentrations have greater influence in the prediction of air particle concentrations than meteorological parameters such as wind direction and temperature. On the other hand, wind speed remains the most decisive independent variable in the proposed linear model.

The influence of sulphur dioxide on the measurement of air particle concentrations can be explained as a consequence of the presence of secondary or neo-formation air particles which appear in the atmosphere in the form of inorganic components, generally inorganic sulphate salts.

(*b*) *Grao*

The proposed multiple linear regression model establishes that there is no linear dependence between air particle concentrations and sulphur dioxide.

5. *Conclusions*

The proposed regression models are statistically significant and validated by their residues. As such, they can be taken into account when we predict air particle concentrations linearly. We have only dealt with the linear relationship although a large part of the variations in the dependent variables could be explained using a non-linear relationship. The accuracy of our predictions is affected by the R-square coefficient. Note how the R-square coefficient rises or the variation explained by the model when the new SO_2 variable in Model 2 is considered. This leads us to think of the possibility of considering relevant new variables in order to increase the explained variation and as such, improve the accuracy of our predictions.

The study of wind direction is important for making predictions for the measurement of air particle concentrations at Grao station.

Generally speaking, a decrease in air particle concentrations occurs when temperatures go up, if winds are blowing in the fourth quadrant, and they increase when they blow in the first, second and third quadrants.

In general, we see slight decreases in air particle concentrations when the temperature rises. In conditions of high wind density, SO_2 concentrations are not a determining factor in the prediction of air particle comtamination.

Finally, it is important to remark that those anomalies found in this work may have been caused due to the fact that a unique mathematical model has been used to explain the large variability of meteorological and environmental situations occurring throughout the year.

Acknowledgements—For the final version of this paper we are indebted to the interesting and detailed comments of referees.

References

Anderson, T.W., 1984: *An Introduction to Multivariate Statistical Analysis*. 2nd Edition. Wiley Series, 285-369.

Boix, A., 1992: Estudio la contaminación atmosférica en el área de Castellón y su relación con el regimen de vientos locales. *Tesis de Licenciatura*. Universitat Jaume I., Castellón.

Del Monte, M., 1987: The origin of calcium oxalates on historical buildings monuments and natural out crops. *The Science of the Total Environment 73*, 159-179.

Draper, N.R. and *Smith, H.*, 1981: *Applied Regression Analysis*. 2nd edition. John Wiley and Sons, New York.

Graedel, T.E. and *Mcgill, R.*, 1986: Degradation of materials in the atmosphere. *Env. Sci. Technol, 20,* 1093-1100.

Hallez, S., Goedertier, S. and *Derouane, A.*, 1984: Etude de l'evolution des concentrations en SO2 dans l'air ambiant a Bruxelles de 1968 a 1981. *The Science of the Total Environment 38*, 199-212.

Harrison, R. and *Chirgawi, M.B.*, 1989: The assessment of air and soil as contributors of some trace metals to vegetable plants. II. Translocation of atmospheric and laboratory generated cadmium aerosols and within vegetable plants. *The Science of the Total Environment 83*, 35-45.

Horvath, H., Havenreich, T.A., Kreiner, I. and *Norek, C.*, 1989: Temporal and spatial variations of the Vienna aerosol. *The Science of the Total Environment 83*, 127-159.

Hoskuldsson, A., 1988: PLS regression methods. *Journal Chemometrics 2*, 211-228.

Jaenicke, R., 1984: Physical aspects of the atmospheric aerosol. In *Aerosols and Their Climatic Effects* (eds.: *H.E. Gerber* and *A. Dee*). A. Deepak Publishing Hampton, Va., USA.

Leysen, L., 1989: Air pollution induced chemical decay of a sandy limestone cathedral in Belgium. *The Science of the Total Environment 78*, 263-278.

Lipnick, R.L., 1991: Outliers: Their origin and use in the classification of molecular mechanisms of toxicity. *The Science of the Total Environment 109-110*, 131-153.

Liu, W.K., Tam, J.S.K. and *Wong, M.H.*, 1988: Size dependent citotoxicity as fly ash particles. *Environment International 14*, 473-477.

Matyniak, Z., 1989: Contribution of SO_2 sortion on particulate surface to the air pollution level in the vicinity of coal-fired power plants. *The Science of The Total Environment 83*, 173-179.

Rondia, D. and *Closset, J.*, 1985: Aerosol versus solution composition in occupational exposures. *The Science of the Total Environment 46,* 107-112.

ANNEX

lntdvel	wind speed (km/h)
0.5	4.5
1.0	6.5
1.5	10.0
2.0	16.0
2.5	27.0

tddirec	wind direction (degrees)
0	10
100	135
200	190
300	233
400	270
500	300

rSO_2her	SO_2 concentration ($\mu g/m^3$)
2.0	7.82
4.0	21.00
6.0	40.82
8.0	67.00

rpargra	particle concentration ($\mu g/m^3$)
-15	0.00
-10	6.81
-5	27.20
0	61.30
5	109.00

rparher	particle concentration ($\mu g/m^3$)
-4	0.00
-2	3.02
0	11.90
2	26.62
4	47.19
6	73.61
8	105.88

IDŐJÁRÁS
Quarterly Journal of the Hungarian Meteorological Service
Vol. 100, No. 4, October–December 1996

Influence of terrain configuration on air pollutant concentration

Radmila Cvijović and **Viktor Pocajt**

Faculty of Technology and Metallurgy,
University of Belgrade,
Karnegijeva 4, Belgrade, Yugoslavia

(Manuscript received 15 May 1995; in final form 24 October 1995)

Abstract—This paper is concerned with the evaluation of air pollutant in situ concentration measurement data in Belgrade and the possibility of utilizing information obtained by physical modeling in air pollution prediction and air quality evaluation. The influence of meteorological parameters and objects layout on measurement results is discussed. The results are in accordance with the results of previous investigations, which showed significant influence of control station locations on errors in detecting in situ concentration values. With the advanced technique of physical modeling, it is possible to establish an optimal layout of control stations in air pollution monitoring.

Key-words: air pollution, measurements 'in situ', hydraulic modeling.

1. Introduction

The explanation of the influence of meteorological parameters on the air quality is very significant in solving air pollution problems in cities. If appropriate, scientifically grounded investigations and a well-organized network of control stations are provided, air pollution problem can be successfully analyzed. By using meteorological parameters, it is possible to show their influence on the concentration of pollutants in the atmosphere and to develop methods for prediction of air pollution.

A great number of papers have been presented in which air pollution is correlated to wind direction and velocity and atmosphere stability parameters (*Sonkin et al.*, 1965). It was already pointed out that air pollution diminishes in cities under conditions of increased wind. Maximum of pollutant concentrations was detected in the periods of weak wind and calm conditions. Theoretical and empirical investigations on diffusion from warm sources show the presence of 'danger', when maximum air pollution is detected in the plume trace. This indicates the relation of the pollutant concentrations with wind direction (*Berlyand*, 1975).

All investigations on the correlation between air pollution in cities and atmospheric stability agree that increased atmospheric stability results in increased air pollution. This conclusion was drawn as a consequence of investigating dominantly low sources. Investigations on atmospheric pollution from high, warm sources lead to the opposite results: in most cases, the pollutant concentrations increase with increasing turbulence and instability. In conditions of low wind velocity, the effect of plume rise is more significant and the site concentration is decreased.

In cities with a larger number of low sources, a significant increase in the air pollution level is detected in the wind velocity range between 1 and 2 m/s. According to measurement data from several cities (*Bezuglaya*, 1986), the average level of air pollution by particles, SO_x and NO_x is increased by 30–140%, compared to levels recorded under conditions of other wind velocities. In the latest investigations, where the average daily SO_x concentrations are correlated with different meteorological parameters, influence of wind has been definitely established and only its significance varies (*Annand* and *Hudson*, 1981).

In monitoring air pollution levels and the influence of human activities on their changes, different reports have been made. These reports and data are bases for the implementation of solutions oriented to decrease atmospheric pollution. Chosen alternatives and solutions, therefore, depend highly on the air pollution reports and data reliability.

2. Investigations and results

This paper is concerned with the evaluation of data, originating from air pollutant in situ concentration measurement data in Belgrade, and the possibility of utilizing the information obtained by physical modeling in air pollution prediction and establishing the optimal control stations layout. Application of modeling enables the investigation and simulation of atmospheric diffusion phenomena under various flow conditions and neutral atmosphere stability (*Cleroux et al.,* 1981; *Alessio et al.*, 1983).

Basic idea was to handle complexity of the air quality determination problem by using the possibilities of hydraulic modeling and to investigate simultaneously and under the same conditions influence of meteorological parameters and terrain configuration on SO_2 concentration.

In situ SO_2 concentration measurements were performed during three months, in winter of 1981, at two locations in Belgrade (the corner of Ivana Milutinovića and Sv. Save streets, and in front of the Main Post building).

Total of 60 air samples was taken by Cassela samplers, and SO_2 concentration was determined by the pararosanilyne method. Test models were made, which were imposed to fluid flow, in regimes analogous to the conditions of mild and moderate wind. In the hydraulic channel (4.5 m long and 0.85 m wide) with recirculation, wind was simulated by water flow and the pollutant was simulated by methylene blue color, released from a point source-stack. The pollutant (i.e. color) concentration was detected indirectly, by measuring color intensity on white adsorbent. Thin sondes, coated with white adsorbent silica gel, were posed at marked places. Adsorption method gives very reliable information on the color concentration above the sonde and, since the diameter of the sonde is only 2 mm, it does not affect fluid flow. The turbulence, which originates from fluid bypassing the objects, is affected only by the terrain configuration and fluid flow, and results in mass transfer, which is analogous to momentum transfer (*Končar-Đurđević*, 1953; *Cvijović*, 1982; *Cvijović* and *Cvijović*, 1992).

The crossroads model

The plume rise above the building is shown in *Fig. 1*; the concentration near to the 'ground' is lower. More intensive wind leads to plume drop and higher pollutant concentrations near the ground and in local turbulence zones.

The pollutant concentration distribution was controlled in situ (*Fig. 2,* measurement units 1 to 4). The dominant wind directions for Belgrade are east-southeast (ESE) and west-northwest (WNW).

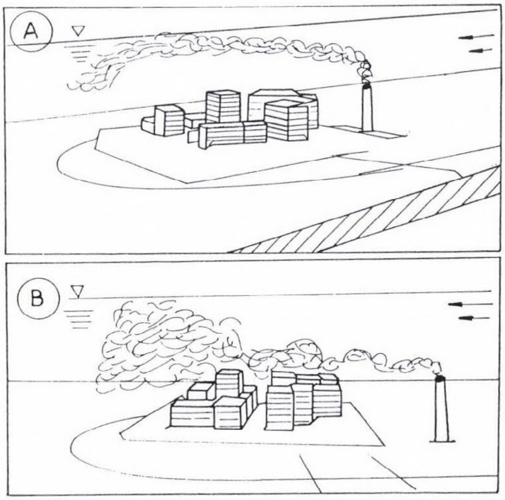

Fig 1. Model with stack in the hydraulic channel.
(*a*) mild wind conditions (Re = 2000); (*b*) moderate wind conditions (Re = 5300).

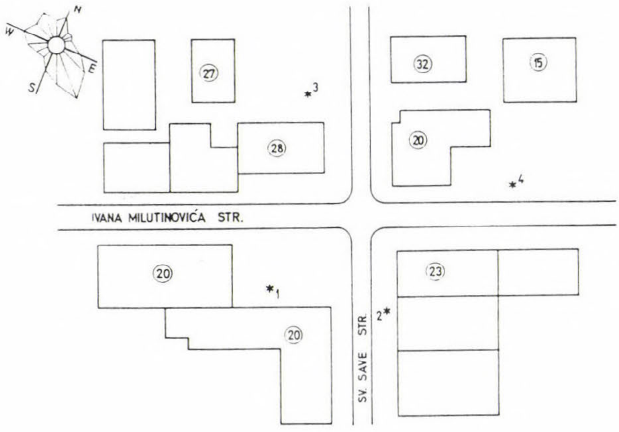

Fig 2. Scheme of the crossroads model, with the measurement units (*) and building height, in meters (numbers in circle). Orientation corresponds to dominant wind directions (ESE and WNW).

The source of the pollutant is the local boiler room stack. Measurement unit 1, managed by the City Health Institute, has been used for air quality control purposes for several years. In order to prove in situ concentration dependence on the meteorological conditions and on the measurement unit position, we posed samplers at the marked places and simultaneously measured SO_2 concentration. Results, in the form of average relative concentration (i.e., the quotient of concentration and average concentration), are shown in *Fig 3*. Histograms are plotted for mild (a) and moderate wind (b) conditions, with parallel model and terrain data.

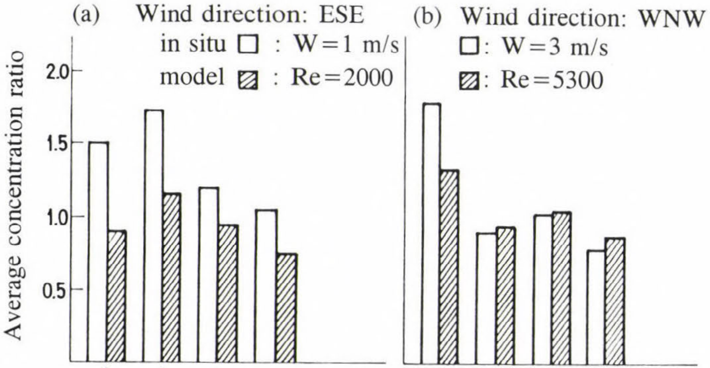

Fig 3. Concentration histogram (corner of Ivana Milutinovića and Sv. Save streets), for mild (*a*) and moderate wind (*b*) conditions.

The agreement of the model results with reality is good, specially for ESE wind direction. Measured pollutant concentration differs for different measurement units. For case (a), measurement unit 1 is the closest to the average concentration (four measurement units), but for case (b) (wind direction WNW) unit 3 is the most representative. It can be concluded that the pollutant distribution on measurement units varies for different wind directions.

For determining the influence of the meteorological parameters on SO_2 concentration, relations between the concentrations for the same wind velocity but different directions were calculated on the basis of model data. In that conditions, concentrations differ by a factor of 1.36.

The influence of the wind velocity was estimated in the same manner, by using model data for the same wind direction but different velocities. Concentration ratio varies by up to 1.26 times.

The influence of the measurement unit position was estimated using the maximum and minimum pollutant concentration ratio. For in situ measurements and ESE wind, the ratio is 1.6; for model measurement and the same wind, the ratio is 1.62.

It can be concluded that for a 'canyon' crossroads wind direction and velocity have similar significance, but the unit position on the measured pollutant concentration is the most significant parameter.

The Main Post model

This model is different from the previous one, since there is no street 'canyon'. In the wind direction (ESE), there is a wide area in the front of the House of Parliament and the park. The pollutant distribution was measured with three units in December, 1979 and January, 1980. The SO_2 source is the local boiling room stack on the Main Post building. The model, which reproduces terrain situation and measurement units layout is shown in *Fig. 4*.

The average concentration ratio (ratio of measured concentrations and average concentration) for ESE wind is shown in the histogram (*Fig. 5*). It can be noticed that with increasing distance from the source, the pollutant concentration decreases. In situ and model measurements are in good accordance for moderate velocity wind from the same direction. High concentration was detected by measurement unit 1, in the 'building shadow' zone, which provides conditions for concentrating the pollutant.

Interesting in situ measurement results were obtained for high wind velocity (up to 13,6 m/s). The concentration measured by unit 1 was slightly decreased, but by units 2 and 3 was increased. This is probably caused by the plume dropping effect - higher wind velocity increases SO_2 concentration. Unfortunately, model measurements for conditions of very strong wind were not performed, due to limited possibilities of flow regulation in the hydraulic channel.

The influence of the wind velocity, described by the ratio of maximal to minimal in situ concentration is significant: the ratio difference is 1.58 times.

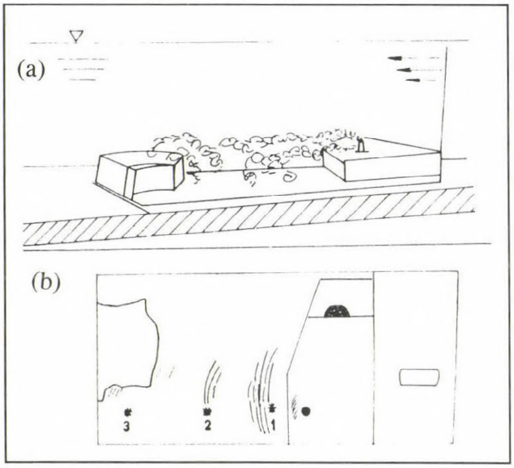

Fig. 4. Model in the hydraulic channel. (*a*) moderate wind velocity (Re = 5300); (*b*) model with measurement units layout.

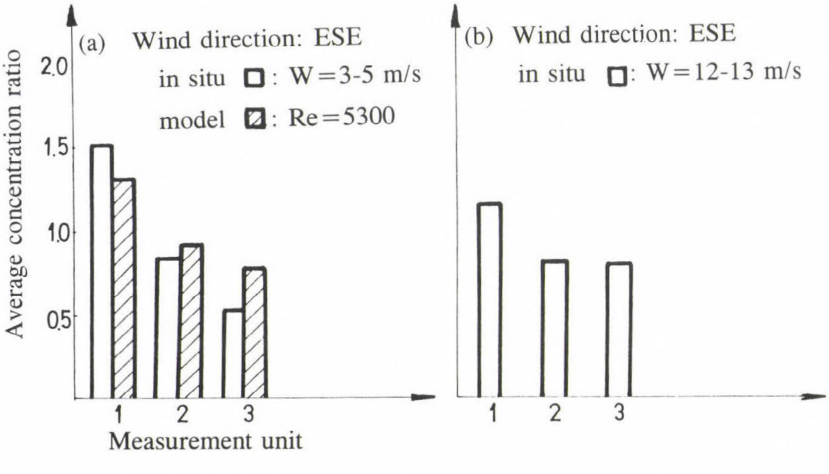

Fig 5. Concentration histogram, location: in front of the Main Post. (*a*) moderate wind; (*b*) strong wind.

The influence of the measurement unit position, which is described by the ratio of maximal to minimal in situ concentration, is very significant: for conditions of moderate wind the ratio differs 2.7 times and for strong wind the difference is 1.54 times. According to model measurements, predicted difference is 1.54 times.

On the basis of these results, it can be concluded that physical modeling provides a satisfactory degree of analogy of momentum and mass transport phenomena, which are cause of the distribution of pollutant in nature. Influence of objects layout and local turbulence on the concentration was also confirmed.

3. Conclusions

Model measurements exhibit very good accordance with in situ measurements; they are relatively simple, velocity and direction of the wind can be easily changed and objects' layout corresponds to the real situation.

Our investigations have shown that under the conditions of moderate wind velocity (1 to 5 m/s) significance of wind velocity and wind direction are approximately equal. For the model with a street 'canyon' measured concentrations for different velocities (other conditions were same) varied by up to 1.26 times; measured concentration for different wind directions varied by up to 1.36 times. For measurements without a street 'canyon' (Main Post building) and moderate wind velocity, the results varied by up to 1.58 times.

In the analysis of the influence of the measurement unit position, for small and moderate wind velocities, it was found that concentrations varied by up to 1.6 times. Therefore, the influence of the measurement unit position on measured pollutant concentrations is as important as the influence of meteorological parameters.

These investigations can give useful information for establishing a rational and functional network of representative measurement units in the complex structure of cities.

References

Alessio, S., Briatore, L., Elisei, G. and *Longetto, A.*, 1983: A laboratory model of wake-affected stacks emissions. *Atmospheric Environment 17*, 1139-1143.

Annand, W.Y. and *Hudson, A.M.*, 1981: Meteorological effects on smoke and sulfur dioxide concentrations in the Manchester area. *Atmospheric Environment 15*, 799-806.

Berlyand, M.E., 1975: *Contemporary problems of atmospheric diffusion and atmospheric pollution* (in Russian). Gidrometeoizdat, Leningrad.

Bezuglaya, E., 1986: *Atmospheric air-pollution monitoring* (in Russian). Gidrometeoizdat, Leningrad.

Cleroux, R., Roy, R. and *Robert, A.*, 1981: Relationships between sulfur dioxide pollution and meteorological factors in Montreal. *J. Environ. Syst. 10,* 165-181.

Cvijović, R.S., 1982: *Application of Adsorption Method and Hydraulic Analogy in Pollutant Distribution Modeling* (in Serbian). *Ph. D. Thesis*, University of Belgrade, Belgrade.

Cvijović, R.S. and *Cvijović, S.D.*, 1992: Some characteristic hydraulic models of pollutant transfer. *J. Serb. Chem. Soc. 57 (5-6)*, 375-384.

Končar-Đurđević, S., 1953: Application of a new adsorption method in fluid flow. *Nature 172*, 858.

Sonkin, L.R. and *Hrapachenko, V.*, 1965: Dependence of pollution in cities on meteorological conditions in summer season (in Russsian). *Trudy, G.G.O.,* No. 293, 68-77.

IDŐJÁRÁS

Quarterly Journal of the Hungarian Meteorological Service
Vol. 100, No. 4, October–December 1996

The effect of Belgrade on urban precipitation

Miroslava Unkašević

Institute of Meteorology, University of Belgrade,
11001 Belgrade, Dobračina 16, Yugoslavia

(Manuscript received 6 June 1995; in final form 27 December 1995)

Abstract—In this study daily, monthly, seasonal and yearly precipitation in the Belgrade area network during the period 1951–1985 are analyzed. Daily precipitation amounts were expressed in millimeters, which included the melted water equivalent for snow. Averaged annual minimum precipitation which refers to the spatial pattern is recorded northeasterly and maximum precipitation southwesterly from Belgrade confirming that the direction southwest-northeast is the direction of decreasing of station elevations.

It is shown that the average annual increase of precipitation on urban stations is about 11% in comparison with rural stations. This indicates that some individual rain intensity centres of showers or thunderstorms that develop or pass over Belgrade industrial area appear to be significant (*Ćurić* and *Janc*, 1987).

However, monthly precipitation in the Belgrade urban area does not seem to follow the rule that urban precipitation is always higher than rural, since contrary results have been found during the analyzed period.

The examined frequency distributions of mean daily temperature and distributions of total precipitation amounts as a function of mean daily temperature for Belgrade-Observatory for January and October (1951–1985) show that most of precipitations are observed below the median of daily temperatures.

Key-words: precipitation, urban effect, Belgrade area network.

1. Introduction

In a review of urban effects on precipitation in the United States, *Changnon* (1969) stated that if topographic effects are eliminated, urban produced increases in annual precipitation have been found to be from 5–8%. In the mid-western cities of Chicago, Champaign-Urban and Tulsa, warmer half-year precipitation totals were 4–6% higher in urban than rural areas; while for the colder half-year, the values were 6–11%. *Thomas* (1971) reports that in Toronto (Canada), with 35 precipitation observing stations, many in operation for 10–15 years, no urban effect on precipitation has been discovered. *Huff* and *Changnon*

(1972) report that for St. Louis, urban effects caused an increase in precipitation in and downwind of the city in all seasons, and that the average summer rainfall was increased by 6–15% for distances up to 40 km downwind of the city. The controversial results in La Porte data (*Changnon*, 1969) with differences reported as 30–35% for warm and cold season precipitation, perhaps should be considered a special case. Although the urban area or microscale precipitation pattern did not appear to differ on an annual basis from the regional precipitation pattern, *Sanderson et al.* (1973) concluded that, on a seasonal basis, Detroit received less precipitation than the surrounding rural areas in autumn and winter and about 20% more in summer.

Oke (1984) suggests that the greater frequency of rain initiation over urban and industrial areas is tied to three urban-related factors:

(1) thermodynamic effects which lead to more clouds, higher cloud bases and greater cloud instability,
(2) mechanical and thermodynamic effects that produce confluence zones where clouds and rain initiate,
(3) the enhancement of the cloud droplet coalescence process due to the addition of giant nuclei.

These factors appear to combine to initiate more cloud cells over urban-industrial regions in summer which, increase the probability of cell merger and the probability of heavier rain.

2. Precipitation in Belgrade area network

It is evident that there is an important gap in basic knowledge concerning small-scale rainfall processes which is important for design and analysis of urban precipitation and runoff (*Allerup*, 1991). There is an urgent need for coupling meteorology, hydrology and statistics in order to make improvements in urban precipitation characterization. The lack of densely spaced precipitation stations with good historical records, inadequate instruments for air-borne measurements of the effects on precipitation systems, and difficulties associated with delineating orographic, maritime, and gage-exposure effects are the primary reasons for insufficient research.

However, the recent development of air-borne nuclei measuring instruments has led to selected measurements of condensation and freezing nuclei over several urban areas. These facts give evidence that urban-induced nuclei concentration is high and probably sufficient to produce the observed changes in precipitation, whereas other studies (*Chandler*, 1976; *Landsberg*, 1981; *Goldreich*, 1985; *Oke,* 1986) have indirectly shown the importance of the urban thermal effects.

In this Section daily, monthly, seasonal and yearly precipitation in Belgrade area network during the period 1951–1985 are analyzed because in this period most of precipitation stations were in operation (48). The stations in the major area of Belgrade used in this work are shown in *Fig. 1*. The area, with its particularities (changes in height from 70 m (Boljevci) to 310 m (Avala)) presents characteristics making it particularly interesting for such studies. The Belgrade basin covers approximately 560 km^2 area with the hill of Avala to the south and two great rivers (Sava and Danube) and lowlands to the east, north and west. The precipitation stations taken into account (*Table 1*) are representative of the different areas present in this district: rural, suburban and urban territories. The Meteorological Station of the National Observatory of Belgrade which is situated at 132 m above mean sea level is the basic station.

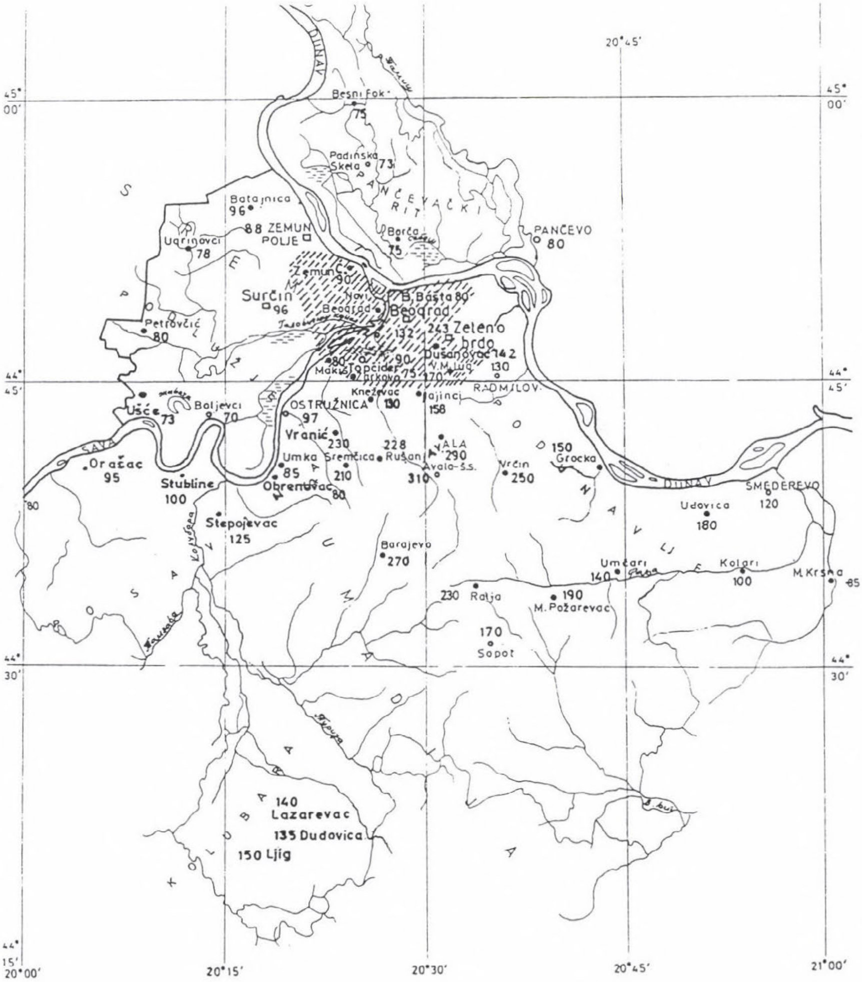

Fig. 1. Map of Belgrade precipitation network. The shaded area represents the Belgrade urban area. The numbers are related to the station altitude (m).

Table 1. Averaged monthly and annual precipitation (mm) during the period 1951–1985 in the Belgrade area

			MONTH												
No	Station	H(m)	Jan	Feb	Mar	Apr	May	June	July	Aug	Sep	Oct	Nov	Dec	Σ
1	Avala - Šum. upr.	290	52.4	48.7	51.7	60.0	76.7	90.8	71.2	60.4	57.2	47.5	59.1	62.8	738.3
2	Avala - Šuplja st.	310	48.5	46.0	46.6	56.5	74.9	87.7	69.0	53.7	54.9	45.8	56.5	59.3	699.4
3	Batajnica	96	43.7	41.2	41.2	46.2	60.2	92.9	62.3	52.1	45.9	41.3	52.1	58.5	637.6
4	Barajevo	270	59.3	43.3	45.0	54.7	81.6	92.3	67.5	64.2	51.6	51.6	52.6	61.8	719.1
5	Beograd (Obs)	132	49.1	46.4	46.5	55.9	72.2	95.6	70.4	53.9	53.1	42.5	55.7	58.7	700.2
6	Besni Fok	75	39.0	41.1	36.8	44.1	57.3	82.1	63.8	46.4	44.0	39.3	49.1	51.6	594.5
7	Botanička Bašta	80	48.6	47.1	46.3	57.4	73.9	95.8	71.8	54.7	52.0	42.8	58.1	62.3	710.7
8	Borča	75	47.2	44.1	42.2	52.4	64.3	93.3	63.5	51.8	47.2	41.4	53.1	57.9	658.4
9	Boljevci	70	46.1	46.1	42.3	50.9	68.5	89.7	63.1	59.1	51.4	45.0	54.4	59.7	672.3
10	Veliki Mokri Lug	160	56.0	50.5	51.6	59.7	74.2	102.4	75.7	52.7	54.7	45.8	57.8	62.7	743.6
11	Vranić	230	53.0	48.8	50.1	60.3	79.5	93.5	73.8	64.5	56.0	48.1	61.1	65.7	754.4
12	Vrčin	250	53.3	49.0	50.2	59.8	74.7	92.3	71.2	51.2	53.4	45.2	58.7	60.3	719.3
13	Grocka	250	41.7	40.0	40.8	52.3	66.3	76.1	60.0	47.5	43.7	43.0	52.5	50.3	614.2
14	Dudovica	135	57.3	53.6	59.2	67.8	95.7	97.0	82.0	72.0	60.1	54.2	67.4	67.8	834.0
15	Dušanovac	142	52.8	47.0	48.5	57.5	72.7	95.7	69.4	53.9	50.2	43.1	55.9	62.6	709.2
16	Žarkovo	75	48.5	44.8	43.5	53.4	70.2	87.7	64.4	51.1	50.3	44.5	54.3	58.5	671.3
17	Zeleno brdo	243	44.4	41.6	45.0	54.0	75.8	97.3	75.1	50.6	51.3	44.8	54.4	57.7	692.0
18	Zemun Ćukovac	90	49.0	45.0	44.8	54.8	68.9	91.9	68.1	53.8	53.1	43.6	54.3	59.5	686.7
19	Zemun Polje	88	39.4	39.6	37.7	49.4	67.7	85.3	67.9	50.8	45.5	42.9	50.5	52.9	629.6
20	Jajinci	158	47.5	44.3	44.9	57.5	74.4	97.7	71.7	54.2	52.3	43.2	55.0	58.1	692.6
21	Kneževac	130	49.7	45.6	46.9	57.9	71.9	94.1	71.0	59.1	53.9	44.8	55.5	60.1	710.5
22	Kolari	100	49.8	48.5	43.9	57.1	68.3	76.7	62.6	53.1	46.8	43.9	54.5	56.4	661.6
23	Lazarevac	140	59.8	55.0	60.8	63.7	85.1	99.3	76.8	69.2	56.3	49.8	64.1	68.4	799.8
24	Ljig	150	58.1	59.5	59.4	72.0	91.7	99.5	85.6	73.5	59.0	55.1	63.3	73.1	856.8
25	Makiš	80	47.4	42.5	42.2	50.7	70.2	86.9	61.9	56.3	49.4	42.1	50.5	57.4	640.5
26	Mala Krsna	85	46.2	40.9	43.0	53.9	73.0	85.5	65.9	51.5	45.1	42.5	53.8	55.1	655.8
27	Mali Požarevac	190	42.1	36.5	40.7	52.4	68.1	79.7	60.0	56.0	49.3	42.5	50.6	52.2	631.1
28	Obrenovac	80	45.8	41.8	43.5	52.8	65.5	89.4	67.4	62.8	52.6	46.7	53.0	57.3	678.6
29	Orašac	95	47.8	45.4	47.5	56.5	62.5	95.8	63.1	59.5	52.2	45.4	55.9	55.7	690.3
30	Ostružnica	97	49.6	44.1	44.3	51.5	71.8	85.7	63.6	57.8	50.5	44.1	54.2	59.2	676.3
31	Pančevo	80	40.8	40.2	40.7	52.2	71.5	90.7	63.5	52.5	43.7	40.0	55.1	56.0	647.0
32	Padinska skela	73	38.0	40.6	38.6	48.5	60.2	81.0	67.4	50.0	43.3	40.9	52.5	52.2	613.0
33	Petrovčić	80	47.2	46.2	44.5	52.6	65.8	88.6	62.3	58.2	50.7	45.4	53.3	61.8	676.6
34	Radmilovac	130	46.4	42.9	42.5	56.0	71.8	85.7	71.5	50.1	47.3	43.7	54.9	55.8	668.4
35	Ralja	230	50.3	43.4	47.5	58.0	73.0	90.7	70.7	55.1	52.9	49.1	55.3	59.9	706.1
36	Rušanj	228	52.8	47.5	46.9	58.5	72.5	93.1	63.9	64.5	57.3	46.5	57.1	61.2	721.9
37	Smederevo	120	46.7	43.0	43.1	55.5	71.2	88.0	62.7	51.5	49.1	44.5	55.2	53.5	664.0
38	Sopot	170	52.6	50.2	50.4	59.9	74.0	88.7	63.6	59.0	51.4	44.9	55.2	60.3	710.2
39	SremčIca	210	53.4	46.1	47.8	60.0	78.6	97.1	77.1	63.1	52.8	51.0	58.9	65.8	751.7
40	Stubline	100	46.6	48.7	51.5	58.4	71.4	91.8	74.0	58.4	54.8	50.6	59.3	56.4	721.9
41	Stepojevac	125	51.4	46.6	46.7	55.1	76.6	87.7	71.3	56.0	50.5	50.2	59.1	59.2	710.4
42	Surčin (Airport)	96	45.9	43.5	42.5	49.9	68.2	88.9	63.4	58.6	51.9	41.4	52.5	56.2	662.9
43	Topčider	90	55.3	47.7	49.8	57.1	75.7	93.3	76.4	58.0	53.0	43.2	57.1	60.8	727.5
44	Ugrinovci	80	41.5	41.5	36.7	43.8	59.8	81.2	60.8	56.2	46.4	44.3	51.2	55.5	618.7
45	Udovice	180	48.3	47.1	47.2	64.0	83.1	96.1	65.0	55.3	53.3	46.7	60.9	60.3	727.4
46	Umka	85	49.0	43.2	44.7	56.7	72.2	91.3	66.8	59.2	51.4	47.2	56.7	59.4	697.7
47	Umčari	140	46.6	45.5	46.0	55.8	66.7	77.9	62.4	53.0	44.1	44.2	50.3	58.7	651.2
48	Ušće	73	48.1	46.0	49.7	55.3	64.5	85.7	65.9	58.1	52.5	49.8	58.7	60.6	695.0

The numbers: 5, 7, 10, 15, 16, 18 are related to urban, 3, 4, 8, 17, 23, 24, 25, 26, 27, 28, 29, 31, 32, 37, 38, 39, 42, 43, 46, 48, to suburban and 1, 2, 6, 9, 11, 12, 13, 14, 19, 20, 21, 22, 30, 33, 34, 35, 36, 40, 41, 44, 45, 47, to rural stations. The station altitude (m) is given on the right-hand side of the station name.

Table 1 shows the annual and monthly data patterns for precipitation, as recorded in the different stations. Changes in annual precipitation are less than changes in monthly precipitation. Maximum changes occur in May, June and October and minimum in January. It may be concluded that greatest changes in warm season are caused by different thunderstorm precipitation. Annual precipitation in the Belgrade network area depends on the elevation of stations. Regional patterns of annual and seasonal precipitation are shown in *Fig. 2*.

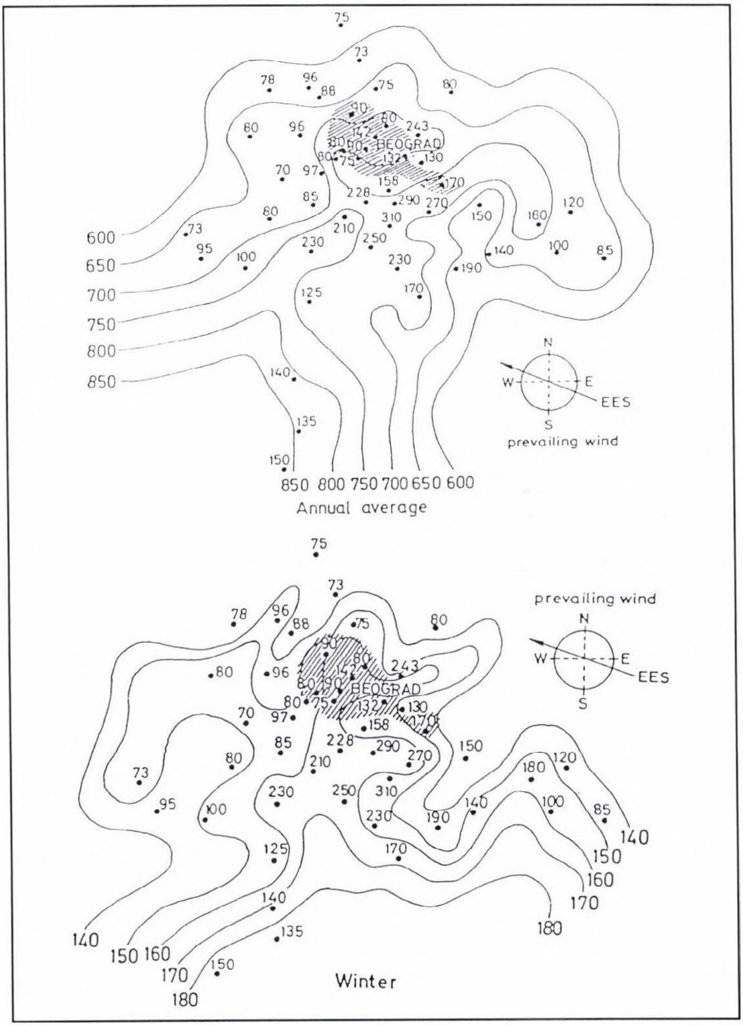

Fig. 2. Annual and seasonal precipitation patterns (mm), during the period 1951–1985 in the Belgrade area. The shaded area represents the Belgrade urban area. The numbers are related to station altitude (m).

Continued Fig. 2.

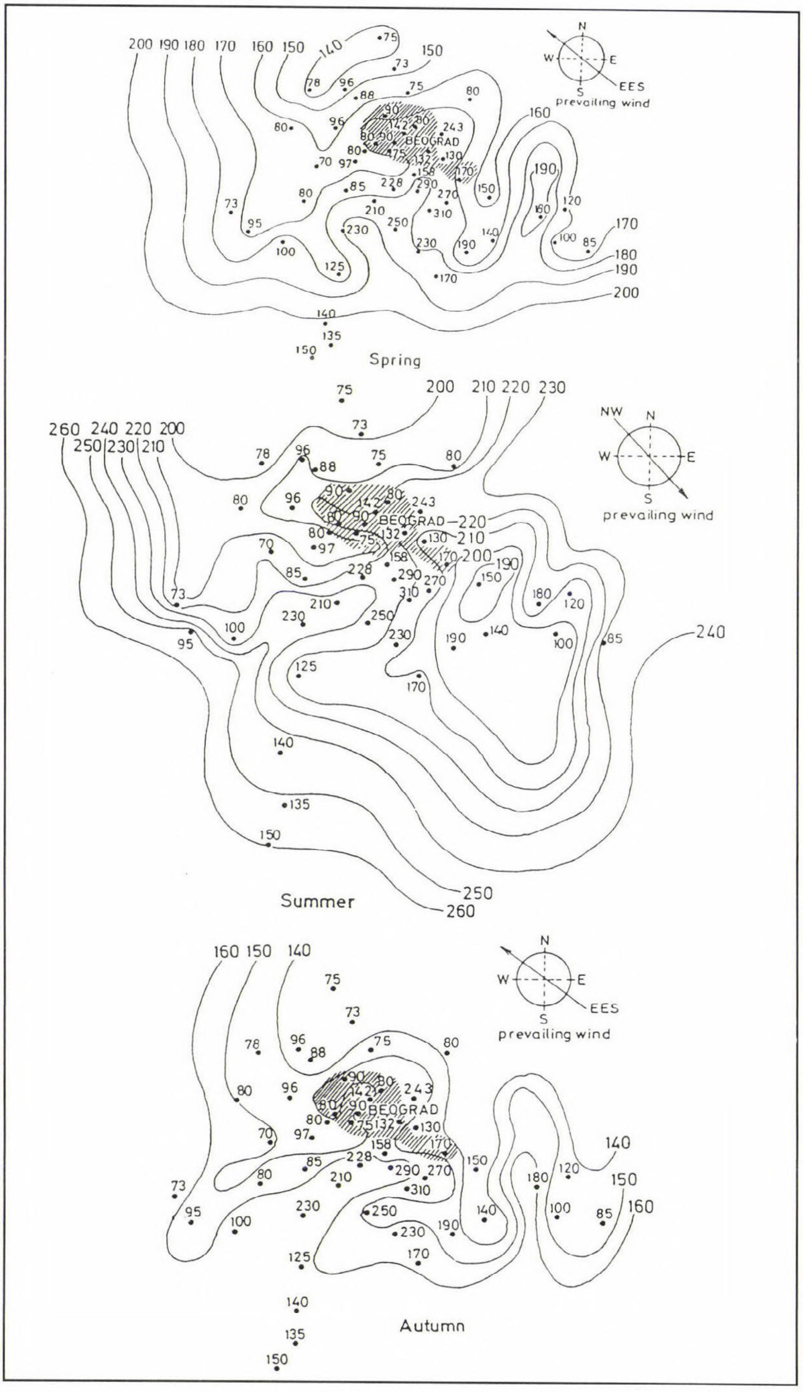

Averaged annual minimum precipitation amounts are recorded to the northwest from Belgrade in the area between precipitation stations Besni Fok and Zemun, i.e. in the area with the lowest elevations of the stations. Higher values over these precipitation amounts are recorded on stations Batajnica, Ugrinovci, Petrovčić Surčin, Pančevo and on stations along Danube river towards to the station Smederevo. Precipitation stations along Sava river and at the western border of Belgrade area have more of annual average precipitation by 20 to 50 mm than those stations on the eastern border of Belgrade area. This could be caused by updraft and cooling air on the west side of the Belgrade area which gave less precipitation than the east side of the Belgrade area.

However, the greatest precipitation amounts are registered in the region of Lazarevac towards Ljig, confirming that the direction southwest-northeast is the direction of decreasing in the station elevations.

The seasonal precipitation distribution (Fig. 2) shows that during spring and summer the relatively high amounts of precipitation are recorded in central parts of Belgrade city. In spring, the minimum precipitation amounts are recorded at the stations Besni Fok (138 mm) and Ugrinovci (140 mm), increasing to the south. The similar space distribution of precipitation is observed during summer but with greater amounts towards the prevailing wind. The precipitation amount decreases in the cold part of the year in all stations (Fig. 2). So in autumn and winter the amounts between 150 and 160 mm are registered in the Belgrade area (Fig. 2) giving evidence to more uniform distribution in the cold part of the year.

3. *The effect of urban heat island on urban precipitation*

First, we used the Student's t-test (*Brazel* and *Balling*, 1986) to determine differences in the means in periods 1888 to 1969 and 1970 to 1991 (period of great urbanization) in Belgrade-Observatory.

This statistic is determined as

$$t = \frac{(\bar{P}_2 - \bar{P}_1)}{\left(\left[\left(N_1 S_1^2 + N_2 S_2^2\right)/\left(N_1 + N_2 - 2\right)\right]\left[1/N_1 + 1/N_2\right]\right)^{1/2}},$$

where $(\bar{P}_2 - \bar{P}_1)$ represents the difference in group means, N_1 and N_2 are the number of cases within each subsample, and S_1 and S_2 are the standard deviations in the subsamples. When t is outside the bounds of the two-tailed probability of the Gaussian distribution tg (equal to 1.96 at the 0.95 confidence level), a significant shift in the means is assumed. The results are represented in *Table 2*.

The Student's test indicates that October have been characterized by slight decrease and January and February by slight increase in precipitation, so that there are significant changes in precipitation in the urban area during the period of examination.

Table 2. Precipitation time series descriptive statistic during the period 1888–1991 for Belgrade-Observatory

	Jan	Feb	Mar	Apr	May	Jun	Jul	Aug	Sep	Oct	Nov	Dec
t	1.99	2.03	0.49	-0.30	-0.06	1.64	0.92	–0.09	1.24	-2.13	0.33	1.79
tg	1.96	1.96	1.96	1.96	1.96	1.96	1.96	1.96	1.96	1.96	1.96	1.96

The 1951–85 frequency distributions of mean daily air temperature for Belgrade Observatory for January and October are shown in *Fig. 3* (*Isaac* and *Stuart*, 1992). Superimposed on Fig. 3 are the distributions of total precipitation amount as a function of mean daily temperature. The mean daily temperature was obtained by averaging the daily maximum and minimum temperatures. As it is evident from these graphs, most of the precipitation in October is observed at temperatures below the median of daily temperatures (65.6% represented by the hatched area on Fig. 3). This fraction of the total monthly precipitation for January is 46.9%. This shows that average daily temperatures can be used to identify other temperature-dependent phenomena as freezing rain or fog which is significant for urban climate.

In order to determine the effect of the urban heat island relative to the surrounding areas on urban precipitation, a spatial-temporal section was used with the mean values of the minimum temperatures collected at stations located on the line from station Zemun Polje to station Radmilovac. The section gives month by month trends of the minimum temperature from the rural station Zemun Polje through the city up to the rural station at Radmilovac during the period 1970–1989 and is represented in *Fig. 4* (*Unkašević*, 1991).

Taking into consideration these minimum temperatures, the presence of the heat island appears clearly either during the winter months or during the summer months, it increases from winter to summer.

ΔT_{S-S} and ΔT_{u-S} in *Table 3* concern the temperature differences between two suburban stations Padinska Skela and Pančevo (with elevation difference of 7 m) as well as the urban station Dušanovac and suburban station Surčin (Airport) (with elevation difference of 46 m). The terms ΔT_{S-r} and ΔT_{u-r} refers to the temperature differences between suburban and rural station located in Zeleno Brdo and Radmilovac (with elevation difference of 113 m), and urban station Beograd (Observatory) and rural station Ostružnica (with elevation difference of 35 m).

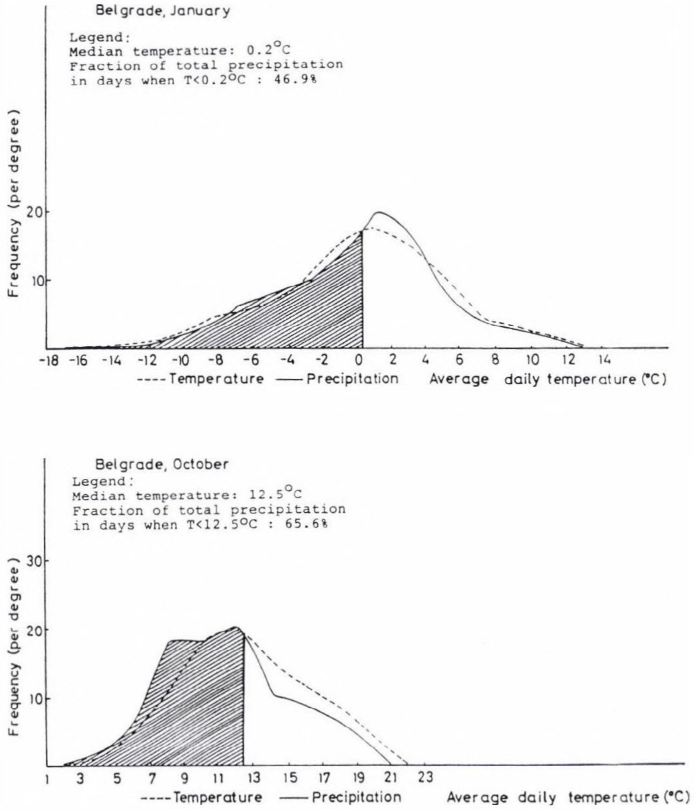

Fig. 3. Frequency distribution of temperature and total precipitation during January and October at Belgrade-Observatory during the period 1888–1991.

In a general sense, it is obvious that the city generates the heat island with temperatures increasing from suburbs to the center. Due to topographic (changes in elevation) and other complicating factors it is hard to place a definite value on the magnitude of the heat island, but it seems reasonable to suggest a figure of at least 2–3°C (*Unkašević*, 1991).

Research on the effect of the urban area on precipitation patterns has been done by a comparison of seasonal precipitation patterns for adjacent urban-rural pairs of stations of similar heights. The results, being represented in *Table 4*, show that maximum differences are obtained in four pairs of stations during spring and summer (rainy season) and in two pairs of stations during winter (Veliki Mokri Lug – Jajinci and Zemun Ćukovac – Zemun Polje). These maximum differences are registered downwind of the city in all seasons.

In the Belgrade area, warmer half-year precipitation totals were 3.4–37.4 mm higher in urban than in rural areas; while for the colder half-year, the differences were 4.9–30.6 mm. In the average value, for all pairs of stations, the rate of precipitation change has minimum in autumn (11.5 mm) and maximum in winter (20.4 mm). Namely, it is obvious that the average annual increase in precipitation of urban stations is about 11% in comparison with adjacent rural stations of similar heights, i.e. maximum annual increase was registered on urban station located in strong industrial zone of the Belgrade area (stations: Botanička Bašta, Dušanovac and Zemun Ćukovac).

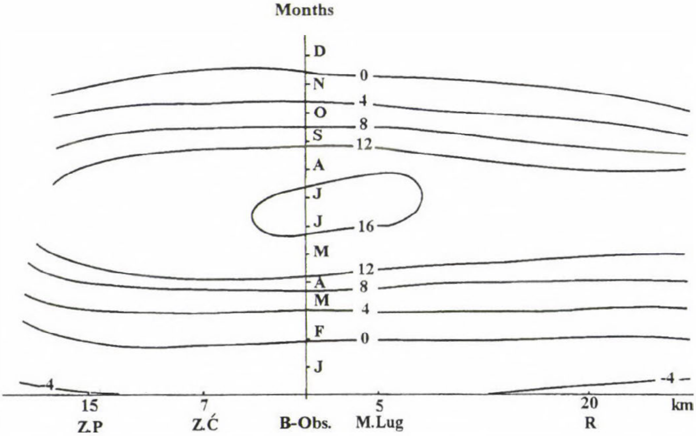

Fig. 4. Time-space section of the mean minimum temperature (˚C).

Table 3. Minimum mean monthly temperature differences between the city and the surroundings (˚C)

Temp. differ.	Jan	Feb	Mar	Apr	May	Jun	Jul	Aug	Sep	Oct	Nov	Dec	Year
$\Delta T_{s\text{-}r}$	1.9	2.0	2.3	2.5	3.0	2.5	3.0	2.7	3.3	3.2	1.3	2.3	2.5
$\Delta T_{s\text{-}s}$	1.3	2.2	1.6	1.7	2.0	1.2	2.3	2.3	1.4	15	1.0	1.1	1.8
$\Delta T_{u\text{-}r}$	1.5	2.0	1.7	2.5	3.4	3.3	3.6	3.3	3.8	3.7	3.0	1.8	2.8
$\Delta T_{u\text{-}s}$	1.9	1.6	1.9	2.2	1.5	1.6	2.2	1.0	1.9	1.1	2.0	1.0	1.6

Examination of the effect of urban heat island on urban precipitation is continued by using minimum temperature differences and precipitation differences from choice urban-rural pairs of stations during the period of strong industrialization in that part of the Belgrade area. The chosen urban-rural pairs of stations are: (a) Belgrade – Radmilovac (with minimum annual precipitation difference), (b) Zemun Ćukovac – Zemun Polje (with mean annual precipitation difference) and (c) Botanička Bašta – Besni Fok (with maximum annual precipitation difference). The obtained results, represented on *Figs. 5a, b* and *c*, indicates that there are insignificant correlations between urban-rural differences in monthly total precipitation and mean minimum monthly temperatures i.e., that urban heat island (shown in Fig. 4) has no effect on increase of precipitation in strong urban zone of the Belgrade area. It might be concluded that the direct thermal effect on increase in urban precipitation is small and that the other effects as increase of nuclei concentration in urban atmosphere from anthropogenic activities and cloud dynamics are dominant.

Table 4. Seasonal precipitation differences ΔP (mm) between urban-rural pairs of stations (numbers 5, 6, 7, 10, 13, 15, 16, 18, 19, 20, 34 and 44 are related to stations assigned in Table 1)

ΔP (mm)	Winter	Spring	Summer	Autumn	Annual value (mm)	%
5-34	9.8	3.4	12.5	4.9	30.6	4.6
7-6	27.1	37.4	29.9	19.3	113.7	19.1
10-20	19.6	8.6	7.2	7.8	43.2	6.2
15-13	30.6	19.3	35.4	9.9	95.2	15.5
16-44	13.6	27.2	5.1	6.9	52.8	8.5
18-19	22.0	13.7	10.0	20.4	66.1	10.5
Average	**20.4**	**18.3**	**16.7**	**11.5**	**66.9**	**10.8**

4. Conclusions

Precipitation stations at the west edge of the Belgrade area show 20 mm to 50 mm more precipitation than stations on the eastern border of Belgrade area in annual average, confirming that the direction southwest-northeast is the direction of decreasing of station elevations.

Monthly precipitation in the Belgrade urban area does not seem to follow the rule that urban precipitation is always higher than rural.

However, seasonal precipitation amounts are changed by the presence of the city. In autumn and winter Belgrade receives between 5 mm and 31 mm and in spring and summer between 3 mm and 37 mm more precipitation than the surrounding area. It is obvious that the average annual increase of precipitation in urban station is between 5 and 19% in comparison with adjacent rural stations of similar heights.

It seems to be most likely that any urban effects upon rainfall are related to cloud dynamical effects associated with the heat island and surface roughness.

Because there is a gap between existing and needed rainfall data (usually not provided by national weather services), an urgent need exists for further research on data acquisition by traditional (i.e. rain gauge) and modern methods (i.e. radar and satellites).

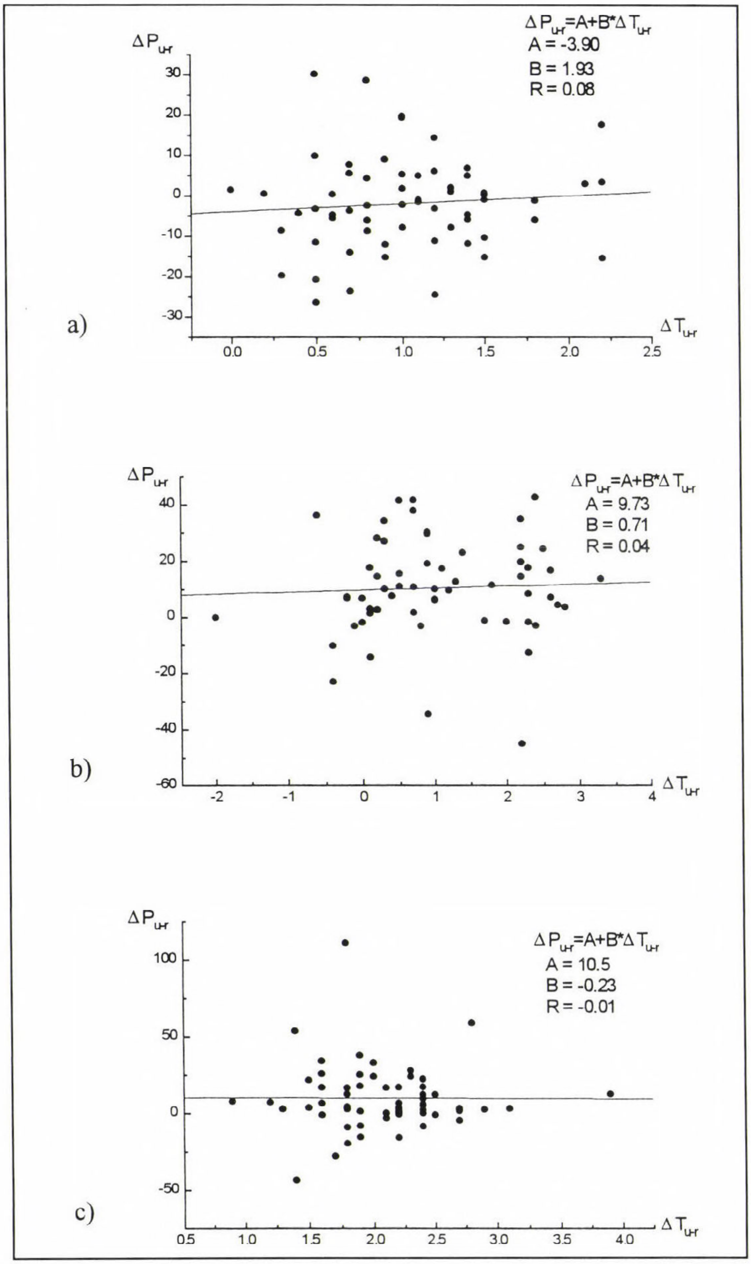

Fig. 5. Regression of differences in monthly total precipitation against differences in minimum monthly temperature between: (*a*) Belgrade (u) and Radmilovac (r) during the period 1987–1991; (*b*) Zemun Ćukovac (u) and Zemun Polje (r) and (*c*) Botanička Bašta (u) and Besni Fok (r) during the period 1987–1982.

References

Allerup, P., 1991: Statistical modelling of urban-scale precipitation data. *Atmos. Research 1-3*, 67-80.

Brazel, W.S. and *Balling, R.J.*, 1986: Temporal analysis of long term atmospheric moisture levels in Phoenix, Arizona. *J. Clim. Appl. Meteor. 25*, 112-117.

Chandler, T.J., 1976: *Urban Climatology and its Relevance to Urban Design*. Techn. Note, No. 149, WMO, Geneva.

Changnon, S.A., 1969: Recent studies of urban effects on precipitation in the United States. *Bull. Amer. Meteor. Soc. 50*, 411-421.

Ćurić, M. and *Janc, D.*, 1987: The effect of Belgrade on cloudiness during convective nights. *Bull. Serb. Meteor. Serv. 14,* 137-139.

Goldreich, Y., 1985: Urban topo-climatology. *Progress in Phys. Geog. 8,* 336-364.

Huff, F.A. and *Changnon, S.A.*, 1972: Climatological assessment of urban effects on precipitation at St. Louis. *J. Appl. Meteor. 11*, 823-842.

Isaac, G.A. and *Stuart, R.A.*, 1992: Temperature-precipitation relationships for Canadian stations. *J. Clim. 8*, 822-830.

Landsberg, H.E., 1981: *The Urban Climate*. Int. Geophys. Ser. 28, Academic Press, New York.

Oke, T.R., 1984: Methods in urban climatology. In *Applied Climatology*. Zurcher Geog. Schriften, Zurich, 19-29.

Oke, T.R., 1986: Urban climatology and the tropical city. In *Proc. Technical Conference on Urban Climatology and Its Applications with Special Regards to Tropical Areas*. WMO No. 652, Geneva, 1-25.

Sanderson, M., Kumanan, J., Tanguay, T. and *Schertzer, W.*, 1973: Three aspects of the urban climate of Detroit-Windsor. *J. Appl. Meteor. 12*, 629-638.

Thomas, M.K., 1971: A survey of the urban effect on the climates of Canadian cites. *Canadian Science*, No. 11-71, Environment Canada, Toronto.

Unkašević, M., 1991: Evidence of the urban heat island in Belgrade. *Beitr. Phys. Atmos. 1*, 55-63.

IDŐJÁRÁS

Quarterly Journal of the Hungarian Meteorological Service
Vol. 100, No. 4, October–December 1996

Analysis of harmattan dust over Accra, Ghana

K. Oduro-Afriyie and **K. Anderson**

Department of Physics, University of Ghana
Legon, Accra, Ghana

(Manuscript received 31 July 1995; in final form 13 June 1996)

Abstract—Harmattan aeolian dust from the Sahara desert which occurs in West Africa was monitored at Accra (5°32'N, 0°12'W) during the 1993/94 harmattan season. Dust deposition for 1993/94 harmattan season at Accra amounted to 4.8287×10^{-3} kg m^{-2}. Particle size analysis as well as X-ray fluorescence and neutron activation analyses were carried out on the harmattan dust. The particle size analysis indicated that the great majority of the particles deposited have a diameter above 1 μm with mean, mode and median diameters of 2.11, 2.00 and 1.73 μm, respectively. The deposition velocities, calculated by the Stokes formula, are 3.51×10^{-4}, 3.15×10^{-4} and 2.36×10^{-4} m s^{-1}, for these sizes respectively. X-ray fluorescence analysis of the dust showed the presence of the following elements, with the order of abundance as Fe > Ca > Cu > Ti > Zr > Pb > Sr > Rb > Y > Nb. In addition to these elements, neutron activation analysis also revealed the presence of elements: Na, K, Mn and Mg.

Key-words: harmattan dust, dry deposition, particle elemental composition.

1. Introduction

In West Africa, large quantities of dust particles are transported every year between November and March from the Sahara desert towards the Gulf of Guinea. The dust is transported by a cold dry wind, called the harmattan, which brings about one of the severest winter conditions and dust haze in the region (*Kalu*, 1977). The harmattan dust particles are kept air-borne for considerable length of time, and thereby produce a dusty atmosphere, which subsequently reduces visibility.

The harmattan dust has several source areas. One of such source areas is the Faya Largeau in Chad, off the western slope of the Tibesti-Massif (*Kalu*, 1977). According to *Wilson* (1971), the region responsible for the dusty atmosphere over West Africa is the Bilma-Faya Largeau area (see *Fig. 1*). Most of the dust settle over the coastal countries of West Africa (*Tiessen et al.*, 1991).

The Saharan dust also affects some parts of North Africa at certain periods of the year. For instance in summer, when the dust is essentially absent in West Africa south of the Intertropical Discontinuity (ITD), the trajectory of the dust changes to a westward direction to affect areas in the south western part of North Africa, such as Southern Algeria and Morocco, and further west to the Caribbean Islands across the Atlantic Ocean (*Prospero*, 1968).

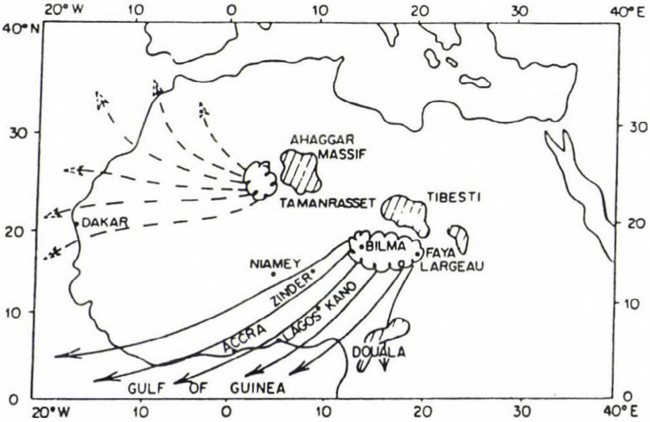

Fig. 1. Map of West Africa showing main source of harmattan dust; —— trajectory during winter; - - - trajectory during summer (*Kalu*, 1977).

The north-easterly winds blowing from the Sahara gives rise to high atmospheric turbidity and consequently, poor visibility in West Africa. The more turbid the atmosphere, the shorter the horizontal visibility (*Adeyefa* and *Adedokun*, 1991). Poor visibility, often caused by thick harmattan haze, frequently results in disruption of aviation schedules and sometimes aviation accidents over the West African sub-region. For example, because of the harmattan dust, visibility was only 300 m at Kano Airport, Nigeria, in the morning of 22 January, 1973, when 176 people lost their lives in the crash of a Jordanian airliner (*Hayward* and *Oguntoyinbo*, 1987).

Harmattan dust consists of atmospheric aerosol particles, and has some effect on climate. It interacts with solar radiation reaching the Earth's surface through scattering and absorption processes. It also affects the size distribution of cloud droplets and their optical characteristics (*Munn* and *Machta*, 1979).

Healthwise, harmattan brings an increase in viral diseases such as pneumonia, tuberculosis and meningitis. *Hayward* and *Oguntoyinbo* (1987) point out that outbreaks of cerebrospinal meningitis, irritation in the throat, cold symptoms and catarrh are associated with the onset of harmattan condition in West Africa.

Water bodies are polluted, and exposed foods become contaminated. These adversely affect the health and economy of a country.

On the positive side, harmattan dust may help to locally improve the structure and the micro-nutrient content of marginal soils (*Hayward* and *Oguntoyinbo*, 1987). It has been found to be the source of potassium and other basic materials in Volta shale soils in Northern Ghana (*Tiessen et al.*, 1991).

Adedokun et al. (1989) found in the harmattan dust the following major elements: Fe, Al, Ti, Si, Ca, Mg, Na and K with trace elements like Zn > Mn > Ni > Cu > Cr > Co > V > Li (in order of abundance) over Ile-Ife, Nigeria, during the harmattan seasons of 1983/84 and 1984/85. The mean and standard deviation of the particle sizes were 3.12 and 1.59 μm, respectively. They also found quartz, crodine and kaslinite as the main minerals in the harmattan dust.

The current study is intended to examine the physical and chemical characteristics of harmattan dust over Accra (5°32'N, 0°12'W) with a view to enhancing our knowledge on the harmattan dust in Accra. This would enable policy makers to tackle some of the problems associated with the harmattan dust.

2. *Materials and methods*

2.1 Sample collection

Harmattan dust samples were collected at five locations in Accra between December, 1993 and March 1994. These sites (*Table 1*) were chosen to give a fair representation of Accra. In order to avoid the intrusion of fugitive dust from local sources, the locations were sited far from any major road or bare land.

Table 1. Sites from which harmattan dust samples were collected

Site	Description
Atomic (AT)	Top of Radiation Protection Board building, Ghana Atomic Energy Commission, Kwabenya.
Legon (LEG)	Department of Physics, University of Ghana, Legon.
Meteo (MET)	Top of building in the weather observatory enclosure, Ghana Meteorological Services Department, Accra.
Airport (AP)	Top of a platform in the weather observatory enclosure, Kotoka International Airport.
Korle-Bu (KB)	Top of Medical School Laboratory building, Korle-Bu Teaching Hospital.

The dust was collected using locally constructed deposit gauges. Each deposit gauge consisted of a large funnel of cross-sectional area between 0.1052 and 0.1089 m^2. The nozzle of the funnel was fitted with a transparent polyethylene bag, which trapped the harmattan dust. Except at the Airport where sampling was done monthly because of stringent security measures, the dust was collected fortnightly at all sites.

For the particle size analysis, some of the dust particles were collected on clean glass slides mounted for 4 hours between 8.00 a.m. and 1.00 p.m. at the sampling sites.

2.2 *Analyses*

2.2.1 Particle size analysis

The particle size analysis was carried out with the aid of an Olympus CH2 optical microscope. The diameters of 5414 particles were measured.

Taking the density of a dust particle as 2.65×10^3 kg m^{-3} and the viscosity of air at 300K as 18.325×10^{-6} Ns m^{-2} (*Adedokun et al.*, 1989), the deposition velocities were computed for the various particle diameters using the well-known Stokes equation (see e.g. *Ludlam*, 1980).

2.2.2 Chemical analysis

An X-ray fluorescence spectrometer was used to determine quantitatively the chemical composition of the harmattan dust. The spectrometer was first calibrated against standards.

Dust samples collected from each site were put into pellets. Each side of a sample pellet was irradiated for 400 seconds. This was done to check the homogeneity of the sample.

Elemental analysis of the harmattan dust was also done using neutron activation analysis. This analytical technique was able to detect the elements with lower atomic numbers which the X-ray fluorescence analysis could not detect.

3. Results and discussion

Between 1.2015×10^{-3} kg m^{-2} and 10.8813×10^{-3} kg m^{-2} were collected at the five locations for 75 days. Deposition rates were low from December 22 to January 17, when the harmattan was relatively weak. The mean deposition and mean daily deposition rate for the entire harmattan season were 4.8287×10^{-3} kg m^{-2} and 0.0644×10^{-3} kg m^{-2} $(\text{day})^{-1}$, respectively (*Table* 2).

Table 2. Dust collected at various sites

Station	Cross-sectional area of catchment funnel m^2	Total deposit $\times 10^{-3}$ kg	Deposit per unit $\times 10^{-3}$ kg m^{-2}	Deposit rate $\times 10^{-3}$ kg m^{-2} day^{-1}
MET	0.1052	0.1264	1.2015	0.0160
AT	0.1061	0.2276	2.1451	0.0286
KB	0.1070	0.7712	7.2075	0.0961
AP	0.1078	1.1730	10.8813	0.1451
LEG	0.1089	0.2949	2.7080	0.0361
	Mean	0.5186	4.8287	0.0644

3.1 Results of particle size analysis

Fig. 2 shows the mean frequency of deposited particles versus their diameter.

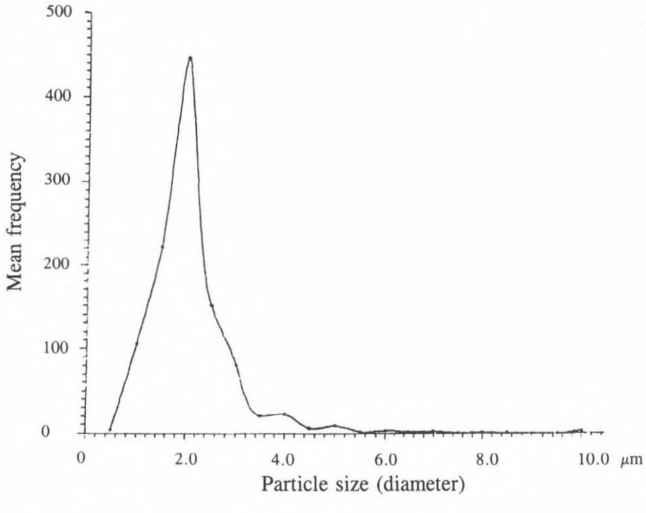

Fig. 2. Particle size distribution of harmattan dust over Accra.

The figure shows that:

(i) most of the particles (98.7%) have diameters less than or equal to 5.0 μm;

(ii) the mean diameter of the harmattan dust particles in Accra is 2.11 μm, with a standard deviation of 0.94 μm; 75.8% of particle diameters lie in the range (2.11 ± 0.94) μm;

(iii) the frequency distribution is close to a Gaussian distribution function, with mode at 2.00 μm. This value compares favourably with the 2.5 μm modal diameter obtained by *Adedokun et al.*, (1989) for Ile-Ife, Nigeria, which is nearer to the source region of the harmattan dust. The harmattan dust over Accra has a median particle diameter of 1.73 μm. This agrees with the findings of *El-Fandy* (1953) that, harmattan dust arriving in West Africa has particle diameter of 1.3 to 2.0 μm.

Bagnold's (1971) identification scheme on the deposited dust particles shows that 10.2% constitute haze. These have diameters ranging between 0.1 to 1.0 μm. The small percentage of particles in this size range among the deposited particles indicates that the majority of this range of particles remain suspended in the atmosphere for a long time. A typical diameter of about 0.50 μm can stay aloft for much longer periods, thereby causing atmospheric turbidity and poor visibility. They could only be washed out from the atmosphere by precipitation. These particles have diameters comparable to the wave-length of light (0.1 to 1.0 μm) and are therefore effective in scattering sunlight.

According to our observations, about 89.8% of the harmattan dust deposited have particle diameters greater than 1.0 μm. These are called coarse nuclei.

Head (1980) has shown that silt particles have diameters ranging from 2.0 to 6.0 μm, while clay particles have diameters less than 2.0 μm. Based on this classification, harmattan dust in Accra is composed of silt and clay in a relative quantity of 69.3% and 30.7%, respectively.

According to *Adefolalu* (1984) dust particles with diameters below 2 μm can reach the lungs of humans and bring about worsening conditions in respiratory ailments. 30.7% of the harmattan dust in Accra fall into this category. This might explain the outbreak of respiratory diseases in Accra during the harmattan season.

The particle diameters and their deposition velocities are presented in *Table 3*. The low values of the deposition velocities indicate that the particles do settle on surfaces at very slow rates. Their collision with human skins are therefore not felt.

3.2 Results of chemical analysis

X-ray fluorescence analysis of the dust particles revealed the presence of the following elements: Fe, Cu, Ti, Rb, Sr, Y, Zr, Nb and Pb. The dominant element detected was Fe and had an average value of 1.664% in abundance on mass basis. The least element in abundance was Nb with an average value of 5.5 ppm (*Table 4*). The order of abundance of the elements was Fe > Ca > Cu > Ti > Zr > Pb > Sr > Rb > Y > Nb.

The pattern of the elemental composition was the same for all the sampling sites. The high relative occurrence of Pb in the dust deposited at Legon might be attributed to exhaust fumes from the large concentration of vehicles on the campus, and which might have been trapped by the numerous trees.

Table 3. Particle diameters and computed deposition velocities of 1993/94 season of harmattan dust over Accra

Particle size	Diameter (μm)	Deposition velocity (ms^{-1})
Largest	10.00	7.87×10^{-3}
Mean	2.11	3.51×10^{-4}
Modal class	2.00	3.15×10^{-4}
Median	1.73	2.36×10^{-4}
Smallest	0.50	1.97×10^{-5}

Qualitative analytical results of the dust samples by neutron activation analysis showed the presence of the following elements: Ti, Na, K, Mn, Mg, Cu, Sr and Rb. These elements could not be quantified since the quantity of dust available at each site was less than 16×10^{-3} kg, which is the minimum amount required for such analysis.

The presence of these chemical elements in the harmattan dust, and the possibility of their deposition in the lungs and dissolution in the blood, might explain the high incidence of such ailments as cerebrospinal meningitis, irritation in the throat, colds and catarrh associated with harmattan in Accra. On the positive side, the presence of K and Na in the dust may help to improve the micro-nutrient content of the marginal soils in Accra.

Table 4. Elemental composition of harmattan dust at various sites (the relative quantities are expressed on mass basis)

Sample site	Ca ppm	Ti ppm	Fe %	Cu ppm	Rb ppm	Sr ppm	Y ppm	Zr ppm	Nb ppm	Pb ppm
KB	4800	2138	1.821	5982	16	42	12	175	7	98
AP	4121	2048	1.433	3582	13	30	9	133	8	64
LEG	7472	1653	1.704	4409	13	29	8	113	4	263
AT	3406	1503	1.697	1979	10	16	6	54	3	66
Mean	4949.8	1834.8	1.664	3969	13	29.3	8.8	118.8	5.5	122.8

4. Conclusions

The harmattan dust in Accra during the 1993/94 harmattan season was composed of 69.3% silt and 30.7% clay. The mean deposition of the dust during the entire sampling period was 4.8287×10^{-3} kg m^{-2}, with a mean deposition rate of 6.440×10^{-5} kg m^{-2} day^{-1}.

This study shows that 98.7% of the dust particles deposited have diameters less than or equal to 5.00 μm. The modal, mean and median diameters are 2.00, 2.11 and 1.73 μm, respectively. The particles have deposition or settling velocities of 3.15×10^{-4}, 3.51×10^{-4} and 2.36×10^{-4} m s^{-1} for the modal, mean, and median sizes, respectively.

Among the elements analyzed, the harmattan dust in Accra contained the following chemical elements: Fe > Ca > Cu > Ti > Zr > Pb > Sr > Rb > Y > Nb in order of abundance. Neutron activation analysis showed the presence of the following additional elements: Na, K, Mn and Mg.

Although the scope of this study was limited by the non-availability of X-ray diffractometer for mineralogical analysis, the results have thrown some light on the nature and chemical composition of harmattan dust in Accra.

Acknowledgements—The authors are grateful to the Director and staff of the Ghana Atomic Energy Commission, Accra, for the use of their X-ray spectrometer and neutron activation analyzer. They are also grateful for the hospitality offered to the first author by the International Centre for Theoretical Physics, Trieste, Italy where the final write-up was done during his Associateship visit in 1996; and to the Swedish Agency for Research Co-operation with Developing Countries for sponsoring the visit.

References

Adedokun, J.A., Emofurieta, W.O. and *Adedeji, O.A.*, 1989: Physical, mineralogical and chemical properties of harmattan dust at Ile-Ife, Nigeria. *Theor. Appl. Climatol. 40,* 161-169.

Adefolalu, D.O., 1984: On bioclimatological aspects of harmattan dust haze in Nigeria. *Arch. Met. Geoph. Biocl. Ser. B. 33*, 387-404.

Adeyefa, Z.D. and *Adedokun, J.A.*, 1991: Pyrheliometric determination of atmospheric turbidity in the harmattan season over Ile-Ife, Nigeria. *Renewable Energy 1*, 555-566.

Bagnold, R.A., 1971: *The Physics of Blown Sand and Desert Dunes*. Chapman and Hall, London.

El-Fandy, M.G., 1953: On the physics of dusty atmosphere. *Q. J. Roy. Meteorol. Soc. 79,* 284-287.

Hayward, D.F. and *Oguntoyinbo, J.S.*, 1987: *Climatology of West Africa.* Hutchinson Education, New Jersey.

Head, K.H., 1980: *Manual of Soil Laboratory Testing, vol. 1: Soil Classification and Compact Tests.* Pentech Press Limited, Plymouth, Devon.

Kalu, A.E., 1977: The African dust plumes; Its characteristics and propagation across West Africa in winter. In *Saharan Dust* (ed.: *A. Morales*). Wiley, New York.

Ludlam, F.H., 1980: *Clouds and storms.* University Park and London, Pennsylvania State Univ. Press.

Munn, R.E. and *Machta, L.*, 1979: Human activities that affect climate. *Proc. of the World Climate Conference,* Geneva, February, 1979.

Prospero, J.M., 1968: Atmospheric dust studies on Barbados. *Bull. Amer. Meterol. Soc. 49*, 645- 652.

Tiessen, H., Hauffe, H.K. and *Mermut, A.R.*, 1991: Deposition of harmattan dust and its influence on base saturation of soils in Northern Ghana. *Geoderma 49*, 285-299.

Wilson, I.G., 1971: Desert sand flow basins and a model for the development of ergs. *Geogr. J. 137,* 180-198.

BOOK REVIEW

Attila Kerényi: **Global Problems–Possible Solutions (General Questions of the Environmental Protection)** (in Hungarian with English summary). Mozaik Oktatási Stúdió, Szeged, Hungary, 1995, 383 pages.

A new book is published in the rich series of books on environmental protection. The book is warmly recommended to everybody who has any connection with environmental protection, deals with any topic of it, teaches it, or a member of any environmental movement, works for an environmental office in a council or he or she only is simply interested in the happening of our days.

We have the honour to Hungarian publishers for having published many translated books on environmental protection since the 70's. Lately, Hungarian authors have written too on the topic so the numbers of books concerning in the subject have grown into a small library. In these circumstances it is very hard to write a book that gives newer and more information than the earlier ones. Attila Kerényi fulfilled this requirement in many respects.

The book, 'General Environmental Protection' looks over the development of the earthly environment, the qualitative changes of it from the beginnings to nowadays. It displays the connection of the human being with its natural environment from the ancient time. The historical view and the system conception both characterise the chapters throughout the book. Logical argument and extremely many facts illustrate the deepest roots of the environmental problems that have grown global nowadays.

The author not only draws the problems. As the subtitle of the book signs too, he takes more care of the possible solutions than most of the earlier authors. From the most general principle of solutions to the most concrete solutions he presents many ways and real means on several areas of environmental protection.

The book redefines the basic environmental concepts and analyses their connections and relations. It deals with the action system of the environmental movement and emphasises the environmental tasks of different fields. The longest chapter presents the mutual connection between the human population and the environment as well the damaging effect of the production and consumption on environment. The author considers the action to slow the human demographic expansion and to produce energy with technology saving the environment, to be key factors. He discusses both topics in detail and gives real prospects on the future of atomic energy and recycling energy sources. The effect of mining, metal industry, transport, chemical industry and agriculture are analyzed later. Alternatives are suggested for the prevention of the damaging effects of these activities.

The book contains the consequences of the different forms of consumption and offers methods to learn to live with less as an alternative. Besides the usage of home garbage and sewage we can find chapters on the connection of tourism and environment and sport and environment.

The author deals with those environmental damages which do not connect with the pollution directly such as deforestation, overfishing, overgrazing, the effect of the change in field usage, soil erosion, deflation and the adverse effect of secondary alkalisation in the soil. Afterwards, basic knowledge on environmental pollution and waste follows.

The sixth chapter reveals the human effects on the changing operation of the global earth system. The subtopics in this chapter are the following: climate change, desertification, thinning of the ozone layer, acidification of the environment, pollution of the oceans, damage and extinction of species.

The chapter on the basic principles of environmental protection is a novelty. These principles 'work like lighthouses on seaside helping too determine the right way'. Among the principles a few ones are defined at the first time in the book.

The chapters on the economics and legal regulation of environmental protection are written by *Tibor Szász* and *Gyula Bándi*, respectively. A short chapter on chemical industry is the work of *Jenő Borda*.

In the last chapter, the author draws attention to the development of the environmental awareness. It is worth citing the last sentence: ‘Considering all the facts we mentioned here on environmental education and training, we can be certain that the future of our environment depends on what is happening at schools'.

Summarising, the real worth of the book is the followings: presents the problems without extremity, gives many alternatives for solutions, it is highly systematised, informative, wide scaled and it has mind changing approach. The book can serve as a manual too, because it has a good index of about 1500 words and a glossary to understand the basic notions.

We are sure that the book is one of the most remarkable Hungarian books published on environmental protection lately (by Mozaik Oktatási Studió, Szeged).

Imre Berki

NEWS

IDŐJÁRÁS Centenary Session

This issue of IDŐJÁRÁS (No. 4, 1996) closes the 100th volume of the journal. Previously (No. 1–3) a brief summary of the 99-year history reminded the readers of this special event.

For more than a quarter of a century, every year, the Hungarian meteorological community has been holding a two-day session under the title: Meteorological Scientific Days (MSD). In 1996 the second part of MSD was dedicated to IDŐJÁRÁS as its Centenary Session. For this occasion *Dr. Iván Mersich,* President of the Hungarian Meteorological Service, invited the 14 foreign members of the Editorial Board of IDŐJÁRÁS. From them nine colleagues came to Budapest to attend the meeting:

H.-W. Georgii, Germany
D. Möller, Germany
F. Neuwirth, Austria
S. Panchev, Bulgaria
J. Pretel, Czech Republic
A. Renoux, France
D. Spänkuch, Germany
D. A. Wilhite, USA
D. Závodsky, Slovakia.

Best wishes were expressed in writing for the other members and for the future of the journal by *B. Fisher* (U.K.) and *K. Ya. Kondratyev* (Russia), and also by *P. Brimblecombe* (U.K.), executive editor of the journal Atmospheric Environment.

The speakers of the Centenary Session and the titles of their presentations were the followigs:

Ernő Mészáros, academician, professor of Veszprém University (Hungary), he teaches environmental sciences. He was editor-in-chief of the journal for 15 years. **The role and tasks of IDŐJÁRÁS.**

Tibor Braun, professor of Eötvös Loránd University of Budapest, on the one hand he teaches and investigates chemistry, on the other hand he is a very well known scientometrist of the Library of the Hungarian Academy of Sciences. **The demography of scientific journals**.

Donald A. Wilhite, professor of University of Nebraska, Lincoln, USA, and director of Drought Research Center. **International nature of drought monitoring, response and mitigation efforts.**

Stoycho Panchev, professor of Clement Okhridsky University of Sofia, he teaches dynamic meteorology. **Nonlinear dynamics, chaos theory and applications as presented in meteorological journals and university education.**

Dietrich Spänkuch, scientist with the German Weather Service in Potsdam. He deals with IR atmospheric sounding. **UV radiation forecast and ozone monitoring at the Meteorological Observatory Potsdam**.

Dusan Závodsky, chief scientist of the Slovak Hydrometeorological Institute, president of the Slovak Meteorological Society. He deals with air chemistry. **Cooperation of Slovak and Hungarian meteorologists**.

The full session has been recorded on VIDEO tape.

At the end of the Centenary Session a reception was given by *Dr. Iván Mersich*. He expressed his thanks to all the contributors and editors for the past 100 years and invited the international and Hungarian meteorological community to help in the operation of IDŐJÁRÁS for the next 100 years!

G. Major

IDŐJÁRÁS

VOLUME 100 * 1996

Editor-in-Chief
G. MAJOR

Executive Editor
Ms. M. ANTAL

BUDAPEST, HUNGARY

AUTHOR INDEX

TABLE OF CONTENTS

I. Papers

II. Book review

III. News

IV. Subject index

The asterisk denotes book reviews or news